THE PHYSICAL REVIEW

VOLUME 83 Number 5

SEPTEMBER 1, 1951

Published by the
AMERICAN PHYSICAL SOCIETY
at
Lancaster, Pa. and Concord, N. H.

THE PHYSICAL REVIEW

A journal of experimental and theoretical physics established by E. L. Nichols in 1893

Published by the American Institute of Physics
for the
AMERICAN PHYSICAL SOCIETY

Officers

President

C. C. LAURITSEN
California Institute of Technology
Pasadena, California

Vice-President

J. H. VAN VLECK
Harvard University
Cambridge, Massachusetts

Secretary

K. K. DARROW
Bell Telephone Laboratories
Office:
Columbia University
New York 27, New York

Treasurer

G. B. PEGRAM
Columbia University
New York 27, New York

Local Secretary
for the Pacific Coast

J. KAPLAN
University of California at Los Angeles
Los Angeles, California

Managing Editor

S. A. GOUDSMIT
Brookhaven National Laboratory
Upton, Long Island
New York

BOARD OF EDITORS

Editor

S. A. GOUDSMIT

Assistant Editor

S. PASTERNACK

Associate Editors

J. BARDEEN — HARVEY BROOKS — M. GOLDHABER
T. BONNER — R. F. CHRISTY — R. HOFSTADTER
R. G. HERB — C. L. CRITCHFIELD — A. W. LAWSON
W. E. LAMB, JR. — M. DEUTSCH — A. PAIS
A. J. F. SIEGERT — T. H. JOHNSON — R. SERBER
W. E. STEPHENS — BRUNO ROSSI — C. H. TOWNES

Manuscripts for publication should be submitted to S. A. Goudsmit, Brookhaven National Laboratory, Upton, Long Island, New York. The authors' institutions are requested to pay a publication charge of $10 per page which, if honored, entitles them to 100 free reprints. Instructions will be sent with galley proofs.

Proof and all correspondence concerning papers in the process of publication should be addressed to the Publication Manager, American Institute of Physics, 57 East 55 Street, New York 22, New York.

Subscription Price

United States and Canada.....$25.00
Elsewhere.....$27.00

Back Numbers[1]

Yearly back number rate when complete year is available:
Prior to 1949: $20.00
Thereafter: $27.00
Single copies: $2.00 each, prior to July, 1929;
$1.00 each, July, 1929–December, 1941;
$2.00 each, January, 1942–December, 1946;
$1.00 each, January, 1947–December, 1948;
$1.25 each, thereafter.
General Index, 1893–1930: $4.00.

Subscriptions, renewals, and orders for back numbers should be addressed to the American Institute of Physics, 57 East 55 Street, New York 22, New York.

Changes of address in the case of members of the American Physical Society should be addressed to the Treasurer; in the case of other subscribers, to the American Institute of Physics.

[1] For Series I Index of Physics Department, Cornell University, Ithaca, New York.

The Physical Review is published semi-monthly at Prince and Lemon Streets, Lancaster, Pennsylvania.

Entered as second-class matter March 6, 1917, at the Post Office at Lancaster, Pennsylvania, under the Act of March 3, 1879.

Acceptance for mailing at special rate of postage provided for in paragraph (d-2), section 34.40, P. L. & R. of 1948, authorized January 1, 1949.

THE
PHYSICAL REVIEW

A journal of experimental and theoretical physics established by E. L. Nichols in 1893

SECOND SERIES, VOL. 83, NO. 5 SEPTEMBER 1, 1951

The Interaction of the Dirac Magnetic Monopole with Matter*

W. V. R. MALKUS
University of Chicago, Chicago, Illinois
(Received February 19, 1951)

It has been previously determined that an electron has no bound states in the field of the magnetic monopole. Seeking to establish the character of the monopole's interaction with the more complex fields of atoms and molecules, this paper investigates charged particles, of arbitrary magnetic moment, moving simultaneously in the field of the monopole and an external electric field. It is concluded that the monopole can be coupled to matter with energies comparable to, but not significantly greater than, the chemical bond, reservations being made in the case of hydrogen where the lowest energy state depends upon the mass of the monopole.

Speculation regarding the creation of monopoles by primary cosmic radiation and their consequent motion in the earth's magnetic field instigated an experimental attempt to arrive at an upper limit for the rate of such creation. The results of this experiment determine that the number of monopoles arriving at the surface of the earth is less than 10^{-10} per cm^2 per sec.

INTRODUCTION

PAST work[1] has shown that in the absence of an external electric field, an electron cannot be bound to the magnetic monopole.[2] Normal matter, however, is built upon such external electric fields. Hence, this work was undertaken to determine whether the presence of the magnetic monopole could reduce the energy of the electronic structure of an atom and so lead to bound states. The problem is clearly quite complex and is approached by consideration of the extreme cases. The total electric energy of an atom is therefore determined with the monopole first at or very near the nucleus, and second, removed to considerable distance. Conclusions may then be drawn concerning the magnitude of binding energy for intermediate cases.

The program of this investigation is: (I) to determine the eigenstructure of a charged particle with arbitrary magnetic moment in the field of a magnetic monopole and, using these results, to discuss the interaction energy of the atomic nuclei and the monopole; (II) neglecting, for the moment, the foregoing interaction energy, to find the eigenstructure of an electron in the combined field of a monopole and an atomic nucleus both situated at the origin; (III) to perform a variation-perturbation calculation on the many-electron problem built with the eigenfunctions found in (II) in order to determine whether the resulting total electronic energies are greater or less than that of the corresponding normal atom; (IV) to consider the approximate diamagnetic and paramagnetic energies of an electronic structure at some distance from a magnetic monopole, and to summarize these various findings in a conclusion regarding the monopole's interaction with matter.

In the last section, consideration of the possibility of monopole creation by cosmic radiation and the consequent motion of these particles in the earth's magnetic field leads to the description of an experiment which has set an upper limit on the arrival of monopoles at the earth's surface.

I. THE DETERMINATION OF THE EIGENSTRUCTURE OF A SPIN 1/2 PARTICLE OF CHARGE $Z|e|$ WITH ARBITRARY MAGNETIC MOMENT IN THE FIELD OF A MAGNETIC MONOPOLE

1. A vector potential of a monopole of charge M, situated at $r=0$, satisfying $\mathrm{div}\mathbf{A}=0$, $\mathrm{curl}\mathbf{A}=\mathbf{H}=M\mathbf{r}/r^3$, is

$$A_\phi = M/r(1-\cos\theta/\sin\theta)$$

* This paper is based on a thesis submitted in partial fulfillment of the requirements for the degree of Doctor of Philosophy at the University of Chicago.

[1] P. Banderet, Helv. Phys. Acta **19**, 503 (1946).

[2] E. Teller has observed that this conclusion is an immediate consequence of the Dirac equation for an electrically charged particle, since in the absence of an external electric field, yet with any magnetic field describable by a vector potential, Dirac's equation can have no energy eigenvalue whose absolute magnitude is less than mc^2.

and

$$A_\theta = A_r = 0. \tag{I 1.1}$$

2. The separated hamiltonian, to the Pauli approximation including an arbitrary radial electric field, but neglecting the spin orbit interaction and terms of higher order, is:

$$H = \frac{1}{2\mu}\left(\mathbf{P} - \frac{Z|e|}{c}\mathbf{A}\right)^2 + V(r) - B_z\frac{|e|\hbar}{2m_z c}\frac{M}{r^2}\sigma_r, \tag{I 2.1}$$

where B_z is the number of magnetons carried by the particle of charge $Z|e|$ and mass m_z. $B_z = Z$ for a Dirac particle. H may be written

$$H = -\frac{\hbar^2}{2\mu r^2}\left\{\frac{\partial}{\partial r}r^2\frac{\partial}{\partial r} + \frac{1}{\sin^2\theta}\left[\sin\theta\frac{\partial}{\partial\theta}\sin\theta\frac{\partial}{\partial\theta} + \left\{\frac{\partial}{\partial\phi} - i\kappa_z(1-\cos\theta)\right\}^2\right] + \gamma\sigma_r\right\} + V(r), \tag{I 2.2}$$

in which

$$\gamma = B_z(\mu/m_z)\kappa_{z=1} \tag{I 2.3}$$

and

$$\kappa_z = Z|e|M/\hbar c \tag{I 2.4}$$

where, as first concluded by Dirac,[3] $2\kappa_z$ must be an integer.

3. Solution of the angular operator when $\gamma = 0$. Consider

$$\mathfrak{L}^2 = \frac{1}{\sin^2\theta}\left[\sin\theta\frac{\partial}{\partial\theta}\sin\theta\frac{\partial}{\partial\theta} + \left\{\frac{\partial}{\partial\phi} - i\kappa_z(1-\cos\theta)\right\}^2\right], \tag{I 3.1}$$

which commutes with $L_z = -i\hbar(\partial/\partial\phi)$ (but not L^2).

Hence, if it is assumed that

$$\mathfrak{L}^2\Theta\Phi = -\beta_0\Theta\Phi,$$

then

$$\Phi = e^{im\phi}$$

where

$$m = 0, \pm 1, \pm 2, \cdots. \tag{I 3.2}$$

Therefore

$$\left[\frac{1}{\sin\theta}\frac{\partial}{\partial\theta}\sin\theta\frac{\partial}{\partial\theta} - \frac{1}{\sin^2\theta}\{m - \kappa_z(1-\cos\theta)\}^2\right]\Theta = -\beta_0\Theta. \tag{I 3.3}$$

Now let

$$x = \sin^2\tfrac{1}{2}\theta = (1-\cos\theta)/2. \tag{I 3.4}$$

Then

$$\left[\frac{\partial}{\partial x}x(1-x)\frac{\partial}{\partial x} - \frac{(m/2)^2}{x(1-x)} - \frac{\kappa_z(\kappa_z - m)}{(1-x)} + \kappa_z^2\right]\Theta = -\beta_0\Theta. \tag{I 3.5}$$

[3] P. Dirac, Proc. Roy. Soc. (London) **A133**, 60 (1931); Phys. Rev. **74**, 817 (1948).

The form of the two middle terms suggests trying

$$\Theta = x^{\frac{1}{2}|m|}(1-x)^{\frac{1}{2}|m-2\kappa_z|}u, \tag{I 3.6}$$

which leads to

$$x(1-x)\partial^2u/\partial x^2 + [(1+|m|) - 2(1+P)x]\partial u/\partial x - [P(P+1) - \kappa_z^2]u = -\beta_0 u, \tag{I 3.7}$$

where

$$P = \tfrac{1}{2}(|m| + |m - 2\kappa_z|). \tag{I 3.8}$$

If u is written as a series in x,

$$u = \sum_n C_{n+s}x^{n+s} \tag{I 3.9}$$

then $s = 0, -|m|$, the latter indicial being unacceptable and

$$\frac{C_{n+1}}{C_n} = \frac{[n(n-1) + 2(1+P)n + P(P+1) - \kappa_z^2 - \beta]}{[n(n+1) + (1+|m|)(n+1)]}. \tag{I 3.10}$$

The condition that this series terminates is

$$\beta_0 = l'(l'+1) - \kappa_z^2, \tag{I 3.11}$$

where

$$l' = n + P = |\kappa_z|, |\kappa_z| + 1, |\kappa_z| + 2 \cdots. \tag{I 3.12}$$

This eigenvalue has previously been obtained by Tamm[4] and Fierz.[5]

4. The solution of the angular operator for arbitrary γ. Since

$$\sigma_r = \begin{vmatrix} \cos\theta & \sin\theta e^{-i\phi} \\ \sin\theta e^{+i\phi} & -\cos\theta \end{vmatrix},$$

consider

$$\mathfrak{J}^2 = \begin{vmatrix} \mathfrak{L}^2 + \gamma\cos\theta & \gamma\sin\theta e^{-i\phi} \\ \gamma\sin\theta e^{+i\phi} & \mathfrak{L}^2 - \gamma\cos\theta \end{vmatrix} \tag{I 4.1}$$

where $\mathfrak{J}^2$ commutes with $J_z = -\hbar(\partial/\partial\phi) + \frac{1}{2}\hbar\sigma_z$.

Hence, if it is assumed that $\mathfrak{J}^2\Theta\Phi = -\beta\Theta\Phi$, then

$$\Phi = \begin{vmatrix} e^{i(m-1)\phi} \\ e^{im\phi} \end{vmatrix}, \quad m = 0, \pm 1, \pm 2, \cdots. \tag{I 4.2}$$

Therefore,

$$\left[\frac{1}{\sin\theta}\frac{\partial}{\partial\theta}\sin\theta\frac{\partial}{\partial\theta} - \frac{1}{\sin^2\theta}\{(m-1) - \kappa_z(1-\cos\theta)\}^2 + \gamma\cos\theta\right]\Theta_1 + \gamma\sin\theta\Theta_2 = -\beta\Theta_1$$

$$\left[\frac{1}{\sin\theta}\frac{\partial}{\partial\theta}\sin\theta\frac{\partial}{\partial\theta} - \frac{1}{\sin^2\theta}\{m - \kappa_z(1-\cos\theta)\}^2 - \gamma\cos\theta\right]\Theta_2 + \gamma\sin\theta\Theta_1 = -\beta\Theta_2. \tag{I 4.3}$$

[4] J. Tamm, Z. Physik **71**, 141 (1931).

[5] M. Fierz, Helv. Phys. Acta **17**, 27 (1944).

As in (I 3.3) to (I 3.7), the form of solution attempted is

$$\Theta_1 = x^{\frac{1}{2}|m-1|}(1-x)^{\frac{1}{2}|m-1-2\kappa_z|}u,$$
$$\Theta_2 = x^{\frac{1}{2}|m|}(1-x)^{\frac{1}{2}|m-2\kappa_z|}v \qquad \text{(I 4.4)}$$

leading to

$$x(1-x)\frac{\partial^2 u}{\partial x^2}+[(1+|m-1|)-2(1+\bar{P})x]\frac{\partial u}{\partial x}-\bar{\alpha}u$$
$$+\gamma(1-2x)u+2\gamma(1-x)^{1-A}x^{1-B}v=-\beta u \qquad \text{(I 4.5)}$$
$$x(1-x)\frac{\partial^2 v}{\partial x^2}+[(1+|m|)-2(1+P)x]\frac{\partial v}{\partial x}-\alpha v$$
$$-\gamma(1-2x)v+2\gamma(1-x)^{A}x^{B}u=-\beta v,$$

with $\alpha=P(P+1)-\kappa_z^2$ where P is defined in Eq. (I 3.8) and $\bar{P}$ and $\bar{\alpha}$ are similar expressions with (m) replaced by $(m-1)$, and

$$A=1 \text{ for } (m-2\kappa_z)\leqslant 0, \quad B=1 \text{ for } m\leqslant 0$$
$$A=0 \text{ for } (m-2\kappa_z)>0, \quad B=0 \text{ for } m>0. \qquad \text{(I 4.6)}$$

The symbol ϵ_{AB} is used to distinguish the four cases, where

$$\epsilon_{10}=\begin{cases}1 \text{ when } (m-2\kappa_z)\leqslant 0,\ m>0\\ 0 \text{ all other cases}\end{cases}$$
$$\epsilon_{01}=\begin{cases}1 \text{ when } (m-2\kappa_z)>0,\ m\leqslant 0\\ 0 \text{ all other cases}\end{cases}$$
$$\epsilon_{00}=\begin{cases}1 \text{ when } (m-2\kappa_z)>0,\ m>0\\ 0 \text{ all other cases}\end{cases}$$
$$\epsilon_{11}=\begin{cases}1 \text{ when } (m-2\kappa_z)\leqslant 0,\ m\leqslant 0\\ 0 \text{ all other cases.}\end{cases}$$

This notation permits writing all four cases at once.

If the further substitution

$$u=(-1)^{\epsilon_{01}+\epsilon_{00}}x^{\epsilon_{00}}u' \quad \text{and} \quad v=x^{\epsilon_{11}}v' \qquad \text{(I 4.7)}$$

is made, then

$$x(1-x)\partial^2 u'/\partial x^2+[\epsilon_{00}2(1-x)+(1+|m-1|)$$
$$-2(1+\bar{P})x]\partial u'/\partial x-[\bar{\alpha}+\epsilon_{00}\{2(1+\bar{P})$$
$$-(1+|m-1|)/x\}]u'+\gamma[(1-2x)u'$$
$$+2(-1)^{\epsilon_{01}+\epsilon_{00}}(1-x)^{\epsilon_{01}+\epsilon_{00}}x^{\epsilon_{11}+\epsilon_{10}}v']=-\beta u' \qquad \text{(I 4.8)}$$

and

$$x(1-x)\partial^2 v'/\partial x^2+[\epsilon_{11}2(1-x)+(1+|m|)$$
$$-2(1+P)x]\partial v'/\partial x-[\alpha+\epsilon_{11}\{2(1+P)$$
$$-(1+|m|)/x\}]v'-\gamma[(1-2x)v'$$
$$-2(-1)^{\epsilon_{01}+\epsilon_{00}}(1-x)^{\epsilon_{11}+\epsilon_{10}}x^{\epsilon_{01}+\epsilon_{00}}u']=-\beta v', \qquad \text{(I 4.9)}$$

where it is to be noted that in no case (ϵ_{AB}) does an x^2 term actually appear in the brackets multiplied by γ. In subtracting the foregoing equations,

$$x(1-x)\frac{\partial^2(u'-v')}{\partial x^2}-2(1+P+\epsilon_{11})x\frac{\partial(u'-v')}{\partial x}$$
$$-(\alpha+2\epsilon_{11}(1+P))(u'-v')+(-1)^{\epsilon_{11}+\epsilon_{10}}\gamma(u'-v')$$
$$+(1+|m|+2\epsilon_{11})\frac{\partial(u'-v')}{\partial x}+\epsilon_{00}\frac{|m|}{x}u'-\epsilon_{11}\frac{1+|m|}{x}v'$$
$$+\{2(\epsilon_{01}+\epsilon_{00})-1\}\frac{\partial u'}{\partial x}=-\beta(u'-v'), \qquad \text{(I 4.10)}$$

since

$$1+P+\epsilon_{11}=1+\bar{P}+\epsilon_{00}; \quad \alpha+2\epsilon_{11}(1+P)=\bar{\alpha}+2\epsilon_{00}(1+\bar{P}).$$

Now expressing u' and v' as descending series in x,

$$u'=x^n+C_1x^{n-1}+\cdots; \quad v'=x^n+C_2x^{n-1}+\cdots \qquad \text{(I 4.11)}$$

then the coefficient of x^n in (I 4.9) is

$$-n(n-1)-2(1+P+\epsilon_{11})n-[\alpha+2\epsilon_{11}(1+P)]$$
$$-(-1)^{\epsilon_{11}+\epsilon_{10}}-2\gamma(C_1-C_2)=-\beta, \qquad \text{(I 4.12)}$$

while the coefficient of x^{n-1} in (I 4.10) is

$$(C_1-C_2)[(n-1)(n-2)+2(1+P+\epsilon_{11})(n-1)$$
$$+\{\alpha+2\epsilon_{11}(1+P)\}-(-1)^{\epsilon_{11}+\epsilon_{10}}-\beta]$$
$$=[1-2(\epsilon_{11}+\epsilon_{10})]n+|m|(\epsilon_{00}-\epsilon_{11})-\epsilon_{11}. \qquad \text{(I 4.13)}$$

Eliminating (C_1-C_2) between these last two equations, and letting $l''=n+P+\epsilon_{11}$, then

$$\beta=l''^2-\kappa_z^2\pm[l''^2+2\gamma\{|m|(\epsilon_{11}-\epsilon_{00})$$
$$-P(-1)^{\epsilon_{11}+\epsilon_{10}}\}+\gamma^2]^{\frac{1}{2}},$$

which reduces to

$$\beta=l''^2-\kappa_z^2\pm[l''^2-\kappa_z^2+(\kappa_z-\gamma)^2]^{\frac{1}{2}}. \qquad \text{(I 4.14)}$$

Since ϵ_{11} is implicitly contained in β, it is here represented in terms of m and κ_z,

$$\epsilon_{11}=\tfrac{1}{4}(|m-2\kappa_z-1|+1$$
$$-|m-2\kappa_z|)(|m-1|+1-|m|). \qquad \text{(I 4.15)}$$

To understand the lowest roots of β, it is observed that both when $\epsilon_{01}=1$ and $\epsilon_{10}=1$, $P=|\kappa_z|$ and therefore $l''^2-\kappa_z^2=0$ for $n=0$. In these cases $C_1=C_2=0$ when $n=0$ and Eq. (I 4.13) becomes identically zero so that Eq. (I 4.12) alone determines β. Indeed when $\epsilon_{10}=1$, $\beta=\kappa_z-\gamma$ while when $\epsilon_{01}=1$, $\beta=\gamma-\kappa_z$, which are the two possible roots of the general form (I 4.14) when $l''^2-\kappa_z^2=0$. However when $\epsilon_{10}=1$, $\kappa_z>0$ while when $\epsilon_{01}=1$, $\kappa_z<0$, hence this lowest root may be written

$$\beta=|\kappa_z|-(\kappa_z/|\kappa_z|)\gamma \qquad \text{(I 4.16)}$$

in agreement with the results of (I 3.10) as γ approaches zero.

TABLE I. The energy levels and degeneracies of normal hydrogen compared with those of Eq. (II 1.8).

Degeneracy	n'	Hydrogen degeneracy
1	1	2
3	$\sqrt{2}$	
1	2	8
6	$1+\sqrt{2}$	
5	$\sqrt{6}$	
1	3	18
6	$2+\sqrt{2}$	
10	$1+\sqrt{6}$	
7	$\sqrt{12}$	
1	4	32
6	$3+\sqrt{2}$	
10	$2+\sqrt{6}$	
14	$1+\sqrt{12}$	
9	$\sqrt{20}$	
1	5	50

When the monopole is very massive compared to the charged particle, then the reduced mass $\mu \cong m_2$, and if this is true for the electron, where $Z=-1$, $B_2=-1$ and if κ_2 has its smallest value $\kappa_{2=-1}=-\frac{1}{2}(M/|M|)$, $\gamma=-\frac{1}{2}(M/|M|)$ then β can be reduced to

$$\beta=l(l+1)\pm[l(l+1)]^{\frac{1}{2}}, \qquad \text{(I 4.17)}$$

where $l=0, 1, 2, \cdots$. This last result has also been obtained by Banderet[1] as the eigenvalue of the angular operator in the relativistic treatment for an electron in the field of an infinitely massive monopole.

5. The lowest states of the atomic nuclei in the field of the monopole.

The radial equation is, in this case

$$(1/r^2)(\partial/\partial r)r^2(\partial/\partial r)R-(k^2+\beta/r^2)R=0, \qquad \text{(I 5.1)}$$

where $k^2=-2\mu E/\hbar^2$ and μ is the reduced mass of the monopole-nucleus system.

For the spin zero nuclei, the lowest value of β is $\beta_1=|\kappa_z|$ from (I 3.11), while for nuclei where $|\kappa_z| \gg \gamma$ (i.e., $1 \gg |B_z|$), $\beta_1 \cong |\kappa_z|$ from (I 4.16). However, in the case of the proton where $B_{z=1}=2.79$,

$$\beta_1=|\kappa_{z=1}|[1-B_{z=1}(\mu/m_{z=1})]$$

from (I 4.16), (I 2.2), and it is seen that this may be negative for sufficiently large values of the reduced mass.

It has been shown[6] that Eq. (I 5.1) has only solutions of positive energy for $\beta \geqslant -\frac{1}{4}$ but when $\beta < -\frac{1}{4}$ the interaction is such that arbitrarily low energy eigenvalues may be found. Hence, relativistic effects must be considered around this critical value of β. The monopole, then, can be bound to the proton if its mass is comparable to the proton mass, but the exact character of this situation is not clear.[7]

On the other hand, these considerations indicate that in the interaction of the magnetic monopole with all other atomic nuclei, no bound state exists.

TABLE II. The total electronic energies of normal atoms and atoms with a monopole in their nucleus, assuming no electronic interaction. Energy in units of $Z^2(-e^2/2a)$.

Z	Atom	Normal	Monopole
1	H	1	1
2	He	2	1.500
3	Li	2.250	2
4	Be	2.500	2.500
5	B	2.750	2.750
6	C	3	2.922
10	Ne	4	3.508
16	S	4.666	4.613
28	Ni	6	5.575
40	Zr	6.750	6.662
60	Nd	8	7.638
80	Hg	8.800	8.690

II. THE ENERGY LEVELS AND EIGENFUNCTIONS OF AN ELECTRON IN THE FIELD OF A MONOPOLE AND A PARTICLE OF CHARGE $Z|e|$ BOTH SITUATED AT THE ORIGIN

1. The radial equation obtained from separation of the more general hamiltonian of Sec. A is:

$$(1/r^2)(\partial/\partial r)r^2(\partial/\partial r)R-(k^2+U(r)+\beta/r^2)R=0 \qquad \text{(II 1.1)}$$

where $k^2=-2\mu/\hbar^2 E$ and $U(r)=-(2\mu/\hbar^2)(Ze^2/r)$. For the electron then, where $\beta=l(l+1)\pm[l(l+1)]^{\frac{1}{2}}$ when $|\kappa_z|=\frac{1}{2}$, and for positive Z, we consider negative E.

Let $\rho=2kr$ and let $n'=(\mu/\hbar^2)(Ze^2/k)$, exactly as for the normal Laguerre polynomials, then

$$(1/\rho^2)(\partial/\partial\rho)\rho^2(\partial/\partial\rho)R + (-\tfrac{1}{4}+n'/\rho-\beta/\rho^2)R=0 \qquad \text{(II 1.2)}$$

asymptotically $R=e^{-\frac{1}{2}\rho}F$,

$$F''+\left(\frac{2}{\rho}-1\right)F'+\left[\frac{n'-1}{\rho}-\frac{\beta}{\rho^2}\right]F=0 \qquad \text{(II 1.3)}$$

let $F=\rho^s L(\rho)$,

$$s=\frac{-1+(1+4\beta)^{\frac{1}{2}}}{2}=|\tfrac{1}{2}\pm[l(l+1)]^{\frac{1}{2}}|-\tfrac{1}{2} \qquad \text{(II 1.4)}$$

the other root leading to unacceptable origin divergence. Therefore

$$\rho L''+[2(s+1)-\rho]L'+(n'-s-1)L=0, \qquad \text{(II 1.5)}$$

where L is a polynomial of order n'' if

$$n'=n''+s+1=n''+\tfrac{1}{2}+|\tfrac{1}{2}\pm[l(l+1)]^{\frac{1}{2}}|. \qquad \text{(II 1.6)}$$

Hence,

$$R=e^{-\frac{1}{2}\rho}\rho^s L(\rho) \qquad \text{(II 1.7)}$$

[6] N. F. Mott and H. S. W. Massey, *The Theory of Atomic Collisions* (Oxford University Press, London, 1933), p. 40.

[7] A paper is being prepared which considers a monopole with spin in its interaction with the proton. The results indicate that the monopole mass which gives rise to the critical value, $\beta=-\frac{1}{4}$, is equal to the proton mass.

TABLE III. The unnormalized eigenfunctions of an electron in the field of a charged particle and a monopole, from Eqs. (I 4.4) and (II 1.7).

$$\psi_{100}=(-\sin\tfrac{1}{2}\theta e^{-i\phi}\uparrow+\cos\tfrac{1}{2}\theta\downarrow)e^{-\varrho/a}$$

$$\psi_{\sqrt{20}+1}=(-\cos\tfrac{1}{2}\theta[\sin^2\tfrac{1}{2}\theta+(3-\beta)]\uparrow+\sin\tfrac{1}{2}\theta\cos^2\tfrac{1}{2}\theta e^{+i\phi}\downarrow)e^{-\varrho/\sqrt{2}a}\varrho^{\sqrt{2}-1}$$

$$\psi_{\sqrt{21}0}=\left(\sin\tfrac{1}{2}\theta\left[\cos^2\tfrac{1}{2}\theta-\frac{1}{\beta}\right]e^{-i\phi}\uparrow+\cos\tfrac{1}{2}\theta\left[\sin^2\tfrac{1}{2}\theta-\frac{1}{\beta}\right]\downarrow\right)e^{-\varrho/\sqrt{2}a}\varrho^{\sqrt{2}-1}$$

$$\psi_{\sqrt{20}-1}=(\cos\tfrac{1}{2}\theta\sin^2\tfrac{1}{2}\theta e^{-i2\phi}\uparrow-\sin\tfrac{1}{2}\theta[\cos^2\tfrac{1}{2}\theta+(3-\beta)]e^{-i\phi}\downarrow)e^{-\varrho/\sqrt{2}a}\varrho^{\sqrt{2}-1}$$

$$\psi_{200}=(-\sin\tfrac{1}{2}\theta e^{-i\phi}\uparrow+\cos\tfrac{1}{2}\theta\downarrow)e^{-\frac{1}{2}\varrho/a}(1-\tfrac{1}{2}\varrho/a)\quad\text{where}\quad\beta=2-\sqrt{2}.$$

and

$$E_{n'}=-(e^2/2a)(Z^2/n'^2), \qquad \text{(II 1.8)}$$

where $a=\hbar^2/\mu e^2$.

The multiplicity of each eigenvalue in Eq. (II 1.8) follows from the $(2l+1)$-fold degeneracy of each l value and from the fact that, for a given $l\geq 1$, each n' value resulting from (II 1.6) with the upper sign is obtained once more by using the lower sign and replacing n'' by $n''+1$.

2. Table I implicitly compares the energy levels of Eq. (II 1.8) and the degeneracy of each level with those of normal hydrogen. The table actually lists the values of this parameter n' of (II 1.6) which is inversely proportional to the square root of the energy.

Table II compares the total electronic energies of various normal atoms with those containing a monopole on the assumption that there is no electronic interaction. The values tabulated after $Z=6$ are alternately those corresponding to maxima and minima of the energy difference between the normal and monopole atoms. It is to be noted that, in this approximation, the monopole increases the total electronic energy in all cases except hydrogen, beryllium, and boron. A perturbation calculation should indicate whether the monopole-electron interaction can cause binding of the monopole in beryllium and boron, while the total energy in hydrogen depends upon the monopole-proton interaction discussed in (I 5).

Table III lists the unnormalized eigenfunctions, obtained from (I 4.4), (I 4.7), (I 4.11), and (II 1.7), which are necessary in the calculation mentioned above. The vectors $\uparrow$ and $\downarrow$ indicate the orthogonal eigenfunctions of σ_z. The total eigenfunction is identified by the three indices n', n, and m, where n' is the energy parameter of (II 1.6), while n and m are the parameters defining the angular part of the wave function as in (I 4.4) and (I 4.11).

3. The perturbation variation computation of the total electronic energies of the beryllium-like and boron-like atoms proceeds in a conventional and somewhat tedious fashion. The technique and results were checked by performing the identical manipulations to approximate the energies of the normal atoms as well. These computed energies are listed in Table IV and compared with the observational values for the normal atoms. These results demonstrate that a monopole at or near an atomic nucleus markedly increases the total electronic energy. However one might have expected that normally paramagnetic atoms would attract the monopole. While such attraction is overcompensated by diamagnetic effects when the monopole is at $r=0$, the behavior of the monopole at other distances must still be investigated.

III. APPROXIMATE CONSIDERATIONS WITH THE MONOPOLE AT SOME DISTANCE FROM THE NUCLEUS

1. The previous sections have determined the energetic consequences of a magnetic monopole near the nucleus of the atom. The problem of the monopole at an arbitrary distance from the nucleus is far more complex and is dealt with here in a most approximate way.

When the monopole is at considerable distance from an electronic structure, the change in its energy, ΔE, is the sum of the normal paramagnetic and diamagnetic terms,

$$\Delta E=E_p+E_d=-(e\hbar/2\mu c)\mathfrak{IC}\textstyle\sum_i(m_z{}^i+2s_z{}^i)$$
$$+(e^2/\mu c^2)\mathfrak{IC}^2\textstyle\sum_i(x_i{}^2+y_i{}^2) \qquad \text{(III 1.1)}$$

where the magnetic field is $\mathfrak{IC}=M/R^2$ and R is the distance of the monopole of charge M from the structure, where i is summed over the various electrons and $m_z{}^i$, $s_z{}^i$, $x_i{}^2$, and $y_i{}^2$ are the eigenvalues of the usual operators of the z component of angular momentum, spin, and coordinate position, respectively.

In an attempt to judge the minimum energy a normally paramagnetic substance may have in the field of the monopole, the minimum of ΔE will be found for the case of the hydrogen atom where $m_z=0$, $s_z=\frac{1}{2}$, and $x^2=y^2=(\hbar^2/\mu e^2)^2=a_0{}^2$. Then

$$\partial\Delta E/\partial R=0=2eM\hbar/2\mu cR^3-4e^2M^2\cdot 2a_0{}^2/8\mu c^2R^5 \qquad \text{(III 1.2)}$$

TABLE IV. The computed total electronic energies of helium, beryllium, and singly ionized boron for normal and monopole atoms. Energy in units of $(-e^2/2a)$.

		Perturbation computation		Observed
Z	Atom	Normal	Monopole	Normal
2	He	5.70	4.63	5.81
4	Be	28.4	25.2	29.35
5	B^+	47.2	43.5	48.76

but $eM/\hbar c=\frac{1}{2}$, so $(\hbar^2/2\mu R^3)(1-a_0^2/2R^2)=0$. Hence,

$$R=a_0/\sqrt{2} \qquad \text{(III 1.3)}$$

and the minimum energy

$$\Delta E_{\min}=-\hbar^2/2\mu a_0^2+\hbar^2/4\mu a_0^2=-6.76 \text{ ev.} \qquad \text{(III 1.4)}$$

2. This last result is drawn in a region of R outside the valid range of the approximation (III 1.1). However the use of a trial wave function and the complete hamiltonian corresponding to (III 1.1) permits the establishment of both an upper and lower limit for the binding energy. This has been done for a trial function similar to ψ_{100} in Table III and, after lengthy computation leads to a maximum value for $\Delta E_{\min}\simeq -7$ ev at $R\simeq 0.56a_0$, quite similar to the approximation (III 1.4). For the many-electron configuration, one sees from Eq. (III 1.1) that while each electron still contributes a diamagnetic term, only the few electrons in unfilled shells or excited states may be paramagnetic. Hence, one would anticipate that the monopole could be coupled to matter with energies comparable to the chemical bond but not significantly greater.

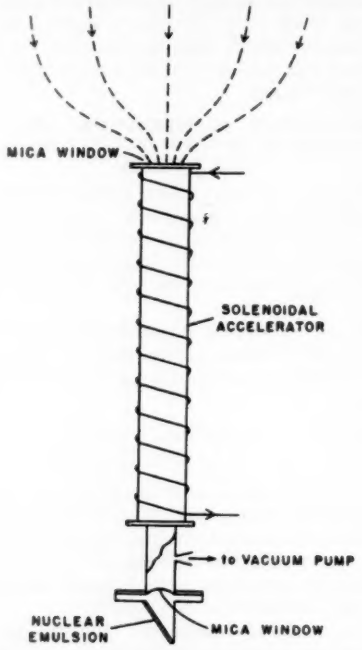

FIG. 1. Schematic diagram of an instrument to detect magnetic monopoles arriving at the earth's surface.

Of course, no estimate of nuclear forces is possible and these may be attractive, repulsive, or neutral. However, a sizable barrier confronts the monopole before it can be influenced by the nucleus.

IV. SOME CONSEQUENCES OF THE CREATION OF MAGNETIC MONOPOLES BY PRIMARY COSMIC RADIATION AND EXPERIMENTAL CONSIDERATONS WHICH SET AN UPPER LIMIT FOR SUCH CREATION

1. The energy needed for the production of a monopole pair is available in the primary cosmic radiation even if the monopole is considerably heavier than the proton.[8] Once created[9] in the atmosphere the initially energetic monopole would reach a low terminal velocity in the earth's magnetic field in a few meters because of its large and velocity independent ionization loss (about 5 Mev/cm N.T.P.). No conventional cosmic-ray techniques would have detected these monopoles moving along the field lines at terminal velocity while the relatively few energetic monopoles created near a nuclear emulsion or a cloud chamber would probably stop in the protective covering of these instruments. For example, one-fourth of a millimeter of brass would stop a monopole with 1 Bev of energy.

If the monopole were strongly bound to matter by unknown nuclear forces or, if more massive than the proton, bound to it by the forces discussed in Sec. I-5, then it would be possible for monopoles to depolarize the earth. Indeed, if this is so, a monopole arrival rate at the surface of the earth of one per cm² per sec would cancel the earth's magnetic field in a month. Hence one could tentatively conclude that if monopoles have been accumulating in the earth's crust for the last billion years, then their arrival rate must be less than 10^{-10} per cm² per sec, for there is no measurable magnetic charge associated with surface matter.

However, if the conclusions of Sec. III are correct and the monopole is bound only weakly to paramagnetic material, then monopoles could diffuse through the earth and would have little effect on the magnetic field. In this case as many positive monopoles would be moving one way as negative monopoles the other, and once beyond the earth's atmosphere, the monopoles would be hurled free of the earth's dipole due to their inertia. The only effect then is to dissipate part of the energy stored in the earth's magnetic field which could be restored by the internal regenerative processes hypothesized in recent literature.

2. A simple experiment has been performed to detect those monopoles arriving at the surface that can diffuse through the earth at any rate greater than one kilometer in a billion years. Figure 1 is a schematic diagram of

[8] Although postulated as a particle completely analogous to the electron, the magnetic monopole has a "fine" structure constant $M^2/\hbar c=137/4$, and consequently such processes as monopole pair production cannot be dealt with by the conventional weak coupling approximation. However, a computation based on the assumption of weak coupling would conceivably be correct within several orders of magnitude. Such a computation, for monopole masses comparable to the proton mass, implies that the arrival of monopoles at the surface of the earth would be roughly one per cm² per sec.

[9] The monopole, to conserve its charge, will continue to exist indefinitely since the probability of an annihilation collision will be vanishingly small.

the instrument constructed. A long solenoid draws monopoles moving at terminal velocity along the earth's field lines through a thin window into its evacuated core. The monopoles are then accelerated to several hundred Mev and pass through a second window to strike a photographic emulsion. The experimental requirements and the conclusions drawn from operating the instrument are described in the following paragraphs.

The monopole, of charge $M=(137/2)e$ emu, gains $(137/2)300H$ ev/cm in free fall in a field of H gauss. Hence in a field of 250 gauss, one meter long, the monopole gains 500 Mev. As indicated in the figure, monopoles moving along the earth's field lines would be drawn to the upper surface of the evacuated[10] brass tube which forms the core of the solenoid. Here they diffuse through a 10 mg/cm² mica window and attain 500 Mev in the one-meter fall. On passing through a second mica window at the lower end of the solenoid the monopole will lose less than 50 Mev, while its loss in the photographic emulsion which it then strikes will be roughly 1 Mev per micron.

The effective cross-sectional area, A_E, of the earth's field lines drawn into the solenoid can be found by observing that all the flux drawn into the upper end of a solenoid comes from the earth's field in any solenoid for which

$$H_a=H_s\cdot A_s/4\pi a^2<H_E, \qquad \text{(IV 2.1)}$$

where H_a is the external field due to the solenoid alone near its midpoint; H_s is the internal field of the solenoid; A_s is the cross-sectional area of the solenoid and a its half-length; H_E is the earth's field. In the solenoid constructed this inequality (IV 2.1) holds, hence

$$A_EH_E=A_sH_s. \qquad \text{(IV 2.2)}$$

It should be noted that no ferromagnetic material which might distort the magnetic field was placed near the solenoid and that it was directed along the local field lines in an exposed place.

[10] The pressure was kept well below one micron.

Careful scanning of the emulsions exposed during the two week period of operation showed no heavy tracks other than the few short and randomly oriented tracks of alpha-particles. (The monopole tracks should be heavier than those of alpha-particles, several hundred microns long, and oriented in only one direction.)

The upper limit[11] of the monopole arrival rate set as a consequence of this negative result is $1/A_ET$, where $A_E=H_sA_s/H_E$ from (IV 2.2) and T the time of observation, which was 1.2×10^6 sec. In this equipment $H_s=250$ gauss; $A_s=20$ cm², while $H_E=0.6$ gauss. Therefore $A_E\cong8300$ cm² and

$$1/A_ET\leqslant10^{-10} \text{ monopoles per cm}^2 \text{ per sec.} \qquad \text{(IV 2.3)}$$

The corresponding cross section for monopole production by primary cosmic radiation is

$$\sigma_{\max}\leqslant1\Big/A_ET\int CNdx \qquad \text{(IV 2.4)}$$

where C is the number of primary cosmic particles crossing a cm² per sec at altitude x and N is the number of atmospheric nuclei per cm³ at altitude x. The value[12] of $\int CNdx$ is approximately 3.8×10^{24} per cm² per sec for primary protons alone; hence,

$$\sigma_{\max}\leqslant3\times10^{-25} \text{ cm}^2. \qquad \text{(IV 2.5)}$$

The author wishes to thank Professor E. Teller for suggesting this topic and for his invaluable criticism as the work progressed. He is also greatly indebted to Professor G. Wentzel for his careful consideration of the theoretical conclusions, to Professor E. Fermi for stimulating discussions concerning the validity of various possible experiments, and for their generous assistance to Dr. John Marshall and Mr. Philip Shevick of the Institute of Nuclear Studies at the University of Chicago where the experiment was performed.

[11] The statistical significance of the phrase "upper limit" is that an arrival rate n times as great as that established has a probability of e^{-n}.

[12] B. Rossi, Revs. Modern Phys. **20**, 566 (1948).

Classification of Nuclear Isomers*†

M. GOLDHABER AND A. W. SUNYAR
Brookhaven National Laboratory, Upton, New York

(Received May 25, 1951)

The lifetime-energy relations of Axel and Dancoff and the K/L ratios calculated by Hebb and Nelson are shown to yield spin differences ΔI which are one unit too high for long-lived electric transitions ($\Delta I \geq 3$). These transitions are also slower than expected from Weisskopf's one-particle model and have approximately the same lifetime as magnetic transitions of equal ΔI. The lifetimes of magnetic transitions agree approximately with Weisskopf's formula. If the statistical weight of the initial state is introduced into the lifetime formula, the "scatter" of the square of the matrix elements is greatly reduced for these transitions. Most long-lived isomers show $M4$ transitions, in agreement with shell theory. Some isomeric transitions which were previously assumed to show no parity change are now interpreted as $E3$. Their occurrence in the $1g_{9/2}$ shell may be explained by assuming that for the configurations $(g_{9/2})^{3,5 \text{ or } 7}$, $7/2+$ and $g_{9/2}$ states are comparable in energy. The $7/2+$ state is lower in more than half of the cases. Empirical curves of K/L ratios plotted against Z^2/E are given. They are consistently lower than the existing theoretical curves based on nonrelativistic calculations of internal conversion coefficients. Spins of metastable and ground states are assigned for a number of nuclei. For even-even nuclei the following rule is found: the first excited state usually has spin 2 and even parity. The only mixed transitions found are $M1+E2$. Sufficiently many $E3$ transitions are established to permit the conclusion that electric transitions are slower for odd-neutron nuclei than for odd-proton nuclei. This gives strong support to a one-particle model. Among electric transitions only some $E2$ transitions are faster than expected on the one-particle model. This is interpreted as a cooperative phenomenon, related to the existence of large quadrupole moments.

INTRODUCTION

AMONG nuclei of odd mass number nuclear isomers occur predominantly just before the number of protons or neutrons, whichever is odd, reaches a "magic number."[1,2] The position of these "islands," as well as the value of the magic numbers, can be most easily explained in terms of the strong spin orbit coupling model.[3,4] However, in the island which precedes magic number 50, where $g_{9/2}$ and $p_{1/2}$ levels should be adjacent and should give rise to isomeric transitions of spin change $\Delta I=4$ with change of parity ($M4$ transitions),[5] there are two families of isomers which differ in half-life by factors of the order of 10^5 for similar energy and similar nuclear charge. Two typical examples, representative of the short-lived and the long-lived families respectively, are ${}_{47}Ag^{107m}$ ($T_{1/2}=44$ sec, $E=94$ kev) and ${}_{41}Nb^{91m}$ ($T_{1/2}=60$ days, $E=104.5$ kev). In the classification of nuclear isomers which Axel and Dancoff[6] have carried out, Nb^{91m} appeared as an isomeric transition of multipole order 5, and Ag^{107m} as one of multipole order 4. While the isomeric transition in Nb^{91m} could therefore be considered as an $M4$ transition, in agreement with shell theory, the transition in Ag^{107m} was ascribed no parity change. This is in contradiction to the strong spin-orbit coupling model, as emphasized by several authors.[2,7,8]

In the next shell, closing at magic number 82, the long-lived isomeric transitions are expected to be of the $M4$ type, according to the strong spin-orbit coupling model: $h_{11/2} \rightarrow d_{3/2}$, followed by a second step, $d_{3/2} \rightarrow s_{1/2}$ whenever the ground state is $s_{1/2}$. This is indeed found to be so, but a search for internal conversion electrons[9] or unconverted γ-rays[10] from the expected ($E5$) cross-over transitions ($h_{11/2} \rightarrow s_{1/2}$) has so far been unsuccessful. The new lifetime-energy relations recently derived by Weisskopf[11] give considerably smaller radiation probabilities for $E5$ transitions than the old ones.[12]‡ Although

* Preliminary reports of this work were given at the American Physical Society Meeting in New York, January, 1951, M. Goldhaber, Phys. Rev. **82**, 323 (1951); and at Washington, April, 1951, A. W. Sunyar and M. Goldhaber, Phys. Rev. **83**, 216 (1951). Related work was reported at Washington by S. A. Moszkowski, Phys. Rev. **83**, 240 (1951).

† Research carried out under contract with the AEC.

[1] E. Feenberg and K. C. Hammack, Phys. Rev. **75**, 1877 (1949).

[2] L. W. Nordheim, Phys. Rev. **75**, 1894 (1949).

[3] M. G. Mayer, Phys. Rev. **78**, 16, 22 (1951).

[4] Haxel, Jensen, and Suess, Z. Physik **128**, 301 (1950).

[5] The following designations of isomeric transitions are used here:

	$E1$	$M1$	$E2$	$M2$	$E3$	$M3$	$E4$	$M4$	$E5$
$\lvert\Delta I\rvert$	1	1	2	2	3	3	4	4	5
Parity change	yes	no	no	yes	yes	no	no	yes	yes
Multipole order (Λ)	1		2		3		4		5

[6] P. Axel and S. M. Dancoff, Phys. Rev. **76**, 892 (1949).

[7] E. Feenberg, Phys. Rev. **77**, 771 (1950).

[8] P. Axel, Phys. Rev. **80**, 104 (1950).

[9] R. D. Hill, Phys. Rev. **76**, 186 (1949); J. C. Bowe and G. Scharff-Goldhaber, Phys. Rev. **76**, 437 (1949); Katz, Hill, and Goldhaber, Phys. Rev. **79**, 781 (1950); J. W. Mihelich and R. D. Hill, Phys. Rev. **79**, 781 (1950).

[10] E. der Mateosian and M. Goldhaber, unpublished.

[11] V. F. Weisskopf and J. Blatt, privately circulated chapter from forthcoming book on *Nuclear Theory*.

[12] The lifetime-energy relations used by Axel and Dancoff for transitions of multipole order Λ are:

$$\tau_\gamma \text{ (sec)} = 3(\Lambda!)^2 \frac{1}{\rho^{2\Lambda}} \left(\frac{137}{W}\right)^{2\Lambda+1} \frac{\hbar}{mc^2},$$

where ρ is a dimensionless quantity equal to the nuclear radius $R=1.5\times10^{-13}A^{\frac{1}{3}}$ cm divided by $e^2/mc^2=2.82\times10^{-13}$ cm, W = transition energy in mc^2 and $\hbar/mc^2=1.31\times10^{-21}$ sec. Weisskopf's lifetime-energy relations for electric transitions of spin change ΔI are:

$$\tau_\gamma \text{ (sec)} = \frac{\Delta I[1\cdot3\cdots(2\Delta I+1)]^2}{2(\Delta I+1)} \frac{1}{\rho^{2\Delta I}} \left(\frac{137}{W}\right)^{2\Delta I+1} \frac{\hbar}{mc^2}.$$

For magnetic transitions of spin change ΔI they are: $(\tau_\gamma)_{\Delta I,\,\text{magn}} = (\tau_\gamma)_{\Delta I,\,el} \times (McR/\hbar)^2$, where M is the mass of a nucleon. For

this goes a long way towards explaining the absence of $E5$ crossover transitions, as was pointed out by Hill,[13] the theoretical values are still larger than the experimental upper limits for these transition probabilities. On the other hand, in apparent contradiction to this fact, the "K/L ratios" obtained experimentally for some $M4$ transitions are found to lie between the theoretical values[14] for $M4$ and $E5$, and have been interpreted in the past as indicating a mixture of $M4$ and $E5$ radiations. This seemed reasonable as long as lifetime energy relations were used which were identical for $M4$ and $E5$ transitions (identical for equal multipole order Λ).

In this paper it will be shown how the above three difficulties, as well as some others, can be resolved. They are, in short:

(1) Occurrence of isomers of apparently no parity change in the $1g_{9/2}$ shell (10 cases):[15] Se^{77}, Se^{79}, Se^{81}, Kr^{79}, Kr^{81}, Kr^{83}, Rh^{105}, Rh^{105}, Ag^{107}, Ag^{109}; and in the $1h_{11/2}$ shell (3 cases): Cd^{111}, Xe^{127}, Au^{197}.
(2) Absence of $E5$ (crossover) transitions in the $1h_{11/2}$ shell.
(3) Interpretation of the experimental K/L ratios as indicating that $E5$ transitions have half-lives of the same order as $M4$ transitions of similar energy.

Two further difficulties of the previous classifications are:

(4) Absence of isomers of multipole order $\Lambda=3$, and
(5) Absence of isomers in the millisecond region.

These two difficulties were sometimes believed to be closely connected.

We have used a semi-empirical approach, using only experimental results and well-founded theoretical calculations, e.g., the relativistic internal conversion coefficients computed by Rose, Goertzel, Spinrad, Harr, and Strong.[16] We shall show that the assumption of strong spin-orbit coupling is compatible with the empirical results concerning isomers, provided we give up the rule[3] that $j-j$ coupling of an odd number of particles in the $1g_{9/2}$ shell leads always to a $g_{9/2}$ state as the configuration of lowest energy. Theoretically, this rule can only be expected to hold for zero range forces, and it is known to break down in some other shells ($1d_{5/2}$, $1f_{7/2}$), where forces of finite range can be shown to yield lowest configurations different from j, in agreement with experiment.[17]

In the course of this investigation some other results have been obtained of which the most important are:

Empirical curves of K/L ratios are given (Sec. IV) which may replace for the time being the less accurate non-relativistic theoretical curves.[14]

An empirical law connecting the lifetime of $M4$ transitions with energy, mass number of isomer and spin of the metastable state is found and compared with Weisskopf's formula for $M4$ transitions (Sec. I).

For $E3$, $E4$, and $E5$ transitions the multipole order is shown to have been previously overestimated by one unit (Secs. I and II).

Electric transitions (except some $E2$ transitions) have a slower rate than that given by Weisskopf's formula, and have half lives comparable to magnetic transitions of the same spin change (Secs. III and IV).

The only mixed transitions that occur are $M1+E2$ (Sec. III).

For even-even nuclei the first excited state has in most cases the spin $I=2$ and even parity (Sec. V).

I. $\Delta I=4$ OR 5

It is convenient to start with the long-lived isomers which contain most of the well-investigated examples. Axel and Dancoff's[6] classification contained among the isomers of $\Lambda=5$ only one example of an isomer which appeared to show an $E5$ transition: In^{114m}. Here the experimental K/L ratio[18] of 1.1 agrees well with Hebb and Nelson's[14] theoretical value for an $E5$ transition, 1.2. The experimental K conversion coefficient,[18] 2.1, does not agree with that expected for an $E5$ transition from the table of Rose *et al.*,[16] *viz.*, 12, but rather with the value computed for an $E4$ transition, 2.4. However, for an $E4$ transition, the theoretical K/L ratio[14] would be 2.6. Since the K conversion coefficients of Rose *et al.* can be considered as practically exact and the nonrelativistic K/L ratios as only approximate, we conclude that the isomeric transition in In^{114} is $E4$ rather than $E5$ and that the K/L ratios of Hebb and Nelson[14] for $E4$ transitions are too high. A further example of an $E4$ transition occurs in the first step of the isomeric transition of $Mo^{92\pm1}$ (7 hr),[19] recently investigated in more detail in this Laboratory.[20]

Two more examples of isomers tentatively identified as $E4$ transitions, Sc^{44}, and Pa^{234} (UX_2), are included in Table I, which summarizes the experimental and theoretical information on $E4$ transitions. The conversion coefficient of Sc^{44} is compatible either with an $E4$ or $M4$ transition, but an empirical rule for $M4$ transi-

electric transitions where $\Lambda=\Delta I$ the two formulas differ only by numerical factors. The lifetimes predicted by Weisskopf's formula compared with those obtained from Axel and Dancoff's formula are larger by the following factors:

$E1$	$E2$	$E3$	$E4$	$E5$
0.75	6.25	~38	~207	~1040

‡ *Note added in proof:* Dr. J. Blatt has kindly informed us of a recent modification of Weisskopf's formulas. All lifetimes should be multiplied by $((\Delta I+3)/\Delta I)^2$ and those for the magnetic transitions by ~1/10 to take account of the effect of the intrinsic magnetic moment of the nucleons.

[13] R. D. Hill, Phys. Rev. **81**, 470 (1951).
[14] M. H. Hebb and E. Nelson, Phys. Rev. **58**, 486 (1940); N. Tralli and I. S. Lowen, Phys. Rev. **76**, 1541 (1949).
[15] Sr^{80m} should probably be added to this group, but its decay is complicated due to the existence of a K-branch. [M. Terpogossian and F. Porter, Phys. Rev. **81**, 1057 (1951); Deutsch, Goldhaber, Scharff-Goldhaber, and Sunyar, unpublished.]
[16] Rose, Goertzel, Spinard, Harr, and Strong, privately circulated tables.
[17] D. Kurath, Phys. Rev. **80**, 98 (1950); I. Talmi, Phys. Rev. **82**, 101 (1951).
[18] F. Boehm and P. Preiswerk, Helv. Phys. Acta **22**, 331 (1949).
[19] Kundu, Hult, and Pool, Phys. Rev. **77**, 71 (1949).
[20] der Mateosian, Alburger, Friedlander, Goldhaber, Scharff-Goldhaber, and Sunyar, unpublished. The mass number of the Mo isomer is not yet definitely assigned.

TABLE I. Summary of information on $E4$ group of isomers.[a]

	$T_{\frac{1}{2}}$	E (kev)	Theor. K conv. coeff. α	Exp. K/L ratio	Total conv. coeff. Exp.	Calc.	$\log_{10}\tau_\gamma$	$\lvert M\rvert^2$
Sc^{44}	2.44 day	269	0.12	8	0.07	0.14	5.54	4.8×10^{-2}
$Mo^{93\pm1}$	7 hr	256	0.58	2.8	0.7	0.78	4.81	5.5×10^{-2}
In^{114} [b]	50 day	192	2.4	1.1	4	4.6	7.54	8×10^{-4}
$Pa^{234}(UX_2)$	5.7×10^4 sec[c]	394	0.3	<0.3	$\alpha_{L+M}\approx1$	~1.3	5.28	3.3×10^{-5}

[a] Values in this and the following tables for which no references are given are taken from "Nuclear Data" by K. Way *et al.*, Natl. Bur. Standards circular 499 and from the supplement 1 to this circular.

[b] Further evidence in favor of an $E4$ assignment for In^{114} has been recently given by R. M. Steffen (private communication).

[c] The partial half-life for the isomeric branch is given here.

tions, discussed below, makes it unlikely that Sc^{44} belongs to the $M4$ group. It decays ~50 times faster than expected for an $M4$ transition.

In this and the following tables, theoretical internal conversion coefficients $\alpha=N_e/N_\gamma$ are taken from the tables of Rose *et al.*[16] for $E>150$ kev. For lower energies an extrapolation suggested by Axel and Goodrich[21] is used. The ratio of the relativistic K conversion coefficients obtained from Rose *et al.* to the nonrelativistic coefficients of Hebb and Nelson[14] is plotted above $E=150$ kev and extrapolated to one at zero electron energy. K conversion coefficients below 150 kev are then obtained by multiplying Hebb and Nelson's values with a correction factor obtained from the ratio plot.

To calculate the total conversion coefficient, the K/L ratio is taken either from experiment or from empirical curves obtained from measured K/L ratios for $M4$, etc., transitions (Fig. 1 and later figures). Conversion in the M, N, etc., shells is neglected, wherever measurements are not available.

Most known long-lived isomers belong to the $M4$ group in agreement with expectations from shell theory. Table II summarizes the experimental and theoretical data on the $M4$ group of isomers. Some of the transitions take place in two successive steps. The initial and final spins of the states between which the longer lived isomeric transition takes place are indicated by I_i and I_f, respectively. Whenever a second transition takes place before the ground state (I_0) is reached, information about the second step is given. The spins and configurations tabulated are based either on existing measurements, or deductions from β-decay schemes and shell theory.

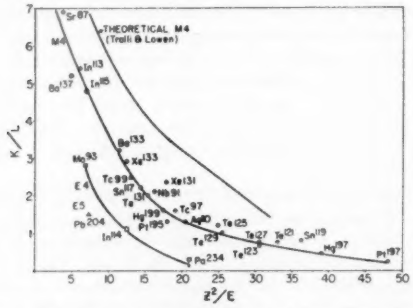

FIG. 1. Experimental K/L ratios for $M4$, $E4$, and $E5$ transitions. The nonrelativistic theoretical curve for $M4$ is shown for comparison. The theoretical curves for $E4$ and $E5$, which are not shown, are also higher than the corresponding experimental points (E in kev).

The information which exists on $E5$ transitions is rather meager. Only one such transition can be identified with certainty. It occurs in Pb^{204} and was previously believed to be an $E6$ transition. Its properties are as follows:[22] $T_{1/2}=68$ min; $E=905$ kev; $K/L=1.5\pm0.2$; ϵ (total)≃10 percent; α_6 (theoretical)=10 percent.§ Lower limits for radiation lifetimes may be computed for two other transitions (Te^{121} and Cd^{115}) which are expected to be $E5$ transitions. The spin assignments leading to this expectation are based on investigations which do not involve the direct observation of the isomeric transition: the two-step isomeric transition[9] in Te^{121} and the β-decay of the two isomers[23] of Cd^{115}.

In Fig. 2, $\log_{10}\tau_\gamma$ (sec) is plotted *vs* $\log_{10}E$ (kev) for isomers of the $E4$, $M4$, and $E5$ group, where

$$\tau_\gamma=T_{1/2}(1+\alpha_{\text{total}})/\ln2.$$

Some points appear twice, with different internal conversion corrections made, e.g., Mn^{52}, once assuming an $E4$ correction, and once assuming an $M4$ correction. To calculate τ_γ, the experimental value of α_{total} was used wherever it agrees approximately with the theoretical value. In the few cases where there are large discrepancies and where there exists supporting evidence for assigning the isomeric transition, the theoretical value was used.

The following empirical rule follows from Fig. 2: For a given energy and a spin change $\Delta I=4$ the γ-lifetime of a transition is not appreciably affected by the fact that the parity may or may not change. This rule is contrary to previous theoretical expectations. A rough empirical formula for the γ-lifetime for $\Delta I=4$ can be deduced from Fig. 2: $\log\tau_\gamma$ (sec)≃$27.7-\log E$(kev).

[21] P. Axel and R. F. Goodrich, Technical Report, University of Illinois, 1950.

[22] Sunyar, Alburger, Friedlander, Goldhaber, and Scharff-Goldhaber, Phys. Rev. **79**, 181 (1950).

§ We designate experimental conversion coefficients by ϵ and theoretical conversion coefficients for 2^l electric or magnetic transitions by α_l and β_l, respectively.

[23] The Cd^{115} isomers have been studied by R. W. Hayward and A. C. Helmholz, Phys. Rev. **75**, 1469(A) (1949) and by D. W. Engelkemeier, Argonne National Laboratory, unpublished.

TABLE II. Summary of information on $M4$ isomers.

Isomer	$T_{1/2}$	E (kev)	Theor. K conv. coeff.	K/L Ratio Exp.	K/L Ratio Emp. curve	Total conv. coeff. Exp.	Total conv. coeff. Calc.	$\log_{10}\tau_\gamma$ (sec)	$\lvert M\rvert^2$	Spins I_i	Spins I_f	$\lvert M'\rvert^2$	Second step E (kev)	Second step $T_{1/2}$	Second step I_g	Second step K/L	Reference
Mn^{52}	1.26×10^6 sec*	390	~0.05		>8		~0.05	5.28	1.40	low	high				···†		
Zn^{69}	13.8 hr	439	0.05		~8	0.06	~0.06	4.88	0.685	$g_{9/2}$	$p_{1/2}$	0.455			···		
Kr^{85}	21.2 hr*	300	0.46		~6.5		0.53	5.23	5.97	$p_{1/2}$	$g_{9/2}$	0.795			···		a
Se^{87}	2.80 hr	394	0.23	6.9		0.29	0.27	4.27	5.25	$p_{1/2}$	$g_{9/2}$	0.63			···		b, c
Y^{87}	14 hr	389	0.23	8.3			~0.27	4.97	1.05	$g_{9/2}$	$p_{1/2}$	0.63			···		b, c
Y^{89}	14 sec	920	0.008		>8	0.01	$\sim9\times10^{-3}$	1.31	1.67	$g_{9/2}$	$p_{1/2}$	1.11			···		d
Y^{91}	51 min	610	0.035		>~7	~0.1	$\sim4\times10^{-2}$	3.68	0.322	$g_{9/2}$	$p_{1/2}$	0.21			···		
Zr^{89}	4.5 min	555	0.07		~7		$\sim8\times10^{-2}$	2.62	0.08	$p_{1/2}$	$g_{9/2}$	1.23			···		
Nb^{91}	60 day	104.5	~180	2.1		100	~270	8.90	15.3	$(p_{1/2})$	$(g_{9/2})$	2.05			···		e
Nb^{96}	90 hr	216	3.4		4.5	large	4.2	6.39	6.66	$p_{1/2}$	$g_{9/2}$	0.89			···		
Nb^{97}	60 sec	749	0.0165	≥~4		0.015	$\sim2\times10^{-2}$	1.94	2.47	$p_{1/2}$	$g_{9/2}$	0.33			···		f
Tc^{96}	~5 yr*	39	~16,000		0.33		~64,000	~13.16	~5.52	$p_{1/2}$	$g_{9/2}$	~0.725			···		g
Tc^{97}	90 day	97	~250		1.5	large	~420	9.67	4.46	$p_{1/2}$	$g_{9/2}$	0.59			···		
Tc^{98}	432 hr*	142.3	31	~2.5			46.5	8.03	6.12	$p_{1/2}$	$g_{9/2}$	0.835			···		h
Ag^{110}	5.4×10^8 sec*	116	~100	~1.3		large	~177	~10.98	~0.034	(5 −)	(1 +)	~2.5 $\times10^{-2}$			···		
In^{113}	1.73 hr	390	0.44	5.4		0.7	0.55	4.144	4.05	$p_{1/2}$	$g_{9/2}$	0.542			···		
In^{115}	5.11 hr*	338	0.8	4.8		0.33	0.98	4.702	3.91	$p_{1/2}$	$g_{9/2}$	0.523			···		
Sn^{117}	14.5 day	159	33	2.2			48	7.95	1.91	$h_{11/2}$	$d_{3/2}$	1.30	162		$s_{1/2}$		
Sn^{119}	245 day	69	~1900	~0.8			~4300	11.12	2.26	$h_{11/2}$	$d_{3/2}$	1.82	24.2		$s_{1/2}$		i
Te^{121}	154 day	82	~950	0.75		large	~2450	10.67	1.24	$h_{11/2}$	$d_{3/2}$	1.00	213		$s_{1/2}$	7.3	j
Te^{123}	104 day	88.5	620	0.68			1740	10.35	1.32	$h_{11/2}$	$d_{3/2}$	1.06	159		$s_{1/2}$	8.6	j
Te^{125}	58 day	109	205	1.2		>100	375	9.43	1.62	$h_{11/2}$	$d_{3/2}$	1.30	35.4		$s_{1/2}$	~7.3	
Te^{127}	90 day	88.5	620	0.75		≥5.7	1635	10.263	1.545	$h_{11/2}$	$d_{3/2}$	1.24			···		k
Te^{129}	33.5 day	106	245	1		$\sim\infty$ ≥1.9	490	9.34	2.46	$h_{11/2}$	$d_{3/2}$	1.95			···		k
Te^{131}	3.0 day*	183.2	16.5	2		≥0.6	24.7	6.98	4.10	$h_{11/2}$	$d_{3/2}$	3.32			···		k
Xe^{129}	8 day	196	16	$\frac{K}{L+M}$ 2.1			23.6	7.39	0.86	$h_{11/2}$	$d_{3/2}$	0.70	(39?)		$s_{1/2}$		l
Xe^{131}	12 day	163	34	2.34			53	7.91	1.33	$h_{11/2}$	$d_{3/2}$	1.06			···		m
Xe^{133}	2.30 day	232	6.6	2.9			9.6	6.42	1.57	$h_{11/2}$	$d_{3/2}$	1.26			···		n
Xe^{135}	15.3 min	520	0.22		5.5		0.26	3.22	1.78	$h_{11/2}$	$d_{3/2}$	1.43			···		
Ba^{133}	38.9 hr	276	3.5	3.2		2.45	4.6	6.05	0.784	$h_{11/2}$	$d_{3/2}$	0.63			···		
Ba^{135}	28.7 hr	300	2.3		3.5		3	5.77	0.705	$h_{11/2}$	$d_{3/2}$	0.564			···		
Ba^{137}	2.6 min	669	0.1	5.2		~0.12	0.12	2.40	1.18	$h_{11/2}$	$d_{3/2}$	0.945			···		o
Pt^{196}	~80 min	337	5.2	1.3		large	9.2	4.86	0.97	$i_{13/2}$	$f_{5/2}$	0.90	?		$p_{1/2}$		
Pt^{197}	3.5 day	126	170	0.23			910	8.60	1.21	$i_{13/2}$	$f_{5/2}$	1.15	?		?		
Hg^{197}	23 hr	164	85	0.45		~4.5	360	7.65	1.00	$i_{13/2}$	$f_{5/2}$	0.937	133	7×10^{-9} sec	$p_{1/2}$	0.39	p
Hg^{199}	44 min	368	4.4	1.6		>11	7.2	4.50	0.975	$i_{13/2}$	$f_{5/2}$	0.91	158.5		$p_{1/2}$	0.37	
Pb^{207}	0.9 sec	1050	0.103		~5.2		~0.12	0.164	1.54	$i_{13/2}$	$f_{5/2}$	1.45	520		$p_{1/2}$		q

* Partial half-life for isomeric transition is given wherever branching is known to occur.

† Whenever the ground state is also the final state of the first isomeric transition, this is indicated by ····.

[a] L. Bergström and S. Thulin, Phys. Rev. **79**, 537 (1950).

[b] L. G. Mann and P. Axel, Phys. Rev. **80**, 759 (1950) and private communication.

[c] E. K. Hyde and G. D. O'Kelley, Phys. Rev. **82**, 944 (1951).

[d] Goldhaber, der Mateosian, Scharff-Goldhaber, Sunyar, Deutsch, and Wall, Phys. Rev. **83**, 661 (1951).

[e] J. Ovadia and P. Axel, private communication.

[f] Burgus, Knight, and Prestwood, Phys. Rev. **79**, 104 (1950).

[g] H. Medicus and P. Preiswerk, Phys. Rev. **80**, 1101 (1950).

[h] Mihelich, Goldhaber, and Wilson, Phys. Rev. **82**, 972 (1951).

[i] J. W. Mihelich, private communication of K/L ratio. The second step in Sn^{119} has recently been found (Scharff-Goldhaber, der Mateosian, Goldhaber, Johnson, and McKeown, Phys. Rev. **83**, 480 (1951) and R. D. Hill, Phys. Rev., Aug. 15, 1951.

[j] R. D. Hill, Phys. Rev. **81**, 470 (1951).

[k] J. W. Mihelich and E. Church, private communication; R. R. Williams, Jr., J. Chem. Phys. **16**, 513 (1948), finds by a Szilard-Chalmers separation that approximately 40 percent of the transitions of Te^{131m} lead to the 25-min Te^{131} ground state. This he interprets as indicating ~40 percent internal conversion for the isomeric transition. Theoretically we should expect ~96 percent. We therefore interpret the experimental result tentatively as indicating that the isomeric branch is only ~40 percent, the remainder being β-decay from Te^{131m} to I^{131}. *Note added in proof:* If we similarly re-interpret Williams' results for Te^{127} and Te^{129} where he finds Szilard-Chalmers yields of ~85 percent and ~50 percent, respectively, and use new lifetime values obtained by R. D. Hill and M. T. Piggott (Te^{127}, $113\pm5d$; Te^{129}, $38\pm2d$) we find $|M'|^2\cong1$ for these isomers.

[l] I. Bergström, Nature **167**, 634 (1951). C. J. Borkowski and A. R. Brosi, ORNL 607, report a 39-kev transition in the decay of I^{129}. This may be also the hitherto undiscovered second step in the decay of Xe^{129m}.

[m] I. Bergström, Phys. Rev. **80**, 114 (1950).

[n] I. Bergström, Phys. Rev. **81**, 638 (1951).

[o] D. E. Alburger, private communication. J. W. Mihelich, private communication (K/L ratio).

[p] Frauenfelder, Huber, De-Shalit, and Zünti, Phys. Rev. **77**, 139 (1950).

[q] E. C. Campbell and M. Goodrich, Phys. Rev. **78**, 640(A) (1950). *Note added in proof:* An unpublished analysis of Pb^{207} levels by M. H. L. Pryce lends further support to the level assignment given here.

To compare the empirical and theoretical mean lifetimes in detail, it is convenient to multiply τ_γ by the appropriate power of ρ (e.g., ρ^6 for $M4$ transitions) and to plot the logarithm of the product *vs* $\log E$. This is done for $M4$ transitions in Fig. 3, for $E4$ and $E5$ transitions together with $E3$ transitions in Fig. 9. We can define the ratio of the experimentally obtained τ_γ (exp) to the τ_γ (theor) obtained from Weisskopf's formula as $1/|M|^2$ if we take Weisskopf's squares of matrix elements as unity for comparison. The values of $|M|^2$ are given in the tables.

It is remarkable how well most points of Fig. 3 agree with the theoretical straight line. However, some points appear to be systematically lower by approximately a factor 5. This fact is illustrated more clearly by Fig. 4(a) where the distribution in $|M|^2$ is plotted indicating two

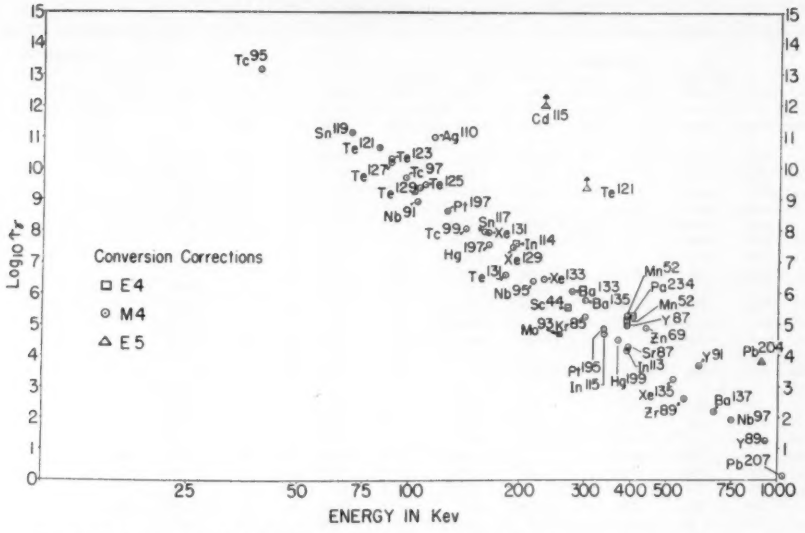

FIG. 2. Lifetime-energy relation for $E4$, $M4$, and $E5$ transitions. Mn^{52} appears twice, once with an $E4$ correction and once with $M4$ correction for internal conversion.

groups of isomers differing in $|M|^2$ by ~ 5. Especially interesting is the pair of isobars, Sr^{87m} and Y^{87m}, which have the same ρ correction, similar energy, (394 and 389 kev, respectively),[24] and a very similar internal conversion correction ($Z=38$ and 39, respectively), but half-lives of 2.80 ± 0.03 hr and 14 ± 1 hr, respectively. Thus, the half-lives are in the ratio of 1:5.[25] This is the same as the ratio of the statistical weights $(2I_i+1)$ of the initial states, *viz.* 2:10 for these two nuclei where I_i takes on the values 1/2 and 9/2, respectively.

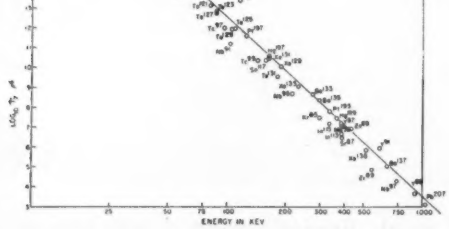

FIG. 3. Normalized lifetime-energy relation for $M4$ transitions. The theoretical relation due to Weisskopf is plotted for comparison.

Such a ratio of life times would be expected for the ideal case where the ψ-functions of the initial and final state are exactly reversed for the two isomers.[26] If we plot [Fig. 4(b)] the distribution of isomers *vs* $|M'|^2=(2I_i+1)|M|^2$, normalized at the mean value, we find that this quantity shows remarkably little deviation from the mean; it has a half-width at half-maximum of about 40 percent.

The lifetime of $M4$ transitions is given by the empirical law (see Fig. 5)

$$\tau_\gamma \text{ (sec)} = 1.0\times10^4(2I_i+1)/A^2E^9,$$

where A = mass number, I_i = spin of metastable state, and E = energy in Mev. Considering that a good part of the deviation found must be due to experimental errors and approximations made in the computations, the mean deviation from the lifetime given by this formula is estimated to be <30 percent.

It is perhaps significant that the point which deviates most from the mean, Ag^{110}, where the value of $(2I_i+1)|M|^2$ is 40 times smaller than the mean, corresponds to a transition in an odd-odd nucleus, whereas all other transitions, except Mn^{52}, occur in nuclei with a single odd particle. According to shell theory, the odd particle suffers a change of three units of orbital angular momentum and a reversal of its spin in each case. The transition probabilities are approximately the same for odd-proton nuclei as for odd-neutron nuclei, with perhaps a slight tendency for larger transition probabilities

[24] E. Hyde and G. O'Kelley, UCRL 1064; L. G. Mann and P. Axel, Phys. Rev. **80**, 750 (1950) and private communication (Mann and Axel give energies of 390 and 385 kev for Sr^{87m} and Y^{87m} respectively).

[25] A possible K capture branch in Y^{87m} has a negligible effect on the lifetime. (L. G. Mann and P. Axel, private communication.)

[26] A similar spin correction was introduced in β-decay theory by R. E. Marshak, Phys. Rev. **61**, 431 (1942).

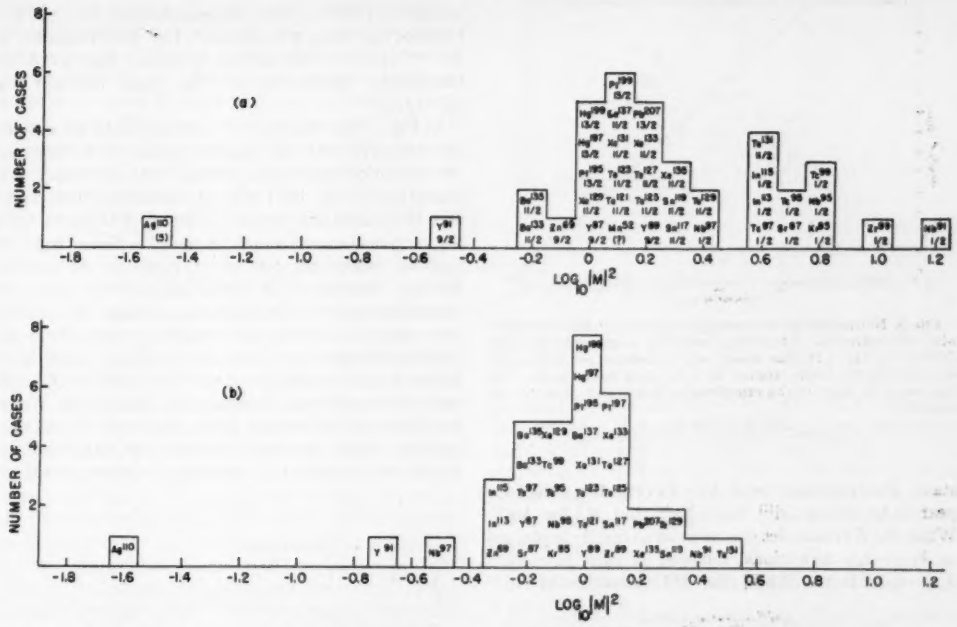

FIG. 4. Distribution of the squares of matrix elements for nuclei showing $M4$ transitions. In (a) it is plotted against $\log|M|^2$, taking Weisskopf's squares of matrix elements as unity. The spin I_i of the metastable state is indicated for each nucleus. In (b) it is plotted against the relative values of $\log[(2I_i+1)|M|^2]$, normalized at the mean value.

for odd-neutron nuclei [see Fig. 4(b)]. This tendency, if real, may also be connected with the fact that most odd-neutron nuclei shown are heavier nuclei which have $h_{11/2}\rightarrow d_{3/2}$ and $i_{13/2}\rightarrow f_{5/2}$ transitions, whereas the odd-proton nuclei shown have $g_{9/2}\leftrightarrow p_{1/2}$ transitions only. Within the $g_{9/2}\leftrightarrow p_{1/2}$ group there appears to be no distinction between odd-neutron and odd-proton nuclei.

II. $\Delta I=3$

We have seen that $E4$ and $M4$ transitions have similar lifetimes. This statement carries an important implication. The group of isomers previously identified as $M3$ and $E4$ ($\Lambda=4$) may really consist of $M3$ and $E3$ transitions. The previously "absent" $E3$ group of isomers would thus be accounted for in a very simple manner. One of the well-studied isomers of this group is Ag^{107m}. The spin and magnetic moment of the ground state are known, and it may be designated confidently as a $p_{1/2}$ level, in agreement with shell theory. For the excited state ($E=94$ kev) shell theory would predict a $g_{9/2}$ configuration and a resultant $M4$ transition, leading to a mean lifetime $\tau_\gamma=1.34\times10^{10}$ sec and a conversion coefficient, $\beta_k\approx390$; thus we should expect $T_{1/2}\approx132$ days, instead of the observed value of 44 sec. The experimental K/L ratio agrees with the theoretical one for an $E4$ transition, but we have seen above that the K/L ratios for $E4$, $E5$, and $M4$ transitions were found to be lower than the theoretical ratios. A better guide than the K/L ratio is the K conversion coefficient. Its value can be calculated from the experimental total conversion coefficient ($\epsilon=16$) and the experimental $K/(L+M)$ ratio obtained by Bradt and collaborators.[27] One finds $\epsilon_K=7.1$. In Fig. 6 we compare this value with the extrapolated values for the conversion coefficient. We see that only the $E3$ curve is close to the experimental value, indicating a 7/2+ state[28] for Ag^{107m}.[29] Low-lying 7/2+ states have been recently established in Tc^{99} [30,31] and Kr^{83} [32] and interpreted as due to $(g_{9/2})^3$ or ^{7} configurations.[31] To understand the decay of Ag^{107m}, and a number of similar isomeric transitions, we would have to generalize this interpretation by saying: For the configurations $(g_{9/2})^{3,5,7}$ in the $1g_{9/2}$ shell there exist two low-lying states: 7/2+ and $g_{9/2}$. In more than half of the cases the 7/2+ state is lower than the $g_{9/2}$

[27] Bradt, Gugelot, Huber, Medicus, Preiswerk, Scherrer, and Steffen, Helv. Phys. Acta **20**, 153 (1947).

[28] Following the usual convention, we designate even parity by a + sign and odd parity by a − sign.

[29] Because of conflicting reports on the properties of Ag^{109m} this isomer has been recently restudied carefully by J. Ovadia and P. Axel (University of Illinois) with results which are similar to those discussed here for Ag^{107m} (private communication).

[30] Medicus, Maeder, and Schneider, Helv. Phys. Acta **24**, 72 (1950).

[31] Mihelich, Goldhaber, and Wilson, Phys. Rev. **82**, 972 (1951).

[32] I. Bergström, Phys. Rev. **81**, 638 (1951).

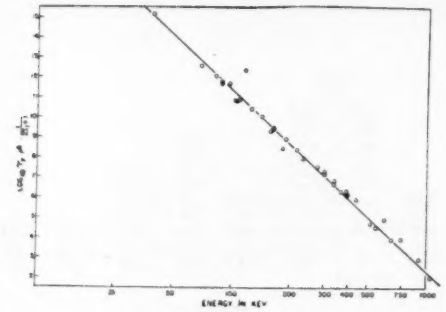

FIG. 5. Normalized lifetime-energy relations for $M4$ transitions with spin correction. The points from Fig. 3 are replotted after division by $(2I_i+1)$. The names of the isomers are left out to demonstrate the linear relation on a log scale more clearly. The line shown is fitted to the experimental points and given by the equation

$$\tau_\gamma \text{ (sec)} = \frac{1.0\times 10^4 (2I_i+1)}{A^2 E^9} \quad (E \text{ in Mev}).$$

state. The transitions with $\Delta I=3$ in the $1h_{11/2}$ shell appear to be $E3$ for Cd^{111} [33] and Xe^{127}, but $M3$ for Au^{197}. While the $E3$ examples can be most naturally explained as $h_{11/2}\rightarrow d_{5/2}$ transitions, followed in each case by a $d_{5/2}\rightarrow s_{1/2}(E2)$ transition, the $M3$ transition in Au^{197} appears to involve a new configuration e.g., $h_{11/2}\rightarrow 5/2$— followed by more transitions.[34] The $M3$ transition in Hf^{179m} which is followed by a second step has been tentatively interpreted as $h_{9/2}\rightarrow p_{3/2}$, followed by $p_{3/2}\rightarrow p_{1/2}$.[35]

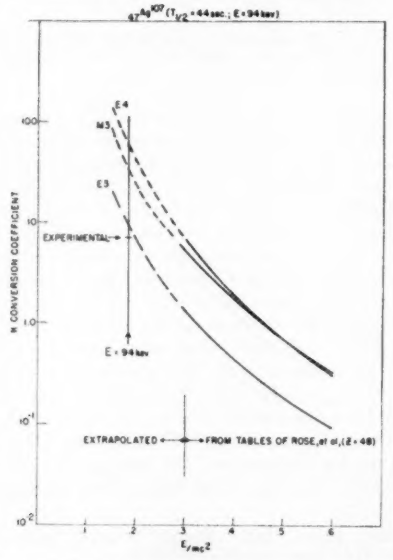

FIG. 6. Theoretical extrapolated K-conversion coefficients for Ag^{107m}. The plotted values are for the neighboring element ($Z=48$) and would be slightly lower for $Z=47$.

In Fig. 7 the empirical K/L ratios for $E3$ transitions are compared with the theoretical ones. K/L ratios for $M3$ transitions are shown together with other magnetic transitions in Fig. 16. Table III summarizes data on $E3$ and $M3$ transitions, based in part on K/L ratios from the empirical curve. Figure 8 shows a plot of $\log\tau_\gamma$ *vs* $\log E$ for transitions with $\Delta I=3$. Again we see that the lifetime dependence is approximately the same for transitions with or without parity change. An approximate empirical formula for transitions with $\Delta I=3$ can be deduced from Fig. 8: $\log\tau_\gamma$ (sec) $=17.5-7\log E$ (kev). Figure 9 shows plots of $\log(\tau_\gamma\rho^{2\Delta I})$ *vs* $\log E$ for $E3$, $E4$, and $E5$ transitions. Experimental points and Weisskopf's theoretical lines are given. For nuclei of odd mass number, where reasonably certain spin assignments of the metastable states can be made, we have plotted the

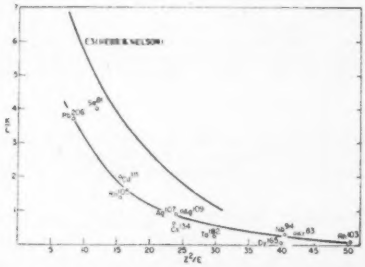

FIG. 7. Experimental K/L ratios for $E3$ transitions. The nonrelativistic theoretical curve is shown for comparison (E in kev.)

distribution of isomers *vs* $|M'|^2=(2I_i+1)|M|^2$ (relative values) in Fig. 10. It can be seen that odd proton transitions appear to be on the average faster than odd neutron transitions. $M3$ transitions are shown in Fig. 14, together with $M2$ and $M1$ transitions, on a plot of $\log(\tau_\gamma\rho^{2\Delta I-2})$ *vs* $\log E$. It is interesting to note that the three high points Br^{80m}, Hf^{179m}, and Au^{197m} probably have a high spin; a correction by the statistical weight factor would reduce the deviation from the theoretical $M3$ line.

III. $\Delta I\leq 2$

For a few isomeric transitions with a spin change $\Delta I\leq 2$ the lifetime has been measured, usually by the method of delayed coincidences. K/L ratios for $E2$ transitions are shown in Fig. 11, for $M1$ and $M2$ transitions in Fig. 16. Table IV summarizes some of the

[33] Recent work on the K conversion coefficient of the 149-kev transition in Cd^{111}, carried out in this Laboratory (A. W. Sunyar) and in Berkeley (C. L. McGinnis, private communication from A. C. Helmholz) confirms the assignment of $E3$, in agreement with the decay scheme proposed by S. Johansson, Phys. Rev. **79**, 896 (1950).

[34] Recent work at E. T. H. Zürich (private communication from D. C. Peaslee).

[35] Burson, Blair, Keller, and Wexler, Phys. Rev. **83**, 62 (1951) and E. der Mateosian and M. Goldhaber, Phys. Rev. **83**, 843 (1951).

existing data and Fig. 12 gives a plot of $\log\tau_\gamma$ *vs* $\log E$ for these transitions. A rough empirical formula for transitions with $\Delta I=2$ is $\log\tau_\gamma$ (sec)$=4-5\log E$ (kev) but the large scatter of the experimental points makes the formula of very limited practical use. Figure 13 shows a plot of $\log(\tau_\gamma\rho^4)$ *vs* $\log E$ for $E2$ transitions. Unlike the other electric transitions, some $E2$ transitions are faster than expected from Weisskopf's one particle formula. The magnetic transitions $M1$, $M2$, and $M3$ shown in Fig. 14, where $\log(\tau_\gamma\rho^{2\Delta I-2})$ is plotted *vs* $\log E$, agree fairly well with Weisskopf's formula.

IV. K/L RATIOS

The K/L ratios for some transitions have been shown above (Figs. 1, 7, and 11). It is useful to summarize the K/L ratios for electric and magnetic transitions (Figs. 15 and 16). One point, Hg^{196}, which can be identified as an $E1$ transition from a comparison of its observed K conversion coefficient $\epsilon_K=0.116$[36] with the theoretical $\alpha_1\cong0.095$ from the tables of Rose *et al.*,[17] has been added to the previously discussed K/L ratios for electric transitions. The data on magnetic transitions, except $M4$, are rather sketchy. The curves $M1$–$M3$ should therefore be taken only as a rough guide to the identification of transitions. Some experimental points called $M1$ may be low due to possible admixture of $E2$ to $M1$. A case which can be identified from its experimental K conversion coefficient as a mixed transition is Tl^{203}. Here a 286-kev transition has a total conversion coefficient of 0.24 and a K/L ratio of 3.[37] Thus, $\epsilon_K=0.18$. For this energy and atomic number, the theoretical K conversion coefficients of Rose *et al.*[16] are as follows: $E2$ (7.6×10^{-2}); $M1$ (0.52). From Fig. 11, the K/L ratio expected for an $E2$ transition ($Z=81$) would be 1.3. From this it follows that about 25 percent of the emitted quanta are $M1$ quanta and 75 percent are $E2$ quanta and that the K/L ratio for the $M1$ transition is approximately 7. The exact amount of mixing of $M1$ and $E2$ depends very sensitively on the value used for ϵ_K. A somewhat smaller value for the K/L ratio of the $M1$ transition follows from the data of Slätis and Siegbahn.[38]¶

V. FIRST EXCITED STATE OF EVEN-EVEN NUCLEI

For many nuclei where the transition from the first known excited state to the ground state has been identified, the spin and parity of the excited state can be deduced. This is particularly so for even-even nuclei which have a ground-state spin of zero and presumably even parity. The spin and parity of the first excited state then follow wherever the transition from this state to the ground state is identified from a study

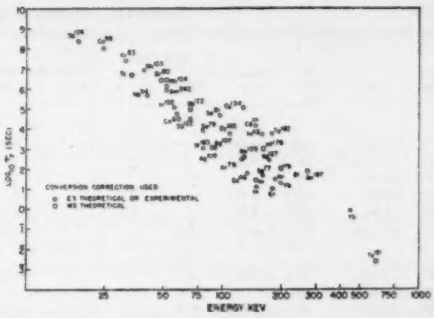

FIG. 8. Lifetime-energy relations for $E3$ and $M3$ transitions. Some points appear twice, once with an $E3$ correction and once with an $M3$ correction for internal conversion.

of one or more of the following: conversion coefficient, pair creation, lifetime, K/L ratio, angular correlation, and nuclear reactions. In Fig. 17 we show the distribution in spin and parity of the first excited state for even-even nuclei. The following rule follows: For even-even nuclei the first excited state usually has spin 2 and even parity.

VI. SUMMARY AND INTERPRETATIONS

It is useful to summarize the analysis which we have given and to discuss some tentative interpretations of our results. Long-lived isomers can be divided into two classes: Those which appear systematically in islands just before the magic numbers are reached, and those which appear unrelated to magic numbers, especially among odd-odd nuclei, as well as occasionally in even-even or even-odd nuclei. Among the systematic ones there are two main groups, one of the $M4$ type,

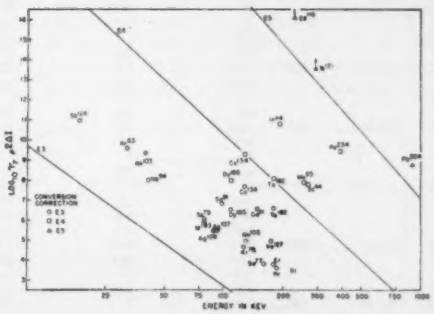

FIG. 9. Normalized lifetime-energy relations for $E3$, $E4$, and $E5$ transitions. Some points appear twice, once as $E3$ and once as $E4$, because there is at present no explicit proof existing for one or the other assignments. The theoretical lines obtained from Weisskopf's formula are shown for comparison. *Note added in proof:* A. W. Sunyar, Phys. Rev., **83**, 864 (1951), shows that Cs^{134} and Ta^{180} are $E3$ transitions. R. D. Hill, private communication, finds that the lower limit for the partial lifetime of the $E5$ crossover transition in Te^{121m} is still higher than shown here by a factor of ~20.

[36] Steffen, Huber, and Humbel, Helv. Phys. Acta **22**, 167 (1949).
[37] D. Saxon, Phys. Rev. **74**, 849 (1948).
[38] K. Slätis and K. Siegbahn, Phys. Rev. **75**, 318 (1949) and and Arkiv. Mat. Astron. Fysik **36**, No. 21 (1949).
¶ *Note added in proof:* Dr. D. Saxon has kindly informed us that the value for ϵ_{total} quoted in Natl. Bureau Standards circular 499 is actually the value for ϵ_K. The K/L ratio for the $M1$ transition then becomes ~4.8.

TABLE III. Summary of information on $E3$ and $M3$ isomers.

Isomer	$T_{1/2}$	E (kev)	K/L ratio: Theor. α_K	K/L ratio: Exp.	K/L ratio: Emp. curve	Total conv. coeff.: Exp.	Total conv. coeff.: Calc.	$\log_{10}\tau_\gamma$	$\lvert M\rvert^2$	Spins: I_i	Spins: I_f	Second step: E (kev)	Second step: $T_{1/2}$	Second step: I_s	K/L	Reference
							E3 isomers									
Se^{77}	17.5 sec	162	0.74		4.5		0.9	1.68	2.36×10^{-3}	$7/2+$	$p_{1/2}$			···†		a
Se^{79}	3.9 min	80	14.5		2		21.7	3.89	1.94×10^{-3}	$p_{1/2}$	$7/2+$			···		b
Se^{81}	59 min	98	6	4			7.5	4.64	8.0×10^{-5}	$7/2+$	$p_{1/2}$			···		c
Kr^{79}	55 sec	127	2.1		3.3		2.7	2.47	1.96×10^{-2}	$p_{1/2}$	$7/2+$			···		
Kr^{81}	13 sec	187	0.42		4.6		0.5	1.45	1.37×10^{-2}	$p_{1/2}$	$7/2+$			···		
Kr^{85}	114 min	32.2	~650	$\frac{K}{L+M}$ 0.35			~2500	~7.39	3.27×10^{-4}	$p_{1/2}$	$7/2+$	9		$g_{9/2}$		d
Nb^{94}	6.6 min	41.5	~200	0.31			~850	~5.68	2.2×10^{-3}							e
Tc^{99}	6 hr	2.0								$p_{1/2}$	$7/2+$	140.3	$<10^{-6}$ sec	$g_{9/2}$	7.3	f
Rh^{103}	57 min	40	~165	~0.1			~1800	~6.95	1.29×10^{-4}	$7/2+$	$p_{1/2}$			···		g
Rh^{105}	45 sec	130	2.6	1.4			4.5	2.55	8×10^{-4}	$(7/2)+$	$(p_{1/2})$			···		h
Ag^{107}	44 sec	93.9	9.2	0.92		16 ±3	20.8	3.03	2.36×10^{-3}	$7/2+$	$p_{1/2}$			···		
Ag^{109}	39 sec	89	11	1.0		19 ±3	23.8	3.04	3.39×10^{-3}	$7/2+$	$p_{1/2}$			···		
Cd^{111}	48.6 min	149	1.4	2.0		2.25	2.1	4.12	7.2×10^{-5}	$h_{11/2}$	$d_{5/2}$	247	8×10^{-9} sec	$s_{1/2}$	5.12	i
Sb^{124}	21 min	18.5					α_L: 1.34×10^5	~8.39	7.06×10^{-4}	0−	3+					
Xe^{127}	75 sec	175	0.85		1.6		1.4	2.41	9.48×10^{-5}	$h_{11/2}$	$d_{3/2}$	96(125)		$s_{1/2}$		j
Cs^{134}	3.15 hr	128	2.5	0.64		5.6	6.4	5.08	1.59×10^{-5}	low	high					i
Dy^{165}	1.2 min	109	~3.5	0.076			~50	3.72	7.55×10^{-5}	$i_{13/2}$	$f_{7/2}$					e
Er	2.5 sec	180	0.75		~0.8		~1.75	0.99	1.19×10^{-5}							i
Ta^{180}	16 min	180	0.69	0.25		4.0	2.8	3.72	1.85×10^{-5}	low	high					
W^{180}	5.5 sec	80	~2	small			$\alpha_L\cong128$	~3.02	2.71×10^{-3}	$7/2+$	$p_{1/2}$					
							M3 isomers									
Br^{80}	4.4 hr	49	~100	5.3		>57	~120	~6.45	~1.55 ×10⁻³	4 or 5	1 or 2	37			6.8	k
Tc	51.5 min	34.4	~530	1.2			~970	~6.64	~1.0							l
Hf^{179}	19 sec	161	21	~2		>19	~32	~2.95	~2.8 $\times10^{-2}$	$h_{9/2}$	$p_{1/2}$	215	$<3\times10^{-7}$ sec	$p_{1/2}$		m
Ta^{181}	1.22×10^3 sec*	610	0.24		high		~0.3	3.36	1.41	$1/2+$	$g_{7/2}$			···		n
Au^{197}	7.5 sec	273	4.2	3.4			5.5	1.85	1.0×10^{-2}	$h_{11/2}$	$5/2-$	191		$d_{5/2}$		o
							E3 or M3 isomers									
Sc^{46}	20 sec	135	*E3* 0.66 *M3* 0.42		*E3* >6 *M3* high	~1	*E3* ~0.7 M3 ~0.47	1.76								p
Co^{58}	8.8 hr	24.9	*E3* ~1500	1.9			*E3* ~2300	*E3* ~8.02		5 ±	2+					q
Co^{60}	~11 min	59	*E3* ~50	4.55			*E3* ~60	*E3* ~4.76		2+	5 ±					e, r
Rh^{104}	4.7 min	52	*E3* ~75 *M3* ~450		*E3* ~0.25 *M3* ~1.7	~0.65	*E3* ~375 *M3* ~715	*E3* ~6.18 *M3* ~6.47								p
In	2.5 sec	150	*E3* 1.35 *M3* 5.2		*E3* 1.8 *M3* ~5		*E3* 2.1 *M3* ~6	*E3* 1.05 *M3* ~1.40								s
In^{113}	23 min	160	*E3* 1.05 *M3* 4.5		*E3* 1.9 *M3* ~5		*E3* 1.6 *M3* ~5.5	*E3* 3.71 *M3* ~4.11								
Sb^{122}	3.5 min	69	*E3* ~24 *M3* ~200		*E3* ~0.3 *M3* ~1.8		*E3* ~104 *M3* ~310	*E3* ~4.50 *M3* ~4.99								p
Yb	6 sec	~200	*E3* 0.55 *M3* ~8		*E3* ~0.85 *M3* ~3		*E3* ~1.2 *M3* ~10.5	*E3* ~1.28 *M3* ~2.0								
Yb	0.5 sec	450	*E3* 0.046		*E3* 3		*E3* 0.06	*E3* 1.88								s
Ir^{192}	1.5 min	57					*E3* α_L~890	*E3* ~5.06								
Am^{242}	80 hr*	52				~1		5.92								t

* Partial half-life for isomeric transition is given wherever branching is known to occur.

† Whenever the ground state is the final state of the first isomeric transition, this is indicated by ···.

[a] W. C. Rutledge and S. B. Burson, private communication. A. C. G. Mitchell, private communication.

[b] A. Flammersfeld and W. Herr, Z. Naturforsch. **5a**, 569 (1950).

[c] The values given by I. Bergström and S. Thulin, Phys. Rev. **76**, 1718 (1949), make the value for $|M|^2$ somewhat smaller.

[d] I. Bergström, Phys. Rev. **81**, 638 (1951).

[e] R. L. Caldwell, Phys. Rev. **78**, 407 (1950).

[f] Mihelich, Goldhaber, and Wilson, Phys. Rev. **82**, 972 (1951).

[g] Sauer, Axel, Mann, and Ovadia, Phys. Rev. **79**, 237(A) (1950), and private communication.

[h] R. B. Duffield and L. M. Langer, Phys. Rev. **81**, 203 (1951).

[i] A. W. Sunyar, Phys. Rev. **83**, 864 (1951).

Footnotes continued on following page

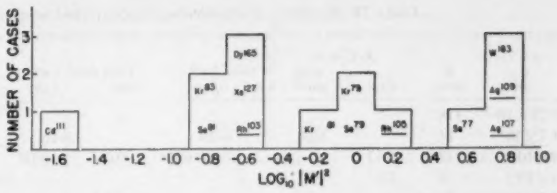

FIG. 10. Distribution of the squares of matrix elements for nuclei of odd mass number which show $E3$ transitions. They are plotted against the relative values of $|M'|^2=(2I_i+1)|M|^2$. Nuclei with an odd proton are underlined.

another of the $E3$ type. The first group fits the strong spin orbit coupling model: $g_{9/2}\leftrightarrow p_{1/2}$ transitions below magic number 50, $h_{11/2}\rightarrow d_{3/2}$ transitions below magic number 82, $i_{13/2}\rightarrow f_{5/2}$ transitions below magic number 126. The $h_{11/2}\rightarrow d_{3/2}$ transitions are followed by $M1$ transitions wherever the ground state is known to be $s_{1/2}$ (with Xe^{129} still insufficiently investigated). The $i_{13/2}\rightarrow f_{5/2}$ transitions are followed by $E2$ transitions wherever the ground state is known to be $p_{1/2}$ (with $Pt^{195,197}$ still insufficiently investigated). The $M4$ transitions follow an empirical law: $\tau_\gamma=C(2I_i+1)/A^3E^9$.‖ This formula is equivalent to Weisskopf's formula if the statistical weight factor $(2I_i+1)$ is introduced. The energy dependence is definitely E^9 rather than E^{11}. The most remarkable fact appears to be the small amount of "scatter" found in the experimental points, indicating a mean deviation of the squares of the matrix elements which does not exceed 30 percent. One cannot take this lack of scatter in itself as evidence for the one-particle radiation model. If that model were true in its extreme form, one would expect lower radiation probabilities for odd-neutron nuclei than for odd-proton nuclei.[39] This is not found to be so for magnetic transitions. For electric transitions, however (Fig. 10), there is a strong indication that odd-neutron nuclei have indeed lower radiation probabilities than odd-proton nuclei, thus supporting the one-particle model in a very direct way. It may be that magnetic transition probabilities are determined largely by "interaction effects"[40] which involve an average over many nucleons and are essentially the same for odd-neutron and odd-proton nuclei. The reduction in the square of the matrix element for the odd-odd nucleus, Ag^{110}, may speak for the existence of a two-nucleon jump here.

The $E3$ group of "systematically" occurring isomers contains two kinds: one for which $j-j$ coupling can account without any new assumption, showing $h_{11/2}\rightarrow d_{3/2}$ transitions, and one occurring in the $1g_{9/2}$ shell and implying the existence of a low-lying $7/2+$ state. In most of these cases the $7/2+$ state is the metastable state. In two cases where it corresponds to the ground state of long-lived radioactive nuclei, Se^{79} and Kr^{81} (see Table III), it may be possible to check the predicted spin of $7/2$ experimentally. The existence of a low-lying state of spin $7/2$ and even parity would be in contradiction to the strong spin orbit coupling if it were interpreted as a $g_{7/2}$ level. This level should be 1–2 Mev higher than the $g_{9/2}$ level, as the change in the binding energy at magic number 50 indicates.[41] It is therefore plausible to interpret the occurrence of a low-lying $7/2+$ level as due to a breakdown of the rule that $j-j$ coupling of a number of odd nucleons of equal j leads to a spin j as the lowest state. This rule is known to break down for Na^{23} and Mn^{55} where the configurations $(d_{3/2})^3$ and $(f_{7/2})^5$ have lowest states of spin $3/2$ and $5/2$ respectively. If the finite range of forces is taken into account, $j-j$ coupling is found to be compatible in these cases with the experi-

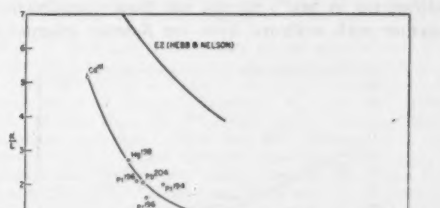

FIG. 11. Experimental K/L ratios for $E2$ transitions. The nonrelativistic theoretical curve is shown for comparison. (E in kev.)

‖ It would seem better to use three different constants for the three different families ($g_{9/2}\leftrightarrow p_{1/2}$, $h_{11/2}\rightarrow d_{3/2}$, $i_{13/2}\rightarrow f_{5/2}$). However, empirically these constants are found to be nearly equal. Had we used the equivalent formula $\tau_\gamma=c/(2I_f+1)A^3E^9$ the three empirical constants would differ considerably.

[39] In a one particle model the orbital motion of a neutron contributes to the radiation probability only indirectly through the recoil of the charged core. For electric transitions the rate is reduced by a factor $\sim(Z/A^{\Delta I})^2$. The transition probability thus becomes negligibly small for large spin changes when compared to that for nuclei with an odd proton. In spite of the contribution from the intrinsic magnetic moment of the neutron one should expect on this model a small reduction in the transition probability for magnetic transitions in odd-neutron nuclei compared with odd-proton nuclei.

[40] N. Austern and R. G. Sachs, Phys. Rev. **81**, 710 (1951).

[41] J. A. Harvey, Phys. Rev. **81**, 353 (1951).

[j] Creutz, Delsasso, Sutton, White, and Barkas, Phys. Rev. **58**, 481 (1940). These authors find two γ-rays, 175 and 125 kev. For the second one they find only a single electron line, interpreted as a K-line. We prefer to interpret this line tentatively as an L-line of a 96-kev γ-ray, because our empirical K/L ratios would indicate that the L-line of a 125-kev $E2$ transition should be sufficiently intense to be visible.

[k] Lidofsky, Macklin, and Wu, Phys. Rev. **78**, 318(A) (1950).

[l] Medicus, Preiswerk, and Scherrer, Helv. Phys. Acta **23**, 299 (1950).

[m] E. der Mateosian and M. Goldhaber, Phys. Rev. **83**, 843 (1951). S. B. Burson, private communication.

[n] Burson, Blair, Keller, and Wexler, Phys. Rev. **83**, 62 (1951), and private communication. J. L. Wolfson (Chalk River) unpublished.

[o] Frauenfelder, Huber, De-Shalit, and Zünti, Phys. Rev. **79**, 1029 (1950).

[p] E. der Mateosian and M. Goldhaber, Phys. Rev. **82**, 115 (1951).

[q] K. Strauch, Phys. Rev. **79**, 487 (1950).

[r] Spin assignments are those given by M. Deutsch and G. Scharff-Goldhaber, Phys. Rev. **83**, 1059 (1951).

[s] E. C. Campbell, private communication.

[t] O'Kelley, Barton, Crane, and Perlman, Phys. Rev. **80**, 293 (1950).

TABLE IV. Summary of information on short-lived isomers: $M1$, $E2$, and $M2$.

Isomer	$T_{1/2}$ (sec)	E (kev)	K/L ratio Exp.	K/L ratio Emp. curve	K conv. coeff. Exp.	K conv. coeff. Calc.	Total conv. coeff. Exp.	Total conv. coeff. Calc.	Type	$\text{Log}_{10}\tau_\gamma$	$\lvert M\rvert^2$	Spins I_i	Spins I_g	Reference
Li^{7}	0.75×10^{-13}	478							$M1$	13.03	15.9	$p_{3/2}$	$p_{1/2}$	a
Fe^{57}	1.1×10^{-7}	14		high		~14		~16	$(M1)$	$\bar{6}.43$	0.025			
Cd^{111}	8×10^{-6}	247	5.12			0.053	0.06	0.06	$E2$	$\bar{7}.09$	3.2×10^{-2}	$d_{5/2}$	$s_{1/2}$	b
Eu^{150}	3×10^{-9}	70	1.3						$M1+E2$					c, d
Er^{168}	1.7×10^{-9}	80					$\alpha_L\cong0.4$		$E2$	$\bar{8}.09$	55	2+	0+	e
Tm^{171}	2.5×10^{-6}	113					1.3							
Yb^{170}	1.6×10^{-9}	84	0.14		0.4		4.0		$E2$	$\bar{8}.06$	43	2+	0+	f
Lu^{177}	1.3×10^{-7}	150	3			6.6		8.8	$M2$	$\bar{6}.27$	25			g
Ta^{181}	2.2×10^{-6}	134	0.5			0.48		1.44	$E2$	$\bar{5}.89$	5.6×10^{-4}	1/2+	3/2+	g
Ta^{181}	$\frac{1.1\times10^{-8}}{1/9}$	345		~2.6		0.03		~0.042	$E2$	$\bar{7}.18$	2.6×10^{-3}	3/2+	7/2+	h
Ta^{181}	$\frac{1.1\times10^{-8}}{8/9}$	481	3–5	~4.3		0.017	~0.02	~0.021	$E2$	$\bar{8}.26$	4×10^{-3}	3/2+	$g_{7/2}$	h
Re^{187}	5.5×10^{-7}	133	5			~13.5		~16	$M2$	$\bar{5}.13$	5.7		$d_{5/2}$	g, i
Os^{186}	8×10^{-10}	137	0.6			~0.44	~1		$E2$	$\bar{9}.37$	16	2+	0+	j
Ir^{191}	5.7×10^{-9}	65											$d_{3/2}$	k
Hg^{197}	7×10^{-9}	133	$\frac{K}{L+M+N}$ 0.29			~0.45	~2.4	~2	$E2$	$\bar{8}.53$	1.25	$f_{5/2}$	$p_{1/2}$	l
Pb^{204}	3×10^{-7}	374	2			0.04	~0.05	0.06	$E2$	$\bar{7}.66$	5×10^{-4}	2+	0+	

[a] R. E. Bell and L. G. Elliot, Phys. Rev. **76**, 168 (1949).
[b] C. L. McGinnis, Phys. Rev. **80**, 842 (1950).
[c] F. K. McGowan, Phys. Rev. **80**, 482 (1950).
[d] J. W. Mihelich, private communication.
[e] F. K. McGowan, Phys. Rev. **80**, 923 (1950). K. Siegbahn and H. Slätis, Arkiv. Physik **1**, 559 (1950).
[f] R. E. Bell and R. L. Graham, Phys. Rev. **78**, 490 (1950).
[g] F. K. McGowan, ORNL 952, 104.
[h] A. Hedgran and S. Thulin, Phys. Rev. **81**, 1072 (1951).
[i] *Note added in proof:* F. K. McGowan (private communication), has measured the conversion coefficient and finds it smaller than expected for an $M2$ transition. This may thus be an $(M1+E2)$ transition.
[j] F. K. McGowan, Phys. Rev. **81**, 1066 (1951). F. R. Metzger and R. D. Hill, Phys. Rev. **81**, 300(A) (1951).
[k] F. K. McGowan, Phys. Rev. **79**, 404 (1950).
[l] F. K. McGowan, Phys. Rev. **77**, 138 (1950). M. Deutsch and W. Wright, Phys. Rev. **77**, 139 (1950). Frauenfelder, Huber, De-Shalit, and Zünti, Phys. Rev. **79**, 1029 (1950).

mental results.[17] The lowest states of the $(g_{9/2})^{3,5,7}$ configurations have not yet been calculated for forces of finite range. If we accept the interpretation that these configurations contain low-lying 7/2+ states, one of the main objections to the strong spin orbit coupling model is removed. On this interpretation no low-lying state of spin 7/2 should occur for either a single particle or a single hole in the $g_{9/2}$ shell. All isomeric transitions observed at the beginning or end of the shell are indeed of the $M4$ type. Where isomers exist, but no isomeric transition has been observed because of β-decay competition (as in Se_{49}^{83}) we can use these considerations together with evidence from the β-decay schemes to assign spins to the excited and ground states ($p_{1/2}$ and $g_{9/2}$, respectively, for the Se^{83} isomers).

The "unsystematically" occurring isomers do not appear to favor any particular spin or parity change, except that their number appears to drop off as ΔI increases, as might be expected.

Electric transition probabilities are usually considerably smaller than predicted by Weisskopf's one particle formula and their matrix elements scatter considerably. Such a behavior appears quite reasonable, as any deviation from one particle wave functions should lead, as a rule, to a reduction of the transition probability by an amount which will vary from nucleus to nucleus. The

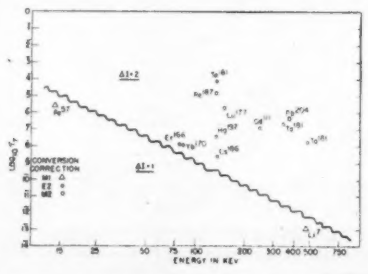

FIG. 12. Lifetime-energy relations for $E2$, $M2$, and $M1$ transitions. [The □ for Pb^{204} should be ○.]

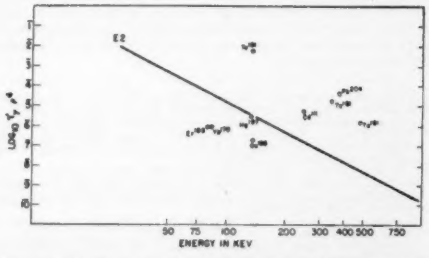

FIG. 13. Normalized lifetime-energy relation for $E2$ transitions. The theoretical line from Weisskopf's formula is shown for comparison. The existence of transitions faster than expected from the one particle model is noteworthy.

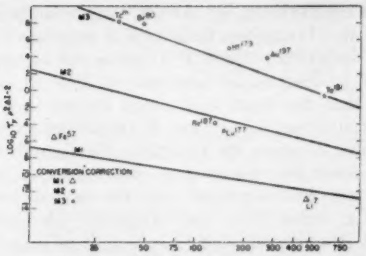

FIG. 14. Normalized lifetime-energy relations for $M1$, $M2$, and $M3$ transitions. The theoretical lines from Weisskopf's formula are shown for comparison.

tendency of odd-neutron nuclei to have lower electric transition probabilities than odd-proton nuclei may become a measure of the "purity" of the one particle wave functions: The more nearly the wave functions are represented by one particle wave functions, the shorter should be the lifetime for the case of an odd-proton nucleus and the longer for that of an odd-neutron nucleus; e.g., $_{47}Ag^{107}$ has an $E3$ transition of 44-sec half-life with an energy of 94 kev, whereas Cd_{69}^{111} has one of 48.6-min half-life in spite of its considerably higher energy of 149 kev. The large fluctuations of the squares of the matrix elements which are found for electric transitions do not permit any precise predictions for the relative probabilities of transitions which can take place competitively from an excited state to two different lower states whenever one or both are electric transitions. The capricious behavior of such ratios has often been noticed, e.g., in studies of cross-over transitions of the $E4$ type competing with $E2$ transitions.

Some $E2$ transitions have squares of matrix elements >1; these are unique among the electric transitions considered here. It is conceivable that we are dealing here with a radiation analog of the "cooperative" phenomenon which is believed[42] to be responsible for the large

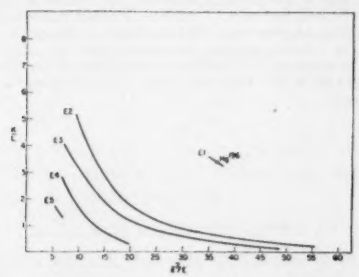

FIG. 15. Summary of empirical K/L ratios for electric transitions. For both $E5$ (see Fig. 1) and $E1$ only one point is known. For $E2$, $E3$, and $E4$ many points are known (see Figs. 1, 7, and 11). (E in kev.)

[42] J. Rainwater, Phys. Rev. **79**, 432 (1950). A. Bohr, Phys. Rev. **81**, 134 (1951).

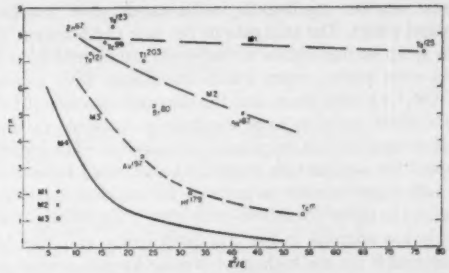

FIG. 16. Summary of empirical K/L ratios for magnetic transitions. Many points are known for $M4$ (see Fig. 1) but few are known for the other transitions where the curves must be considered as preliminary. (E in kev.) *Note added in proof:* Later work on Au^{197m} [Huber, Humbel, Schneider, de Shalit, and Zunti, Helv. Phys. Acta **24**, 127 (1951)] and Hf^{179m} [S. B. Burson and H. B. Keller, private communication] indicates that the K/L ratios for these points are higher than plotted.

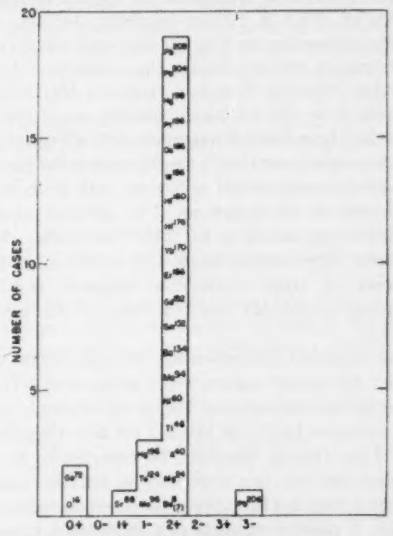

FIG. 17. Spin and parity of first excited state of even-even nuclei. The assignments given here are based in part on data given in Tables III and IV and Figs. 7, 11, and 15, as well as on the review article of Hornyak, Lauritsen, Morrison, and Fowler, Revs. Modern Phys. **22**, 291 (1950) and on "Nuclear Data" (including Supplement 1) by K. Way *et al.* (1950 and 1951). The following cases are based on more recent publications and unpublished data: Te^{124} [Langer, Moffat, and Price, Jr., Phys. Rev. **79**, 808 (1950)]; A^{40} [P. Morrison, Phys. Rev. **82**, 209 (1951)]; Sm^{148} and Gd^{160} (J. W. Mihelich, to be published); Er^{166} and Hf^{178} (Scharff-Goldhaber, Mihelich and der Mateosian, to be published); Hf^{180} (R. A. Becker, University of Illinois, private communication); W^{186} and Os^{186} [F. R. Metzger and R. D. Hill, Phys. Rev. **81**, 300(A) (1951)]; Pb^{208} (Recent results on angular correlation, obtained by H. E. Petch and M. W. Johns, Phys. Rev. **80**, 478 (1951) favor the assignment 2+ for the first excited state, in contradiction with results on internal conversion obtained by D. G. E. Martin and H. O. W. Richardson, Proc. Phys. Soc. (London) **A63**, 223 (1950) which favor 1+.)

static electric quadrupole moments of some nuclear ground states. The existence in the rare earth region of low lying excited states in even-even nuclei with spin 2 and even parity, from which transitions with values of $|M|^2>1$ take place, and the easy deformation of the core which leads to large quadrupole moments in this region may in fact be related phenomena. One should expect the one-particle model to break down for nuclei of odd mass number as soon as the excitation energy suffices to excite their even-even core. This will occur at fairly low energies in the rare earth region and may be responsible for the high level density known to exist in this region.

Because of the empirical rule that the lifetime of a γ-ray transition depends mainly on the spin change and not on the parity change, we can usually not expect an appreciable admixture of electric $(\Delta I+1)$ radiation to magnetic ΔI radiation. The only exceptions are the $M1+E2$ transitions. The existence of such a mixed transition was first established in angular correlation studies of Y^{88}.[43] A further example, deduced from internal conversion studies, was discussed above (Tl^{203}). There can be two reasons for the occurrence of these mixtures: Selection rules may make the $M1$ transition forbidden,[40] or the $E2$ transitions may be of the "cooperative" type which can compete with $M1$ transitions. We have seen above that in the Te isomers the $d_{3/2}\rightarrow s_{1/2}$ transitions consist of $M1$ radiations with little, if any, admixture of $E2$ radiations. The lifetimes of these transitions are known to be $\lesssim 10^{-9}$ sec. If $d_{3/2}$ and $s_{1/2}$ represent pure configurations, this would indicate the existence of large interaction magnetic moments, according to the $M1$ selection rules of Austern and Sachs.[40]

The empirical lifetime-energy relations allow us to predict the energy regions where millisecond activities might be expected to occur. For $\Delta I=2$ we should expect such activities for $E\sim 50$ kev and for $\Delta I=3$ for $E\sim 800$ kev. They cannot, therefore, be expected to be very common and the fact that they so far have escaped detection need not be entirely due to experimental difficulties. A possible example of a millisecond transition may be the 803-kev γ-ray in Pb^{206} [44] which can be identified as an $E3$ transition from its K/L ratio (see Fig. 7).

The empirically found K/L ratios can be approximately represented as functions of Z^2/E. It is very likely that the exact K/L ratios depend in a more complicated manner on Z and E. Deviations are noticeable: low Z points are sometimes higher and high Z points lower than the average empirical curve. Such a trend may be compatible with the deviation of the empirical curve from the calculated nonrelativistic curves. The nonrelativistic curves may be expected to agree better with experiment for lower Z values, but better data are needed before a definite conclusion can be drawn.

The rule that the first excited state of an even-even nucleus usually has spin 2 and even parity would follow in those cases where the ground state and the first excited state are formed by a pair of identical nucleons in equivalent orbits, both for $j-j$ coupling and $L-S$ coupling. The excited state could also be caused by excitation of the even-even nucleus as a whole (liquid drop model). A more detailed experimental and theoretical study of this question seems desirable.

From a theoretical point of view, the most important results of our analysis of isomeric transitions seem twofold: Important objections to the strong spin-orbit coupling model have been removed, and the need for a refinement in the radiation probability formula has been pointed up by the recognition of the remarkable constancy of the squares of matrix elements for magnetic transitions and their large variability for electric transitions.

We should like to thank Doctors H. S. Snyder, G. Scharff-Goldhaber, E. J. Kelly, M. Neuman, and G. Snow of this laboratory, and J. Blatt of the University of Illinois for valuable discussions.

[43] E. L. Brady and M. Deutsch, Phys. Rev. **78**, 558 (1950). D. S. Ling and D. L. Falkoff, Phys. Rev. **74**, 1224 (1948).

[44] D. E. Alburger and G. Friedlander, Phys. Rev. **81**, 523 (1951). *Note added in proof:* Grace, Allen, West, and Halban, Proc. Phys. Soc. (London) **64**, 493 (1951), have measured the internal conversion coefficient of this 803-kev γ-ray which is emitted following α-decay from Po^{210}. They find $\epsilon=6.7$ percent, from which they conclude that this is an $M2$ transition. The theoretical values are $\beta_2=7.8$ percent, and $\alpha_3=2.1$ percent. Excited states formed by α-decay from an even-even nucleus should be expected to have even parity for even angular momentum and odd parity for odd angular momentum. The gamma-ray transitions from these states to the ground state should therefore be expected to be electric transitions.

The Nuclide P^{33} and the P^{32} Spectrum*

RAYMOND K. SHELINE, RICHARD B. HOLTZMAN, AND CHANG-YUN FAN
Institute for Nuclear Studies, University of Chicago, Chicago, Illinois

(Received May 21, 1951)

P^{33} has been produced by the bombardment of sulfur, sodium sulfide, and lithium chloride with the 48-Mev gamma-ray spectrum of the University of Chicago betatron. The reactions involved are $S^{34}(\gamma,p)P^{33}$, $Cl^{35}(\gamma,2p)P^{33}$, and $Cl^{37}(\gamma,\alpha)P^{33}$. The P^{33} activity has a 25 ± 2 day half-life with a 0.27 ± 0.02-Mev negative beta-ray. There is less than one (0.5-Mev) gamma for every fifteen betas. The activity was observed in the presence of P^{32}, and its ratio to the P^{32} activity did not change with chemical purification. Beta-ray spectra of the weak component observed in Oak Ridge carrier-free P^{32} indicate that this weak activity is P^{33} produced by the reaction $S^{33}(n,p)P^{33}$. The cross section for pile neutrons for this reaction is approximately 0.029 barn. The Fermi plot of the beta-ray spectrum is straight with a log ft value of 5.2. A decay scheme for P^{33} is proposed.

I. INTRODUCTION

IN looking at a table of isotopes in the vicinity of P^{33} one finds that P^{33} is largely surrounded by stable and known radioactive isotopes, yet itself is unknown. Often when such a circumstance arises it is because the nuclide in question has either a very short half-life, a very long half-life and a weak radiation, or because it has the same half-life as a known activity. In each of these cases its detection is difficult. P^{33} in particular would be expected to have a long half-life and a weak radiation, for it is an odd-even isotope like the stable P^{31} to which just one excess neutron pair has been added. Thus, in the case of chlorine, which has an additional proton pair, the stable Cl^{35} corresponds to stable P^{31}, whereas Cl^{37}, which corresponds to P^{33}, is now stable. Indeed, if one calculates the decay energy for P^{33} by calculating the masses of S^{33} and P^{33} from the Fermi-Weizsäcker equation, one obtains 0.23 Mev. Assuming this energy and that the transition $P^{33}\rightarrow S^{33}+\beta^-+\nu$ is allowed ($ft=10^5$), the half-life is about 70 days. In some preliminary experiments in which phosphorus fractions were separated from chlorine irradiated at the betatron, the separated activity showed a half-life longer than 14 days when counted with a thin window counter. This evidence indicated that P^{33} might indeed be longer lived than P^{32}. In experiments at the Chalk River Pile, however, Yaffe and Brown[1] found a 22-sec activity which they assigned to P^{33}.

Since one should be able to make P^{33} from sulfur by the $S^{34}(\gamma,p)P^{33}$ reaction, and also from chlorine by the $Cl^{37}(\gamma,\alpha)P^{33}$ and $Cl^{35}(\gamma,2p)P^{33}$ reactions, it seemed advisable to look for P^{33} in the irradiation of sulfur and chlorine with 48-Mev gamma-rays from the University of Chicago betatron.

II. SEARCH FOR SHORT-LIVED P^{33}

In order to look for very short-lived activities a sample was counted in place, without chemistry, immediately after turning off the betatron beam. The sample of sulfur was a pressed pill cylinder, 8 inches in length, and $\frac{3}{4}$-inch in diameter. It was mounted directly in the beam in such a way that the axis of the cylinder was the axis of the beam. A Geiger tube was placed parallel to it and about 2 inches off the beam center. The counter was shielded from the beam by 6 inches of lead. The betatron and the Geiger tube were controlled by a motor-driven timing switch which executed a duty cycle: betatron—on 3 sec, off 5 sec, on 3 sec, etc., synchronous with counter—off 3 sec, on 5 sec, off 3 sec, etc. The scaler pulse was fed directly to one pen of a two-channel Brush recorder. The other pen was fed 60 cycle ac to act as a timer. In this way it was possible to irradiate samples for 3 sec and then to count them within milliseconds after the beam was turned off for a period of 5 sec. This apparatus was used to look for a new activity of half-life from 0.2 second to 2 minutes where no chemical separation was effected. No indication of a new short-lived activity was found within the experimental error of the measurement, which was very small.

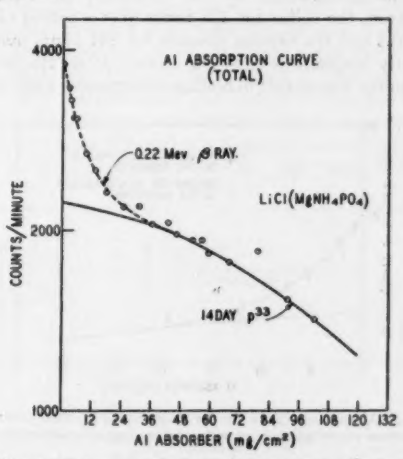

FIG. 1. Absorption curve on the phosphorus fraction from the gamma-ray irradiation of lithium chloride.

* Part of this work was reported at the Washington, D. C., meeting of the American Physical Society, April, 1951. Phys. Rev. 83, 215 (A) (1951).

[1] L. Yaffe and F. Brown, Phys. Rev. 82, 322 (1951).

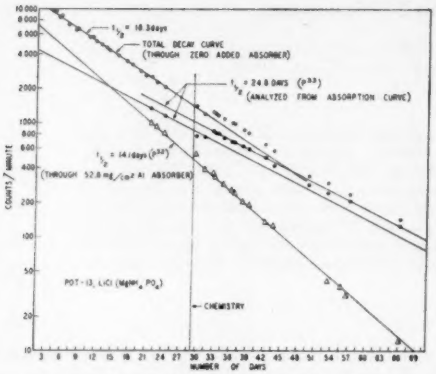

FIG. 2. Decay of the phosphorus fraction analyzed for strong and weak beta-ray components.

Using, then, a "rabbit" to transport the sample quickly after irradiation, and the traditional end-window Geiger tube and counting setup, we irradiated chlorine and sulfur with gamma-rays. In each case the phosphorus was separated as the ammonium phosphomolybdate.[2] No indication of a new activity of half-life from 2 minutes to 14 days was found. Thus, no new activity was found in the half-life region from 0.2 second to 14 days with the exception of the 1 to 3 second and 1 to 3 minute regions, which would be obscured by the strong activities of S^{31} (2.6 sec) and P^{30} (2.55 min), respectively. Accordingly, it seemed advisable to look for a longer lived activity.

III. 25-DAY PHOSPHORUS NEGATIVE BETA-EMITTER

Samples of sulfur and lithium chloride were irradiated by the gamma-rays of the University of Chicago betatron, the sulfur for 225 hours over a period of $1\frac{1}{2}$ months and the lithium chloride for 244 hours over a slightly longer time than the sulfur. After irradiation the sulfur was melted in boiling concentrated nitric acid in the presence of phosphate carrier, and the phosphate was precipitated twice as ammonium phosphomolybdate in 1*N* nitric acid. The lithium chloride was dissolved in hot concentrated nitric acid and after the reaction had stopped the solution was diluted to 1*N* nitric acid. Phosphate carrier and sodium sulfate holdback carrier were added. Ammonium phosphomolybdate was precipitated and washed with ammonium molybdate solution. The precipitate was dissolved in dilute ammonia and ammonium sulfide was added to hold back sulfide and sulfur. The phosphate was then precipitated twice as the magnesium ammonium phosphate.

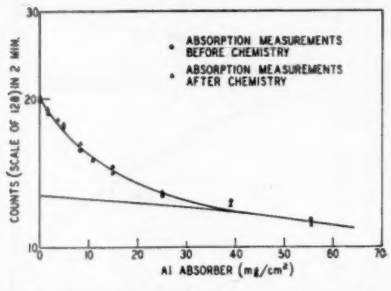
ABSORPTION MEASUREMENTS BEFORE CHEMISTRY
ABSORPTION MEASUREMENTS AFTER CHEMISTRY
COUNTS (SCALE OF 120) IN 2 MIN.
Al ABSORBER (mg/cm²)

FIG. 3. Absorption curve on the phosphorus fraction from the gamma-ray irradiation of sulfur before and after chemistry.

[2] W. F. Hillebrand and G. E. F. Lundell, *Applied Inorganic Analysis* (John Wiley and Sons, Inc., New York, 1929), pp. 38, 581.

Absorption curves were taken on these samples (Fig. 1). A 0.22-Mev beta-ray component was observed. Decay curves were also taken on these samples, utilizing appropriate absorbers to diminish the counting rate of the weak beta-ray component. In this way, the gross decay curve (Fig. 2) was broken into two components, one the 14-day P^{32} and the other a new 25-day activity. The thin window counter used to take the decay curves of Fig. 2 was replaced after the 60th day. The new tube had a thinner window, so that the weak beta-ray component was counted more efficiently and consequently the decay curve deviated discontinuously. It may be noticed that the total decay curve deviated also, but the decay of the hard beta-ray component is constant.

If this activity were an impurity, it would most probably be S^{35} (0.167 Mev β^-, half-life 87 days), Ca^{45} (0.25 Mev β^-, half-life 152 days), or Pa^{233} (0.23 Mev β^-, half-life 27.4 days).[3] Since protoactinium has several gamma-rays and conversion electrons associated with its decay, and no indication of these was found, it was eliminated from consideration.

A chemical purification of phosphorus was made in the presence of sulfur and calcium carriers. The sulfur was in the form of sulfate, sulfite, and sulfide, and the calcium was in the Ca^{++} state.

The chemistry consisted of dissolving the samples in 6*N* HCl, adding calcium, sulfate, and sulfite carriers and then adding concentrated nitric acid to oxidize the sulfite to sulfate and precipitating the sulfate with barium. After centrifuging to remove the barium sulfate, the phosphate was precipitated as ammonium phosphomolybdate to separate it from calcium. As before the phosphomolybdate was washed and dissolved in ammonium hydroxide, and ammonium sulfide was added to hold back sulfide and sulfur. Two precipitations as the magnesium ammonium phosphate were done before counting. This rather extensive chemistry in no way affected the relative amount of P^{32} to the new low energy component. The absorption curves before and after chemistry are shown in Fig. 3. Therefore, this new activity is certainly a phosphorus activity. Magnetic deflection experiments show the activity to be a

[3] Way, Fano, Scott, and Thew, *Nuclear Data* (Circular of the Natl. Bur. of Standards 499, 1950), pp. 28, 38, 264.

negative beta-emitter. Therefore, the activity is a 25-day negative-beta-emitting phosphorus of approximately 0.22 Mev.

IV. THE BETA-SPECTRA OF P^{33} AND THE 25-DAY PHOSPHORUS ACTIVITY

Earlier work by Agnew[4] in this laboratory on the beta-spectrum of P^{32} revealed the presence of an anomaly in the low energy region. This anomaly becomes pronounced below 250 kev and was not observed with certainty before.[5] Agnew's result was subsequently confirmed by Warshaw *et al.*,[6] whose spectrum shows an even more pronounced "bump" in the momentum plot at low energies. The interpretation that the anomaly was due to a complex beta-spectrum seemed improbable, since P^{32} is known not to emit gamma-rays.[7] The work reported here, along with that of Jensen and Nichols,[8] shows that the anomaly is due to the presence of a hitherto unknown beta-emitter, having just the half-life and energy to account for all the observations.

The beta-spectrum of various samples of radioactive phosphorus were studied with the same double lens

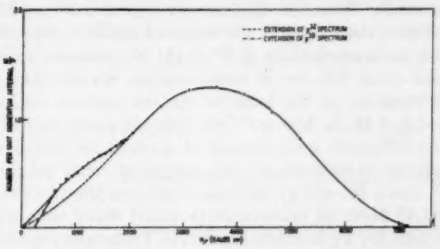

FIG. 4. The beta-spectrum of 27-day-old carrier-free phosphorus from Oak Ridge.

beta-ray spectrometer as was used by Agnew.[9] The samples studied were carrier-free P^{32} obtained from the Isotopes Division at Oak Ridge and measured (a) 27 days after end of irradiation, (b) 242 days after end of irradiation, and (c) 308 days after the end of the irradiation; and also phosphorus purified radiochemically from (d) sulfur and (e) chlorine, which had been irradiated with gamma-rays up to 48 Mev from the University of Chicago betatron.

The spectrometer was used with 9 percent resolution and 4 percent transmission. Samples (*a*) and (*b*) were measured by using a Nylon window counter of window thickness approximately 80 $\mu g/cm^2$ which cuts off electrons below 3 kev. This window is supported on a grid

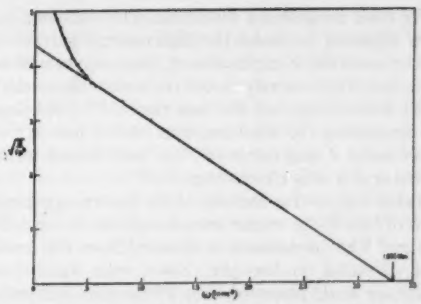

FIG. 5. Fermi plot of the beta-spectrum of 27 day old carrier-free phosphorus from Oak Ridge. $E_{max} = 1.695 \pm 0.005$ Mev.

which reduces the transmission by a factor of 3. Due to the weakness of samples (*c*), (*d*) and (*e*) a counter was used without a grid but with a mica window with a window thickness of 0.96 mg/cm^2. The mica window cuts off electrons below about 12 kev. The cut-off energies of the beta-rays were determined from the beta-ray spectra. The sources were deposited on 15 $\mu g/cm^2$ Nylon foil made conducting by evaporating aluminum of thickness approximately 5 $\mu g/cm^2$. The internal conversion line of Cs^{137} was used to check the energy calibration and resolution of the instrument at each setting used.

Figure 4 shows the beta-spectrum of the 27-day-old carrier-free phosphorus from the Isotopes Division at Oak Ridge. This curve is quite similar to the one obtained by Agnew and Warshaw and shows the anomalous "bump" at low energy. The conventional Fermi plot is shown in Fig. 5. It is straight from 1.7 Mev to about 300 kev and then rises abruptly at low energy.

Figure 6 shows the momentum plot of samples of the 308-day-old phosphorus, curve *I*; the 242-day-old phosphorus, curve *IV*; and the gamma-irradiated samples of chlorine, curve *II*; and of sulfur, curve *III*. Curves *II* and *III* were taken about 27 days after the end of the irradiation. The source thicknesses were about 5 mg/cm^2 for the 242-day-old phosphorus, 20 mg/cm^2 for the 308-day-old phosphorus, and 15 mg/cm^2 for both bombardment samples. All these samples

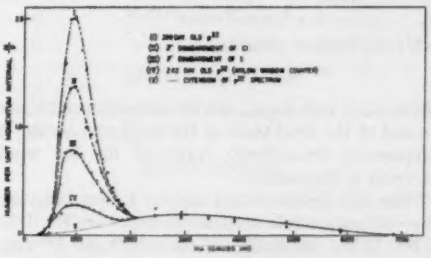

FIG. 6. The beta-spectra of various phosphorus fractions in which the P^{32} component has been normalized.

[4] H. M. Agnew, Phys. Rev. **77**, 655 (1950).
[5] E. M. Lyman, Phys. Rev. **51**, 1 (1937); J. L. Lawson, Phys. Rev. **56**, 131 (1939); K. Siegbahn, Phys. Rev. **70**, 127 (1946); E. J. Scott, Phys. Rev. **74**, 1240 (1948); L. M. Langer and H.C. Price, Phys. Rev. **76**, 641 (1949).
[6] Warshaw, Chen, and Appleton, Phys. Rev. **80**, 288 (1950).
[7] Kurie, Richardson, and Paxton, Phys. Rev. **49**, 368 (1936).
[8] E. N. Jensen and R. T. Nichols, Phys. Rev. **83**, 215(A) (1951).
[9] H. M. Agnew and H. L. Andersen, Rev. Sci. Instr. **20**, 869 (1949).

suffer from thick-source distortion. The ordinates have been adjusted to make the high energy part of the spectra coincide. Examination of these curves makes it clear that the anomaly is due to some other activity which has a longer half-life than that of P^{32} (14.1 days). By comparing the total amounts of the new activity uncer curve *I* and curve *IV*, the half-life can be estimated and is about twice that of P^{32}.

Table I shows the increase of the low energy component of Oak Ridge carrier-free phosphorus as a function of time. This phosphorus is obtained from the irradiation of sulfur in the pile. Since both Agnew[4] and Warshaw *et al.*[6] observed their P^{32} samples over only 5 and 3 half-lives respectively, it is easy to understand from this table why they observed no change in the low energy "bump."

A determination of the end point energy of the new activity from these spectra is $E_{max}=0.27\pm0.02$ Mev, as shown in Fig. 7.†

V. ASSIGNMENT, DECAY SCHEME, AND MASS

Using an end-window counter and an appropriate absorber to cut out all betas, an upper limit for the number of gamma-rays was determined. There is less than one 0.5-Mev gamma to every fifteen low energy component betas.

TABLE I. Variation of percentage of low energy component in Oak Ridge carrier-free phosphorus.

No. of half-lives of P^{32} ($T_{\frac{1}{2}}=14.1$ days)	Percent of low energy component ($T_{\frac{1}{2}}=25$ days)
0	1.9
1	2.5
2	3.4
3	4.7
4	5.9
5	8.6
10	38.8

A run was done in which a sample of sulfur and a sample of lithium chloride were irradiated in the betatron for 21 hours over a period of three days. The ratios of the yields of the weak beta-ray component to the strong beta-ray component, correcting for half-life and absorption are, from sulfur,

$$A_{weak}/A_{strong}=0.79$$

and, from lithium chloride,

$$A_{weak}/A_{strong}=1.02,$$

where A_{weak} and A_{strong} are the saturation activities at the end of the irradiation of the weak and strong (P^{32}) components, respectively, corrected for the window thickness of the counter.

These two pieces of data suggest a mass assignment. The various possible mass assignments are P^{32}, P^{33}, P^{34} or P^{35}. In the irradiation of sulfur, P^{34} and P^{35} can be produced only by the gamma-ray irradiation of S^{36} which is present in 0.016 percent isotopic abundance. Therefore, the relative amounts of P^{34} or P^{35} to that of P^{32} should be very small, since P^{32} can be produced by the gamma-ray bombardment of either S^{33} or S^{34} which have the isotopic compositions 0.75 percent and 4.2 percent respectively. The results quoted above show that the yield of the weak component is almost equal to the yield of P^{32}. The results of the chlorine irradiation are similar. Therefore this activity is neither P^{34} nor P^{35}.

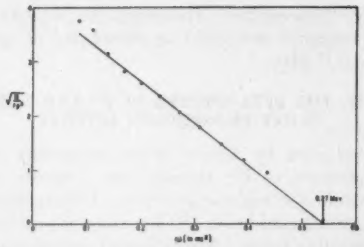

FIG. 7. Fermi plot of the weak component in 27-day old carrier-free phosphorus from Oak Ridge. $E_{max}=0.27\pm0.02$ Mev.

The evidence against the observed radiation resulting from an isomeric state of P^{32} is (1) No isomeric transitions occur this low in mass number, nor are they to be expected on the basis of the one particle nuclear model of M. G. Mayer.[10] One does not expect to find a spin difference great enough to account for long-lived isomeric transitions in this region of mass number. (2) Since the energy difference between the two betas is 1.45 Mev, an isomeric state would decay with high probability by isomeric transition. From spin considerations at least one isomeric transition must not be strictly forbidden. However, no gammas are found associated with the transition. Therefore the activity cannot be an isomeric state of P^{32} or S^{32}.

By elimination, this 0.27-Mev 25-day negative beta-emitting phosphorus must be P^{33}. The decay scheme is shown in Fig. 8. P^{33} is either an $s_{\frac{1}{2}}$ or a $d_{\frac{1}{2}}$ state. Using the rule that adding two neutrons to a nucleus does not change the spin one obtains the same state for P^{33} as for P^{31} which is known to be $s_{\frac{1}{2}}$. The transition

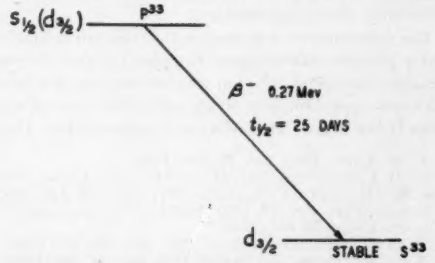

FIG. 8. Decay scheme of P^{33}.

† *Note added in proof:* Our new measurements show the end-point energy to be 0.26±0.01 Mev.

[10] M. G. Mayer, Phys. Rev. **78**, 16 (1950).

$s_{\frac{1}{2}} \rightarrow d_{\frac{1}{2}}$ is L-forbidden with an expected log$ft \sim 7$. The measured logft is 5.2. This is evidence in favor of a strict shell model $d_{\frac{1}{2}}$ state for P^{33}. S^{33} is known to be in a $d_{\frac{1}{2}}$ state.

Low and Townes[11] report the atomic mass of S^{33} as 3.298058 ± 10. This is not an absolute mass but is relative to the mass chosen for S^{32}, which is 31.98089. If one assumes the simple decay scheme shown in Fig. 8, the mass for P^{33} is 32.98088 ± 10.

At Oak Ridge, P^{32} is produced by the $S^{32}(n,p)P^{32}$ reaction. This explains the existence of a small amount of P^{33} in the P^{32} sample because the same reaction will transform S^{33} into P^{33}. The ratio of P^{33} activity to that of P^{32}, after correction for decay, is 1.9 percent. Taking the cross section of the reaction $S^{32}(n,p)P^{32}$ to be 0.012 barn for pile neutrons[3] the cross section of the reaction $S^{33}(n,p)P^{33}$ is then ~ 0.029 barn, assuming that the sulfur was in the pile for the usual 6 weeks.

VI. DISCUSSION AND CONCLUSION

The isotope P^{33} has also been reported by Yaffe and Brown[1] to exist as a 22-sec beta-activity of high energy. This was produced by bombarding P^{32} with neutrons in the pile. The P^{32} was made by $S^{32}(n,p)P^{32}$. An (n,γ) reaction on P^{33} would produce P^{34} previously reported as a 12.4-second half-life with 5.1 and 3.2-Mev betas. In view of the complexity of the decay curve of Yaffe and Brown this may be the 22-sec activity observed by them. If this short-lived activity is actually P^{34}, this would be strong evidence in favor of its assignment as P^{33} since P^{34} could only be produced by (n,γ) on P^{33}.

This isotope may have some value as a phosphorus tracer because of its long half-life. Its use in plant physiology is especially apparent. Thus, for example, at the end of a 150-day growing season the activity of P^{33} would have 15 times as much activity as P^{32}.

The low energy of the radiation may be a defect in making detection difficult; however, it makes it possible to use higher specific activities because the radiation damage would be less than with the high energy beta of P^{32}.

It is suggested that the P^{33} can be best obtained by allowing samples of very intense carrier-free P^{32} from Oak Ridge to decay over a period of 10–12 months. The resulting activity would be from 90–98 percent P^{33}.

The authors wish to acknowledge the interest and advice of Professors Nathan Sugarman, Herbert L. Anderson, and Willard F. Libby in this work. Thanks are also due Mr. Charles McKinney and the betatron operating crew.

[11] W. Low and C. H. Townes, Phys. Rev. **80**, 608 (1950).

PHYSICAL REVIEW VOLUME 83, NUMBER 5 SEPTEMBER 1, 1951

Experiments on Proton-Proton Scattering from 120 to 345 Mev*

O. CHAMBERLAIN, E. SEGRÈ, AND C. WIEGAND
Radiation Laboratory, Department of Physics, University of California, Berkeley, California

(Received April 30, 1951)

The differential scattering cross section for elastic collisions of 345-Mev protons with protons has been measured in the angular range 11° to 90° (center of mass system). The same cross section has been measured over more limited ranges of angles at lower energies. The cross section (in the center of mass system) at 90° is remarkably independent of energy. The cross section at 345 Mev is very independent of angle, being close to 3.8×10^{-27} cm²/steradian (center of mass system). The agreement with existing phenomenological theories based on static potentials is rather poor, especially in the case of scattering at small angles at 345 Mev.

INTRODUCTION

THE results of experimental investigations of n-p scattering have previously been reported and we have given preliminary reports on our study of p-p scattering.[1,2]

At the end of one preliminary report, we indicated some possible improvements in technique which we have now accomplished. In this paper we give our final results on the differential cross section of proton-proton scattering as a function of the angle of scattering and of the energy of the protons. The results of our preliminary paper are confirmed, but the present investigation extends the data to lower energies and increases the precision of the determinations. While these experiments were in progress, Oxley, Schamberger, and Towler[3] have investigated the p-p scattering at 240 Mev, and Birge[4] has done the same at 100 Mev. Their results overlap our own in part, and agree with us in the common part.

A summary of the results is presented in Tables I, II, and III and in Fig. 10.

EXPERIMENTAL

Our source of high energy protons is the external beam of the 184-inch Berkeley cyclotron. In this beam is placed a hydrogenous target, either polyethylene

* Through the Radiation Laboratory this work has been supported by the U.S. AEC.

[1] Hadley, Kelly, Leith, Segrè, Wiegand, and York, Phys. Rev. **75**, 351 (1949); Kelly, Leith, Segrè, and Wiegand, Phys. Rev. **79**, 96 (1950).

[2] O. Chamberlain and C. Wiegand, Phys. Rev. **79**, 81 (1950); Chamberlain, Segrè, and Wiegand, Phys. Rev. **81**, 284, 661 (1951).

[3] Oxley, Schamberger, and Towler, Phys. Rev. **82**, 295(A) (1951).

[4] R. W. Birge, Phys. Rev. **80**, 490 (1950).

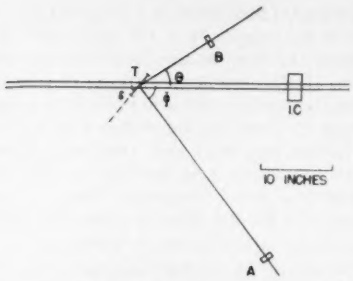

FIG. 1. Arrangement of the coincidence apparatus, top view. The angles used in the text are shown on this figure.

(CH_2) or liquid hydrogen. The protons scattered out of the beam (and out of the target) are counted either singly (method I) or else both the scattered and struck protons are detected simultaneously by two counters in coincidence (method II). In the latter case the two protons emerge from the target at about 90° from each other, a characteristic which helps very greatly in the separation of *p-p* scattering from other scattering processes. Both methods are aided by two developments: the invention by Leith of a method for obtaining a fairly long (25-microsecond) beam pulse time, using deflection by multiple scattering within the cyclotron vacuum tank;[5] and the development of *trans*-stilbene crystal counters and associated equipment,[6,7] with a resolving time for coincidence of about 4×10^{-8} sec.

A schematic diagram of the apparatus (method II) is presented in Fig. 1. The beam deflected from the cyclotron and collimated through the shielding walls impinges on the target T (a foil of polyethylene). The protons, scattered and recoil, are detected in the stilbene crystals A and B, each viewed by a 1P21 photomultiplier tube. A subtends the smaller solid angle Ω, and B is such that every proton through A sends its counterpart through B; as a matter of fact, B subtends a larger solid angle than would be necessary to satisfy the condition stated above in order to be safe from losses of coincidences due to multiple scattering effects and defects in alignment. The beam is monitored by measuring the ionization produced in a shallow ionization chamber full of argon which has (in turn) been calibrated against a faraday cup.

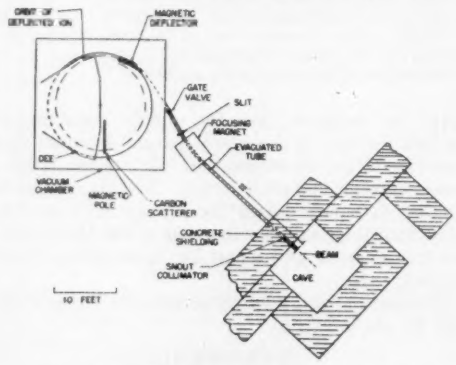

FIG. 2. Schematic diagram of the cyclotron, deflecting magnet, and collimator.

Let us call N the number of hydrogen atoms per cm² in the target measured in the direction of the incident beam, n the number of protons that crossed the target, and H the number of coincidence counts between A and B due to hydrogen in the target. Let Φ be the angle between the line from the target to counter A and the direction of the primary beam. We have $\sigma(\Phi)$, the differential scattering cross section (laboratory system) given by

$$\sigma(\Phi)=H/(n\Omega N). \tag{1}$$

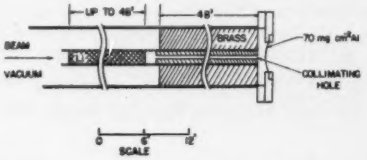

FIG. 3. Collimator for the proton beam. In this figure we also show the lithium absorbers occasionally used to reduce the energy of the beam. The mechanism for moving the collimator hole is not shown.

Passing to the center of mass system,

$$\sigma(\theta)=\frac{[1+(E/2Mc^2)\sin^2\Phi]^2}{1+(E/2Mc^2)}\left(\frac{1}{4\cos\Phi}\right)\sigma(\Phi), \tag{2}$$

$$\tan(\theta/2)=[1+(E/2Mc^2)]^{\frac{1}{2}}\tan\Phi, \tag{3}$$

where $\sigma(\theta)$ is the differential scattering cross section in the center of mass system, at angle θ from the beam in the center of mass system of coordinates, E is the kinetic energy of the incident protons (laboratory system), Mc^2 is the proton rest energy.

We shall now describe our operations and the measurements of the single factors entering into Eq. (1).

PROTON BEAM

Figure 2 gives a general plan of the cyclotron showing the path of the protons in the external beam. At large radii (about 81 inches) the proton orbits show large vertical oscillations and much of the internal beam strikes either of two graphite blocks placed above and below the normal beam plane. A few of the protons are deflected by multiple scattering in the graphite in such a way as to enter the magnetic shielding tube ("magnetic deflector") through which the protons are led away from the main field of the cyclotron.

[5] C. E. Leith, Phys. Rev. **78**, 89 (1950).
[6] Ginston, Hewlett, Jasberg, and Noe, Proc. Inst. Radio Engrs. **36**, 956 (1948).
[7] C. Wiegand, Rev. Sci. Instr. **21**, 975 (1950).

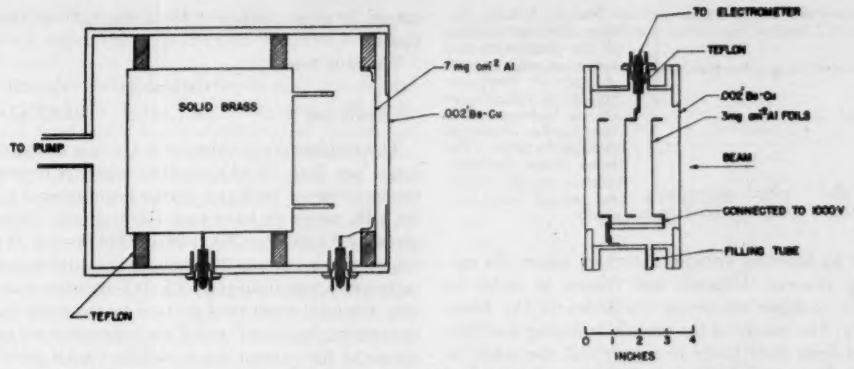

FIG. 4. Detail of the monitoring ionization chamber and of the faraday cup as assembled for calibration of the ionization chamber.

The collimator C is shown in more detail in Fig. 3. Its aperture can be changed from two inches to $\frac{1}{4}$ inch; we used it in the range $\frac{1}{2}$ inch to 1 inch. The axis of the collimator hole was adjusted to be parallel to the beam to within 0.001 radian. The central hole of the collimator could be preceded by cylindrical boxes full of lithium metal in order to reduce the energy of the emerging protons.

The homogeneity in energy of the emerging beam is very satisfactory as shown by the Bragg curve given in another article.[8] This is obtainable by putting 2 shallow ionization chambers in the beam between which is a variable copper absorber. The ratio of the current in the second chamber to that in the first chamber is plotted as a function of absorber thickness. The sharp peak at the end of the curve is an indication of the homogeneity in the energy of the beam.

The bending magnet in combination with the three collimating holes through which the beam must pass gives a momentum selection to about one percent. Evidence that few very low energy protons are generated in the collimator tube material is obtained from the coincidence counting method (as explained in connection with Fig. 8).

The current in the beam was measured in an ionization chamber of the type shown in Fig. 4, which was calibrated against a faraday cup at the highest energy used (345 Mev). The faraday cup, which is our primary standard for determination of the beam intensity, was built by Peterson. It consists of a 6-inch by 6-inch cylindrical brass block, as shown in Fig. 4. Across the face of the faraday cup is a thin foil (bias foil) which can be biased to test for the effect of secondary electron emission from the electrodes. The whole faraday cup structure is in an evacuated enclosure into which the beam passes through a thin window. A magnetic field of 100 gauss across the face of the faraday cup serves to reduce drastically the secondary electron emission.

[8] R. Mather and E. Segrè (to be published).

In operation, change of the bias foil potential from -500 v to $+500$ v caused only $\frac{1}{2}$ percent change in the apparent calibration of the ionization chamber, indicating that secondary electron emission was sufficiently small.

We call the multiplication factor M of the ionization chamber the ratio between the saturation current collected in the chamber and the current in the faraday cup. We can write

$$M=(t/w)(-dE/dx), \tag{4}$$

where t is the thickness of the chamber in g/cm^2 of argon, dE/dx is the specific energy loss in ev g^{-1} cm^2 and w is the energy in ev spent for producing one ion pair. Assuming at the maximum energy $-dE/dx=3.08\times10^6$ for argon[9] we find that the energy w spent per ion pair produced is 25.5 ev. Assuming this quantity to be independent of energy, and the range energy relations of reference 9 to be correct, we can calculate the multiplication factor of the chamber at the other energies.

The intensity of the beam used varied from 5×10^5 to 5×10^7 protons/sec. The pulses during which the particles come out occupied about one thousandth of the "beam on" time. The diameter of the beam was usually 1.25 cm. The integrated current in the ionization chamber was measured by passing it into a condenser and measuring the potential across the condenser with an electrometer circuit similar to that of Vance.[10] The leakage resistance of the system was about 10^{13} ohms. When necessary, the energy of the beam was

FIG. 5. Relative size and position of defining and coincident crystal viewed from the direction of the beam. The two crystals and the beam are shown on scale. The separation distances of each crystal from the beam are reduced to $\frac{1}{4}$ that scale.

[9] Aron, Hoffman, and Williams, AECU—663.
[10] A. W. Vance, Rev. Sci. Instr. 7, 489 (1936).

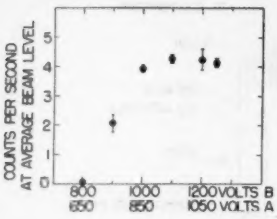

FIG. 6. Voltage plateau. Abscissa: voltage on the photomultipliers connected with crystals *A* and *B*. Ordinate: number of coincidences due to hydrogen for a fixed number of protons crossing the target. (The figure shows the coincidence counting rate at the average beam level used.)

reduced by inserting lithium absorbers before the collimating channel. Lithium was chosen in order to minimize multiple scattering which lowers the beam intensity. The energy of the protons emerging was then deduced from their range in copper and the tables of Aron, Hoffman, and Williams[9] which were also checked by a direct experiment.[8]

TARGETS

The targets used were foils of polyethylene $(CH_2)_n$ which weighed 283 mg cm^{-2}. The composition of this substance was kindly checked by the late Dr. Otto Beeck of the Shell Development Company; it was found to contain 14.44 percent hydrogen by weight (theoretical for CH_2 is 14.37). In spite of the coincidence system, the coincidence counting rate did not vanish if we replaced CH_2 by carbon of equal stopping power. These residual coincidences were mainly accidentals and their rate could be kept low (1/10) with respect to the main effect by controlling the intensity of the primary beam. In order to subtract them we used a carbon target containing 1.43 times as many carbon atoms per cm^2 as the CH_2 target. This target has approximately the same stopping power for protons as the CH_2 target. Since the way in which the background should be subtracted is not completely unambiguous it is important to keep it small with respect to the main effect.

We calculate H, the effect due to hydrogen, by the formula,

$$H = CH_2 - 0.6C - 0.4B, \tag{5}$$

where CH_2, C and B are the number of counts obtained if the same number of protons crossed the polyethylene target, C target, or no target (blank run). The justification of this formula is as follows: Data from preliminary work show that for 1 single count due to hydrogen there are about 5 single counts due to carbon. On this assumption, taking into account the solid angles subtended by the A and B crystals, we have for one count due to hydrogen in crystal A when using a CH_2 target

	Crystal A	Crystal B
Counts due to H	1	9
Counts due to C	5	45

Accidental coincidences arise from 5 counts in crystal A and $45+8=53$ counts in crystal B. If we use a carbon target having the same stopping power as the CH_2 target, it must contain 1.43 as much C as the CH_2 target.

We have thus

	Crystal A	Crystal B
Counts due to C	$5\times1.43=7$	$45\times1.43=64$

The accidental coincidences in the case of the carbon target are then $7\times64\times\alpha=448\alpha$ where α depends on the instruments used and on the beam intensity. With the CH_2 target we have an accidental coincidence rate given by $5\times53\times\alpha=265\alpha$; $265\alpha/(448\alpha)=0.6$. We thus subtract the carbon background by subtracting the carbon effect multiplied by 0.6. It is important that not only the total number of protons be the same but also the current, because C and B are approximately proportional to the current for a constant total number of protons as is to be expected for accidental coincidences. Experimental verification that this procedure is adequate has come from the agreement of cross sections measured over a considerable range of beam intensities.

GEOMETRY

The angle between the protons emerging from the target, which would be 90° in a nonrelativistic case is given by:

$$\tan(\Theta+\Phi)=[(2Mc^2/E)+1]\tan\Phi+(2Mc^2/E)\cot\Phi. \tag{6}$$

The deviation of $(\Theta+\Phi)$ from 90° may conveniently be approximated by

$$(\pi/2)-\Theta-\Phi\simeq(E/4Mc^2)\sin(2\Phi), \tag{7}$$

where E is the kinetic energy of the incident proton in the laboratory system.

The defining crystal A and the larger crystal B are located as in Fig. 1. Given the dimensions and distance of crystal A, which define Ω, the dimensions and distance of B must be so chosen that all p-p scattering processes which register in A register also in B. The condition on the height of crystal B is indicated in Fig. 5 which is a projection in a direction parallel to the beam direction. The analogous condition on the width of crystal B involves the width of crystal A as well as the thickness of the target measured in the direction of crystal A. The size of crystal B must be further increased to allow for the effect of multiple scattering of both emerging protons in the target material. In a typical case the dimensions of A are 1.8 cm high×3.80 cm wide; of B 3.80 cm×2.51 cm wide; the distances TA and TB in projection are 64 cm and 16 cm. The actual distances

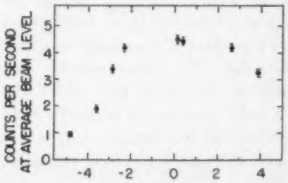

FIG. 7. Number of coincidences due to CH_2 for a fixed number of protons crossing the target *versus* height of the plane containing crystals AB and the target. This plane is initially parallel to the beam and is adjusted to contain the beam by lifting the whole apparatus.

between the target and the fronts of A and B are 80 cm and 30 cm respectively. In the case described $\Phi = 52.5°$ and $\Theta = 32.8°$.

The distance between the target and the crystal which defines the solid angle has been arbitrarily measured from 4 mm inside of the crystal. We do not know exactly how far a particle must penetrate the crystal in order to be counted, but since the total distance between A and T is more than 80 cm, this uncertainty of 2 or 3 mm cannot make more than an error of about 0.8 percent in the measurement of the solid angle. A more serious problem is to make sure that the whole front of the crystal is sensitive. The best evidence on the subject is given by the plateaus of the counting rate *versus* voltage on the photomultiplier, which we have repeatedly checked, and by the fact that several different pairs of crystals in different geometries gave the same cross section within statistics. In a previous paper we reported cross sections obtained with gas counters. They were systematically somewhat higher than the ones obtained with crystal counters.[2] The origin of this discrepancy has been traced to the fact that the brass walls of the counters were thick (0.3 cm). Protons hitting the brass could, by multiple scattering, be deviated into the gas and thus counted. The order of magnitude of this effect calculated in a crude way was comparable with the disagreement between the gas counter cross sections and the present crystal cross sections. To make certain that our explanation is correct, we put in front of our crystal a brass tube to simulate the geometry of the gas counters. Measurement of the cross sections with this device gave again high values in agreement with the gas counter results.

The angle between the target and the beam was chosen in such a way that the plane of the target was tangent to a circle defined by the two crystals and the point where the beam intersects the target. This minimizes the deviations from the optimum geometry for the various points of the target and is essential if crystal A and crystal B are to have approximately the same dimensions.

We checked many times that upon changing the distance between A and T or B and T or both, within the limits prescribed by the geometrical criteria, the cross sections remained unchanged.

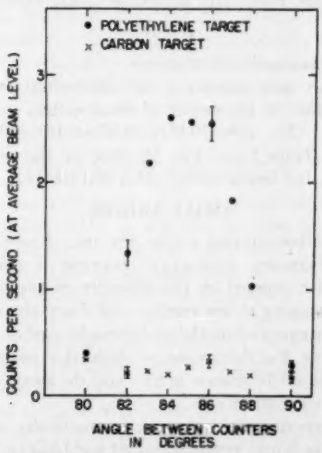

FIG. 8. Coincidence counting rate as a function of the angle $(\Theta+\Phi)$ between the two crystals for $\Theta = 43°$. According to Eq. (6) a maximum at 84.7° corresponds to $E = 345$ Mev.

TABLE I. Complete results obtained at the full beam energy with the coincidence counting technique (method II) and polyethylene targets.

Angle θ cm system in degrees	Differential cross section $\sigma(\theta)$ in 10^{-27} cm²/sterad	Error in $\sigma(\theta)$ in 10^{-27} cm²/sterad	E lab. system in Mev
35.6	4.31	0.21	345
36.4	3.93	0.15	345
43.4	3.79	0.15	345
44.0	4.17	0.13	345
45.8	3.64	0.07	345
46.1	3.99	0.11	345
52.4	3.77	0.10	345
60.8	3.83	0.13	345
64.0	3.55	0.11	345
64.0	3.74	0.14	345
70.6	3.67	0.16	345
72.2	3.67	0.11	345
80.2	3.95	0.12	345
87.6	3.86	0.10	345
88.2	3.91	0.08	345
88.2	3.70	0.08	345
88.6	3.85	0.06	345
88.6	3.54	0.09	345
89.2	4.15	0.36	345

EXPERIMENTAL PROCEDURE

A typical run proceeded as follows: The deflected beam of the cyclotron was aligned photographically by replacing the target T and ionization chamber M of Fig. 1 with x-ray films which had fiducial marks accurately located with respect to the scattering table.

After this the plateaus of the coincidence counting rate H *versus* voltage in the photomultiplier tubes were taken. Results are shown in Fig. 6.

Following this the height of the whole scattering apparatus was changed in small steps and the coincidence counting rate maximized. (Fig. 7.) This guaranteed that the beam, crystal A and crystal B were in a plane. Finally, keeping Θ constant, Φ was varied to maximize the H count. This last check shows very clearly that the energy of the impinging proton is about 345 Mev (and that the relativistic elastic collision laws are obeyed) (Fig. 8). The effect vanishes at 90°, indicating that there were few very low energy protons in the beam.

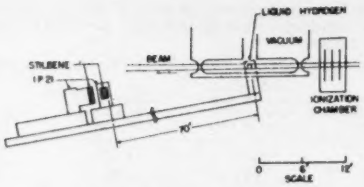

FIG. 9. Vertical section of the liquid hydrogen apparatus for measuring scattering at small angles to the beam. The counter arm pivots around an axis through the center of the liquid hydrogen container. Not shown is a thin heat shield which surrounds the liquid hydrogen container and is maintained at liquid nitrogen temperature.

After these tests a measuring run started and we report the numbers obtained in a typical case.

We give as an example the detailed calculation of the eleventh line of Table I. The angle Φ, measured directly, is 52.5°. Knowledge of the incident proton energy allows calculation of the center of mass angle, $\theta=70.6°$ using Eq. (3). (Here we always use whichever angle is less than 90°.) The target thickness is 0.283 g/cm^{-2} of CH_2, and the surface of the target makes an angle of 54.1° with the beam. The number of target atoms per cm^2 along the beam direction is $N=0.283\times2\times6.023\times10^{22}/(14.03\times\sin 54.1°)=3.000\times10^{22}$ target protons/cm^2. The defining crystal (A) has a face of 1.81 cm $\times3.80$ cm$=6.88$ cm^2, and is located at the effective distance 80.2 cm from the target. The solid angle subtended by the counter, Ω, is then $6.88/(80.2)^2=1.070\times10^{-3}$ sterad. Crystal B is 3.80 cm high by 2.51 cm wide and is located 30 cm from the target. The ionization chamber for beam monitoring is 5.10 cm deep, and is filled with argon gas to a pressure of 89.6 cm Hg at 22°C (82.9 cm Hg at 0°C). The total capacity in the integration circuit is 1.007×10^{-7} f; the integrator circuit is observed to read full scale with 0.993 volt at the input. From these figures and the data obtained in the calibration with the faraday cup we calculate that $n=6.86\times10^8$ protons for full scale integrator reading ("integrator volt").

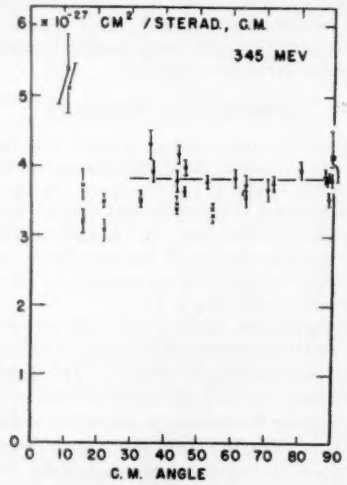

FIG. 10. Differential scattering cross section in center of mass coordinate system, $\sigma(\theta)$. The errors shown are standard deviations from counting statistics only. Circles: CH_2 target, coincidence method (method II). Crosses: liquid hydrogen, single counter (method I). Square: CH_2 target, single counter (method I).

The number of counts per integrator volt registered was as follows:

$$CH_2\text{: } 228\pm6,$$
$$C\text{: } 52\pm4,$$
$$\text{Blank: } 26\pm7;$$

the time required for one integrator volt was about 100 seconds. From this, according to Eq. (5) we obtain

$$H=187$$

and ϵ_H (standard deviation)$=8$.

We can now calculate the differential scattering cross section in the center of mass system using Eqs. (1) and (2), $\sigma(\theta=70.6°)=(3.67\pm0.16)\times10^{-27}$ cm^2 $sterad^{-1}$. Table I and Fig. 10 show all the results obtained at full beam energy with this method.

TABLE II. Complete results obtained at the full beam energy using a liquid hydrogen target. Only the proton at the smaller angle from the beam was detected (method I).

Angle θ CM system in degrees	Differential cross section $\sigma(\theta)$ in 10^{-27} cm^2/sterad	Error in $\sigma(\theta)$ in 10^{-27} cm^2/sterad	E lab. system in Mev
11.3	5.1	0.36	345
11.3	5.38	0.49	345
15.2	3.71	0.22	345
15.2	3.21	0.17	345
21.1	3.51	0.10	345
21.7	3.06	0.15	345
32.5	3.52	0.09	345
33.1	3.51	0.11	345
42.8	3.48	0.10	345
42.8	3.40	0.08	345
53.2	3.40	0.08	345
53.2	3.28	0.10	345

SMALL ANGLES

At small scattering angles the use of polyethylene targets becomes impractical because a coincidence system is hampered by the difficulty of measuring the proton escaping at low energy, and if one abandons the coincidence procedure the scattering by carbon becomes prohibitive. For this reason we decided to use method I with a liquid hydrogen target and do away with the coincidence method.

The experimental setup is schematically shown in Fig. 9. The liquid hydrogen target was built by Dr. L. J. Cook and will be described by him in another article.[11]

[11] To be published soon, probably in the Rev. Sci. Instr.

The hydrogen containing part of it is a stainless steel tube 34.92 cm long and 5.08 cm in diameter closed by two hemispherical foils of stainless steel 0.1 g/cm² thick. Also two identical hemispherical foils form part of the vacuum jacket. The beam, 1.3 cm in diameter, passes through this target hitting only the four terminal hemispheres and the hydrogen but not the side walls. The crystal counters A and B were connected in coincidence and could detect particles from the whole length of the hydrogen target. The measurement proceeded as follows: first, the coincidence counting rate was determined with T full of air, next with T full of liquid hydrogen boiling at atmospheric pressure, and finally the liquid hydrogen was evaporated and the background redetermined. This cycle was repeated twice. The angle Φ was varied from 5 to 25 degrees in order to overlap with measurements obtained by the coincidence system. The results are contained in Table II. It will be noted that the consistency of the data is good, but there is a deviation of about 10 percent between these data and those obtained with the coincidence system. More work on this point would clearly be desirable, because the discrepancy is not yet accounted for.

LOWER ENERGIES

Results at redd uceenergies are reported in Table III, and the differential cross sections at 90° (CM) are shown in Fig. 11. Only the coincidence method (method II) has been used at reduced energies. The beam is greatly attenuated (to 1/100 normal intensity) by multiple scattering in the lithium and the beam loses its parallelism so the only effective collimation is by the 48-inch-long collimating tube shown in Fig. 3. The effect of previous collimating slits is reduced drastically by the multiple scattering. Therefore, the beam is more spread and more divergent than the full energy beam and larger crystals of stilbene have been necessary to obtain satisfactory geometry. Relative to the proton beam intensity the background is considerably increased, presumably due to neutrons formed in the lithium and in the brass of the collimator.

PRECISION OF THE RESULTS

The errors quoted in Table I are standard deviations due to statistics only. In addition to these we have to consider errors in the various quantities H, N, n, Ω, and Φ which enter in the expression for $\sigma(\theta)$. For the target: area, mass, uniformity, composition. These all together may make 1 percent. The effective thickness of the target depends on the angle δ of Fig. 1. The imprecision of the adjustment of this angle may make another 1 percent error.

The measurement of H is affected by statistical errors and by the uncertainty inherent in the background subtraction method. The measurement of the solid angle of the crystals is affected by the precision of the geometrical measurements which is good (1.5 percent) but is subject to the assumption that all the crystal is sensitive. This in turn is proved by the plateaus of the coincidence counting rate *versus* voltage. The error introduced here is hard to estimate and is probably one of the weakest points of this investigation. We give as an estimate 3 percent error. Some reassurance on this point was obtained by using various sets of crystals and distances. The cross sections obtained were identical within the statistical accuracy of the measurements.

Multiple scattering in the target and in the crystals

TABLE III. Complete results obtained at reduced beam energies. Polyethylene targets and the coincidence method (method II) were used.

Angle θ CM system in degrees	Differential cross section $\sigma(\theta)$ in 10^{-27} cm²/sterad	Error in $\sigma(\theta)$ in 10^{-27} cm²/sterad	E lab. system in Mev
47.4	3.97	0.51	250
47.4	3.23	0.29	250
62.0	4.38	0.27	247
64.6	3.84	0.20	250
78.4	3.69	0.15	250
78.4	3.53	0.18	250
87.2	3.67	0.21	250
87.4	3.69	0.10	249
87.6	3.95	0.22	250
87.6	3.59	0.21	250
89.6	3.56	0.27	247
89.6	3.28	0.16	247
59.9	3.38	0.23	164
60.8	4.08	0.45	163
88.6	3.88	0.26	163
88.8	3.54	0.35	164
90.0	3.60	0.17	164
63.0	3.67	0.56	120
63.0	4.40	0.50	120
77.8	4.25	0.33	120
85.2	3.85	0.25	120
89.2	3.95	0.12	118

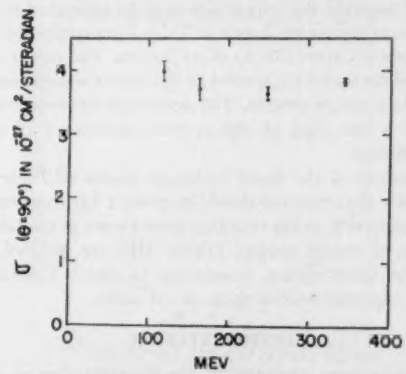

FIG. 11. Differential scattering cross section for $\theta=90°$ as a function of energy, in 10^{-27} cm²/steradian. Errors indicated are standard deviations from counting statistics only.

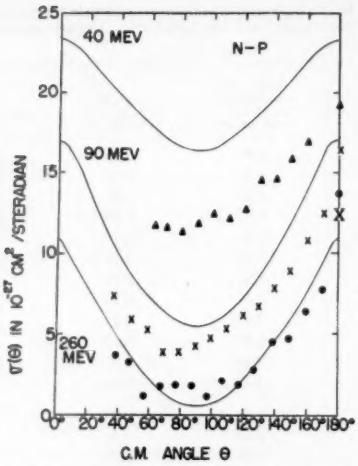

FIG. 12. The curves show the calculated differential cross sections of Christian and Hart. The points are experimental values, taken from the papers of reference (1), except the large X which was obtained from private communication from Dr. Robert H. Fox. The experimental total cross sections might be in error by as much as 20 percent, as would be needed to give good fit. In the calculations Christian and Hart used the following potential: For singlet states $V=(-35.3\text{ Mev})(\frac{1}{2}+\frac{1}{2}P_x)(r_0/r)\exp(-r/r_0)$; for triplet states

$$V=(-25.3\text{ Mev})(\tfrac{1}{2}+\tfrac{1}{2}P_x)(r_0/r)\exp(-r/r_0)$$
$$+(-48.2\text{ Mev})(0.37+0.63P_x)(r_0/r)\exp(-r/r_0)S_{12},$$

where S_{12} is the tensor force operator and $r_0=1.35\times10^{-13}$ cm in all cases. P_x is the space exchange operator.

is negligible, since crystal B was in all cases sufficiently larger than dictated by geometrical considerations alone.

The measurement of the current in the primary beam is subject to the uncertainty of the electrical apparatus, saturation of the current in the ionization chamber, and calibration with the faraday cup. Two percent error may be a fair estimate for this part of the measurement.

All together the imprecision may be estimated to be the counting errors shown in Table I superimposed on a 5 percent error due to other factors. The points obtained are each independent of the others and represent absolute measurements. The agreement between them gives a fair idea of the over-all consistency of the experiment.

Analysis of the liquid hydrogen results of Table II indicate that they too should be given a 5 percent error superimposed on the counting error shown in the table. Reduced energy results (Table III) are subject to greater uncertainties, amounting to about 7 percent error superimposed on those of the table.

INTERPRETATION

A maximum program for the interpretation of n-p and p-p scattering experiments would be to deduce the cross section from meson theory. At the present stage of the theory this is clearly impossible and we must be content with more modest procedures.

An attempt has been made by many people to interpret the scattering experiments with velocity independent forces.[12] Accepting the usual symmetry restrictions one is left, for particles of spin $\frac{1}{2}$, with a fairly broad class of potentials:

$$V=V_1+\boldsymbol{\sigma}_1\cdot\boldsymbol{\sigma}_2V_2+S_{12}V_3, \tag{8}$$

where V_1, V_2 and V_3 are functions of the separation distance and may be different for even and odd quantum numbers of the orbital angular momentum. $\boldsymbol{\sigma}_1$ and $\boldsymbol{\sigma}_2$ are the spin operators and S_{12} is the tensor force operator. These attempts have been reasonably successful in several cases in explaining high energy scattering with potentials which also show proper agreement with the low energy properties of the n-p or p-p system respectively. As an example of these attempts we report the results of calculations by Christian and Hart for the n-p scattering in Fig. 12.

It will be noticed that whereas the form of the curves fits reasonably well, the calculated cross sections are in all cases higher than the observed cross sections.[1,13] The theoretical curves are to be considered the best fits in

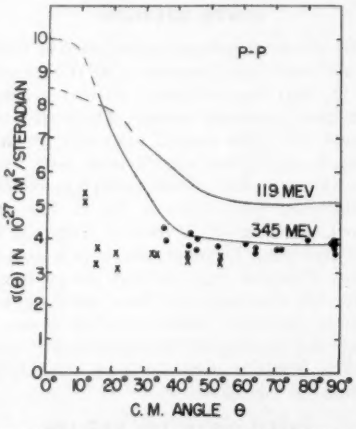

FIG. 13. Points represent experimental results, 345 Mev. Curves are those calculated by Swanson using the method of Christian and Noyes. In the calculations the following potentials were used: For singlet states $V=(-13.273\text{ Mev})(\frac{1}{2}+\frac{1}{2}P_x)$ for $r<r_1$ and $V=0$ for $r>r_1$; for triplet states

$$V=(-25.3\text{ Mev})(\tfrac{1}{2}+\tfrac{1}{2}P_x)(r_2/r)\exp(-r/r_2)$$
$$+(-48.3\text{ Mev})(\tfrac{1}{2}+\tfrac{1}{2}P_x)(r_2/r)\exp(-r/r_2)S_{12}$$
$$+(-15.25\text{ Mev})(\tfrac{1}{2}-\tfrac{1}{2}P_x)(r_3/r)^3\exp(-r/r_3)S_{12}.$$

$r_1=2.615\times10^{-13}$ cm, $r_2=1.35\times10^{-13}$ cm, and $r_3=1.6\times10^{-13}$ cm.

[12] A partial list includes M. Camac and H. A. Bethe, Phys. Rev **73**, 191 (1948); T. Wu, Phys. Rev. **73**, 934 (1948); J. Ashkin and T. Wu, Phys. Rev. **73**, 973 (1948); Massey, Burhop, and Hu, Phys. Rev. **73**, 1403 (1948); Burhop and Yadav, Proc. Roy. Soc. (London) **A197**, 505 (1949); R. S. Christian and E. W. Hart, Phys. Rev. **77**, 441 (1950); R. S. Christian and H. P. Noyes, Phys. Rev. **79**, 85 (1950); Robert Jastrow, Phys. Rev. **79**, 389 (1950).

[13] Cook, McMillan, Peterson, and Sewell, Phys. Rev. **75**, 7 (1949); J. DeJuren and N. Knable, Phys. Rev. **77**, 606 (1950).

this case, for the angular distributions are thought to be better known than the total cross sections. For instance, at 90 Mev the angular distribution is probably known to about 5 percent while the total cross section is known only to 15 percent. (The uncertainties in the total cross sections stem not from the cross section measurements themselves, but from the uncertainties in the effective energies at which the observed cross sections should be considered to apply.) Nevertheless there is a fairly clear discrepancy between calculated and observed cross sections for n-p scattering at 90 Mev, for the experiments indicate that the product $E\sigma_t$ is definitely less than 8×10^{-24} Mev-cm^2, while the calculated value of Christian and Hart is 9.3×10^{-24} Mev-cm^2.

For the p-p scattering we show in Fig. 13 the results of Christian and Noyes. The parameters have been changed for us by Swanson, to give the best fit to the present results. The forces used here differ from those

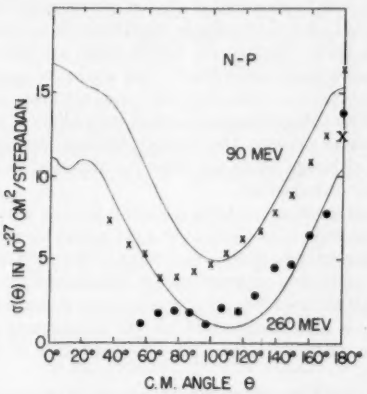

FIG. 14. n-p scattering calculated with the same potential used for p-p scattering in Fig. 13.

used in the n-p calculations of Fig. 12 mainly in the addition of a strong odd-wave tensor force with a singularity at the origin. Within this framework no way has been found to remove the large discrepancy between observed and calculated cross sections near 15°, 345 Mev. Omission of the tensor part of the force would create an insurmountable difficulty inasmuch as it would produce a vanishingly small cross section at 90°.

In view of the strong arguments from low energy phenomena favoring the identify of the n-n and p-p forces it is very tempting to extend this result and try the hypothesis of the identity of the n-p, p-p, and n-n interactions. Qualitative support for this hypothesis has recently been given by Jastrow. The low energy n-p and p-p scattering experiments do not conflict with this viewpoint. The large apparent differences between high energy n-p and p-p scattering cross sections do not rule out this possibility because the Pauli principle eliminates half of the states (triplet s, singlet p, etc.)

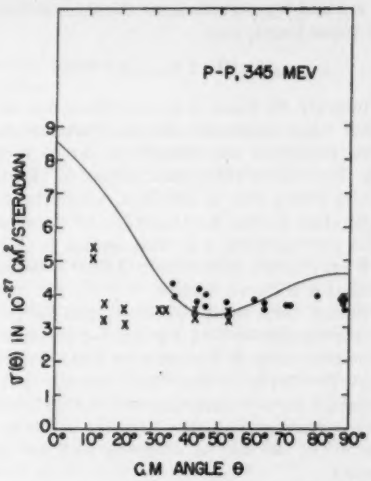

FIG. 15. Experimental points and curves as calculated by Jastrow using the following potential: In singlet states $V=\infty$ when $r<r_0$, $V=(-375\ \text{Mev})(\frac{1}{4}+\frac{1}{4}P_x)\exp[-(r-r_0)/r_t]$, when $r>r_0$, where $r_0=0.60\times10^{-13}$ cm, $r_t=0.40\times10^{-13}$ cm; in triplet states $V=(-69\ \text{Mev})[\frac{1}{4}+\frac{1}{4}P_x+(0.3+0.7P_x)\times1.84S_{12}]\exp(-r/r_t)$ where $r_t=0.75\times10^{-13}$ cm.

from p-p or n-n scattering. The absence of half of the states in the case of systems with identical particles gives a large leeway in the choice of potentials to fit both problems.

Actually the most that we can hope to do with the semi-empirical line of approach followed is to exhibit a special potential compatible with all the experimental material available including high energy p-p and n-p scattering.

It might be possible, however, to do the opposite, namely, to prove that the potentials are different. The only simple theorem now known to us is the following:

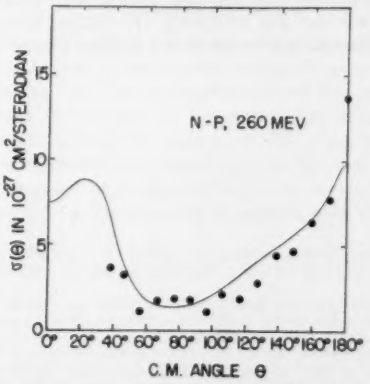

FIG. 16. Experimental points and curves as calculated by Jastrow using the potential given in Fig. 15.

If the n-p and p-p potentials are the same and if there are no tensor forces, then

$$\sigma_{p-p}(\theta=90°) \leqslant 4\sigma_{n-p}(\theta=90°). \quad (9)$$

Unfortunately, we know of no such limitation for cases in which tensor forces are allowed. Furthermore even this relationship is not violated as far as it is now known. The case which comes closest to violation of the above rule is that at 260 Mev, where the p-p differential cross section is $(3.6\pm0.2)\times10^{-27}$ cm²/sterad, and the corresponding n-p cross section is $(1.3\pm0.2)\times10^{-27}$ cm²/sterad. The ratio is 2.8 ± 0.5, so the rule (limited as it is) is not broken.

It remains, then, to try to show at least one potential which corresponds to both p-p and n-p scattering. We mention three cases of interest with which we have the greatest familiarity. First, the Christian and Hart potential for the n-p scattering used in Fig. 12 gives for the p-p scattering negligible intensity in the range of angles 50° to 90° and so disagrees with the p-p experiments.

Secondly, the Christian and Noyes potential developed for p-p scattering may be applied to the n-p scattering. Figure 14 shows the cross sections for n-p scattering, as calculated for us by Swanson with experimental points, using the same potential as in the p-p case of Fig. 13. The agreement is not excellent, but the qualitative features are reasonably well represented. The calculations have been made using Born approximation in odd states, but a more exact method has been used in even states. The unexpected behavior near 30° may be the result of the approximation used. The calculated total cross section is, as usual, too high. These curves are included here because they give a better fit to the n-p experiments than was at first supposed, and for comparison with the calculations of Jastrow.

The third case of interest is that of Jastrow,[12] who chooses a potential with a strong repulsion at short distances. The same potential has been used to calculate both n-p and p-p scattering. His results, along with experimental points, are shown in Figs. 15 and 16. He has kindly extended his calculations for us to include in the angular distribution the effect of tensor forces in odd states. The calculations were made using Born approximation except in the case of the s-wave, where a more exact method has been used. The n-p curve of Fig. 16 shows unexpected maxima near 30° and 130° which are thought to be peculiar to the approximation used.

In Jastrow's results, as in those of Christian and Noyes, a large discrepancy appears in the p-p scattering at 15°, 345 Mev. Coulomb effects have not been included in the calculation. However the coulomb effect, even in the form of interference with the specifically nuclear scattering, cannot account for more than a small part of the discrepancy at 15°. The n-p results (Fig. 16) are remarkably good, but the calculated total cross section is still slightly too high. All together one can say that these attempts are only moderately successful.

If we abandon the restriction to velocity independent forces, then the variety of choices becomes practically unlimited. One of the simple possibilities is to introduce a spin orbit coupling for which there are also independent indications in the nuclear shell structure. This has been done by Case and Pais[14] and they also conclude that with this generalized form of interaction it may be possible to preserve the identity between n-p and p-p force, although we do not know the quantitative results of their calculations.

In all these calculations relativity has not been taken into account. The changes brought about by relativity are guessed to be of the order of 0.2 of the cross sections.

In conclusion we must rather disappointingly admit that all the evidence accumulated on n-p and p-p scattering at high energy does not yet allow a sure answer to the question of the charge independence of nuclear forces.

The authors are grateful to the cyclotron operating crew for their lasting patience and to Dr. V. Z. Peterson for his helpfulness with both the liquid hydrogen target and the faraday cup. Mr. D. R. Swanson has kindly extended the calculations of Christian and Noyes.

[14] K. M. Case and A. Pais, Phys. Rev. **80**, 203 (1950).

Form of Transient Currents in Townsend Discharges with Metastables

J. P. MOLNAR
Bell Telephone Laboratories, Murray Hill, New Jersey
(Received December 8, 1950)

The form of the current is calculated for a Townsend discharge stimulated by a pulsed light beam, with particular reference to the current component initiated by metastable effects. The calculation is directed particularly to the development of methods for quantitative interpretation of current patterns observed experimentally.

A. INTRODUCTION

THE electrtical currents caused by the action of metastable atoms in a Townsend discharge are characterized by their relatively slow time of build-up to a steady-state value. In a typical experiment this time is of the order of one millisecond and is set essentially by the lifetime of the metastables in the space between the electrodes. Because of this slow build-up, a study of the transient character of Townsend currents initiated by pulsed light-illumination of the cathode permits separating currents attributable to the action of metastables from those caused by ions and photons, which build up much more rapidly. Such experiments are described in an accompanying paper (hereafter designated as II). Our purpose here is to develop a theoretical basis for interpreting the current forms obtained in these experiments.

This problem has been discussed by Engstrom and Huxford[1] and Newton.[2] The treatment here follows closely that of Engstrom and Huxford and represents an extension of their analysis to include higher order terms and the volume destruction of metastables, as well as the diffusion loss they considered.

B. STATEMENT OF PROBLEM

We assume we have a gas-filled tube with two plane-parallel electrodes, an anode and cathode, and that beginning at time $t=0$, a current of electrons, i_0, leaves the cathode as a result of photoeletric action of light shone on the cathode.[3] This electron current we assume is amplified to a value, i_f, in a time of the order of ten microseconds, which we take to be instantaneous on our time scale. The value i_f is given by the well-known Townsend equation,

$$i_f = i_0 \exp[\alpha_i(X-x_0)]/1-\gamma_f(\exp[\alpha_i(X-x_0)]-1), \quad (1)$$

where α_i = the first Townsend coefficient for ionization, defined specifically as the number of electron-ion pairs generated per electron per cm of path in a direction perpendicular to the electrode surfaces; X = the electrode separation; x_0 = the electrode separation at which ionization begins,[4] γ_f = the number of electrons released at the cathode and entering the discharge stream (i.e., not diffusing back) per ion generated in the gas by the fast processes, which include both ion and photon bombardment of cathode (γ_f is defined and discussed in greater detail in II).

The action of metastable atoms in the discharge results in a slowly rising current component, $i_s(t)$ (see Fig. 1); and it is the form and magnitude of this component which we wish to calculate.

We assume that the i_s-component originates either from (1) the emission of electrons from the cathode caused by metastables striking the cathode directly, or (2) the conversion of metastables into radiating atoms from which the emitted photons can photoelectrically eject electrons from the cathode.[5]

We shall see that the form and magnitude of $i_s(t)$ can quite readily be computed for any assumed set of parameters describing the efficiencies of metastable production and of electron emission by the different processes. The inverse problem of establishing these parameters from observed current patterns is less straightforward. For this purpose various approximations are introduced into the analysis.

C. INTEGRAL EQUATIONS

Following Engstrom and Huxford, we start by considering the flow of metastables produced by one electron leaving the cathode, crossing the gap, and causing ionization and excitations. The metastables generated by this electron and its progeny (resulting from ionizations) will diffuse to the containing walls (the electrodes in this case) and be destroyed there unless they are first "destroyed" by special types of collision with normal

[1] R. W. Engstrom and W. S. Huxford, Phys. Rev. **58**, 670 (1940).
[2] R. R. Newton, Phys. Rev. **73**, 570 (1948).
[3] Our analysis is for a "step-function" cycle of light stimulation, and furthermore we consider only the rising part of the transient. The falling part which starts at the removal of the stimulating light has a form exactly the inverse of the rising part. The general method of analysis can, of course, be applied equally well to any form of the stimulating light. For more complicated forms, say, that of a sinewave-modulated light beam, the analysis is probably most easily carried through by first calculating the current form resulting from a "delta-function" type of stimulation, and then integrating a series of these currents modulated according to the assumed form of the light modulation.

[4] This definition of x_0 is rough. In practice x_0 is adjusted to a value such that the experimental values of i_f for $X>x_0$ fit closely Eq. (1).
[5] Metastables can probably also produce electrical effects in pure gases by such processes as a metastable-metastable collision yielding an ionized and a neutral atom plus an electron, or an electron-metastable collision yielding an ion and another electron. These processes come into importance only at high metastable densities, and they are easily reduced to negligible importance by using sufficiently small values of current.

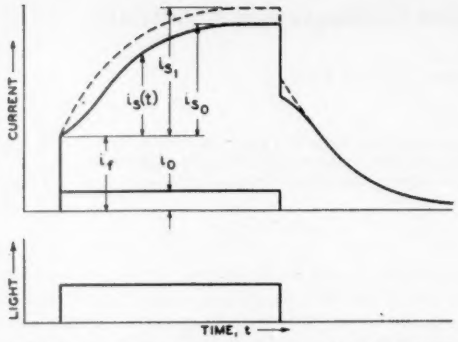

FIG. 1. The current form (schematic) in a pulsed Townsend discharge with metastables. The light pulse is assumed here to have a duration of about 0.005 second. The fast component of current, i_f, is shown here to rise instantaneously. Actually it rises with a time constant of 1 to 30μsec in a typical experiment. The dashed line indicates the form the current would have with a $P(t)$-function described by a single exponential. The effect of higher terms, having a net negative amplitude, is to give the solid curve, although the difference is exaggerated here for purpose of clarity.

atoms.[6] We define a function $P_K(t)$ as the rate of arrival at the cathode of the metastables produced by such an electron leaving the cathode at $t=0$. Similarly, $P_A(t)$ is the rate of arrival at the anode, while $P_G(t)$ is the rate of disappearance of metastables in the volume. Hence, the total rate of flow of the metastables, created by one single electron leaving the cathode, out of the gap is the sum of these three P-functions. We shall calculate their individual forms in Sec. D.

Let us first restrict ourselves to the case in which $i_s(t)$ arises from the release of electrons at the cathode caused only by direct bombardment by metastables. The component $i_s(t)$ will then consist of an electron current at the cathode, initiated by the metastables, enhanced by the same processes which amplify the primary photocurrent i_0 to i_f. Thus, we have

$$i_s(t)=i_f/i_0 \text{ (rate of release of electrons at the cathode by metastables).} \quad (2)$$

The term in the parenthesis is given by the product of the rate of arrival of metastables at the cathode and their efficiency of electron emission. The latter quantity is given $\gamma_m f_{esc}$, where γ_m is the number of electrons released per metastable striking the surface and f_{esc} is the fraction of these electrons which actually enter the discharge stream and do not diffuse back to the cathode. The rate of arrival is given by

$$\int_0^t P_K(t-t')(\text{current of electrons leaving the cathode at } t=t')dt'.$$

[6] Assuming there are no impurities present, such "destruction" is usually assumed to be caused by the conversion of the metastables into atoms excited into nearby radiating states, which for all the noble gases, except helium, lie within 0.1 electron volt. In the case of helium this spacing is much larger. Here the destructive mechanism is less well understood and probably involves the formation of helium molecules. See R. Meyerott, Phys. Rev. **70**, 671 (1946).

The current of electrons leaving the cathode at time t' is given by the total current, $i_f+i_s(t)$, divided by the gas amplification factor, $\exp[\alpha_i(X-x_0)]$. Hence, we have

$$i_s(t)=\left(\frac{i_f}{i_0}\right)(\gamma_m f_{esc})\int_0^t P_K(t-t')\frac{i_f+i_s(t')}{\exp[\alpha_i(X-x_0)]}dt'. \quad (3)$$

By making use of Eq. (1) and introducing the notation $R_f\equiv\gamma_f(\exp[\alpha_i(X-x_0)]-1)$, we can rewrite Eq. (3) as

$$\frac{i_s(t)}{i_f}=\frac{\gamma_m f_{esc}}{1-R_f}\int_0^t P_K(t-t')\left(1+\frac{i_s(t')}{i_f}\right)dt'. \quad (4)$$

This is the fundamental equation describing the problem we are here discussing.

If we assume instead that metastable atoms give rise to a current by being converted into radiating atoms in the gas from which the emitted photons cause photoelectric emission at the cathode, then by analogous reasoning we come out with the equation,

$$\frac{i_s(t)}{i_f}=\frac{\gamma_r f_{rk}' f_{esc}}{1-R_f}\int_0^t P_G(t-t')\left(1+\frac{i_s(t')}{i_f}\right)dt', \quad (5)$$

where γ_r = the number of electrons emitted per gas photon striking the cathode; f_{rk}' = the fraction of the photons emitted by the converted metastables which reach the cathode. For infinite plane-parallel geometry and in the absence radiation imprisonment effects, $f_{rk}'=0.5$. In a practical situation, the lack of perfect plane-parallel geometry and imprisonment effects will tend to make f_{rk}' somewhat smaller. If both processes are acting, then obviously $i_s(t)/i_f$ is given by sum of the right-hand sides of Eqs. (4) and (5).

D. CALCULATION OF P-FUNCTIONS

To calculate the functions $P_K(t)$, $P_A(t)$, and $P_G(t)$, defined earlier, we assume the metastables have a diffusive motion, and so we proceed by solving the diffusion equation. This we write in the form,

$$\partial\rho/\partial t=D_m(\partial^2\rho/\partial x^2)-G\rho, \quad (6)$$

where ρ = the linear density of metastables created by a single electron leaving the cathode at $t=0$, D_m = the diffusion coefficient of metastable atoms in the parent gas, x = the distance from the cathode, and G = the probability of a metastable being destroyed in the gas per second.

We assume that the metastables are destroyed when striking either electrode, so that our boundary conditions are

$$\rho=0 \text{ for } x=0 \text{ and } x=X. \quad (7)$$

It is readily shown that the following solution fulfills our requirements:

$$\rho=\sum_n a_n \sin(n\pi x/X)\exp\{-[(\pi^2n^2D_m/X^2)+G]t\}, \quad n=1, 2, 3, \cdots, \quad (8)$$

where the a_n's are coefficients determined by having ρ as given by Eq. (8) describe the initial distribution of

metastables. Since at $t=0$ the exponential factors are all unity, it is evident that the a_n's are coefficients in a fourier expansion of the initial distribution function. For this we assume that metastables are initially formed in the space between electrodes in a density α_m/α_i times that at which the ions are formed, where α_m is the first Townsend coefficient for metastable excitations and is specifically the number of metastable excitations per electron per centimeter.[7] Since the ion distribution is zero for $x<x_0$ and $\alpha_i \exp[\alpha_i(X-x_0)]$ for $x>X$, we can write the initial metastable distribution as

$$\rho=0, \qquad 0<x\leq x_0,$$
$$=\alpha_m \exp[\alpha_i(X-x_0)], \quad x_0<x\leq X. \tag{9}$$

Using the standard formula for fourier coefficients, we have

$$a_n=(2/X)\int_{x_0}^{X} \alpha_m \exp[\alpha_i(X-x_0)]\sin(n\pi x/X)dx. \tag{10}$$

The integration is readily carried out. We shall not take space here to do so, but simply note that a_n is positive for all odd values of n, and negative for all even values.

When ρ, the metastable density, is calculated by the method outlined above, the P-functions are obtained from the following relations,

$P_K(t)\equiv$ (diffusion current to the cathode)
$$=D_m(\partial\rho/\partial x)_{x=0};$$
$P_A(t)\equiv$ (diffusion current to the anode)
$$=-D_m(\partial\rho/\partial x)_{x=X}; \tag{11}$$
$P_G(t)\equiv$ (rate of destruction in the gas)
$$=G\int_0^X \rho dx.$$

With ρ in the form given by Eq. (8), the formulas in Eq. (11) yield

$$P_K(t)=D_m \sum\left(\frac{n\pi}{X}\right)a_n \exp\left[-\left(\frac{\pi^2n^2D_m}{X^2}+G\right)t\right], \qquad n=1, 2, 3, \cdots, \tag{12}$$

$$P_A(t)=D_m \sum\left(\frac{n\pi}{X}\right)a_n(-1)^{n+1} \times\exp\left[-\left(\frac{\pi^2n^2D_m}{X^2}+G\right)t\right], \qquad n=1, 2, 3, \cdots, \tag{13}$$

$$P_G(t)=G\sum\left(\frac{2X}{n\pi}\right)a_n \exp\left[-\left(\frac{\pi^2n^2D_m}{X^2}+G\right)t\right], \qquad n=1, 3, 5, \cdots \text{(only odd)}. \tag{14}$$

[7] This assumption is obviously approximate. On the other hand, for the experiments we are here trying to explain, only the gross exponential form of the initial distribution is important.

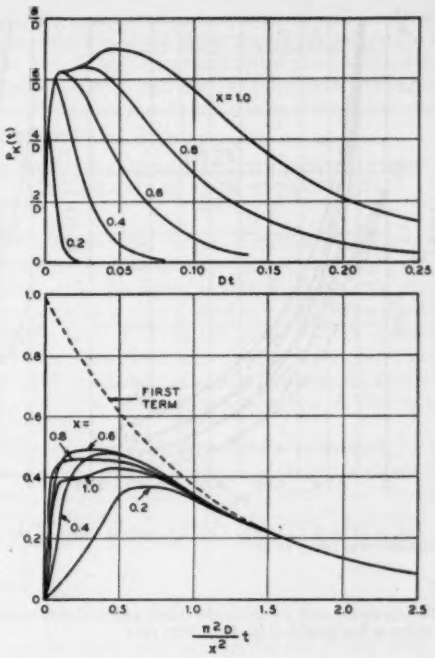

FIG. 2. Typical plots of $P_K(t)$ *vs* t for various values of the electrode spacing, X, computed for an initial distribution of metastables given by

$$\rho=0, \qquad 0\leq x\leq 0.1,$$
$$\rho=e^{\beta(x-0.1)}, \quad 0.1\leq x\leq X,$$

and with $G=0$. The lower set of curves gives $P_K(t)$ for the same conditions, but plotted here in a manner such as to permit direct comparison with the first term of each series. The scales of ordinates and abscissas are adjusted in each case so that the first term falls on the dashed curve. Note that for large X the curves have roughly the same shape when plotted in this form.

We note from the foregoing relations that all the P-functions are described by a series of exponentials with the same time constants but different constant multipliers. Since, as indicated, a_n alternates in sign, the constant multipliers alternate in sign for $P_K(t)$, while for $P_A(t)$ they have the same magnitude, but are all positive. In $P_G(t)$ only the odd terms are present; and, furthermore, because of the appearance of n in the denominator, the constant multipliers get small rapidly with n.

P-functions calculated by the equations are shown in Figs. 2 and 3 for various assumed values of the various parameters. On examination of these curves, it can be seen that $P_G(t)$ is closely represented by a single exponential. The first term of the expansion for $P_G(t)$ given by Eq. (14) contains 95 percent of the area under the $P_G(t)$ curve for a variety of typical cases we calculated. For $P_K(t)$ a single exponential approximation is somewhat worse. Except for the very small values of

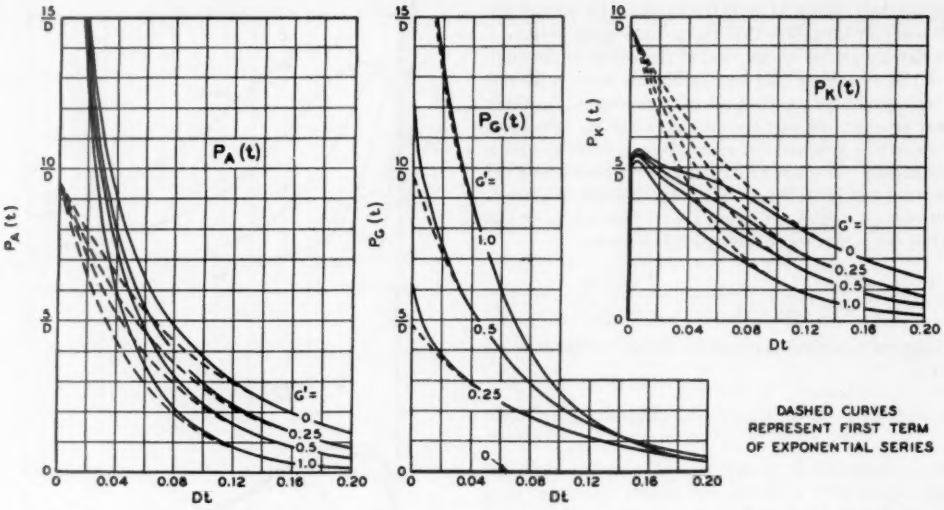

FIG. 3. Plots of $P_A(t)$ and $P_K(t)$ for various values of the gas destruction parameter. Here $G' \equiv GX^2/\pi^2 D_m$, and the initial distribution was taken to be

$$\rho = 0, \qquad 0 \leq x \leq 0.1,$$
$$\rho = e^{3(x-0.1)}, \quad 0.1 \leq x \leq 1.0.$$

The curves for $\rho_G(t)$ are seen to be closely approximated by the first term of their series expansions, whereas for $P_K(t)$ that approximation is less good and for $P_A(t)$ very poor.

X, the area under the $P_K(t)$ curve was 75 to 90 percent of the area under the first term of the expansion as given by Eq. (12), for a variety of typical cases which we computed. Here a two-term approximation, however, is quite satisfactory, as illustrated in Fig. 4.

E. SOLUTION OF INTEGRAL EQUATION

Having outlined the methods of calculating the P-functions, we are now in a position to discuss the solution of the integral Eqs. (4) and (5).

For simplicity let us use for the P-functions the notation

$$P(t) \equiv P_1 e^{-t/\tau_1} + P_2 e^{-t/\tau_2} + \cdots = \sum_1^N P_j e^{-t/\tau_j}. \quad (15)$$

Although $P(t)$ in the strict sense requires an infinite number of terms, we have seen that both $P_K(t)$ and $P_G(t)$ can be closely approximated by a limited number of terms; and, in fact, $P_G(t)$ can be described very well by a single term, while for $P_K(t)$ two terms provide a satisfactory approximation.

With such a series representation of $P(t)$, it is readily shown that $i_s(t)$ can be described by a similar series of exponentials,

$$i_s(t) = i_{s0} - i_{s1} e^{-t/T_1} - i_{s2} e^{-t/T_2} - \cdots = i_{s0} - \sum_1^N i_{sl} e^{-t/T_l}, \quad (16)$$

having the same number of exponential terms as the $P(t)$ series. If this $i_s(t)$ series is substituted into Eq. (4), then we find the following relations between the time constants and coefficients:

$$i_{s0} = i_f \left(\frac{\gamma_m f_{esc}}{1-R_f} \right) \sum_1^N P_j \tau_j \Big/ 1 - \left(\frac{\gamma_m f_{esc}}{1-R_f} \right) \sum_1^N P_j \tau_j, \quad (17)$$

$$1 = \left(\frac{\gamma_m f_{esc}}{1-R_f} \right) \sum_{j=1}^N \frac{P_j}{(1/\tau_j) - 1/T_l} \text{ for each value of } l, \quad (18)$$

$$0 = \sum_{l=1}^N \frac{i_{sl}}{(1/\tau_j) - 1/T_l} - \frac{i_f + i_{s0}}{1/\tau_j} \text{ for each value of } j. \quad (19)$$

In addition we have

$$i_{s0} = i_{s1} + i_{s2} + i_{s3} + \cdots = \sum_{l=i}^N i_l$$

simply from the physics of the situation.[8]

A similar set of equations apply in the case of Eq. (5) with γ_m replaced by $\gamma_r f_{rk}'$.

The accuracy with which $i_s(t)$ can be calculated obviously depends on the number of terms used to express $P(t)$, and the labor involved in solving Eq. (18) and (20) correspondingly depends on the number of terms involved. If, for example, four terms are used, then Eq. (18) is a quartic algebraic equation, from which T_1, T_2, T_3, and T_4 can be obtained. The coefficients i_{s1},

[8] In his paper R. R. Newton (see reference 2, p. 580) derives these relations by another method and discusses them briefly.

i_{s2}, i_{s3}, amd i_{s4} are obtained by solving four linear equations given by Eq. (19).

We carried out such a solution for the case corresponding to an initial metastable distribution given by

$$\rho=0, \quad 0\leq x\leq 0.1,$$
$$\rho=e^{2(x-0.1)}, \quad 0.1\leq x\leq 1.0, \tag{20}$$

and G assumed to be zero. Then we approximated $P_K(t)$ by four-, three-, and two-term series (see Fig. 4). In each case the coefficients of the exponentials were made the same as those corresponding to an infinite series representation, except for the term with the smallest value of τ. For this the coefficient was adjusted so that the value of $P\tau$ for this term was equal to the sum of the $P\tau$'s for this and all higher terms in the infinite series representation. Thus, the quantity $\sum_{j=1,N} P_j\tau_j$ was the same for all three cases, and hence i_{s0} as calculated from Eq. (17) was not dependent on the number of terms used in $P(t)$.

Values of i_{s1} and T_1 as calculated from Eq. (18) and (19) for the four-term series are plotted in Figs. 5 and 6 as a function of the quantity,

$$R_m/1-R_f\equiv(\gamma_m f_{esc}/1-R_f)\sum P_j\tau_j.$$

Over the range of this plot i_{s1} differed less than 0.2 percent for the three series representations, while T_1 differed by less than 0.6 percent.[9] Similarly, the sum of the amplitudes of the higher terms, i_{s2}, i_{s3}, and i_{s4} was maintained within 10 percent.

Note that for small values of $R_m/(1-R_f)$ the relative amplitudes of the various terms remain fixed, while the values of T_1 are close to those of corresponding τ_j's in the $P(t)$ series. As $R_m/(1-R_f)$ is made larger, the first terms shows a marked increase in both amplitude and time constant, while the higher terms deviate little from the earlier trends. Note also that the total amplitude of the higher terms, $i_{s2}+i_{s3}+i_{s4}$, is always negative.

These observations suggest that a fairly satisfactory description of $i_s(t)$ is obtained with a two-term description of $P_K(t)$, yielding a two-term description of $i_s(t)$ in which the fundamental or first term becomes the increasingly dominant fraction as $R_m/(1-R_f)$ is made larger. Such a description fits well the experimental situation, in which case it turns out to be feasible to describe any observed $i_s(t)$ curve by only two terms.[10]

For the case in which metastables are converted into radiating atoms which emit light and thereby give rise to photoelectric emission at the cathode [Eq. (5)], the calculation is even simpler. Here $P_G(t)$ is closely represented by a single exponential. If a second term is added, however, it will have an amplitude with the same sign as the first, and so the higher term in $i_s(t)$ will *add* to the first term. If both electron emission processes are simultaneously active, then Eqs. (4) and (5) can be combined in an obvious way, and a solution carried out in a manner as outlined for Eq. (4).

F. CALCULATION OF FUNDAMENTAL TIME CONSTANT, τ_1, FROM EXPERIMENTAL DATA

In the preceding section a method is outlined for calculating $i_s(t)$ for given values of $\gamma_m f_{esc}/(1-R_f)$ or $\gamma_r f_{rk} f_{esc}/(1-R_f)$ and $P_K(t)$ or $P_G(t)$. In the experimental situation we are faced with the inverse problem, namely, that of calculating these various quantities from data describing $i_s(t)$. The quantity most easily obtained in this way is τ_1, the fundamental time constant of decay of the metastables, and we discuss this problem first.

The experimental arrangements described in the accompanying paper permit fairly accurate determination of i_f, i_{s1}, T_1, and i_{s2}. No accurate time constant corresponding to i_{s2} can be measured. We proceed by applying Eq. (19), which for this case reduces to

$$0=\frac{i_{s1}}{(1/\tau_1)-1/T_1}+\frac{i_{s2}}{(1/\tau_1)-1/T_2}-\frac{i_f+i_{s0}}{1/\tau_1}. \tag{21}$$

If now we recall that $i_{s0}=i_{s1}+i_{s2}$, and further that T_2 does not deviate much from τ_2, so that we can set

$$\beta=\tau_1/\tau_2\approx\tau_1/T_2, \tag{22}$$

where β is a constant, then by rearranging Eq. (21) we have

$$\tau_1=T_1\left[\frac{i_f+(\beta/\beta-1)i_{s2}}{i_f+i_{s1}+(\beta/\beta-1)i_{s2}}\right]. \tag{23}$$

The value of β will depend on whether the function $P_k(t)$ or $P_G(t)$ is involved, and what the relative values

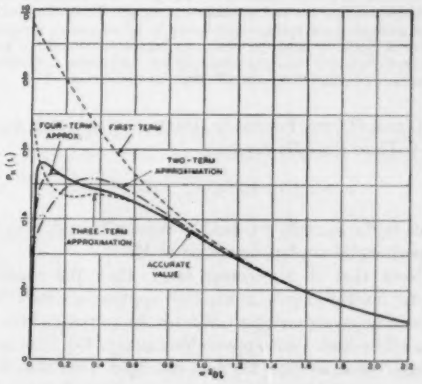

FIG. 4. Various approximations to $P_K(t)$ used in the calculation of $i_s(t)$. $P_K(t)$ here corresponds to an initial metastable distribution same as that in Fig. 3 with $G=0$.

[9] These differences were too small to show up on the scale used in Fig. 5.

[10] Even in a theoretical description, the higher terms depend closely on the assumed spatial distribution of metastables when formed, which we know only approximately. Furthermore, the diffusion equation itself breaks down as a description of the metastable motion for short distances, which in effect correspond to the higher terms of $P_K(t)$. Thus, we lose very little in our knowledge of the actual $i_s(t)$ by approximately $P_K(t)$ is indicated.

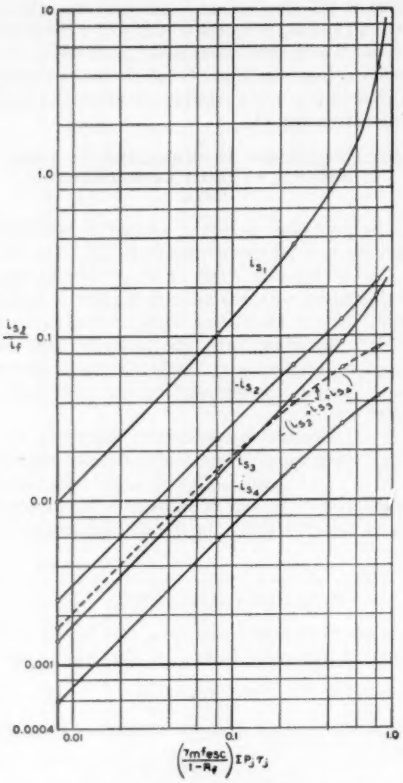

FIG. 5. The amplitudes of the exponential terms in the $i_s(t)$ series *vs* the quantity shown as the abscissas calculated for the case described in the text. In this $(\gamma_m f_{esc})(\Sigma P_j\tau_j)$ gives the number of electrons released at the cathode by the metastables generated by a single electron (and its progeny) leaving the cathode and crossing the gap. The factor $1/(1-R_f)$ gives the multiplication of such electrons by the fast secondary processes. Thus, the abscissa scale gives the total replacement factor by all secondary processes. When it becomes equal to unity, i_{s1} becomes indefinitely large. For small values of the replacement factor, the various i_{sj}'s increase linearly, as indicated by the 45° slope of the curves.

of G and D_m are. For many situations β is closely equal to 4. Then Eq. (23) becomes

$$\tau_1 = T_1(i_f+1.3i_{s2})/(i_f+i_{s0}+1.3i_{s2}). \tag{24}$$

This is the formula we used to reduce T_1 and τ_1 in the experimental studies described in II.

Note that if β becomes large, then the constant factor multiplying i_{s2} in Eq. (23) approaches unity, and i_{s2} can be considered part of i_f for the purposes here. In the other limit of β approaching unity, Eq. (22) is no longer valid, so Eq. (23) does not hold. This case illustrates the problem of evaluating τ_1 when $P(t)$ is made of exponentials with time constants that differ little from term to term.

In Eq. (24) the quantities on the right side are all easily measurable, and only relative values of the current magnitudes need be known. Such quantities as γ_f, α_i, or i_{s0}, which in general are harder to obtain, are not involved. Thus, in a given experimental situation τ_1 is quite readily evaluated.

G. CALCULATION OF $\alpha_m\gamma_m f_{esc}$ FROM EXPERIMENTAL DATA

Here we make no use of time constant data and use only the value of the total slow component of current, i_{s0}. We rearrange Eq. (17) to give

$$\gamma_m f_{esc}\sum_1^N P_j\tau_j = \frac{(1-R_f)i_{s0}}{i_f+i_{s0}}. \tag{25}$$

The quantity $\sum_{1,N} P_j\tau_j$ is just $\int_0^\infty P_K(t)dt$, in other words, the total number of metastables created by a single electron leaving the cathode which return to the cathode. For our purposes here, we may represent this number by f_{mk} times the total number of metastables created by this electron (and its progeny from ionization), where f_{mk} is the fraction of the metastables which diffuse to the cathode. Now the total number of metastables is found by integrating Eq. (9), which describes the initial distribution, giving

$$\sum_1^N P_j\tau_j = \frac{\alpha_m}{\alpha_i}\{\exp[\alpha_i(X-x_0)]-1\}f_{mk}. \tag{26}$$

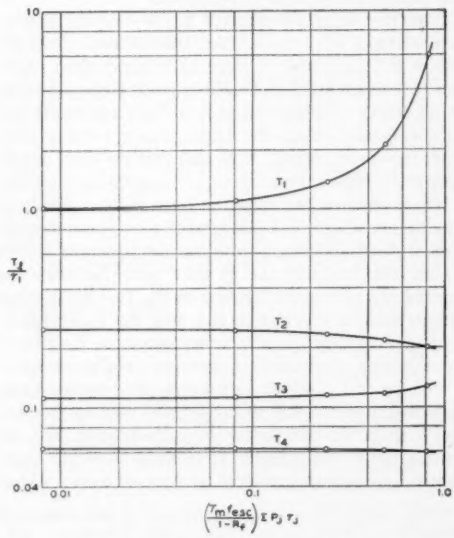

FIG. 6. Time constants, T_i, computed for the same case for which the amplitudes are given in Fig. 5. The time constants start with values in the ratio of $1:\frac{1}{2}:\frac{1}{3}:\frac{1}{16}$, as in the corresponding $P_K(t)$-function. Note that only in the case of T_1 is there a large deviation as the replacement factor approaches unity, while T_2, T_3, and T_4, vary only by a smaller amount. These variations are discussed by Newton [see reference 2, particularly Fig. 2].

Hence, we have finally

$$\alpha_m\gamma_m f_{esc} f_{mk}=\frac{\alpha_i(1-R_f)i_{s0}}{(i_f+i_{s0})\{\exp[\alpha_i(X-x_0)]-1\}}. \quad (27)$$

On the right-hand side, every term can be either directly measured or evaluated by fitting the Townsend equation to i_f/i_0 *vs* X data. Newton[2] showed that f_{mk} is given for the case of $G=0$, by

$$f_{mk}=\frac{1}{\alpha_i X}-\frac{1-x_0/X}{\exp[\alpha_i(X-x_0)]-1}. \quad (28)$$

For the more general case in which $G\neq 0$, we have computed values of f_{mk} by numerically evaluating

$$f_{mk}=\frac{\int_0^\infty P_K(t)dt}{\int_0^\infty P_K(t)+\int_0^\infty P_G(t)+\int_0^\infty P_A(t)dt}. \quad (29)$$

Some typical results are given in Fig. 7. Here we also plot f_{mr} and f_{ma}, which give the fraction of the metastables which are destroyed in the gas and at the anode, respectively.[11] We note that f_{mk} has a maximum value of about 0.4, and if G is not zero, it is less and decreasing at large values of X.

For rough evaluations and under conditions in which G is known to be small, Eq. (27) is probably useful with f_{mk} taken as 0.4. When G is not zero, then the second process of electron emission (i.e., by photoelectric effect of photons from "destroyed" metastables) may also be contributing to i_{s0}. For this situation we outline a method of analysis in the following section.

H. APPROXIMATE ANALYSIS FOR COMBINED PROCESSES

When both emission processes are active, then it is readily shown that Eq. (17) becomes

$$i_{s0}=i_f\frac{\left(\frac{f_{esc}}{1-R_f}\right)\left[\gamma_m\sum_1^N P_{Kj}\tau_j+\gamma_r f_{rk}'\sum_1^N P_{Gj}\tau_j\right]}{1-\left(\frac{f_{esc}}{1-R_f}\right)\left[\gamma_m\sum_1^N P_{Kj}\tau_j+\gamma_r f_{rk}'\sum_1^N P_{Gj}\tau_j\right]}, \quad (30)$$

where the subscripts K and G after P should be interpreted to indicate that the coefficients refer to the $P_K(t)$ and $P_G(t)$ series, respectively.

Now to reduce Eq. (30) to a manageable form, we make the approximation that $P_K(t)$ and $P_G(t)$ are each represented by the first term of their infinite series expansion. Then $f_{rk}'=0.5$, since the first term has a sine-wave distribution in x, and so exactly one-half of the photons go to each electrode. For PK_1 and PG_1 we apply Eqs. (12) and (14), and with these substitutions, Eq. (30) becomes

$$f_{esc}\left(\gamma_m+\gamma_r\frac{GX^2}{\pi^2 D_m}\right)=\frac{(1-R_f)i_{s0}}{i_{s1}+i_f}\frac{(\pi D_m/X)+GX/\pi D_m}{a_1}. \quad (31)$$

If the integration indicated by Eq. (10) is carried out for a_1, and if we recall the definition of R_f and apply Eq. (1), then Eq. (31) becomes

$$\alpha_m f_{esc}\left(\gamma_m+\gamma_r\frac{GX^2}{\pi^2 D_m}\right)=\alpha_i\frac{i_0 i_{s1}}{i_f(i_f+i_{s1})}\left(1+\frac{GX^2}{\pi^2 D_m}\right)H, \quad (32)$$

where

$$\frac{1}{H}\equiv\frac{2\alpha_i X}{(\alpha_i X)^2+\pi^2}\left\{1-e^{(\alpha_i x_0-\alpha_i X)}\left[\frac{\alpha_i X}{\pi}\sin\left(\pi\frac{\alpha_i X}{\alpha_i x_0}\right)-\cos\left(\pi\frac{\alpha_i x_0}{\alpha_i X}\right)\right]\right\}. \quad (33)$$

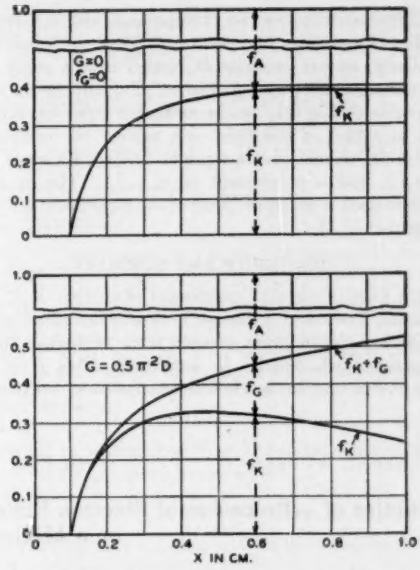

FIG. 7. The fraction of metastables lost at the cathode, f_k, in the gas, f_G, and at the anode, f_A, plotted as function of the electrode spacing for two values of G and an assumed initial distribution of metastables given by

$$\rho=0, \quad x\leq 0.1,$$
$$\rho=e^{(x-0.1)}, \quad x\geq 0.1.$$

Note that in the text the notation f_{mk}, f_{mr}, f_{ma} is used for these quantities.

[11] For the limiting case in which the P-functions are represented by a single exponential, it is readily shown that

$$f_{mk}=0.5\pi^2 D_m/(\pi^2 D_m+GX^2).$$

The curves in Fig. 7 can be closely approximately at large X by this expression multiplied by 0.76. Note also that if D_m is inversely proportional to the gas pressure, and G is proportional to the pressure, then f_{mk} is a function of pX alone.

Experimentally, we can evaluate $\alpha_i x_0$ and $\alpha_i X$ from studies of i_f/i_0 as a function of X. Thus, we know H. Similarly, we can evaluate D_m and G from a study of the variation of τ_1 with X. Hence, all quantities on the right side of Eq. (32) can be measured experimentally, and so a plot of the right side against the quantity $GX^2/\pi^2 D_m$ should give a straight line with a slope of $\alpha_m\gamma_r f_{esc}$ and a y intercept of $\alpha_m\gamma_m f_{esc}$. This is the method used to interpret some of the experimental data presented in II.

I. DISCUSSION AND SUMMARY

The form of the slow component of current, $i_s(t)$, in a pulsed Townsend discharge is closely described by a single exponential plus second term of higher time constant much smaller in amplitude. This term is negative in amplitude when the metastables initiate a current by releasing electrons in the process of bombarding the cathode. The amplitude is positive (i.e., adds to the first term) when the electrons are released through photoelectric action of photons from metastables converted in the gas.

From a study of experimental current patterns one can get with little trouble the fundamental time constant of decay, τ_1, of the metastables in the gap. This is valuable, because by studying the variation of τ_1 with electrode spacing and gas pressure, the diffusion constant and volume destruction probability of metastables are readily obtained. In addition the quantities $\alpha_m\gamma_m$ and $\alpha_m\gamma_r$ can be obtained. Applications of these methods of analysis are described in II.

The author wishes to express his appreciation to Miss C. L. Froelich and her co-workers for assistance in carrying out computations.

PHYSICAL REVIEW VOLUME 83, NUMBER 5 SEPTEMBER 1, 1951

Studies of γ-Processes of Electron Emission Employing Pulsed Townsend Discharges on a Millisecond Time Scale

J. P. MOLNAR
Bell Telephone Laboratories, Murray Hill, New Jersey
(Received December 8, 1950)

The relative amounts of electron emission from the cathode in a Townsend discharge caused by ions, photons, and metastables have been studied experimentally for several cathodes in argon, using pulsed-light stimulation of the discharge. The current initiated by metastables exhibits a slow build-up and decay, thus permitting easy separation from the faster rising effects of gas ionization and electron emission by photons and ions. Time constant studies of the slow component yielded a diffusion constant for metastable argon atoms of 45 cm² sec⁻¹ at one millimeter pressure. The efficiencies of electron emission by metastables and ions was found to be closely the same, while the quantum yield for photon emission was found to be generally smaller.

I. INTRODUCTION

ELECTRON emission from the cathode in Townsend or glow discharges is generally believed to arise from the bombardment of the cathode by ions, metastable atoms, and photons.[1,2] These processes are commonly called the γ-processes, or sometimes the γ-mechanism, after the coefficient γ used in the Townsend equation to describe the part of the amplification of an electron current between electrodes in a gas attributable to these processes. The experiments in this paper were directed towards an evaluation of the relative amount of electron emission produced by the ions, the metastables, and the photons in the case of argon gas with several cathode materials. An incidental by-product of these studies was a determination of the lifetime of metastable argon atoms.

The method employed was similar to that described by Engstrom and Huxford.[3] A Townsend discharge was stimulated by photoelectrons generated by a shuttered light beam shone on the cathode of a gas-filled tube, and the transient character of the resultant current between the electrodes was observed by an oscilloscopic technique. The current is found to be composed of a component closely in step with the stimulating light pulse and a component which lags by an amount of the order of a millisecond. The second component is initiated by the action of metastables, which have lifetimes in the discharge space of this amount of time. The fast component includes the primary electron current amplified by gas ionization and electron emission from the cathode caused by ion and photon effects, all of which reach a steady-state value in a time of the order of ten microseconds.[4] From an analysis of these patterns the fractions of the electron emission produced by metastables and by ions and photons were obtained.[5]

[1] L. B. Loeb, *Fundamental Processes of Electrical Discharge in Gases* (John Wiley and Sons, Inc., New York, 1939).
[2] M. J. Druyvesteyn and F. M. Penning, Revs. Modern Phys. **12**, 87 (1940).
[3] R. W. Engstrom and W. S. Huxford, Phys. Rev. **58**, 67 (1940).
[4] A parallel study of pulsed Townsend discharges on a microsecond time scale, in which these effects can be resolved, has been carried out by J. A. Hornbeck of these laboratories.
[5] A theoretical analysis of transient form of the current in the Townsend discharge under these conditions is described in a companion paper (hereafter referred to as I), and reference will be made to the relations derived in that paper.

The relative emission efficiencies of photons and metastable atoms were measured by an experiment in which metastable atoms are converted into radiating atoms by irradiation of the discharge space with light of the proper wavelength.

II. GENERAL PROCEDURE

The usual procedure employed in Townsend experiments[6] is to measure the current, i, between plane-parallel electrodes when a primary photocurrent, i_0, is liberated by light shone on the cathode, and the cathode-anode spacing, X, is varied with the electric field, E, maintained constant. The measured values of i/i_0 are then fitted to the Townsend equation,

$$i/i_0=\exp[\alpha_i(X-x_0)]/1-\gamma(\exp[\alpha_i(X-x_0)]-1), \quad (1)$$

where α_i is the number of electron-ion pairs generated per electron per cm of path in a direction perpendicular to the electrode surfaces and is commonly called the First Townsend Coefficient, x_0 is the minimum value of the electrode spacing at which ionization can occur, and γ is defined loosely as the number of electrons liberated at the cathode per ion striking it.

For our purposes γ is defined more specifically as the number of electrons which are liberated at the cathode and enter the discharge stream per ion formed in the gas. Such a definition permits us to include in γ the metastable and photon contributions by writing

$$\gamma=f_{esc}\left\{\gamma_i+\frac{\alpha_r}{\alpha_i}f_{rk}\gamma_r+\frac{\alpha_m}{\alpha_i}[f_{mk}\gamma_m+f_{mr}f_{rk}'\gamma_r]\right\}, \quad (2)$$

where γ_i, γ_r, γ_m = number of electrons liberated at the cathode per ion, per photon, and per metastable, respectively; α_i, α_r, α_m = number of ions, photons, and metastables produced per cm per electron; f_{esc} = fraction of the electrons liberated at the cathode which escape the back diffusion effect and enter the discharge stream; f_{rk}, f_{mk} = fraction of the photons and metastables generated in the gas which reach the cathode; f_{mr} = fraction of the metastables generated in the gas which are converted to radiating atoms; f_{rk}' = fraction of the photons from these radiating atoms which reach the cathode.[7] In this expression f_{rk}, f_{mk}, f_{mr}, and f_{rk}' are not independent of X; and so γ is not strictly a constant when one measures i/i_0 *vs* X, as in an ordinary Townsend experiment.[8]

In our experiments the fast component of current is assumed to be described by a Townsend equation with the γ-coefficient given by γ_f, where

$$\gamma_f=f_{esc}[\gamma_i+(\alpha_r/\alpha_i)f_{rk}\gamma_r]. \quad (3)$$

The total current is described by a Townsend equation with $\gamma=\gamma_f+\gamma_s$, where

$$\gamma_s=f_{esc}(\alpha_m/\alpha_i)(f_{mk}\gamma_m+f_{mr}f_{rk}'\gamma_r). \quad (4)$$

By means of light of appropriate wavelength shone on the space between the electrodes, metastable atoms can be converted into radiating atoms. In this way we were able to vary, in effect, the quantities f_{mk} and f_{mr}, and from the resultant variation in γ_s compute a value of γ_r/γ_m. The small value we found for this ratio indicates that at high values of E/p_0, where $(\alpha_r/\alpha_i)f_{rk}<1$, the second or photon part of γ_f is small, and therefore the variation of γ_f with X is negligible. Thus, in this high E/p_0 region we fitted the fast component of current to the Townsend equation assuming a constant value of γ_f throughout the range of X variation. From this fit, $\exp[\alpha_i(X-x_0)]$ was obtained and used to evaluate $\gamma_f+\gamma_s$ from the values of the total current; and γ_s as thus obtained was found in general not to be constant with X.

Examination of the Townsend equation quickly reveals that the accuracy with which γ can be evaluated is closely dependent on the accuracy with which the term $\exp[\alpha_i(X-x_0)]$ is known. The latter term is most accurately evaluated when the Townsend experiment is conducted on a surface with a low value of γ, because then the denominator in the Townsend equation does not depart appreciably from a value of unity until large values of X are reached. We therefore found it expedient to make our measurements on two or more surfaces of different γ-values in tubes interconnected so as to have exactly the same gas filling. Then the quantity $\exp[\alpha_i(X-x_0)]$ was evaluated from the data taken on the low γ-surface and used to evaluate both γ_f and γ_s from the data taken on the high γ-surface.

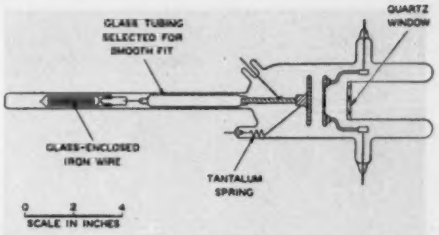

FIG. 1. Townsend tube used in later experiments. The drawing is simplified for purposes of clarity. The anode (right-hand electrode) is supported in three places, instead of two as shown, with the inner section held with two glass-insulated wires. The upper wire contact to the cathode support rides in a slot to prevent rotation. Holes in the inner glass tubing provide a means of pumping the left-hand side of the tube. The inside of the tube is coated with Aquadag with a ring ½ in. wide left clear in the region near the electrodes. Connections are provided to each half of the coating.

[6] An excellent summary of studies in the rare gases is given by A. A. Kruithof, Physica **7**, 519 (1940).

[7] This expression for γ is obviously simplified, because we have lumped into one both types of metastables ($^3P_0$ and $^3P_2$) and into one all types of photons. Furthermore, f_{esc} may be different for electrons released by the various processes. In addition there may be conversion of radiating atoms back to the metastable states, a process which probably becomes important at higher pressures.

[8] Although most previous experimenters have assumed γ to be a constant in their interpretation of Townsend data, this has probably not affected seriously their values of α_i, since the evaluation of α_i from experimental data is rather insensitive to the value of γ employed.

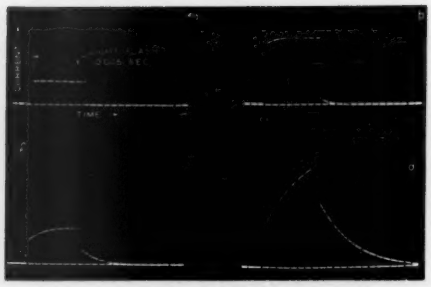

FIG. 2. Typical oscillograms of the current in a Townsend discharge with pulse light stimulation. The traces were taken with a fixed electrode separation and increasing values of applied voltage going from *a* to *d*. The amplifier gain was reduced 5× for traces *c* and *d*. Trace *a* corresponds to a current consisting entirely of photoelectrons released from the cathode by the stimulating light. The other traces show the effect of gas amplification and γ_f-processes by the increase of the in-phase component and the effect of the γ_s-processes by the appearance in successively larger amounts of a delayed component.

Actually, it is very difficult to fit the Townsend equation to i/i_0—data from a surface with $\gamma \approx 0.25$, because the value of α_i has barely stabilized at the value of X at which breakdown occurs.[9]

In the first set of experiments we employed two tubes, one with a BaO—Ni surface (high γ) and the other with a nickel surface (low γ). In a second set of experiments four tubes were set up, three with surfaces of tantalum, molybdenum, and barium oxide on tantalum and one intended to be barium on tantalum. Unfortunately, the barium was accidentally lost in the processing and so this surface was essentially like the plain tantalum also. In fact, however, the pure metal surfaces undoubtedly did not represent atomically clean surfaces but were to some extent contaminated by adsorbed gases. Furthermore, we were unable to vary the gas pressure in the tubes without altering the cathode surface properties. Thus, we shall present here only a limited amount of γ-data. They are intended to illustrate the composition of γ for the surfaces as they were studied, which we recognize were neither in a clean nor necessarily in a very stable condition.

Our experiments were limited, in the main, to the higher range of E/p_0, i.e., from about 50 to 200 volts/cm ×mm, for two reasons. At lower values of E/p_0 the increased generation of photons make their contribution to γ_f sizable, and therefore γ_f can no longer be assumed constant with X. Furthermore, the higher gas pressures required for experiments at lower values of E/p_0 result in having a large fraction of the metastables destroyed in the volume rather than at the electrodes. Both of these effects make any measurements of Townsend currents much more difficult to interpret in the low E/p_0 region.

[9] The Philips workers showed that α_i varies periodically with x for small values of x and becomes constant only when $x>3$ to $5x_0$. This arises from a changing velocity distribution of electrons with x, and it is only when this distribution becomes independent of x that α_i becomes constant.

III. EXPERIMENTAL ARRANGEMENTS

Two types of Townsend tubes were used in the course of these studies. The first type was similar to that described by Engstrom and Huxford.[3] The second type of tube, shown in Fig. 1, has a smaller outside diameter so that both anode and cathode can be outgassed by rf induction heating. Wall charge effects are minimized by coating the interior walls of the tube with Aquadag. The coatings were in two halves, one connected to the anode, the other to the cathode potential.

The electrodes were two inches in diameter and one-eighth inch thick, with rounded edges. The anode in the first type was drilled with approximately 200 holes 0.013 in. in diameter grouped in the central area inside a circle $\frac{3}{8}$ in. in diamater. In the second tube the anode was made in two parts to permit separate measurement of the current to the central and to the outer parts of the electrode. The central part was made in the shape of a hexagon approximately 0.6 in. in "diameter" with 331 holes 0.016 in. in diameter. The inner half of the outer part was drilled with 864 holes of the same diameter. The current measurements to the two parts did not, in general, reveal anything very interesting, so for the most part the total current alone was measured.

By trial-and-error methods the cathode-supporting section of the tube could be adjusted so as to achieve a parallelism of the electrodes to about 0.1°. During bakeout and outgassing operations the supports sometimes sagged. If the angle increased to a value greater than 0.4°, the tubes were corrected. Electrode spacing was measured with a traveling microscope to a precision of about 0.01 mm.

Baking and outgassing operations were conducted alternately over a period of several days. With the apparatus cold a vacuum of 1×10^{-8} mm of mercury was indicated on an ionization gauge. The barium oxide surfaces were prepared according to conventional practice.[10] The pure metal surfaces were operated at high currents in a glow discharge. For molybdenum the "contraction" phenomenon was observed.[11] In the case of tantalum at high currents the discharge tended to go to the Kovar support on the rear side and no contraction effects could be produced. After several flushings with argon, a Batalum getter was flashed, gas was admitted at the desired pressure, and the tubes were sealed off. Pressure was measured at an accuracy of about 0.5 percent with a carefully calibrated McLeod gauge.

[10] The metal electrodes are coated with a mixture of $BaCO_3$ and $SrCO_3$ 0.5 mg per cm². During outgassing of the electrodes the carbonates are converted to oxides. Then with argon at a pressure of about 20 mm, a high frequency discharge from a spark generator is operated between the electrodes until the cathode reaches a state of constant activation. The sustaining voltage for a newly prepared surface can be as low as 55 volts.

[11] F. M. Penning and J. H. Moubis, Philips Research Repts. **2**, 119 (1946).

A system of multiple seal-off constrictions and break-off tips described by Engstrom and Huxford[3] was incorporated to permit subsequent change in the gas pressure without exposure of the system to the atmosphere. In practice, however, when this was attempted, the cathode surfaces never appeared to retain their original emission efficiencies, and so one was then left with the very small area of opening in the shattered break-off tips for use in pumping during the subsequent preparation of the surfaces.

In all Townsend experiments it is of prime importance to use gas of the highest purity. Small impurities have two kinds of effects: (1) they may destroy the argon metastables by collisions of the second kind, and (2) they may affect the cathode emission efficiency. Our main effort toward purification consisted of exposing the gas[12] to a surface of barium metal flashed from a Batalum getter and then passing it through two liquid nitrogen traps, one of which was in the form of a long helical coil. Some measure of the purity could be obtained from the time-constant studies described in Sec. IV. Kruithof and Penning[13] have described techniques of purifying rare gases by operating a discharge between barium or other electrodes. Although we tried similar techniques, we cannot definitely state that beneficial effects were observed generally, at least as measured by the lifetime of the metastables.

The source of stimulating light was an AH-4 high pressure mercury lamp, with its glass envelope removed, operated on dc. The light was shuttered by a rotating sector disk which produced a pulse five milliseconds in duration every one-thirtieth of a second. When the amount of light was ample, the slit behind the disk through which the light was directed could be reduced to 0.2 mm so as to give a rise time for the light pulse of about 20 μsec.

Current through the tube was measured by letting it flow through a resistor from one electrode to ground, amplifying the resultant IR drop, and displaying on a cathode-ray oscilloscope. In order to permit measurement of the smallest possible current, careful attention was paid to the problem of inherent noise in the amplifier. By using a selected tube for the first stage operated on batteries, the amplifier noise, with a grid input resistor of 200,000 ohms, was about 10 microvolts or the equivalent of 5×10^{-11} amp flowing through this resistor. Thus, to measure a current through the tube with an accuracy of 0.5 percent, the current had to be roughly 200 times this amount, or 1×10^{-8} amp. Space charge effects began to distort the observed patterns at currents greater than about 2×10^{-7} amp, and we had, therefore, only a twentyfold range of current over which accurate measurements were possible. An improved signal-to-noise ratio could, of course, be obtained by employing a larger grid resistor; but the resultant rounding of the pattern then made it impossible to separate clearly the fast and slow components of current. Typical patterns are shown in Fig. 2.

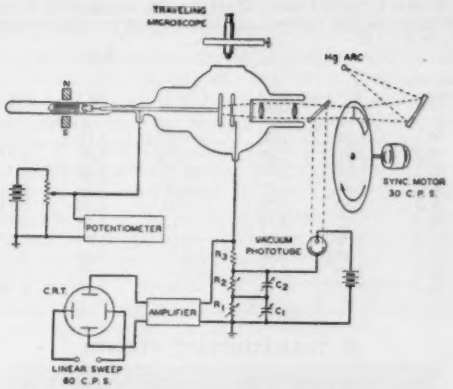

FIG. 3. Schematic diagram of arrangement of apparatus. The resistance of R_3 is large compared with R_1+R_2, so that the effect of the capacitance of C_1 and C_2 on the Townsend tube current is small. The horizontal sweep on the cathode-ray tube is operated at twice the disk frequency to provide a zero-line reference.

The actual current measurement was made by employing a null method. By means of a partially reflecting mirror, some of the light was directed into a vacuum phototube, which then generated a current pulse exactly in step with the primary current in the Townsend tube. This current flowed through two resistor-capacitor combinations, R_1C_1 and R_2C_2, as shown very schematically[14] in Fig. 3, by means of which a voltage pulse could be formed having a shape and size very similar to that of the total Townsend current but opposite in sign. The fast component of the Townsend current could usually be matched closely with an RC combination having a time constant of from 0 to 30 sec. A large part of the slow component could be matched with an RC combination having a time constant from 0.1 to 30 milliseconds. When these components were adjusted to a "best" fit to the Townsend current, there remained nearly always a component negative in amplitude and intermediate in time constant.[15] The amplitude of this component was measured by the decrease necessary in the fast component to bring the current trace up to the baseline. Under favorable conditions the fast component could be measured with an accuracy of 0.2 percent, and the slow time constant with an accuracy of 2 percent.

[12] One liter flasks of the "spectroscopically pure" grade were purchased from Air Reduction Company and Linde Air Products. Mass spectrometric tests revealed no impurities above the level of detection of the instrument, which was about 0.005 percent for the common gases.

[13] A. A. Kruithoff and F. M. Penning, Physica **3**, 515 (1936).

[14] The circuit was actually arranged in such a manner as to permit independent adjustment of the R and RC values of both the fast and slow components.

[15] See I for an interpretation of this component.

TABLE I. Sample data illustrating the computation of the fundamental time constant, τ_1, from the observed time constant T_1 by Eq. (5).

Applied potential (volts)	i_f (10^{-8} amp)	i_{s1} (10^{-8} amp)	i_{s2} (10^{-8} amp)	T_1 (10^{-2} sec)	τ_1 (10^{-2} sec)
76.5	2.28	1.20	−0.075	1.17	0.76
78.5	2.61	1.69	−0.078	1.29	0.77
79.5	2.87	2.05	−0.10	1.38	0.79
80.5	3.07	2.55	−0.11	1.46	0.78
81.0	3.17	2.89	−0.10	1.50	0.78
82.0	3.43	3.73	−0.12	1.65	0.78
83.0	3.80	5.09	−0.15	1.85	0.77
83.5	4.00	6.06	−0.18	2.00	0.77
84.0	4.29	7.34	−0.21	2.19	0.78
84.5	4.52	9.15	−0.21	2.45	0.78

IV. TIME CONSTANT STUDIES

The current-measuring apparatus described in the preceding section made it possible to make detailed time constant studies of the slow component of current with relatively little effort. The procedure employed was to measure the time constant of the slow component, T_1, and the amplitudes of the fast (i_f), slow (i_{s1}), and intermediate (i_{s2}) components for various applied voltages at a series of electrode spacings. As explained in the companion paper, T_1, can then be related to the fundamental time constant of decay of metastables in the gap, τ_1, through the relation,

$$\tau_1 = T_1[(i_f+1.3i_{s2})/(i_f+1.3i_{s2}+i_{s1})]. \qquad (5)$$

The value of τ_1 obtained from this relation should be the same for a given electrode-spacing independence of the applied voltage as well as the electrode material, provided the electrical effects caused by the destruction of the metastables originates at the cathode (see I). In other words, the slow component must arise from electron emission caused either by direct impact of the metastables on the cathode, or by the conversion of metastables into radiating atoms in the gas from which the light radiation causes photoelectric emission at the cathode. Should the slow component of current arise from an ionization of impurity atoms by collision with the metastables (Penning effect), then analysis shows the value of τ_1 should be calculated from the observed quantities by a different equation. Thus, τ_1 from Eq. (5) will not be independent of the voltage.

For the most part Eq. (5) appeared to be applicable in all the argon studies. (See sample data given in Table I.) Occasionally, for large values of T_1/τ_1, i.e., three or larger, deviations as large as 25 percent were found. The voltages at which such large ratios are observed are usually close to breakdown, and the accompanying unsteadiness of the pattern along with possible space charge distortions might explain the failure of the relation.

The quantity τ_1 represents the fundamental time constant of decay of metastables and is related to the diffusion constant, D_m, and the probability of volume destruction of metastables per second in the gas, G, by the relation,

$$1/\tau_1 = (\pi^2 D_m/X^2)+G. \qquad (6)$$

Plots of $1/\tau_1$ *vs* π^2/X^2 should, therefore, yield straight lines with slopes given by D_m and a y-intercept equal to G. Several such plots are shown in Fig. 4 for various pressures in argon. Both the slopes and intercepts are seen to vary with pressure. The slopes fit a $1/p$ variation, as might be expected for the diffusion coefficient. The points for different electrode materials are seen to fall satisfactorily on the same line, which is gratifying, because the surfaces had widely different γ_m-values and so the measurements were made at widely different values of applied voltage.

The diffusion coefficient for argon metastables in argon, D_m, as obtained from these measurements is 45 ± 4 cm^2 sec^{-1} for a pressure of one millimeter at 25°C.[16] This may be compared with the diffusion coefficient, D_n, obtained by Hutchinson[17] for radioactive argon atoms of mass 41 in normal argon (largely mass 40), which is 139 cm^2 sec^{-1} when reduced to this pressure and temperature. If we assume that in a collision between a metastable and an unexcited argon atom the "radius" of the normal atom, r_n, has the same value as in a collision between two unexcited atoms, then, if r_m is the "radius" of the metastable atom, we

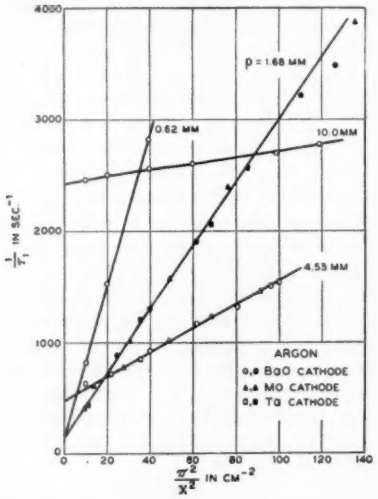

FIG. 4. Plots of $1/\tau_1$ *vs* π^2/X^2 for argon metastables in argon. The slopes of these curves give D_m, while the y intercepts give G. The measurements were made at room temperature ($T=25$°C).

[16] The pressure here is not the reduced pressure p_0, defining the concentration of gas at 0°C. We did not reduce the data here to 0°C, because we do not know how D_m varies with temperature.

[17] F. Hutchinson, J. Chem. Phys. **17**, 1081 (1949) (argon); W. Grath and E. Sussner, Z. physik. Chem. **193**, 296 (1944) (neon); and W. Grath and G. Dickel, Z. Elektrochem. **47**, 167 (1941) (krypton and xenon).

have from kinetic theory that

$$D_n/D_m=(r_n+r_m)^2/(2r_n)^2. \quad (7)$$

This yields $r_m/r_n=2.52$, which appears to be a reasonable value.

Similar time constant studies carried out in neon and xenon gave values of $D_m=120\pm10$ cm² sec⁻¹ for neon, and $D_m=13\pm1$ cm² sec⁻¹ for xenon, both at one millimeter pressure and a temperature of 25°C. These can also be compared with diffusion coefficients obtained by isotope tracer techniques[17] and values of r_m/r_n can be computed, which come out to be 2.45 for neon and 2.22 for xenon.

Once the value of the diffusion coefficient had been established for argon, the plot of $1/\tau_1$ *vs* π^2/X^2 in any later experiment served as a useful check of the proper behavior of the metastables. The effect of the presence of impurity molecules in the gas which destroy the metastables on collision with them but are not ionized in the process can be detected by an increase in the value of the y intercept in a plot of $1/\tau_1$ *vs* π^2/X^2.

In one instance the presence of a large amount of nitrogen (probably in a concentration of about 0.1 percent) produced a more striking effect in that these molecules destroyed all the argon metastables in a time of 100 microseconds. However, the nitrogen molecules when thus excited ended up in a metastable state, as evidenced by the fact that a slow component of current was observed in the Townsend tube of milliseconds duration. When a study of the fundamental time constant, τ_1, of this component was made, however, it was found that the lifetimes of the metastables in this case were substantially different from that of the argon metastables. The data gave a diffusion constant for nitrogen metastable in argon of 157 cm² sec⁻¹ at one-mm pressure and 25°C, with an immeasurably small volume destruction.

Nitrogen was not intentionally introduced into the argon in this experiment and probably was present through faulty handling of the gas. Its presence was indicated by the appearance of the nitrogen band spectrum in the positive column of a glow discharge operated between two electrodes in the tube. The fact that the argon metastables were destroyed in a very short time was established by studying the decay of argon metastables by a light absorption experiment.[18]

In spite of all efforts at purifying the argon, the y intercept of the $1/\tau_1$ *vs* π^2/X^2 plots was finite; in other words the constant G is finite, indicating a measurable volume loss of metastables. This observation agrees with the findings of the light absorption experiments, and so we believe that our measured values of G cannot for the most part be ascribed to impurities, but instead they represent a measurement of the instability of metastables under impact with neutral atoms.[19] The accuracy of measurement of G in these experiments was not great, but up to a few millimeters of pressure G appeared to increase linearly with pressure and for higher pressures more rapidly. At one millimeter, G for argon metastables was found to be 80 sec⁻¹. If we assume a collision diameter for normal argon atoms of 3.2A and utilize the r_m/r_n ratio given above, we can compute a collision frequency between metastables and normal atoms at one millimeter and 25°C of 1.6×10^7 sec⁻¹. Thus, a value of $G=80$ sec⁻¹ corresponds to the argon metastables having a lifetime of 2×10^6 impacts with normal atoms at room temperature.

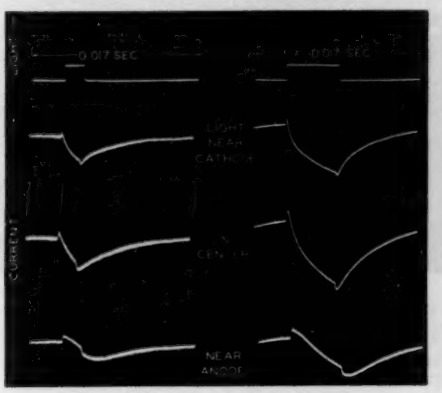

FIG. 5. Oscillograms of the current in a Townsend discharge with the primary stimulating light on steadily and light from a pulsed argon discharge directed across the gap between the electrodes. The left-hand group of traces were taken with the pulsed light 0.002 second in duration, the right group for the light 0.004 second in duration. These traces represent only small variations in a large dc current. Trace *h* in Fig. 6 illustrates a similar pattern obtained with a higher intensity of illumination.

V. CONVERSION OF METASTABLES INTO RADIATING ATOMS BY LIGHT RADIATION

The conversion of metastables to radiating atoms by light radiation is a well-known phenomenon. Penning[20] used this method in breakdown studies to reduce the number of neon metastables in tubes filled with neon and small admixtures of argon and thereby reduce the number of argon atom ionizations by collisions of the second kind. In our work this conversion process was utilized to measure the relative amount of electron emission produced by a metastable drifting to the cathode compared with that produced by a photon of the same energy striking the surface.

[18] This experiment is similar to those of Meissner and others in which the presence of metastables in a volume of gas is detected by their absorption of appropriate lines of the argon spectrum arising from transitions between the $3p^54s$ and $3p^44p$ configurations. As a separate project we have studied metastable lifetimes with this method also and will report our findings in a separate paper.

[19] We can rule out impacts between metastables and electrons, ions, or other excited atoms as a cause of this effect, because then the observed time constant would be dependent on the magnitude of the current, which is not observed except at currents above 10^{-7} amp (see Fig. 8).

[20] F. M. Penning, Z. Physik **57**, 723 (1929).

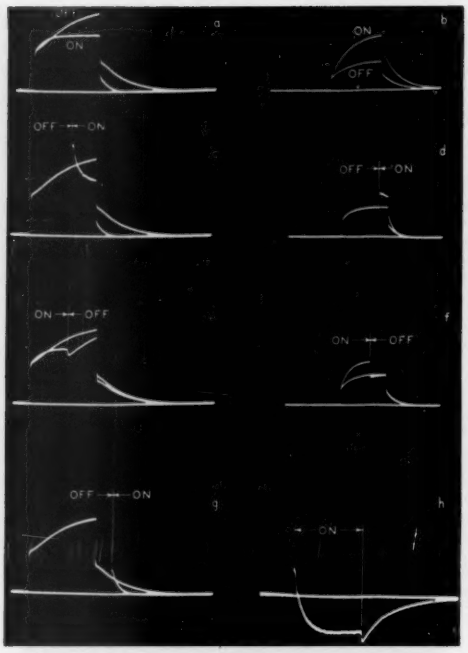

FIG. 6. Oscillograms of the current in a pulsed Townsend discharge with the side light on during alternate cycles of the primary light, except in *h*, for which the primary light was on continuously. The traces, *a*, *c*, *e*, *g*, and *h* were taken with a tantalum cathode for which $\gamma_r/\gamma_m=40$ percent. The traces *b*, *d*, and *f* were taken with a nickel cathode for which $\gamma_r>\gamma_m$. Note in traces *a* and *e* that with the side light on, the slow component rises at first more rapidly than when the side light is off. This effect is caused by the finite diffusion time required for the metastables to traverse the distance from $x=x_0$ (where they are first formed) to $x=0$ (the cathode) in the latter case, in contrast to the rapid flow of the energy in the form of photons in the former case.

Spectroscopically, the energy levels involved are as follows. The first excited configuration in argon is the $3p^54s$, which gives rise to four states, $^1P_1$, (radiating) $^3P_0$, metastable $^3P_1$ (radiating), and $^3P_2$ (metastable). If now light from an external argon discharge shines on the space between the electrodes, then those lines corresponding to transitions between the configurations $3p^54p$ and $3p^54s$ can be absorbed by atoms which are in states of the $3p^54s$ configuration. In general, only atoms in the two metastable states will be present in an appreciable density. On absorption of this radiation, the metastables are raised to various states in the $3p^54p$ configuration, from which they may decay downward either by going back to one of the metastable or one of the radiating states. In the former case, there will be no net effect on the density of metsastables. In the latter case, the atom will very soon decay to the ground state by radiating a photon. Thus, it is seen that effect of the light radiation is to convert some of the energy stored in the metastables into radiant energy. The four states of the $3p^54s$ configuration have energies differing at most by 0.29 ev (out of about 11.5 ev) so that the photon energies are very nearly the same as that of the metastables.

Our experiments were conducted with two arrangements. In the first the external light from a line source was focused so as to go through a small region between the electrodes near the anode, in the middle or near the cathode. In the second arrangement a ring-shaped discharge tube surrounding the Townsend tube was employed with which a much larger conversion factor was possible, but the light could not then be concentrated in any particular region.

In the first arrangement the most interesting results were obtained when the primary stimulating light for the Townsend discharge was maintained steady and the side illumination was pulsed. Typical oscillograms of the current through the Townsend tube are shown in Fig. 5. The current is seen to increase immediately on the application of the side light and then decrease slowly. When the side light is cut off, the current drop suddenly and then returns slowly to its steady-state value. The slow decrease and slow recovery is seen to start more rapidly when the sidelight crosses the gap near the cathode than when it crosses near the anode.

The interpretation of these patterns is as follows. The sidelight has two effects, that of increasing the number of photons striking the cathode and that of decreasing the metastable density in the region through which the light is passing. The sudden increase in currents when the light goes on is caused by the increase in the number of high energy photons striking the cathode. The slow decrease is caused by the diminution of the number of metastables available to diffuse to the cathode. Furthermore, the time for this diminution to "diffuse" to the cathode is longer when the light crosses the gap near the anode than when it crosses near the cathode; hence, the slow decrease occurs with a time lag when the light crosses near the anode. Finally, the net reduction in current through the tube with the side light on shows that in this case the photons are less effective than the metastables in producing electron emission at the cathode.

In the second arrangement a light source was used consisting of a piece of $\frac{3}{4}$-in. glass tubing bent into a circular shape to fit around the Townsend tubes of the second type. Electrostatic effects produced by noisy discharge conditions made it necessary to interpose grounded copper screening between the light source and the Townsend tube. This probably reduced the available light by at least 75 percent. The outer side of the discharge tube was aluminized to increase the light going in the inward direction. With this arrangement oscillograms were obtained as shown in Fig. 6.

The light source was pulsed at a frequency of 15 cps (as compared with 30 csp for the stimulating light), so as to permit direct comparison of the patterns with and without the side light. In the top two patterns (*a* and *b*),

oscillograms are shown for the case in which the side light was turned on before the stimulating light, and kept on during the entire cycle. In oscillogram *a* the effect of the light was to decrease the amplitude and the fundamental time constant, τ_1, of the slow component. In *b* the effect was the opposite, although the change in τ_1 is less evident, since the increased regeneration brought about by the increased value of i_s increases T_1 and masks the actual decrease in τ_1. The other oscillograms in Fig. 6 illustrate cases in which the side light was either turned on or turned off during the time the normal current pattern was visible.

For nearly every case studied the net effect of the side light was to reduce the magnitude of the slow component. Patterns *b*, *d*, and *f* in Fig. 6 illustrates the opposite case. They were obtained with nickel surface in an unknown state of contamination, a situation we did not observe in later work. The oscillograms are shown here only because they illustrate clearly the effect γ_r being greater than γ_m, when this is the case.

In order to obtain quantitative information from these patterns, we apply a first-term analysis similar to that described in I. First, the time constant of the slow component was measured with and without the side light on, and from these data, τ_1 computed for the two cases. Now, as indicated in Eq. (6), π^2D_m/X^2 includes the contribution of diffusion losses to $1/\tau_1$ and G the effect of volume destruction. For the side light off G includes only the normal volume loss due to collisions between metastables and normal argon atoms, G_c. With the side light on G includes, in addition, the volume loss caused by the side light, G_s. Thus, the difference between $1/\tau_1$ with and without the side light is a measure of G_s. With our light source the maximum value we could obtain for G_s was about 1500 sec^{-1}.

If one is concerned only with those metastables described by the first-term of the fourier analysis of the initial distribution, then the quantities (π^2D_m/X^2), G_c, and G_s are also a measure of the rate at which the metastables are destroyed at the electrodes, in the gas by collision, and in the gas by the side light. Furthermore, since we are dealing with the first term, exactly one-half of the electrode destruction will be at the cathode and one-half of the photons released in either type of volume destruction will go to the cathode. Thus, the quantities

$$\frac{\pi^2D_m/2X^2}{(\pi^2D_m/X^2)+G_c} \quad \text{and} \quad \frac{G_c/2}{(\pi^2D_m/X^2)+G_c}$$

represent the fractions of the excitation energy in the metastables which without side light reach the cathode by metastables and by photons, respectively. Immediately after the side light is turned on, the rate of arrival of metastables remains unchanged, but the rate of arrival of photons increases suddenly by the factor $(G_c+G_s)/G_c$. Then, gradually, a new steady-state is set up, for which the fractional carriers of energy are given by expressions above, except that G_c is replaced by G_c+G_s.

The measurement of γ_r/γ_m can be made using the amplitude of the slow component either immediately after the light is turned on or using the value of this component after the new equilibrium has been attained. We have found the former method better. A pattern of the type shown in trace *g* in Fig. 6 is used. The quantities π^2D_m/X^2, G_c, and G_s, are established from time constant studies. Then the magnitude of the slow component just before the side light is turned on, s, and its value just afterwards, $s+\Delta s$, is measured. Both s and $s+\Delta s$ will be directly proportional to the electron currents leaving the cathode due to the combination of metastables and photons from converted metastables striking the cathode, i.e.,

$$\Delta s/s=\gamma_rG_s/\gamma_m(\pi^2D_m/X^2)+\gamma_rG_c,$$

so that

$$\gamma_r/\gamma_m=(\Delta s/s)(\pi^2D_m/X^2)/[G_s-(\Delta s/s)(G_c)]. \tag{8}$$

In this equation all quantities on the right-hand side are measurable, so that γ_r/γ_m can be evaluated directly. In case the normal volume loss, as measured by G_c, is caused by impurities which do not yield photoelectrically active photons, then the second part of the denominator should be omitted.

The accuracy of measurement of the various quantities involved was not great, probably ±20 percent, mainly because of the presence of the electrical noise induced in the Townsend current by the operation of the discharge tube in close proximity. Nevertheless, a large difference between the γ_r/γ_m ratio for the tantalum cathode as compared with those of molybdenum and BaO cathodes was clearly discernible. The average value of γ_r/γ_m as determined by this method was 0.40 for tantalum, 0.08 for molybdenum, and 0.10 for barium oxide.

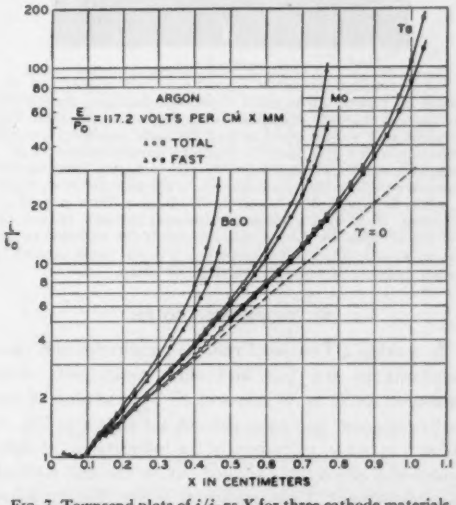

FIG. 7. Townsend plots of i/i_0 vs X for three cathode materials in argon at E/p_0 = 117.2 volts/cm×mm taken with p_0 = 1.535 mm.

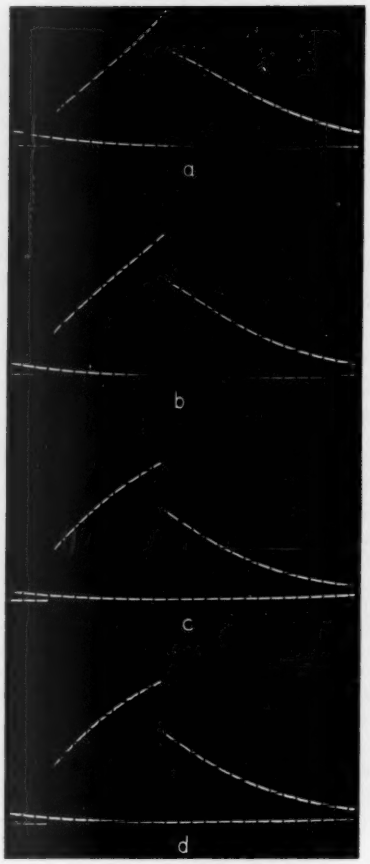

FIG. 8. Oscillograms of the current in a pulsed Townsend discharge for various intensities of the stimulating light, the applied voltage and electrode separation being maintained constant. The amplifier gain was adjusted to give the same maximum vertical deflection in each case. In *a* the maximum current value $=5\times10^{-7}$ amp, in *b*, one-half, in *c*, one-fourth, and in *d*, one thirty-second that amount. The pattern is seen to be the same for both *c* and *d*, while in *b*, and more so in *a*, the trace exhibits a positive curvature. If the light is left on continuously in case *a*, breakdown will ensue. While we did not examine closely the variation of the distortion with current, it appeared as if it was never present in serious amounts for currents less than 10^{-7} amp.

VI. TOWNSEND RUNS

In making a Townsend run the amplitudes and time constants of the fast and slow components were measured for 20 to 50 values of X. Typical plots of the fast component and total current are shown in Fig. 7. In such runs any variations in the intensity of the light source was effectively canceled out by the null method of measurement. Time variations in the photoemission sensitivity of the cathode in either the Townsend tube or the vacuum phototube could, however, introduce errors. We tried to minimize such errors by allowing the apparatus to "warm up" for several hours before starting a run and then periodically repeating complete runs to check the reproducibility of the data. For values of i/i_0 less than about ten, the measurements were in general reproducible to better than 1 percent. At higher ratios the accuracy of setting of the electrode spacings, and possibly slight variations in γ, made the variations larger. In general, if the gap had been allowed to break down between runs, there would be a noticeable change in the i/i_0 values.

We have labeled the distortions at high currents as being caused by space charge, although we have no direct proof that this is the cause. The oscillograms in Fig. 8 illustrate current forms for several values of the current as indicated in the caption. The distortion appeared to be of the kind which would make the slow component larger than expected by an exponential form at high currents.

The Townsend curves shown in Fig. 7 illustrate the back diffusion loss of electrons at applied voltages below 12 volts. They also exhibit a wave-like form for applied voltages below about 70 volts, caused by the lack of a constant value of α_i. Both of these effects have been discussed by the Eindhoven-Phillips workers.[6] We used for our value of i_0 the minimum value of the current which was normally observed for applied voltages in the range 12 to 15 volts. The value of x_0 was established by drawing a smooth tangent to the data for the fast component of current on the low γ-surface and taking the value of X where this line intersected the current value of i_0.

The best value of α_i corresponding to a set of data for a particular E/p_0 value was determined by a trial-and-

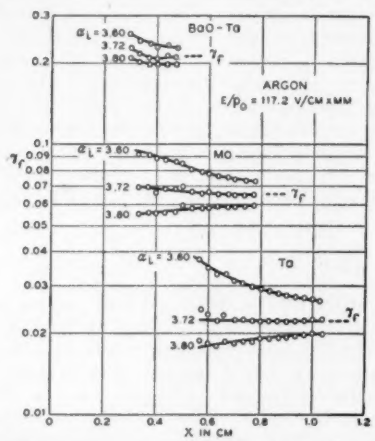

FIG. 9. Values of γ_f computed from i_f/i_0 data for three assumed values of α_i. Here the value of $\alpha_i=3.72$ cm^{-1} and the value of γ_f indicated by the dashed line was taken as the "best" fit of these parameters in the Townsend equation to the experimental data.

error method. A value of α_i was assumed, and then, measured values of i_f/i_0 being taken, γ_f-values were computed, using the Townsend equation. For the "best" value of α_i these γ_f-values should not vary with X. In Fig. 9 such computed values of γ_f are plotted *vs* X for three assumed values of α_i, of which the middle one was taken as "best." Note the sensitivity of the resultant γ-values to relatively small differences in the α_i-values.

The values of γ and γ_f were computed from i/i_0 and i_f/i_0 data. The value of γ_s, obtained by subtracting γ_f from γ, in general decreased with increasing X especially for lower values of E/p_0, for which the fraction of metastables destroyed in the gas is larger (see Fig. 10). The main cause of the decrease is the increasing fraction of the metastables which are lost in the volume of the gas as the electrode spacing is made larger coupled with the fact that the photons emitted in this process are usually less effective in causing electron emission at the cathode than the metastables (i.e., $\gamma_r < \gamma_m$).

In an attempt to take into account the varying fractions of metastables diffusing to the cathode and being lost in the volume, we applied the so-called first-term analysis described in I. In this analysis it is shown [Eq. (35)] that

$$f_{esc}\left[\alpha_m\gamma_m+\alpha_m\gamma_r\left(\frac{GX^2}{\pi^2 D_m}\right)\right] = \alpha_i\frac{i_0 i_{s1}}{i_f(i_{s1}+i_f)}\left[1+\frac{GX^2}{\pi^2 D_m}\right]H, \quad (9)$$

where H is a function of $\alpha_i X$ and $\alpha_i x_0$ as defined by Eq. (36) in I. Thus, if the right-hand side of this equation is plotted as a function of $(GX^2)/(\pi^2 D_m)$, then there should result a straight line having a slope $\alpha_m\gamma_r f_{esc}$ and a y intercept of $\alpha_m\gamma_m f_{esc}$. A typical plot is shown in Fig. 11. This method of analysis seems about as satisfactory as any for evaluating $\alpha_m\gamma_m$, but for obtaining $\alpha_m\gamma_m$ the light destruction scheme, described in Sec. V is probably better.

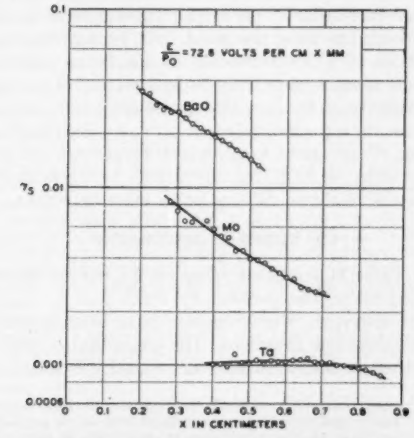

FIG. 10. γ_s and a function of X for three cathodes.

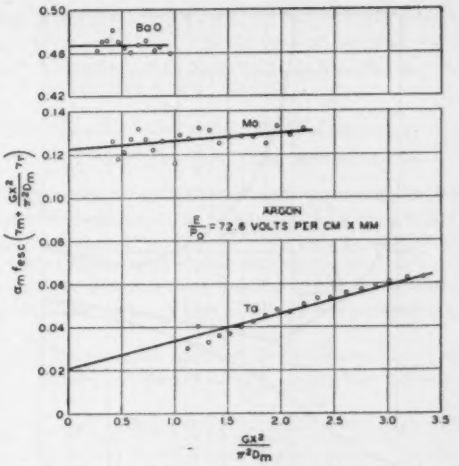

FIG. 11. Plots for three cathode materials showing application of "first-term" analysis of slow component for determining $\alpha_m\gamma_m$ and $\alpha_m\gamma_r$.

The quantity f_{esc} in the expression for γ was evaluated by making detailed measurements of the current in the Townsend tube at low voltages. Such data are shown in Fig. 12. We assumed that the current of elec-

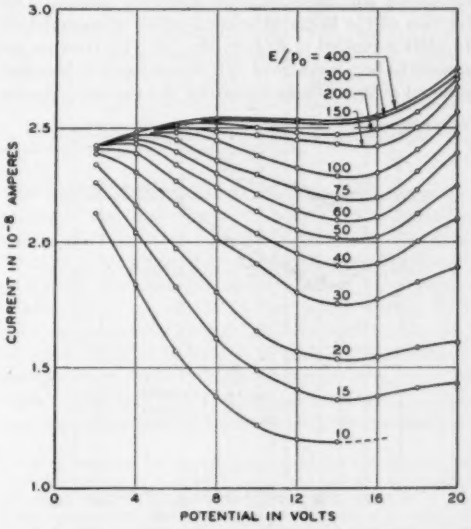

FIG. 12. "Low-voltage" Townsend plots obtained with a molybdenum cathode and argon gas with $p_0 = 1.535$ mm and E/p_0 varied by changing E only.

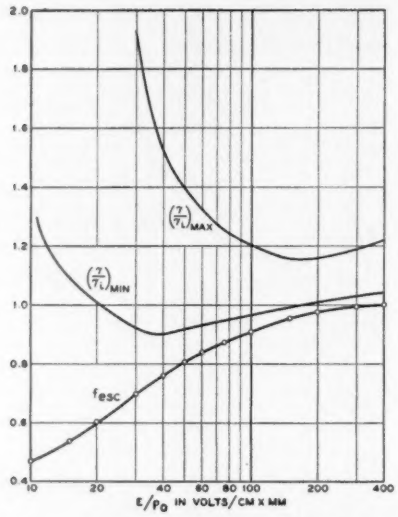

FIG. 13. f_{esc} as obtained from the 14-volt values of current in Fig. 11, and values of γ/γ_i as calculated by Eq. (11) for the extreme cases of no volume destruction and complete volume destruction of metastables along with other assumptions given in the text.

trons liberated from the cathode was given by 2.56×10^{-8} amp, the value observed for the $E/p_0=400$ curve in the region of 8 to 14 volts. The fall-off at six volts and below for the higher E/p_0 curves was due, we believe, to the influence of the size of the holes in the anode compared with the electrode spacing. The fraction of the liberated current which is observed at 14 volts is plotted *vs* E/p_0 in Fig. 13. This fraction we assume to be a measure of f_{esc}. It was found to be independent of the cathode surface for the various cathodes

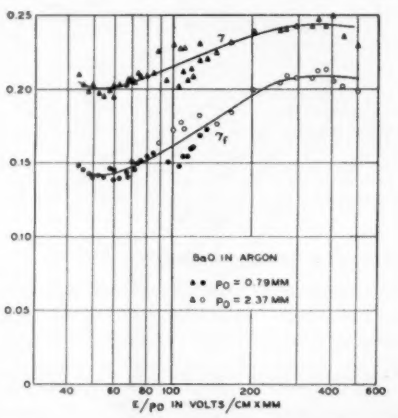

FIG. 14. γ and γ_f for a BaO-Ni surface using Eq. (10) and current amplification data obtained on a BaO-Ni surface and a pure Ni surface.

at our disposal, Ta, Mo, and BaO. (Crude measurements of the long wavelength photoelectric threshold indicated a work function of about 4.5 ev for the first two and 2.25 ev for the last.)

As indicated earlier we were unable in these studies to change the pressure in the tubes and retain the same efficiency of cathode emission. Thus, we were unable to obtain γ-measurements from complete Townsend runs as a function E/p_0, since at a given pressure complete runs for all surfaces could not be made over a range of E/p_0 greater than a factor of two. The data obtained from complete Townsend runs served mainly to establish the breakdown of γ into various parts.

The variation of γ_f with E/p_0 was obtained for the BaO surface, however, by comparing the ratios of i_f/i_0 of the BaO surface with that of a low γ-surface, in this case, nickel. (These measurements were made with the first type of tube.) Now, it can be readily shown that if $H=i/i_0$ for the high γ-surface ($\gamma=\gamma_H$) and $L=i/i_0$ for the low γ-surface ($\gamma=\gamma_L$), we have

$$(\gamma_H-\gamma_L)/(1-\gamma_L)=(H-L)/H(L-1). \qquad (10)$$

Although γ_L was not known percentagewise with great accuracy, its value was somewhere close to 0.02. On the other hand, γ_H had values between 0.15 and 0.20. Thus, a determination of γ_H by means of this relation could be made with reasonable accuracy, and without making a complete Townsend run. The γ-data as obtained by this method are shown in Fig. 14 for a BaO on Ni surface. Comparison of the curve of γ_f with that of f_{esc} in Fig. 13 suggests strongly that the variation of γ_f over a range of E/p_0 covered is caused mainly by the variation of f_{esc}.

This observation implies that the quantity $[\gamma_i + (\alpha_r/\alpha_i)f_{rk}\gamma_r]$ is constant over this range. Since α_r/α_i is certainly increasing for decreasing E/p_0, one must assume either that γ_i decreases with decreasing E/p_0, or that γ_i is constant and that the value of $[(\alpha_r/\alpha_i)f_{rk}\gamma_r]$ though increasing is still small compared with γ_i. We are inclined to favor the latter, first, because the data available of γ_i measurements by ion beam methods, though meager, show very little variation of γ_i with ion velocity in the low velocity range,[21] and, second, because the measured values of γ_r/γ_m for BaO as given in Sec. V are quite small, about 10 percent. At still lower values of E/p_0, the contribution of the radiation term will, of course, become much more important.

VII. GENERAL DISCUSSION

In Table II are listed values of the various factors making up γ. The methods by which f_{esc}, α_i, γ_f, γ_s, $\alpha_m\gamma_m$, and γ_r/γ_m were evaluated have been described in the preceding discussion. The quantities α_m and α_r could not be measured, and so we used the calculated

[21] Private communication of H. D. Hagstrum of these Laboratories. His studies now underway indicate that γ_i as measured by an ion beam method increases only very slowly in the range from 10 to 100 ev of ion energy for He^+ on a Mo target.

values of Kruithof,[6] who evaluated the ratio

$$N_r=(\alpha_m+\alpha_r)/\alpha_i$$

as a function of E/p_0 for the various rare gases. We further assumed that $\alpha_m=\alpha_r$, which seems to be a reasonable guess, lacking more detailed information on which to base an estimate.[22] The γ_m-values were then calculated from α_m calculated in this way and from the values of $\alpha_m\gamma_m$. Next, using the γ_r/γ_m data, γ_r was computed. Finally, $(\alpha_r/\alpha_i)f_{rk}\gamma_r$ was computed assuming $f_{rk}=0.4$. Then γ_i was evaluated from γ_f and f_{esc}.

Considering the accuracy of the original data and the many operations required on them, the values of γ_i, γ_m, and γ_r as listed can hardly be more accurate than 10 to 20 percent. Bearing in mind these limitations, we see that γ_m and γ_i have closely the same value, while, on the other hand, there is no such simple relationship between γ_r and γ_i or γ_m.[23]

The physics of electron emission caused by ion impact on surfaces has been discussed most recently by Cobas and Lamb.[24] They have investigated theoretically the process in which ions are assumed to be first neutralized by electrons being captured in excited states. The excited atom on closer approach to the surface then gives rise to the electron emitted into the gas. If the second process is the limiting one (i.e., assuming all electrons are captured in excited states),[25] then our observation of $\gamma_m\approx\gamma_i$ is not unreasonable.

The lack of any correlation between γ_r and γ_m or γ_i may be due to the fact the photoelectric process involved in these studies involve high energy photons. These photons enter the cathode probably to a depth of several atomic layers (volume photoelectric effect). The subsequent escape of the electron from the cathode depends on a variety of effects not all of which involve the detailed nature of the surface.

The variation of γ with E/p_0 has been shown to be dependent on a variety of factors which will depend on the conditions of the experiment. One can calculate, however, two limiting cases, namely, that in which all metastables are converted into radiating atoms by collisions and that in which none are so converted. We shall take $f_{rk}=f_{rk}'=0.4$,[26] and for the first case assume $f_{mk}=0$, $f_{mr}=1$, while for the second we shall take $f_{mk}=0.4$ and $f_{mr}=0$. Assuming, as before, $\alpha_m=\alpha_r=\frac{1}{2}N_r\alpha_i$, and that $\gamma_m=\gamma_i$, we have

$$\gamma=f_{esc}\gamma_i(1+0.4N_r\gamma_r/\gamma_m) \text{ for the first case,}$$
$$\gamma=f_{esc}\gamma_i[1+0.2N_r(1+\gamma_r/\gamma_m)] \text{ for the second case.} \quad (11)$$

The quantity γ/γ_i is plotted *vs* E/p_0 in Fig. 13 for these two cases assuming $\gamma_r/\gamma_m=0.1$, f_{esc} given by data in the plots in Fig. 12, and N_r by the calculations of Kruithof.[6] The actual observed values of γ will be somewhere between these limiting curves being closer to the higher value at high E/p_0 and vice versa at low E/p_0.

The literature contains numerous measurements of γ.[1-3] In view of dependence of γ on X which we mentioned earlier, it seems likely that some of these measurements may have been in error for not properly taking this effect into account. Nevertheless, the data for argon as summarized by Druyvesteyn and Penning[27] appear for the most part accountable in terms of the relation given above. It is also worth noting that γ-values given by Kruithof and Penning,[28] for the case of small argon admixtures in neon, which show a decrease in γ for very small values of E/p_0, may be explained by lack of a γ_r-contribution here if the neon atoms in the radiating (as well as in the metastable)

TABLE II. Data giving the various factors making up γ. The data for the two higher values of E/p_0 were obtained with $p_0=1.535$ mm and the surfaces in the same condition. The data for the lowest value of E/p_0 were obtained with $p_0=4.135$ mm and the surfaces having a reduced efficiency.

Gas-dependent factors:

E/p_0 volts/cm×mm	f_{esc}	α_i cm^{-1}	α_r, α_m cm^{-1}
195.4	0.97	6.63	2.6
117.2	0.91	3.72	2.4
72.6	0.86	5.10	7.0

Cathode-dependent factors:

$\frac{E}{p_0}$	Cathode	γ_f	γ_r near breakdown	$\alpha_m\gamma_m$	$\frac{\alpha_r}{\alpha_i}f_{rk}\gamma_r$	γ_i	γ_m	γ_r
195.4	Ta	0.026	0.0025	0.062	0.0014	0.026	0.023	0.009
195.4	Mo	0.076	0.0074	0.160	0.0008	0.071	0.060	0.005
195.4	BaO-Ta	0.23	0.050	0.83	0.005	0.23	0.31	0.031
117.2	Ta	0.022	0.0026	0.056	0.002	0.022	0.023	0.009
117.2	Mo	0.065	0.011	0.158	0.001	0.071	0.065	0.005
117.2	BaO-Ta	0.21	0.065	0.65	0.007	0.22	0.27	0.027
72.6	Ta	0.0060	0.0009	0.025	0.0017	0.0053	0.0035	0.0021*
72.6	Mo	0.030	0.0025	0.14	0.001	0.034	0.020	<0.001*
72.6	BaO-Ta	0.073	0.013	0.54	···	0.085	0.078	···

* No γ_r/γ_m-measurements were made by the light destruction method for the cathodes in this condition, so we use here the less reliable data obtained from the slopes of the curves in Fig. 11.

[22] From the data obtained in studies of the Penning effect, A. A. Kruithof and M. J. Druyvesteyn [Physica 4, 450 (1939)] calculated a value of $\alpha_m/(\alpha_m+\alpha_r)$ as high as 95 percent for some values of E/p_0. We believe this high value could have been caused by the ionization of argon atoms by neon atoms not only in the metastable states, but in the nearby radiative states also. The lifetime of the latter when enhanced by the phenomenon of the "imprisonment of resonance radiation" could well have been adequate in the conditions of their experiments to permit this process.

[23] If our assumption that $\alpha_r=\alpha_m$ is widely in error, then, obviously, the measurements do not give $\gamma_i\approx\gamma_r$, but merely that γ_i/γ_m is roughly constant for the cathodes we studied. This observation is still in contrast to the lack of such a fixed ratio between γ_m and γ_r.

[24] A. Cobas and W. E. Lamb, Phys. Rev. **65**, 327 (1944).

[25] Here, the excited states need not be metastable, because the time spent by the excited atom in the proximity of the surface is short compared to the lifetime of even radiative states.

[26] If it were not for the phenomenon of the imprisonment of resonance radiation, f_{rk} would be 0.5 for infinite plane-parallel geometry. Instead, the radiation flows in something like a diffusion process [see T. Holstein, Phys. Rev. **72**, 1212 (1947)]; hence, f_{rk} will be less than 0.5, though probably still greater than f_{mk} with $G=0$.

[27] See Fig. 20 in reference 2.

[28] A. A. Kruithof and F. M. Penning, Physica **4**, 430 (1937).

states are destroyed in collisions of the second kind with argon atons. Thus, γ here would follow simply the f_{esc} curve.

It is unfortunate that we were unable to get good γ-data over a larger range of E/p_0. With the techniques developed by Penning[11] and his co-workers for producing stable, high γ-surfaces it may be possible to carry out such experiments.[29] Our tubes were not very suitable for this purpose because of the massive cathode we employed, the large gas volumes involved, and difficulties presented by the extended sputtering required by his techniques. It would also be desirable to obtain experimental values of α_m and α_r, which obviously play an important role in the interpretation of γ. Similarly, there is need for a clearer understanding of the physical process involved in the destruction of metastables by collisions in the gas, an effect which may be different in magnitude for the two metastable states.

The author is indebted to numerous members of these Laboratories for assistance, for which he wishes to express his appreciation; in particular to H. W. Weinhart, who designed all the tubes and supervised their construction, to A. A. Manner, who built the mechanical apparatus, and to R. G. Brandes, who assisted in the conduct of the experiments. I am also very much indebted to my colleagues, A. H. White, H. D. Hagstrum, W. A. Depp, and R. A. Newton (now located at the University of Tennessee, Knoxville, Tennessee), for many valuable discussions, and particularly to J. A. Hornbeck, who actually participated in the early conduct of these experiments.

[29] The pressure changes could probably be made most easily by starting the measurements at high pressure, and then proceeding to lower pressures (and hence higher E/p_0's), letting the gas expand into evacuated glass bottles, by shattering "break-off" tips. In this way the gas purity would be unchanged during the pressure change.

PHYSICAL REVIEW VOLUME 83, NUMBER 5 SEPTEMBER 1, 1951

Range of High Energy Electrons in Aluminum

H. E. JOHNS, J. R. CUNNINGHAM, AND L. KATZ
Betatron Group, University of Saskatchewan, Saskatoon, Saskatchewan, Canada

(Received May 16, 1951)

An electron beam has been extracted from the 25-Mev betatron of the Physics Department of the University of Saskatchewan by using a magnetic peeler similar in design to that developed at the University of Illinois. The high energy electron beam was analyzed by bending it through an angle of 90° with a magnetic field. The high energy electrons were passed in turn through a flat ionization chamber, the aluminum absorber and a second ionization chamber. By measuring the ratio of the two ionization currents for different thicknesses of the absorber, the range of the electrons was determined. The ranges of electrons having energies from 12 to 16 Mev were obtained in this way and found to be in agreement with an empirical formula previously proposed by one of the authors (see reference 7 of this paper).

INTRODUCTION

EXPERIMENTAL determinations of the ranges of high energy electrons in the region above 3 Mev have been almost nonexistent until the recent measurements on nuclear beta-rays by Hereford[1] on B^{12} (13.4 Mev) and Alvarez[2] on N^{12} (16.6 Mev) and measurements by Hereford and Swann[3] on monoenergetic electrons. Short-lived nuclear activities having energies in this high energy region have been reported in the literature. The energies of these beta-rays are most readily determined by their range in aluminum. For this reason the authors felt that further investigations on the ranges of high energy electrons was justified. The ranges of monoenergetic electrons from the University of Saskatchewan betatron with energies from 12 to 16 Mev have been measured and are reported in this paper.

[1] F. L. Hereford, Phys. Rev. **74**, 574 (1948).
[2] L. W. Alvarez, Phys. Rev. **75**, 1815 (1949).
[3] F. L. Hereford and C. P. Swann, Phys. Rev. **78**, 727 (1950).

EXPERIMENTAL ARRANGEMENT

Electrons were removed from the betatron using a magnetic shunt peeler device very similar to that developed by Skaggs *et al.*[4] The electron beam was passed through a 1-cm aperture one meter from the betatron and was deflected through 90° in a magnetic field as indicated in Fig. 1. After passing through an aluminum ionization chamber, 5 cm in diameter and 6 mm thick, the electrons pass through an absorber of aluminum as indicated, and through a second ionization chamber of the same diameter as the first but five times the thickness. The central electrodes of both ionization chambers were connected through shielded cables to a detecting device in the control room of the betatron. The details of this device are shown in Fig. 2. The central electrode and the outer walls of the chambers were made of aluminum 0.001 in. thick. A voltage of

[4] Skaggs, Almy, Kerst, and Lanzl, Phys. Rev. **70**, 95 (1946). The porcelain electron doughnut was obtained through the courtesy of D. W. Kerst.

+200 volts was applied to the outer electrode of chamber 1 and −200 volts to the outer electrode of chamber 2.

The energy of the electrons was determined by their path in the known magnetic field (Fig. 1). A defining slit 1 mm wide was placed at A, and the beam was made to pass through photographic films at positions B and C. The path of the electrons through the magnetic field was thus determined and from knowledge of the magnitude of the magnetic field the energy was determined. Magnetic fields were measured with a flux meter which had been calibrated against a magnetic resonance device at Chalk River through the kindness of J. G. Bayly. It is felt that the energies of the electrons selected were known to an accuracy of 1.5 percent.

A schematic diagram of the circuit is shown in Fig. 2. This device is essentially that which has been developed by Kemp[5] and measures the ratio of the two ionization currents. It can be shown that when the ratio of the

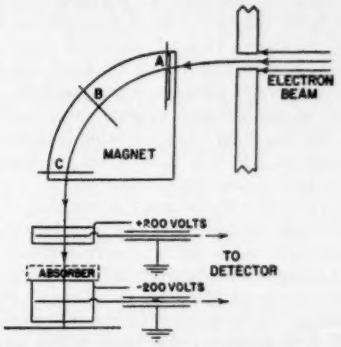

FIG. 1. Experimental arrangement of apparatus. The electron beam is collimated, bent in a magnetic field, and passed through two ionization chambers between which the absorber is placed.

ionization currents I'/I'' is given by Eq. (1), the potential of the point P will not change when the ganged switches, S_1, S_2, and S_3, are momentarily opened. This condition of balance is found using a VX32B Victoreen electrometer triode in the circuit shown in Fig. 2. As indicated above, at balance, Kemp[5] has shown that

$$\frac{I''}{I'}=\frac{(C''+C)}{(C'+C_1)}\cdot\frac{C_1}{C}, \tag{1}$$

where C' and C'' are the capacities to ground of the two cables and their connected ionization chambers. C is a variable capacity which can be set precisely with a micrometer dial and C_1 is a fixed capacity. Suppose n is the numbers of electrons/sec of energy E_0 which pass through ion chamber 1. The ionization current I' will be given by

$$I'=K_1 n(dE_0/dx), \tag{2}$$

[5] L. A. Kemp, Brit. J. Radiol. **19**, 233 (1946).

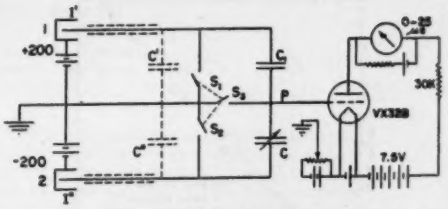

FIG. 2. Circuit diagram of the device for measuring the ratio I'/I''. For the proper setting of C momentary opening of S_1, S_2, and S_3 will not change the plate current of the VX32B.

where K_1 is a constant determined by the size of the chamber and (dE_0/dx) is the rate of energy loss in air of an electron of energy E_0. The ionization current in chamber 2 for no absorber between the chambers is given by a similar expression,

$$I''=K_2 n(dE_0/dx). \tag{3}$$

It is assumed that the electron beam is well enough collimated so that the number passing through both chambers is the same when no absorber is present. When C is adjusted for balance to a value C_0 we have

$$\frac{I_0''}{I'}=\frac{K_2}{K_1}=\frac{(C''+C_0)}{(C'+C_1)}\cdot\frac{C_1}{C_0}. \tag{4}$$

This equation enables one to evaluate the ratio of the sensitivities of the two chambers.

Suppose now an absorber of thickness x is placed in front of chamber 2, the number of electrons which enter chamber 2 will be a certain fraction "f" of the original number, and the mean energy of the emerging electrons will be E_x. When balance is restored by adjusting C to a new value C_x we have

$$\frac{I_x''}{I'}=\frac{K_2 nf(dE_x/dx)}{K_1 n(dE_0/dx)}=\frac{(C''+C_x)}{(C'+C_1)}\cdot\frac{C_1}{C_x}. \tag{5}$$

In Eq. (5) it is not necessary to assume that the

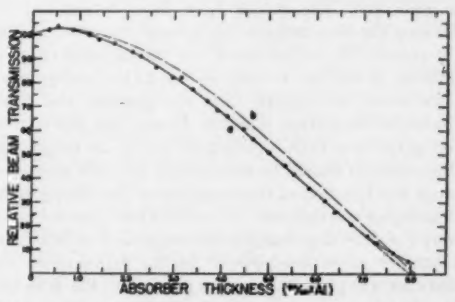

FIG. 3. Typical transmission curve. Curve "a" obtained by evaluating Eq. (6), neglecting the correction term $(dE_0/dx)/(dE_x/dx)$. Curve "b" was obtained from a by applying this correction factor.

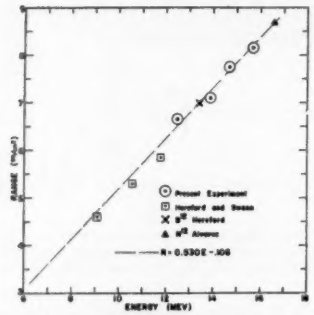

FIG. 4. Range-energy relation for aluminum in the region 6 to 18 Mev. The squares represent range measurements for monoenergetic electrons by Hereford and Swann [reference (3)]; the cross represents nuclear beta-rays from B^{12}, range due to Hereford [reference (1)] and energy due to W. F. Hornyak and T. Lauritsen [Phys. Rev. 77, 160 (1950)]; the triangle represents nuclear beta-rays from N^{13} due to Alvarez [reference (2)]; the circles represent the present investigation of monoenergetic electrons; the dashed line is an empirical relation due to Katz and Penfold [reference (7)].

number of electrons passing through chamber 1 remains constant with time for "n" cancels out of the expression. Using Eqs. (4) and (5) we obtain

$$f=\frac{(C''+C_x)}{(C''+C_0)}\cdot\frac{(C_0)}{(C_x)}\cdot\frac{(dE_0/dx)}{(dE_x/dx)}. \tag{6}$$

The quantity $(dE_0/dx)/(dE_x/dx)$ is a correction term which amounts to some 20 percent for the energies of electrons herein considered, but its effect on the practical range is less than 2 percent and will be discussed later. From Eq. (6) it is seen that an evaluation of the capacities C'', C_x, and C_0 enable one to determine f.

RESULTS

A typical transmission curve is shown in Fig. 3. It will be seen that the curve initially rises above the 100 percent and then falls in a nearly linear manner. Near the extreme range the transmission curve bends upwards as indicated. The ranges have been determined by drawing the best straight line through the latter half of the points. The initial rise of the transmission curve is difficult to explain. It may be due to low energy electrons which are ejected from the absorber and enter the second ionization chamber. In any case this part of the graph has little significance as far as ranges are concerned. It should be emphasized that the measured range is a function of the geometry of the arrangement of absorber and detector. If the absorber is moved away from the detecting chamber the response is reduced and a smaller range is obtained. In the experiments the absorber was placed as close as possible to the detector.

TABLE I. Range of monoenergetic electrons in aluminum.

Energy (Mev)	Range (g/cm²)
12.5	6.65
13.9	7.10
14.7	7.75
15.7	8.15

This is the usual arrangement when ranges of beta particles are measured using a Geiger counter. When the detector and absorber are separated some electrons which are deflected through large angles will miss the detector.

In Fig. 3 the dashed curve gives the percentage transmission when correction is made for the change in sensitivity of the lower chamber with the energy of the electrons. This correction cannot be carried out accurately since the electrons which emerge from the absorber are not monoenergetic. From Eq. (6) the correction is $(dE_0/dx)/(dE_x/dx)$. To evaluate this function we must know the energy E_x of the electrons for each absorber thickness. This was obtained approximately as follows: For an absorber of thickness one-half the range, the emerging electrons were considered to have an energy of one-half their original value E_0, etc. This implies that the range energy relation is strictly linear, an assumption which is fairly good for high energy electrons. In any case examination of Fig. 3 will show that the correction to the range is less than 2 percent. Values for (dE/dx) were obtained from Heitler.[6]

Ranges corrected in this way were obtained for four different energies and are given in Fig. 4 along with the measured values of Hereford and Swann,[3] Hereford,[1] and Alvarez.[2] The actual values obtained are shown in Table I. It is estimated that these ranges were determined to an accuracy of ± 1.5 percent. The magnitude of these possible errors are shown in Fig. 4. However, their absolute values may be in error more than this because of the difficulty of estimating the corrections which should be applied for the geometrical arrangement. Katz and Penfold have proposed[7] an empirical range equation in the energy region 3 to 20 Mev. $R=0.530E-0.116$, where R is the range in g/cm² and E the energy in Mev. This has been plotted in Fig. 4. It is in agreement with the measurements of Hereford and Alvarez and with our measurements.

The authors wish to acknowledge the financial assistance of the National Research Council and the University of Saskatchewan for grants in aid of this research. Thanks are due to Mr. S. B. Mauchel, betatron technician, for his help.

[6] W. Heitler, *Quantum Theory of Radiation* (Oxford University Press, London, 1944).

[7] L. Katz and A. S. Penfold (to be published). June 1951 Meetings of the Royal Society of Canada. Abstract 119 Section III.

Radiations from Br^{77} and Ni^{67}

ROBERT CANADA AND ALLAN C. G. MITCHELL
Physics Department, Indiana University, Bloomington, Indiana*
(Received May 14, 1951)

The nuclear spectra of Br^{77} (58 hr) and Ni^{67} (36 hr) have been investigated in a magnetic lens spectrograph.

Br^{77} decays by orbital electron capture and positron emission to Se^{77}. Br^{77} emits a single positron group of energy 0.336 Mev together with gamma-rays of energy 0.160, 0.237, 0.284, 0.298, 0.520, 0.641, and 0.813 Mev, of which the lines at 0.160, 0.237, and 0.520 Mev are internally converted. Br^{77} is the parent of the metastable state Se^{77m} of 17-sec half-life, and the energy of the gamma-ray associated with this transition is 0.160 Mev.

The radiations from Ni^{67} consist of one positron group whose end point is 0.835 Mev together with one strong gamma-ray of energy 1.375 Mev and two weaker gamma-rays whose energies are 1.91 and 0.128 Mev, the latter being internally converted.

I. INTRODUCTION

THE radiations from Br^{77} and Ni^{67} have been studied with the help of a magnetic lens spectrometer. The spectrum of Br^{77} is of interest because the transition goes to Se^{77}, which contains a metastable state of 17 sec half-life, and, in addition, the spectrum of As^{77}, which also goes to Se^{77}, has been measured. The present experiments have fixed the energy of the transition associated with the metastable state since the short-lived metastable state is in equilibrium with the long-lived parent and measurements can be made at leisure. Measurements on Ni^{67} were undertaken to obtain a more detailed picture of the disintegration scheme than that given by the earlier coincidence experiments published from this laboratory.

II. RADIATIONS FROM Br^{77} AND Se^{77m}

The radiations from the decay of Br^{77} (58 hours) have been shown to consist of positrons, gamma-radiation, and x-rays resulting from the capture of orbital electrons. Woodward, McCown, and Pool[1] found a positron end point of 0.36 Mev by absorption techniques. These investigators report that there is gamma-radiation in addition to annihilation quanta, and also that there are abundant x-rays. They give a value of 20 for the ratio of the number of disintegrations which take place by K-capture to those which go by positron emission. Hopkins and Cunningham[2] are reported to have measured a maximum positron energy of 0.36 Mev and a gamma-ray of 0.7 Mev.

Since no complete spectrometric study of the radiations from this disintegration has been reported, it was decided to study the radiations from Br^{77} with the use of a magnetic lens type beta-ray spectrometer. Since it has recently been shown[3] that the 17-second selenium isomer, Se^{77m}, is not the daugher of As^{77}, it is of particular interest to investigate whether this selenium activity grows from Br^{77}.

The source material for these experiments was prepared by alpha-particle bombardment of arsenic in the Indiana University cyclotron. Metallic arsenic powder was pressed into the grooves of a target plate and covered with aluminum foil to prevent the escape of the bromine. Bombardments of 150 micro-ampere-hours gave sufficient activity to allow the preparation of adequate beta- and gamma-ray sources.

The bromine was separated and purified chemically in the following manner. The target material was dissolved in concentrated HNO_3, care being taken to catch any escaping fumes in a water trap cooled in ice. Carrier amounts of iodine and bromine ion were added. Oxidation and extraction cycles designed to separate the bromine from iodine and other impurities were then repeated several times. The last aqueous solution of Br^- was then made 1N in HNO_3 and heated. Upon the addition of $AgNO_3$ the source was precipitated as AgBr in which form it was used in the spectrometer.

The spectrometer used in most of these experiments was a magnetic lens with ring-type focusing. The instrument has been described previously.[4,5] During these investigations the spectrometer was adjusted to give maximum transmission, for which the instrument resolution is 2 percent. The zapon window of the Geiger counter had a low energy cutoff at 11 kev. This window was not supported by any kind of grid.

The beta-ray source was made by allowing a water suspension of AgBr to dry on a zapon backing. Because of the small particle flux from Br^{77} it was necessary to use a source which was quite thick. The source was approximately 10 mg/cm^2 in surface density and was 5 mm in diameter.

The electron spectrum is shown in Fig. 1, in which the number of counts per minute, corrected for decay, is plotted against the magnetic rigidity in gauss-cm. The large peak at 1381 gauss-cm is a K internal conversion line corresponding to a gamma-ray energy of

* Supported by the joint program of the ONR and AEC.
[1] Woodward, McCown, and Pool, Phys. Rev. **74**, 870 (1948).
[2] H. H. Hopkins, Jr., and B. B. Cunningham, private communication, listed in G. T. Seaborg and I. Perlman, Revs. Modern Phys. **20**, 585 (1948).
[3] R. Canada and A. C. G. Mitchell, Phys. Rev. **81**, 485 (1951).
[4] Bunker, Canada, and Mitchell, Phys. Rev. **79**, 610 (1950).
[5] R. Canada and A. C. G. Mitchell, Phys. Rev. **83**, 76 (1951).

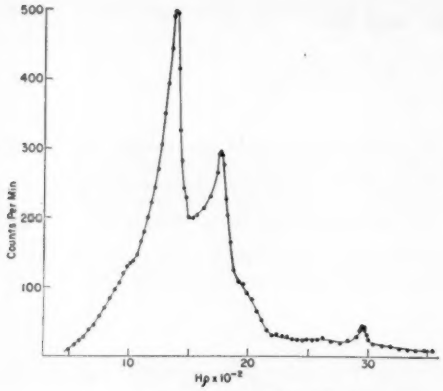

FIG. 1. The electron spectrum of Br^{77}.

0.160 Mev. Similarly the peak at 1756 gauss-cm is a K line for a 0.237-Mev gamma-ray. The L lines are not resolved. There is also a weak internal conversion line at 2946 gauss-cm corresponding to a gamma-ray of 0.521-Mev energy. The positron distribution is somewhat obscured by the two larger internal conversion lines.

For that reason the positron spectrum was measured in a 180° type spectrometer. A plot of the Fermi analysis, using the approximation to the coulomb correction factor given by Bethe and Bacher,[6] yields an end-point energy of 0.336 Mev. There is only one group and the shape indicates an allowed transition. The data from the 180° type instrument shows that the particles causing the continuous distribution beyond 0.336 Mev are negative electrons. They are probably Compton recoils, appearing in some abundance because of the thick source.

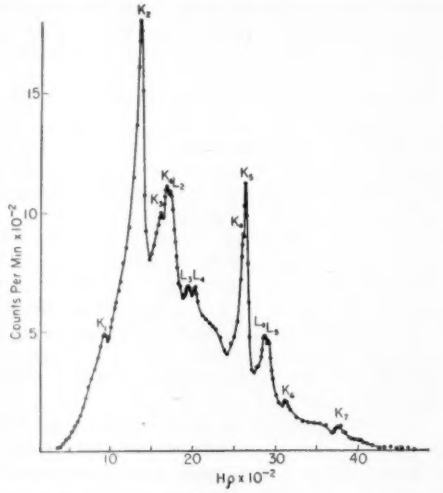

FIG. 2. The distribution of secondary electrons ejected from lead by the gamma-radiation of Br^{77}.

The distribution of secondary electrons ejected from a 16 mg/cm² lead radiator by the gamma-radiation of Br^{77} was examined with the lens and the result is shown in Fig. 2. The peak at 948.9 gauss-cm (K_1) is the K photoelectron peak corresponding to a gamma-ray of 0.160 Mev. The K and L peaks at 1395 and 1742 gauss-cm (K_2L_2) are due to a gamma-ray of 0.237 Mev. The K and L peaks which appear at 1629 and 1947 gauss-cm (K_3L_3) are due to a 0.284-Mev gamma-ray and the peaks at 1700 and 2039 gauss-cm (K_4L_4) correspond to a 0.298-Mev gamma-ray. The large peak at 2648 gauss-cm (K_5) is the K photoelectron line for a 0.520-Mev gamma-ray and its L line falls at 2918 gauss-cm (L_5). The weaker annihilation radiation rides under this line and, of course, distorts its intensity. The peaks for the photoelectrons for the annihilation radiation come at K_a and L_a. There are small peaks at 3116 and 3753 gauss-cm (K_6 and K_7) which are K lines for 0.641- and 0.813-Mev gamma-rays.

A comparison of the gamma-ray intensities was made using the curves of Gray[7] to obtain the photoelectric efficiencies of the various gamma-rays. The results are shown in Table I.

It should be emphasized that, since the intensity of most of the lines is quite weak, the relative intensities given in Table I may contain large errors. They can serve only as a guide to a proposed scheme.

IIa. The Isomer Se^{77m}

In order to investigate whether Se^{77m} is a daughter of Br^{77} a rapid chemical procedure was developed which would separate any selenium from the Br^{77} source material quickly enough to allow a measurement of a very short half-life. Upon the performance of this experiment a 17.5-second selenium activity was found to grow from the Br^{77}. This experiment has been described in detail elsewhere.[8] Since others have measured a gamma-ray of about 0.15 Mev,[9–11] associated with the decay of Se^{77m}, it seems probable that the 0.160-Mev gamma-ray is associated with the 17.5-second Se^{77m} isomeric transition.

IIb. Discussion of the Br^{77}-Se^{77} Decay

The energies and intensities of the gamma-rays observed are given in Table I. From a purely energetic standpoint it will be seen that the gamma-rays have

[6] H. A. Bethe and R. F. Bacher, Revs. Modern Phys. **8**, 194 (1936).

[7] L. H. Gray, Proc. Cambridge Phil. Soc. **27**, 103 (1931).

[8] Canada, Cuffey, Lessor, and Mitchell, Phys. Rev. **82**, 750 (1951).

[9] J. A. Arnold and N. Sugarman, J. Chem. Phys. **15**, 703 (1947).

[10] Gideon, Miller, and Waldman, Phys. Rev. **75**, 329 (1949).

[11] E. der Mateosian and M. Goldhaber, Phys. Rev. **82**, 115 (1951).

energies which suggest that they can be fitted into a decay scheme. Thus the energies of the lines at 0.237 and 0.284 Mev add together to give an energy of 0.521 Mev which agrees with the observed line at 0.520 Mev. In addition the sum of the energies 0.520 and 0.298 Mev gives 0.818 Mev, and that of 0.160 and 0.641 gives 0.801, in reasonable agreement with the observed line at 0.813 Mev. This suggests that the energy relations are given by the decay scheme shown in Fig. 3. In order to explain the relative intensities of the various lines it is necessary to suppose that orbital electron capture takes place to the three levels at 0.237, 0.520, and 0.813 Mev.

The pair at 0.641 and 0.160 Mev, which have been put in series, deserve some special discussion. Since the line at 0.641 Mev has a relative intensity of approximately 8 and that at 0.160 Mev approximately 0.6, it would appear at first sight that these two lines cannot be in series. However, the line at 0.160 is highly internally converted and comes from a metastable state. According to the shell model[12] this line is a transition between a $g_{9/2}$ and a $p_{1/2}$ configuration and the polarity of the radiation should be magnetic 2^4, and N_e/N_γ should be approximately[13] 6. The corrected intensity of this line would then be approximately 4, which is in reasonable agreement with that of the 0.641-Mev line.

Finally, the positron transition is assumed to take place between the ground state of Br^{77} and the ground state of Se^{77}. This is done for several reasons. In the first place, the ratio of the number of internal conversion electrons in the line at 0.160 Mev to the total number of positrons is approximately 0.3. If the character of the 0.160-Mev transition is magnetic 2^4-pole, one would expect about 0.9. Secondly, the shell model predicts that the ground state of both As^{77} and Br^{77} is $p_{3/2}$, and for this reason it would be very difficult to understand why the metastable state is not excited in the As^{77} decay and is excited from Br^{77}. However, if this state is excited via orbital electron capture followed by cascade gamma-rays, as indicated above, the configurations of the ground states of As^{77} and Br^{77} can both be $p_{3/2}$ and that of the ground state of Se^{77} can be $p_{1/2}$, as indicated by the work on As^{77}. In addition the value of $\log_{10}ft$ for the transition from Br^{77} has been calculated and is approximately 5, indicating an allowed transition.

III. THE RADIATIONS FROM Ni^{57}

Absorption and coincidence experiments of Maienschein and Meem[14] showed that Ni^{57} (36 hours) decays by the emission of a 0.725-Mev positron followed by gamma radiation. They showed that at least two gamma-rays are present in cascade and that the energy of the most energetic gamma-ray is 1.97 Mev.

[12] M. Goeppert-Mayer, Phys. Rev. **78**, 16 (1950).
[13] P. Axel and R. F. Goodrich, Internal Conversion Data, University of Illinois (unpublished).
[14] F. Maienschein and J. L. Meem, Jr., Phys. Rev. **76**, 899 (1949).

TABLE I. Relative intensities of the gamma-rays.

Gamma-ray energy	Relative intensity	Remarks
0.160±0.001	0.64	K photoelectron line, I.C. (strongly)
0.237±0.002	20.	K, L photoelectron lines, I.C.
0.284±0.003	0.22	K, L photoelectron lines
0.298±0.003	0.25	K, L photoelectron lines
0.520±0.002	100.	K, L photoelectron lines, I.C.
0.641±0.003	8.6	K photoelectron line
0.813±0.005	25.	K photoelectron line

Friedlander, Perlman, Alburger, and Sunyar[15] examined the radiations from this nuclide using absorption, coincidence, and scintillation techniques as well as a magnetic lens type spectrometer. They found the positron spectrum to be simple, of an allowed shape, and to have an end-point energy of 0.845±0.01 Mev. The electron spectrum showed a weak line of internal conversion electrons corresponding to a 0.120-Mev gamma-ray. They reported that the gamma-ray intensity was too small to allow the determination of the energies of the quanta by examining the secondary electron distribution in the spectrometer. Lead absorption experiments indicated the occurrence of 1.9-Mev gamma-radiation, annihilation radiation, and 0.120-Mev quanta. They state that the presence of other low-energy components of the gamma-ray spectrum cannot be excluded. These investigators found that the radiations from Ni^{57} produce photoneutrons in Be but not in deuterium. This shows that there must be a gamma-ray present with energy between 1.7 and 2.2 Mev. Comparison measurements with a variably biased scintillation counter gave a gamma-ray energy of 1.9±0.1 Mev. Their coincidence experiments showed that there is hard gamma-radiation in series with the beta-rays and also that the hard gamma-radiation is in coincidence with quanta having energy of less than 0.5 Mev.

The source material used in the present experiments was prepared by bombarding chemically pure iron with

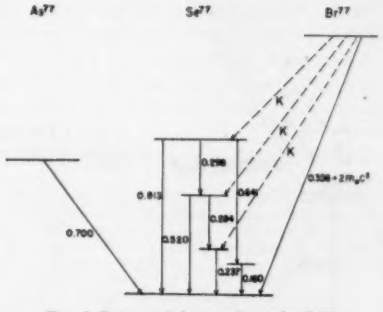

FIG. 3. Suggested decay scheme for Br^{77}.

[15] Friedlander, Perlman, Alburger, and Sunyar, Phys. Rev. **80**, 30 (1950).

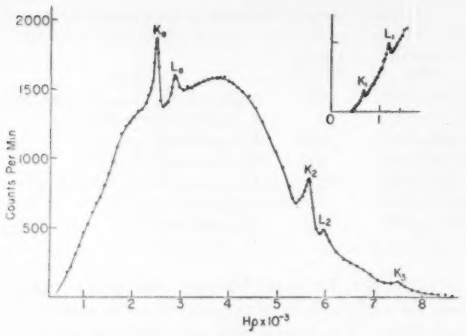

FIG. 4. Spectrum of secondary electrons ejected by gamma-rays of Ni^{57}.

alpha-particles in the Indiana University cyclotron. The iron was in the form of a thin sheet which was hard-soldered to the end of the copper probe. Bombardments of 40 micro-ampere-hours produced enough Ni^{57} activity to allow the examination of both the beta- and gamma-ray spectra in the spectrometer.

The nickel activity was separated and purified chemically by a procedure essentially the same as that described by Friedlander[15] *et al*, the nickel being finally precipitated as the dimethylglyoxime salt. The nickel dimethylglyoxime was used as source material for the study of the gamma-radiation. For the beta-ray sources the material was converted to nickel sulfide and deposited on zapon from a water suspension.

The gamma-rays emitted by Ni^{57} were investigated by examining the momentum distribution of the secondary electrons ejected from a radiator. Figure 4 shows the spectrum of the photoelectrons produced from a uranium radiator of considerable thickness (50 mg/cm²). The strong line at 5651 gauss-cm (K_2) corresponds to a gamma-ray of 1.375-Mev energy converted in the K shell of uranium. The L line for this gamma-ray is at 5945 gauss-cm (L_2). The peaks at 2493 gauss-cm and 2861 gauss-cm (K_aL_a) are photoelectron lines for annihilation radiation. There is an indication of a small peak at 7500 gauss-cm (K_3) which corresponds to a K photoelectron line for a 1.914-Mev gamma-ray.

A later experiment in which a lead foil of 16 mg/cm² surface density was used as a radiator showed weak lines at 680 gauss-cm and 1190 gauss-cm (K_1L_1) which indicate a gamma-ray of 0.128-Mev energy. These lines are shown in the inset of Fig. 4. All parts of the gamma-ray spectrum appeared to decay with the same 36-hour half-life.

A comparison of gamma-ray intensities, using Gray's[7] formula for the photoelectric cross-section shows that the ratio of the intensity of annihilation radiation to that of the 1.375-Mev gamma-ray is 0.69. The 1.375-Mev line is approximately six times as intense as that at 1.91 Mev.

The positron spectrum of Ni^{57} has been reported previously[16] and will not be discussed here in detail. The present experiments show that the positron distribution is simple with an end point at 0.835±0.010 Mev. A weak internal conversion line, which corresponds to a gamma-ray energy of 0.128 Mev, was found.

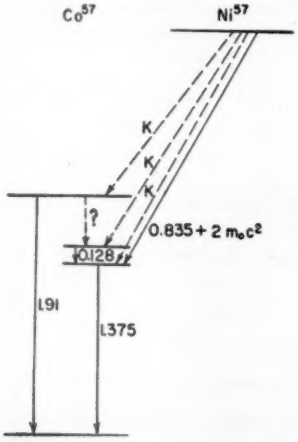

FIG. 5. Proposed disintegration scheme for Ni^{57}.

IIIa. Discussion of the Ni^{57} Experiments

The strongest line in the Ni^{57} spectrum is the gamma-ray at 1.375 Mev. From the coincidence experiments of Maienschein and Meem[14] it is clear that this state is fed by the positron disintegration whose end-point energy is 0.835 Mev. Since the ratio of the number of annihilation quanta to the number of 1.375-Mev quanta is 0.69, it follows that this state is also fed directly by orbital electron capture. The state at 1.9 Mev, from which the line of energy 1.9 Mev arises, is produced entirely by orbital electron capture. The weak internally converted line at 0.128 Mev is probably in parallel with the 1.9-Mev line and in series with the 1.375-Mev line, since gamma-gamma coincidences have been found. It is necessary to assume that the states at 1.9 and 1.50 Mev are populated by orbital electron capture since the positron spectrum is simple. The state at 1.375 Mev is populated both by positron emission and orbital electron capture. Since no other gamma-rays were found besides those mentioned, it would appear that the state at 1.9 Mev loses its activation almost entirely through the emission of the 1.9-Mev gamma-ray to the ground state with very little, if any, emission to the states at 1.50 and 1.375 Mev. This no doubt comes about through the action of selection rules. The decay scheme shown in Fig. 5, while incomplete, is in agreement with all of the information which is available to date on Ni^{57}.

According to the shell model,[12] the ground state of

Ni^{57} should have the configuration $p_{3/2}$ and that of Co^{57} $f_{7/2}$. The present experiments are in agreement with this prediction, since there is no positron decay to the ground state. Since the positron transition to the 1.375-Mev state of Co^{57} is allowed, the configuration of this state is probably $p_{3/2}$. In addition, since the $p_{3/2}$ and $f_{5/2}$ states have nearly the same energy in this region, it is probable that the state at 1.50 Mev has the configuration $f_{5/2}$.

The authors are indebted to Dr. M. B. Sampson and the cyclotron crew for making the bombardments, to Mr. Arthur Lessor for making the chemical separations, and to Dr. R. G. Wilkinson and Mr. Harvey Israel for help with the investigation of the positron spectrum.

PHYSICAL REVIEW VOLUME 83, NUMBER 5 SEPTEMBER 1, 1951

Z Dependence and Angular Distribution of Bremsstrahlung from 17-Mev Electrons*

L. H. Lanzl† and A. O. Hanson
Department of Physics, University of Illinois, Urbana, Illinois

(Received April 16, 1951)

The relative bremsstrahlung cross section for the upper portion of the spectrum as a function of Z, for 17-Mev electrons from a 22-Mev betatron, has been measured. The radiation was detected by means of the $Cu^{63}(\gamma,n)$ induced activity, which has a 10.9-Mev threshold. The effect of atomic screening is small for the quantum energies to which this detector responds, but was taken into account. The results are in agreement with the Bethe-Heitler theory for electron-nuclear interactions within 1 percent. Electron-electron interactions give 0.75 times the intensity for electron-proton interactions, as measured with a copper detector.

The total cross section for radiative energy loss of electrons has been measured with an ionization chamber. The experimental Z dependence of the relative cross section indicates that the yield from gold for a given $N(Z^2+Z)$ is somewhat less than that from low Z elements. This discrepancy might be accounted for by improved corrections for screening, and by more accurate consideration of the radiation produced by electron-electron impacts. Rough measurements of the absolute cross section are in agreement with the Bethe-Heitler theory.

The intrinsic angular distribution of bremsstrahlung, produced in a small amount of cellophane and air, was measured by film and ion chamber, and was found to fit a $1/[1+(E\theta/\mu)^2]^2$ distribution. The angular distribution was measured with three detectors, for one Be and several Au targets. The results are in agreement with calculations in which the above intrinsic distribution and Molière's multiple scattering theory are used.

The central intensity of bremsstrahlung as a function of target thickness, measured with a small ion chamber, is in approximate agreement with a calculation in which the energy loss of the primary electrons has been taken into account.

INTRODUCTION

THE amount of energy radiated during the passage of electrons through matter has been studied by two methods: (1) by measuring the electron energy before and after passage through a given material, the difference in energy being a measure of the total energy loss, which is caused mainly by ionization or excitation, and by radiation; (2) by measuring the bremsstrahlung itself. This latter method was the one used in the experiments to be presented in this paper, the electron source being a betatron.

Blackett[1] and Anderson and Neddermeyer[2] performed cloud-chamber experiments in which the total energy loss of cosmic-ray electrons in lead was determined by the first method. Some typical results obtained by Anderson and Neddermeyer near 30 Mev were about 16 percent lower than predicted by the Bethe-Heitler theory.[3] Although a number of experiments on energy loss have been performed with β-rays, those at energies below about 9 Mev are of little use in a direct check of the theory because of the multiple scattering which the electrons undergo.[4] Results for β-rays of 9 to 13.5 Mev indicate energy losses of about 1.4 times the theoretical values.[5–7]

The electrostatic generator was used by Ivanov *et al.*[8] for calorimetric measurements of the radiation output from a thick lead target, with results lower than given by the Bethe-Heitler theory for bremsstrahlung production and by that of Bloch[9] for collision loss. Buechner and Van de Graaff[10] found experimentally, with 2-Mev electrons from a Van de Graaff generator, and by using a very thick calorimeter, that no energy is carried away by any means other than radiation, e.g., in the form of neutrinos.

Van Atta, Petrauskas, and Myers[11] measured the

* This work was assisted in part by the joint program of the ONR and AEC.

† Now at Argonne Cancer Research Hospital, University of Chicago, Chicago, Illinois.

[1] P. M. S. Blackett, Proc. Roy. Soc. (London) **165**, 11 (1938).

[2] C. D. Anderson and S. H. Neddermeyer, Phys. Rev. **50**, 263 (1936).

[3] H. Bethe and W. Heitler, Proc. Roy. Soc. (London) **146**, 83 (1934); see also H. Bethe, Proc. Cambridge Phil. Soc. **30**, 524 (1934).

[4] M. M. Slawsky and H. R. Crane, Phys. Rev. **56**, 1203 (1939).

[5] W. A. Fowler and J. Oppenheimer, Phys. Rev. **54**, 320 (1938).

[6] A. J. Ruhlig and H. R. Crane, Phys. Rev. **53**, 618 (1938).

[7] J. J. Turin and H. R. Crane, Phys. Rev. **52**, 63 (1937).

[8] Ivanov, Walther, Sinelnikov, Taranov, and Abramovich, J. Phys. (U.S.S.R.) **4**, 319 (1941).

[9] F. Bloch, Z. Physik **81**, 363 (1933).

[10] W. W. Buechner and R. J. Van de Graaff, Phys. Rev. **70**, 174 (1946).

[11] Van Atta, Petrauskas, and Myers, Am. J. Roentgenol. Radium Therapy **50**, 803 (1943).

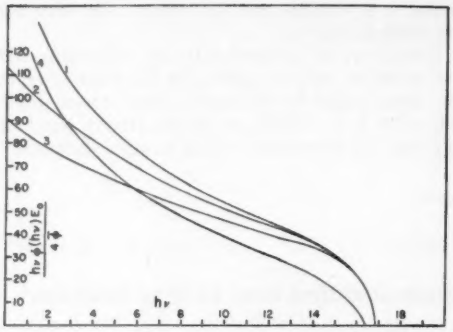

FIG. 1. Bremsstrahlung intensity distribution as a function of quantum energy, $h\nu$, from 16.93-Mev monokinetic electrons. The ordinate is in units of $E_0/4\bar{\phi}$, where $\bar{\phi}=Z^2r_0^2/137$, and E_0=total electron energy in Mev. Curve 1: Unscreened nucleus. Curve 2: Beryllium. Curve 3: Gold. Curve 40: Bremsstrahlung from electron-electron collisions.

angular distribution and efficiency of production of bremsstrahlung in a $\frac{1}{2}$-in. gold target, by monokinetic electrons of incident energies between 0.7 and 2.5 Mev, using a small ion chamber with air-equivalent wall material. The efficiency of bremsstrahlung production, when compared to the Bethe-Heitler theory, was found to be 12 percent lower at 0.9 Mev, 4 percent higher at 1.63 Mev, and 20 percent higher at 2.35 Mev.

Korsunsky *et al.*[12] investigated the Z dependence of the bremsstrahlung cross section over the upper portion of the spectrum by using a wide range of target elements, and found that the amount of radiation produced was proportional to the square of the atomic number as given by the Bethe-Heitler theory. The accuracy of the experimental results, however, was not indicated.

It appeared desirable to obtain information on the efficiency of bremsstrahlung production and the angular distribution of radiation intensities in the neighborhood of 20 Mev, where a larger fraction of the electron energy loss is due to radiation. Experiments were performed in which the bremsstrahlung was produced by an external electron beam from the 22-Mev betatron[13] at the University of Illinois. Measurements on the Z dependence of the bremsstrahlung cross section will be discussed in Part I, while experiments on the angular distribution of radiation from a number of targets will be presented in Part II.

I. Z DEPENDENCE OF BREMSSTRAHLUNG PRODUCTION

A. Theory

Bethe and Heitler[3] have calculated the cross section for the production of bremsstrahlung by relativistic electrons impinging both on an unshielded nucleus and on a nucleus whose field is screened by the orbital electrons of the atom. The bremsstrahlung cross section, $\phi(h\nu)$, is the integral of the differential cross section over all possible directions which the electron may have after radiating, and over all possible directions of the quanta emitted in a given energy interval. The calculations of Bethe and Heitler are based on the Born approximation, the condition of validity of which is $Z/137\ll 1$, if the initial and final electron velocities approach c. Thus, it is by no means certain that this calculation is valid for high-Z elements.

For the case of the unshielded nucleus, Bethe and Heitler found that the cross section for bremsstrahlung production depends on the square of the atomic number. However, the cross section for the shielded nucleus in general does not have a simple Z dependence. The effect of screening by the orbital electrons is to decrease the cross section for the production of low energy relative to high energy quanta. Figure 1 gives the theoretical bremsstrahlung spectra for Be and Au as well as for an unscreened nucleus to be expected from monokinetic electrons of 16.93 Mev. An experimental determination of the bremsstrahlung spectrum from a thin platinum target has been made by Koch and Carter,[14] who found overall agreement with the Bethe-Heitler theory.

In the experiments discussed in Sec. IB, wide-angle detectors were used which had a threshold energy high enough that the difference, between the unscreened and screened cases, of the product of detector sensitivity and number of quanta was only a few percent.

Since the energy sensitivity of the threshold detector used in these experiments is known, the theoretically predicted Z dependence of the bremsstrahlung cross section for a screened nucleus can be compared with the experimental measurements. If the corrections for screening are sufficiently accurate, the experimental results may be adjusted to give the Z dependence of the bremsstrahlung cross section for the bare nucleus.

In addition to the radiation considered above, there is the radiation emitted from the collisions of the incident electrons with the orbital electrons of an atom. Heitler[15] has shown by means of the Weizsacker-Williams semiclassical method of calculating cross sections that the radiation emitted in the collision of two electrons (see Fig. 1) is slightly less than, but has a spectrum similar to, that emitted in a collision of an electron with a nucleus of $Z=1$. Thus, since there are Z orbital electrons for each nucleus, one would expect that the Z dependence of the cross section would be approximately Z^2+gZ for low Z, where g is a numerical factor less than unity, whose value depends on the energy sensitivity of the detector.

The threshold detectors which were used in all of the experiments discussed in Sec. IB were copper foils, in

[12] Korsunsky, Walther, Ivanov, Zypkin, and Ganenko, J. Phys. (U.S.S.R.) **7**, 129 (1943).
[13] D. W. Kerst, Rev. Sci. Instr. **13**, 387 (1942).
[14] H. W. Koch and R. E. Carter, Phys. Rev. **77**, 165 (1950).
[15] W. Heitler, *The Quantum Theory of Radiation* (Oxford University Press, London, 1944), second edition, p. 266.

which the radioactivity induced by the nuclear reaction $Cu^{63}(\gamma,n)Cu^{62}$ was measured. The threshold of this reaction is 10.9 Mev.[16] The average energy of the quanta which activated the copper, assuming the bremsstrahlung spectrum of Bethe and Heitler and the measured[17,18] cross section for the (γ,n) reaction of Cu^{63}, was calculated to be 14.3 Mev for a bremsstrahlung spectrum with a peak energy of 16.93 Mev.

The experiments of Sec. IB give information about the production of high energy quanta. The experiments to be discussed in Sec. IC are concerned with the total energy loss of electrons due to radiation. The cross section for this energy loss is obtained by integrating the intensity, $h\nu\phi(h\nu)$ (see Fig. 1), over the complete energy range, and is given by Heitler[15] as

$$U=E_0\phi_{\text{rad}}=\int_0^{h\nu_{\max}} h\nu\phi(h\nu)d(h\nu). \qquad (1)$$

This total radiation energy loss can be measured fairly directly by the use of ionization chambers, which are sensitive to the total energy incident on them, and whose sensitivity is nearly independent of the energy of the incident quanta.

The primary purpose of the experiments discussed in Sec. IC, as in IB, was to obtain relative rather than absolute cross sections. However, the measurements in Sec. IC were such that some rough absolute values for the cross section for radiation energy loss could be obtained.

B. Cross Section for Upper Portion of Spectrum

For these experiments, the electrons were removed from the betatron by means of a peeler.[19] They were then focused by means of a magnetic lens while passing through an evacuated cylindrical tube which was connected directly to the evacuated donut (see Fig. 2). The focal length of the lens used for these experiments was about 125 cm. Since the electrons, upon leaving the betatron, have a single energy, they can be focused to form a very small image, the size of which is of the order of a few square millimeters.

Just before emerging from the evacuated tube, the electrons passed through a low pressure, cylindrical ion chamber, which served as a monitor for the electron beam current. The ionization current was amplified and kept constant by the betatron operator during an irradiation. To keep multiple scattering of the beam electrons to a minimum, very thin windows were used on the ion chamber. The window between the vacuum system and the ion chamber was made of 0.6 mg/cm² rubber hydrochloride, which can support a maximum air pressure of about 10 cm of mercury. The exit window consisted of 5.21 mg/cm² of Cellophane. The air pressure in the ion chamber was kept at approximately 3 mm of mercury. This ion chamber was calibrated by means of a thick-walled aluminum faraday cage connected to a vibrating reed electrometer. The beam current used in these experiments was about 3×10^{-9} ampere.

The method of electron energy control used was that described by Baldwin and Koch[16] and by others.[20] The energy of the electrons is proportional to the setting of an integrator circuit. In the following experiments, the integrator was calibrated by means of the $Cu^{63}(\gamma,n)$ reaction, which has a threshold of 10.9 Mev.

1. X-Ray Beam With Primary Electrons

In the first technique used to measure the Z dependence of the bremsstrahlung cross section, the x-ray beam was not cleared of electrons. Therefore, the threshold detector was activated by both x-rays and the primary electrons. In the second technique, the primary electrons were removed from the x-ray beam. The first, which was used for two pairs of elements, will be discussed briefly.[21]

Two stacks of seven thin foils each, one composed of copper and the other of alternate copper and gold foils, were irradiated with electrons in the target position shown in Fig. 2. (For this method, the magnetic shield, the final deflecting magnet, and the detector foil shown in Fig. 2 were not used.) The two stacks were irradiated in a holder mounted on a synchronous motor in such a way that alternate electron bursts from the betatron activated the two stacks successively. The motor was operated from the frequency tripler of the betatron power supply, so that the motor and the betatron had a fixed phase relationship. This method insured that

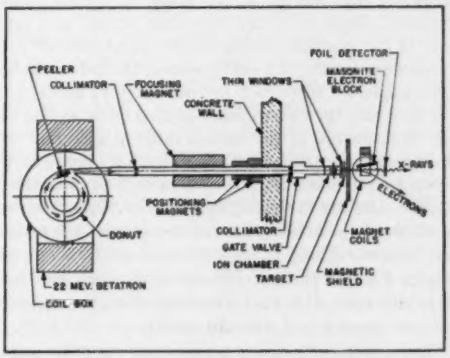

FIG. 2. Schematic drawing (top view) of betatron, focusing magnet, ion chamber, deflecting magnet, and detector position.

[16] G. C. Baldwin and H. W. Koch, Phys. Rev. **67**, 1 (1945).
[17] Johns, Katz, Douglas, and Haslam, Phys. Rev. **80**, 1062 (1950).
[18] B. C. Diven and G. M. Almy, Phys. Rev. **80**, 407 (1950).
[19] Skaggs, Almy, Kerst, and Lanzl, Phys. Rev. **70**, 95 (1946); Radiology **48**, 215 (1948).
[20] McElhinney, Hanson, Becker, Duffield, and Diven, Phys. Rev. **75**, 542 (1949); Katz, McNamara, Forsyth, Haslam, and Johns, Can. J. Research **A28**, 113 (1950).
[21] See L. H. Lanzl, Ph.D. thesis, University of Illinois (1951), for more complete discussion.

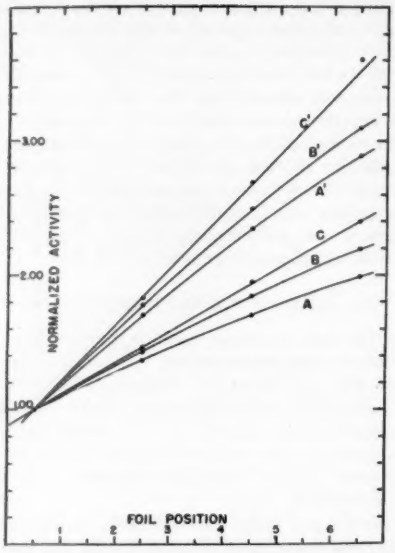

FIG. 3. Normalized activities in Cu−Cu and Cu−Au stacks *vs* foil position for 16.18-Mev electrons. Upper set of curves: Cu−Au stack. Lower set of curves: Cu−Cu stack. *A*, *A'*: Normalized activity. *B*, *B'*: Curves *A*, *A'* corrected for decrease in electrodisintegration cross section with electron energy. *C*, *C'*: Curves *B*, *B'* corrected for decrease of peak photon energy caused by energy loss of electrons. Foil thicknesses: 46.58 mg/cm² (Cu); 52.35 mg/cm² (Au). Each stack contained 7 foils.

the two foil stacks were irradiated with the same electron beam current.

After irradiation, the activities induced in the four odd-position copper detector foils of each stack were measured by means of an array of Geiger-Müller counters. These activities were then plotted as a function of foil position, giving nearly linear curves[22] after corrections for electron energy loss in the foil stacks had been applied. Corrections are necessary to account for the fact that the electrodisintegration cross section and the peak energy of the bremsstrahlung spectrum produced decrease with decreasing electron energy as the electrons traverse a foil stack, since both of these effects cause a decrease in the induced activity. Using the ratio of slopes of the activity curves, one obtains the ratio of the bremsstrahlung cross sections of gold and copper. Figure 3 shows the activity curves obtained for 16.18-Mev electrons, with the corrections which were applied, for the Cu−Cu and Cu−Au stacks.

This experiment gave a bremsstrahlung cross section ratio for gold to copper of 7.15 ±1.0 percent. This result is to be compared with the cross-section ratio as calculated from the Bethe-Heitler theory for a copper detector. The theoretical ratio is 7.28 for $g=0$ (g is defined in Section *A*), and 7.13 for $g=1$. It is to be noted that these calculated values differ from the simple Z^2 ratio by only 2 percent. In an early report on this method,[23] some preliminary results were given for which the energy loss corrections had been neglected. The ratio of bremsstrahlung cross sections thus found was about 8 percent higher than that obtained when the corrections had been applied.

From a similar measurement, the cross section ratio of aluminum and copper was found to be 0.210 ±1.7 percent. The corresponding theoretical ratios are 0.203 and 0.211, for $g=0$ and 1, respectively.

A modification of this method involved the irradiation of two stacks of thin foils in which the theoretical collision and radiation losses had been made equal. One stack consisted of copper and the other, of gold and aluminum foils. The radiation produced was detected by a copper foil placed behind each stack. The bremsstrahlung cross section ratio of gold to copper was found using the measurement of the Al−Cu ratio given above. The experimental value thus obtained was 7.21 ±1.2 percent. For this experiment, the kinetic energy of the electrons was 17.98 Mev. At this energy, the theoretical values are 7.25 and 7.10 for $g=0$ and 1, respectively.

For this latter method, the corrections for the degradation of the primary electron energy amounted to only 0.7 percent since the energy losses in the two stacks had been closely matched.

2. *X-Ray Beam Free of Primary Electrons*

(*a*) *Apparatus and Procedure.*—Figure 2 shows schematically the experimental setup for the technique using an electron-free x-ray beam.[24] The radiators were placed as close as possible to the exit window of the ion chamber. They were supported in a holder which was guided by ways rigidly fastened to a 1 in.-thick iron magnetic shield. The purpose of this shield was to avoid deflecting the beam electrons before they passed through the target.

An electromagnet with wedge-shaped poles which subtended a half-angle of 10° at the target provided the magnetic field. In the vertical direction, the two poles would intercept the few electrons which underwent large angle scattering. In the horizontal direction, an electron block, consisting of masonite, was used for the same purpose, absorbing electrons scattered at angles greater than 10° as measured from the target position. Thus, scattered primary electrons were kept from reaching the detector.

The detector foils were accurately cut circular sheets, 3 in. in diameter, 0.005 in. thick. These were paired and selected so that the weight of any pair differed by no more than 0.15 percent from the mean weight. During irradiation, the detectors were held in place by means

[22] Skaggs, Laughlin, Hanson, and Orlin, Phys. Rev. **73**, 420 (1948).

[23] Lanzl, Laughlin, and Skaggs, Phys. Rev. **74**, 1261 (1948).

[24] Some results obtained by this method were reported recently: L. H. Lanzl and A. O. Hanson, Phys. Rev. **81**, 309 (1951).

of a foil holder mounted rigidly on the magnet base. The center of the holder, which corresponded to the center of the detector, was adjusted to be on the axis of the x-ray beam. The alignment of the holder was checked radiographically. The detector subtended a half-angle of 5.7° at the target position.

During each irradiation, two detector foils were exposed, one being placed directly behind the other. The activated foils were counted simultaneously, being mounted above and below a Geiger-Müller counter, in a cylindrical holder whose axis coincided with the central wire of the counter. During irradiation, the detector foils were held flat and perpendicular to the beam; during the counting period, the foils were bent so as to lie in complete contact with the inner surface of the cylindrical holder.

(*b*) *Measurements and Results.*—Two sets of radiator thicknesses were used. Within each set, the quantity $N(Z^2+Z)$, where N is the number of atoms per cm², and $Z=4$, 13, 29, 47, 79, was made approximately the same for each target. Between sets, $N(Z^2+Z)$ differed by a factor of 2 for each element. Except for the Be, the targets were cut by a 1 in.×$\frac{3}{4}$ in. die. The Be had been obtained in the form used for the experiments.

Since the beam electrons lose energy, due to ionization and radiation, as they penetrate a target, an appropriate correction has to be applied to the measured activity. For this purpose, the activity induced in a detector as a function of the energy of the incident electrons must be known. This relation was determined (Fig. 4) by irradiating one of the thin gold targets at various electron energies and measuring the activity induced in a pair of detector foils. In this gold target, the ionization energy loss is practically negligible, namely 0.050 Mev for 16.93-Mev electrons. The activity of the detector in this geometry increases slightly faster than the function $(E-E_{th})^3$, where E_{th} is the threshold energy, 10.9 Mev, of the copper detector. The activities in this and in all the other irradiations under this method were normalized to the same electron beam current.

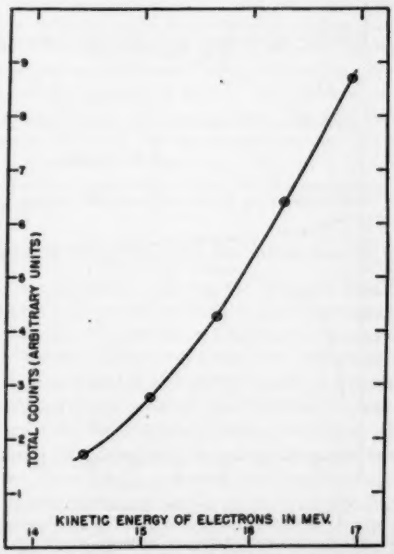

FIG. 4. Activity in copper detector, induced by x-rays from gold radiator, vs energy of incident electrons. Target: 37.28 mg/cm² of Au.

TABLE I. Results of experiment on bremsstrahlung production as a function of Z. Incident electron energy = 16.93 Mev.

Element	Thickness (mg/cm²)	Incident energy minus ½ ionization energy loss = average energy (Mev)	Average net activity (original data)	y_a / $\overline{N(Z^2+0.75Z)}$ normalized to Au	Theory (Bethe-Heitler) ϕ/Z^2 normalized to Au
Thin series					
Be	257.0	16.69	3921	1.042±0.9%	1.046
Al	84.11	16.85	4266	1.021±1.9%	1.033
Cu	41.00	16.90	4338	1.016±0.5%	1.021
Ag	29.26	16.91	4748	1.020±1.3%	1.011
Au	18.31	16.92	4554	1.000±0.7%	1.000
Thick series					
Be	491.3	16.47	6128	1.045±0.5%	1.046
Al	168.2	16.77	7546	1.031±0.5%	1.033
Cu	90.91	16.85	8465	1.022±0.8%	1.021
Ag	54.52	16.89	8036	1.019±1.2%	1.011
Au	37.28	16.90	8353	1.000±0.5%	1.000

[a] Y is the activity corrected for energy loss of electrons and fraction of radiation intercepted by detector.

A background count, induced in a pair of detectors when the betatron was run without a target, i.e., when radiation was produced by the electrons in the exit window and in the intervening air, was measured and later subtracted from the counts obtained with targets.

To determine the fraction of the radiation produced in the targets which passed through the detector foils, measurements of the angular distribution of intensities were made, using copper detectors. These measurements indicated that 82 percent of the radiation from the series of thick targets was intercepted by the detector. The measurements on Be and Au appear in Fig. 12. It may be noted here that, in doubling $N(Z^2+Z)$, the relative total induced activity was increased by a factor of 1.9 rather than 2, the difference being due to additional radiation bypassing the detector in the case of the thicker series.

The irradiation times for this experiment were 6 minutes each, and the counting periods, 8 minutes. Including the background measurements, a total of 64 irradiations was made and the activities measured. The average original data for the thick and thin targets, corrected for the air and window background, and also

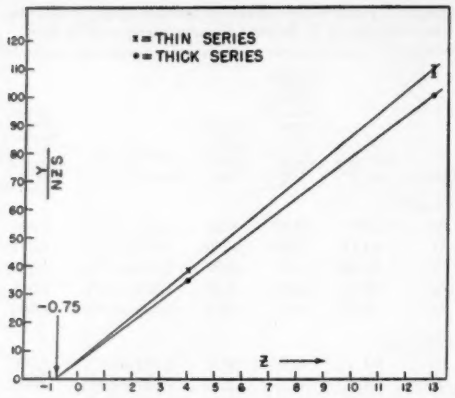

FIG. 5. Graph of relative activity divided by NZS, *vs* Z, for thin and thick series. The intercept with the Z axis gives the value of $g=0.75$.

the values of the thicknesses of the targets are presented in Table I.

(*c*) *Analysis of Results.*—The measured activities were corrected for electron energy loss by means of the experimentally determined relation (Fig. 4) between induced activity and electron energy. Each activity was increased by the ratio of the activity at the incident electron energy, 16.93 Mev, to the activity at the average energy of the electrons in the target, this ratio being obtained from Fig. 4. For each target, the average energy used was the incident energy reduced by one-half that lost by ionization.

A further correction of the measured activities was made for slight variations in the fraction of the total radiation intercepted by the detector, from each target within a series. Figure 11 shows that the angular distribution of radiation for the thick Be foil very nearly matched that of the thick Au foil. Therefore, the fractional amount of radiation intercepted by the detector was considered to be the same, and no correction was applied. The $N(Z^2+Z)$ value for the thick Be foil was 10 percent less than that of the thick Au foil. Corrections were made for the other targets by interpolating between Be and Au. However, since the $N(Z^2+Z)$ values of these targets were fairly well matched, these corrections were small, their average amounting to 0.5 percent.

It follows from the discussion in Sec. IA that the cross section for bremsstrahlung production can be represented approximately by $NS(Z^2+gZ)$, where S is the screening factor and g, the fractional effectiveness of electron-electron relative to electron-proton radiation. The data of the present experiment can be used to determine g. The corrected activities, divided by SNZ, were plotted as a function of Z. A simple analysis shows that g is given by the intercept of this curve with the Z axis. As shown in Fig. 5, this value was found to be 0.75, with an error of approximately ±0.05.

This may be compared to a theoretical value of 0.54, as obtained by the relation,

$$g=\frac{\int_{10.9\ \text{Mev}}^{16.93\ \text{Mev}}\beta_{\text{Cu}}(h\nu)\phi_{e-e}(h\nu)d(h\nu)}{\int_{10.9\ \text{Mev}}^{16.93\ \text{Mev}}\beta_{\text{Cu}}(h\nu)\phi_{e-p}(h\nu)d(h\nu)},$$

where $\phi_{e-p}(h\nu)$ and $\phi_{e-e}(h\nu)$ are, respectively, the bremsstrahlung cross sections given by Heitler[25] for electron-proton and electron-electron collisions, and $\beta_{\text{Cu}}(h\nu)$ is the photodisintegration cross section for copper.[17,18] The experimental value of g will be used in the subsequent analysis.

The relative activities, divided by $N(Z^2+0.75Z)$, are

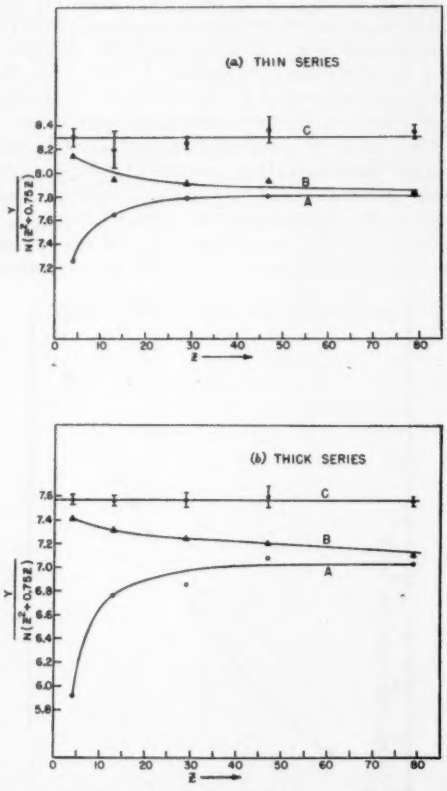

FIG. 6. Graphs of relative activity divided by $N(Z^2+0.75Z)$, *vs* Z. Curve A: uncorrected activities. Curve B: activities corrected for ionization loss of the electrons in the target and for the fraction of radiation intercepted by the detector. Curve C: adjusted for screening. (*a*) Thin series; (*b*) Thick series.

[25] See reference 15, pp. 165, 266.

shown as a function of Z in Figs. 6(a) and 6(b), for the thin and thick target series, respectively. The points on curve A in each of the figures are the uncorrected activities. Curve B, a plot of the corrected activities, gives the variation of the relative bremsstrahlung cross sections as a function of Z, as measured by a copper detector. The corresponding theoretical values, which appear in column 6 of Table I, include the small screening corrections and are calculated for electron-nuclear collisions only. For comparison with the experimental values, they are divided by Z^2 rather than by Z^2+Z.

(d) *Discussion of Results.*—It can be seen from Table I that the experimental results are in very good agreement with the theoretical values when the value of g is taken as 0.75. It should be pointed out that this value will be changed only slightly even if there are large errors in the screening calculations. The remaining variation of curves B indicated in Figs. 6(a) and 6(b) must represent the variation in the Z dependence of the cross section for electron-nuclear collisions not accounted for by the Z^2 term.

If one raised the corrected measurements, shown in curves B, by the screening factor, $1/S$, one would obtain values which represent the bremsstrahlung from radiative collisions with unscreened nuclei and electrons. The screening decreases the radiation by 2.1 percent for beryllium and 6.2 percent for gold. The experimental yields, modified in this manner, appear in the upper curves, C, of Figs. 6(a) and 6(b) for the thin and thick target series, respectively. These points lie very close to a line parallel to the abscissa, i.e., a line where the yield varies as $N(Z^2+0.75Z)$, and therefore indicate that the radiation from an unscreened nucleus varies as Z^2 within the experimental error of about 1 percent.

A comparison of the results from both series, adjusted for screening, appears in Fig. 7. The yields were normalized to the gold foil in each series. The solid lines on this graph represent the variation of the expected yield with Z, assuming g values of 0, 0.75, and 1. It can be seen that the shape of the curves is very sensitive to the choice of g.

C. Cross Section for Total Radiative Energy Loss

The measurements with copper detectors, which are sensitive to the upper portion of the bremsstrahlung spectrum, are of value in determining the dependence of the bremsstrahlung cross section on nuclear charge, since the production of high energy quanta is, relatively, little affected by the presence of orbital electrons. In the experiment to be discussed here, a detector whose response is almost independent of the quantum energy was used, thus giving a measurement of the total energy loss of electrons due to radiation, U [Eq. (1)]. It can be seen from Fig. 1 that relatively more low energy quanta are radiated from the lower Z elements. This additional radiated energy appears as an increase in the total radiation loss, which amounts to 10 percent

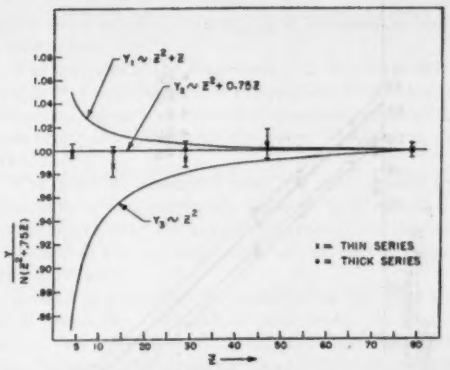

FIG. 7. Graph of $N(Z^2+gZ)/N(Z^2+0.75Z)$ *vs* Z, for $g=0$, 0.75, and 1. The experimental values, normalized to 1 at gold, are also given for the thin and thick series.

for a beryllium as compared to a gold target with the same value of $N(Z^2+Z)$.

Although the primary purpose of these experiments was to investigate the Z dependence of the total radiative energy loss of electrons, it was also possible to obtain rough measurements of the absolute values.

1. Victoreen R Thimble in Aluminum Block

The experimental setup for the absolute radiative energy loss of electrons was nearly the same as that used in the determination of the Z dependence of the bremsstrahlung cross section with copper detectors. As before, the electron beam was deflected magnetically after passing through the target (see Fig. 2). For this experiment, a stack of three copper foils, three inches in diameter, and with a total thickness of 0.1991 g/cm², was used as a radiator. The detectors were placed in an aluminum block containing two holes, each of such a size that a 25-roentgen Victoreen thimble could be inserted. During irradiation, one of these holes contained the thimble and the other, a fourth copper disk which was folded in such a way that it subtended very nearly the same solid angle at the target as did the thimble. The holes were aligned with the axis of the x-ray beam, the copper foil occupying the position behind the Victoreen thimble. The thickness of aluminum in front of the detector foil was 5.08 cm, and in front of the thimble, 4.05 cm. The thimble was located 112 cm behind the target, a distance which is great enough that the x-ray beam is considerably wider than the detectors. The thickness of the detector foil was 0.0471 g/cm². This was also the thickness of the first and third radiator foils.

Following an irradiation of 20 minutes, the activities of the first and last foils in the target stack, and of the foil in the aluminum block, were counted. The counting geometry was the same as that described in Sec. IB2. The measured counts were corrected for differences in

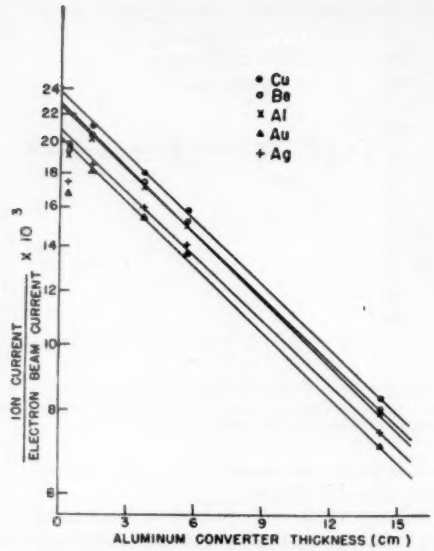

FIG. 8. Ionization current from wide-angle ionization chamber *vs* converter thickness, for five radiators.

the activity distributions on the three foils, and were reduced to the same time interval. The R meter, which had been exposed simultaneously, was read at the end of the irradiation period.

The activity induced in the first foil of the target stack is mainly due to electrodisintegration, whereas that in the last foil is due to the sum of electrodisintegration and photodisintegration activities, the quanta being produced in all three foils. The difference between the activities of the first and third foils is thus a measure of the integrated intensity or total x-ray flux, C_t. The activity per unit area, C_d/A, in the foil placed in the aluminum block is, on the other hand, a measure of the radiation intensity at the R meter.

Since the detector foil was placed at a depth of 5.08 cm within the aluminum block, a correction for absorption of the x-rays had to be applied to the measured activity. In the calculation of the total relative activity due to photodisintegrations produced in the last target foil, several corrections have to be applied. The decrease of the electron energy, and the subsequent decrease of the electrodisintegration cross section, were taken into account. The corrected activities of the first and last copper foils were plotted as a function of foil thickness, at the midpoints of their respective thicknesses. The activity extrapolated to the total thickness of the target, minus the extrapolated zero-thickness activity (electrodisintegration activity), is C_t.

The ratio between the integrated yield, C_t, and the count per unit area for the foil at the position of the R thimble, C_d/A, represents the effective area of the x-ray beam at the position of the R thimble. This ratio, C_tA/C_d, was found to be 327 cm². The ratio of the R meter reading in roentgens/min to the saturated activity in counts/min induced in the copper detector, for the particular counting geometry used, is about 3.8×10^{-4} roentgen per count. The total energy radiated can then be obtained from the central yield, Y, as measured by the thimble. Specifically, the total energy radiated is

$$U=(C_tA/C_d)(Y/K),$$

where K is the ionization produced at a depth x in the aluminum by one Mev of bremsstrahlung incident on the surface of the block. K is calculated from the formula,

$$K=\frac{\int_0^{16.93\ \text{Mev}} I(h\nu)\phi(h\nu)\exp(-\mu(h\nu)x)d(h\nu)}{\int_0^{16.93\ \text{Mev}} h\nu\phi(h\nu)d(h\nu)}, \quad (2)$$

where $h\nu$ = quantum energy; $I(h\nu)$ = ionization in units of ion pairs/cc per quantum/cm², as given by Fowler *et al.*;[26] $\phi(h\nu)$ = number-of-quanta spectrum (bremsstrahlung cross section; ordinate of Fig. 1 divided by $h\nu$) for copper; x = thickness of aluminum converter; μ = absorption coefficient in cm⁻¹ for x-rays in aluminum, where $\mu=\mu_{ph}+\mu_c+\mu_p$ and μ_{ph} = photoelectric absorption coefficient, μ_c = Klein-Nishina (Compton) absorption coefficient, and μ_p = pair production absorption coefficient. The values of these coefficients were taken for the most part from graphs by Evans.[27] K is relatively insensitive to the exact shape of the bremsstrahlung spectrum. At a depth $x=4.05$ cm, K has a value:

$$K=0.633 \text{ ion pair/cm Mev}$$
$$=3.02\times10^{-10} \text{ roentgen cm}^2\text{/Mev}. \quad (3)$$

The yield, Y, as measured by the Victoreen thimble, was 1.11×10^{-3} roentgen per second per 10^{-9} ampere of incident electron current. This gives

$$U=1.20\times10^{9} \text{ Mev/sec per } 10^{-9} \text{ amp.}$$

The theoretical value for copper, based on the Bethe-Heitler theory, was calculated to be 1.33×10^{9} Mev/sec per 10^{-9} amp. The error to be assigned to the Victoreen reading is about 5 percent, and errors of approximately this magnitude may be expected in the measurement of the incident beam current. Thus, the result appears to be in agreement with theory.

[26] Fowler, Lauritsen, and Lauritsen, Revs. Modern Phys. **20**, 236 (1948). J. D. Lawson, A.E.R.E. Report G/R 555, reports a result for K about 4 percent lower than the one used here. The difference is probably smaller than the errors in the calculations.

[27] R. D. Evans and R. O. Evans, Revs. Modern Phys. **20**, 305 (1948).

2. Wide-Angle Ionization Chamber

(*a*) *Experimental Apparatus and Procedure.*—The apparatus used in this experiment was the same as the foregoing, with the exception that the detector was a thick-walled ionization chamber, with a flat, air-filled cylindrical cavity 10.2 cm in diameter and 0.389 cm deep. The axis of the cylinder was aligned radiographically with the axis of the x-ray beam. The chamber was completely surrounded by grade 2S aluminum. The aluminum converter thickness was varied in the course of the experiment. The ionization current was measured with a vibrating reed electrometer. The ion chamber subtended a total angle of 11.6° at the target.

The radiators were the thick series used in the experiment discussed in Sec. IB2. The incident kinetic energy of the electrons was again 16.93 Mev.

The yield from this series of targets was also measured by two other ion chambers of smaller diameters, which subtended angles of 1.73° and 0.78°.

(*b*) *Results and Analysis.*—The results of the yield measurements using the 11.6° ion chamber with various thicknesses of an aluminum converter are presented in Fig. 8. The ordinate is the ratio of the detector ion current to the electron beam current, both of which were known by absolute measurements. The abscissa gives the thickness of the converter in cm.

As in the previous measurement of the total radiative energy loss, the ionization, $I(h\nu)$, of Fowler *et al.*,[26] for an air ion chamber with an aluminum converter, was used. Although their calculation was carrried out for a small air cavity ion chamber embedded in a large block of aluminum, upon which a wide, parallel beam was incident, the use of the above ionization function is nevertheless valid, since the ion chamber in this experiment intercepted nearly all of the radiation, and was used to obtain the integral of the intensity over a large fraction of the total radiation.

The constant K of the ion chamber, given by Eq. (2) above, was calculated for Be, Cu, and Au targets, and for a converter thickness of 4 cm. In this calculation, the spectra given in Fig. 1 were used, the nuclear spectrum being weighted by the factor $Z^2/(Z^2+Z)$ and the electron spectrum, by $Z/(Z^2+Z)$. For these three target elements, the value of K was found to be the same within 1 percent. Also, K (for gold) was calculated[28] from Eq. (2) for $t=0$, 1, 2, 8, and 16 cm, as well as for 4 cm. For these converter thicknesses, it was found that K could be very well represented by an exponential function,

$$Kd=1.263\times10^{-19}e^{-\lambda t}d \text{ coulombs/Mev}, \qquad (4)$$

where d=thickness of the air gap of the ion chamber, t=thickness of the aluminum converter, and $\lambda=0.056$ cm^{-1} is the calculated absorption coefficient. This representation is exact for $t=0$ and 1 cm, and differs from the exact value by only 2 percent for a thickness of 16 cm of aluminum.

The fraction of the total energy in the beam intercepted was calculated from the angular distribution of radiation, measured with a small ion chamber, from the gold target of 37.28 mg/cm^2 thickness. The fraction was 0.843.

The yield as measured with the two smaller ion chambers, which subtended angles of 1.73° and 0.78° at the target, gave the same Z dependence for the relative yield as did the larger detector, within the experimental accuracy.

Instead of using the data presented in Fig. 8 for any finite converter thickness in comparing the experimental and theoretical yields, the yield extrapolated to zero thickness (neglecting the smallest converter thicknesses, where equilibrium of radiation and secondary electrons has not yet been reached) was used in connection with Eq. (4) to obtain the radiative energy lost by the electrons as they pass through a target. It is to be noted that the experimental slopes as given in Fig. 8 fit a value of $\lambda=0.07$ rather than the calculated value of 0.056. The absolute cross section as a function of atomic number is presented in Fig. 9, along with the theoretical values times $(Z^2+Z)/Z^2$ as calculated from the Bethe-Heitler theory for electron-nuclear radiative collisions. The ordinate is plotted in terms of $\phi_{rad}/(Z^2+Z)$, where ϕ_{rad} is the cross section for the total radiative energy loss, as given earlier, and has the dimensions of cm^2.

The curve indicates that the measured absolute cross section is about 10 percent lower than theory for gold. The experimental errors are estimated to be of the order of 10 percent. The discrepancy is probably due to the measurement of the electron beam current and to the ion chamber response.

The variation of the experimental cross section with Z is expected to be more reliable than the absolute values. It can be seen in Fig. 9 that relatively more energy is radiated from low Z materials than is pre-

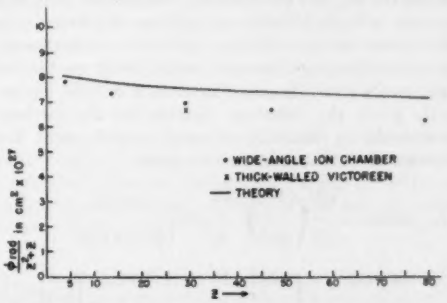

FIG. 9. Cross section, ϕ_{rad}, for radiative energy loss by electrons, divided by (Z^2+Z), vs Z. Solid line is calculated from Bethe-Heitler theory. (Z^2 replaced by Z^2+Z in formula for electron-nuclear interactions.) Experimental results are from measurements using ionization chambers.

[28] This calculation was carried out by D. Schiff.

dicted by theory, for foils of the same $N(Z^2+Z)$ value. This discrepancy amounts to about 10 percent between beryllium and gold.

D. Summary

The experimental results on the Z dependence of bremsstrahlung cross sections with a threshold detector and an ion chamber can be summarized as follows:

1. The radiation cross section for the unshielded nucleus is proportional to Z^2 to within 1 percent for the upper portion of a spectrum having a maximum energy of 16.93 Mev. This is in agreement with the theory based on the Born approximation.

2. Electron-electron collisions are found to give 0.75 times the radiation, in the high energy region, expected for electron-proton collisions. The value calculated for this number from theory is 0.54.

3. Rough measurements of the absolute yields of x-rays are in agreement with the Bethe-Heitler theory. There is, however, an indication that the relative yield from a gold target with the same $N(Z^2+Z)$ is somewhat less than that from low Z elements. It is possible that the discrepancy may be accounted for by improved corrections for screening and more accurate consideration of the radiation produced by electron-electron impacts.

II. ANGULAR DISTRIBUTION OF RADIATION FROM FAST ELECTRONS

A. Theory

Measurements were made to determine the angular distribution of radiation emitted at small angles with respect to the direction of the primary electron beam, from targets of various thicknesses. Besides being of intrinsic interest, the angular distribution of radiation is important in many experiments, especially in those for which some knowledge of the total amount of radiation in a given beam is desired.

Stearns[29] and Hough[30] have derived expressions concerning the angular distributions of radiation from fast electrons in a single radiative collision. However, these calculations are not directly applicable in the energy region and the range of angles, respectively, used in the experiments to be discussed here. L. I. Schiff[31] has recently given the following formula for the intrinsic bremsstrahlung intensity at small angles about the direction of the incident electron beam:

$$\sigma(K,x)dKdx=\frac{4Z^2}{137}\left(\frac{e^2}{mc^2}\right)^2\frac{dK}{K}xdx\left\{\frac{16x^2E}{(x^2+1)^4E_0}-\frac{(E_0+E)^2}{(x^2+1)^2E_0^2}+\left[\frac{E_0^2+E^2}{(x^2+1)^2E_0^2}-\frac{4x^2E}{(x^2+1)^4E_0}\right]\ln M(x)\right\},$$

where

$$\mu=mc^2,\quad K=h\nu=E_0-E,\quad x=E_0\theta_0/\mu,$$

$$\frac{1}{M(x)}=\left(\frac{\mu K}{2E_0E}\right)^2+\left(\frac{Z^{\frac{1}{3}}}{111(1+x^2)}\right)^2.$$

For the present work the angular distribution was represented by a simpler expression which does not take into account the variation of the angular distribution with the energy of the radiation, namely,

$$F(\theta_0)=1/[1+(E_0\theta_0/\mu)^2]^2. \tag{5}$$

The fact that the average intrinsic angular distribution is fairly well represented by Eq. (5) will be seen from data using a thin target, which will be presented in the next section.

In an actual experiment, however, either a foil or a volume of gas is employed, so that the angular distribution of the resulting quanta is modified by the multiple scattering of electrons in the target material before radiation takes place. The effect of a large number of target nuclei is to increase the width of the radiation beam over that produced by an infinitely thin foil. Lawson[32] and Schiff[33] have derived expressions for the ratio of the radiation intensity per unit solid angle at an angle θ to the intensity at $\theta=0$. Schiff's calculation uses the theory of multiple scattering developed by Williams,[34] whereas Lawson's calculation uses the theory of Rossi and Greisen.[35]

The experimentally observed x-ray beam widths are somewhat narrower than those calculated using either of the two formulations of the theory mentioned above. This disagreement is consistent with the observation that the multiple scattering widths used in these theories are too large.[36] Baldwin *et al.*[37] have also reported narrower widths for high Z elements with 70-Mev x-rays.

In order to calculate the expected x-ray beam widths more easily than is possible with the form of Eq. (5), the above angle factor was represented by the sum of two gaussian distributions, with constants chosen graphically:

$$1/[1+(E_0\theta/\mu)^2]^2\leqq 0.85\exp[-(E_0\theta/\mu\theta_1)^2]+0.15\exp[-(E_0\theta/\mu\theta_2)^2],$$

with $\theta_1^2=0.553$ rad^2 and $\theta_2^2=2.85$ rad^2. The greatest deviation from Eq. (5), over the range of angles from 0° to 10°, amounts to less than 5 percent.

To obtain an expression for the angular distribution of the x-ray beam from the above expressions, it is necessary to consider the multiple scattering distribution at any depth t. Experiments on multiple scattering of electrons[36] in gold are in good agreement with

[29] M. Stearns, Phys. Rev. **76**, 836 (1949).
[30] P. V. C. Hough, Phys. Rev. **74**, 80 (1948).
[31] L. I. Schiff, Phys. Rev. **83**, 252 (1951).
[32] J. D. Lawson, Proc. Phys. Soc. **A63**, 653 (1950).
[33] L. I. Schiff, Phys. Rev. **70**, 87 (1946).
[34] E. J. Williams, Phys. Rev. **58**, 292 (1940).
[35] B. Rossi and K. Greisen, Revs. Modern Phys. **13**, 240 (1941).
[36] Lyman, Hanson, Lanzl, and Scott, Phys. Rev. **81**, 309 (1951).
[37] Baldwin, Boley, and Pollock, Phys. Rev. **79**, 210 (1950).

Molière's theory,[38] but give $1/e$ widths 10 percent narrower than predicted by the theories of Williams, Snyder and Scott, and Goudsmit and Saunderson.[39] Molière's expression was approximated by a gaussian function of the form $\exp(-E_0^2\theta^2/ct)$ (E_0 = effective electron energy in the foil), with c chosen to give the same $1/e$ value as the exact expression. The factor c was determined from Molière's theory for gold, which agrees with the experimental measurements; for beryllium, the experimental values were used.

The convolution of the multiple scattering distribution with that for the intrinsic distribution, when integrated over the total target thickness, gives the following form:

$$P(\theta, E_0)=\frac{0.85\theta_1^2\left[-\mathrm{Ei}\left(-\frac{E_0^2\theta^2}{ct+(\mu\theta_1)^2}\right)+\mathrm{Ei}\left(-\frac{E_0^2\theta^2}{(\mu\theta_1)^2}\right)\right]+0.15\theta_2^2\left[-\mathrm{Ei}\left(-\frac{E_0^2\theta^2}{ct+(\mu\theta_2)^2}\right)+\mathrm{Ei}\left(-\frac{E_0^2\theta^2}{(\mu\theta_2)^2}\right)\right]}{0.85\theta_1^2\ln[1+ct/(\mu\theta_1)^2]+0.15\theta_2^2\ln[1+ct/(\mu\theta_2)^2]}, \quad (6)$$

where Ei is the exponential integral function. This expression is similar to that given by Lawson.[32]

Experiments which have been performed using targets such as the standard betatron target or metal wires cannot be compared with theory because the target thickness is not uniform. Measurements on the angular distribution were made by Lawson[32] at 10 Mev, with a thin, uniform gold target, and by Koch and Carter[14] at 19.6 Mev, with a thin platinum target. The angular width found by Lawson is somewhat greater than that given by Schiff's theory, while the measurement of Koch and Carter is in agreement with this theory.

B. Measurements and Procedure

A number of measurements on the angular distribution of radiation were made, using a focused 16.93-Mev electron beam from the betatron. The experimental arrangement was the same as that described earlier, in which an electron-free x-ray beam was used to measure the Z dependence of the cross section for bremsstrahlung production (Fig. 2). Again, the beam, before striking a target, passed through the two thin windows of the ion chamber monitor, and through approximately 2 inches of air, about one inch of this path being in front and one inch behind the target.

Measurements were made on uniform Be and Au targets. For Be, only one target thickness was used, while the thicknesses of gold ranged from 0.7 mil to 600 mils. One of the three types of detectors used was Industrial-A x-ray film, exposed with and without a $1\frac{3}{4}$ inch thick presdwood converter. This film, used because of the linearity of its dose-density curve,[40] was developed in D-19b under standard conditions of developing time, temperature, agitation, and fixing time. During exposure, the film was held in a standard Eastman cardboard cassette containing five mils of lead backing, placed perpendicular to the beam, $15\frac{1}{8}$ inches from the target. Densities were measured by means of a Weston photographic analyzer, calibrated against an Eastman transmission densitometer. The angular resolution, determined by the diameter of the densitometer field, was 0.15°.

A second detector used was a small cylindrical, lead-walled ion chamber of $\frac{1}{2}$ in. inside diameter, $1\frac{1}{2}$ in. inside length, and a wall thickness of $\frac{1}{8}$ in. The ion chamber was placed 30.75 in. behind the target, its axis parallel to the central ray of the x-ray beam, and subtended an angle of 0.9° at the target. Its current was measured with a vibrating reed electrometer. For measuring the current at various angles, the chamber was moved by remote control both horizontally and vertically by means of a pair of Selsyn motors.

A row of copper cylinders, 1 in. in outside diameter and $1\frac{1}{2}$ in. long, with a $\frac{1}{16}$-in. wall, was another type of detector used. These cylinders were placed $51\frac{1}{16}$ in. behind the target with their axes vertical, and set side by side in a straight line perpendicular to the beam axis. By this method, only the horizontal distribution of intensities was measured, with an angular resolution of 1.1°. A number of cylinders was thus irradiated simultaneously, and the induced activities then counted successively with a Geiger counter.

The angular distribution of x-rays from the windows of the ion chamber and the short air path gives a fair measurement of the intrinsic angular distribution. The distributions from the thicker targets, on the other hand, are determined primarily by multiple scattering.

A special run was made in which the small lead-walled ion chamber was held in a fixed position along the central ray of the x-ray beam, and the yields from the various gold foils were measured. An analysis of these data is given in Sec. IID.

A series of measurements was made in which wide-angle copper detectors were used to find the relative amount of radiation produced in various gold targets. One detector subtended an angle of 180° and the other, 11.4° at the target.

C. Results Using Small-Angle Detectors

The angular distribution measurements, made with the small lead ion chamber and with film, on the radiation produced in the monitor windows and in the air traversed by the electrons near the target were in good

[38] G. Molière, Z. Naturforsch. **3a**, 78 (1948).
[39] E. J. Williams, Proc. Roy. Soc. (London) **169**, 531 (1939); S. Goudsmit and J. L. Saunderson, Phys. Rev. **58**, 39 (1940); H. Snyder and W. T. Scott, Phys. Rev. **76**, 220 (1949).
[40] G. D. Adams, Ph.D. thesis, Part II, University of Illinois (1942).

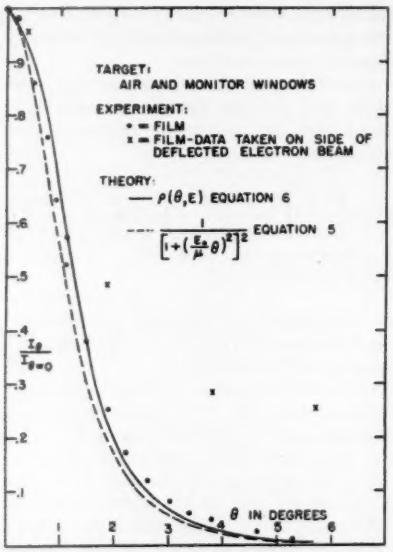

FIG. 10. X-ray intensity, as determined by the net film density, *vs* angle, for monitor windows and air, normalized to 1 at $\theta=0°$. The theoretical intrinsic x-ray distribution, and this distribution modified by multiple scattering, are also given. The crosses are those points measured on the side of the deflected electron beam.

agreement with each other. The increase in the x-ray beam width due to multiple scattering and due to the inherent angular spread of the electron beam over the width of a parallel, unscattered electron beam is small. Therefore, the measurements made can be used to check Schiff's formula for the intrinsic x-ray beam width, Eq. (5). Figure 10 is a plot of film density *vs* angle, with the peak density normalized to unity. Equations (5) and (6), for electrons of kinetic energy equal to 16.93 Mev (E_0 is the total energy of the electrons), are shown in this figure. From Molière's theory, the $1/e$ width of multiple scattering was calculated for the windows and the air. Under the assumption that the multiple scattering and primary electron beam shapes are gaussian, an assumption which is reasonable because its overall effect is small, the squares of the $1/e$ angles of these two distributions were added, the square root of their sum giving the $1/e$ width of the combined gaussian function. It was this combined distribution which was used in Eq. (6) for the theoretical curve in Fig. 10. Although the plot of Eq. (6) does not quite pass through the experimental points at the lower end of the distribution, the shape of a curve drawn through these points indicates that the intrinsic width may be represented by Eq. (5). A better fit to the experimental data in Fig. 10 would be obtained if an approximation to Schiff's intrinsic distribution were used which is more accurate than the two gaussian functions.

For the film data, the angular distribution of radiation was the same in the two vertical directions from the beam center, and in the horizontal direction opposite to that in which the electrons were deflected. On the side of the electrons, the film measurements indicated an asymmetric distribution, due to electrons which radiated while being deflected by the magnet. The crosses in Fig. 10 show this effect. The asymmetry becomes negligible for the thicker foils. The ion chamber measurements were in complete agreement with the film measurements for the radiation from the air and the monitor windows.

The fog density in the film measurements, for all targets, was between 0.18 and 0.21. It was this background which was subtracted to obtain the net density. The maximum density for all films measured ranged from 0.5 to 3.0; for each target, at least two exposures were made whose peak densities differed by about two. This was done in order to check the linearity of the film response.

Some of the data obtained using ion chamber and copper detectors are plotted in Figs. 11 to 13. The thicknesses of the gold targets, as well as the detectors used, are indicated on these graphs. The theoretical curves were calculated by means of Eq. (6), in which gaussian distributions for the multiple scattering were used whose $1/e$ angles were those calculated from Molière's theory for gold, modified to account for multiple scattering in the windows and air, and for the primary electron beam width. The electron energy used in these calculations was the incident energy of 16.93 Mev, reduced by one half the ionization loss as calculated from Heitler's[41] formula. Since the Molière theory of multiple scattering cannot be represented in its entirety without appropriate tables, the resulting $1/e$ widths for the gold foils are given in Table II. For the beryllium foil, the experimental $1/e$ width for multiple scattering, obtained from scattering chamber measurements,[36] was used for the distribution of radiation.

The theoretical x-ray distributions were not calculated for gold thicknesses greater than 967 mg/cm² because x-ray absorption in the target itself begins to become appreciable. In fact, in the experiment on central yields discussed in Sec. IID, it is shown that photon absorption outweighs photon production for

TABLE II. $1/e$ widths of multiple scattering.

Element	Thickness	$(\theta_{1/e})^2$	$(\theta_{1/e})^2$ modified by window and air multiple scattering and divergence of the electron beam	Source of $(\theta_{1/e})$
Be	491.3 mg/cm²	15.60 deg²	16.38 deg²	Expt. Molière
Au	37.28 mg/cm²	12.62 deg²	13.40 deg²	Expt. Molière
Au	51.5 mg/cm²	18.55 deg²	19.32 deg²	Expt. Molière
Au	247.1 mg/cm²	101.16 deg²	101.94 deg²	Expt. Molière
Au	967.0 mg/cm²	563.78 deg²	564.56 deg²	Expt. Molière

[41] See reference (15), p. 217.

gold foils thicker than 1700 mg/cm², for 16.93-Mev electrons.

Figure 11 shows a comparison of the measurement on the angular distribution of x-rays from 491.3 mg/cm² of beryllium and 37.28 mg/cm² of gold. These were the thicker targets used in the experiment on the Z dependence of bremsstrahlung [Sec. IB2]. Measurements of the angular distribution using x-ray film were in close agreement with those using copper threshold detectors. Since the film is most sensitive to low energy x-rays, while the copper is sensitive only to high energy quanta, the result indicates that there is no marked energy change with angle for such thin targets. This is not the case for targets of greater thickness. Although the angular distributions for the gold and beryllium targets were very nearly the same, the absolute values of the film densities differed by about a factor of two. More precisely, the maximum film densities minus the fog background density, normalized to the same number of incident electrons (7×10^{11} electrons), were 1.50 and 0.69 for these beryllium and gold targets, respectively. This striking effect can be attributed to the difference in the relative number of low energy quanta from these beryllium and gold targets. The beryllium nucleus is screened less by the orbital electrons and, therefore, should yield more low energy quanta than gold.

Figure 12 is a graph of the angular distribution of radiation from a 51.5 mg/cm² gold target, as measured with film and ion chamber. Besides the experimental data, this figure includes the theoretical angular distribution as given by Schiff.[33] In the derivation of this formula, Schiff used the electron multiple scattering theory by Williams, which gives a distribution wider than that of Molière's theory. The closer agreement of the experiment with Eq. (6) indicates that, at least for high Z, Molière's theory is more accurate than that of Williams. Also, Fig. 12 shows the distribution as given by Lawson's formula, modified in that the multiple scattering gaussian of Rossi and Greisen[35] assumed by him has been replaced with Molière's theory, and the $1/e$ angle of radiation for an infinitely thin foil was made equal to the $1/e$ angle from Schiff's formula, Eq. (5). In Lawson's expression, the radiation width is assumed to be a single gaussian. Equation (6), however, agrees somewhat better with the experimental results.

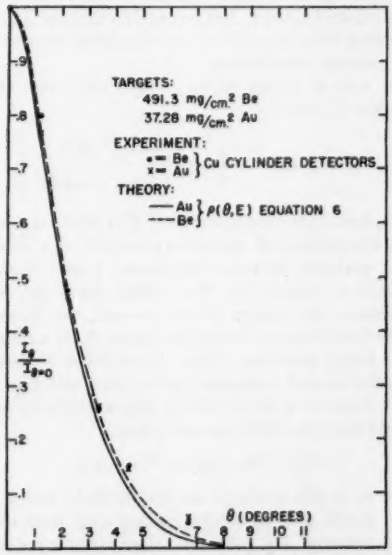

FIG. 11. Angular distribution of radiation from 491.3 mg/cm² Be target and 37.28 mg/cm² Au target, measured with Cu threshold detectors. Theoretical curves from Eq. (6).

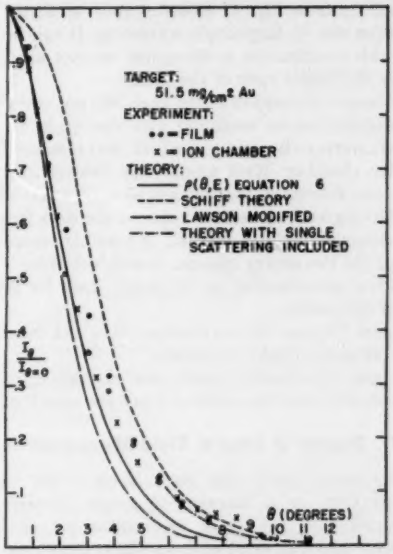

FIG. 12. Angular distribution of radiation from 51.5 mg/cm² Au target, measured with film and ion chamber. Theoretical curves from Eq. (6), Schiff (reference 33) and Lawson (reference 32). Estimate of theory including single scattering of electrons is indicated.

The lack of agreement between the experimental and the theoretical curves at large angles can be explained at least in part by the fact that the gaussian approximation to the electron scattering distribution is definitely poor at large angles. The contribution by electrons which have undergone large-angle scatterings can be estimated by comparing the actual scattering to that accounted for by the gaussian approximation. If one assumes that these electrons make radiative collisions during the remainder of their path in the target, one can estimate the contribution of these electrons to the angular distribution of the x-rays. To a first approximation, this contribution varies as $1/\theta^4$. The

dashed curve in Fig. 12 indicates this calculated contribution due to large-angle scattering. It can be seen that this contribution is the major one not accounted for by the simple form of the theory.

At target thicknesses larger than 100 mg/cm² of Au, the distribution as measured with film (thin Pb converter) starts to become wider than that measured with the ion chamber. With successively thicker foils, this difference becomes more pronounced until, at a thickness of 3910 mg/cm², agreement between the data from the two detectors is again reached. A possible explanation is that the low energy quanta, to which the film is very sensitive, are absorbed in the target itself for greater target thicknesses.

Figure 13 gives the ion chamber data and the theory for a number of gold thicknesses.

In the ion chamber data, the random errors are estimated to be of the order of 1 percent near the peak.

D. Results of Central Yield Measurements

This section deals with the analysis of the data on central yield as a function of target thickness, as measured with the small lead-walled ion chamber. Lawson[22] gives an expression for the central yield as a function of primary electron energy and target thickness. This expression involves multiple scattering and the beam width expected for radiative collisions. Lawson used Rossi and Greisen's multiple scattering formula and a gaussian distribution for radiative collisions. Instead, an expression approximating Molière's theory of multiple scattering by a gaussian, and the radiative distribution described by two gaussian functions (see Sec. A), is compared with the experimental results. This expression for the central yield per unit solid angle is given by

$$R(E_0, t) = (E_0^2\sigma/c)\{1.102\ln(1+ct/\mu^2\theta_1^2) + \ln(1+ct/\mu^2\theta_2^2)\}, \quad (7)$$

where E_0 is the total energy (inlcuding the rest mass) of the electrons incident on the foil, and where $\theta_1^2=0.553$ rad² and $\theta_2^2=2.85$ rad², as in Sec. A. This expression is the denominator of Eq. (6), multiplied by the square of the incident electron energy which, in Eq. (6), cancelled with a factor E_0^2 in the numerator. σ is a constant proportional to the radiation loss in the foil ($NE_0\phi_{\text{rad}}$). The factor c is not strictly a constant, but is a slowly varying function of the thickness, as well as of the electron energy. However, since the initial layer of a target contributes more than any subsequent layer to the forward yield, the factor c was determined from Molière's theory for the smallest target thickness used, and regarded to be the same for all thicknesses, for the sake of simplicity of analysis. The thinnest target used in this series was 0.0515 g/cm² of gold. The multiple scattering distribution from a target of this thickness is very nearly gaussian to angles well beyond the $1/e$ width. For this target, and an incident electron kinetic

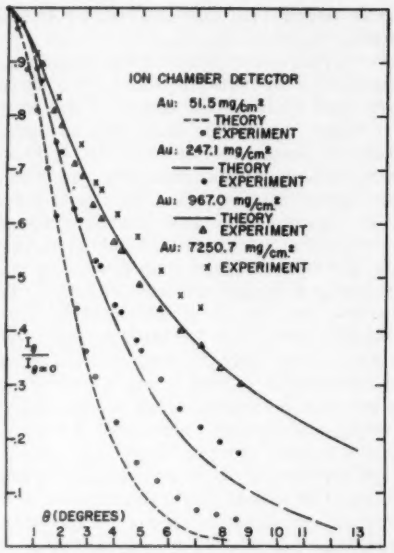

FIG. 13. Angular distribution of radiation for four Au targets, measured with ion chamber. The three corresponding theoretical curves are given, as calculated from Eq. (6).

energy of 16.93 Mev, the value of c was calculated to be 1.090×10^5 deg² Mev²/(g/cm²). To summarize, the logical choice of c would be that calculated for a thin foil, since most of the radiation is produced in the initial layer of a target, but not so thin that the multiple scattering from this foil is not adequately represented by a gaussian distribution.

The rate of change of the central yield with target thickness is given by

$$dR(E_0, t) = \frac{E_0^2\sigma}{c}\left\{1.102\frac{k_1dt}{1+k_1t}+\frac{k_2dt}{1+k_2t}\right\}, \quad (8)$$

where, $k_1=c/\mu^2\theta_1^2$ and $k_2=c/\mu^2\theta_2^2$. This expression, then, gives the amount of radiation produced in a layer of target material between thicknesses t and $t+dt$, for electrons of energy E_0. Now, since, for large target thicknesses, the energy is not constant, but decreases due to radiation and ionization losses, E_0 is a function of the target thickness. Using the formulas of Heitler[41] for radiation and ionization loss in gold, which is very nearly linear in a plot of energy loss *vs* incident energy, one obtains the following expression:

$$E(t) = [(\alpha_0+\beta E_0)e^{-\beta t}-\alpha_0]/\beta, \quad (9)$$

where α_0 is the intercept on the ordinate and β, the slope, in the plot of energy loss per unit thickness *vs* electron energy. For gold, the values of these constants were determined graphically to be

$$\alpha_0=17.8\text{ Mev/cm}=0.921\text{ Mev/g/cm}^2$$

and

$$\beta=3.13\ \text{cm}^{-1}=0.162\ [\text{g/cm}^2]^{-1}.$$

If the electron energy loss is appreciable in a given target, E_0 in Eq. (8) must be replaced by $E(t)$ of Eq. (9).

Introducing Eq. (9) into Eq. (8) and integrating from 0 to t, one obtains the expression for the forward yield from a target of thickness t,

$$R(E_0,t)=\frac{\sigma}{c\beta^2}\Big\{(\alpha_0+\beta E_0)^2\int_0^t e^{-2\beta t}\Big(\frac{1.102k_1}{1+k_1t}+\frac{k_2}{1+k_2t}\Big)dt$$
$$-2\alpha_0(\alpha_0+\beta E_0)\int_0^t e^{-\beta t}\Big(\frac{1.102k_1}{1+k_1t}+\frac{k_2}{1+k_2t}\Big)dt$$
$$+\alpha_0^2\int_0^t\Big(\frac{1.102k_1}{1+k_1t}+\frac{k_2}{1+k_2t}\Big)dt\Big\}. \quad (10)$$

The last of these integrals is easily found to have the value

$$\frac{\sigma\alpha_0^2}{c\beta^2}\{1.102\ln(1+k_1t)+\ln(1+k_2t)\}.$$

In order to evaluate $R(E_0, t)$, the exponential in Eq. (9) was expanded for a value of $\beta t_1 \ll 1$. For large target thicknesses, t_n, where βt_n was not necessarily less than 1, the first two integrals of Eq. (10) were evaluated numerically from t_1 to t_n, and the results added to that from 0 to t_1.

Figure 14 is a plot of the relative net yield, i.e., of the net current from the ion chamber, from gold as a function of target thickness. The plot shows that the larger thicknesses were such that photon absorption in the targets became appreciable. For these thicknesses, even though the radiation spectrum is far from being monochromatic, the measured yield falls off exponentially with target thickness. The absorption coefficient, λ, in the factor $e^{-\lambda t}$, was determined experimentally to be 0.0555 $(\text{g/cm}^2)^{-1}$ for gold.

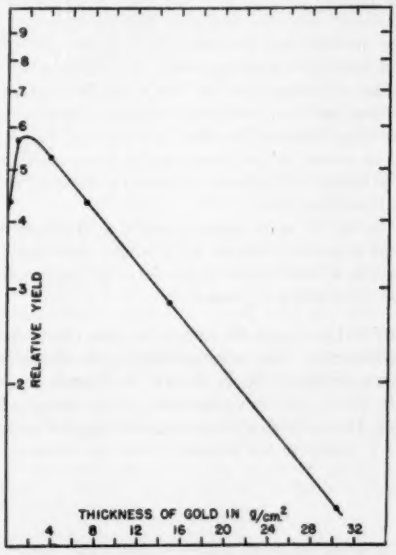

FIG. 14. Experimental measurement of central yield (logarithmic scale) vs gold target thickness, for 16.93-Mev electrons.

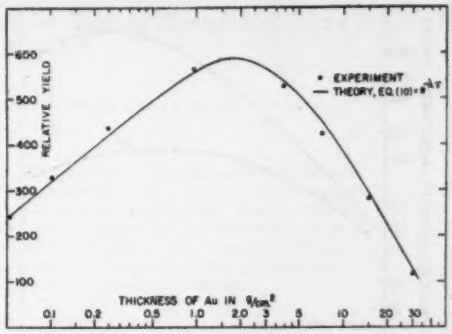

FIG. 15. Comparison of theory and experiment for central yield vs target thickness in gold (logarithmic scale). Incident kinetic energy of electrons is 16.93 Mev. $R(E_0, t)e^{-\lambda t}$ is the theoretical expression, where $R(E_0, t)$ is given by Eq. (10) and λ is the effective photon absorption coefficient.

The theoretical expression given by Eq. (10) does not include photon absorption. Therefore, for a comparison of theory and experiment, $R(E_0, t)$ is multiplied by $e^{-\lambda t}$. Equation (10) no longer applies for foil thicknesses such that the energy loss would be more than the incident electron energy. Thus, for target thicknesses greater than the maximum electron range, the thickness equivalent to this range is used in comparing the theoretical expression, including the absorption factor, with experiment. The thickness corresponding to this maximum range for gold, as determined from Eq. (9), was 8.66 g/cm².

The experimental results are plotted in Fig. 15, together with $R(E_0, t)e^{-\lambda t}$ as given by Eq. (10). The values are normalized to the yield of the first foil, of thickness 0.0515 g/cm². The peak yield as determined experimentally occurs at about 1.7 g/cm², while the theoretical peak is at approximately 1.8 g/cm².

The increase in yield for small thicknesses, calculated as described above, appears to be slightly slower than the experimental values indicate; however, the shape of the experimental rise agrees with theory in being proportional to the logarithm of the target thickness.

E. Results Using Wide-Angle Copper Detector

A wide-angle copper threshold detector was used to measure the radiation produced in gold and copper by 16.93-Mev electrons. As in Sec. IB2, the detectors were flat copper disks, 3 inches in diameter. These subtended a total angle of 11.4° at the radiator position.

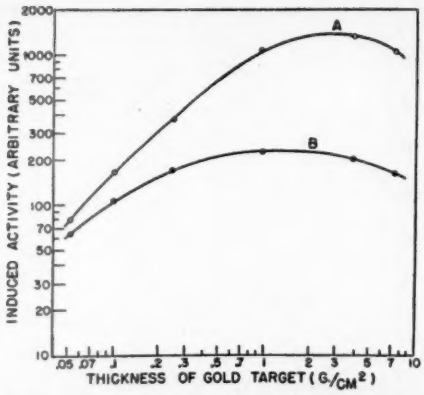

FIG. 16. X-ray induced copper activity from gold targets of various thicknesses. Curve A: detector subtending 180° at target. Curve B: detector subtending 11.4° at target. Electron energy = 16.93 Mev, where effective energy response of detector = 14.3 Mev.

Two series of measurements were made, with the set of gold radiators used for the central yield experiment. In one series, gold foils served as radiators, a copper disk at a distance of $15\frac{1}{8}$ inches behind them being the detector. In the second series, in addition, a copper disk of the same dimensions and weight as the detector disk was placed directly behind the gold foils, and served both as a radiator and a detector. The thickness of the copper disks was 0.1088 g/cm²; the gold target thicknesses ranged from 0.0515 to 7.25 g/cm².

The activities in the two copper foils of the series in which both gold and copper acted as radiators were measured, while the activity in the one detector was measured for the series having only a gold radiator foil. In order to correct for radiation produced in the monitor windows, an irradiation was made without a target foil. Also, to correct the activity, in the copper detector immediately behind the gold, for electrodisintegration and bremsstrahlung activity produced in the detector itself, a measurement was made in which a copper foil alone acted as a target. The irradiations were monitored with the ion chamber mentioned previously. All of the measured activities were reduced to the same counting interval and normalized to the same beam current. The relatively small activity produced in the detectors due to the air and the monitor windows was subtracted.

The activity induced in the copper foil directly behind the gold radiators measured the total radiation, from 0° to 90°, leaving a target. The radiation leaving the target is, of course, not the actual total amount produced, since some absorption takes place. To reduce the activity induced in the total radiation detector to that due to the gold alone, a correction was applied, eliminating the induced activity due to electrodisintegrations and bremsstrahlung produced in the detector. The results of these measurements appear in Fig. 16. No analysis will be given here.

F. Summary

The results of the experiments discussed in this part may be summarized as follows:

1. The experimental measurements on the angular distribution of radiation from a very thin foil were used to check Schiff's expression (see Eq. (5)) for the intrinsic angular distribution of bremsstrahlung and were found to be in good agreement.

2. The angular distributions of radiation from foils of various thicknesses were measured. The results are in agreement with an expression given by Eq. (6) if a correction is applied at large angles for the single scattering tail. This expression differs from those of Schiff[33] and Lawson[32] in that the intrinsic distribution of radiation is taken into account more accurately. A gaussian approximation of Molière's theory of multiple scattering in Eq. (6) agrees more closely with experiment than does the gaussian approximation based on Williams' theory, as used by Schiff.

3. An approximate expression is given for the central yield as a function of target thickness. This expression ($e^{-\lambda t}R(E_0, t)$, where $R(E_0, t)$ is given by Eq. (10) and λ is the photon absorption coefficient) is similar to that of Lawson,[32] with the exception that an improved form of the intrinsic angular distribution of bremsstrahlung and of multiple scattering is used. It includes a different gaussian approximation for the multiple scattering of electrons, and the decrease in primary electron energy in the target material is taken into account. The experiment on central radiation intensities, using a wide range of gold target thicknesses, was found to be in agreement with this calculation.

4. In Sec. E, some measurements on the total intensity of radiation emitted by a target and that intercepted by a wide-angle copper detector as a function of target thickness are presented.

The setting up of the apparatus and the making of measurements were accomplished with the able assistance of Messrs. D. E. Riesen, W. Unruh, D. Schiff, M. B. Scott, and other members of the electron beam group. The authors wish to acknowledge the assistance of E. F. Lanzl in the preparation of the manuscript.

Relation of Antiferromagnetic Structure to the Binding Energies of Some b.c.c. Transition Metals*

YEE-CHUANG HSU
Institute for the Study of Metals, University of Chicago, Chicago, Illinois
(Received May 7, 1951)

Zener's theory of antiferromagnetic structure for V, Cr, Nb, Mo, Ta, and W is discussed from the point of view of binding energy. According to such a picture the large binding energies must come from coulomb interaction between cores. The importance of the outer *d* electrons in achieving large coulomb attraction is pointed out. A mathematical scheme for treating binding energy in the case of extensive overlap of cores is discussed. By dismissing the contribution of a Wigner-Seitz type calculation, the remaining contributions to the binding energy of tungsten are calculated at the observed lattice constant. Results obtained demonstrate the importance of the coulomb attractive energy in an antiferromagnetic structure.

I

IN a recent paper by Zener[1] the body-centered cubic structure of certain transition metals like V, Nb, Ta, Cr, Mo, and W is explained by the following two assumptions: (1) The interaction between the incomplete *d* shells of the transition elements is insufficient to disrupt the coupling between the *d* electrons in the same shell, in which the spins of the *d* electrons are aligned in such a manner as to attain the largest possible net spin. (2) The exchange interaction between adjacent *d* shells always has the same sign as in the case of the H_2 molecule, thus favoring an antiferromagnetic arrangement of *d* spins. In these two columns of elements maximum net *d* spin is achieved. This large net spin results in a big exchange interaction between adjacent *d* shells of parallel spins. Since the b.c.c. lattice is of such a structure that nearest neighbors of an atom cannot themselves be nearest neighbors to each other, atoms of parallel *d* spins can be kept as far apart as possible in such a lattice if we assume an antiferromagnetic structure for such metals. According to this theory, the binding energy of these metals must come primarily from the classical coulomb interpenetration.

By assuming the interactions between tungsten atoms to be short range interactions, Isenberg[2] has been able to show that it is possible to get some information from the elastic constants regarding the interactions between neighboring atoms and between atoms next nearest to each other. He finds that it is not inconsistent with the observed elastic constants to say that the interaction of an atom with its nearest neighbor is attractive, while the interaction of an atom with its next nearest neighbor is repulsive. This substantiates Zener's theory.

The band theory of transition metals is roughly as follows.[3] When atoms are put together, the outer *d* and *s* electrons are strongly perturbed by the proximity of other atoms. The result is that all the outer electrons can move more or less freely to all parts of the crystal. Corresponding to the case of molecular orbitals it is now appropriate to use crystal orbitals, that is, Bloch wave functions. These wave functions represent a piling-up of an electron cloud in the regions halfway between the cores, thereby resulting in a binding.

In the Pauling resonating valence bond theory[4] of the transition metals it is necessary to take into consideration np orbitals in addition to $(n-1)d$ and ns orbitals. On the average, for each atom $2.44d$ orbitals show only weak interatomic interactions. They are considered to be atomic orbitals. The remaining $2.56d$ orbitals combine with *s* and *p* orbitals to form hybrid bond orbitals. Taking tungsten as an example, one can say that of the four $5d$ electrons and two $6s$ electrons, 0.44 electron are in the atomic *d* orbitals, while 5.56 electrons are engaged in bonding. The introduction of $6p$ orbitals means promotion of electrons to higher energy levels. Pauling's contention is that the bonding energy obtained through hybridization more than compensates for the energy of promotion.

These three theories represent three different approaches to the understanding of the binding of the transition metals. An actual transition metal probably does not conform precisely to any one of these three models, but rather has certain features characteristic of each model. The purpose of the present paper is to find whether the simple antiferromagnetic model of the b.c.c. transition metals is adequate to give the major part of the binding energy, and thereby to explain the position of these non-close-packed lattices in the periodic table. We use the word "non-close-packed" here because at least in the case of the diamond structure and the simple cubic lattice an antiferromagnetic arrangement can also be realized.

We are therefore led to the question of binding energy in an antiferromagnetic b.c.c. crystal. In such a model the attraction between two nearest neighbors is mainly the electrostatic interaction between two rigid charge

* A dissertation submitted to the faculty of the Division of the Physical Sciences in candidacy for the degree of Doctor of Philosophy, Department of Physics.

[1] C. Zener, Phys. Rev. **81**, 440 (1951).

[2] I. Isenberg, private communication.

[3] F. Seitz, *Modern Theory of Solids* (McGraw-Hill Book Company, Inc., New York, 1940), pp. 430–432. M. F. Manning and M. I. Chodorow, Phys. Rev. **56**, 787 (1939).

[4] L. Pauling, Phys. Rev. **54**, 899 (1938). L. Pauling, Physica **15**, 23 (1949).

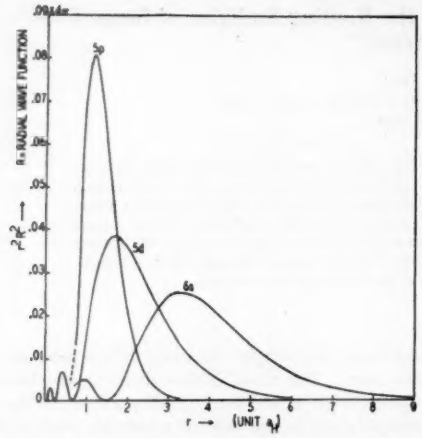

FIG. 1. Plot of r^2R^2 as a function of r for tungsten. The radial wave function R is obtained from Manning and Millman's calculation for W.

distributions. There is no additional piling-up of negative charge clouds. Accordingly, we would like to have a large coulomb attractive energy along with a small exchange repulsive energy so as to account for the large binding energies of metals like Mo and W. In Sec. II we discuss qualitatively how this is achieved via the charge distribution of the d electrons and the antiferromagnetic arrangement.

To carry out some quantitative calculation we want to formulate the mathematics in such a manner as to permit easy handling. If we assume that in the column Cr, Mo, W a single s electron per atom goes into the conduction band, we must carry out a Wigner-Seitz calculation for this electron. Since we are mainly interested in evaluating the contribution of the electrostatic attraction, we want to separate, in our mathematical formulation, the Wigner-Seitz type contribution from all other contributions. Unlike the case of alkali metals, the cores (containing electrons of the incomplete d shells) of neighboring atoms overlap quite appreciably. As a result, near the surface of a Wigner-Seitz sphere the s electron is subjected to a field deviating appreciably from the field owing to its core alone. Such an effect provides for additional electrostatic attraction. A detailed discussion is given in Sec. III.

Quantitative support to the qualitative discussion in Sec. II can be obtained only through calculation for special elements. In Sec. IV, tungsten is treated as an example because a self-consistent field calculation of the Hartree type has been carried out for free tungsten atoms by Manning and Millman.[5] Since their calculation is for the configuration $(5d)^4(6s)^2$, we have not taken into consideration the possible demotion of a $6s$ electron into the $5d$ shell. Also, since we are interested only in comparing the various contributions to the binding energy, calculation is made for the observed lattice constant. The numerical results so obtained indicate that the classical electrostatic attraction between neighboring cores is the major contributor to the binding energy. The antiferromagnetic interpretation of the b.c.c. transition metals is thereby placed upon a satisfactory quantitative basis.

II

To discuss the source of binding in an antiferromagnetic structure we can, without loss of generality, take the case of tungsten and investigate the various kinds of interaction involved. It must be emphasized that we do not know the degree of demotion of $6s$ electrons. We shall consider that no demotion has taken place. Allowing for demotion would, of course, increase the calculated binding energy.

It seems advantageous to begin our discussion by presenting the charge distributions of $5p$, $5d$, and $6s$ electrons of a W atom. From Fig. 1, in which r^2R^2 (R=radial wave function) is plotted instead, one sees that the charge distribution of the $6s$ electrons extends to a very large distance from the nucleus. In the formation of a crystal the $6s$ electrons are first subjected to strong perturbation. They can therefore be more appropriately represented by crystal orbitals.

Now let us consider an idealized crystal consisting of idealized atoms each of which contains a nucleus of charge $4e$ and only four $5d$ electrons. Suppose this crystal has an antiferromagnetic structure. The interaction between two nearest neighbors is then a pure coulomb interaction. At sufficiently large separation this is attractive. To see how large this attractive energy may be, we may mention the coulomb attraction in Heitler-London's calculation[6] for an H_2 molecule. At the optimum separation of $2a_H$ this attractive energy is 0.04 ry. It is expected that in the present case of four electrons per atom the coulomb attractive energy between two atoms would be an order greater (4^2) than this value through a certain range of separation. The contribution of the coulomb interaction to the binding energy per atom in a b.c.c. lattice will be four times this interaction. The observed heat of vaporization is 0.68 ry per atom. In the absence of all other types of interaction, the coulomb interaction between nearest neighbors would therefore give rise to a binding energy far greater than is observed.

In an antiferromagnetic b.c.c. lattice next-nearest neighbors have a parallel alignment of d shell spins. An exchange repulsion therefore acts between next-nearest neighbors. This exchange repulsion would, by itself, prevent nearest neighbors from coming so close as to attain their maximum coulomb attraction.

In real tungsten atoms we have also electrons inside the $5d$ shell. While these inner electrons of one atom

[5] M. F. Manning and J. Millman, Phys. Rev. **49**, 848 (1936).

[6] W. Heitler and F. London, Z. Physik **44**, 455 (1927).

do not overlap appreciably with those of a neighboring atom, they do overlap appreciably with the 5*d* electrons of neighboring atoms. This overlap gives rise to a second exchange repulsive interaction which keeps the atoms so far separated as to prevent the coulomb interaction from attaining its maximum value.

III

According to our present picture, in a metal like W the outermost *s* electrons go into the conduction band, while the incomplete *d* shells remain localized. To treat the outer *s* electrons by means of the Wigner-Seitz method, it is necessary to bear in mind several features not shared by the alkali metals, for which this method is highly successful. In the first place, the antiferromagnetic structure requires us to consider a b.c.c. lattice as a composite lattice obtained by the superposition of two simple cubic lattices. It is therefore incorrect to say that we can introduce a Wigner-Seitz sphere around each atom. All we can hope is that the spin interaction between *s* and *d* electrons can be taken into account using a wave function obtained by Hartree's method. This wave function is obtained by neglecting the exchange effect and by introducing a Wigner-Seitz sphere around each atom. In what follows the exchange effect between conduction and core electrons has been neglected.

Secondly, when one applies the Wigner-Seitz method to alkali metals, one usually argues in the following manner. Since in each cell the total charge of free electrons is just equal to the net charge of the core, the total potential due to such a cell for an electron moving in an adjacent cell is essentially zero. So when we limit ourselves to considering the motion of an electron in a cell, it is necessary to use only the potential due to the core. This contention is true only when the core is so small that the charge density due to the core electrons does not extend to the outside of the cell. In the present case the charge distribution of the incomplete *d* shell extends far outside of the Wigner-Seitz cell assigned to a tungsten atom at the observed lattice constant. As a result, the screening of the effect of a neighboring core by the almost uniform distribution of conduction electrons is rather incomplete. This necessarily complicates the calculation.

Perhaps the following is the easiest way to take such an effect into consideration. Let us first work out a Wigner-Seitz calculation using the potential due to the core of a free atom. The energy of the whole system is then calculated with this approximate wave function. It is expected that a first-order error in the wave function used will give rise to a second-order error in the energy calculated. The effect on the conduction electrons due to the overlap of cores, being a first-order one, is therefore properly taken into account in this type of calculation. The correction term so obtained for the total energy can be visualized in the following manner. Let us divide the whole space into Wigner-Seitz cells. In each cell we have an almost uniform distribution of conduction electrons with a core, which extends to the outside of the cell. The energy correction is then obviously the electrostatic interaction of the almost uniform charge distribution of conduction electrons in one cell with the conduction electrons as well as the core of another cell. This can be calculated readily if the distribution of the conduction electrons is assumed to be uniform.

The above-mentioned correction occurs whenever the overlap of cores becomes not negligible. In Fuchs' calculation for the binding energy of copper,[7] exchange repulsion between cores is taken into consideration. This is of sizable amount only when there is appreciable overlap. But then we must also take into account the electrostatic correction. At the theoretical lattice constant 4.2A the contribution to binding energy by this correction term is 0.5 ev per atom. This changes the calculated binding energy from 1.45 ev per atom to 2.0 ev per atom. The observed heat of vaporization is 3.1 ev per atom.

The case of two conduction electrons has been studied by Herring and Hill[8] for Be and recently by Raimes[9] for Mg. According to the latter, since electrons with parallel spins rarely approach each other within a distance of smaller than the radius of the Wigner-Seitz sphere,[10] it is reasonable to assume that in each sphere an electron is moving only in the field of another electron of opposite spin in addition to the field due to the core. To obtain the wave function for the conduction electron a self-consistent field calculation is therefore required.

Now we are ready to write down the formula for the binding energy per atom. The formulation, except for the above-mentioned correction and the core-core interactions, is the same as that given in Raimes' paper.[9] The binding energy per atom is found to be[11]

$$E_b = -E_I - 2\epsilon - 2E_k - 2E_{ex} - \frac{1}{2N}\sum_{a\neq b}^{N}\left(V_{ab} - \frac{4}{r_{ab}} - 2V_{ab}'\right). \quad (1)$$

The summation is to be carried over all the N lattice points. Here E_I means the energy required to ionize the two 6*s* electrons; ϵ, the eigenvalue obtained in the Wigner-Seitz method; E_k, the average Fermi kinetic energy per conduction electron; E_{ex}, the average exchange energy per conduction electron. V_{ab} represents the interaction between two cores, one situated at lattice point a, the other at point b. V_{ab}' represents the electrostatic correction due to the overlap of cores. The presence of the term $4/V_{ab}$ can be understood in

[7] K. Fuchs, Proc. Roy. Soc. (London) **151**, 585 (1935).
[8] C. C. Herring and A. G. Hill, Phys. Rev. **58**, 132 (1940).
[9] S. Raimes, Phil. Mag. **41**, 568 (1950).
[10] E. Wigner and F. Seitz, Phys. Rev. **46**, 509 (1934).
[11] The units used here are: length, a_H Bohr radius; energy, 2 Rydberg.

TABLE I. Contributions to the binding energy for tungsten.

	Nearest neighbors (antiparallel spins)	Next-nearest neighbors (parallel spins)
r_{ab}	$5.17a_H$	$5.97a_H$
C_{ab}	−0.149 ry	−0.038
$2V_{ab}'$	−0.120 ry	−0.039
K_{ab}	+0.223 ry	+0.137
X_{ab}	−0.061 ry	−0.057
Total	−0.107 ry	+0.003

the following manner. If we say that the correction term V_{ab}' is zero and that the core interaction V_{ab} can be represented by the coulomb repulsion between two positive centers each of charge +2, then every term in the summation becomes zero and we obtain the usual formula for the binding energy.

The task now reduces to the calculations of V_{ab} and V_{ab}'. Assuming a uniform distribution for the conduction electrons it can be shown that

$$V_{ab}'=\frac{2}{\Omega_0}\int_{\Omega_0}\frac{Z_p(|\mathbf{r}-\mathbf{r}_a|)}{|\mathbf{r}-\mathbf{r}_a|}d^3r. \tag{2}$$

In this expression the lattice point b is taken as the origin, and $\mathbf{r}_a$ represents the position vector of point a with respect to b. The integration is to be carried over the space bounded in the Wigner-Seitz sphere around b, its volume being Ω_0. $Z_p(r)/r$ is the potential due to a nuclear charge of Z_0-2 as well as the core electrons surrounding it, Z_0 being the total nuclear charge of the atom. Since Z_p is usually tabulated in the self-consistent field calculation for a free atom, V_{ab}' can be evaluated easily by numerical integration.

To calculate the interaction V_{ab} between the cores, we shall use the Thomas-Fermi-Dirac gas model, the charge density of the cores being regarded as superposed without any redistribution. The charge density of the cores will be taken as identical to that given by the Hartree solution for the isolated atom.

The calculation of the coulomb electrostatic contribution to V_{ab} is straightforward. The noncoulombic interaction consists of two parts. The first part, a repulsive interaction, arises from the increase in kinetic energy which comes from the superposition of two Thomas-Fermi distributions. The second part arises from the exchange interaction between electrons of parallel spin. This exchange interaction, which is of a negative sign, always increases when two charge distributions are superposed. There is no necessity for writing down the formula. We shall write only

$$V_{ab}=(4/r_{ab})+C_{ab}+K_{ab}+X_{ab}, \tag{3}$$

where $4/r_{ab}$ takes care of the net positive charge of the core, C_{ab} represents the rest of the electrostatic interaction, and K_{ab} and X_{ab} represent, respectively, the interactions arising from Fermi kinetic energy and exchange energy. $K_{ab}+X_{ab}$ is equivalent to the exchange repulsion usually understood in a quantum-mechanical calculation of the interaction between cores. It is to be noticed that, owing to the antiferromagnetic arrangement, K_{ab} and X_{ab} assume different forms for nearest neighbors and for next-nearest neighbors. For nearest neighbors they are due to the overlap of d orbitals of one atom with inner orbitals of the other. For next-nearest neighbors they are due mainly to the overlap of incomplete d shells.

For later use let us write

$$\begin{aligned}E_B'&=-\frac{1}{2N}\sum_{a\neq b}^{N}\left(V_{ab}-\frac{4}{r_{ab}}-2V_{ab}'\right)\\&=-\frac{1}{2N}\sum_{a\neq b}^{N}(C_{ab}+2V_{ab}'+K_{ab}+X_{ab}).\end{aligned} \tag{4}$$

Since all the interactions drop rapidly with increasing r_{ab}, we need to carry out the summation over nearest and next-nearest neighbors, obtaining

$$\begin{aligned}E_B'&=-4(C_{ab}+2V_{ab}'+K_{ab}+X_{ab})\text{ nearest}\\&=-3(C_{ab}+2V_{ab}'+K_{ab}+X_{ab})\text{ next nearest.}\end{aligned} \tag{5}$$

IV

To illustrate in a quantitative way the importance of the electrostatic energy, tungsten is chosen as an example. As mentioned before, to make use of Manning and Millman's calculation for the configuration $(5d)^4(6s)^2$, we assume that two electrons per atom go into the conduction band. In the expression

$$E_B=\{-E_I-2-2E_k-2E_{ex}\}+E_B',$$

the first part $\{-E_I-2-2E_k-2E_{ex}\}$ may be regarded as essentially the same in W as in Hg, which has, in fact, two electrons in the conduction band. Now in Hg the $5d$ shells are so small as to have no appreciable interaction, so that the binding energy may be taken as given by the first part of E_B. Since this binding energy is very small compared with that of W, we shall hereafter neglect this first part of E_B, and thus consider only that part of the binding which arises from the extension of the $5d$ shells outside of the Wigner-Seitz cells.

E_B' has been evaluated through numerical integrations. The following table gives the various contributions calculated at the observed lattice constant $5.97a_H$. Using Eq. (5) we get $E_B'=0.42$ ry/atom. The observed heat of vaporization is 0.68 ry/atom. Considering the crudeness of our method, the agreement is quite satisfying.

In Table I one may notice that the term C_{ab}, arising from the coulomb interaction between cores, is indeed the major contributor to the calculated binding energy. In the formation of tungsten crystal this source of energy must be fully explored. The demotion of a $6s$ electron into the $5d$ shell will certainly increase the

attractive term C_{ab}; but the attractive energy $2V_{ab}'$, being proportional to the density of the conduction electrons, will be decreased to approximately half its present value. Further, the repulsive energies will be increased. It is difficult to say what will be the over-all effect. Such considerations must be preceded by a calculation of the wave functions using the Hartree-Fock method. In all cases the coulomb energy arising from the overlap of d shells will continue to play an important role in the binding energy consideration for tungsten.

From the table one sees that the exchange repulsion $K_{ab}+X_{ab}$ between nearest neighbors is quite large, being 0.162 ry. Assuming nearest neighbors to have parallel spins we obtain for $K_{ab}+X_{ab}$ a value of 0.260 ry. Comparing the two values, one can see that the antiferromagnetic arrangement is really quite effective in minimizing the repulsive energy. As the binding energy calculated from this model is of the right order of magnitude, one may be inclined to believe that the preference of b.c.c. lattice over the common close-packed lattice is coupled to the tendency of such atoms toward antiferromagnetic arrangement.

It is a pleasure for the author to express his gratitude to Professor C. Zener for suggesting this problem and for his constant advice.

PHYSICAL REVIEW VOLUME 83, NUMBER 5 SEPTEMBER 1, 1951

Stability of Short Arcs in Oxygen, Hydrogen, and Helium

W. M. BRUBAKER
Westinghouse Research Laboratories, East Pittsburgh, Pennsylvania
(Received November 1, 1950)

An arc drawn between separating contacts is known to be very unstable, in the absence of oxygen, in the usual power circuit. To study this instability experiments have been made in which a four-ampere arc in a 125-volt dc resistive circuit was repeatedly restruck between separating contacts. Various metals were used as cathodes, with spectroscopically pure carbons as anodes, in various gases.

Data have been obtained showing the dependence of average arc duration after ignition on the cathode material and on the pressure and kind of surrounding atmosphere for a number of metals in oxygen, hydrogen, and helium. Oxygen exhibits an extraordinary stabilizing influence for most metals, whereas in hydrogen the mean life of the arc is generally less than ten milliseconds even at atmospheric pressure.

ELECTRIC arcs have been used by engineers for many years. The conduction of electricity in gases is as old as electricity itself, yet no one has developed a generally accepted theory of the physics of the concentrated cathode arc spot. Welding engineers desire stable arcs; circuit breaker engineers want unstable arcs; designers of rectifiers strive to eliminate cathode arc spots from their anodes at all times.

As long ago as 1932, Professor G. E. Doan[1-3] reported extreme instability for arcs drawn in very pure argon, between electrodes of very pure iron. Yet none of the theories proposed to describe the cathode spot suggests the influence of oxygen. Doan observed instabilities at low currents of a few amperes and also at welding currents of more than 100 amperes. Besides the reports of Doan and his collaborators, other references can be found to the difficulty of arc spot formation in the absence of oxygen.[4] Fan[5] found glow discharges between copper electrodes in hydrogen to exist for currents above ten amperes before transition to the low voltage arc occurred. When oxygen is present in even small amounts, the transition occurs at currents of the order of one ampere.

This paper presents the results of a study of the relative stability of dc arcs as a function of the composition and pressure of the surrounding gas atmosphere. Tests were made with cathodes of aluminum, carbon, cobalt, chromium, copper, iron, molybdenum, nickel, tungsten, titanium, and zirconium. These cathodes were used with spectroscopically pure carbon anodes. Observations of arc stability were made for each electrode pair in atmospheres of tank oxygen, tank hydrogen, and tank helium.

The phenomenon under investigation involves the cathode. When a source of electrons is provided, as with a thermionic cathode, no difficulty is experienced in maintaining a discharge through a gas under conditions similar to those of this experiment. Arcs in gas-filled thermionic diodes or in thyratrons are extremely stable. The instability we have observed seems to be peculiar to the self-maintaining concentrated cathode spot.

The instabilities observed in this investigation are found at high currents as well as low currents. A momentary improvement in stability is found when the arc current is increased. However, after the cathode spot has roamed over the available cathode material,

[1] G. E. Doan and J. L. Myer, Elec. Eng. **51**, 624 (1932).
[2] G. E. Doan and J. L. Myer, Phys. Rev. **40**, 36 (1932).
[3] G. E. Doan and A. M. Thorne, Phys. Rev. **46**, 49 (1934).
[4] J. D. Cobine and C. J. Gallagher, Phys. Rev. **74**, 1524 (1948).
[5] Hsu Yun Fan, Phys. Rev. **55**, 769 (1939).

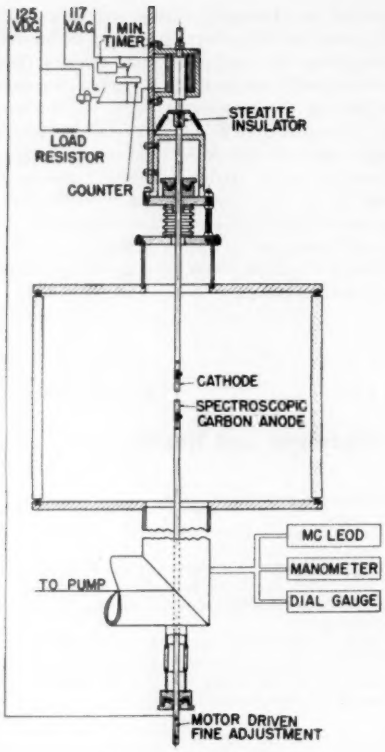

FIG. 1. Arcing chamber.

the arc again becomes unstable. A suggested explanation of this behavior is the presence of some oxide of the metal which is always present unless it has been removed under vacuum. Apparently, an initial oxide film on the metal, which makes the arc stable, is removed by the arcing in the oxygen-free gas.

A similar phenomenon is observed in the welding of aluminum metal or alloy with tungsten anode in an oxygen-free gas such as argon. So long as the arc is kept moving to fresh metal, it is stable. When the arc is kept in one small region, however, instability is soon experienced.

APPARATUS

A diagram of the apparatus used is shown in Fig. 1. A vacuum is drawn in the arcing chamber by a small size Kinney high vacuum pump. The pressure is measured by either a McLeod gauge, a mercury manometer, or a dial gauge depending on the pressure range of interest. Horizontal motion for the alignment of the electrodes is provided by the sylphon bellows on the upper plate of the vacuum chamber. Axial motion for arc electrode adjustment is made through the lower Wilson seal. In operation the lower electrode is raised slowly until it makes contact with the upper. When current flows, the dc relay in parallel with the load resistor closes, energizing the ac solenoid. The arc electrodes are separated 0.05 inch by the solenoid and are held apart as long as anode current flows. Upon arc extinction the relay and solenoid are de-energized and the upper electrode drops. When contact between the electrodes is re-established, the cycle starts all over again. The cycle counter registers each restriking.

When the arcing time is of the order of milliseconds or less, the frequency of restriking is limited to about 1000 per minute by the mechanical forces and the inertia of the relay, solenoid, and upper electrode rod. The state of lubrication on the Wilson seal and the adjustment of the lower electrode have a relatively small influence on the maximum frequency, but are responsible for the variations noted from one test to another.

The carbon anodes of the type and purity used in spectroscopy were one-fourth inch in diameter, one-half to three-quarters inch long. The cathodes were all of exceptional purity. They varied in diameter from one-eighth inch to one-quarter inch, and were of the same lengths as the anodes.

METHOD

The load resistor in the 125-volt dc circuit is adjusted to give five amperes in the arc circuit when the electrodes are in contact. The current during arcing falls to about four amperes. For aluminum the currents are reduced to three amperes short circuit or 2.4 amperes arcing to avoid melting the cathode.

Each new electrode pair was arced first at the lowest pressure, about 20 microns. The gases were introduced in the order oxygen, hydrogen, and helium. At the lowest pressure the duration of the arc was very short for all metals tested. At the beginning of each series of runs the lower electrode was adjusted to give a maximum re-striking rate, as judged audibly. This adjustment had to be remade at higher pressures because expansion of the vacuum vessel prevented the electrodes from making contact.

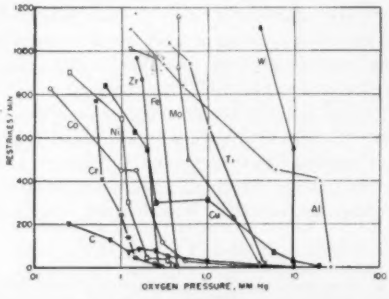

FIG. 2. Arc instabilities in oxygen.

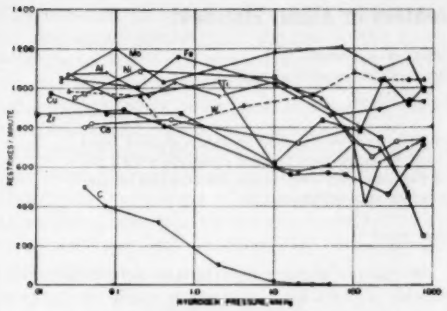

FIG. 3. Arc instabilities in hydrogen.

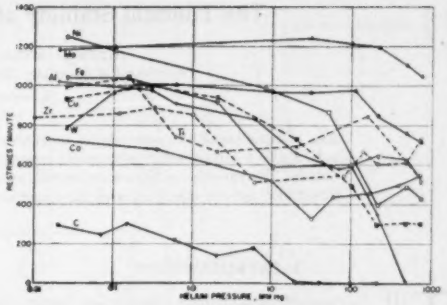

FIG. 4. Arc instabilities in helium.

With the lower electrode adjusted as described, the one-minute time switch to the cycle counter was closed. The counts registered during the timed interval were recorded, and the procedure was repeated for each set of electrodes at a number of pressures in each of the three test gases. In general, only a one-minute observation was made for each point on the curves. The lines joining the points have no significance other than to guide one's eye from one point to the next.

The time between successive countings was just that required for the adjustment of the pressure to a new, higher value. This was a minute or less. In regions where the counting rate was falling rapidly with an increase in oxygen pressure, as in iron, equilibrium conditions were not established before the counting was started. If smaller pressure increments had been used in these cases, the data with oxygen would have shown greater arcing stability at lower pressures.

DATA AND CONCLUSIONS

The data for oxygen are shown in Fig. 2. The points on the horizontal portion of each curve have been deleted to avoid confusion. It is seen that a pressure of millimeters is sufficient to have a pronounced influence on the stability of arcs draw from most cathode materials.

Stability observations for hydrogen and helium are plotted in Figs. 3 and 4. There is a great similarity between the results in these two gases. The striking difference between either of these and the data for oxygen in Fig. 2 is apparent.

These tests indicate a much greater dependence of arcing stability upon the gaseous atmosphere surrounding the electrodes than upon the material of the electrodes themselves. In particular, they show for all metals tested the stabilizing influence of oxygen relative to hydrogen, a reducing gas, and helium, a chemically inert gas. The arc voltages were not recorded, but the constancy of the arc current at four amperes indicates an arc voltage of the order of 25 volts. This is a sufficiently small portion of the 125-volt line voltage to ensure stable arcing conditions in the positive column. That is, the energy input to the arc increases almost linearly with the arc voltage. For this reason the increased cooling and hence de-ionizing effect of the lighter gases hydrogen and helium should be expected to increase the voltage drop in the positive column, but should not lead to arc instability. Heavier gases have not been used in this experiment; the emphasis has been on the cathodes rather than on a great variety of gases. However, Doan[3] has reported instabilities with several metals in argon, helium, and neon, when all traces of oxygen have been removed.

Water vapor at a pressure of 18 mm had but a weak stabilizing influence on an iron cathode. It would seem that the arc with metal cathode, as it is found in practice, is completely dependent on the presence of some oxygen in the atmosphere for its stability. So remarkable a fact should be an important point in any satisfactory theory of the arc cathode spot. However, none of the hitherto proposed theories refers to it.

The attention of the author was directed to the phenomena described in this paper during the course of another experiment with Dr. J. Slepian. His interest and encouragement in this work is greatly appreciated.

The Thermal Stability of *F*-Centers in Alkali Halides*

ALLEN B. SCOTT AND WILLIAM A. SMITH
Department of Chemistry, Oregon State College, Corvallis, Oregon
(Received May 7, 1951)

The *R'*-band reported previously in additively colored KCl has been found to contain a distinct band which, above a certain total color-center concentration, is in heterogeneous thermal equilibrium with the *F*-centers. The variation of the saturation concentration of *F*-centers with temperature has been studied and a latent heat for the dissociation of the coagulated centers has been determined.

I. INTRODUCTION

THE formation of a broad absorption band (the *R'*-band) on the long-wavelength side of the *F*-band by optical and thermal treatment of additively colored KCl has been discussed recently.[1,2] By analogy with a similar band frequently observed[3,4] in NaCl, this band might be ascribed to colloidal metal; but, except for the temperature-insensitivity of the band shape, the presence of a second phase could not be demonstrated. This was in large part the result of the simultaneous presence of absorbing centers caused by illumination in the *F*-band, such as *R*-, *M*-, and *N*-centers, in addition to any formed solely by thermal coagulation of *F*-centers. As a consequence, the shape and wavelength of maximum absorption of the *R'*-band varied considerably with the combined thermal and optical treatment.

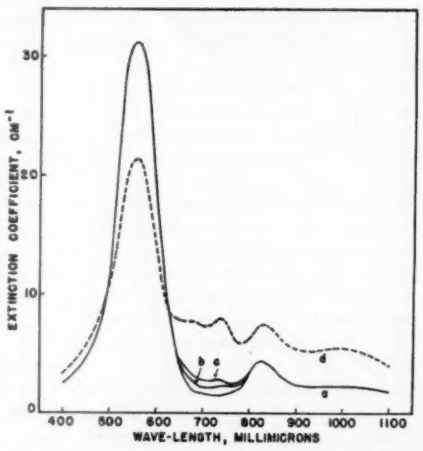

FIG. 1. Growth of *R*-bands during illumination.

Several preliminary experiments were undertaken to provide a basis for a systematic study of the purely thermal coagulative process. The absorption at −195°C of about fifty different additively colored crystals covering a concentration range from 9×10^{16} to 1×10^{18} *F*-centers/cc, which were exposed to daylight and heated at several temperatures and rapidly quenched, was measured. It was observed that the prominence of the *R*-, *M*-, and *N*-bands bore no particular relation to the total color-center concentration or treatment temperature. The broad *R'*-band was both temperature and concentration dependent. On the other hand, crystals prepared and handled in complete darkness or under red light showed only the development of *F*- and *M*-bands and a quite narrow, symmetrical band in the neighborhood of 760 mμ (at room temperature) in crystals having a high concentration or after treating at the lower temperatures. Anticipating conclusions to be drawn later, we will call this band the colloidal band. Curve a, Fig. 1, and curve c, Fig. 2 illustrate the appearance of these bands at room temperature. The initial presence of the *M*-band is surprising, as it has previously been considered primarily as an optical product.[5,6]

The effect of brief illumination in the *F*-band during measurement of the spectrum is shown in Fig. 1. Curve *a* is that of a crystal prepared in the dark, the measurements made from 1100 working toward 400 mμ. Curve b was taken for the region 625–800 mμ immediately following a; curve c was obtained after 5 minutes irradiation by 560-mμ light in the spectrophotometer, and d after 2 days' exposure to daylight. It is apparent that *R*- and *N*-bands are absent prior to the measurement, and that brief exposure in the *F*-band causes some, but not an objectionable, growth in the *R*-bands and consequently a slight decrease in the *F*-band.

Slices of crystal containing *F*- and *M*-centers were mounted in small Al-foil holders having a horizontal slit as a spectrophotometer aperture; and, without recutting or repositioning the crystal, the absorption spectrum was measured prior to and after heat treatment to develop the colloidal band. The Smakula dispersion formula[7] was applied to the bands both before and after to obtain concentrations; and it was found

* This work has been supported by the ONR. Presented before the one-hundred-and-nineteenth meeting of the American Chemical Society, Cleveland, Ohio, April 10, 1951. Published with the approval of the Oregon State College Monographs Committee as Research Paper No. 180, Department of Chemistry, School of Science.

[1] A. B. Scott and L. P. Bupp, Phys. Rev. **79**, 341 (1950).
[2] Scott, Hrostowski, and Bupp, Phys. Rev. **79**, 346 (1950).
[3] E. Mollwo, Nachr. Ges. Wiss. Göttingen **II**, 254 (1932).
[4] M. Savostianowa, Z. Physik **64**, 262 (1930).
[5] J. P. Molnar, Phys. Rev. **59**, 944(A) (1941).
[6] S. Petroff, Z. Physik **127**, 443 (1950).
[7] A. Smakula, Z. Physik **59**, 603 (1930).

in all cases that the apparent gain in the colloidal band was very much greater than the loss in the *F*- and *M*-bands, so that it was concluded that the dispersion formula, intended to apply to electronic oscillators, cannot be applied to other types of absorbing centers even qualitatively, as has been suggested.[1,3]

To obtain quantitative information about the thermal equilibrium between *F*-centers and the coagulation product, the dependence of the equilibrium *F*-center concentration upon total color-center concentration and upon temperature was determined by the experiments to be described.

II. EXPERIMENTAL

(A) Preparation and Thermal Treatment of Crystals

All crystals were additively colored by the method previously described.[1] The time of heating was materially reduced in the case of the more dilute crystals by keeping the end of the copper pipe containing the KCl at a temperature of about 650°C and allowing the other end to extend out of the furnace. By varying the length of tube extending out of the furnace, the temperature of the cool end, and thus the vapor pressure of *K*, was varied to give crystals having from 1 to 10×10^{17} color centers/cc after two hours heating. The crystal having 9×10^{16} color centers/cc was prepared by using Na instead of K and heating the entire bomb at 500°C for 23 hours. After the bombs were quenched in cold water, the crystals were removed and stored in light-proof containers.

Pieces of crystal considerably larger than needed for spectrophotometric measurements were wrapped in Al foil and brought to equilibrium at a series of temperatures in a small automatically controlled muffle furnace. Temperatures were measured by means of a Chromel-Alumel thermocouple and microvoltmeter, the couple and meter being calibrated at the normal boiling point of water and the temperature of freezing KCl. Allowing for thermal gradients in the furnace and small time drifts in the controlling mechanism, the temperatures reported are correct within 5°. Following attainment of equilibrium, the foil-wrapped crystals were plunged into cold CCl_4. Numerous experiments with several quenching methods showed this to yield the highest and most reproducible concentration of *F*-centers at any given temperature.

Slices taken from the interior of the crystals were used for absorption measurements in the Beckman Model D-U Spectrophotometer. For the more concentrated samples, the slices could not be more than about 0.25-mm thick to avoid optical density beyond the range of the instrument; the difficulty of preparing thin sections imposed an upper concentration limit of about 8.0×10^{17} color centers/cc for absorption determinations. These slices were cut and mounted on metal holders having horizontal apertures 1.0×2.5 mm, by red safelight. They were transferred to the instrument

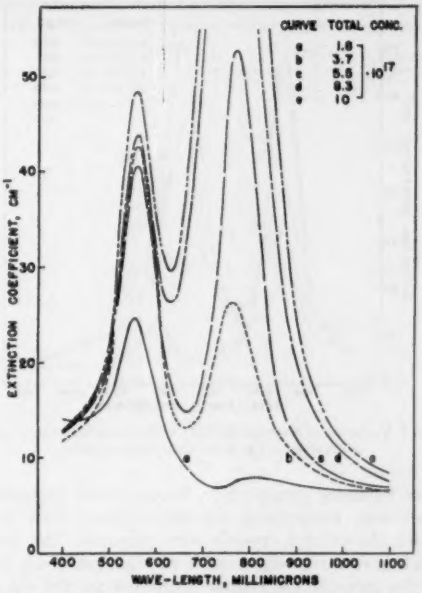

FIG. 2. Absorption curves for a series of crystals of varying concentration. Quenched from 400°C after 15 minutes.

with a minimum of exposure of subdued light, and in no case was a development of *R*- or *N*-bands noted. Following the absorption measurement, the thickness was measured by a calibrated eyepiece micrometer; only sections showing accurately parallel faces were included in the computation of concentrations.

Initially, the thermal treatments were carried out on crystals already cut to the proper thickness for absorption measurements; but a good deal of bleaching and evaporation occurred on the surface, which would tend to make measured concentrations low.

(B) Analytical Methods

For colored crystals in this concentration range, the application of the dispersion formula to absorption data is the only practicable analytical means available. An attempt was made to extend the *p*H-change method[1] to this concentration range, in the hope of verifying Kleinschrod's value[4] for the oscillator strength for *F*-centers in KCl. A small cell of about 2-ml capacity was fitted with a suitable inlet and outlet for purified nitrogen. A slightly acidified solution, boiled to expel CO_2, and having a *p*H in the neighborhood of 5.2, was thermostated at 25°C and the *p*H of the solution measured by means of a Beckmann *p*H meter and "micro" electrodes inserted in the cell. While nitrogen was streaming out of the cell, a crystal of KCl weighing about 200 mg was inserted and the change in *p*H noted

[4] F. G. Kleinschrod, Ann. Physik **27**, 97 (1936).

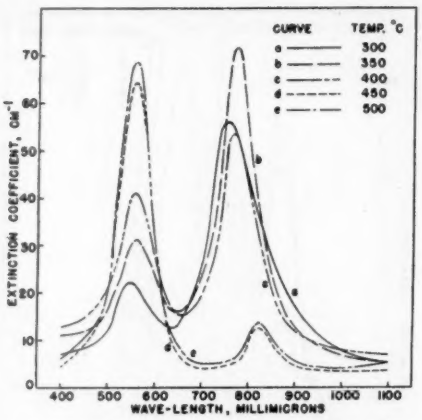

FIG. 3. Variation of F-center stability with temperature for a series of crystals of the same total concentration.

after regaining temperature. Several blank determinations were made using the single-crystal stock from which the colored crystals were prepared. The blank stock gave extremely variable pH changes which were of the order of the change computed for the colored crystals to be analyzed, so that the method could not be relied upon. Some experiments using Baker's analyzed cp KCl on a larger scale showed that it caused no significant change in pH of slightly acid CO_2-free water, so that with sufficient care in the preparation of fused single crystals, this method might prove to have sufficient sensitivity to provide an analytical method for color centers.

Kleinschrod gives no specific data on blank determinations but states that the stock material was tested and only unobjectionable pieces were used to prepare colored crystals. He did not exclude CO_2 but states the indicator used as a measure of pH was unaffected by CO_2. In general, the concentration of color centers used was considerably lower than in these experiments. While his ratios of chemically-determined to optically-determined concentration are satisfactorily constant, it is felt that his value for the oscillator strength, 0.81, cannot be considered as established without further investigation by independent means.

For this reason, the oscillator strength has been assumed to be unity, and all concentrations reported may be readily converted to the basis of any other chosen oscillator strength by dividing by the oscillator strength. The Smakula equation, using modern values for the physical constants involved then reduces to

$$n = 1.095 \alpha_M W$$

for F-centers having maximum absorption at room temperature at 560 mμ in KCl, where n is the number of F-centers/cc, α_M the absorption coefficient at the maximum absorption in cm^{-1}, and W the width of the absorption curve at half-maximum in electron volts. For M-centers, having a maximum at 825 mμ, the numerical multiplier has the value 1.120; and α_M for the F-band, in the absence of an overlapping band, was taken as the difference between α at 560 mμ and the lowest value of α on the absorption curve, which generally lay in the region 1000–1100 mμ. The reference aperture used to establish 100 percent transmission was slightly narrower than those upon which crystals were mounted, so that negative optical densities were avoided and the minimum α had thus always a small, positive value. When the colloidal band is present, α_M and W of the F-band are both somewhat increased by overlapping. In the absence of more accurate means of correction for the overlap, the colloidal band was assumed symmetrical (which is not strictly true largely because of a small contribution to the absorption by M-centers) and α_M was taken as the difference between α at 560 and at 960 mμ. W should be a constant characteristic of the band at a constant temperature and was obtained by taking the average value of 30 measurements made on crystals containing F-centers, varying in concentration from 14 to 85×10^{16}/cc, and having such small concentrations of other centers that no overlapping was possible. At 25°C, W was found to be 0.359 ± 0.002 ev. This value could then be used with confidence when the F-band was broadened by overlapping of the colloidal band, and, in fact, was used in preference to individually determined W values even in the absence of the colloidal band.

Errors in absorption measurements were greatest in the case of dense crystals and, since optical densities measured were sometimes as high as 2, were of considerable magnitude. However, these errors, arising from random inaccuracies in dark-current, 100 percent transmission, and optical density settings, are random and were largely eliminated by taking the mean of sufficient concentration determinations at each temperature to reduce the probable error in the mean to less than 3 percent. However, errors in concentration arising from the foregoing choice of method for arriving at α_M and W are systematic and affect all concentrations about the same way. Estimation of this error is difficult; but an inspection of the curves showing both F- and colloidal bands will show that uncertainty in the choice of the 960-mμ absorption, rather than some other neighboring value, as the proper base for α_M calculation might introduce an error as high as 10 percent in the crystals showing greatest overlapping. In most cases the overlapping was not serious, and the probable systematic error from this source was at the outside 5 percent. The over-all probable error in the reported F-center concentrations, noting that the error in W is negligible, is thus about 7 percent. It must be emphasized that the assumption of an oscillator strength other than unity would introduce a corresponding change in all the concentrations, which are on a consistent basis among themselves.

III. DISCUSSION OF RESULTS

(A) Stability of F-Centers as a Function of Temperature

Figure 2 shows typical absorption curves for a series of crystals of varying total concentration held at 400°C for 15 minutes and quenched. The total concentrations were estimated from curves taken prior to the 400° treatment on neighboring sections of the crystals used, and include the concentration of M-centers; due to some inhomogeneity throughout large regions, these total values cannot be considered exact and actually do not enter the calculation of the equilibrium F-center concentration. It will be noted that α_M for the F-band, as defined in Sec. II, is quite constant for all crystals in which both F- and colloidal bands are present, regardless of total concentration. Since α_M and F-center concentration are proportional, this shows the equilibrium F-center concentration to be independent of total concentration and the equilibrium is consequently heterogeneous. A further indication is the complete absence of the 760-mμ band in the crystal having less than the saturation concentration of F-centers.

Curves b and c were obtained for crystals which had been previously brought to equilibrium at 300°; the fact that the saturation concentrations are the same for these two as for those in which the equilibrium was approached from the opposite direction shows that 15 minutes is a sufficient time at 400°. The time required for attainment of equilibrium was determined either in this way or by treating individual crystals for varying times and determining the time after which the F-concentration remained unaltered.

These times varied from 90 minutes at 300° to 45 seconds at 500°.

Figure 3 shows the variation of F-center stability with temperature for a series of crystals all of approximately the same total concentration. Especially to be noted is the fact that, at temperatures as low as 300°, there is a definite stable concentration of F-centers which is readily measurable when the total concentration is not too high and when optical bands are suppressed.

From 7 to 15 separate crystals covering a range of total concentration were studied at each of four temperatures, and the mean of the F-center concentrations in equilibrium with colloidal centers was obtained (Table I). Concentrations in brackets are for crystals in which the F-center concentration was below the mean equilibrium value and in which no colloidal band was observed. Three crystals, at or somewhat above the concentration for quantitative determination, were treated at 500° with no development of the colloidal band.

The attainment of equilibrium at 300° was tested by heating part of the samples for 90 and part for 150 minutes. It will be noted there is no significant difference in the average F-center concentration for the two groups. The time required at each temperature gives a rough indication of the rate of the coagulation of F-centers; but, until further rate studies are made, little can be said about the actual value of the activation energy.

However, ΔH for the process, colloid = F-centers, can readily be evaluated from the slope of the curve of Fig. 4, in which the logarithm of the equilibrium concentra-

TABLE I. Concentration of F-centers in equilibrium with colloid

t, °C, and time	Approx. total concentration centers/cc $\times 10^{-18}$	F-centers/cc $\times 10^{-18}$	Av. equilibrium conc., F-centers/cc $\times 10^{-18}$
500, 45 sec	55	[56]	
	83	[>80]	
	100	[>80]	>80
450, 3 min	37	[34]	
	55	[54]	
	83	62, 73, 70	
		69, 69	
	100	58, 53, 54	64±2
400, 15 min	17	[17]	
	37	32, 28	
	55	29, 25	
	83	29	
	100	28, 30, 32	29±1
350, 50 min	9	[9.2]	
	23	20, 18, 17	
	34	19	
	55	22, 21	19±0.5
300, 90 min	18	9.9, 9.4, 8.3, 9.0	
	37	10.8, 11.2, 12.4	
	55	11.9, 13.6, 12.4	10.8±0.5
150 min	9	[9.2]	
	18	12.8	
	37	10.1, 9.4	
	55	12.4	11.2±0.7; mean for 300° = 11.0±0.5

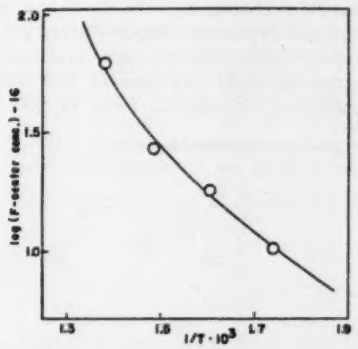

FIG. 4. Variation of the saturation concentration of F-centers with temperature.

tion is plotted against $1/T$; and it is found to be 8.0 ± 0.3 kcal/mole of F-centers formed at 350° and is reasonably constant over the range 300°–400°. From Fig. 4 it may also be seen that a concentration of F-centers in the neighborhood of 7.0×10^{17}/cc would be stable at 500°, while at 250° the stable concentration would be about 3×10^{16}. Further extrapolation in either direction would yield stability values of qualitative value only. Errors due to changes during quenching may be expected to play an increasing part at temperatures above 400°; and, even if analytical means for the denser crystals were available, it would be necessary to make the absorption measurements at the equilibrium temperature, where broadening of the bands would cause serious interference.

Whether or not the coagulated centers are considered colloidal depends on the definition of the term "colloidal." Since a phase change occurs during the coagulation, the term appears appropriate, though light-scattering experiments have not as yet demonstrated the presence of colloidal material as was accomplished in the case of NaCl. E. Burstein and J. J. Oberly[9] have observed only slight photoconductance for KBr containing the R'-band, when illuminated with light of wavelength lying within the band, which is to be expected if the centers are mainly colloidal. It would be interesting to carry out the experiments on crystals in which the colloidal band has been developed in the absence of R- and N-bands.

(B) Shift of the Colloidal Band Maximum

The maximum absorption of the colloidal band was observed between 750 and 775 mμ, but a definite shift toward longer wavelength was observed at the higher treatment temperatures. This may be caused either by a change in the size distribution of the colloidal centers or by a thermal equilibrium between F- and M-centers, which have a maximum absorption at 825 mμ. A systematic study of the purely thermal relation between these two centers would add much to the understanding of the nature of M-centers.

No particular dependence of band shape or maximum other than an approximately symmetrical braodening and increase in height was observed with increasing concentration of the colloidal form. In the case of R'-bands observed[1] in very dense crystals (1×10^{19} color centers/cc) there was a broadening which included most of the spectrum from 600 to 1200 mμ and having a maximum absorption wavelength varying with thermal and optical treatment.

The colloidal band was virtually unaltered when measured at the temperature of liquid nitrogen.

(C) Additional Conclusions

R- and N-bands were never observed either accompanying the colloidal band nor following its reconversion to the F-band, which shows that these centers are not the initial steps in the thermal coagulation of F-centers.

The homogeneity of the $F-R'$ equilibrium previously described[1] is readily accounted for by the fact that both crystals studied were unsaturated with respect to F-centers at 450°, and therefore no second phase was present. Owing to the interference of the optically-produced centers, this was not discernible from the absorption curves alone, although with the present knowledge that the colloidal centers absorb strongly at 760 mμ it may be inferred from the general shape of the curves.

A reason, in addition to the possibilities already suggested,[2] for the extremely variable susceptibility change when F-centers were converted to R'-centers by 15 minutes' heating at 300°, is that equilibrium was not attained in that time. Complete conversion to a colloidal form should result in a loss of 98 percent of the paramagnetism of the F-centers; complete attainment of the saturation concentration of F-centers, in the absence of any small paramagnetic centers of the R- and M-type, should result in a loss of about 96 percent. The smaller change, on the average, may be accounted for on the basis of either incomplete conversion, the presence of other paramagnetic centers, or both. The acceleration of the conversion as indicated by the results with the faraday balance, by combined illumination and heat treatment, is at present under study in this laboratory. Unfortunately, the extension of magnetic investigations to the concentration range in which optical analytical means may be used would be a problem involving extreme experimental difficulties.

The interest and support of the Office of Naval Research, and the valuable assistance of Ray F. Palmer in conducting some of the pH experiments, is gratefully acknowledged.

[9] E. Burstein (private communication).

Pressure Broadening in the Microwave Spectrum of Ammonia

C. A. POTTER,* A. V. BUSHKOVITCH, AND A. G. ROUSE
St. Louis University, St. Louis, Missouri

(Received May 14, 1951)

Half-widths of five pressure-broadened lines of the ammonia inversion spectrum have been measured as a function of total pressure. The perturbing gases were oxygen, helium, and nitrous oxide in various mix ratios. The results indicate a decrease in the collision diameters with increasing mix ratio of perturber to absorber. In the case of the nonpolar helium and oxygen the observed variation of collision diameter with quantum numbers of the lines can be compared with the predictions of the theory of collision broadening developed by P. W. Anderson. The general trend of the variation agrees with the theory, but its observed magnitude is considerably greater than predicted.

INTRODUCTION

PRESSURE broadening of the absorption spectrum lines of ammonia gas has been the subject of several experimental and theoretical investigations. Self-broadening has been observed by Bleaney and Penrose[1] for 17 lines in the inversion spectrum of ammonia. Broadening due to foreign perturbers was also investigated by Bleaney and Penrose and by Smith and Howard.[2] A rigorous quantum-mechanical theory has been developed by Anderson.[3]

This paper describes the results of measurements of microwave collision diameters correlated with quantum numbers, perturbing gas, and ratio of the number of perturbing molecules to the number of ammonia molecules at a constant total pressure. Five lines of the ammonia inversion spectrum were studied in the pressure range from 0.8 to 5×10^{-2} mm of Hg. The perturbing gases were oxygen and helium (nonpolar) and nitrous oxide (dipole, linear, nonsymmetric) in each case, each gas being used in at least two mix ratios. No ternary mixtures were used. In the case of oxygen, four mix ratios were used for the 3, 3 line.

The relations between half-width and collision diameter are[2]

$$\Delta\nu = n_1 v_1 b_1^2/\sqrt{2} \qquad (1)$$

for self-broadening, where $\Delta\nu$ is half-width in Mc-sec^{-1}, n_1 is number of ammonia molecules per unit volume, v_1 is mean velocity, and b_1 is collision diameter.

For broadening by a foreign gas, we have

$$2\Delta\nu = \sqrt{2} n_1 v_1 b_1^2 + n_2 v_{12} (b_{12})^2, \qquad (2)$$

where n_2 is the number of perturber molecules per unit volume, v_{12} is root-mean-square velocity of perturbing molecules with respect to ammonia molecules, and b_{12} is collision diameter of perturbing gas.

The half-widths at a pressure of 0.5 mm of Hg were used to calculate collision diameters.

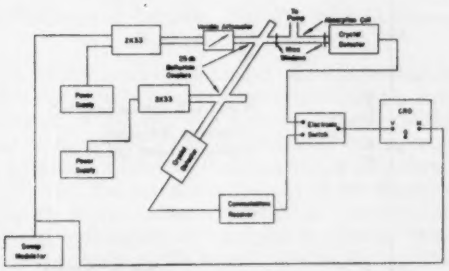

FIG. 1. Block diagram of microwave system.

EXPERIMENTAL

The spectrograph used in this investigation is a relatively low sensitivity unbalanced type, shown in Fig. 1. The data was permanently recorded as a photograph of the oscilloscope trace. For a given absorption line, the desired mix ratio was prepared and let into the absorption cell. It was then pumped out rapidly by a high speed forepump. The pressure was continuously monitored by a modified Pirani gauge. At convenient pressure intervals the pump was stopped and photographs taken. Usually twelve pressures were used, three photographs being taken at each pressure. The film strips were projected and measurements of half-width made directly. Marker pips provided the scale factor. Approximately 1500 exposures were used.

The apparatus which was used to make gas mixtures of known ratio is shown in Fig. 2. The calibrated burettes were filled with ammonia and perturber, respectively. The pressure of the gases in each tube

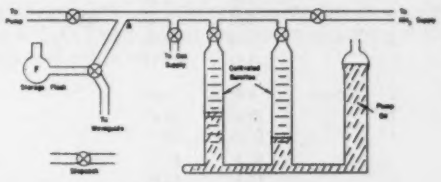

FIG. 2. Gas mixing apparatus.

* The material in this paper is a part of the author's thesis submitted in partial fulfillment of the requirements for the degree of Doctor of Philosophy at Saint Louis University.

[1] B. Bleaney and R. P. Penrose, Proc. Phys. Soc. (London) **60**, 540 (1948).

[2] W. V. Smith and R. Howard, Phys. Rev. **79**, 132 (1950); R. Howard and W. V. Smith, Phys. Rev. **79**, 128 (1950).

[3] P. W. Anderson, Phys. Rev. **76**, 647 (1949).

TABLE I. Collision diameters for ammonia inversion lines at 0.5-mm Hg pressure ($\times 10^8$ cm).

J	K	Bleaney and Penrose	This paper
2	1	10.5	10.3
8	7	13.2	13.2
3	3	13.8	13.9
4	4	13.8	13.9
6	6	14.1	14.0

was very close to atmospheric, differing from it negligibly because of unequal heights of liquid in each tube. The space A above the burettes and the storage flask F were evacuated. Then a measured amount of gas was let into space A, and allowed to diffuse into flask F. The region A was again evacuated and the procedure repeated with the ammonia. The ratio of volumes of A to F is known and appears as a correction factor to the mix ratio, which is otherwise determined by the changes in height of the oil columns in the burettes. To check the reliability of the gas mixer, a sample of each gas mix was withdrawn from the wave guide and the percentage of ammonia checked, using volumetric absorption by water of NH_3 gas. The mixes checked within a few percent in all cases.

The vacuum gauge which was used to record pressure was a modified Pirani, using a very small filament as the active element in a standard bridge circuit. The gauge was calibrated *in situ* for each gas involved, using a McLeod gauge as standard. Curves for each pure gas were plotted. The indication with a known mix ratio was taken to be linearly related to the reciprocal of the sum of the partial pressures. The variation between gases was somewhat less than might be expected from a true Pirani gauge because of the small size of the filament, so that it was not possible to calculate the response of the gauge using kinetic gas theory. The advantages of such a gauge are a comparatively fast response to pressure changes and a somewhat more linear calibration curve than with a true Pirani gauge.

TABLE II. Collision diameters of ammonia inversion lines with foreign perturbers ($\times 10^8$ cm). Mix A = 45 percent perturbing gas by volume. Mix B = 70 percent perturbing gas by volume.

J	K	Gas	Mix A	Mix B	Smith and Howard	Bleaney and Penrose
2	1	O_2	3.14	2.48		
8	7		4.05	3.78		
3	3		4.31	4.02	3.86	4.85
4	4		4.52	4.28		
6	6		5.05	4.71		
2	1	He	1.88	1.52		
8	7		2.62	2.28		
3	3		2.81	2.42	2.00	2.35
4	4		2.94	2.50		
6	6		3.14	2.73		
2	1	N_2O	9.51	8.85		
8	7		10.8	10.4		
3	3		11.2	10.7		
4	4		11.4	11.1		
6	6		12.5	12.0		

TABLE III. Collision diameter of ammonia 3, 3 line in oxygen.

Percent O_2	40	45	54	70
$b_{12}\times 10^8$ cm	4.38	4.31	4.22	4.02

The half-width was determined by measurement of an absorption line which was superimposed on the mode of the klystron tube used. Because of mode curvature, half-widths greater than approximately twelve Mc-sec^{-1} were not used. The low pressure limit was determined by the gas mixture, as the pump began to pump out the gases selectively at about one-tenth of a millimeter so that the mix ratio was no longer constant. In the case of self-broadening this limitation, of course, did not appear.

Since the measurements of the trace depend on faithful reproduction of line shape, the crystal detector which was used was calibrated. Actually, it was always operated in the region where the departure from square-law characteristic was negligible.

This spectrograph is capable of producing measurements at a relatively rapid rate. All that need be recorded for a given line, perturber, and mix is the pressure-gauge reading and the marker pip setting for each photograph. A mix can be prepared and observed in less than an hour, data being taken at as many pressures as desired.

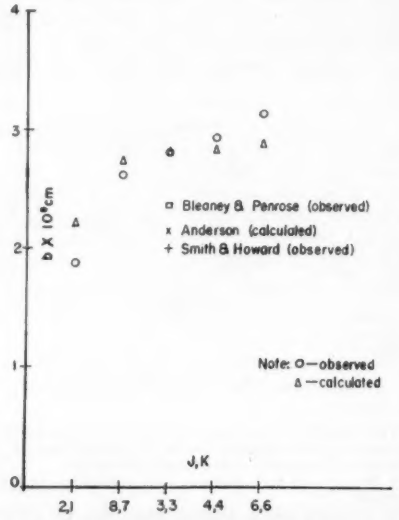

FIG. 3. Variation of collision diameter with quantum numbers of lines.

RESULTS

A. Variation of Collision Cross Sections with Mix

In all cases, the collision cross sections b_{12} decrease with increasing admixture of perturber, although Eq. (2) used for computing b_{12} should yield a constant value of b_{12}, the effect of mixture having already been allowed for. This result is disturbing, and its cause is, for the present, obscure. Experiments are under way to study this effect further. In the meantime, it seems best to take as the best value of b_{12} the result of extrapolating to 100 percent of perturber.

B. Effect of Pressure and Accuracy of Results

For any mixture, the half-width is directly proportional to total pressure in the pressure range from 0.1 to 0.6 mm of Hg. The accuracy which is claimed for our measurements is not better than about five percent in the case of broadening by foreign gases. The self-broadening collision diameters of ammonia are within one percent.

C. Self-Broadening of Ammonia

Table I gives our collision cross sections for self-broadening of ammonia, as well as those obtained by Bleaney and Penrose. Agreement is good.

D. Broadening by Foreign Perturbers

Table II gives the collision diameters as a function of mix ratio and absorbing line, for the three perturbers used: O_2 and He (nonpolar), and N_2O (dipole, linear, nonsymmetric). Values for the 3, 3 line obtained by Bleaney and Penrose and by Smith and Howard are also given; agreement with these is only fair. Table III gives the collision diameter of ammonia 3, 3 line in oxygen for several mixes, exhibiting most clearly the variation of cross-section diameter with mix, discussed under A.

E. Variation of Collision Diameter with Quantum Numbers of Lines

In the case of self-broadening of ammonia, our values agree closely with those of Bleaney and Penrose, and, therefore, in the main with Anderson's theory. In the case of nonpolar He and O_2, Anderson[4] has recently given a formula based on the interaction of the induced dipole with the quadrupole moment of the ammonia molecule which makes it possible to compute the collision cross sections as a function of quantum numbers. The results of this computation for the 3, 3 line perturbed by He and O_2 are in good agreement with the observed values obtained by Smith and Howard and are, therefore, a good deal smaller than our observed values (see Table III and Fig. 3). The variation with quantum number as given by Anderson's formulas is also a good deal smaller than observed by us, but the general type of variation is correctly given. This is exhibited in Table IV and Fig. 3. In both of these, the values for the 3, 3 line are our observed values, and the values for the other lines are computed (for He, mix A; the other cases are similar) from this using Anderson's factor depending on the quantum numbers [Eq. (14) of reference 5].

Table IV. Comparison with Anderson's theory. Agreement is assumed for the 3, 3 line; and the values for the other lines represent, therefore, variation from the 3, 3 line.

J	K	b, observed	b, calculated	b, Anderson
		Mix A, 45 percent of perturber, by volume		
		He		
3	3	2.81	(2.81)	2.15
2	1	1.88	2.21	
8	7	2.62	2.77	
4	4	2.94	2.85	
6	6	3.14	2.89	
		O_2		
3	3	4.31	(4.31)	3.35
2	1	3.14	3.39	
8	7	4.05	4.25	
4	4	4.52	4.37	
6	6	5.05	4.44	
		Mix B, 70 percent of perturber		
		He		
3	3	2.42	(2.42)	2.15
2	1	1.52	1.91	
8	7	2.28	2.38	
4	4	2.50	2.45	
6	6	2.73	2.49	
		O_2		
3	3	4.02	(4.02)	3.35
2	1	2.48	3.16	
8	7	3.78	3.96	
4	4	4.28	4.08	
6	6	4.71	4.14	

Broadening of ammonia lines by N_2O is markedly less than by the nonpolar O_2 and He. Unfortunately, an explicit formula based on Anderson's theory is not at present available for this case.

We are very grateful to Dr. P. W. Anderson for interesting and helpful discussions and correspondence and for the loan of his thesis. We would like also to thank Drs. W. V. Smith and R. Howard for sending us their results prior to publication. Our thanks are also due to J. V. Bonet, S.J., for assistance with some of the numerical computations.

[4] P. W. Anderson, Phys. Rev. **80**, 511 (1950).

A Search for Short Period Activities from U^{235} Fission Products*

J. E. Brolley, Jr., D. H. Cooper, Wm. S. Hall, M. S. Livingston,† and L. K. Schlacks
Los Alamos Scientific Laboratory of the University of California, Los Alamos, New Mexico
(Received May 17, 1951)

A search for gamma-ray activities with period 1–100 msec from thermal neutron fission of U^{235} gave negative results. 0.43±0.03 sec was the shortest observed. The period of B^{13} was found to be 27±3 msec. The cyclotron beam was pulsed to supply 1–10 msec neutron bursts. Coincidence scintillation detectors were employed.

INTRODUCTION

THE shortest period of radioactivity arising from U^{235} fission that has been published is a delayed neutron period of 0.05 sec; the next shortest neutron period is 0.43 sec.[1] It is to be expected that delayed neutrons follow a β- or γ-ray transition, but none such has been reported with half-lives shorter than about 1 sec.[2] Isomeric γ-ray transitions have been observed with periods ranging from 10^{-9} sec to months or years. The very short periods have been observed using electronic time delay techniques.[3] However, there is a conspicuous absence of periods in the millisecond region, although it might be assumed to be due to experimental difficulties. Unpublished studies of fission activities of 3- to 7-millisecond period made at Los Alamos[4] in 1943–1945 are contradictory, and it seems possible that the observations were the result of instrumental limitations. If β-ray activities of such periods exist in the medium weight elements resulting from fission, it would have considerable significance in the interpretation of β-ray theory. This paper reports a search for β-ray and γ-ray activities in the range between 1 and 1000 milliseconds. No periods were found shorter than the known 0.43-sec period corresponding to a delayed neutron activity.

EXPERIMENTAL ARRANGEMENTS

The emergent 11-Mev deuteron beam from the cyclotron was used to provide a pulsed source of neutrons. The beam was passed between electrostatic deflecting plates, through a focusing and analyzing magnet, and through a water tank shielding wall where it could strike a Be target at the end of an evacuated spout. A potential was applied to the deflecting plates which directed the beam off the target, then it was shorted out by an electronic switch for a time interval adjustable between 1 and 10 milliseconds, allowing a pulse of deuterons to strike the target. Neutrons from the Be target were slowed in a paraffin moderator and produced fissions in a U^{235} foil target surrounding a scintillation crystal, which was viewed by two RCA 5819 photomultiplier tubes. Gamma-radiation from the target was attenuated in a Pb cylinder 8 in. long between the target and the crystal. The experimental arrangement is shown in Fig. 1. Pulses from the two tubes were amplified and put through a discriminator coincidence circuit. Coincidence pulses were shaped and applied to the deflection plates of a cathode-ray oscillograph. The trace, to which millisecond time marks were also applied, was photographed by a moving film camera. Data consisted of plots of the number of pulses in each time interval against time.

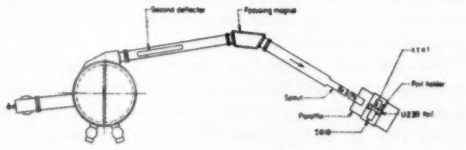

FIG. 1. Arrangement for pulsing and focusing the cyclotron emergent beam and for observing fission activities.

The electronic control circuits for pulsing the cyclotron and operating the camera were activated by a manual switch when the cyclotron beam was tuned to maximum, and performed a sequence of operations as follows:

(a) the camera film drive motor was started and allowed a 0.2-sec run to bring it up to speed;
(b) timing pulses of 1 to 10 millisecond spacing were applied to an electronic switch to turn off and on the electrostatic deflecting field;
(c) a coincident 1 to 10 millisecond square pulse was applied to the fifth dynodes of the photomultipliers to defocus them and prevent circuits from overloading during irradiation;
(d) the first timing pulse started a 100 kilocycle self-excited oscillator with frequency dividers to give 1 and 10 millisecond time marker pulses applied to the cathode-ray tube deflection plates;
(e) the second timing pulse turned off the cyclotron ion source voltage and the cyclotron radio frequency supply voltage;
(f) the camera motor was turned off 100 milliseconds (or more) after the second timing pulse.

Output pulses from the coincidence amplifier were too short (1 μsec) to give photographically observable marks on the film. A pulse-shaping circuit was developed to stretch the pulses to 5 μsec and provide a triangular shape. Amplitude controls for pulse height and timing signals were provided. Films were counted in a projec-

* Work performed under the auspices of the AEC.
† Now at the Massachusetts Institute of Technology, Cambridge, Massachusetts.
[1] Hughes, Dabbs, Cahn, and Hall, Phys. Rev. **73**, 111 (1948).
[2] Plutonium Project, Revs. Modern Phys. **18**, 513 (1946).
[3] S. DeBenedetti and F. K. McGowan, Phys. Rev. **74**, 728 (1948).
[4] LAMS-255, LA-253, LA-253A (unpublished).

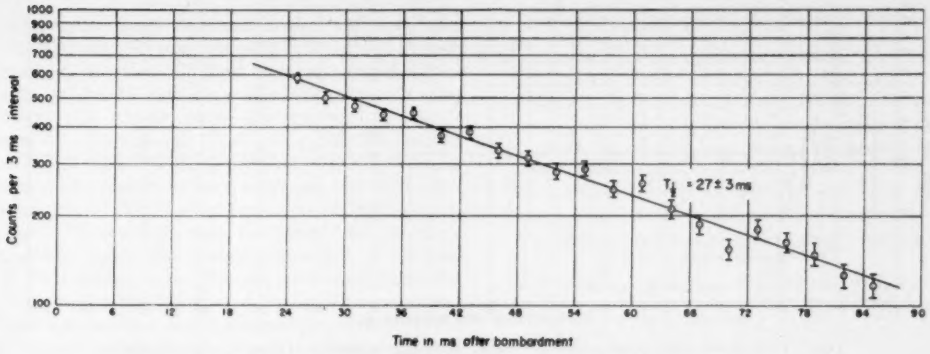

FIG. 2. Decay of B^{12} activity used to check performance of the instruments.

tion microscope. Pulse width, oscilloscope spot size, and photographic resolution limited countable intensities to about 20 per millisecond. Sufficient duplicate runs were made and the counts were added to obtain statistically significant data.

A ballistic galvanometer connected to the insulated Be target measured the total deuteron current pulse during the 1- to 10-millisecond bombardment. The galvanometer was calibrated with standard capacitances. A typical 5-millisecond pulse would record about 5 milli-microcoulombs, indicating an average deuteron beam of 1 microampere on the target.

Amplifiers, discriminator coincidence circuits, scalers, and power supplies were standard laboratory equipment developed by others at Los Alamos. The camera was a General Radio Type 651AE with rebuilt motor drive to give a speed of 100 milliseconds per foot of film. Films used were Eastman Photoflure and Linagraph Pan.

The fission sample was a foil of U^{235}, 0.010 in. thick, 2 in. wide, and 9.5 in. long, bent into a cylindrical shape around a 3-in. diameter crystal holder so as to offer a large solid angle to the crystal for fission-product γ-rays. The 10-mil thickness was chosen because it is approximately one radiation length for 1-Mev γ-rays. Three foils were available, for alternate use in case fission activity was built up in the one in use to give undesirably large background intensities. All three foils could be used simultaneously to obtain maximum intensity of fission activity if required.

The crystal was a cylinder 2 in. in diameter and 1 in. thick, with faces machined to a concave shape to fit the ends of the 5819 photomultiplier tubes. It was cut from a crystalline block of naphthalene having a concentration of 5 percent anthracene. One crystal holder had 0.62 in. of Al between the U^{235} sample and the crystal to absorb β-rays. Another holder was a frame with no absorber to observe both β-rays and γ-rays from the U^{235}. A third crystal holder of Pb 0.62 in. thick and with a Cd foil adjacent to the crystal was used to observe Cd γ-rays from delayed neutrons via the capture process.

The crystal holder and the two photomultiplier tubes were mounted in a light-tight cylinder located in a block of paraffin used as a neutron moderator. A cylindrical mu-metal shield around the cylinder shielded the photomultiplier tubes from the small stray field due to the cyclotron and focus magnets.

The "static" background arising from radioactivity in the uranium was observed by camera runs in which no beam was generated. It was usually small, of the order of 0.1 per millisecond, and could be subtracted directly from runs made with the beam. Background counts with the beam on, arising from causes other than uranium fission, were observed by replacing the U^{235} foil with a Pb foil having the same γ-ray absorption in alternate runs. These were due to activities induced in the surrounding materials and other causes. The "dynamic" background was assumed to be proportional to beam pulse intensity, and so was subtracted in proportion to the intensity as observed by the ballistic galvanometer in the several runs.

Preliminary runs were made to check the operation of the instruments, the sharpness of the pulse and recovery of the amplifiers after an irradiation pulse. In one test the deuteron beam was brought out into air through a thin window, and through a narrow slit onto the moving film of the camera. A direct photograph of the beam pulse was obtained. No tail was found following the pulse beyond the first 0.1 millisecond after termination of bombardment that was more than 0.1 percent the intensity of the main pulse. This proved that the pulsing was sufficiently sharp to carry observations down to one millisecond.

To check the effectiveness of the defocusing pulse on the photomultipliers, runs were made with a strong Co^{60} source placed adjacent to the crystal, pulsing the circuits but with no cyclotron beam. Counting rates were found to be identical in the intervals just before and after the pulse, and no counts were observed during the pulse.

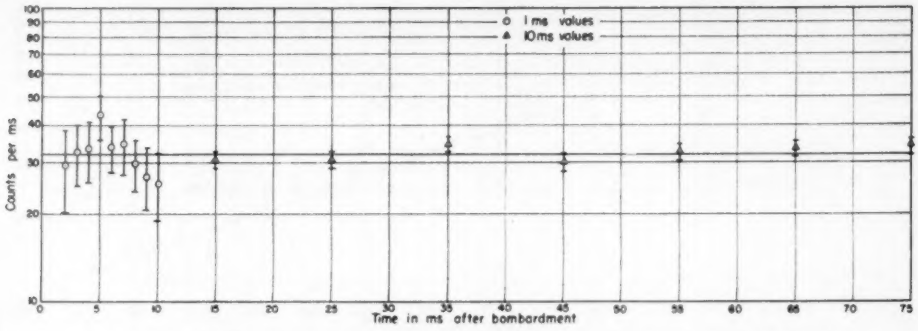

FIG. 3. Total β- and γ-ray activity from U^{235} fission products as a function of time after bombardment showing no millisecond decay periods.

In the preliminary runs a discontinuity in counting rates was observed at about 90 milliseconds, due to the heavy load of the cyclotron radio frequency power supply going off the line. This long time delay was caused by the slow action of several heavy relays and contactors in the circuit. As a consequence, no data are reported in the interval between 75 and 100 milliseconds. The continuous character of the data on both sides of this interval justify the conclusion that no significant information was missed.

As an over-all check on the performance of the system, the decay of B^{12} (produced by $B^{11}(d,p)B^{12}$) was measured, using a 10-millisecond pulse. Absorption between the boron and crystal was sufficiently small to permit the most energetic electrons (end point $\sim$13 Mev) to enter the crystal. Irradiations were made at high and low intensity levels. The high intensity run could not be counted much below 25 milliseconds. Background was negligible. The results are shown in Fig. 2. The observed period of 27 ± 3 milliseconds may be compared with another recent measurement of 27 ± 2 milliseconds.[8] The low intensity run had poorer statistics but could be satisfied by a 27-millisecond period down to the time of termination of bombardment.

RESULTS

No difference was observed, except for intensity, in preliminary runs using 1, 2, 5, and 10 millisecond bombardment pulses. The final runs to accumulate statistically significant data were made with 5 or 10 msec pulses. Runs were also made with 1, 2 or 3 U^{235} foils and found to be identical except for intensity. Three layers were used in the final runs. Five sets of

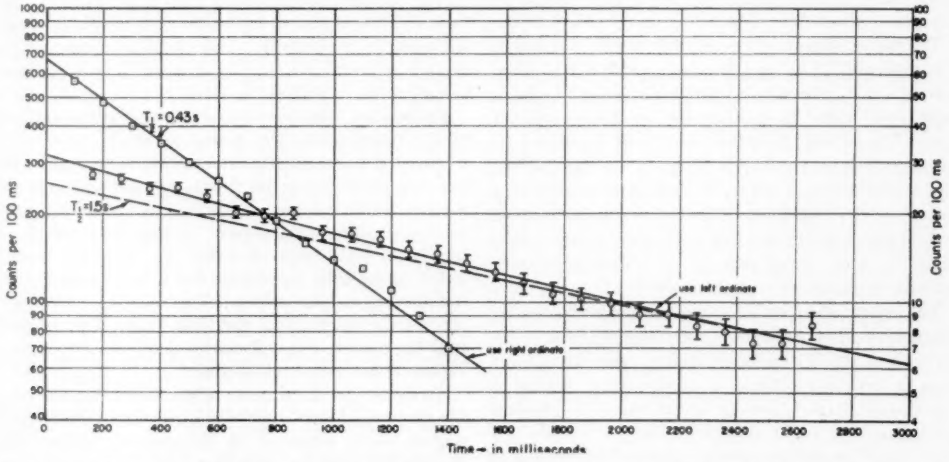

FIG. 4. γ-ray activity for U^{235} fission products as a function of time after bombardment from 100 to 2700 milliseconds. The observed period of about 1 sec can be resolved into 1.52- and 0.43-sec periods if the 1.52-sec period is assumed.

[8] J. V. Jelly and E. B. Paul, Proc. Cambridge Phil. Soc. **44**, 133 (1948).

fission measurement runs were made: (1) 5 msec pulse —no absorber—75 msec counting interval; (2) 10 msec pulse—Al absorber—75 msec counting interval; (3) 10 msec pulse—Al absorber—100–2700 msec counting interval; (4) 10 msec pulse—Pb absorber—no Cd—75 msec counting interval; (5) 10 msec pulse—Pb absorber —Cd—75 msec counting interval. Three variations were made in each set except (4) and (5): (a) U in—beam pulsed; (b) U in—no beam; (c) Pb foil in—beam pulsed. To correct the data, the results from (b) which represent chiefly the natural radioactive background of the uranium, were directly subtracted from (a). (c) represents the background arising from substances other than uranium and is assumed proportional to the beam pulse intensity. (a), (b), and (c) were normalized to unit galvanometer deflection and the difference taken. Corrected data from each run in a given set were added together and plotted on a semi-log scale as a function of time.

The results of set (1), which represent the total β-ray and γ-ray intensity, are plotted in Fig. 3. The first point is not plotted, since it represented an interval shorter than 1 msec due to persistence of the defocusing pulse. There was also a strong decay in the first half of the interval in both the U and Pb background runs, not due to fission, which would make large errors in the difference count. The source of this apparent decay period of a few tenths millisecond is not known, but may be associated with the finite slowing down time of neutrons in the moderator. Figure 3 shows clearly that there are no decay periods in the millisecond range, and this is illustrated by passing a horizontal line through the data. It is of course decaying with a period long compared to the interval displayed, which is determined in the longer duration runs. The vertical lines in this and other figures represent statistical errors in the total count for each time interval.

Identical results were obtained with set (2), which measured γ-ray activity only. The lower counting rates made the data less accurate, so the results are not plotted separately.

An estimate of the shortest period occurring in fission comes from the data of set (3), in which the camera was run for the maximum length of film available (100 ft), about 2700 milliseconds. The resulting decay curve shown in Fig. 4 indicates a period of the order of 1 sec. The curve does not extend for a long enough time to analyze it easily for components. However, if it is assumed that the predominant component at 2700 msec is the known 1.52-sec period[1] in the delayed neutron family, and this period is subtracted from the data, a residual activity of 0.43 ± 0.03 sec is revealed as the shortest period in fission activities. This value is in exact agreement, possibly fortuitous, with the shorter delayed neutron period of 0.43 ± 0.05 sec.[1] The analysis showing two periods is also indicated in Fig. 4.

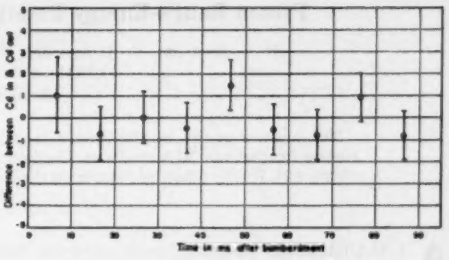

FIG. 5. Difference between runs with Cd in and Cd out plotted against time in an attempt to observe the 50-msec delayed neutron period. Results are negative.

Sets (4) and (5) with and without a Cd radiator surrounding the crystal and with a thick Pb absorber for U β- and γ-rays were made in the hope of accentuating the delayed neutron activities, and to search for a 50-msec period. No measurable difference was observed with and without Cd, the results were consistent with the results from sets (1) and (2). The difference between counts with Cd in and Cd out is plotted in Fig. 5, and shows no evidence for a 50-msec period.

CONCLUSIONS

From the results of this study it seems unlikely that any short period β- or γ-rays (1 to 100 milliseconds) arise from the products of slow neutron fission of U^{235}. Specifically, no periods were observed in the 3- to 7-msec region or in the 50-msec region where previous experiments had indicated the existence of activities. An activity of 5 percent the intensity of the observed 1-sec period could have been detected. The shortest period observed was of the order of 1 sec, which is resolvable into two periods of 1.52 and 0.43 sec if the 1.52-sec period is assumed. No evidence has been obtained for delayed neutron activities, but the β- and γ-ray results throw considerable doubt on the validity of the reported 50-msec neutron period.

These negative results are in agreement with present β-ray theory, which requires excitation energies above the neutron binding energy for medium weight elements in order to have a half-life of less than 0.5 sec. The absence of gamma-ray activity in the millisecond range from isomeric transitions is also significant, since fission products cover such a wide spread of elements.

We are indebted to B. Watt for advice and loan of equipment, to C. Sewell, H. Fishbine, and W. Johnstone for the design and construction of the electronic control circuits, to Dr. Alice Armstrong for supervising the counting by the microscope observing group and to the cyclotron crew for their generous cooperation.

Proton Range-Energy Relation for Eastman NTA Emulsions*

H. T. RICHARDS, V. R. JOHNSON,† F. AJZENBERG, AND M. J. W. LAUBENSTEIN‡
University of Wisconsin, Madison, Wisconsin

(Received May 10, 1951)

The ranges of protons recoiling from monoergic neutrons have been used to determine a range-energy relation for Eastman NTA emulsions. The experimental results for proton energies from 1 to 17 Mev agree closely with Webb's computed range-energy relation.

A CALCULATED stopping power curve for Eastman NTA and NTB emulsions has been published by Webb.[1] This calculated stopping power was in considerable disagreement with an experimental calibration for NTB plates reported by Peck,[2] but was in fair agreement with the data of Lattes, Fowler, and Cuer[3] for Ilford B-1 emulsions which have approximately the same chemical composition. More accurate range-energy data for the Ilford C-2 emulsions have been recently published by Roblat.[4] Rotblat also reports some data which indicate that Kodak NT-2A (Eastman NTA?) emulsions have a few percent greater stopping power than the Ilford C-2.

During the past year several reactions have been investigated at Wisconsin by observing in Eastman NTA emulsions the proton recoils from neutrons. The reactions studied were $Li^7(p,n)Be^7$, $Be^9(p,n)B^9$, $Be^9(d,n)B^{10}$, $B^{10}(d,n)C^{11}$, $B^{11}(d,n)C^{12}$, and $O^{16}(d,n)F^{17}$. Details of the exposure and the measurement criteria are given in the original papers.[5–9] These data can

TABLE I. Calibration data for the range-energy curve of protons in Eastman NTA emulsions.

Reaction	Q (Mev)	Angle of observation	Mean energy of incident particles (Mev)	Mean energy of recoil protons (Mev)	Mean range of recoil protons (microns)
$Li^7(p,n)Be^7$	-1.646 ± 0.002[a]	0	3.36	1.67	32±1
		80	3.91	1.83	36±1
		0	3.91	2.23	51±2
$Be^9(p,n)B^9$	-1.852 ± 0.002[b]	90	3.80	1.37	23±1
		45	3.80	1.73	35±1
		0	3.80	1.91	39±2
		0	3.93	2.03	44±2
$Be^9(d,n)B^{10}$	$+4.363\pm0.016$[c]	80	3.41	6.66	296±7
		0	3.41	7.78	387±12
$B^{10}(d,n)C^{11}$	$+6.473\pm0.011$[d]	80	3.40	8.78	503±16
		80	3.64	8.94	492±17
		0	3.64	10.15	634±11
$B^{11}(d,n)C^{12}$	$+13.740\pm0.014$[e]	80	3.40	15.57	1271±55
		0	3.40	16.93	1536±48
$B^{11}(d,n)C^{12*}$	$+9.302\pm0.020$[f]	80	3.40	11.44	752±25
		0	3.40	12.63	897±16
		0	3.64	12.88	971±18
$O^{16}(d,n)F^{17}$	-1.63 ± 0.01[g]	0	3.06	1.32	22±1
		10	3.06	1.32	21±1
		20	3.06	1.30	21±1
		30	3.06	1.28	20±1
		90	3.06	1.01	14±1

[a] Herb, Snowdon, and Sala, Phys. Rev. **75**, 246 (1949).
[b] Richards, Smith, and Brown, Phys. Rev. **80**, 524 (1950).
[c] Computed from $Q=(2D-He^4)-(Q_d+Q_{d_p}+Q_{d\alpha})$, where $(2D-He^4)=23.842\pm0.008$ Mev [Ewald, Z. Naturforsch. **5**, 1 (1950)]. $Q_d=2.226\pm0.003$ [Mobley and Laubenstein, Phys. Rev. **80**, 309 (1950)] and Q_{d_p} and $Q_{d\alpha}$ are the MIT values for $B^{10}(d,p)B^{11}$ and $B^{11}(d,\alpha)Be^9$ [Strait, Van Patter, Buechner, and Sperduto, Phys. Rev. **81**, 747 (1951)].
[d] Computed from $B^{10}(d,p)B^{11}$ and $B^{11}(p,n)C^{11}$ with Q_{d_p} from Strait, *et al.* (footnote c); and Q_{p_n} is from Richards, *et al.* (footnote b).
[e] Computed from $Q=(2D-He^4)-(Q_d+Q_{d_p}'+Q_{d\alpha}')$, where the quantities are the same as in footnote c except the primed Q's refer to Strait, *et al.*'s values for $C^{12}(d,p)C^{13}$ and $C^{12}(d,\alpha)B^{11}$.
[f] Computed from Malm and Buechner's value for the C^{12} excited state, 4.438 ± 0.014 Mev (Phys. Rev. **81**, 519 (1951)) and the above Q value for the ground-state transition.
[g] F. Ajzenberg, unpublished threshold determination.

* Work supported by the AEC and the Wisconsin Alumni Research Foundation.
† Now at Midwest Research Institute, Kansas City, Missouri.
‡ Now at North American Aviation, Downey, California.
[1] J. H. Webb, Phys. Rev. **74**, 511 (1948).
[2] R. A. Peck, Phys. Rev. **72**, 1121 (1947).
[3] Lattes, Fowler, and Cuer, Proc. Phys. Soc. (London) **A59**, 883 (1947).
[4] J. Rotblat, Nature **165**, 3871 (1950); Nature **167**, 550 (1951).
[5] Johnson, Laubenstein, and Richards, Phys. Rev. **77**, 413 (1950).
[6] Johnson, Ajzenberg, and Laubenstein, Phys. Rev. **79**, 187 (1950).
[7] F. Ajzenberg, Phys. Rev. **82**, 43 (1951).
[8] V. R. Johnson (to be published).
[9] F. Ajzenberg (to be published).

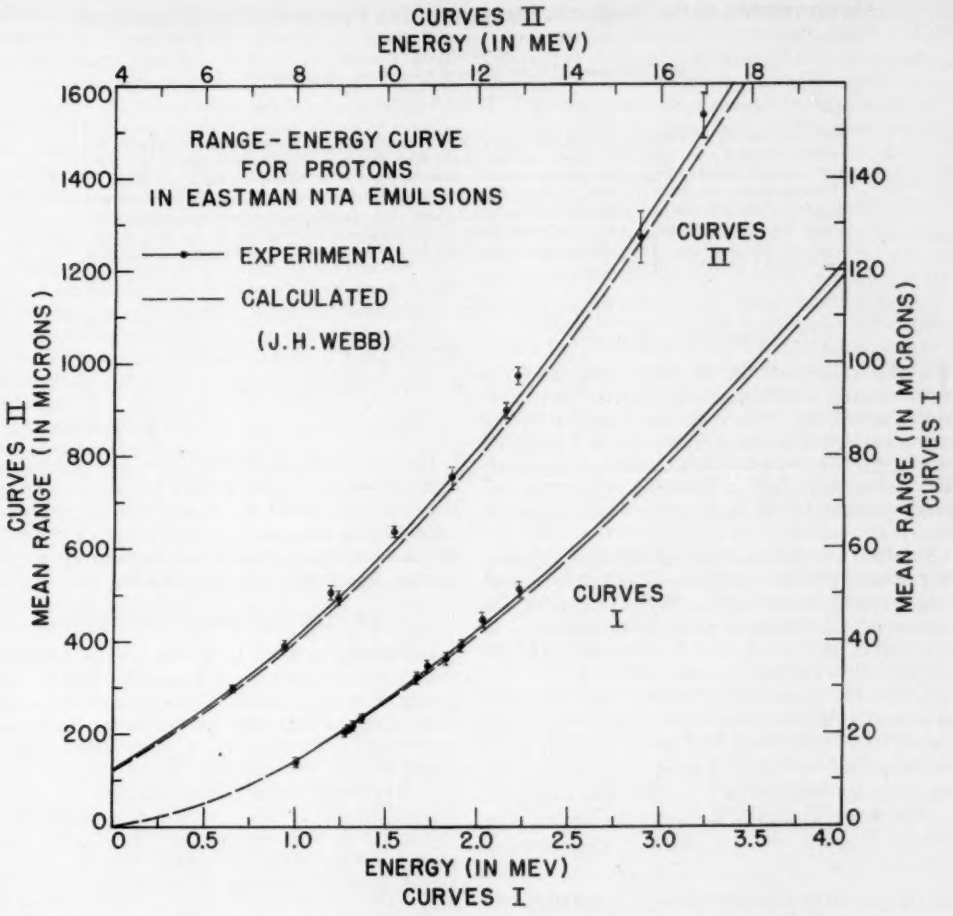

FIG. 1. Range-energy curve for protons in Eastman NTA emulsions. Both curves refer to emulsions used under ordinary laboratory humidity conditions.

be used for calibration points on a range-energy curve for protons stopped in Eastman NTA emulsions. The data cover a range of proton energies from about 1 to 17 Mev. The uncertainty in recoil proton energy is much smaller than the experimental mean range determination in most cases since the reaction Q values are known to about 0.5 percent or better, the bombarding energy to 0.1 percent, and the uncertainty in target thicknesses does not appreciably increase the energy uncertainty. The uncertainty in mean range indicated in Table I and in the figure is 0.675 times the root-mean-square deviation of all track lengths in the group.

All the data are summarized in Table I and in Fig. 1. The figure also includes Webb's range-energy curve[1] which is calculated for an emulsion whose effective stopping power is closely the same as the Eastman NTA, NTB, and the Ilford B-1 and C-2 emulsions. The calculated and observed range-energy curves are now in satisfactory agreement, though the experimental data do indicate a slightly lower stopping power than Webb's calculations. In fact, the smooth curve drawn through the experimental points of Fig. 1 is exactly 2 percent higher than Webb's calculated curve.

It should be emphasized that Webb's calculations and our experimental data refer to plates used under ordinary relative humidity conditions (around 60 percent), and if emulsions are used under vacuum conditions the stopping power may be several percent higher (for example, see reference 4.)

Measurement of the Magnetic Moment of the Proton in Bohr Magnetons*

J. H. GARDNER†
Lyman Laboratory, Harvard University, Cambridge, Massachusetts
(Received April 5, 1951)

An experimental determination of the ratio of the precession frequency of the proton, $\omega_p=\mu_p H_0$, to the cyclotron frequency, $\omega_e=eH_0/mc$ of a free electron in the same magnetic field has been carried out. The result, ω_p/ω_e, is the magnitude of the proton magnetic moment, μ_p, in Bohr magnetons, since $\gamma_p=2\mu_p/\hbar$.

Possible sources of systematic error were carefully investigated and in view of the results of this investigation and the high internal consistency of the data it is felt that the true ratio, uncorrected for diamagnetism, lies within the range $\omega_e/\omega_p=657.475\pm0.008$. If the diamagnetic correction to the field at the proton for the hydrogen molecule is applied here the proton moment in Bohr magnetons becomes $\mu_p=(1.52101\pm0.00002)\times10^{-3}(e\hbar/2mc)$.

1. INTRODUCTION

IN this experiment the magnetic moment of the proton, μ_p, is obtained in terms of the Bohr magneton, $\mu_0=eh/2mc$. The cyclotron frequency in the microwave region of the free electron in a magnetic field, $\omega_e=eH/mc$, is measured by the resonance method, and the magnetic field is measured in terms of the proton moment, $\omega_p=2\mu_p H/h$, by the nuclear resonance absorption method.

In addition to the importance of the ratio μ_p/μ_0 as a fundamental physical constant its significance as here measured is increased by its ability to provide further experimental confirmation to recent developments in quantum electrodynamics and by its utility in the calculation of the constants α, e/mc, and M/m.

In 1947 Kusch and Foley[1] measured, by the method of atomic beams, the ratios of the g-factors of various atomic states and showed that the spin g-factor is not precisely twice the orbital g-factor. This anomaly was explained by Schwinger[2] who showed that a radiative correction to the magnetic moment of the electron in an external magnetic field was necessary. This correction gives the value

$$g_s/g_0=2(1+\alpha/2\pi-2.973\alpha^2/\pi^2)=2(1.001147)$$

to fourth order in e. Kusch and Foley's experimental value of this quantity is $g_s/g_0=2(1.00119)$.

More recently Taub and Kusch compared the proton g-factor, g_p, with the g-factors of the ground states of indium and of cesium, which in turn were known in terms of the g-factor of the ground state of sodium from the experiments of Kusch and Foley and of Kusch and Taub.[3] Since the g-factor of the ground state ($^2S_{\frac{1}{2}}$) of sodium is simply the spin g-factor of the electron g_s[3] one can calculate the ratio of the proton moment to the Bohr magneton by using either the experimental or theoretical value of g_s/g_0 as follows:

$$\frac{g_p}{(g_J)_{\text{In}}}\times\frac{(g_J)_{\text{In}}}{(g_J)_{\text{Na}}}\times\frac{(g_J)_{\text{Na}}}{g_0}=[g_s]=\frac{g_p}{g_0}=\frac{\mu_p}{(\frac{1}{2}e\hbar/mc)}. \quad (1)$$

The experiment described in this paper permits the direct measurement of g_p/g_0 using free electrons rather than electrons bound in atoms. One can therefore calculate g_s/g_0 where g_0 here refers to free electrons, to give an additional experimental confirmation of the electron spin magnetic moment anomaly.

2. THE ELECTRON RESONANCE METHOD

The general problem is to measure the cyclotron frequency ω_e, of electrons in a magnetic field by subjecting them to an alternating electric field transverse to the magnetic field. In order to obtain a sharp resonance effect as the frequency, ω, of the electric field is varied through the frequency ω_e, the electrons must have long transit times through the field and ω and hence ω_e must be as high as possible. Long transit times correspond to slow electrons and long paths. This suggests the use of thermal velocity electrons, or some means of velocity selection to obtain even lower velocities.

The cyclotron frequency, ω_e, is limited by the magnetic fields obtainable and the electric field frequency, ω, is limited by the equipment and techniques available. We chose 9400 mc/sec for ω, largely because of the immediate availability of equipment working at this frequency. The corresponding magnetic field is about 3300 gauss.

To detect the resonance one could use some means of observing the reaction of the electron resonance on the microwave circuit. We chose the more direct method of observing the effect of the resonance on the current through a circuit involving the electron beam.

A ribbon-shaped beam of slow electrons drifting parallel to the magnetic field is formed by a slit. The beam is kept from expanding by the field inasmuch as the helical trajectories of the individual electrons have axes parallel to the field and radii determined by their initial transverse velocities, assuming no interaction

* This research was assisted by the joint program of the ONR and AEC.
† Now at Brigham Young University, Provo, Utah.
[1] P. Kusch and H. M. Foley, Phys. Rev. **74**, 250 (1948).
[2] J. Schwinger, Phys. Rev. **73**, 416 (1948); R. Karplus and N. M. Kroll, Phys. Rev. **77**, 536 (1950).
[3] P. Kusch and H. Taub, Phys. Rev. **75**, 1477 (1949).

between the electrons. A ribbon rather than a pencil beam is used to minimize the effect of this interaction on the resonant frequency. This will be discussed later. This beam is subjected to a weak transverse microwave electric field. At resonance the beam expands since the effect of the alternating electric field is then to increase the transverse velocity of the electrons cumulatively so that the radii of their orbits increase.

The beam is selected by a rectangular slit on one side of the short dimension of a $1\times\frac{1}{2}$-in. rectangular wave guide. The wave guide propagates only the TE_{10} mode so that inside the guide the beam is expanded by the transverse electric field. A second slit on the opposite side of the guide permits the unexpanded beam to pass through and be collected at an anode but fails to admit all the expanded beam. Hence one could recognize the resonance condition by a decrease in the current at the anode.

The radius of the electron orbits under the influence of the magnetic field alone is given by

$$r=cmv/eH. \tag{2}$$

For a field of 3300 gauss and thermal velocity electrons ($\sim 2\times 10^7$ cm/sec) this is approximately 0.003 mm. The width of the slit is 0.1 mm or approximately 30 electron-orbit radii. In the presence of the microwaves if this initial radius is neglected the radius of the orbit after the electron has traveled across the guide of width a with a velocity u parallel to the field is given by

$$r_a=\left|\frac{eEa}{m\omega\pi u}\frac{\cos(\frac{1}{2}a\delta\omega/u)}{1-(a\delta\omega/\pi u)^2}\right|, \tag{3}$$

where $\delta\omega=\omega-\omega_c$ is the difference between the microwave frequency and the cyclotron frequency and E is the maximum amplitude of the microwave electric field. This formula assumes standing waves in the guide excited in the TE_{10} mode. At resonance ($\delta\omega=0$), for the radii to expand to approximately the original width of the beam upon traversal of the guide, an electric field of 0.03 esu is required. This corresponds to a power of 20 milliwatts propagating into the guide if the beam is at a voltage maximum. For $a\approx 2.3$ cm, thermal electrons revolve about 1000 times during their transit through the guide.

If one assumes that the only factor serving to diminish the number of electrons arriving at the anode as resonance is passed through is the action of the second slit which discriminates against electrons with large radii one obtains for the current at the anode as a function of the initial velocities of the electrons,

$$I(\alpha)=I_0(\alpha)\left(1-\frac{AeE}{m\omega w}\left|\frac{\cos(\frac{1}{2}\pi\delta\omega/\alpha)}{\alpha(1-(\delta\omega/\alpha)^2)}\right|\right), \tag{4}$$

where

$$I_0(\alpha)=2N(\alpha)eLw;\quad \alpha=\pi u/a. \tag{5}$$

$2w$ is the width of the slit, L the length, and $N(\alpha)$ is the number of electrons with velocity between u and $u+du$. A is either 1 or $1/\pi$, depending upon whether one assumes that no electron striking the wall of the slit is collected or all electrons entering the slit are collected, respectively. The full width at half-value, $I_{\frac{1}{2}}$, of the dip in current as resonance is passed through may readily be calculated for electrons all having the same velocity to be

$$I_{\frac{1}{2}}=3.30\alpha/2\pi. \tag{6}$$

For thermal velocity electrons (approximately 2×10^7 cm/sec) and a guide width of 2.3 cm, this is of the order of 14 mc or 4.3 gauss. If one were to take into account the maxwellian distribution of initial velocities in calculating $I_{\frac{1}{2}}$ this value would be somewhat reduced.

It may be noted that the formula for the current admits the possibility of side lobes on the current dip and these were observed in the experiment. One would expect the first return of the current to full value after passing resonance to occur for that frequency at which the electrons gain energy from the field during the first half of their journey across the guide but completely lose it again by the time they reach the second slit. Of course, these side lobes would be smoothed out by a maxwellian velocity distribution in the beam.

In the preceding discussion the effect of the interaction of the electrons on each other was completely neglected. Under certain conditions of operation this space charge effect becomes of considerable importance and in fact provides a means of detection of the resonance which depends to a large extent upon the more slowly moving electrons in the beam. In this sense it provides velocity selection. By making use of this effect we were able to make measurements with resonance widths of the order of 0.3 gauss. This will be discussed after the apparatus is described.

The effect of the space charge on the resonant frequency must be considered. Each electron is moving in the average field due to the other electrons. If one assumes that the only electrons contributing to a change in the resonant frequency are those inside a pencil beam whose circumference is defined by the orbit of the electron, the effect of the others being averaged out over many cycles, then the force on this electron, neglecting the microwaves, is

$$F=mr\omega^2=(Hev/c)-eE. \tag{7}$$

The field due to this cylindrical distribution of charge is

$$E=2\pi r\rho, \tag{8}$$

where ρ is the space charge density and r is the radius of the electron orbit. Then

$$m\omega^2=(He\omega/c)-e2\pi\rho. \tag{9}$$

Solve for ω

$$\omega=\frac{eH}{2mc}\pm\frac{1}{2}\left(\left(\frac{eH}{mc}\right)^2-\frac{8\pi\rho e}{m}\right)^{\frac{1}{2}}. \tag{10}$$

If we assume the space charge effect to be small, we

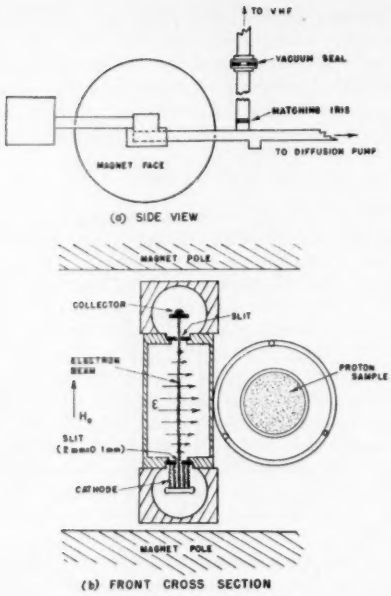

FIG. 1. Electron resonator.

have approximately

$$\omega=\frac{eH}{mc}\left(1-\frac{2\pi\rho e/m}{(eH/mc)^2}\right)=\omega_0\left(1-\frac{2\pi\rho e/m}{\omega_0{}^2}\right). \quad (11)$$

3. ELECTRON RESONANCE APPARATUS

The electron resonance apparatus consisted essentially of $1\times\frac{1}{2}$-in. shorted wave guide with a 0.080 $\times$0.004-in. slit in the narrow dimension of the guide on either side located at a voltage maximum $\lambda/4$ (0.440 in.) back from the short. An indirectly heated oxide-coated cathode was located just outside of the slit on one side and a collector plate was similarly located near the other slit. These elements were contained in a copper sheath and a $\frac{3}{8}$-in. hole between the sheath and the guide on either side allowed rapid evacuation. The holes were located $\lambda/2$ back from the short to avoid disturbing appreciably the rf currents in the guide (see Fig. 1). The flat rectangular cathode was heated by a tungsten filament folded back and forth several times and stuffed inside the cathode sheath. Batteries supplied the filament current.

The tube was evacuated to a pressure of 2×10^{-6} mm Hg by an oil diffusion pump (Distillation Products, Inc., VMF-20-W) backed by a Cenco Hyvac. This was attached at the end of the guide opposite to the location of the short. The microwaves were introduced between these through a T. These were kept out of the vacuum pump end by means of a stub designed to present an apparent short circuit adjacent to the T on the pump side. A Corning 707 glass window sealed to Kovar was soldered to the guide between the T and the oscillator by means of an asymmetrical E plane iris. The pressure was measured by means of an ionization gauge made from a 24-C(3-C-24) triode.

The rf source was a 723-A klystron in a TS-13/AP test set. An attenuator in the output provided a convenient control of the power available at the position of the electron beam.

The wave guide was maintained at some voltage V_a relative to the cathode. This is an important parameter in the operation of the tube. The collector plate was maintained at approximately 20 volts positive relative to the guide so as to collect all of the electrons that came through the second slit. The anode current could be measured by means of a galvanometer or be amplified and displayed on a CRO. A simple audio amplifier was used for this latter purpose.

The magnetic field was provided by a water-cooled electromagnet. The magnetizing current was furnished by storage batteries. The pole faces of the electromagnet were 8 in. in diameter and were separated by a 2-in. gap. The gap was uniform aside from 0.062-in. thick by 0.320-in. wide raised rims at the perimeters of the pole faces which were provided to correct for edge effects. Coarse control of the magnetic field was effected by a sliding rheostat made from strips of Advance alloy connected in series with the magnet. Fine control was provided by an auxiliary coil around a pole cap.

A second auxiliary coil on the pole cap of the magnet provided 60-cycle modulation of the magnetic field when the resonance was to be displayed on the CRO. The gross magnetic field was set approximately at the resonance value and this small modulation carried the field back and forth through the resonance. The same variac that supplied the current to this coil provided the CRO sweep. A phase-shifting network in this circuit made it possible to adjust the phase of the sweep relative to that of the modulation.

4. OPERATION OF THE ELECTRON RESONATOR

The electron apparatus was first operated with the voltage V_a between guide and cathode at approximately 5 volts and above (guide positive with respect to cathode) and the anode current was observed with a sensitive galvanometer (sensitivity approximately 0.04 microampere per millimeter deflection). Under these circumstances a dip in the current was observed as the magnetic field passed through resonance and the width of the dip turned out to be approximately that predicted by the foregoing equations. Side lobes were observed as predicted by Eq. (4). The current was of the order of magnitude of 0.4 microampere and the dip brought it to approximately 0.3 microampere.

When the anode current, i_p, was amplified and displayed on the CRO it was found possible to obtain peaks in the current rather than dips if V_a was less than about 3 volts. These peaks were considerably

narrower than the dips, being of the order of magnitude of 0.5 gauss as opposed to approximately 5 gauss for the dips. The anode current under these circumstances was something less than 0.0005 microampere when away from resonance and could be made to go several hundred times this value at resonance.

This behavior can be understood by noting that owing to the presence of the magnetic field to a first approximation one has in effect two infinite plane diodes in series. The magnetic field confines the electrons to a cylindrical sheath thus making it possible to obtain an approximate one-dimensional treatment of the space charge problem. Since the static electric field inside the guide is due to the electrons alone a potential minimum is present in this region and space charge limitation may exist here. As one passes through reonance the space charge limitation, and the current through the tube, i_p, shows a peak. This is evidently very sensitive to the character of the potential minimum due to the space charge. The electrons contributing most to the potential minimum are those moving with small velocities at the minimum, and these are the ones which are acted on for a long time by the microwaves, with the result that the resonance width is very small.

For the plane one-dimensional case[4] space charge limitation may exist for V_a between about 0.7 and 2 volts with an anode current of 10^{-9} ampere which is roughly the value obtained. This checks as well as could be expected with the range of V_a over which the peak in anode current may be observed.

Inasmuch as this space charge detection was made use of in the measurements the remainder of the discussion will have reference only to this type of detection.

The important parameters studied in connection with the resonance were the effect of the microwave power level and the effect of the voltage, V_a.

The microwave power input could be varied over a wide range. It was observed that if one started with the smallest power for which the resonance was observable and increased the power the magnitude of the resonance peak would increase very rapidly. The width would remain constant for low power but would eventually beging to broaden. Side lobes would develop. In some cases the region in the neighborhood of the peak would begin to invert for very large power. This effect may be due to the fact that some electrons getting through the potential minimum were spiraling to large enough radii to miss the second slit. This explanation is not entirely satisfactory because the dip in the peak was less than one gauss wide and one would expect a width of about 3 gauss in this case. It is very likely possible, however, to narrow the width of the dip for this sort of situation by misaligning the two slits so that the expanded beam does not completely fill the second slit. Then, of those electrons reaching the second slit, only those with the smaller velocities would be effective in changing the current through the tube. This type of arrangement would amount to velocity selection for those electrons getting past the potential minimum.

The voltage V_a between the wave guide and the cathode controls the initial velocities of the electrons in the beam and also the beam current. The value of this voltage was known only with an additive constant since the contact potential was not known. A plot of the current to the collector, i_p, (anode current) and of the current entering the first slit as a function of V_a appears in Fig. 3. The values of the current entering the first slit are only approximate and relative. It was assumed that the ratio of this current to the anode current was approximately proportional to the height of the resonance curve for the power high enough to produce saturation, a situation in which space charge limitation is not present and all the electrons passing the first slit are collected at the anode. The values in the graph are really the heights of the resonance curve, measured under these limiting conditions.

The range of V_a used was about 0 to 3 volts. The resonance width did not vary appreciably with V_a, and in fact the resonance appeared to be at its narrowest for high V_a. It is possible that this is due to the fact that the potential minimum is sharper and more critical for large V_a.

An interesting effect occurs as one increases V_a (refer to Fig. 2). With the magnetic field due to the filament opposing the gross magnetic field, increasing with small V_a of less than 1.0 volt merely increases the height of the resonance peak but on going from 1.0 to 1.2 volts the magnetic field at which the peak occurs shifts over by about 1 part in 10,000. No further shift takes place upon increasing beyond 1.2 volts. The height of the peak does not at first change appreciably, and in fact decreases to some extent, till it eventually begins to rise again and the resonance broadens. The locus of the peaks on the CRO display as one increases V_a is shown in Fig. 2. The oscilloscope picture becomes unsteady and the effect cannot be studied much beyond where the rise begins again. If the variation in V_a is repeated with the field due to the filament current aiding the gross magnetic field the peak begins to shift slightly in the opposite direction by something less than one part in 50,000 and then shifts back again with no further shift above 1.2 volts.

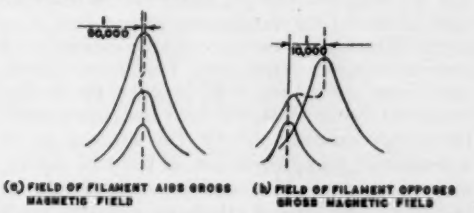

FIG. 2. Effect of changing bias voltage upon frequency at which resonance peaks occur. Dotted line shows locus of peaks as one increases V_a.

[4] Fay, Samuel, and Shockley, Bell System Tech. J. 17, 49 (1938).

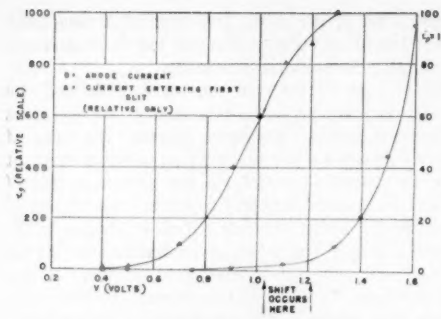

FIG. 3. Current-voltage relationships for electron tube.

This behavior is attributed to the combination of two effects: the change from a maxwellian velocity distribution to one for which a finite minimum velocity exists with a resultant shift of the region of the beam at which the most important contribution to the resonance takes place towards the cathode and hence further into the magnetic field of the heater current; and the accompanying increase in space charge density of this region with a resultant space charge shift in the resonance.

The fact that the heater current actually produced a magnetic field sufficiently large to affect the resonance was verified by momentarily shorting out this current. If the voltage V_a was under 1.0 volt, a shift in the position of the electron resonance of the order of 1 part in 60,000 took place. Furthermore, this shift took place in the opposite direction if the same thing was done with the filament current reversed. For V_a above 1.2 volts the shift is of the order of 1 part in 15,000.

The space charge shift is the same independent of the direction of the filament current and hence in the one case the two effects add and in the other case they compensate one another.

That part of the shift which is attributed to a change in the space charge density in the critical part of the beam is in magnitude about 1 part in 35,000. It has the correct sign to be associated with an increase of space charge density as V_a is increased from 1.0 to 1.2 volts.

The magnetic field of the cathode may be roughly estimated from a knowledge of the filament current and this, in conjunction with the known shift in resonance upon reversal of the filament current may be used to predict the position of the important region of the beam as far as resonance is concerned. The filament current was 1.6 amp and the area of the portion of the filament which was doubled back and forth and pushed inside the cathode was about 0.5 cm². This situation can be approximated by a current loop of this area and the magnetic moment of an equivalent dipole may be calculated. This type of calculation gives the result that the important region is about $\frac{3}{8}$ of the distance across the guide from the cathode side, where the dipole magnetic field is 0.05 gauss, for V_a below 1.0 volt; and about $\frac{1}{4}$ of the same distance where the dipole field is 0.165 gauss, for V_a above 1.2 volts.

If the space charge density in the neighborhood of the potential minimum were known one could readily calculate the shift in resonant frequency one would expect due to the space charge effect. Inasmuch as the calculation of the space charge has not been done it is difficult to obtain an estimate of what this shift should be. One can obtain a value for this space charge at the potential minimum by assuming that equilibrium conditions exist there so that the Boltzmann equation can be used. In this case

$$\tfrac{1}{4}n\bar{c}\approx\tfrac{1}{4}ne(kT/m)^{\frac{1}{2}}=J_0, \tag{12}$$

so

$$\rho=4J_0(2m/\pi kT)^{\frac{1}{2}}, \tag{13}$$

where $\bar{c}$ is the average velocity of the electrons, J_0 is the current density at the anode, and n is the number of electrons/unit volume. Taking J_0 as approximately 10^{-6} ampere/cm² one obtains a value for the shift in resonance of approximately one part in a million.

The important region of the beam for the resonance is likely a little away from this minimum on the cathode side where the density is greater so this shift might be expected to be somewhat larger than that calculated. For large values of V_a it is evident from the increase in the effect of the field of the heater current that this important region has shifted further toward the cathode to a considerably more dense space charge region.

The proper calculation of the space charge density would shed considerable light on the situation and give more confidence in the theory of operation of the tube and the measurements obtained.

In making the final measurements the voltage V_a was kept below 1.0 volt to avoid the space charge shift. Figure 3 shows the region in which this shift takes place. Inasmuch as no shift took place as V_a was increased up to 1.0 volt even though the current entering the first slit shows a large increase in this region with a consequent large increase in space charge it was felt that the space charge had little influence on the position of the resonance below 1.0 volt.

5. THE PROTON RESONANCE

The Larmor frequency, $\omega_p=2\mu_pH/\hbar$, of a sample of protons in the magnetic field is measured by the reonance absorption method. This proton resonance technique is essentially the same as that used by Purcell and collaborators and has been described adequately in the literature.[5] The source of rf was the oscillator stage of a surplus SCR-522 transmitter.[6] This unit is a modified Pierce circuit using a 7.12-mc crystal and gives an output at 14.24 mc. The signal for the proton resonance was coupled off from the tank coil by a single

[5] Bloembergen, Purcell, and Pound, Phys. Rev. **73**, 679 (1948).
[6] War Department Tech. Manual, TM 11-590 (1945).

loop of wire. The proton sample was mineral oil which occupied a volume of about 0.13 cm³ inside a coil consisting of 8 turns of number 20 copper wire ⅛-in. long by 3¼-in. inside diameter. This was supported by a Teflon form and shielded with ¾-in. brass with ⅛-in. wall. The bridge was similar to that described by Bloembergen, Purcell, and Pound.[5] The receiver was a Signal Corp B.C. 312 N.

The proton resonance widths have been studied in some detail by Purcell and others[6] and will not be discussed here. It is sufficient to note that in a liquid the perturbing fields at the nuclei are very small due to the thermal motion of the molecules and consequently very narrow lines are predicted. The line widths actually observed are largely due to the inhomogeneity of the magnetic field. The magnetic field used was sufficiently homogeneous to render the proton line width well below the electron resonance width thus making the latter the limiting factor.

An effect called the "wiggles" [7] was of importance in the measurements. A series of damped oscillations occur after resonance has been passed. These are due to the fact that the proton moments remain coherent for a short time after the resonance and come in and out of phase with the applied rf. An analysis of this effect shows that the persistence of this coherence after resonance causes the main peak of the resonance curve to appear after the resonance has been passed. This would lead to some difficulty if it were not for the fact that it is a time effect, or "before and after resonance" effect, which may be made to take place in exactly the same way going up through resonance as coming down through resonance. Hence the picture on the oscilloscope of the line going up may be made to be the mirror image of that coming down and the point of symmetry of such a scope picture is the true resonance position.

To get an idea of how important symmetry was for locating the true resonance position in this CRO display, the radio frequency bridge was balanced for perfect symmetry ("up" trace mirror image of "down" trace) and then adjusted for noticeable asymmetry and the shift in the cross-over point of the two traces was noted. It was found that this would shift by less than 1 part in 100,000 for readily detectable asymmetry. Great care was taken to adjust the bridge and receiver for symmetry in the measurements. Some of the spread in the numbers taken may be due to slight asymmetry. It should be noted that errors due to this are of no great importance since they are random provided no inherent asymmetry is present.

The proton signal was displayed on the oscilloscope simultaneously with the electron signal by means of an electronic switch (Dumont type 150).

6. FREQUENCY COMPARISON SYSTEM

If the Larmor frequency of the proton is observed in the same magnetic field in which the cyclotron frequency of the electron is measured, the magnetic field may be eliminated by taking the ratio of these two quantities:

$$\frac{\omega_e}{\omega_p}=\frac{eH/mc}{2\mu_p H/\hbar}=\frac{e\hbar/2mc}{\mu_p}=\frac{\mu_0}{\mu_p}. \tag{14}$$

The result is the ratio of the Bohr magneton to the magnetic moment of the proton.

In order to obtain a cyclotron frequency in the X-band region (9365 mc) the proton resonance was chosen to occur at 14.24 mc.

A precise comparison of these frequencies was obtained by multiplying the 14.24-mc signal 657 times and comparing this with the X-band signal on a spectrum analyzer. A spectrum analyzer[8] is an electronic instrument which provides a plot of input signal power as a function of signal frequency on a cathode-ray tube. It consists essentially of a narrow band superheterodyne receiver which is electronically tuned in frequency by a linear modulating voltage applied to the local oscillator. This same sawtooth voltage is applied to the horizontal deflecting plates of a cathode-ray tube and the output of the receiver is applied to the vertical deflecting plates.

The proton signal from the tank circuit of the oscillator was first multiplied nine times by the SCR 522 transmitter itself by means of two tripler stages. This transmitter was designed to give high power output (about 10 watts) at the frequency of this ninth harmonic. The signal was then passed through a selenium crystal 1N21 which excited harmonics to the 73rd and beyond. The crystal was contained in a 1×½-in. wave guide crystal holder of Radiation Laboratory design[5]

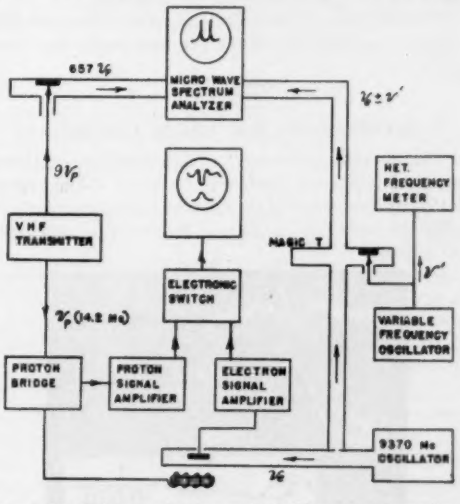

FIG. 4. Block diagram showing method of frequency comparison.

[7] See reference 8, and B. A. Jacobsohn and R. K. Wangsness, Phys. Rev. 73, 942 (1948).

[8] C. G. Montgomery, *Technique of Microwave Measurements*, Rad. Lab. Series (McGraw-Hill Book Company, Inc., New York, 1947).

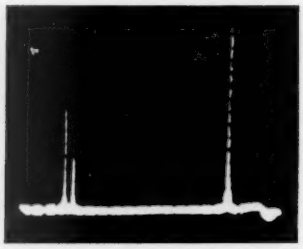

FIG. 5. Scope picture of frequency comparison on spectrum analyzer. Large pips are signal from electron oscillator and side band. Small pip is 657th harmonic of proton oscillator signal.

and the wave guide served as a filter. This signal then passed directly into the spectrum analyzer mixer (see Fig. 4).

A portion of the electron signal was coupled out by means of a probe in the wave guide leading to the electron tube. This signal passed into the H plane arm of a magic T.[8] Into a crystal on one side of the T was passed the output of the microvolter (Ferris model 18C) whose frequency could be varied over a wide range in the megacycle region. A matched load was placed on the other side of the T. The signal taken out at the E plane arm was thus amplitude modulated, at the frequency, ν', of the microvolter by the change in crystal response, then passed directly into the mixer of the spectrum analyzer. The frequency of the microvolter was varied so that the side band of the electron signal coincided with the 657th harmonic of the proton signal. This frequency was measured with a Navy LM-18 crystal calibrated frequency indicating equipment.

This frequency, ν', was all that needed to be measured inasmuch as the ratio of the two frequencies was then given by

$$\omega_e/\omega_p = 9 \times 73 \pm (\nu'/14.24). \tag{15}$$

7. EXPERIMENTAL PROCEDURE AND RESULTS

The process of making a measurement consisted merely in adjusting the frequency of the X-band oscillator until the center of the electron resonance coincided with the center of the proton resonance on the oscilloscope, then adjusting the modulation frequency, ν', of the signal coupled off from the electron oscillator till the pip on the spectrum analyzer of the first side band coincided with the pip due to the 657th harmonic of the proton signal. The frequency of the oscillator providing the modulation was then measured. Then either the magnetic field of the cathode heater (heater current) was reversed or the gross magnetic field was reversed to eliminate the effect of the heater current, and a second measurement was made. The same process was repeated for the positions of the proton sample and electron resonator interchanged. These four numbers were then averaged to constitute a single measurement. All measurements were taken with the bridge adjusted so that the proton signal for field increasing through resonance was the mirror image of the proton signal for the field decreasing through resonance, also the signals were at the center of the sweep. The electron signal was very nearly symmetrical (see Figs. 5 and 6).

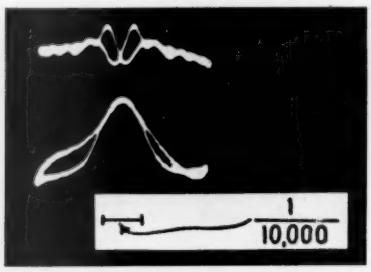

FIG. 6. Scope picture of proton and electron resonances.

For most measurements an 8-mc ($\sim$2.8-gauss) sweep was used although in some cases a 3-mc sweep proved more convenient. The width of the proton resonance was about 0.25 gauss and the width of the electron resonance varied from about 0.3 gauss to 0.75 gauss, depending upon the power used and the voltage V_a between the wave guide and cathode of the electron tube.

The microwave power in the electron tube was turned as low as possible (between 80 and 300 microwatts) for most measurements. If the power was turned very much higher than this the beam began to broaden. This is due to saturation, all the electrons entering the guide being collected at the anode near the peak of the resonance.

A series of nine complete measurements of ν' (megacycles) were taken over a period of five weeks. Within this period the electron tube was torn down and the cathode was replaced; this resulted in no apparent change in the numbers obtained. A tabulation of the numbers taken, together with a deviation from the mean appears in Table I. These represent all the data that were not thrown out at the time of observation for reasons not having to do with the consistency of the data itself. No selection has been made. In Table I F. C. refers to filament current and M.C. to magnetizing current. When both are positive or both negative the two magnetic fields aid. The starred runs were taken by reversing the gross magnetic field current keeping the filament current in the direction defined as positive. All other runs were with the gross magnetic field current in the direction defined as positive.

The 72nd and 74th harmonics of the 9th harmonic of the proton signal could also be observed on the spectrum analyzer. These signals were just 128.16 Mc apart. A cavity wave meter on the spectrum analyzer measured the 73rd harmonic to be at 9356 Mc which is just 4 Mc away from where it should be. This serves as a good check on whether or not we were looking at the

73rd harmonic. Care was taken to ascertain that pips from the electron and proton signals were both associated with the same side band of the spectrum analyzer response. The same sequence of pips was observed 40 Mc away (spectrum analyzer i-f is 20 Mc).

The number obtained gives the desired ratio of the two resonance frequencies from Eq. (15). The fact that we should add rather than subtract the correction was ascertained by noting that the electron signal lay between the 73rd and 74th harmonics of the 9th harmonic of the proton signal.

8. DISCUSSION OF SYSTEMATIC ERRORS

In view of the fact that the measurement is capable of a precision of better than one part in 150,000 if judged solely by internal consistency, it appeared that considerable care was justified in running down small systematic errors. The known possible sources of systematic error were (1) magnetic contamination of the apparatus; (2) magnetic inhomogeneities due to currents; (3) inexact interchange of proton sample and critical portion of electron beam; (4) space charge effects on electron resonance; (5) difference in position of resonances when approaching from below resonance from that in approaching from above; (6) diamagnetic correction to field of proton; (7) relativistic dependence of mass on velocity.

The possibility of magnetic contamination of materials used in the apparatus was carefully explored. Samples of all types of materials that went into the construction of the critical parts were placed in the field in such a way as to have a maximum effect on the resonance. The only material found that did have any observable effect was red Glyptal and this was then removed. To obtain a further check on this after the measurements were completed, a large hole was drilled into the electron tube to permit the proton sample to fit inside at the position at which the electron beam had been. The electron tube was then moved on and off of the proton sample while the proton resonance was observed. No effect was noticed even though a shift of 1 part in 200,000 could have been observed.

Nickel leads were used about 3 inches from the electron beam but moving these leads showed no effect on the resonance.

The cathode base was made of nickel. However, the temperature of the cathode was in the neighborhood of 1600°K which is well above the Curie point for nickel which is 360°. The construction of the cathode was such that the entire nickel base was heated to approximately the same temperature.

The discrepancy in the number due to the magnetic field of the heater current was effectively eliminated to first order at least, by averaging readings for both directions of filament current or for both directions of gross magnetic field.

It was, of course, not possible to make an exact interchange of the proton sample and critical portion of electron beam. The difference between the numbers for the interchange was of the order of one part in fifty thousand. The sample and the beam was $\frac{1}{2}$ in. apart. It should be stated, however, that the center of the beam was interchanged with the sample. It was later found that the critical portion of the beam was something less than $\frac{1}{10}$ in. away from the center towards the cathode. This may have led to some error. The interchange was not precisely the same for each reading and the small spread in the data itself, would lead one to suspect that the error would not be appreciable.

The space charge effects have already been discussed.

The protons used in the experiment were the hydrogen nuclei of the water molecule or of the long chain hydrocarbons which make up mineral oil. The numbers obtained for these two substances were the same within experimental error. The shielding of the protons by the electrons in the molecules is large enough to affect the measurements and must be taken into account. The differences in magnetic shielding for H_2, H_2O, and mineral oil are found to be small[9] so we may apply the correction for the hydrogen molecule which has been calculated approximately by Ramsey[10] to be -2.7×10^{-5}H.

TABLE I. Summary of measurements.

Date	Proton above electron F.C. or M.C.+	Proton above electron F.C. or M.C.−	Proton below electron F.C. or M.C.+	Proton below electron F.C. or M.C.−	Average	Deviation
June 22	6.77	6.48	7.01	6.66	6.73	−0.04
June 27	6.85	6.40	7.07	6.43	6.69	−0.08
June 27	6.92	6.52	7.15	6.61	6.80	+0.03
June 27	6.87	6.31	6.99	6.57	6.69	−0.08
June 27	6.98	6.66	6.99	6.66	6.82	+0.05
June 28	7.00	6.52	7.04	6.62	6.80	+0.03
July 6	6.82	6.49	7.14	6.83	6.82	+0.05
July 6	*6.79	*6.99	*7.00	*6.56	*6.83	+0.06
July 29	*6.73	*6.81	*6.95	*6.40	*6.72	−0.05
				Total	60.90	0.47
				Average	6.77	0.05

It may be some inherent asymmetry exists in the resonance observed on the oscilloscope due to the difference in the behavior of the protons or electrons below resonance from their behavior above resonance. The relativistic dependence of mass on velocity would produce such asymmetry in the electron resonance. An asymmetry due to this should be distinguished from an asymmetry due to the difference in behavior before resonance and after resonance. A time effect such as this latter may be eliminated by adjusting the gross magnetic field so that the up and down resonances are equally spaced in time and, in the case of the proton signal, carefully adjusting the receiver and bridge so that the frequency response is the same for both cases.

[9] H. S. Gutowsky and R. E. McClure, Phys. Rev. **81**, 276 (1951).
[10] N. F. Ramsey, Phys. Rev. **77**, 567 (1950).

A requirement for the fulfillment of this latter condition, however, is that no other causes of asymmetry be present because one uses symmetry to determine whether or not the frequency response of the system has been properly adjusted. It is very unlikely that an appreciable inherent asymmetry could be exactly compensated by tuning the system, and, inasmuch as it was possible to tune for excellent symmetry, it seems unlikely that a difference between behavior above resonance from behavior below resonance which would cause asymmetry was significantly present. Of course one could probably not detect experimentally a shift due to a difference in behavior above and below which did not produce asymmetry.

For electron velocities used the relativistic shift in the resonance frequency is just below where it would be observable.

9. CONCLUSION

Using the equipment and technique discussed it was possible to obtain a value of the ratio of the cyclotron frequency of the electron to the precession frequency of the proton with an accuracy approaching one part in a hundred thousand. The mean value of this ratio, uncorrected for diamagnetism, was 657.4752 with a mean deviation of 0.0037 and a maximum deviation of 0.0056. Inasmuch as the accuracy of the result depends on the extent to which systematic errors can be excluded, possible sources of these were carefully investigated as previously discussed. In view of the results of these investigations and the high internal consistency of the values obtained, it is felt that the true ratio, uncorrected for diamagnetism, lies within the range,

$$\omega_e/\omega_p = 657.475 \pm 0.008. \tag{16}$$

If the diamagnetic correction to the field of the proton for the hydrogen molecule[10] of 2.68×10^{-5} is applied here, the proton moment, in Bohr magnetons, becomes

$$\mu_p = (1.52101 \pm 0.00002)\times10^{-3}(eh/2mc). \tag{17}$$

This result may be compared with the value $(1.52106 \pm 0.0007)\times10^{-3}$ obtained by Taub and Kusch.[11] As mentioned in the introduction, this agreement may be regarded as further confirmation of the correction[2] to the spin-moment of the electron, since the experiment discussed here amounts to a comparison of the orbital g-factor (n very large) of the electron with the proton g-factor, whereas Taub and Kusch compared the proton g-factor and the g-factor of a $^2S_{\frac{1}{2}}$ state, applying the factor $2[1+(\alpha/2\pi)]$ to obtain the number just quoted.

The result stated here, like that of Taub and Kusch, may be used in conjunction with the hydrogen hyperfine structure splitting[12] and cR_∞ to obtain the fine structure constant α, and may be combined with the absolute value of the proton gyromagnetic ratio γ_p measured by Thomas, Driscoll, and Hipple[13] to yield e/mc. Also, with the ratio of the proton cyclotron frequency to the proton precession frequency ω_e/ω_p, measured by Hipple, Sommer, and Thomas,[14] this result gives a precise value for M/m, the ratio of the mass of the proton to that of the electron.

The value of α may be computed from the Fermi hyperfine structure formula,[15] modified to include Breit's relativistic correction,[16] the effect of the reduced mass,[17] and the radiative correction to the electron magnetic moment:[2,12]

$$\Delta\nu = \alpha^2\left[\frac{16}{3}\frac{\mu_p}{\mu_0}cR_\infty(1+\tfrac{3}{4}\alpha^2)\left(1+\frac{m}{M}\right)^{-3}\left(1+\frac{\alpha}{2\pi}\right)\right]. \tag{18}$$

Since Taub and Kusch measure the ratio μ_p/μ_e, where μ_e is the magnetic moment of the electron, the radiative correction (last term in parentheses) must appear twice in this formula when their measurement is used. $\Delta\nu$ is known to 4 parts in a million,[12] c to 3 parts in a million[18] and the result stated here for μ_p/μ_0 to 12 parts in a million. α computed from the measurements referred to would have a root-mean-square error of ±7 parts in a million. The accuracy is thus improved to the point where the uncertainties in the theoretical formula become important.[19]

It is at present felt that the possibilities of narrowing the electron resonance line by exploiting the velocity selection provided by the space charge effect have not been fully realized. It is also felt that the velocity selection scheme mentioned in connection with the dip in the electron peak for high power would be profitably utilized. It appears that the width of the electron dip would be limited only by the sensitivity of the detection apparatus for this sort of scheme.[20]

The author wishes to express his appreciation to Professor E. M. Purcell, who suggested the possibility of making the measurement discussed here and contributed many ideas which permitted the realization of this possibility.

[11] H. Taub and P. Kusch, Phys. Rev. **75**, 1481 (1949).

[12] J. E. Nafe and E. B. Nelson, Phys. Rev. **73**, 718 (1948).

[13] Thomas, Driscoll, and Hipple, Phys. Rev. **75**, 992 (1949); **78**, 787 (1950).

[14] Hipple, Sommer, and Thomas, Phys. Rev. **76**, 1877 (1949); **80**, 487 (1950).

[15] E. Fermi, Z. Physik **60**, 320 (1930).

[16] G. Breit, Phys. Rev. **35**, 1447 (1930).

[17] G. Breit and E. R. Meyerott, Phys. Rev. **72**, 1023 (1947).

[18] Kees Bol, Phys. Rev. **80**, 298 (1950).

[19] For recent calculations of these constants see J. A. Bearden and H. M. Watts, Phys. Rev. **81**, 73 (1951).

[20] A more recent measurement using a different means of detecting the resonance has been made by R. W. Nelson. His value falls within the range quoted here.

Electrical Properties of αFe_2O_3 and αFe_2O_3 Containing Titanium

F. J. MORIN
Bell Telephone Laboratories, Murray Hill, New Jersey
(Received February 9, 1951)

Electrical conductivity, Hall effect, and Seebeck effect have been measured on two sets of polycrystalline samples of αFe_2O_3 and αFe_2O_3 containing from 0.05 to 1.0 atomic percent titanium (n-type impurity). One set of samples contained 0.6 atomic percent excess of iron (n-type impurity), the second set contained 0.6 atomic percent deficiency of iron (p-type impurity).

The conductivity of pure αFe_2O_3 is independent of this amount of stoichiometric deviation. The slope of the log conductivity *vs* reciprocal temperature plot is 1.17 ev and the intercept at $1/T=0$ is 2.1×10^4 ohm^{-1} cm^{-1}. Room temperature conductivity varies from $\sim10^{-14}$ ohm^{-1} cm^{-1} (extrapolated) for pure αFe_2O_3 to 0.2 ohm^{-1} cm^{-1} for αFe_2O_3 containing 1.0 atomic percent titanium.

The measured Hall voltages seem to result entirely from magnetization of the samples, which are weakly ferromagnetic, and disappear above the ferromagnetic Curie temperature.

The temperature variations of the Fermi level are determined from Seebeck data. The temperature variations of carrier concentration are determined from Fermi level and of mobility from carrier concentration and conductivity for some samples. Carrier concentration results indicate that each added titanium ion donates approximately one electron to the conduction process. Mobilities are found to be less than 2.0 cm^2/volt sec, suggesting that conduction involves electrons in the d level of iron.

1. INTRODUCTION

ELECTRICAL conductivity, Hall effect, and Seebeck effect have been measured on polycrystalline samples of αFe_2O_3 containing small deviations from stoichiometry and small amounts of added titanium. These measurements were made in the course of an investigation of the conduction mechanism in oxides whose cations have a partially filled d level. A qualitative discussion of this mechanism was first given by deBoer and Verwey.[1] The addition of titanium to produce an increase in the conductivity of αFe_2O_3 has been reported by Verwey and others.[2] Barth and Posnjak[3] show that tianium enters the αFe_2O_3 lattice substitutionally as Ti^{4+}, thus producing an Fe^{2+} and maintaining the average charge per cation at three. Verwey points out that the Fe^{2+} acts as a donor center with respect to the surrounding Fe^{3+} ions and that an electron thermally excited from the Fe^{2+} can wander in an environment of Fe^{3+} ions and, under the influence of an external field, produce an electric current. No quantitative theory has been developed to describe such a mechanism. Consequently, the experimental results presented in this paper are interpreted, to a limited extent, in terms of the band picture.

1.1 Preparation of Samples

The Fe_2O_3 used was C. K. Williams Company pigment grade *R*2899. Titanium was introduced in the form of TiO_2 obtained as Titanium Pigment Corporation pigment grade Titanox *AMO*. The oxides were compacted into sample bars using a wax binder obtained in a water emulsion as Socony Vacuum Oil Company Ceremul *C*. Chemical analyses of these materials are given in the Appendix.

Oxides were mixed in a colloid mill with distilled water slightly acidified with acetic acid. The emulsion was added to the mixture (0.2 cc emulsion per gram of oxide), the wax precipitating from emulsion onto the oxide particles as the acid neutralized the emulsifying agent. Oxides with binder were filtered and dried. Rectangular samples were compacted in a die using a pressure of about one ton per square inch. Two thermocouple holes were drilled through the sample using a No. 60 drill. Samples were heated at 300°C to evaporate the binder and then sintered, under controlled conditions of heating and cooling, at 1100°C for 16 hours. Contacts were painted on the samples using gold or platinum paste containing a small amount of powdered glass (to bond contact metal to oxide) and fired in air at 700°C for 3 minutes. A typical sample is sketched in Fig. 1.

Samples were made of αFe_2O_3 and αFe_2O_3 containing 0.05, 0.2, and 1.0 atomic percent titanium. One set of samples was sintered in pure oxygen at atmospheric

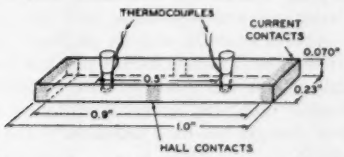

FIG. 1. Diagram of sample showing approximate dimensions and location of contracts and thermocouples.

TABLE I. Composition of samples.

Sample	Atomic % added Ti	Density g/cm^3	Atoms/cm^3 of Fe	Atoms/cm^3 of Ti	
1	0.00	5.179	3.977×10^{22}	0.0	
2	0.05	—	3.975×10^{22}	2×10^{19}	Sintered in oxygen
3	0.20	—	3.969×10^{22}	8×10^{19}	
4	1.00	—	3.937×10^{22}	4×10^{20}	
—	—	5.190	4.000×10^{22}	—	
A	0.00	5.211	4.023×10^{22}	0.0	
B	0.05	—	4.021×10^{22}	2×10^{19}	Sintered in $74N_2+2O_2$
C	0.20	—	4.015×10^{22}	8×10^{19}	
D	1.00	—	3.983×10^{22}	4×10^{20}	

[1] J. H. deBoer and E. J. W. Verwey, Proc. Phys. Soc. (London) **49**, (extra part) (1937).
[2] E. J. W. Verwey *et al.*, Chemisch Weekblad **44**, 705–708 (1948).
[3] T. F. W. Barth and E. Posnjak, Z. Krist. **88**, 265, 271 (1934).

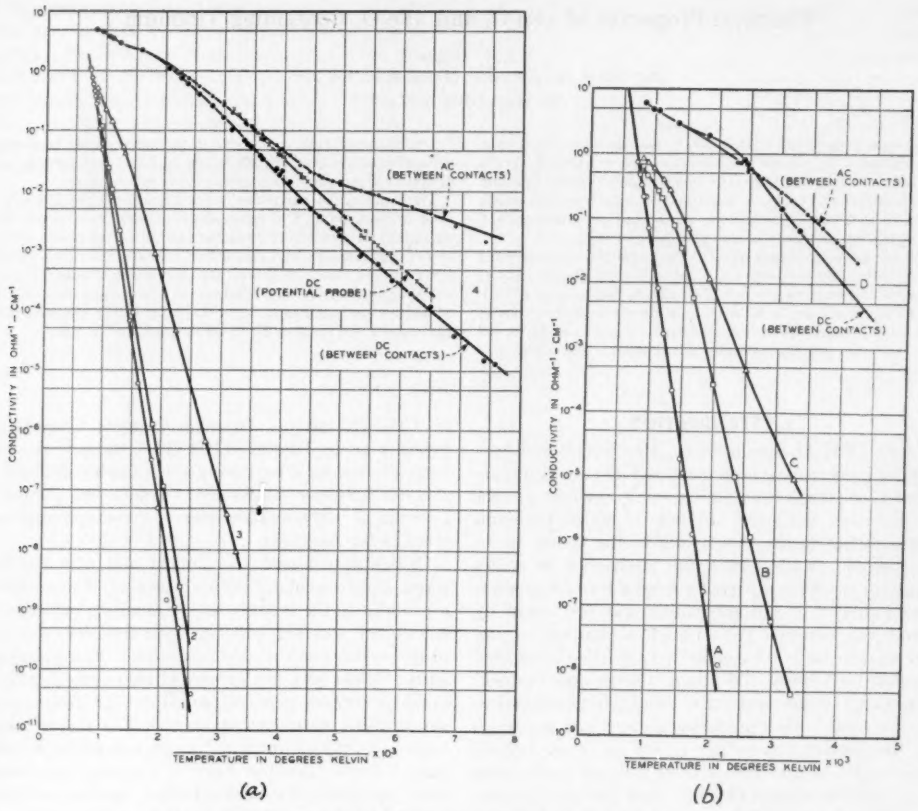

FIG. 2. Conductivity as a function of reciprocal temperature for samples sintered (a) in oxygen; and (b) in $74N_2+2O_2$. Compositions are given in Table I.

pressure to produce a small metal deficiency in the oxide. A second set of samples was sintered in a slightly reducing atmosphere of $74N_2+2O_2$ by volume at atmospheric pressure to produce a small metal excess in the oxide. An idea of the departure from stoichiometry of the αFe_2O_3 was obtained from a determination of the density of the finely powdered material by displacement in carbon tetrachloride. The density of a sample of αFe_2O_3 sintered in air was taken to represent that of a stoichiometric sample since its composition is $Fe_{2.0005}O_3$,[4] a stoichiometric departure too small to detect by the density method used. Assuming a perfect oxygen lattice, the oxidized sample was found to contain an Fe deficit of 2.3×10^{20} atoms per cc and the reduced sample a metal excess of 2.3×10^{20} atoms per cc. Compositions of the samples prepared are shown in Table I. Lattice constants for the samples were determined by K. H. Storks of these Laboratories. The values found agreed with those given in Wyckoff[5] for αFe_2O_3.

2. EXPERIMENTAL PROCEDURE

The data obtained were resistance, Hall voltage, and Seebeck voltage per degree, all as functions of temperature. Direct current resistance was measured by the potential probe method on low resistance samples where contact resistance was appreciable, and was measured directly between contacts with an ohmmeter on high resistance samples. The field used to produce the transverse Hall voltage was measured with a rotating coil and voltmeter calibrated against a permanent magnet whose field strength had been measured by the Bureau of Standards.

Temperatures above room temperature were measured with platinum, platinum-rhodium thermocouples

[4] J. C. Hostetter and H. S. Roberts, J. Am. Ceram. Soc. **4**, 932 (1921).

[5] R. W. G. Wyckoff, "The structure of crystals," A.C.S. Monograph No. 19 (Chemical Catalogue Company, New York, 1931), p. 254.

and below room temperature with Chromel *P*, Alumel couples. The couples were wedged with small ceramic cones into the thermocouple holes of the sample as shown in Fig. 1. Seebeck voltage and potential probe voltage were measured between the platinum or alumel leads of the couples. The temperature difference used to produce the Seebeck effect was about 5°C at low temperatures and 25°C at high temperatures. The ambient temperature was taken to be the average of the temperatures measured by the two couples. All dc voltages were measured with a Leeds and Northrup type *K* potentiometer. Current through the sample was measured with a Model 322 Weston milliampere meter.

After the dc measurements had been made it was realized that grain boundary resistance might be significant in the low resistance samples. To disclose grain boundary resistance, the parallel components of resistance and capacitance were measured as a function of frequency on sample 4 at room temperature using an ac bridge. The ac resistance was found to be the same as the dc resistance up to 10^4 cycles but had decreased to one-third the dc resistance at 10^6 cycles. Because at this point the resistance-frequency curve appeared to have leveled off, 10^6 cycles was used for measuring ac resistance as a function of temperature on samples 4 and *D*. The resistance of the other samples was beyond the limit of the apparatus.

A check of the dc resistance of samples 4 and *D* after all the above described measurements had been made showed that sample 4 had not changed while sample *D* had increased in dc resistance by a factor of 5. For this reason, more detailed measurements were not made on sample *D* as they were on sample 4. Because of its interesting behavior, measurements of ac and dc resistance, Hall voltage, and Seebeck voltage per degree were made to as low temperatures as possible on sample 4. Similar low temperature measurements were not possible on the other samples because of their high resistance.

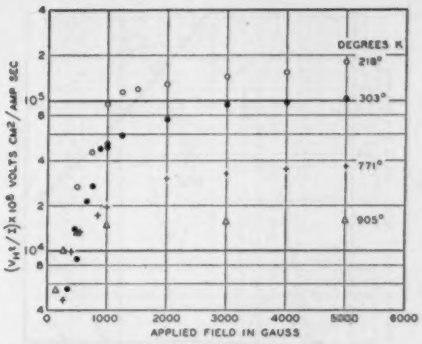

FIG. 3. Dependency of Hall effect on applied field for sample 4.

3. EXPERIMENTAL RESULTS

Conductivity as a function of reciprocal temperature is shown in Fig. 2(a) for oxidized samples and Fig. 2(b)

TABLE II. Hall effect as a function of temperature with and without applied field.

Sample No.	°K	ΔV_H for $H=\pm 5000$ millivolts	ΔV_H for $H=0$ millivolts	t cm	I milliamps	$\Delta V_H t\times 10^8/2I$ for $H=\pm 5000$	$\Delta V_H t\times 10^8/2I$ for $H=0$
1	583	13.0	9.8	0.190	0.022	5.6×10^8	4.2×10^8
	639	12.2	10.1		0.114	1.03×10^8	8.4×10^8
	701	10.8	8.6		0.70	1.47×10^8	1.17×10^8
	823	1.39	0.94		1.80	7.3×10^8	5.0×10^8
	941	0.36	0.24		10.0	3.4×10^8	2.3×10^8
	967	<0.01			19.6	$<5\times 10^8$	
2	561	35.7	29.4	0.185	0.0300	1.10×10^{10}	9.1×10^9
	563	38.5	30.2		0.0325	1.09×10^{10}	8.6×10^9
	715	41.6	31.5		3.6	1.07×10^8	8.1×10^7
	835	9.96	5.27		11.0	8.4×10^8	4.4×10^8
	945	1.27	0.88		13.4	8.8×10^8	6.1×10^8
	953	<0.01			13.55	$<7\times 10^8$	
3	415	42.9	35.9	0.170	0.112	3.26×10^9	2.73×10^9
	546	44.7	35.7		6.5	5.83×10^7	4.66×10^7
	723	5.0	3.7		13.6	3.14×10^8	2.32×10^8
	857	1.48	0.99		14.0	9.0×10^8	6.0×10^8
	933	0.77	0.51		20.0	3.27×10^8	2.16×10^8
	967	<0.005			20.0	$<2\times 10^8$	
4	222	0.43	0.25	0.147	18.5	1.71×10^8	1.00×10^8
	264	0.50	0.34		19.5	1.81×10^8	1.27×10^8
	307	0.425	0.316		20.0	1.56×10^8	1.16×10^8
	391	0.298	0.227		20.0	1.095×10^8	8.35×10^4
	578	0.162	0.119		20.0	5.95×10^4	4.37×10^4
	737	0.107	0.080		20.0	3.94×10^4	2.94×10^4
	855	0.072	0.048		20.0	2.65×10^4	1.77×10^4
	941	0.023	0.015		20.0	8.45×10^3	5.51×10^3
	951	<0.001			20.0	$<3.7\times 10^3$	

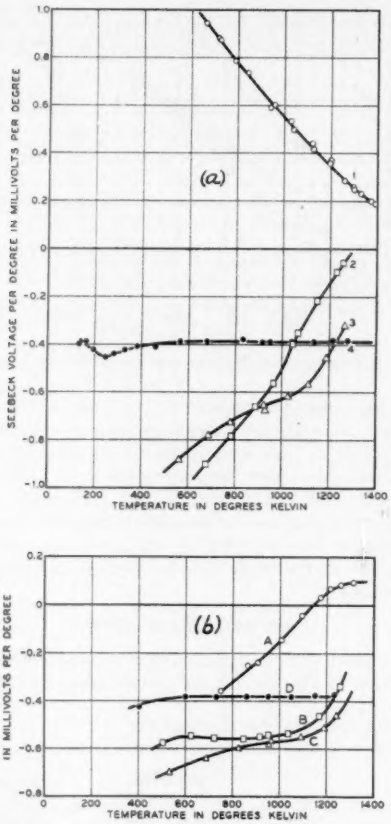

FIG. 4. Seebeck voltage per degree as a function of temperature for samples sintered (a) in oxygen; and (b) in $74N_2+2O_2$. Compositions are given in Table I.

for reduced samples. The general behavior of the data appears similar to that obtained from elemental semiconductors (e.g., silicon and germanium) with added impurities. The straight lines obtained for samples 1 and A suggest some type of intrinsic conductivity which also becomes significant in the impure samples at high temperatures. The conductivity plots for samples 1 and A are identical. This would not be expected if holes and electrons from impurity centers produced by oxidation and reduction contribute to conductivity in the usual way. At low temperature the conductivity of impure samples depends upon added impurity. Samples B and C show greater conductivity than samples 2 and 3, respectively. This probably means that impurity centers produced by oxidation cancel some of those produced by titanium. Sample D is nearly the same as sample 4, indicating that the number of effective impurity centers produced by oxidation is small compared with the number from one percent added titanium.

Conductivity results for sample 4 indicate the presence of a small amount of contact resistance which causes a difference between dc conductivity measured between contacts and by potential probe. The presence of grain boundaries having a higher resistance and higher temperature coefficient of resistance than the grains themselves is suggested by comparison of potential probe with ac conductivity for sample 4. The ac conductivity is used in subsequent computations.

Conduction in samples 1 and A may depend upon a mobility mechanism or an excitation mechanism. If excitation of the usual type, theory indicates that conductivity σ in the intrinsic region should vary as

$$\sigma = A \exp \epsilon_0/2kT, \qquad (1)$$

where A is a constant in ohm^{-1} cm^{-1}, ϵ_0 is the width of the unallowed band in electron volts, k is the Boltzmann constant in electron volts per degree, and T the absolute temperature in degrees Kelvin. From the conductivity of samples 1 and A, $\epsilon_0 = 2.34$ ev and $A = 2.1\times10^4$ ohm^{-1} cm^{-1}.

The Hall coefficient was first measured as a function of

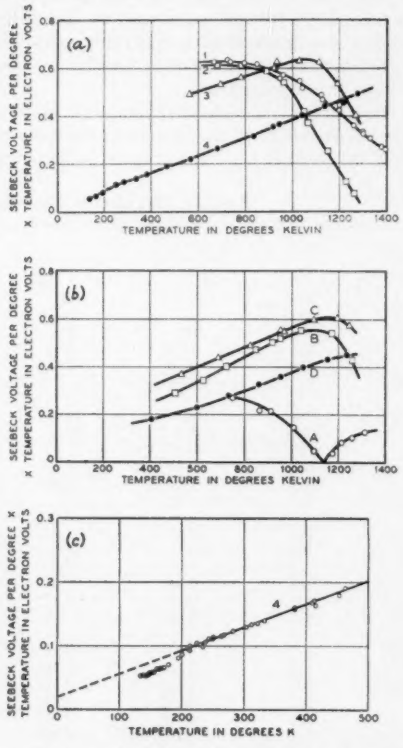

FIG. 5. Seebeck voltage per degree multiplied by temperature plotted as a function of temperature (a) for samples sintered in oxygen; (b) for samples sintered in $74N_2+2O_2$; and (c) detailed plot for sample 4. Compositions are given in Table I.

applied field. It was found to depend on applied field in such a way as to suggest that magnetization of the sample was taking place and producing a large enhancement of the field within the sample. This was unexpected since the magnetic susceptibility per gram for these materials is only about 130×10^{-6}.[6] Results are shown in Fig. 3 for sample 4. Since the effective magnetic field is unknown, the product $R_H H_{eff}=(V_H t/I)\times10^8$ has been plotted against applied field for various temperatures. R_H = Hall coefficient in cm³/coulomb, H_{eff} = effective magnetic field in gauss, V_H = transverse Hall voltage in volts, t = sample thickness in cm, and I = sample current in amperes. Results in Fig. 3 suggested that saturation magnetization occurred at about $H=1000$ since, above this value $(V_H t/I)\times10^8$ increases slowly and linearly with applied field, and that the linear part of the curve resulted from the true Hall effect of the sample. It seemed reasonable to expect, therefore, that R_H for the nonmagnetic part of the sample might be obtained by measuring V_H in the sequence $H=+5000$, $H=0$, $H=-5000$, $H=0$ and computing R_H after subtracting the contribution of the magnetization to the Hall voltage as measured when $H=0$. Results of such measurements for samples 1, 2, 3, and 4 are shown in Table II. The disappearance of Hall voltage above the ferromagnetic Curie point (950°K) indicates that the true R_H for the material cannot be determined from the data in the way described. Carrier concentration computed from Seebeck data predicts a value for V_H just above the Curie point about one decade greater than the limit of the measuring apparatus, consequently, the normal Hall voltage should have been measurable. This apparently small Hall effect may be due to the existence of a mesh-like network of conducting paths in the polycrystalline sample or to peculiarities of the mechanism of d level conduction. The sign of the Hall voltage measured was negative for all samples except for oxidized αFe_2O_3 (sample 1) for which it was plus.

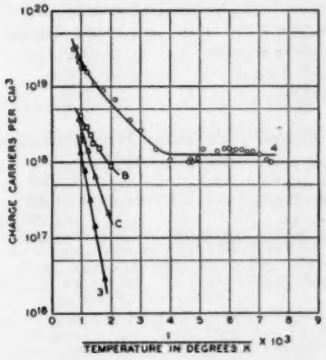

FIG. 6. Charge carrier concentration in the impurity range as a function of reciprocal temperature computed from Seebeck data for samples 3, 4, B, and C.

[6] F. J. Morin, Phys. Rev. **78**, 819–820 (1950).

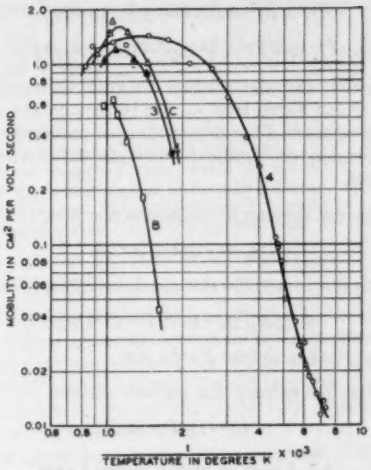

FIG. 7. Electron mobility in the impurity range as a function of reciprocal temperature for samples 3, 4, B, and C.

No further use is made of the Hall data in this paper. However, it is intended to investigate the magnetization effect in more detail, particularly on single crystals, and report on it in a later paper.

The Seebeck voltage per degree as a function of temperature is shown in Fig. 4(a) for oxidized samples and Fig. 4(b) for reduced samples. These data are in agreement with Hall data as to sign. In addition, the Seebeck voltage per degree of reduced αFe_2O_3 (sample A) becomes positive above 1140°K. It is not clear why the mechanism which produces the difference in sign of Hall and Seebeck effects for samples 1 and A fails to change their conductivity.

4. FERMI LEVEL, CHARGE CARRIER CONCENTRATION, AND MOBILITY

In this section, Fermi level, charge carrier concentration and mobility are computed in so far as possible using present theory. Charge carrier concentration is within the range where the electron gas may be considered nondegenerate. The symbols and equations to be used in analyzing the data are as follows.

Symbols: e = charge on electron = 1.6×10^{-19} coulomb. m_e = rest mass of electron = 9.11×10^{-28} gram. k = Boltzman constant = 1.38×10^{-16} erg/degree. h = Planck constant = 6.62×10^{-27} erg second. T = absolute temperature in degrees Kelvin. n_e = concentration of conduction electrons = No./cm³. μ = electron mobility in cm²/volt sec. σ = conductivity in ohm^{-1} cm^{-1}. Q = Seebeck voltage per degree in millivolts/degree. ϵ_0 = distance from top of filled band to bottom of conduction band in electron volts. ϵ_F = location of Fermi level from top of filled band in electron volts.

Equations:

Impurity range for electrons

$$\sigma = n_e e \mu_e \qquad (2)$$

$$-QT\times10^{-3}=\epsilon_0-\epsilon_F+2.5\times10^{-7}kT/e \quad (3)$$

$$n_e=2(2\pi m_e kT)^{\frac{1}{2}}/h^3\exp[-(\epsilon_0-\epsilon_F)e/kT]. \quad (4)$$

Equation (3), the relation between thermoelectric power Q and Fermi level ϵ_F, can be derived as follows. Q is the measure of the entropy flux per unit current due to a temperature gradient.[7] The current carriers are electrons.

Entropy per electron in the conduction band

$$=(\epsilon_0-\epsilon_F)e/T+(5/2)k.$$

Entropy flux in field E = electron flux × entropy/electron

$$=E\mu_e n_e[(\epsilon_0-\epsilon_F)e/T+(5/2)k].$$

Current density in field $E=E\mu_e n_e e$.

Therefore the entropy flux per unit current

$$=(\epsilon_0-\epsilon_F)/T+5k/2e.$$

4.1 Location of the Fermi Level

Observed values of Q have been multiplied by the absolute temperature of observation and QT plotted as a function of absolute temperature in Fig. 5(a) for oxidized samples and Fig. 5(b) for reduced samples. In Fig. 5(c) a detailed plot of QT is shown for sample 4 at low temperatures. These plots necessarily give an incomplete picture of Fermi level behavior since, to determine the Fermi level accurately, the carrier concentration and mobility for both holes and electrons must be known. In the impurity region $-QT$ indicates the distance of the Fermi level below the conduction band, since the impurity centers are donors. As temperature increases and more donors become ionized the Fermi level moves away from the conduction band toward the center of the unallowed band and $-QT$ becomes larger. This behavior is shown for samples 3, 4, B, C, and D. The extrapolation of the impurity region to zero temperature for these samples gives an idea of the location ϵ_D of the donor centers. When, at high temperature, carriers of opposite sign from intrinsic type conductivity become appreciable in relative numbers, QT decreases with increasing temperature as shown by samples 1, 2, 3, A, B, and C. It seems significant that QT for these samples either is positive or is rapidly tending toward a positive value at high temperature. This may mean that hole mobility is greater than electron mobility. More probably, however, a correct explanation of these results depends in some other way upon the mechanism which produces the Seebeck effect.

[7] C. Herring and M. H. Nichols, Revs. Modern Phys. **21**, 185 (1949).

4.2 Computation of n_e and μ_e

Carrier concentration in the impurity range has been computed from Seebeck data using Eqs. (3) and (4) and is shown as a function of reciprocal temperature in Fig. 6 for samples 3, 4, B, and C. Electron mobility has been computed from conductivity and carrier concentration using Eq. (2) and is shown in Fig. 7 for samples 3, 4, B, and C. Results for sample 4 suggest that two mechanisms may be operating, one at low temperatures where conduction changes due to the change in mobility with temperature and a second at higher temperatures where conduction change is more the result of the increase in the number of carriers than the change in mobility. The very low values found for mobility suggest that the conduction is due to electrons confined to the d level. In Fig. 6, the intercept of carrier concentration at $1/T=0$ for the various samples suggests that each added titanium donates an order of one electron to the conduction process.

The author is indebted to P. W. Anderson for suggesting that the Hall voltage was caused by magnetization, to J. Bardeen for stimulating discussions of the data, and to C. Herring for Eq. (3).

APPENDIX I

Chemical analysis of materials Fe_2O_3 by quantitative analysis

Fe_2O_3	99.00 percent
SiO_2	0.06
Fe^{3+}	0.07
Mn	0.08
Al_2O_3	0.04
MgO	0.05
CaO	0.07
Cu	0.0003

TiO_2 by quantitative analysis

TiO_2	98.1 percent
SiO_2	0.46
Fe_2O_3	0.01
P_2O_5	0.21
SO_3	0.06

Ceremul C wax emulsion by spectrochemical qualitative analysis

Na	<0.01 percent
Ca, Fe, Mg, Si	<0.005
Al, Cu, Sn	<0.0005
B, Cr, Ge, Mn, Ni, Pb, Ti	<0.0001

Nuclear Reactions Resulting from the Proton Bombardment of Aluminum*

F. C. SHOEMAKER,† J. E. FAULKNER,‡ G. M. B. BOURICIUS,§ S. G. KAUFMANN,|| AND F. P. MOORING¶
University of Wisconsin, Madison, Wisconsin

(Received April 5, 1951)

The energy dependence of reaction product yields from aluminum bombarded by protons has been measured in the energy range from 1.4 Mev to 4 Mev with fairly high energy resolution. Yield curves are shown for elastically scattered protons, alpha-particles (both full energy and those leaving the residual nucleus Mg^{24} in the first excited state), gamma-radiation, and, over a limited range, inelastically scattered protons leaving the residual nucleus Al^{27} in the first two excited states. The gamma-ray yield at proton energies above 2 Mev is shown to be principally from the excited residual nuclei. All reactions show a pronounced resonance structure.

I. INTRODUCTION

THE interaction of high energy protons with aluminum nuclei was first studied by measurements[1] of the dependence on bombarding proton energy of the yield of gamma-radiation. These yield curves indicated that the gamma-rays are produced by resonance reactions with the resonance energies associated with high-lying levels in the compound nucleus Si^{28}. Secondary electron absorption measurements of the gamma-radiation showed that it must be due to the radiative capture process. Subsequent work on this reaction includes that of Brostrom, Huus, and Tangen,[2] who measured absolute cross sections for resonances up to 1.4 Mev, and Bender, Shoemaker, and Powell,[3] who attempted to determine the total width of one level by bombarding thin targets with a proton beam of small energy spread.

Other reactions have also been studied. The work of Dicke and Marshall[4] and Fulbright and Bush[5] on inelastically scattered protons showed the existence of low-lying energy levels in the Al^{27} residual nucleus. Freeman and Baxter[6] measured the yield of alpha-particles up to a proton bombarding energy of 1 Mev. Their yield curve showed several broad resonances, but no correlation could be made with the gamma-ray yield curves, because of inadequate resolution. The energy dependence of the elastic scattering of protons in the neighborhood of one resonance was recently studied in this laboratory by Bender, Shoemaker, Kaufmann, and Bouricius.[7] From the amplitude of the variation from Rutherford scattering, with the assumption of zero angular momentum for the incident protons, an estimate was made of the width of the level. Although this work was very limited in scope, it showed that proton scattering was potentially a useful tool for studying resonance levels.

A program was planned for continuation of work on proton resonance reactions at this laboratory, with the aim of determining the partial widths (transition probabilities) for the various possible modes of decay of the energy states of compound nuclei, and the eventual assignment of angular momentum quantum numbers to these states. The decision to use aluminum for the target material for the first work was made in view of certain disadvantages—the data for a target nucleus with spin 5/2 is more difficult to interpret than data for a target nucleus with spin zero, and the sharpness of the levels in the low energy region makes the measurement of the widths difficult (reference 7). Aluminum, however, has the advantage of having only one isotope, and targets of this material are easy to prepare. Its high proton-neutron threshold was also thought to be an advantage, since an intense neutron yield could interfere with measurement of other disintegration products.

II. APPARATUS

For the observation of charged reaction products, some form of particle analyzer was needed. After consideration of various possibilities, a focusing homogeneous-field magnetic analyzer was found to satisfy the requirements. Materials were on hand for the construction of a magnet with pole pieces $8\frac{1}{2}$ inches square. For 90° deflection, this size allows a deflection radius of 19.1 cm so that a field of 15,200 gauss is sufficient for 4-Mev protons or alpha-particles. The magnet as constructed gave a maximum field strength of 16,000 gauss with 34,000 ampere turns for a gap of $\frac{1}{2}$ inch. To eliminate fluctuations in the magnetic field, the voltage developed across a resistance in series with the coils was compared with a battery; the error signal so obtained was amplified and applied to the control field of an Amplidyne generator which supplied the coil current. The gain and stability of the circuit were such

* Work supported by the AEC and Wisconsin Alumni Research Foundation.

† Now at Princeton University, Princeton, New Jersey.

‡ Now at Hanford Engineering Works Richland, Washington.

§ Now at Fairchild Engine & Airplane Corporation, Oak Ridge, Tennessee.

|| Now at Argonne National Laboratory, Chicago, Illinois.

¶ Now at Argonne National Laboratory, Chicago, Illinois.

[1] Herb, Kerst, and McKibben, Phys. Rev. **51**, 691 (1937); W. Gentner, Z. Physik **107**, 354 (1937); Plain, Herb, Hudson, and Warren, Phys. Rev. **57**, 187 (1940).

[2] Brostrom, Huus, and Tangen, Phys. Rev. **71**, 661 (1947).

[3] Bender, Shoemaker, and Powell, Phys. Rev. **71**, 905 (1947).

[4] R. H. Dicke and J. Marshall, Phys. Rev. **63**, 86 (1943).

[5] H. W. Fulbright and R. R. Bush, Phys. Rev. **74**, 1323 (1948).

[6] J. M. Freeman and A. S. Baxter, Nature **162**, 196 (1948); J. M. Freeman, Proc. Phys. Soc. (London) **A63**, 668 (1950).

[7] Bender, Shoemaker, Kaufmann, and Bouricius, Phys. Rev. **76**, 273 (1949).

that over a three-hour period the current was constant to 0.01 percent.

In the first parts of the experiment the magnetic field was measured by a flip coil and fluxmeter. The precision of these measurements was marginal, and considerable operator fatigue was involved, so that this was replaced by a balance which measured the torque on a coil carrying a known current.[8]

Figure 1 shows a plan section of the analyzer and target chamber. The incoming proton beam passed through a 2-mm×2-mm tantalum aperture which defined the illuminated area on the target, which in turn acted as the entrance slit of the magnetic analyzer. The solid angle subtended by the analyzer at the target was 0.0028 steradian. It was defined by an aperture located close to the pole pieces so that it prevented secondary small angle scattering from the pole faces. The exit slit was 1.0 cm wide, considerably wider than

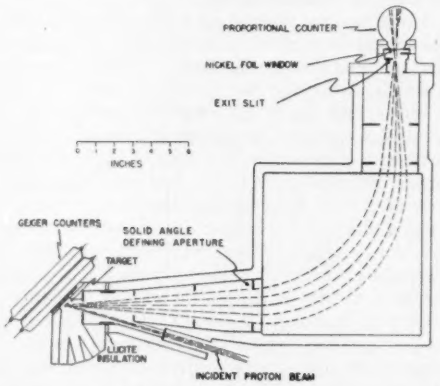

FIG. 1. Schematic of the experimental arrangement. The 90° magnetic analyzer served to separate the various charged particle groups from one another and from the scattering by the target backings. Alpha-particles were distinguished from protons by counter pulse-height discrimination.

the image formed by the magnet, to give a flat-topped window function, and the jaws were staggered so that they lay in the image plane. The energy dispersion was 16.7 cm, and the width of the flat top of the window function was about 4 percent in energy. The target chamber was constructed with four ports for the incoming proton beam, to make possible yield measurements at several angles with respect to the incident beam. The port used in the present experiment was the one which gave the closest approach to the backward direction. Since the analyzer accepted particles over a 10° range, the angle of observation of scattering and charged particle disintegrations extended from 159° to 169° with respect to the incident proton beam.

To inhibit the formation of an oil film on the target surfaces, the targets were mounted on a heated support, and a liquid air trap was used between the diffusion pump and the analyzer chamber. The target support could be moved to change targets without disturbing the vacuum, and without disturbing the vacuum the target support could be transferred to an evaporation chamber for deposition of the target film.

The target chamber was insulated from the remainder of the apparatus by Lucite plates so that it formed a faraday cage. Electrons released by the proton beam striking the target or the beam defining aperture were prevented from passing into or out of the target chamber by electron barriers maintained at minus 300 volts. A circuit[9] was arranged to turn off the scalers after a specified quantity of charge had been collected. This circuit is believed to be dependable to ±0.1 percent.

Charged particles were counted by a proportional counter consisting of a 2-inch brass tube with a 0.003-inch coaxial molybdenum wire for the anode. The window was of nickel foil, 0.0001-inch thick for the first parts of the experiment, and 0.00005-inch thick for the later parts when alpha-particles had to be counted. The counter gas was argon with 2 percent CO_2 added. The pressure varied between 2 cm and 20 cm, depending on the energy and type of particle being counted. Gamma-rays were counted by Radiation Counter Laboratories' thin-wall beta-counters. A sheet of lead was placed between the counters and the target to improve the counting efficiency.

III. EXPERIMENTAL PROCEDURE AND RESULTS

The data were taken in a number of different runs, with somewhat different experimental procedures. Although these data are in some cases grouped together for ease of comparison, the different runs will be discussed individually.

Run 1

Before proceeding with detailed studies on any one resonance or small group of resonances, it appeared desirable to make a relatively rough survey of the elastic scattering and gamma-ray yields, which would indicate where resonance levels were to be found. Since the previous work by Plain *et al.*[1] and Brostrom *et al.*[2] gave a clear picture of the energy region up to 1.4 Mev, it was decided to extend this survey from 1.4 Mev to the limit of the electrostatic generator, about 4 Mev. Targets for this run were prepared by evaporation of aluminum (specified purity, 99.99 percent) onto diamond chips. The diamonds provided smooth surfaces and were sufficiently free from impurities. The magnetic analyzer was thus able to separate the protons scattered by the aluminum film from all other scattering. The field in the analyzer was changed at intervals to follow the energy of the scattered protons. Because of the flat-topped window func-

[8] Buechner, Strait, Sperduto, and Malm, Phys. Rev. **76**, 1543 (1949).

[9] G. M. B. Bouricius and F. C. Shoemaker, Rev. Sci. Instr. **22**, 183 (1951).

tion, the proton energy could be varied 4 percent between changes in the magnetic field. After each change in the magnetic field, the last point taken before the change was repeated as a check on the accuracy of the field setting. Sharp resonances in the elastic scattering could be missed if either the energy spread due to target thickness and proton beam inhomogeneity were large compared with the resonance width, or if the energy steps between points were appreciably larger than this energy spread. Therefore, the energy interval between points, 1.5 kev, was made as small as practicable for a survey covering an energy region this large, and the instrumental energy spread was maintained about equal to this energy step. The data are shown in Fig. 2, labelled "Elastically scattered proton yield." The gamma-ray data taken in this run are now shown because the background from the carbon target backing was so intense as to render them almost meaningless.

Run 2

For comparison of the level structure in this energy region with the structure below 1.4 Mev which had been found by previous workers, it was felt that a gamma-ray yield curve was needed. In addition, because the work of Freeman and Baxter[6] showed that the (p,α) reaction could be an important competing process, it was decided to take an alpha-particle yield curve at the same time. Since the (p,α) reaction is exothermic, the alpha-particles could be separated readily by the magnetic analyzer from the protons scattered by a heavy target backing. Tantalum was chosen for the target backing because its gamma-ray yield under proton bombardment is very small. In this run, the target thickness was chosen about eight times larger than that used in Run 1 so that weak broad resonances would be detected. The resulting increase in the instrumental energy spread allowed a larger energy step between points to be used. The data from this run are shown in Fig. 2, labelled "Gamma-ray yield" and "Alpha-particle yield—full energy group." The gamma-ray yield shown is that recorded by a single Geiger counter. The alpha-particle yield curve was later extended to lower proton energies to overlap the gamma-ray yield curves obtained by previous workers.

Run 3

Although the alpha-particle yield curve showed resonance levels quite well separated, the gamma-ray yield curve showed many more levels which overlap substantially in the high energy region. To get information regarding the origin of this radiation, estimates were made of the gamma-ray energy by coincidence counter absorption measurements[1] on the secondary electrons ejected by the gamma-rays from a lead converter. Absorption curves taken at eight different incident proton energies are shown in Fig. 3, together with the corresponding half-thicknesses of aluminum absorber. At the two lower incident proton energies, the half-thickness corresponds to the order of 10-Mev gamma-ray energy, while for higher incident proton energies, the half-thicknesses correspond to gamma-ray energies of the order of 1 to 2 Mev. The hard gamma-rays observed at the lower proton energies are due to the radiative capture process, but it was believed that some other process, such as inelastic scattering, must be responsible for the soft radiation.

To make possible the detection of inelastically scattered protons, the apparatus was modified so that the proton beam could pass through a thin self-supporting aluminum foil (about 25-kev thick for 3-Mev protons). Momentum analyses of the scattered and disintegration particles were then made at four different incident proton energies, alpha-particles being distinguished from scattered protons by counter pulse-height discrimination. These data are shown in Fig. 4. A reduced energy alpha-particle group appears, as well as several inelastically scattered proton groups. The apparent structure in the full energy alpha-particle group was shown later to be the result of the thickness of the target. From the positions of the peaks, the Q-value for each group was computed. From these the excitation energies of the corresponding states in Al^{27} and Mg^{24} can be obtained. In this work no attempt was made to obtain accurate Q-values. Targets used were relatively thick and the analyzer was adjusted to be as insensitive as possible to magnetic field setting. Values obtained for energy level positions, which are shown in Table I, are sufficiently accurate to show unambiguous correspondence with levels previously observed.

Run 4

The absorption curves indicated that very little, if any, of the gamma-radiation at the higher proton energies was due to the radiative capture process, but the curves for the two lower proton energies, and the work of Plain *et al.*[1] show virtually no soft radiation. To find where the transition between hard and soft gamma-radiation takes place, and to establish that the soft radiation comes from excited residual nuclei, yield curves were obtained for hard gamma-radiation, the reduced energy alpha-particle group, and the inelastically scattered proton groups which leave the aluminum in the 0.82-Mev and 1.05-Mev excited states. Since scattering from a thick target backing would mask these low energy particle groups, and since self-supporting aluminum foils corresponding to the desired target thickness were unavailable, the aluminum was evaporated onto 1000A nickel foil.[10] The target thickness was about the same as that used in Run 2, and the yields were normalized to the same thickness. The hard gamma-radiation was detected by coincidence counters with 3.5 mm of aluminum absorber between

[10] S. Bashkin and G. Goldhaber, Rev. Sci. Instr. **22**, 112 (1951). This technique was developed after the first parts of the present experiment were completed.

FIG. 2. Reaction yield curves from thin aluminum targets bombarded by protons. The charged particle yields were taken at an angle of 164° with respect to the incident proton beam. The solid angle of observation was 0.0028 steradian. The gamma-ray yields are those recorded by a single Geiger counter located about a centimeter from the target. Elastically scattered proton yields were taken with a target about 750 ev thick for 3-Mev protons. Full energy alpha-particle and gamma-ray yields were taken with a target about 6 kev thick for 3-Mev protons. Reduced energy alpha-particle and inelastically scattered proton yields were taken with a target about 7 kev thick for 3-Mev protons and normalized to a target 6 kev thick. Accurate comparison of yields cannot be made because of the possibility of different angular distributions and the variation of peak yields with the ratio of target thickness to resonance width. Yield values are the number of counts, divided by 64, recorded for 48 microcoulombs of incident protons. The low energy extension of the full energy alpha-particle yield curve was taken to overlap the gamma-ray yield curves taken by previous workers. The gamma-radiation at proton energies above 2 Mev is mainly from excited Al^{27} and Mg^{24} residual nuclei. Note that, with few exceptions, for each resonance shown on the yield curves for absorption processes, there is a resonance in the elastic proton scattering. Note also that while the resonances in general are broader for the higher proton energies, very sharp resonances are found up to the highest energies reached.

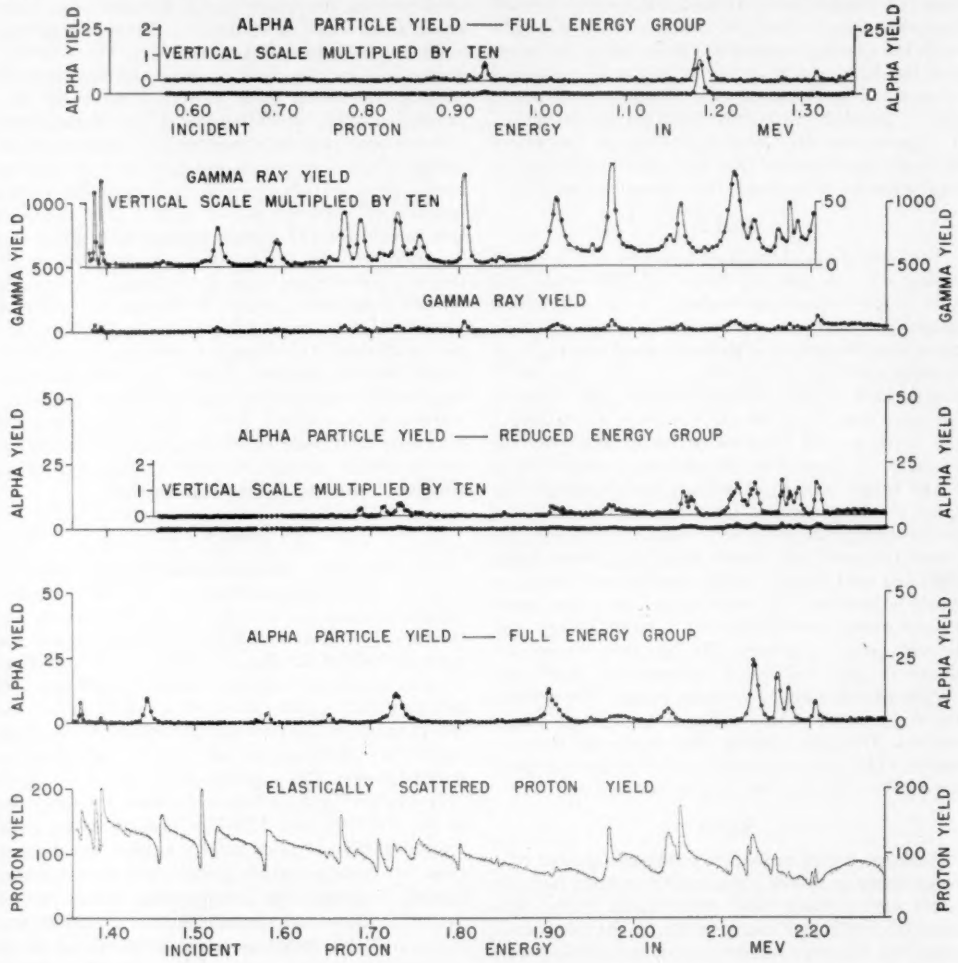
ALPHA PARTICLE YIELD —— FULL ENERGY GROUP
VERTICAL SCALE MULTIPLIED BY TEN
ALPHA YIELD
0.60 0.70 0.80 0.90 1.00 1.10 1.20 1.30
INCIDENT PROTON ENERGY IN MEV
GAMMA RAY YIELD
VERTICAL SCALE MULTIPLIED BY TEN
GAMMA YIELD
ALPHA PARTICLE YIELD —— REDUCED ENERGY GROUP
VERTICAL SCALE MULTIPLIED BY TEN
ALPHA PARTICLE YIELD —— FULL ENERGY GROUP
ELASTICALLY SCATTERED PROTON YIELD
PROTON YIELD
1.40 1.50 1.60 1.70 1.80 1.90 2.00 2.10 2.20
INCIDENT PROTON ENERGY IN MEV

the Geiger tubes. The reduced energy alpha-particle yield and the hard gamma-yield were taken together. The inelastic scattering yield curves were taken over a limited region only, because in the region covered, combined with the reduced energy alpha-yield curve, they satisfactorily accounted for the gamma-ray yield. The data from this run are shown in Fig. 2, labelled "Alpha-particle yield—reduced energy group," and "Inelastically scattered proton yields." The hard gamma-ray yield is not shown, because it was not detected above 1.8 Mev, except for one slight indication at 2.72 Mev. The coincidence counter efficiency was

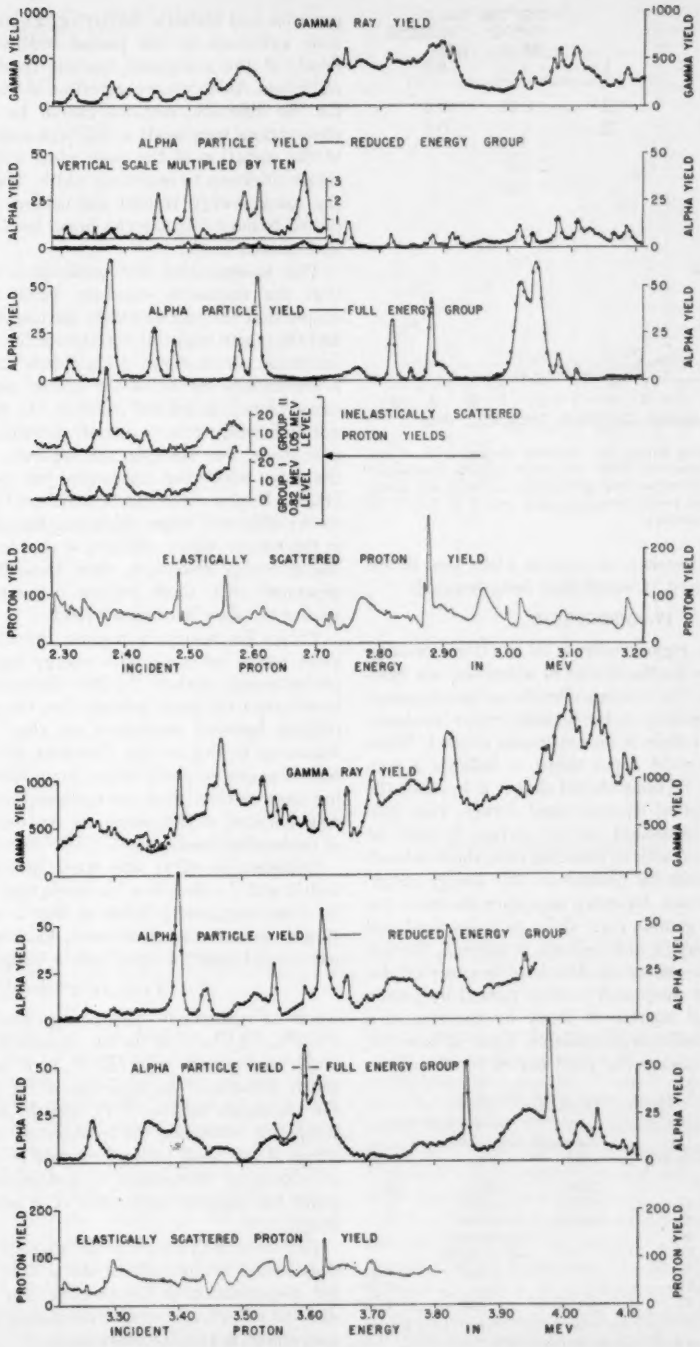
GAMMA RAY YIELD
GAMMA YIELD
1000
500
0
ALPHA PARTICLE YIELD — REDUCED ENERGY GROUP
VERTICAL SCALE MULTIPLIED BY TEN
ALPHA YIELD
50
25
0
3
2
1
ALPHA PARTICLE YIELD — FULL ENERGY GROUP
INELASTICALLY SCATTERED PROTON YIELDS
GROUP II 1.05 MEV LEVEL
GROUP I 0.82 MEV LEVEL
20
10
0
ELASTICALLY SCATTERED PROTON YIELD
PROTON YIELD
200
100
2.30
2.40
2.50
2.60
2.70
2.80
2.90
3.00
3.10
3.20
INCIDENT PROTON ENERGY IN MEV
3.30
3.40
3.50
3.60
3.70
3.80
3.90
4.00
4.10

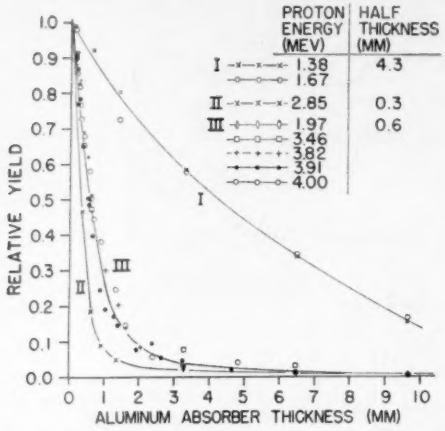

FIG. 3. Absorption curves for electrons ejected from a lead converter by gamma-rays from aluminum targets bombarded by protons. The corresponding gamma-ray energies are about 10 Mev for the two lower proton energies, and 1 to 2 Mev for the higher proton energies.

such that if 10 percent, or in most cases less, of the radiation were hard, it would have been detected.

IV. DISCUSSION

In the energy region covered, all reactions resulting from the proton bombardment of aluminum are resonance processes. The resonance levels are broad enough to overlap appreciably at the highest proton bombarding energies, but there is no continuum evident. While the gamma-ray yield curve seems to indicate a continuum, it must be remembered that it is in effect the sum of a number of separate yield curves. This indicates that the compound nucleus picture is valid for discussion of the reactions resulting from the bombardment of aluminum by protons in this energy range. With few exceptions, for every resonance shown on the yield curves for gamma-rays, alpha-particles (both full and reduced energy), and inelastic scattering, there is resonance elastic scattering. This is to be expected, for any state of the compound nucleus formed by proton capture must be capable of decay by emission of a proton with the full energy available. There is, however, less correlation among the yield curves for the alpha-particles and inelastic scattering. Evidently there are wide variations in the partial widths for modes of decay of the compound nucleus from resonance to resonance. An accurate comparison of the partial widths for the different reactions cannot be made because observations were made at only one angle, and because of the variation of the peak yield with the ratio of target thickness to resonance width. The resonances in the lower energy regions are narrow, but at higher proton bombarding energies broad levels appear mixed with narrow levels.

TABLE I. Energy levels in Al^{27} and Mg^{24}.

Isotope	Levels listed in AEC compilation*	Computed from momentum analyses 14B	14C	14D
	Mev	Mev	Mev	Mev
Al^{27}	+0.84	+0.81	+0.83	···
Al^{27}	+1.07	+1.05	+1.04	···
Al^{27}	+1.48		not observed	
Al^{27}	+1.79		not observed	
Al^{27}	+2.28	···	+2.25	+2.20
Al^{27}	+2.82	···	···	+2.75
Mg^{24}	+1.38	+1.30	+1.35	+1.24

* D. E. Alburger and E. M. Hafner, AEC-549, BNL-T-9.

This investigation was undertaken with the hope that the resonance structure would be sufficiently simple that the partial width, the angular momentum, and the parity might be determined for each level. The excitation curves shown in Fig. 2 were meant to be only a preliminary survey of the energy region. In many cases resonances are well resolved, but the targets were not sufficiently thin to permit determination of their true shape. For example, the apparent overlapping of the three scattering resonances just below 1.40-Mev (Fig. 2, Proton yield) can be attributed almost entirely to the effects of target thickness. Results (not shown) in this energy region, obtained with thinner targets and higher energy resolution, show these levels very well separated with short regions between levels which appear to follow Rutherford yield.

Except for resonance regions, the elastic scattering yield varies inversely with energy squared up to a proton energy of about 2.5 Mev. Estimates from calculated target thickness indicate that the scattering cross sections between resonances are close to Rutherford values up to this energy. However, the data are presented as proton yields rather than differential scattering cross section, since the cross-section values in the neighborhood of the resonances are uncertain because of inadequate resolution.

Considerable effort was spent in trying to assign widths and J-values to a few levels that are sufficiently far from neighboring levels so that a one-level Breit-Wigner formula could be used. Each scattering resonance tried could be fitted with a formula of the form

$$Y=|Y_R^{\frac{1}{2}}+Ae^{i\phi}e^{i\delta}\sin\delta|^2,$$

where Y=observed yield, Y_R=Rutherford yield, $A=Y^{\frac{1}{2}}{}_{\max}\pm Y^{\frac{1}{2}}{}_{\min}$, ϕ is an empirically determined angle, and $\tan\delta=-\frac{1}{2}\Gamma/(E-E_R)$, Γ being the total width. Because of the large spin of the ground state of the aluminum nucleus (5/2), and the large number of competing reactions, the formulation of A and ϕ in terms of the usual parameters used in the description of scattering phenomena is ambiguous. In no case could the angular momentum of a level be uniquely assigned.

Extension of this work to include data on the angular distribution of reaction products had been planned, but consideration of the problem now indicated that such data would not, in most cases, lead to unambiguous assignment of angular momentum.

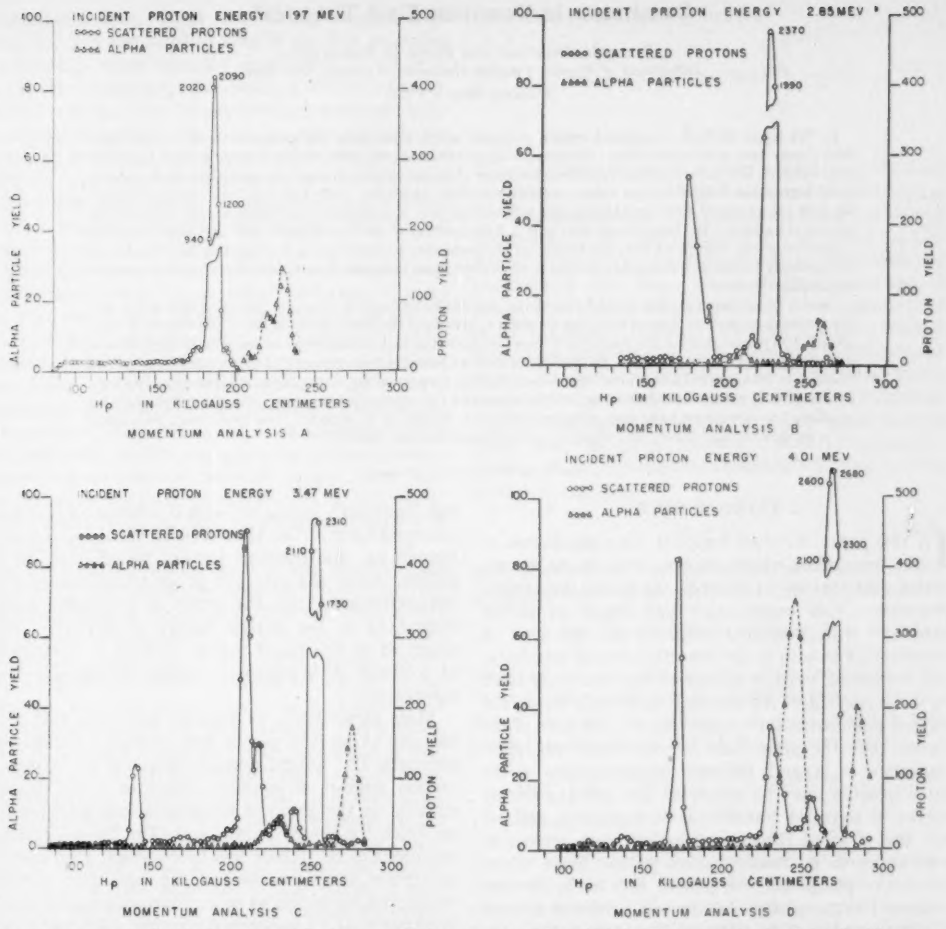

FIG. 4. Momentum distributions of particles from an aluminum target, 25 kev thick for 3-Mev protons, bombarded with protons of four different energies. Four groups of inelastically scattered protons and two alpha-particle groups, corresponding to transitions to the ground state and first excited state of Mg^{24} are evident. The apparent structure of the full energy alpha-particle peak is due to the thickness of the target.

It would appear that the analysis of the angular distribution of the full energy alpha-particles would be particularly revealing, since the spins of the alpha-particles and of the residual Mg^{24} nuclei are both zero. Consequently, the orbital angular momentum of the alpha particles is equal to the J-value of the compound state in Si^{28}. However, according to Eisner and Sachs,[11] the largest power of $\cos\theta$ that can appear in the angular distribution is twice the smaller of the two orbital angular momenta involved—namely, that of the incident proton and of the emitted alpha-particles. For example, if the incident protons are S-protons, the angular distribution of the alpha-particles will be symmetric, regardless of their orbital angular momentum.

Detailed studies of yields with angular distribution measurements might, for certain levels, lead to assignment of angular momentum quantum numbers and parity. However, if such measurements were to be made on a large fraction of the levels observed, the time and effort required would be prohibitive. The work was therefore discontinued.

The authors are indebted to Professors R. G. Herb and R. Rollefson for advice and encouragement throughout the experiment, to M. Cutler and L. J. Koester for their help in taking data, and to G. Goldhaber for the construction of the magnetic balance used for measurement of the magnetic field.

[11] E. Eisner and R. G. Sachs, Phys. Rev. **72**, 680 (1947).

Constraints in Covariant Field Theories*

JAMES L. ANDERSON AND PETER G. BERGMANN
Department of Physics, Syracuse University, Syracuse, New York
(Received May 7, 1951)

In this paper we have considered certain problems which arise when one attempts to cast a covariant field theory into a canonical form. Because of the invariance properties of the theory, certain identities exist between the canonical field variables. To insure that the canonical theory is equivalent to the underlying lagrangian formalism one must require that these identities, once satisfied, will remain satisfied through the course of time. In general, this will be true only if additional constraints are set between the canonical variables. We have shown that only a finite number of such constraints exist and that they form a function group. Our proof rests essentially on the possibility of constructing a generating function for an infinitesimal canonical transformation that is equivalent to an invariant infinitesimal transformation on the lagrangian formalism.

Once a hamiltonian is obtained by one of the procedures outlined in previous papers of this series, and the constraints have all been found, the consistent, invariant canonical formulation of the theory is completed. The main results of the paper have been formulated in such a manner as to make them applicable to a fairly general type of invariance. In the last sections we have applied these results to the cases of gauge and coordinate invariance. In the latter case a hamiltonian, corresponding to a quadratic lagrangian, has been constructed in a parameter-free form; and in both cases the constraints, together with the poisson bracket relations between them, have been obtained explicitly. As was to be expected, two constraints were found for a gauge-invariant theory and eight for a coordinate-invariant theory.

I. INTRODUCTION

IN this paper, we shall complete the examination of the constraints which are met with in the hamiltonian formulation of theories possessing invariance properties. This examination had begun in earlier papers,[1–3] with particular emphasis on the type of covariance met with in the general theory of relativity, and is in some respects similar to the results obtained by L. Rosenfeld.[4,5] All theories dealt with in physics possess some covariance properties, i.e., the laws of the theory take the same form in more than one representation. In general, different representations of the same situation may be converted into one another by means of so-called transformation equations, and we say that a given theory is covariant with respect to such-and-such a transformation group. These transformation groups fall in general into three distinct classes: The group may contain only a finite or at least discrete number of transformations, such as the symmetric group (of permutations), of importance in spectroscopy, and the space group of crystallography. The group may be a continuous set, the members of which can be identified by a finite number of continuously variable parameters, a so-called Lie group; among these groups are the group of orthogonal transformations and the Lorentz group. Finally, the group may again be a continuous set, but so that the number of parameters required to represent it is no longer finite but equivalent to one or several arbitrary functions; examples for this class are the group of canonical transformations, the group of unitary transformations in Hilbert space, the group of gauge transformations in electrodynamics, and the group of coordinate transformations in the general theory of relativity. Our attention in this paper will be focused on covariance of a theory with respect to groups belonging to the third class.

More particularly, we shall be concerned with field theories whose laws can be derived from a variational principle. The Euler-Lagrange equations will possess a certain number of so-called identities which depend directly on the group of transformations with respect to which the theory is invariant. The Euler-Lagrange equations of the theory will be covariant with respect to certain transformations if the lagrangian integral transforms by adding at most a surface integral, which is immaterial for a variational principle. (For continuous groups, it is sufficient to consider the infinitesimal transformations from which the whole group can be constructed.) But this change is an integral over the product of the variational derivatives of the lagrangian and the infinitesimal changes of the field variables. At each point in space-time, this integral must then be a complete divergence (or zero), even when the variational derivatives of the lagrangian are different from zero, i.e., even when the field equations are not satisfied. This condition will lead to identities between the field variables and their derivatives which, depending on the character of the group, will take the form of integrals or will hold at each point separately. In the third class of transformation groups, the identities are generally point-to-point.

For certain groups the identities can be converted into the form of a pure divergence, and hence lead to

* This work was supported by the ONR under Contract 6N-onr-24806.
[1] P. G. Bergmann, Phys. Rev. **75**, 680 (1949), referred to as I.
[2] P. G. Bergmann and J. H. M. Brunings, Revs. Modern Phys. **21**, 480 (1949), referred to as II.
[3] Bergmann, Penfield, Schiller, and Zatzkis, Phys. Rev. **80**, 81 (1950), referred to as III.
[4] L. Rosenfeld, Ann. Physik **5**, 113 (1930).
[5] L. Rosenfeld, Ann. inst. Henri Poincaré **2**, 25 (1932).

conservation laws. These are "strong" conservation laws (I); they are satisfied even if the field equations are not, e.g., when there are singularities in the field. In the case of the gauge invariance of electrodynamics, we have one such law, the conservation of charge, while coordinate covariance leads to the four laws of conservation of energy and linear momentum. It is the existence of the strong conservation laws which leads to equations of motion for the singularities of the field without requiring separate assumptions such as the Lorentz force.

When the theory is carried from the lagrangian over into the hamiltonian (or canonical) formalism, it turns out that the various momentum densities, defined in the customary manner, are not algebraically independent of each other, but satisfy a number of relations, free of time derivatives, which we shall call primary constraints in analogy to the customary terminology of mechanics; these relationships are analogous to the first subsidiary condition of quantum electrodynamics. Unless the momentum densities satisfy these constraints, there will be no conceivable set of "velocities" (time derivatives of the field variables) consistent with the momentum densities.

In the canonical formalism, the field equations are replaced by the first-order canonical field equations. Not all solutions of the canonical field equations satisfy the primary constraints, nor is it sufficient to satisfy the primary constraints on one initial hypersurface to assure that the equations of motion will preserve them elsewhere. But if we were to start with a solution of the lagrangian field equations and translate this solution into the canonical formalism, both the canonical field equations and the primary constraints would be satisfied everywhere. Hence, they are at least compatible with each other. Compatibility, while necessary, is not sufficient. We must discover the totality of all conditions to be satisfied on an initial hypersurface which will guarantee that solutions of the canonical field equations will satisfy the primary constraints everywhere. We shall show that these additional conditions, called the secondary constraints, are finite in number and that their exact number depends on the details of the transformation laws for the field variables and for the lagrangian.

In this paper, we shall derive a number of results for an assumed transformation law for the field variables somewhat more general than that postulated in I and II (though including that law as a special case). Furthermore, we shall carry the argument through without using the parameters introduced in II; their introduction into the theory can be accomplished without difficulty, but contributes little to the developments presented here.

II. INVARIANT TRANSFORMATIONS

In what follows, we shall consider field theories in which the field equations can be derived from a four-dimensional variational principle:

$$S=\int L(y_A, y_{A,\sigma})d^4x, \tag{2.1}$$

$$\delta S=0.$$

The lagrangian density L is to be a function of the field variables $y_A(x^1, \cdots, x^4)$ and their first derivatives $y_{A,\sigma}$. We shall assume that the field equations go over into themselves if the field variables are subjected to any one of a group of transformations; we shall call the members of this group invariant transformations, a designation that is meaningful only with respect to a particular theory or class of theories. We shall further assume that the group structure permits the identification of its members, including the infinitesimal transformations, by a finite number of arbitrary functions. Well-known examples of this type of transformation group are the gauge transformations of electrodynamics, whose infinitesimal transformation law can be written in the form

$$\delta\phi_\mu=\xi_{,\mu} \tag{2.2}$$

and the coordinate transformations, whose infinitesimal (substantive, see I) transformation law taken the form

$$\bar{\delta}y_A=F_{A\mu}{}^{B\nu}y_B\xi^\mu{}_{,\nu}-y_{A,\mu}\xi^\mu, \tag{2.3}$$

provided the field variables transform according to a linear homogeneous law (Christoffel symbols, for instance, do not). Accordingly, we shall adopt as our general transformation law for the field variables

$$\bar{\delta}y_A={}^0f_{Ai}\xi^i+{}^1f_{Ai}{}^\mu\xi^i{}_{,\mu}+\cdots+{}^Pf_{Ai}{}^{\mu\cdots\tau}\xi^i{}_{,\mu\cdots\tau}, \tag{2.4}$$

$$\bar{\delta}x^\rho=0.$$

For the sake of generality, we shall not assume any particular geometric or physical significance for the arbitrary functions ξ^i, the "descriptors," which appear in this infinitesimal transformation law. The coefficients ${}^sf_{Ai}{}^{\mu\cdots\tau}$ are some functions of the field variables and their derivatives, generally such that the sum of the orders of differentiation in the various factors of any one term in Eq. (2.4) does not exceed the finite number P. For the two laws (2.2) and (2.3), this total order P equals one, and these two laws are, moreover, homogeneous with respect to the order of differentiation. To assure group character, we must and shall require that the commutator of two expressions (2.4) with two different sets of descriptors will be an expression of the same kind (with the same coefficients f), with a third set of descriptors.

III. IDENTITIES

By a method similar to that employed in I we find that the field variables satisfy a number of identities. We require that the lagrangian density, in the face of a

transformation of the form (2.4), shall add only a pure divergence. If this is the case then

$$\bar{\delta}L = L^A\bar{\delta}y_A + [(\partial L/\partial y_{A,\rho})\bar{\delta}y_A]_{,\rho} = Q^\rho{}_{,\rho}, \tag{3.1}$$

where the L^A are the field equations, i.e.,

$$L^A \equiv (\partial L/\partial y_A) - (\partial L/\partial y_{A,\rho})_{,\rho}. \tag{3.2}$$

$\bar{\delta}L$ will be a divergence only if

$$L^A{}^0 f_{A i} - (L^{A1} f_{A i}{}^\mu)_{,\mu} + \cdots + (-1)^p (L^A{}^P f_{A i}{}^{\mu\cdots\tau})_{,\mu\cdots\tau} \equiv 0. \tag{3.3}$$

These equations are the generalized "Bianchi identities" of the theory. There are as many of them as there are descriptors in the transformation law. In such identities, the terms containing the highest derivatives of the field variables must vanish by themselves. These terms are of the form

$$L^{A\rho B\sigma}{}^P f_{A i}{}^{\mu\cdots\tau} y_{B,\rho\sigma\mu\cdots\tau} \equiv 0, \tag{3.4}$$

where $L^{A\rho B\sigma}$ is shorthand for $\frac{1}{2}[(\partial^2 L/\partial y_{A,\rho}\partial y_{B,\sigma}) + (\partial^2 L/\partial y_{A,\sigma}\partial y_{A,\rho})]$. Symmetrizing with respect to $\rho\sigma\mu\cdots\tau$, we have

$$\{L^{A\rho B\sigma}{}^P f_{A i}{}^{\mu\cdots\tau}\}_{(\rho\sigma\mu\cdots\tau)} \equiv 0, \tag{3.5}$$

$(\rho\sigma\mu\cdots\tau)$ indicating that the expression is symmetrized with respect to these indices. Of particular interest for what follows are those expressions in which all Greek indices are set equal to 4. They are

$$L^{A4B4} u_{Bi} \equiv 0, \tag{3.6}$$

where

$$u_{Bi} = {}^P f_{Ai}{}^{4\cdots4}. \tag{3.7}$$

IV. HAMILTONIAN FORMALISM

Let us now specialize our problem by assuming that our lagrangian is quadratic in the differentiated quantities; i.e., it has the form

$$L = \Lambda^{A\rho B\sigma} y_{A,\rho} y_{B,\sigma}. \tag{4.1}$$

Momentum densities canonically conjugate to the y_A are defined in the customary manner to be

$$\pi^A \equiv \frac{\partial L}{\partial \dot{y}_A} = 2\Lambda^{A4B4}\dot{y}_B + 2\Lambda^{A4B\sigma} y_{B,\sigma}. \tag{4.2}$$

If we now try to solve these equations for the $y_{A,4}$ in terms of the π^A, we find that we cannot do so directly because of the fact that Λ^{A4B4} is a singular matrix, as shown by Eq. (3.6), and hence has no inverse in the ordinary sense. However, we can circumvent this difficulty by introducing the quasi-inverse (III) to Λ^{A4B4} by the equations

$$E_{AB}\Lambda^{B4C4}E_{CD} = E_{AD}, \qquad \Lambda^{A4B4}E_{BC}\Lambda^{C4D4} = \Lambda^{A4D4}. \tag{4.3}$$

These equations do not determine E_{AB} completely, but only up to a linear combination of the null vectors of the matrix Λ^{A4B4}, the u_{Bi}. It can be shown easily that

$$\Lambda^{A4C4}E_{AB} = \delta_B{}^C - v^{Ci}u_{Bi}, \qquad v^{Ci}E_{CA} = 0, \quad v^{Ci}u_{Cj} = \delta_j{}^i, \tag{4.4}$$

where the expressions v^{Ci} depend on the choice of E_{AB}. If we now multiply Eq. (4.2) by E_{AB} and introduce as a convenient abbreviation

$$\pi^A - 2\Lambda^{A4B\sigma} y_{B,\sigma} = \bar{\pi}^A, \tag{4.5}$$

we find

$$\dot{y}_B = \tfrac{1}{2}E_{BC}\bar{\pi}^C + 2u_{Bi}v^{Ci}\dot{y}_C. \tag{4.6}$$

It is not difficult to see that the expressions $\Lambda^{A4B4}\dot{y}_B$ entering into Eq. (4.2) and the expressions $v^{Bi}\dot{y}_B$ of Eq. (4.6) are completely independent of each other, i.e., all of them can be given arbitrary values without giving rise to inconsistencies. As a result, the $\bar{\pi}^A$ determine the $\dot{y}_B$ only incompletely, and the extent of this incomplete determination is expressed accurately by a set of equations

$$\dot{y}_B = \tfrac{1}{2}E_{BC}\bar{\pi}^C + u_{Bi}w^i \tag{4.7}$$

with arbitrary functions w^i.

If we multiply Eqs. (4.2) by u_{Ai}, we find

$$g_i \equiv u_{Ai}\bar{\pi}^A = 0, \tag{4.8}$$

a set of algebraic relations to be satisfied by the canonical momentum densities together with the field variables y_A. These relations are the primary constraints.

If we wish to form a hamiltonian and to reformulate the whole set of field equations in terms of a canonical formalism, it can be shown that for the quadratic lagrangian density (3.1) the corresponding hamiltonian density H is

$$H = \tfrac{1}{4}E_{AB}\bar{\pi}^A\bar{\pi}^B - \Lambda^{A\tau B\sigma}y_{A,\tau}y_{B,\sigma} + w^i g_i, \tag{4.9}$$

where the functions w^i are arbitrary and identical with those of Eq. (4.7). This result, first obtained by Penfield[6] for the coordinate formalism (which dispenses with the introduction of the parameters), is complete in the sense that it describes the full extent of the arbitrariness remaining in the choice of hamiltonian.[7]

[6] R. Penfield, Ph.D. dissertation, Syracuse University, 1950 (to be published).

[7] Although this result has been obtained using a quadratic lagrangian, it is quite general. The identities (3.6) can be written in the form,

$$u_{Bi}\partial\pi^B/\partial\dot{y}_c = 0$$

and, since by definition u_{Bi} contains no differentiated field variables, we can integrate them and obtain, as primary constraints

$$u_{Bi}\pi^B - K_i(y, y_{,s}) \equiv 0.$$

We then have the problem of solving the set of equations

$$\pi^A = \partial L/\partial\dot{y}_A$$

together with the above constraints. Since we actually have

Naturally, other forms of the hamiltonian density can be obtained by canonical transformations; but the arguments appearing in such new expressions will no longer have the significance of the original field variables y_A and the momentum densities defined by Eq. (4.2). It follows in particular that transformations of the form (2.4) will change the expression (4.9) at most by adding to it further linear combinations of the primary constraints, i.e., by leading to new arbitrary functions w^i. To avoid misunderstandings, it should also be noted that whenever we speak of arbitrary functions, we imply that they are arbitrary in our configuration or phase space; i.e., they may depend on the coordinates as well as the field variables and their derivatives and, in the canonical formalism, on the momentum densities and their derivatives as well.

V. CONTACT TRANSFORMATIONS AND INFINITESIMAL TRANSFORMATIONS

Let us now return to the infinitesimal transformations defined by Eqs. (2.4). We may interpret this transformation law in a number of different spaces. We shall call the function space of all functions $y_A(x^1, x^2, x^3)$ the configuration space of the theory and denote it by S_c. In such a formulation, t appears as a parameter outside the function space, S_c, and the change of the physical system in the course of time appears as the motion of the representative point. Obviously, the transformation (2.4) is not a transformation in S_c, since it involves on its right-hand side $\dot{y}_A, \ddot{y}_A, \cdots$. We might introduce the function space of which the elements are $y_A, \dot{y}_A, \cdots \partial^P y_A/\partial t^P$, and call that space the configuration-plus-"velocity" space, S_{cv}. In that space, the transformation law for the y_A is properly defined, but then the transformation law for $\dot{y}_A$ will involve $P+1$ time derivatives, and so forth indefinitely. A possible way out of this difficulty is to introduce a different type of space, the space of the functions $y_A(x^1, \cdots, x^4)$. A whole trajectory of a representative point in S (its motion as a function of t) becomes a single point in this new space, $\sum_c$. In this new space, the transformation law (2.4) is properly defined, and with the arbitrary functions ξ^i, constitutes a group.

We now ask the following question: if the y_A are subjected to a transformation of the form (2.4), what effect does this have on the corresponding canonical formulation? To answer this question, we shall first introduce as the phase space $\sum$ (without subscript) the function space of all functions $y_A(x^1, \cdots, x^4)$, $\pi^A(x^1, \cdots, x^4)$. Most of its points will not correspond to possible points in $\sum_c$. But $\sum$ is the space in which all canonical transformations

$$\delta y_A = \delta\mathcal{C}/\delta\pi^A, \quad \delta\pi^A = -\delta\mathcal{C}/\delta y_A, \qquad \delta\mathcal{H} = \partial\mathcal{C}/\partial t \tag{5.1}$$

are defined. There is, however, a space which is isomorphic with the space $\sum_c$, although not identical with it; it is a subspace, which we shall designate by $\sum_l$ (lagrangian subspace), consisting of all points of $\sum$ that satisfy the conditions (4.2). We shall call a one-to-one mapping between $\sum_c$ and $\sum_l$ in which the functions y_A of corresponding points are simply the same functions (and they define π^A in $\sum_l$ uniquely), the "identification." Under the identification, each possible transformation in $\sum_c$ corresponds uniquely to one in $\sum_l$, and vice versa. All these transformations can be expanded into canonical transformations in $\sum$ by the following method (and possibly in other ways as well): First, replace the original field variables by the transformed variables in the lagrangian of the variational principle. Then transform this formally new lagrangian theory into a hamiltonian theory. The new hamiltonian theory is equivalent to the original one and, therefore, connected with it by a canonical transformation. We shall call the class of canonical transformations which correspond to transformations in $\sum_c$ "canonical transformations in $\sum_l$," because they map the points of the original $\sum_l$ on the points of the new $\sum_l$. The two subspaces $\sum_l$ are in general not determined by identical Eqs. (4.2), because the lagrangian will have changed its form.

Of special interest are the invariant infinitesimal transformations, Eq. (2.4). We shall call the corresponding infinitesimal canonical transformations "(infinitesimal) invariant canonical transformations." Because of the invariant character of these transformations, we may adopt the same formal expression for the lagrangian density (2.1) before and after the transformation, and we shall do so, because with this choice the identity of the subspace $\sum_l$ remains unaffected by the corresponding canonical transformations.

Given an invariant infinitesimal coordinate transformation, we can expand it into a canonical transformation in $\sum$ in infinitely many ways. If we have obtained one such transformation and its generating functional, we can add to the generator any expression at least quadratic in the primary constraints. These additional terms will have no effect in the subspace $\sum_l$, but they will affect the transformation equations elsewhere in $\sum$.

To each invariant canonical transformation belongs only one invariant transformation in $\sum_c$, because such a transformation leads uniquely to a transformation law in $\sum_l$ and hence in $\sum_c$. The degree of arbitrariness in going from $\sum_c$ to $\sum_l$ and thence to $\sum$ is completely

---

fewer equations than variables, a particular solution can always be found. Let it be of the form,

$$\dot{y}_A{}^0 = \Gamma_A(\pi, y, y_{,s}).$$

It is easy to see that

$$\dot{y}_A = \dot{y}_A{}^0 + w^i u_{Bi}$$

is also a solution. Hence, we can, after forming a hamiltonian according to the equation,

$$H = \pi^A \dot{y}_A{}^0 - L(y, \dot{y}^0)$$

add to it a term of the form $w^i(u_{Bi}\pi^B - K_i)$ and still obtain the same canonical equations.

exhausted by the addition of terms quadratic in g_i and has no effect on the transformation law in $\sum_t$, which is uniquely determined by the transformation law in $\sum_c$. Any nonconstant addition to the generator of a canonical transformation other than terms at least quadratic in the primary constraints would have an effect on the transformation law in $\sum_t$.

We can conclude that the invariant canonical transformations form a group. Because of its importance, this argument will be presented at some length. First of all, the commutator of two invariant transformations in $\sum_c$ must itself be an invariant transformation; under the identification, the corresponding transformations in $\sum_t$ must form a group, too. The only difficulty arises in connection with the expansion into canonical transformations in $\sum$. Let A and B represent two invariant transformations in $\sum_t$, and A' and B' expansions of A and B, respectively, into canonical transformations in $\sum$. Let C be the commutator of A and B in $\sum_t$, and C' some canonical expansion of C in $\sum$. On the other hand, let C'' be the commutator of A' and B' in $\sum$. Obviously, both C' and C'' are canonical transformations by definition, but they might not be identical. Actually, for the proof of group property, it will be necessary and sufficient to show that C'' is an invariant transformation and an expansion of C, that it differs, in other words, from C' at most by terms at least quadratic in the primary constraints. Inasmuch as A' and B' map $\sum_t$ on itself, their commutator must have the same property, and this mapping must be C. Therefore, C'' must be a canonical expansion of C, and that was the burden of the proof. A corollary is that the generators of the infinitesimal invariant canonical transformations form a function group in the terminology of Lie; i.e., their poisson brackets are again generators of infinitesimal invariant canonical transformations.

We now turn our attention to these generators and their relation to the hamiltonian (or hamiltonians) of the theory. We know from the form of the infinitesimal transformations in $\sum_c$ that the generators will be homogeneous linear in the descriptors and their derivatives. The question arises as to the order of the derivatives that appear in the generators. They will, of course, contain no higher derivatives than the transformation laws for the y_A and π^A in $\sum_c$. We have assumed that the order of differentiation of the descriptors in the transformation laws of the y_A is P. In order to find the order of differentiation for the transformation laws of the π^A we proceed as follows. From Eqs. (3.2) we have that

$$\bar{\delta}\pi^A = 2\delta\Lambda^{A4B4}\dot{y}_B + 2\Lambda^{A4B4}\bar{\delta}\dot{y}_A + \cdots. \tag{5.2}$$

According to Eq. (2.4) the $\dot{y}_A$ transform as

$$\bar{\delta}\dot{y}_A = {}^0f_{A_i}\xi^i + \cdots + (-1)^P\, {}^Pf_{A_i}{}^{\mu\cdots\nu}\xi^i{}_{,\mu\cdots\nu}. \tag{5.3}$$

Upon substitution of this expression into (5.2) we see that because of Eq. (3.6), time derivatives of the descriptors appear only up to order P. Space derivatives may appear to a higher order, but that does not concern us, since they can be removed by an integration by parts. In fact, if we restrict ourselves to infinitesimal transformations whose descriptors differ from zero only in a finite spatial domain (a "patch"), we may integrate by parts and assert that the generating density can be brought into the simple form

$$\mathfrak{C} = {}^0A_i\xi^i + {}^1A_i\dot{\xi}^i + \cdots + {}^PA_i\frac{\partial^P\xi^i}{(\partial t)^P}. \tag{5.4}$$

In this form we can ascertain the values for the poisson brackets of the coefficients ${}^nA_i$ by writing down the correct expression for the commutator of two infinitesimal transformations, for, since

$$\bar{\delta}^*(\bar{\delta}y_A) - \bar{\delta}(\bar{\delta}^*y_A) = \bar{\delta}^{**}y_A, \tag{5.5}$$

where $\bar{\delta}$, $\bar{\delta}^*$, and $\bar{\delta}^{**}$ represent transformations of the form (2.4), one has immediately

$$(\mathfrak{C}, \mathfrak{C}^*) = \mathfrak{C}^{**}; \tag{5.6}$$

i.e., the poisson bracket between two generators of the form (5.4) is again of the same form. Hence one can conclude that the poisson bracket between any two functions of the set ${}^nA_i$ must be expressible in terms of members of this set: these ${}^nA_i$ form a function group.

To investigate the poisson bracket relations of the ${}^nA_i$ with the hamiltonian, we proceed as follows. We know from the results of Sec. IV that in the face of an infinitesimal invariant transformation in $\sum_c$ the hamiltonian can change as a function of its arguments only by terms of the form

$$\delta'\mathfrak{IC} = \int \delta' w^i g_i d^3x, \tag{5.7}$$

the $\delta' w^i$ being some functions of the descriptors of the transformation. (Note that $\bar{\delta}$ represents the change produced in a dynamical variable by an infinitesimal transformation, at a point with the same coordinate values, which, depending on the nature of the transformation, may or may not be the same point, while δ' represents the change in $\mathfrak{IC}$ and w^i as a function of their arguments, i.e., of the y_A and π^A.) Under the corresponding canonical transformation in $\sum$ the hamiltonian changes by an amount

$$\delta'\mathfrak{IC} = (\mathfrak{C}, \mathfrak{IC}) + \frac{\partial\mathfrak{C}}{\partial t} = \int \delta' w^i g_i d^3x, \tag{5.8}$$

where $\mathfrak{C}$ is the generator of the transformation. If we restrict ourselves, for the time being, to descriptors that do not depend on the canonical variables, but only

on the coordinates, we can write

$$\int \delta' w^i g_i d^3x = \int \left({}^0A_i \xi^i + \cdots + {}^PA_i \frac{\partial^{P+1}\xi^i}{(\partial t)^{P+1}} \right) d^3x$$

$$+ \int ({}^0A_i, \mathcal{H}) \xi^i d^3x + \cdots + \int ({}^PA_i, \mathcal{H}) \frac{\partial^P \xi^i}{(\partial t)^P} d^3x. \quad (5.9)$$

Now under an infinitesimal transformation $\dot{y}_A$ changes by an amount

$$\bar{\delta}\dot{y}_A = \cdots + u_{Ai} \frac{\partial^{P+1}\xi^i}{(\partial t)^{P+1}}, \quad (5.10)$$

while, according to Eq. (4.7) the change in $\dot{y}_A$ due to the change in the hamiltonian as given by Eq. (5.7) is

$$\bar{\delta}\dot{y}_A = \cdots + u_{Ai} \delta' w^i. \quad (5.11)$$

In each of the above expressions we have explicitly written down only those terms containing $(P+1)$st time derivatives of the descriptors. If Eqs. (5.10) and (5.11) are to agree, as they must if we operate in $\sum_l$, the dependence of $\delta' w^i$ on the $(P+1)$st time derivative of the descriptors is simply

$$\delta' w^i = \cdots + \partial^{P+1}\xi^i/(\partial t)^{P+1} \quad (5.12)$$

and, therefore,

$$g^i = {}^PA_i.$$

However, since $\delta' \mathcal{H}$ is equal to some linear combination of the g_i and hence of the ${}^PA_i$, we can conclude further from Eq. (5.9) that the poisson brackets of all the ${}^nA_i$ with $\mathcal{H}$ can be expressed in terms of the ${}^nA_i$. In fact, since the left-hand side of Eq. (5.9) is nothing more than a linear combination of the ${}^PA_i$, the right-hand side must also have this form. Now, since the ξ^i and all of their time derivatives are independent of each other, the only way in which this can come about is for all of the coefficients of different ξ^i, both with regards to index and differential order, to be linear combinations of the ${}^nA_i$. Comparing terms, we find that

$$({}^0A_i, \mathcal{H}) = \text{linear combination of } g_i,$$

$${}^{n-1}A_i + ({}^nA_i, \mathcal{H}) = \text{linear combination of } g_i,$$

$$n = 1, \cdots, P. \quad (5.13)$$

In particular, we see that the ${}^nA_i$, together with the hamiltonian, form a function group.

These results are the ones needed to establish the total number of constraints that must be set if the canonical equations are to be solved and if the primary constraints are to remain satisfied. A necessary and sufficient condition is that the poisson brackets of the primary constraints with the hamiltonian vanish. In case they do not vanish identically, they must be set equal to zero, and the requirement then becomes that the poisson bracket of these expressions with the hamiltonian vanish, and so on until a point is reached where no new constraints are being obtained. We see that the ${}^nA_i$ (or rather certain linear combinations of them) are just the constraints which must be set equal to zero and, because of Eq. (5.13), only a finite number of them exist. This number is at most $(P+1)$ times the number of descriptors necessary to define our invariant transformation group.

VI. APPLICATION TO ELECTROMAGNETIC THEORY

Here we assume a transformation law of the form (2.1). Recasting this into the form of (2.3), we have

$$\bar{\delta}\phi_\mu = \delta_\mu{}^\nu \xi_{,\nu}. \quad (6.1)$$

The lagrangian of the theory is

$$L = (1/8\pi)(\eta^{\mu\sigma}\eta^{\nu\rho} - \eta^{\mu\nu}\eta^{\rho\sigma})\phi_{\mu,\rho}\phi_{\nu,\sigma}. \quad (6.2)$$

The field equations are

$$L^\mu = -(1/4\pi)(\eta^{\mu\sigma}\eta^{\nu\rho} - \eta^{\mu\nu}\eta^{\rho\sigma})\phi_{\nu,\rho\sigma}. \quad (6.3)$$

The Bianchi identity is

$$-(1/4\pi)(\eta^{\mu\sigma}\eta^{\nu\rho} - \eta^{\nu\mu}\eta^{\rho\sigma})\phi_{\nu,\mu\rho\sigma} \equiv 0. \quad (6.4)$$

The equation which corresponds to (3.6) is simply

$$\eta^{44}\eta^{\nu 4} - \eta^{\nu 4}\eta^{44} \equiv 0. \quad (6.5)$$

The momenta canonically conjugate to the ϕ_μ are

$$\pi^\mu = (1/4\pi)(\eta^{\mu\sigma}\eta^{\nu 4} - \eta^{\mu\nu}\eta^{4\sigma})\phi_{\nu,\sigma}. \quad (6.6)$$

We see immediately that the primary constraint [there is just one, since there is just one descriptor in the definition of the infinitesimal transformation law (6.1)] is simply

$$\pi^4 \equiv 0. \quad (6.7)$$

The generating density which corresponds to Eq. (5.4) can be written down immediately. It is

$$\mathcal{C} = \pi^\sigma{}_{,\sigma}\xi + \pi^4\dot{\xi}. \quad (6.8)$$

At first glance it might appear that this generator is incomplete, since it produces no change in the π^μ. However, examination of the transformation law for the π^μ produced by combining Eqs. (6.1) and (6.6) shows that this is just the case.

The A's for this theory are then just π^4 and $\pi^\sigma{}_{,\sigma}$. Direct calculation then verifies the assertion that together with the hamiltonian they form a function group. In fact, we have that

$$\begin{aligned} (\pi^4, \pi^\sigma{}_{,\sigma}) &\equiv 0, \\ (\pi^4, \mathcal{H}) &= \pi^\sigma{}_{,\sigma}, \\ (\pi^\sigma{}_{,\sigma}, \mathcal{H}) &= 0. \end{aligned} \quad (6.9)$$

Equation (4.6) is thus verifiable directly.

VII. APPLICATION TO COORDINATE-COVARIANT THEORIES

Although the results of the preceding application are well known, it was inserted in order to familiarize the reader with the methodology employed. The application to arbitrary coordinate transformations is not as trivial, and the results are not as well known. We will assume a transformation law of the form (2.3). Here the ξ^μ are the infinitesimal coordinate changes. A thorough discussion of the resulting Bianchi identities has been given in I and will not be repeated here. We merely set down the main result for lagrangians of the form (3.1). For such a langrangian, Eq. (3.6) becomes

$$A^{A4B4}F_{A\mu}{}^{B4}y_B \equiv 0. \tag{7.1}$$

For this type of invariance Eqs. (4.2) to (4.6) can be taken over intact. The primary constraints (four in number, since there are four descriptors in our transformation law) become

$$g_\mu \equiv F_{A\mu}{}^{B4}y_B\bar{\pi}^A = 0. \tag{7.2}$$

The generating density corresponding to Eq. (5.4) is not as easily obtained as was the case for electromagnetic theory. After some considerable calculations it was found to have the form

$$\begin{aligned} C = g_\mu\dot{\xi}^\mu - \Big\{ & L_\mu - (F_{A\mu}{}^{Br}y_B v^{A\alpha}g_\alpha)_{,r} - \delta_\mu{}^r v^{A\alpha}g_\alpha y_{A,r} \\ & + \tfrac{1}{2}F_{C\mu}{}^{B4}y_B\left(\frac{\partial v^{N\alpha}}{\partial y_C} - \frac{\partial v^{C\alpha}}{\partial y_N}\right)E_{ND}\bar{\pi}^D \\ & - \delta_\mu{}^4 v^{A\alpha}g_\alpha\dot{y}_A\Big\}\xi^\mu, \end{aligned} \tag{7.3}$$

where the new quantities which appear are defined as

$$\begin{aligned} L_\mu &= (g_\mu, \mathcal{H}) \\ &= -\frac{1}{2}\left\{F_{A\mu}{}^{C4}E_{CD} - \tfrac{1}{2}F_{C\mu}{}^{B4}y_B\frac{\partial E_{AD}}{\partial y_C}\right\}\bar{\pi}^A\bar{\pi}^D \\ &\quad + F_{C\mu}{}^{B4}y_B\Gamma^{4rC,AE}y_{E,r}E_{AD}\bar{\pi}^D \\ &\quad + F_{C\mu}{}^{Br}y_B\Lambda^{A4C4}(E_{AD}\bar{\pi}^D)_{,r} \\ &\quad + F_{C\mu}{}^{B4}y_B\Gamma^{rsC,AE}y_{A,r}y_{E,s} - 2F_{C\mu}{}^{B4}\Lambda^{ArCs}y_B y_{A,rs}, \end{aligned} \tag{7.4}$$

$$\Gamma^{\mu\nu A,BC} \equiv \frac{\partial\Lambda^{B\mu C\nu}}{\partial y_A} - \frac{\partial\Lambda^{A\mu C\nu}}{\partial y_B} - \frac{\partial\Lambda^{B\mu A\nu}}{\partial y_C},$$

and where the $v^{C\alpha}$ are defined by the equation

$$E_{AB}\Lambda^{B4C4} + v^{C\mu}F_{A\mu}{}^{B4}y_B = \delta_A{}^C. \tag{7.5}$$

The appearance of the $\dot{y}_A$ in the expression for the generator appears at first sight unfortunate, but is unavoidable because the transformation law for field variables in configuration space (including the transport term) depends explicitly on $\dot{y}_A$ [see Eq. (2.3)]. While in $\sum_t$ there exist relationships between y_A, $\dot{y}_A$, and π^A at each point of space-time, these relationships are not sufficient to express $\dot{y}_A$ uniquely as functions of the canonical variables alone. Consequently, there may exist two different fields of $y_A(t)$ in $\sum_t$ which on one spacelike hypersurface have identical values of y_A and π^A everywhere, but nevertheless different $\dot{y}_A$. Thus the transformation law under the canonical transformation cannot be equivalent in $\sum_t$ to the infinitesimal coordinate transformation for all conceivable fields $y_A(t)$ unless the lack of unique determination of the $\dot{y}_A$ by the canonical variables is reflected in their explicit appearance in the generating function.

These "velocities" are all multiplied by primary constraints, and thus in $\sum_t$, at least, transformation laws can be formulated without knowledge of the "poisson bracket" between a velocity and other canonical variables. However, elsewhere in $\sum$, and also for the determination of commutators, these poisson brackets are needed, and we have, as a general rule,

$$(\dot{y}_A, F) = \partial(y_A, F)/\partial t. \tag{7.6}$$

This rule is valid because $\dot{y}_A$ may be interpreted as the difference between two slightly different y_A's, and the poisson bracket is a linear operation with respect to either one of its two components.

We are now in a position to assert that g_μ and L_μ are the only constraints which will appear in a theory because of coordinate invariance, and furthermore, that without or together with the hamiltonian they form a function group. By examining the commutator between various subgroups of transformation laws (2.3) together with the corresponding poisson brackets between the corresponding generators, one can verify that

$$\begin{aligned} &(g_\mu(x), g_\nu(x')) = (\delta_\nu{}^4\delta_\mu{}^\sigma - \delta_\mu{}^4\delta_\nu{}^\sigma)g_\sigma\delta(x-x'), \\ &(\bar{L}_\mu(x), \bar{L}_\nu(x')) = (\delta_\nu{}^r\delta_\mu{}^\sigma - \delta_\mu{}^r\delta_\nu{}^\sigma)\bar{L}_\sigma(\delta(x-x'))_{,r}, \\ &(\bar{L}_\mu(x), g_\nu(x')) = -\delta_\mu{}^4\bar{L}_\nu\delta(x-x') + (\delta_\nu{}^r\delta_\mu{}^\sigma \\ &\qquad\qquad - \delta_\mu{}^r\delta_\nu{}^\sigma)g_\sigma(\delta(x-x'))_{,r}, \end{aligned} \tag{7.7}$$

where $\bar{L}_\mu$ is the coefficient of ξ^μ in Eq. (7.3). All of the above results can, of course, be checked by direct calculation, and one finds that the results are the same. However, owing to the great amount of labor involved in such a calculation and the fact that the calculations cannot be readily carried over to the case of a nonquadratic lagrangian, they will not be presented here.

VIII. CONCLUSION

With this present paper, the canonical formulation of covariant field theories with quadratic lagrangian has been completed. According to our present results,

a field-theoretical situation is completely determined if on a three-dimensional hypersurface the canonical variables are given in such a manner that all the constraints (which are finite in number at each point) are satisfied and a hamiltonian has been chosen for all of space-time. In that case, the solutions are unique and do not permit even a coordinate transformation. A coordinate transformation which leaves the initial situation unchanged is equivalent to the adoption of a new hamiltonian away from the initial hypersurface.

In attempting to quantize this type of theory, we can simplify our problem by first carrying out a canonical transformation that converts the primary constraints into canonical momentum densities. As for the secondary (and higher, if necessary) constraints, it appears that their conversion is neither easy in practice nor desirable, because in singular regions the secondary constraints may not be satisfied. Once we have found a proper formulation for the singular regions, the "sources" and "sinks" of the vacuum field, the examination of the quantized covariant theory can be undertaken in earnest.

PHYSICAL REVIEW VOLUME 83, NUMBER 5 SEPTEMBER 1, 1951

Photon Counter Measurements of Solar X-Rays and Extreme Ultraviolet Light

H. FRIEDMAN, S. W. LICHTMAN, AND E. T. BYRAM
U. S. Naval Research Laboratory, Washington, D. C.
(Received May 10, 1951)

Data telemetered continuously from photon counters in a V-2 rocket, which rose to 150 km at 10:00 A.M. on September 29, 1949, showed solar 8A x-rays above 87 km, and ultraviolet light around 1200A and 1500A above 70 km and 95 km, respectively. The results indicated that solar soft x-rays are important in *E*-layer ionization, that Lyman α-radiation of hydrogen penetrates well below *E*-layer, and that molecular oxygen is rapidly changed to atomic above 100 km.

A V-2 ROCKET, fired in September 1949, carried a set of photon counter tubes which were sensitive to light in the soft x-ray and extreme ultraviolet regions of the spectrum. Each tube responded to a relatively narrow portion of the spectrum in one of four bands covering 0–10A, 1100–1350A, 1425–1650A, and 1725–2100A. The experiment provided an uninterrupted telemetered recording of solar radiation intensities within these wavelength bands throughout the flight of the rocket. Intense solar x-ray emission was detected at altitudes above 87 kilometers. In the atmospheric window near λ 1200A, the photon counters responded strongly above a level of about 70 kilometers. Most of the solar radiation near the peak of the Schumann-Runge absorption band of molecular oxygen, was absorbed between the levels of approximately 95 and 115 km. Only one tube was flown which was sensitive to the longer wavelengths between the oxygen and ozone bands ($\sim$2000A). Its counting rate rose sharply when the rocket reached an altitude of 7 kilometers, but the tube was too sensitive to provide any useful data above 20 kilometers. These measurements support the ideas: that *E*-layer ionization is directly related to soft x-ray emission from the corona; that Lyman α-radiation penetrates the atmosphere well below *E*-layer; and that the transition from molecular to atomic oxygen takes place at altitudes near 100 km.

FLIGHT DETAILS

The rocket (V-2, No. 49) was fired at 10:00 A.M., M.S.T. on September 29, 1949 at the White Sands Proving Ground, New Mexico. The altitude of the sun was 43 degrees. No unusual solar activity was noted at the time of the flight. The telemetering record was continuous over the entire flight period of 336 seconds, during which time the rocket soared to a height of 150 km. Fuel cutoff was made at 64 seconds after take-off. For the first 60 seconds the rocket was in stable flight, after which time it developed a slow, steady roll of approximately 12 seconds average period. The roll persisted until the warhead was blown off at 336 seconds.

EXPERIMENTAL DETAILS

An assortment of 6 photon counter tubes was contained in two pressurized boxes, each unit comprising in effect a photon counter spectroscope. The boxes were located on opposite sides of the warhead, with exposed window areas parallel to the surface of the warhead. In addition to the counter tubes, each box also contained one control tube, sensitive only to cosmic rays, and one photocell for determining the roll orientation of the rocket with respect to the sun.

Each tube consisted of a chrome-iron cathode cylinder, $\frac{3}{4}$ inch in diameter and 2 inches long, and an anode wire, 0.025 inch in diameter. The cathode also served as the envelope of the tube. Glass caps, which supported the anode wire, were sealed to the steel cylinder at each end. A circular aperture $\frac{3}{16}$ in. in diameter was provided in a flat recess, milled midway along the length of the cathode. This aperture was covered by

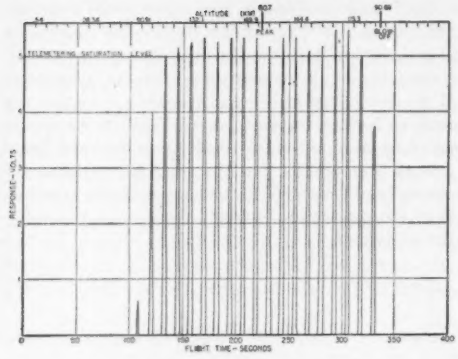

FIG. 1. A plot of data read directly from the telemetered record of the counting rate of an x-ray photon counter. The sharp responses occurred each time the spinning rocket presented the tube to the sun. The telemetered signals were not continuous, but the commutation rate was rapid enough to provide about eight points per exposure. In the illustration, smooth curves are drawn through the experimental points.

an appropriate window material, cemented to the steel body.

The counting rate produced in each tube, when excited by radiation, was determined indirectly by integrating the flow of charge through the tube in an RC circuit of 2 seconds time constant, thereby producing an average dc voltage proportional to the counting rate. The resultant voltage was then impressed on a cathode follower stage, from where it was coupled to the telemetering system. Sufficient voltage was obtained with this simple means of charge integration to satisfy the telemetering requirements, without the necessity of additional amplification. Data originating in all tubes was handled over four telemetering channels by resorting to time sharing mechanical subcommutation.

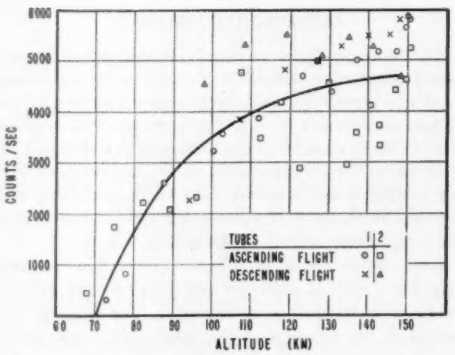

FIG. 2. Intensities measured with two nearly identical photon counters in the 1100A–1350A wavelength band. Four sets of points are plotted representing the telemetered data of the two tubes, corrected for saturation and effect of time constant, in ascending and descending portions of the rocket flight.

Figure 1 is a plot of data read directly from the telemetering record and is representative of the type of record observed for most of the tubes used in the experiment. With every rotation of the rocket, the tube swept through one exposure to the sun. Above 100 km the intensities were strong enough to produce saturated responses with each exposure. The most serious factor affecting the accuracy of the measurements was the error involved in extrapolating these saturated indications. In order to estimate the true maximum intensities, it was assumed that the shape of the response curve was dependent only on the geometrical relationship between the sun and the counter tube window. On this basis, the fraction of the maximum response at any given time earlier or later than the instant of maximum exposure could be determined by examining the shapes of the first few undistorted responses. The corrected maxima were then estimated from measurements made on the slopes of the curves at selected fractions of maximum exposure. In most cases the largest corrections computed in this way brought the true maxima up to twice full scale indication of the telemetering circuit. A second correction was applied to the data to compensate for the effect of time constant in the counter tube circuit. The speed of rotation of the rocket was great enough so that the time of exposure of each tube to the sun was comparable to the time constant of the RC circuit.

In addition to its axial spin, a certain amount of precessional motion is always imparted to a rocket. The yaw angle of the precessional motion of a V-2 rocket has in several high altitude flights been as great as 20 degrees. Since the angular field of view of each photon counter tube was limited to approximately ± 30 degrees about the normal to the window and was not flat over this range, the aspect of the rocket had an influence on the photon counter response. Insufficient aspect data was obtained in this flight to permit complete aspect corrections, but fortunately the flight of V-2 No. 49 appeared to be unusually stable.

Figure 2 is a plot of four sets of data representing the ascending and descending flights of two identical photon counters. To a large degree the scattering of the points may be related to the uncertainties in extrapolating the saturated exposures, and to lack of sufficient rocket aspect information. It would be unjustified to attribute a reliability greater than roughly plus or minus 50 percent to the corrected counting rates. In spite of the scattering of the individual points on the curves, however, certain features of the measurements in three of the four wavelength bands were still quite well defined, such as the level of maximum penetration of the solar radiation and the altitude of maximum rate of absorption.

ULTRAVIOLET PHOTON COUNTERS

The counting action of an ultraviolet photon counter is essentially the same as that of the self-quenching

Geiger counters ordinarily used for detection of x-rays and gamma-rays. The primary electrons which trigger the Townsend avalanches of the discharge are photoelectrically ejected from the surface of the cathode wall.

In contact with gases such as are commonly used in Geiger counters, the photoelectric thresholds of metal surfaces generally fall in the ultraviolet below 3000A. While studying the effects of traces of electronegative gases in Geiger tube fillings, the authors observed a marked increase in the photoelectric work function. An extreme depression of the threshold wavelength occurred when the halogen gases, Cl_2 or Br_2, or halogenated hydrocarbons such as methylene bromide were included in the gas mixture. In the latter case all trace of photosensitivity above 1100A could be eliminated when the partial pressure of the vapor exceeded 1 mm Hg. Since the short wavelength limit of photosensitivity could be controlled by choosing a window from materials such as lithium fluoride, sapphire, quartz, potassium chloride, or Vycor glass, it was possible to make tubes with spectral responses limited to bandwidths of only a few hundred angstroms in the extreme ultraviolet.

Figure 3 shows the spectral response curves of three types of ultraviolet photon counters used in the rocket experiment. The ordinate scales were arbitrarily chosen to permit their combined presentation in one figure. The spectral measurements were carried out with a vacuum monochromator of the type described by Tousey, Johnson, Richardson, and Toran.[1] To derive the indicated efficiencies, comparisons were made of photon counter measurements and thermocouple measurements[2] of the hydrogen arc discharge. At first glance it might appear that the quantum efficiencies, ranging from 10^{-6} to 10^{-3} count per quantum, are extremely low. It should be noted, however, that the wavelength of the peak response for each tube is very close to threshold because of the sharp cut-off characteristics of the window materials on the short wavelength side. If the responses were measured independently of the effect of window absorption, the efficiencies would most likely rise to values of the order of 10^{-4} count per quantum at shorter wavelengths.

The cathodes of all three photon counters were made of chrome-iron. Tube (*A*), with a threshold at 1350A, was filled with 15 mm Hg of Cl_2 and 300 mm Hg of neon, and had a lithium fluoride window which was transparent to about 1100A. An admixture of one-half millimeter of bromine in 300 mm Hg of neon was used in tube *B*, to produce a peaked response at 1500A. The cutoff at 1425A was the limit of transmission of the synthetic sapphire window. A mixture of 10 mm Hg of ethylene and 10 mm Hg of argon yielded the long wavelength characteristic of tube *C*. Its cutoff at 1725A was produced by a crystalline quartz window.

[1] Tousey, Johnson, Richardson, and Toran, J. Opt. Soc. Am. **40**, 264 (1950).
[2] D. M. Packer and C. Lock, J. Opt. Soc. Am. **40**, 264 (1950).

At the time the photon counter tube experiment was proposed for V-2 No. 49, relatively little information had been accumulated about the stability of photon counters for the extreme ultraviolet. It was recognized that the spectral sensitivity altered with aging and with use. Until the very latest stages of preparation for the rocket-experiment, the grating monochromator was not available for detailed studies of the aging characteristics and the rough outlines of the regions of spectral sensitivity were determined by the use of filters.

The schedule of the experiment involved a delay of about one month between final assembly of the tubes in the warhead at NRL and the actual firing at White Sands. As a result it was not possible to check accurately the spectral responses of the tubes at the time of firing. On the basis of tests continued on control tubes at NRL, after shipment of the warhead from NRL to White Sands, it appeared that the tubes for the 1150–1350A band remained virtually unchanged over a period of several months. However, the thresholds of most of the

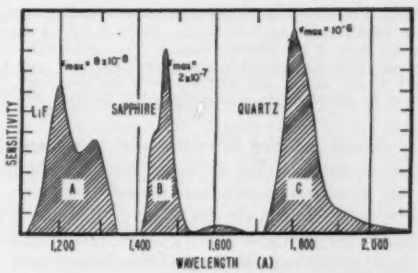

FIG. 3. Spectral response curves of three types of ultraviolet photon counters used in the rocket. The maximum photoelectron yields, ϵ_{max}, for each tube are indicated in units of counts per quantum.

tubes in the longer wavelength bands exhibited a tendency to drift to longer wavelengths. At the time of firing, various rough tests could be made of the reliability of the tubes. For example, the tubes assembled in the warhead were exposed to a hydrogen arc and their responses observed when various filters were inserted and as the air path between the arc and the tubes was varied. It was concluded from such checks that the tubes finally selected to be flown in the rocket had not undergone serious changes in characteristics. At best, however, the efficiencies of the rocket tubes could not have been known to better than an order of magnitude at the time of firing.

X-RAY PHOTON COUNTERS

Two of the photon counters were equipped with beryllium windows 0.005 inch thick, to pass soft x-rays. The transmission of the beryllium window was almost perfect at 2A, but dropped to 10 percent at 6.5A, one percent at 8.5A, and 0.1 percent at 9.5A. Beyond 10A, the window was virtually opaque. The mechanism of

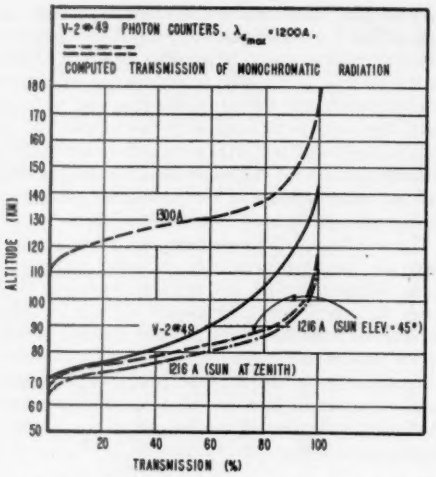

FIG. 4. Penetration of the atmosphere by ultraviolet radiation in the 1100A–1350A spectral region. The solid line is obtained from the data of two photon counters. The dashed line curves were computed from published absorption coefficients (references 4 and 5) at λ1216A and λ1300A for a sun elevation of 45 degrees. The dot-dash curve was computed for the sun at its zenith.

x-ray photon counting differs from that for ultraviolet photon counting in that the x-ray photons transmitted by the window are absorbed almost completely by photoelectric effect in the gas filling of the tube. If it is assumed that each photoelectric absorption of an x-ray quantum produces a discharge of the counter tube, the quantum counting efficiency may be taken as simply the product of the beryllium transmission and the percentage of the photons absorbed in the gaseous volume of the tube. Such an assumption is valid for the majority of counting gas mixtures which use a rare gas in combination with a hydrocarbon quenching vapor. If an electronegative gas impurity is present, however, a certain fraction of the absorbed quanta will fail to produce counts.[3] This effect is especially prominent when a halogen gas is admixed with a rare gas. In the tubes used in the rocket, about one-fifth of the quanta penetrating the beryllium window were effective in triggering counts.

MEASUREMENTS OF EXTREME ULTRAVIOLET RADIATION

All of the photon counters used in the rocket were somewhat too sensitive and produced off-scale signals as the rocket approached the peak of its flight. In the longest wavelength band (~2000A), the degree of saturation was so great as to prevent any reasonable extrapolation of the early portion of each response to the sun. The original set of tubes for the rocket included a second tube with identical spectral response, but having only one-tenth the window area, so as to cover a higher intensity range. Unfortunately this tube failed before the flight. In the shorter wavelength bands, the tubes did not suffer from such extreme saturation. The estimated true maxima were about twice the full scale indication of the telemetering circuit, and were obtained by extrapolating the lower portions of each curve of counting rate relative to angle with respect to sun.

Figure 2 is a plot of all the data obtained from two photon counters, type *A*, sensitive in the 1100–1350 angstrom region. The two tubes were located diametrically opposite each other in the rocket warhead so that their maximum responses to the sun were 180° apart. Although the individual points scattered rather widely, the lowest altitude at which appreciable intensity was detected was defined within ±5 km at about 70 km, and the average curve for the four sets of points approached a maximum asymptotically, near the top of the flight. In Fig. 4 the solid line represents the rocket data. The broken line curves were computed for an atmosphere of uniform composition of molecular oxygen and nitrogen up to the highest altitude, using the absorption coefficient of molecular oxygen at λ1216A reported by Preston[4] and the absorption measurements of Ladenburg and van Voorhis[5] at the

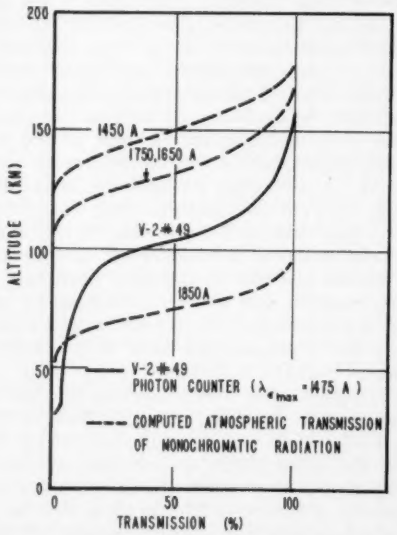

FIG. 5. Penetration of the atmosphere by ultraviolet radiation in the neighborhood of λ1500A. The solid line is obtained from rocket measurements made with tube *B* of Fig. 3. The broken line curves were computed from absorption data of reference 5. Data for λ1750, and λ1650A, on either side of the absorption maximum at λ1450A, almost coincide and are drawn as a single curve.

[3] H. Friedman, Proc. Inst. Radio Engrs. **37**, 791 (1950).

[4] W. M. Preston, Phys. Rev. **57**, 887 (1940).

[5] R. Ladenburg and C. C. van Voorhis, Phys. Rev. **43**, 315 (1933).

longer wavelength. Atmospheric pressure data used were those reported by Havens *et al.*[6]

The maximum depth of penetration indicated by the experimental curve is in agreement with computations for the Lyman alpha-line of hydrogen. Since the photon counter was also sensitive to wavelengths as long as 1350 angstroms the slope of the experimental curve toward the characteristic computed absorption level for λ1300A may be indicative of a response to longer wavelength radiation than the Lyman alpha-line at greater altitudes.

The solid line of Fig. 5 shows the average of the ascending and descending rocket measurements of one photon counter, type *B* (Fig. 3), sensitive to wavelengths in the neighborhood of 1500A, where the absorption coefficient for molecular oxygen is a maximum. The broken line curves were computed for an atmosphere of unaltered composition containing only molecular oxygen and nitrogen up to the highest altitudes. The rapid rate of absorption of radiation, observed in the region of 100 kilometers altitude, is indirect evidence of a rapid transition from molecular to atomic oxygen at that level. Otherwise, the maximum rate of absorption should have occurred at about 145 km, as shown in the computed curve for λ1450A. An unexplained feature of the experimental curve was the small response detected down to levels as low as 50 kilometers. This could perhaps be blamed on the electronics by attributing the early response to some form of electrical crosstalk or commutator noise, but interference tests made just prior to firing showed no signs of such imperfections in the system.

In the longest wavelength band, 1750–2100 angstroms, the photon counter sensitivity was so high that no true intensities could be estimated above 20 kilometers. Radiation in this band was detected at 7 kilometers above sea level and complete saturation developed after only three rotations of the rocket.

Without knowing the detailed features of the spectrum of solar radiation in the ultraviolet, it is impossible from the photon counter measurements to compute the energy flux of radiation incident on the atmosphere. If it is assumed that the source of ultraviolet radiation is a blackbody, then measured intensities in the bands centered at 1200A and 1500A indicated sun temperatures of the order of 6000°K and 4500°K at the respective wavelengths. To a rough approximation, the rocket measurement indicated a flux of from one to ten ergs per cm² per second in the 1150-1350A band. This result agrees in order of magnitude with the flux measured by Tousey, Watanabe, and Purcell, using a thermoluminescent phosphor.

X-RAY MEASUREMENTS

The solid line curve of Fig. 6 represents the averaged x-ray measurements of two photon counters equipped with beryllium windows. Using Havens' pressure data, the transmission of soft x-rays by the upper atmosphere was computed[7] for several wavelengths between 4.6A and 68A. In these computations, illustrated by the broken line curves of Fig. 6, it was assumed that absorption could be attributed entirely to oxygen and nitrogen and that the relative atomic concentration of these elements did not vary with altitude. A significant feature of these curves is the relatively narrow altitude spread within which x-rays of a wide range of wavelengths are absorbed and the approximate coincidence of this altitude region with *E*-layer. The fact that the rocket-borne photon counters detected no x-rays at altitudes below 87 kilometers can be taken as evidence that the high energy limit of the x-ray spectrum occurred at approximately five to seven angstroms. From the observed counting rates at the peak of the flight, the computed flux of x-rays incident on the atmosphere amounted to about 10^{-4} erg per cm² per sec. The production of *E*-layer requires between 10^{-2} and 10^{-1} erg/cm²/sec. Since the beryllium window was essentially opaque above 10A, and since the limit of the x-ray

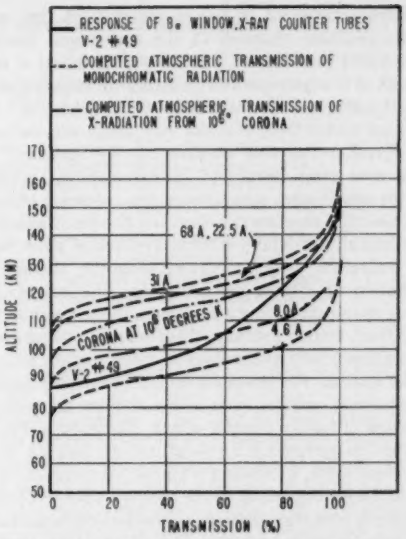

FIG. 6. Penetration of the atmosphere by soft x-rays. The dashed line curves were computed from absorption data listed in Compton and Allison (reference 7) and the pressure data of Havens, *et al.* (reference 6). Because the *K* critical absorption limits of oxygen and nitrogen fall at 23.6A and 32.2A, respectively, the penetration of longer wavelengths is comparable to that of shorter wavelengths, as is shown by the superposition of curves for λ68A and λ22.5A. The dash-dot curve was computed from the spectrum of reference 12. The solid line curve was obtained from the averaged data of two photon counters flown in the rocket.

[6] Best, Durand, Gale, and Havens, Phys. Rev. **70**, 985 (1946).

[7] A. H. Compton and S. K. Allison, *X-Rays in Theory and Experiment* (D. Van Nostrand Company, Inc., New York, 1947), 2nd ed.

spectrum appeared to fall at about 5–7A, the entire x-ray response obtained in the experiment could be attributed to a narrow band centering about a wavelength of 8 angstroms and probably constituting only a small portion of the entire solar x-ray spectrum.

That x-rays from the sun may cause the ionization of *E*-region was first brought out by Hulburt.[8] The idea was later developed in considerable detail by Bates and Hoyle,[9] who derived the spectrum of x-rays necessary to produce the observed *E*-layer. Taking into account all the details of the conversion of x-ray energy to ionization, best agreement with the altitude distribution of *E*-layer ionization was obtained with an x-ray spectrum having a maximum in the neighborhood of 325 ev. Experimentally, there are now several sources of evidence for the emission of x-ray quanta from the solar corona. For example, Edlén[10] identified many of the coronal emission lines with forbidden transitions in spectra of highly ionized atoms, particularly Fe. The ionization potentials involved are as high as several hundred volts, indicating a kinetic temperature of the order of 10^6 degrees K in the corona. Alfven[11] proposed a corona consisting entirely of ions and electrons having thermal energies corresponding to this high temperature. The highly stripped atoms emit soft x-rays in recombining with electrons, the energy of the x-ray quantum being roughly equal to the potential energy of the ion resulting from the recombination. From considerations of the lifetimes of ionized states of Fe atoms in the corona. Alfven concluded that the maximum ionization potential reached was about 900 ev. Hoyle[12] derived the shape of an x-ray spectrum, assuming it due entirely to iron, which consisted of a slowly rising intensity approximately proportional to the quantum energy up to about 500 ev beyond which the intensity fell rapidly as the inverse 5th power of the quantum energy. The absorption characteristic of this latter spectrum of x-rays is included in the illustration of Fig. 6. It differs only slightly from the corresponding absorption curve of blackbody radiation at 10^6 °K, being shifted upward about 3 kilometers with respect to the blackbody curve.

The present experimental measurement of solar x-rays follows earlier detections made by NRL investigators with the aid of photographic film packets[13] and with thermoluminescent powders.[14,15] To check further the hypothesis that x-rays from the corona are responsible for E-layer will require that the x-ray measurements be extended to longer wavelengths, preferably up to 100A. In preparation for V-2 #49, several tubes with very thin aluminum coated nitrocellulose windows were constructed in addition to those with Be windows. Unfortunately, however, those tubes leaked sufficiently during the long interval between filling at NRL and firing at White Sands, to make them unusable in the experiment. To overcome the problem of deterioration, a free-flow counter technique was adopted for an experiment attempted in January, 1951. That experiment was unsuccessful because the rocket engine failed. Another attempt is scheduled for June, 1951, in a V-2 rocket which wlli carry photon counters capable of covering the x-ray region up to at least 50A.

The authors are grateful to Dr. E. O. Hulburt for many discussions of the experiment and to Dr. R. Tousey, Dr. K. Watanabe, and Mr. F. S. Johnson of the Optics Division for their valuable advice and assistance in connection with the ultraviolet spectral sensitivity measurements. The execution of the rocket experiment was possible only with the generous assistance of Dr. Newell and other members of the Rocket Sonde Branch.

[8] E. O. Hulburt, Phys. Rev. **53**, 344 (1938).
[9] D. R. Bates and F. Hoyle, Terr. Mag. Atmos. Elect. **53**, 51 (1948).
[10] B. Edlén, Z. Astrophys. **22**, 30 (1942) and Monthly Notices Roy. Astron. Soc. **105**, 323 (1945).
[11] H. Alfven, Arkiv. Mat. Astron. Fysik. **27A**, 25, (1941).
[12] F. Hoyle, *Some Rrecent Researches in Solar Physics* (Cambridge University Press, Cambridge, Massachusetts, 1949).
[13] T. R. Burnight, Phys. Rev. **76**, 165 (1949).
[14] Purcell, Tousey, and Watanabe, Phys. Rev. **76**, 165 (1949); Watanabe, Purcell, and Tousey, NRL Report No. 3733 (1950).
[15] Tousey, Watanabe, and Purcell, Phys. Rev. **83**, 792 (1951).

PHYSICAL REVIEW VOLUME 83, NUMBER 5 SEPTEMBER 1, 1951

On Relativistic Quantum Mechanics and the Mass Operator

WALTER WESSEL
USAF Institute of Technology, Wright Field, Dayton, Ohio
(Received February 16, 1951)

The theory of the electron developed by Bopp, Hönl, and the author is discussed in relation to the relativistic wave equation of Gelfand and Yaglom, with particular regard to the infinite, hermitian representations of its matrix apparatus. It is shown that the ambiguity left in the work of the Russian authors is completely removed in our formulation. Only the form of the mass operator, which depends, in Bopp's interpretation, on the cut-off function in the Born-Bopp variation principle, remains uncertain. It is shown that in the infinite representations the mass operator must necessarily depend on one of the invariants (K) of the momentum tensor, because otherwise its eigenvalues would have a point of accumulation at zero. In order to avoid this possibility, the diagonal transformation of the invariant in question is accomplished, and a necessary condition for the analytic form of the mass operator is established, which considerably restricts its choice.

I

IN various papers, Bopp and the author have put forward the theory of the electron in an attempt to avoid the difficulties of field quantization by a recourse to some unexhausted possibilities of the older theory. In short, the general idea may be characterized as follows. Surely an electron, if its finer interactions with radiation are considered, is a system of an infinity of degrees of freedom. In quantum electrodynamics, as it is commonly used, these degrees are introduced by the coupling of the moving charge with quantized hohlraum states. This procedure is well known to lead to difficulties by divergence of most of the occurring summations over the frequency spectrum. In the classical theory the energy of a point electron is also infinite, but for a charge extended in space it becomes finite. On the other hand, the equation of motion of an extended electron, if developed in powers of the retardation parameter, includes time derivatives up to an infinite order. This corresponds again to an infinite number of degrees of freedom. In this scheme, however, it is easy to restrict it in a controlled way by breaking off the development at a convenient place. Likewise, one may also get a purely point mechanical or, as Bopp puts it, field-mechanical theory of the electron without infinities in quantum mechanics.

Starting with radiation reaction forces, the author was led to promising analogies with Dirac's theory of the electron.[1] Indeed it is possible to explain the independence of momentum and velocity and some more kinematical details in Dirac's theory by the fact that the equation of motion of a radiating point electron is of the third order. Attempts to write the equations of motion in the form of poisson brackets necessitated the introduction of an acceleration dependent rest mass[2] and of a magnetic moment of the particle as an independent variable.[3] After these accomplishments it was possible to quantize the theory by reinterpretation of the poisson brackets as a closed commutator algebra.[4]

A better foundation of the theory, whose connection with the radiation reaction force had become somewhat indistinct, was given by Bopp,[5] who was able to show that a charge by its mere extension in space gets an acceleration-dependent rest mass and third (and higher) time derivatives in its equation of motion even if the irreversible part of the radiation force is discarded. The motion is then conservative and may be derived from a variation principle first given by Born, which leads automatically to the right poisson brackets. Bopp reached exactly the same quantum-mechanical formalism as the author, although his classical equations of motion look rather different. In fact, they differ from ours only by the disappearance of one of the constants of motion, i.e., by a supplementary condition, that does not affect the system of poisson brackets. The details have been discussed elsewhere.[6] There is no doubt that the supplementary condition, which unduly restricts the quantum-mechanical possibilities, should be removed. Meanwhile, after the quantum-mechanical schemes are coincident and self-consistent, it seems reasonable to go forward with them first.

Another support of the present ideas from a very different standpoint was given by Hönl,[7] who tried to describe the spinning electron by the superposition of a (positive) mass and a (positive-negative) mass dipole. A mass dipole in motion has an angular momentum, just as an electric dipole in motion has a magnetic moment. As Bopp has shown, the Hönl theory just coincides with the first approximation of his own. In this interpretation the appearance of a mass dipole, which makes the point of gravity of the particle noncoincident with its mass, corresponds to the fact that, owing to the emission-reabsorption processes, the energy fluctuates around the

[1] W. Wessel, Z. Physik **92**, 407 (1934).
[2] W. Wessel, Naturwiss. **30**, 606 (1942); Ann. Physik (5) **43**, 565 (1943).
[3] W. Wessel, FIAT Report No. 1131; Z. Naturforsch. **1**, 622 (1946).
[4] W. Wessel, Phys. Rev. **76**, 1512 (1949).
[5] F. Bopp, Z. Physik **125**, 615 (1948); Z. Naturforsch. **1**, 196 (1946); **3a**, 564 (1948).
[6] W. Wessel, Z. Naturforsch. **4a**, 645 (1949).
[7] For the present state and bibliography of this work, accomplished partly in collaboration with A. Papapetrou, see H. Hönl, Z. Naturforsch. **3a**, 573 (1948).

charge.[8] Charge fluctuations may happen even when the total charge is zero; hence, the Bopp-Hönl model admits a spin also for noncharged particles, which were a grave difficulty for the original conception of the author.

Regarding the quantum-mechanical aspect, the three preceding theories coincide in the following statements. In addition to being described by its coordinates and momentum components, the electron is characterized by[9]

(a) a six-vector (momentum tensor) M_{ik}, whose components obey the commutation rules

$$[M_{ik}M^{rs}]=i(\delta_i{}^rM_k{}^s-\delta_k{}^rM_i{}^s-\delta_i{}^sM_k{}^r+\delta_k{}^sM_i{}^r); \quad (1.1)$$

(b) two (!) four-vectors, ι_k and κ_k, $k=1.4$, obeying the relations

$$[\iota_iM^{rs}]=i(\delta_i{}^s\iota^r-\delta_i{}^r\iota^s), \quad (1.2)$$

$$[\kappa_iM^{rs}]=i(\delta_i{}^s\kappa^r-\delta_i{}^r\kappa^s), \quad (1.3)$$

$$-[\iota_i\iota^k]=iM_i{}^k=[\kappa_i\kappa^k]; \quad (1.4)$$

(c) two invariants, I and K, connected with the invariants of the momentum tensor by

$$\tfrac{1}{2}M_{ik}M^{ik}=I^2-K^2-1, \quad (1.5)$$

$$\tfrac{1}{2}M_{ik}{}^*M^{ik}=IK, \quad (1.6)$$

from which I commutes with all quantities, whereas K commutes with the M_{ik} only, being related to the ι_k, κ_k by

$$[\iota_i\kappa^k]=-i\mathrm{K}\delta_i{}^k,\ [\mathrm{K}\iota_k]=i\kappa_k,\ [\kappa^k\mathrm{K}]=-i\iota^k. \quad (1.7)$$

Further relations fulfilled by these quantities may be disregarded for the present purpose.

The momentum-energy relation ("wave equation") reads (sum over repeated indices)

$$\iota_kp^k=-m(\mathrm{I},\mathrm{K})c\cdot(\mathrm{I}^2+\mathrm{K}^2)^{\frac{1}{2}}, \quad (1.8)$$

i.e., the possible energy states are determined by the eigenvalues of cp^4 in this equation, if the momentum components p_1, p_2, p_3 are given. It is a main result of the present theory, that Eq. (1.8) is derived from classical conceptions and not freely postulated as the similar relations in the papers mentioned below. External fields may be introduced in the usual way by their potentials without supplementary conditions. The function $m(\mathrm{I},\mathrm{K})$ is the mass operator, a previously arbitrary function of the character of an invariant, with which this paper will mainly be concerned. The reasons for its arbitrariness are best seen from Bopp's interpretation, where it stems from the arbitrariness of the relativistic "cut-off" function, which determines the "shape" of the electron in the variation principle. The separation of the radical on the right is advised by the fact, that in the classical theory $\iota_k/(\mathrm{I}^2+\mathrm{K}^2)^{\frac{1}{2}}$ is the four velocity.

[8] For a short survey see F. Bopp, Z. angew. Physik **1**, 387 (1949).

[9] For the physical interpretation of the following quantities the reader must be referred to the original papers. Mathematically, they are substitutes for the higher time derivatives in the equation of motion of an electron with a finite extension in space ι_k. The vector is the four velocity but for a factor.

II

Mathematically, the foregoing commutation rules establish a so-called Lie algebra. Owing to its derivation from poisson brackets, it is essentially closed; i.e., the commutator $ab-ba$ of two elements a, b leads to an element c belonging to the system. The number of elements is 16 in our scheme; in the classical interpretation of Bopp and Hönl one of them (I) is identically zero. This algebra is connected with the representation theory of the Lorentz group. The commutation rules (1) of the components of the momentum six-vector M_{ik} are just the "nucleus"[10] which "engenders" such representations. In the frame of our commutation relations (1.1)–(1.4), (1.7) the M_{ik} form a sub-algebra. They are known to admit finite and infinite representations. Accordingly, the matrices of the whole system (1.1)–(1.7) may be finite or infinite.

Finite representations have already been studied by many authors from mathematical points of view.[11] They do not always comply with all of the foregoing requirements; for instance, the representations discussed by Bhabha are not always closed. Closed finite representations of the whole system have been derived by Bopp and Bauer.[12] These authors have been able to show that the Dirac and Duffin-Kemmer equations are contained in the present scheme, so that it is now possible to trace these theories back to purely classical concepts.

Further details about the finite representations lie out of the scope of the present paper. Indeed, as Bopp and Bauer have shown, one obtains (for instance) the Dirac and Kemmer equations in their original forms, but no more. Now, since the starting point of the present theory is the finer interaction of the electron with its own field, one should expect also to have effects like the Lamb-Retherford shift included. Indeed, there exist still the infinite representations mentioned above. They have exactly the same physical basis as the finite ones, but involve a much ampler mathematical apparatus; and it is very suggestive to assume that they provide the necessary generalization, for instance, of Dirac's theory. For the physicist accustomed to ordinary quantum mechanics these representations are particularly attractive because they provide infinite, hermitian matrices, partly with continuous spectra, for all physical quantities, especially for the velocity components. It was primarily this feature, and subsequently the important

[10] van der Waerden, *Die gruppentheoretische Methode in der Quantenmechanik* (Verlag. Julius Springer, Berlin, 1932); H. Weyl, *The Classical Groups* (Princeton University Press, Princeton, New Jersey, 1946).

[11] Kramers, Belinfante, and Lubanski, Physica **8**, 597 (1941); H. Bhabha, Revs. Modern Phys. **17**, 200 (1945); **21**, 451 (1949); Madhavarao, Thiruvenkatachar, and Venkatachaliengar, Proc. Roy. Soc. (London) **A187**, 385 (1946); H. Hönl and H. Boerner, Z. Naturforsch. **5a**, 353 (1950); K. J. Le Couteur, Proc. Roy. Soc. (London) **A202**, 284, 394 (1950).

[12] F. Bopp and F. L. Bauer, Z. Naturforsch. **4a**, 611 (1949).

fact that they permit the setting up of wave equations with purely positive energy,[4] that led the present author to their investigation. Besides, it is a favorite idea of the author that the infinite dimensionality of the Hilbert space is correlate to the infinite number of degrees of freedom of the moving particle, and it seems an advantageous coincidence to get it imposed by so a natural postulate as hermiteity.

The representation theory of the Lorentz group, i.e., the realization of the rules (1.1), by infinite matrices has been analyzed by Gelfand and Neumark, Harish-Chandra, and Bargmann.[13] Just as the representations of the angular momentum (rotation group) are characterized by one parameter, *viz.*, the value of the total angular momentum, so are the momentum components M_{ik} (Lorentz group) characterized by two parameters, for which the quantities I and K of Eqs. (1.5), (1.6) may be chosen. As long as one is only concerned with the Lorentz group, i.e., with (1.1), these parameters are of a scalar (c-number) character, because they commute with all M_{ik}. In our present scheme I is still scalar (although quantized), but K must be represented by a matrix because it does not commute with the ι_k, κ_k-components, which in turn reproduce the M_{ik} in virtue of Eq. (1.4).

We have already shown,[6] starting from Harish-Chandra's paper, how the necessary generalization may be accomplished. In the meantime, papers of Gelfand and Yaglom[14] became known in this country, which come nearer to our aims in so far as they introduce, besides the M_{ik}, a four-vector L^k, which corresponds (*viz.*, for the infinite representations) to our ι^k. The Russian authors postulate, as usual, the relation (1.8), *n.b.*, with constant right side, demanding no more than relativistic invariance of this equation. It is interesting from the physical standpoint to see that this postulate is not sufficient to determine the representations completely. As the authors show, it leads to our formulas (1.2), where the M_{ik} must be known from Eq. (1.1). Moreover, it is easily seen [see also our formula (3.25)[6]], that once ι^4 (resp. L^0) is gained, the other ι^k, $k=1, 2, 3$, may immediately be constructed by

$$\iota_k = i[\iota^4 M_{4k}]. \tag{2.1}$$

Now, without further information, the component ι^4 remains widely undetermined insofar, as a whole set of constants $[c_{rr'}$, Eqs. (3.13), (3.14)[14]] may arbitrarily be chosen. In our representations ι^4 is completely determined, *viz.*, equal to $|I|+1, |I|+2, \cdots$, where I is the minimum spin,[6] and so are all other matrices. Indeed, it is evident from the derivation of our commutation rules that they contain far more physical information than is yielded by the mere principle of invariance. It is exhibited by the existence of another four-vector, κ^k, which in virtue of the relations (1.7) makes the invariant K a matrix, whereas in the work of Gelfand and Yaglom K is still a (complex) number ($=ik_1$) and κ^k does not appear. The question arises, whether these relations (1.7) together with the formulas (1.3) and (1.4), which provide for the closedness of the algebra, make the above choice necessary. In the foregoing paper[6] only its sufficiency has been demonstrated by mere verification. Indeed, it is not very difficult to show, that there exists no other choice. The proof is given in Appendix I.[15]

III

The wave equation (1.8) is now well defined but for the analytic form of $m(I, K)$ on its right side. The origin of this uncertainty has already been mentioned at the end of Sec. I. An analytic dependence exists only on K, because I is discontinuous. For brevity let us write in the following:

$$m(I, K)\cdot(I^2+K^2)^{\frac{1}{2}} = m_I(K). \tag{3.1}$$

As long as K is a scalar, m_I is simply a constant parameter. It is a special feature of our theory, by providing a matrix character of K, to provide a matrix nature of $m_I(K)$, and it is easy to see that m_I must be a matrix in these infinite representations. Indeed, consider a particle in free motion, i.e., with constant momentum vector p_1, p_2, p_3, and chose the system of coordinates so that $p_1=p_2=p_3=0$. The particle will then be "macroscopically" at rest, although its "internal motion" (determined by the ι^k, K, etc., mechanism) persists, and p^4/c will be its rest mass m, so that Eq. (1.8) becomes (note $\iota^4=-\iota_4$):

$$m\iota^4 = m_I(K). \tag{3.2}$$

Now the eigenvalues of ι^4 are of the form $|I|+n$, $n=$integral number; hence, with a constant m_I the eigenvalues of m would be inversely proportional to $|I|+n$, $n=0, 1, 2, \cdots$, i.e., they would have a point of accumulation at $m=0$, an evidently unacceptable consequence. The same thing happens in all examples selected by Gelfand and Yaglom. The seriousness of this argument seems not yet to be recognized, and indeed it could not be as long as the unambiguous character of the infinite representations was not shown. It should be remembered, however, that a similar calamity exists in all finite representations, where the eigenvalues of $(\iota^4)^{-1}$, although, of course, without points

[13] J. M. Gelfand and M. A. Neumark, J. Phys. (U.S.S.R.) **10**, 93 (1946); Bull. Acad. Sci. URSS., Sér. Mat. **11**, 411 (1947); V. Bargmann, Ann. Math. **48**, 568 (1947); Harish-Chandra, Proc. Roy. Soc. (London) **A189**, 372 (1947).

[14] J. M. Gelfand and A. M. Yaglom, Doklady Akad. Nauk SSSR **59**, 655 (1948); Zhur. Eksp. i Teoret. Fiz. **18**, 703 (1948).

[15] For the sake of a complete survey it might seem desirable to derive this result by a direct reduction of the scheme of Gelfand and Yaglom, but this does not seem easily possible, because, in spite of great formal similarities, our representations are not strictly a special case of theirs. We have already shown that the spectrum of our K, that is the ik_1 of the Russian authors, is continuous. (It will be an essential subject of the second half of this paper to accomplish the diagonal transformation of this matrix.) As a consequence, the number of irreducible representations of the Lorentz group involved in the sense of Gelfand and Neumark (labeled by k_0[=our I] and k_1) is not countably infinite, in contradiction to a basic assumption made by these authors.

of accumulation, have far too simple intervals to be actually comparable to the very irregular mass distributions realized in nature.

For this reason a constant m_I should be excluded. On the other hand, it seems possible, after a whole function of K is available, to represent almost every desired mass spectrum by its appropriate choice; but this, too, is not as simple as it seems. Let us formulate the problem more precisely. Our representation is essentially a ι^4-representation, i.e., ι^4 is diagonal, and K is given in the form $\langle \iota^4 | K | \iota^{4\prime} \rangle$. Being all eigenvalues of ι^4 essentially positive, the matrix $(\iota^4)^{-1}$ can immediately be written down; and so, from Eq. (3.2),

$$m = (\iota^4)^{-1} m_I(K), \tag{3.3}$$

provided that the matrix $m_I(K)$ is well defined in ι^4-representation. The admissible values of m are the eigenvalues of the matrix on the right side of Eq. (3.3). For a real computation we have to go over from the ι^4- to a K-representation, because, apart from reasons of practicability, only then is the radical in Eq. (3.1) well defined. The operator $(\iota^4)^{-1}$ becomes a symmetrical integral kernel,

$$(\iota^4)^{-1} = \langle K | (\iota^4)^{-1} | K' \rangle, \tag{3.4}$$

and Eq. (3.3) goes over, after division by m, into an integral equation of the form

$$\psi_m(K) = (1/m) \int \langle K | (\iota^4)^{-1} | K' \rangle m_I(K') \psi_m(K') dK', \tag{3.5}$$

where $\psi_m(K)$ is the eigenfunction belonging to the eigenvalue m of the mass. By a transformation

$$\psi_m(K) = [m_I(K)]^{-\frac{1}{2}} \chi_m(K), \tag{3.6}$$

Eq. (3.5) is easily brought into symmetrical standard form. The difficulty is now that m appears as the reciprocal eigenvalue of this equation. It is well known that the eigenvalues of a symmetrical integral equation increase towards infinity as long as the kernel is regular;[16] hence, the eigenvalues of m will continue converging to zero unless $m_I(K)$ is chosen so as to make the kernel singular. We will see in the next section, that $\langle K | (\iota^4)^{-1} | K' \rangle$ is strongly regular, so that this condition really restricts the choice of $m_I(K)$. At first glance this argument may appear rather artificial, but merely from a physical point of view the mass values occurring in nature look far more like the eigenvalues of a singular than of a regular integral equation; and since the difficulty is of a very general character, it seems worth while to study its consequences thoroughly. For this reason, we compute in the following two sections the $\langle \iota^4 | K \rangle$ transformation function and, with a slight simplification, the operator (3.4) explicitly.

IV

Our first problem will be to bring K into diagonal form. In the ι^4-representation it is given, according to[6] Eq. (3.22), by

$$\langle \iota^4 | K | \iota^{4\prime} \rangle = \tfrac{1}{2} \{ [(\iota^4+\sigma)(\iota^4-\sigma-1)]^{\frac{1}{2}} \delta_{\iota, \iota'+1} + [(\iota^4+\sigma+1)(\iota^4-\sigma)]^{\frac{1}{2}} \delta_{\iota, \iota'-1} \}. \tag{4.1}$$

We use here the symbol σ instead of our former κ, to avoid confusion with the components of κ^k. In the following formulas the index 4 of ι^4 will be dropped, for typographical reasons, when ι^4 is used as an index. There will be a unitary matrix $U_{\iota K}$ depending on σ and I, so that

$$\sum_{\iota' \iota''} U_{K' \iota'}^{\dagger} \langle \iota' | K | \iota'' \rangle U_{\iota'' K''} = \langle K' | K | K'' \rangle. \tag{4.2}$$

By a left side multiplication with $U_{\iota K'}$ we obtain from Eq. (4.2), using Eq. (4.1),

$$\tfrac{1}{2} \{ U_{\iota+1, K} [(\iota^4+\sigma+1)(\iota^4-\sigma)]^{\frac{1}{2}} + U_{\iota-1, K} [(\iota^4+\sigma)(\iota^4-\sigma-1)]^{\frac{1}{2}} \} = U_{\iota, K} \cdot K. \tag{4.3}$$

For simplification put

$$U_{\iota K} = [\Pi(\iota^4-\sigma-1)/\Pi(\iota^4+\sigma)]^{\frac{1}{2}} V_{\iota K}. \tag{4.4}$$

Insertion into Eq. (4.3) gives

$$(\iota^4-\sigma) V_{\iota+1, K} + (\iota^4+\sigma) V_{\iota-1, K} = 2K \cdot V_{\iota, K}. \tag{4.5}$$

From this recurrence formula the $V_{\iota K}$ may easily be determined but for a common factor depending on σ alone. The lowest value of ι^4 is $\sigma+1$.[6] To avoid too much formal complication let us henceforth consider only the case $I=\frac{1}{2}$. The possible values of σ are then[6] $\sigma=\frac{1}{2}, \frac{3}{2}, 5/2, \cdots \iota^4-1$. Instead of considering these values of σ for a given ι^4 we may as well consider the values

$$\iota^4 = \sigma+1+\nu, \quad \nu = 0, 1, 2 \cdots \tag{4.6}$$

for a given σ. Putting for brevity

$$2K = z \tag{4.7}$$

and writing

$$V_{\iota K} = W_{\iota\sigma}(z) N_\sigma^{\frac{1}{2}}(z), \tag{4.8}$$

we obtain from Eq. (4.5), for instance, with $\sigma=\frac{1}{2}$

$$\begin{aligned} &W_{\frac{1}{2}\frac{1}{2}}(z) = 1, \quad W_{7/2,\frac{1}{2}}(z) = \tfrac{1}{2}(z^2-3), \\ &W_{\frac{3}{2}\frac{1}{2}}(z) = z, \quad W_{9/2,\frac{1}{2}}(z) = \tfrac{1}{6}(z^3-11z), \\ &W_{11/2,\frac{1}{2}}(z) = (1/24)(z^4-26z^2+45), \\ &W_{13/2,\frac{1}{2}}(z) = (1/120)(z^5-50z^3+309z) \end{aligned} \tag{4.9}$$

etc.

By the usual methods these polynomials may be shown to be generated, for arbitrary σ, by the function

$$w_\sigma(z, t) = e^{z \arctan t} (1+t^2)^{-\sigma-1} \tag{4.10}$$

as the coefficients of the powers of t in its development at $t=0$:

$$w_\sigma(z, t) = \sum_{\iota=\sigma+1}^{\infty} W_{\iota\sigma}(z) t^{\iota-\sigma-1}. \tag{4.11}$$

[16] We disregard the possibility of a degeneracy of the kernel, which would also settle the problem, but which seems mathematically very unlikely.

To find the normalizing function $N_\sigma(z)$, we start with

$$\int_{-\infty}^{+\infty} d\mathrm{K} U_{\iota\mathrm{K}} U_{\mathrm{K}\iota'}{}^{\dagger} = \delta_{\iota\iota'}. \tag{4.12}$$

With regard to Eqs. (4.4) and (4.7), (4.8) this means

$$\frac{1}{2}\int_{-\infty}^{+\infty} dz N_\sigma(z) W_{\iota\sigma}(z) W_{\iota'\sigma}(z) = \frac{\Pi(\iota^4+\sigma)}{\Pi(\iota^4-\sigma-1)}\delta_{\iota\iota'}. \tag{4.13}$$

Multiplying $w_\sigma(z, t)$ with a given $N_\sigma(z)\cdot W_{\iota\sigma}(z)$ and integrating, we get from Eqs. (4.11) and (4.10) with regard to Eq. (4.13)

$$t^{\iota-\sigma-1} = \frac{\Pi(\iota^4-\sigma-1)}{\Pi(\iota^4+\sigma)} \cdot \frac{1}{2}\int_{-\infty}^{+\infty} N_\sigma(z) W_{\iota\sigma}(z) dz (1+t^2)^{-\sigma-1} e^{\iota\sigma \arctan t}. \tag{4.14}$$

This formula must be an identity in ι^4, and we may use the smallest value of ι^4, i.e., $\iota^4 = \sigma+1$, for the determination of N_σ. The polynomial $W_{\iota\sigma}$ becomes then $W_{\sigma+1,\sigma} = 1$, and with the substitution

$$\arctan t = \vartheta; \tag{4.15}$$

formula (4.14) may be written ($|\vartheta| < \pi/2$)

$$\int_{-\infty}^{+\infty} N_\sigma(z) e^{\vartheta z} dz = 2(2\sigma+1)!(\cos\vartheta)^{-2\sigma-2}. \tag{4.16}$$

Inversion gives immediately

$$N_\sigma(z) = 2(2\sigma+1)!(1/2\pi)\int_{-\infty}^{+\infty} e^{-i\vartheta z}(\cosh\vartheta)^{-2\sigma-2} d\vartheta$$

$$= i^{2\sigma+1} \lim_{\epsilon=0} \frac{d^{2\sigma+1}}{d\epsilon^{2\sigma+1}} \left(\frac{\epsilon}{\sinh\epsilon}\right)^{2\sigma+2} \cdot e^{-\iota\epsilon z} \begin{cases} \sinh^{-1}\tfrac{1}{2}\pi z & \sigma \text{ integral}, \quad (4.17) \\ \cosh^{-1}\tfrac{1}{2}\pi z & \sigma \text{ half odd integral}. \quad (4.18) \end{cases}$$

Of course, N_σ is always real. Especially, we have

$$N_0(z) = z/\sinh\tfrac{1}{2}\pi z, \quad N_{\frac{1}{2}}(z) = (1+z^2)/\cosh\tfrac{1}{2}\pi z, \quad N_1(z) = z(1+\tfrac{1}{4}z^2)/3\sinh\tfrac{1}{2}\pi z. \tag{4.19}$$

It is not very difficult to verify Eq. (4.14) for arbitrary ι^4 by insertion of the integral form (4.17) of $N_\sigma(z)$. A test for Eq. (4.19) is that $N_\sigma(z)$ must be finite for $|z| < 2\sigma+2$. With formulas (4.4), (4.8), (4.9) [resp. (4.10), (4.11)], and (4.18) the desired unitary transformation is completely established. Owing to the real character of the eigenfunctions, there is simply $U_{\mathrm{K}\iota}{}^{\dagger} = U_{\iota\mathrm{K}}$.

V

We now go over to the construction of $(\iota^4)^{-1}$, formula (3.4), in K-representation. For simplicity let us make two unimportant restrictions. First let us be content with the simplest case

$$\sigma = \tfrac{1}{2}.$$

It will be seen that the kernel is regular in this case, and there is no reason to believe that it will behave differently for higher σ-values. Furthermore, to study the asymptotic behavior of the eigenvalues of m, it will make no essential difference if we substitute $(\iota^4)^{-1}$ by $(\iota^4-\tfrac{1}{2})^{-1}$, which may be evaluated in closed form. Owing to the diagonality of ι^4, the transformation corresponding to Eq. (4.2) reduces to a single sum:

$$\langle \mathrm{K}|(\iota^4-\tfrac{1}{2})^{-1}|\mathrm{K}'\rangle = \textstyle\sum_\iota U_{\mathrm{K}\iota}{}^{\dagger}(\iota^4-\tfrac{1}{2})^{-1}U_{\iota\mathrm{K}'}. \tag{5.1}$$

The polynomials $W_{\iota\sigma}(z)$ may be represented, after Eqs. (4.10) and (4.11), by derivations:

$$W_{\sigma+1+\nu,\sigma}(z) = \frac{1}{\nu!}\frac{\partial^\nu}{\partial t^\nu} w_\sigma(z, t)\Big|_{t=0}. \tag{5.2}$$

Thus the series (5.1) has the form (with $\iota^4 = \sigma+1+\nu$, $2\mathrm{K} = z$, as before, and $\sigma = \tfrac{1}{2}$):

$$\langle z/2|(\iota^4-1/2)^{-1}|z'/2\rangle = (N_{\frac{1}{2}}(z)N_{\frac{1}{2}}(z'))^{\frac{1}{2}} \sum_{\nu=0}^{\infty} \frac{\Pi(\nu)(\nu+1)^{-1}}{\Pi(\nu+2)} \times (1/\nu!)^2 \frac{\partial^\nu w_{\frac{1}{2}}(z, t)}{\partial t^\nu}\frac{\partial^\nu w_{\frac{1}{2}}(z', t')}{\partial t'^\nu}\Big|_{t=t'=0}. \tag{5.3}$$

The summation process is described in Appendix II. As a result, we find (the indices $\frac{1}{2}\frac{1}{2}$ of S refer to $\mathrm{I} = \frac{1}{2}$, $\sigma = \frac{1}{2}$):

$$\langle \mathrm{K}|(\iota^4-\tfrac{1}{2})^{-1}|\mathrm{K}'\rangle = S_{\frac{1}{2}\frac{1}{2}}(\mathrm{K}, \mathrm{K}')/(\cosh\pi\mathrm{K}\cdot\cosh\pi\mathrm{K}')^{\frac{1}{2}} \tag{5.4}$$

$$S_{\frac{1}{2}\frac{1}{2}}(z/2, z'/2) = \tfrac{1}{2}\left\{\frac{z-z'}{\sinh\frac{1}{4}\pi(z-z')}\cosh\tfrac{1}{4}\pi(z+z') + \frac{z+z'}{\cosh\frac{1}{4}\pi(z-z')}\sinh\tfrac{1}{4}\pi(z+z') - 2zz'\right\} \times (1+z^2)^{-1}(1+z'^2)^{-1}. \tag{5.5}$$

Of course, S is symmetrical. Introducing this into Eq. (3.5) and using the transformation (3.6), one finds approximately, allowing for the substitution of ι^4 by $\iota^4-\frac{1}{2}$,

$$\chi_m(\mathrm{K}) \simeq \frac{1}{m}\int_{-\infty}^{+\infty} S_{\frac{1}{2}\frac{1}{2}}(\mathrm{K}, \mathrm{K}') \times \left(\frac{m_{\frac{1}{2}}(\mathrm{K})m_{\frac{1}{2}}(\mathrm{K}')}{\cosh\pi\mathrm{K}\cdot\cosh\pi\mathrm{K}'}\right)^{\frac{1}{2}} \chi_m(\mathrm{K}')d\mathrm{K}'. \tag{5.6}$$

It is easily verified that $S_{\frac{1}{2}\frac{1}{2}}(\mathrm{K}, \mathrm{K}')$ is finite for all real values of K and K'; hence, the regularity (quadratic integrability) of the kernel in Eq. (5.6) is entirely determined by the relation $m_{\frac{1}{2}}(\mathrm{K}):\cosh\pi\mathrm{K}$, and one sees immediately that the integral equation will be regular, i.e., that zero-accumulation of the m-values will occur, unless $m_{\frac{1}{2}}(\mathrm{K})$ has either singularities of at least first

order for finite K or else outweighs $\cosh\pi K$ at infinity. In the second case $m_1(K)$ would have to behave at infinity like $K^\delta \cosh\gamma K$ with $\gamma=\pi$, $\delta\geq -1$ or $\gamma>\pi$, δ arbitrary. For $m(I, K)$, formula (3.1), the same conditions hold with $\delta-1$.

With that we have at least a necessary condition, which allows exclusion of a great variety of functions. We shall not enter here into more details about the presumable form of $m(I, K)$, in order not to spoil the conclusiveness of the present arguments by considerations of a necessarily more hypothetical character; it may briefly be mentioned[17] that considerations along the lines of those given in reference 3 favor the choice of an operator $m(I, K)=m_0\cosh[(3\hbar cK/2e^2)+\text{const}]$. On the other hand, a few words should be added about a formal difficulty, which might cause some trouble: evidently, the operator $m_1(K)$ does not exist in ι^4-representation. This means only that the ι^4-representation is inappropriate and that one has to use others. In the present case, one will either continue working with the K-representation, i.e., with the singular integral equation, or else invert formula (3.2) and start with $[mI(K)]^{-1}$, whose matrix elements will be excellently convergent in ι^4-representation.[18]

APPENDIX I

The formulas quoted in the following are those of the author (A)[6] and those of Gelfand and Yaglom (GY),[14] second paper. The relations to be proved are the formulas A (3.23), (3.24) for the a_σ which substitute the B_k in GY (2.2″), (2.3″). The last formula is coincident with A (3.13), if $K=ik_1$ is taken as a scalar. The formulas A (3.11) and GY (2.3′) coincide immediately. Note that our κ, I are the k, k_0 of GY. In the following we write σ instead of κ, with regard to the use in the rest of the present paper.

Starting with A (3.9), which corresponds to GY (2.2″), we obtain in virtue of the relations

$$\iota_k=i[\iota^4 M_{4k}],\quad [\iota^4\iota_k]=iM_{4k}, \tag{I.1}$$

Eqs. (1.2), (1.4) above, and with A (3.11) and (1.7) above:

$$[\iota^4[\iota^4 a_\sigma]]=a_\sigma,\quad [\iota^4[\iota^4 a_\sigma^\dagger]]=a_\sigma^\dagger. \tag{I.2}$$

Owing to the diagonality of ι^4, this gives immediately

$$\{(\iota-\iota')^2-1\}\langle\iota|a_\sigma|\iota'\rangle=0, \tag{I.3}$$

and the same relation for $a_\sigma^\dagger$ (we omit in the following the index 4 of ι^4 throughout); hence, $\iota=\iota'\pm 1$, i.e., a_σ and $a_\sigma^\dagger$ (hermitian conjugate matrix; note that the a_σ need not be hermitian) must have the forms (an asterisk indicates the complex conjugate quantity),

$$\begin{aligned}\langle\iota|a_\sigma|\iota'\rangle&=\zeta(\sigma,\iota)\delta_{\iota,\iota'+1}+\eta(\sigma,\iota)\delta_{\iota,\iota'-1},\\ \langle\iota|a_\sigma^\dagger|\iota'\rangle&=\eta^*(\sigma,\iota')\delta_{\iota,\iota'+1}+\zeta^*(\sigma,\iota')\delta_{\iota,\iota'-1},\end{aligned} \tag{I.4}$$

where the ζ, η are to be determined. We have first to fulfil the first two relations A (3.10), i.e., with regard to A (3.11),

$$\begin{aligned}a_\sigma K_{\sigma-1}&=K_\sigma a_\sigma,\\ K_{\sigma-1}a_\sigma^\dagger&=a_\sigma^\dagger K_\sigma.\end{aligned} \tag{I.5}$$

K is given, in ι^4-representation, by A (3.16) in the form

$$\langle\iota|K|\iota'\rangle=A(\sigma,\iota)\delta_{\iota,\iota'+1}+A^*(\sigma,\iota')\delta_{\iota,\iota'-1}, \tag{I.6}$$

where the A, A^* are determined by A (3.20). They depend on σ by the previously unknown function

$$\rho=\rho(\sigma). \tag{I.7}$$

Substituting (I.4) and (I.6) into (I.5) one obtains, for $(\iota, \iota'+2)$, $(\iota, \iota'-2)$, and (ι, ι') respectively, the three relations

$$\begin{aligned}&\zeta(\sigma,\iota)A(\sigma-1,\iota-1)=\zeta(\sigma,\iota-1)A(\sigma,\iota),\\ &\eta(\sigma,\iota)A^*(\sigma-1,\iota+2)=\eta(\sigma,\iota+1)A^*(\sigma,\iota+1),\\ &\zeta(\sigma,\iota)A^*(\sigma-1,\iota)+\eta(\sigma,\iota)A(\sigma-1,\iota+1)\\ &\qquad=\eta(\sigma,\iota-1)A(\sigma,\iota)+\zeta(\sigma,\iota+1)A^*(\sigma,\iota+1)\end{aligned} \tag{I.8}$$

and a similar triple for the conjugate quantities. The η- and ζ-terms on the right side of the third relation (I.8) are reducible by the two foregoing ones to the corresponding terms appearing on the left, so that the $\eta(\sigma, \iota)$ may be expressed by $\zeta(\sigma, \iota)$:

$$\eta(\sigma,\iota)=g(\sigma,\iota)\zeta(\sigma,\iota), \tag{I.9}$$

where

$$g(\sigma,\iota)=\frac{A^*(\sigma-1,\iota+1)\{|A(\sigma-1,\iota)|^2-|A(\sigma,\iota+1)|^2\}}{A(\sigma-1,\iota)\{|A(\sigma,\iota)|^2-|A(\sigma-1,\iota+1)|^2\}}. \tag{I.10}$$

Finally, the $\zeta(\sigma, \iota)$ are determined, in virtue of the relations A (3.13), by the $a_\sigma a_\sigma^\dagger$ and $a_\sigma^\dagger a_\sigma$. For $(\iota, \iota'\pm 2)$ and (ι, ι') one obtains four relations for the $\zeta(\sigma, \iota)$, which must be fulfilled simultaneously and identically in ι by an appropriate choice of the only available function $\rho(\sigma)$. Hence, the problem is considerably overdetermined; and being sure that a solution exists, one has only to show that its determination by any two of the four relations is complete. In order to avoid reproduction of somewhat complicated formulas, this elementary process will better be left to the reader. As a result one obtains formula A (3.21), i.e.,

$$\rho^2=-\sigma(\sigma+1) \tag{I.11}$$

as the only possible solution, and with that the relations A (3.23), (3.24) to be proved. Hence, our representations[6] are completely determined by the full system of commutation relations (1.1)–(1.4), (1.7), if hermitian character is demanded, with the exception, of course, of a unitary transformation, which may change them, for instance, into the form[4] with which we started originally.

The present proof settles also a question raised occasionally by the author regarding the possible existence of positive values of $I^2+\rho^2$, in the negative sense. Furthermore, it may be mentioned that relation (I.11), which may also be written, because of A (3.18) and (3.6), (3.7),

$$(\kappa^4)^2+K^2-(\iota^4)^2+M^2=0 \tag{I.12}$$

represents one of ten algebraic identities of the Dirac algebra, which seem not yet to be noticed.

APPENDIX II

Consider first series (5.3) without the first factor behind the Σ-sign. Its summation may be accomplished in the following way:

$$\begin{aligned}&\sum_{\nu=0}^{\infty}\left(\frac{1}{\nu!}\right)^2\frac{\partial^{2\nu}}{\partial t^\nu\partial t'^\nu}w_\sigma(z,t)w_\sigma(z',t')\\ &=\frac{1}{2\pi}\int_0^{2\pi}d\varphi\sum_{\mu=0}^{\infty}\sum_{\nu=0}^{\infty}\frac{e^{i\mu\varphi}}{\mu!}\frac{e^{-i\nu\varphi}}{\nu!}\frac{\partial^\mu}{\partial t^\mu}\frac{\partial^\nu}{\partial t'^\nu}w_\sigma(z,t)w_\sigma(z',t')\\ &=\frac{1}{2\pi}\int_0^{2\pi}d\varphi w_\sigma(z,t+e^{i\varphi})w_\sigma(t'+e^{-i\varphi})\end{aligned} \tag{II.1}$$

to be taken with $t=t'=0$. In formula (5.3) this process is rendered more difficult by the factor $\Pi(\nu)/(\nu+1)\Pi(\nu+2)=1/(\nu+1)^2(\nu+2)$. With $(\iota^4)^{-1}$ instead of $(\iota^4-\frac{1}{2})^{-1}$ we would have the still more inconvenient factor $1/(\nu+1)(\nu+\frac{3}{2})(\nu+2)$. The matter would be much simpler, if in (5.3) the quotient of the two Π-functions were inverted, so that we had merely to do with a factor $\Pi(\nu+2)/(\nu+1)\pi(\nu)=\nu+2$ in the numerator, which might easily be generated by differentiation.

Indeed, the determining equation (4.3) is invariant under the substitution $\sigma\to-\sigma-1$, so that instead of Eq. (4.4) one may put as well

$$U_{\iota K}=[\Pi(\iota^4+\sigma)/\Pi(\iota^4-\sigma-1)]^{\frac{1}{2}}\bar{\psi}_{K\iota}. \tag{II.2}$$

[17] See a forthcoming paper, Z. Naturforsch. **6a** (1951).

[18] There exists also an interesting representation of ι^4 as a difference operator, which makes K diagonal; see another forthcoming paper, Z. Naturforsch. **6a** (1951).

Insertion into Eq. (4.3) now gives

$$(\iota^4+\sigma+1)\bar{V}_{\iota+1,\mathrm{K}}+(\iota^4-\sigma-1)\bar{V}_{\iota-1,\mathrm{K}}=2\mathrm{K}\cdot\bar{V}_{\iota\mathrm{K}}. \quad \text{(II.3)}$$

Of course, the polynomials generated by this formula are identical with those arising from Eq. (4.5) but for a common multiple of $\Pi(\iota^4-\sigma-1)/\Pi(\iota^4+\sigma)$. The advantage is that they can again be expressed in the way of formula (5.2) without further factorials:

$$\bar{V}_{\iota\mathrm{K}}=\bar{W}_{\iota\sigma}(z)N_\sigma{}^{\frac{1}{2}}(z), \quad \text{(II.4)}$$

$$\bar{W}_{\sigma+1+\nu,\sigma}(z)=(1/\nu!)\partial^\nu\bar{w}_\sigma(z,t)/\partial t^\nu|_{t=0} \quad \text{(II.5)}$$

$$\bar{w}_\sigma(z,t)=(2\sigma+1)(1+t^2)^\sigma\cdot t^{-2\sigma-1}e^{z\cdot 2\arctan t}$$

$$\times\int_0^t t^{2\sigma}(1+t^2)^{-\sigma-1}e^{-z\cdot 2\arctan t}dt. \quad \text{(II.6)}$$

For proof write the polynomials (II.5) in the form

$$\bar{W}_{\sigma+1+\nu,\sigma}(z)=(1/2\pi i)\oint\bar{w}_\sigma(z,t)dt\cdot t^{-\nu-1}, \quad \text{(II.7)}$$

where the integral is taken in the complex t plane along a path inside the unit circle surrounding the point $t=0$. Separating, in the case of $\bar{W}_{\iota+1,\sigma}$, a factor $t^{-(2\sigma+\nu+3)}$ instead of $t^{-\nu-1}$ and integrating by parts, it is not very difficult to verify formula (II.6) by substitution into (II.3).

The factors are chosen so that the generating functions $w_\sigma(z,t)$ and $\bar{w}_\sigma(z,t)$ render $W_{\sigma+1,\sigma}=\bar{W}_{\sigma+1,\sigma}=1$; hence, the normalizing functions N_σ and $\bar{N}_\sigma$ are the same but for a factor that accounts for the inverted factorials in Eqs. (4.4) and (II.2) for $\iota^4=\sigma+1$:

$$\bar{N}_\sigma{}^{\frac{1}{2}}(z)=[1/(2\sigma+1)!]N_\sigma{}^{\frac{1}{2}}(z). \quad \text{(II.8)}$$

In the case $\sigma=\frac{1}{2}$ formula (II.6) yields

$$\bar{w}_{\frac{1}{2}}(z,t)=2(1+z^2)^{-1}t^{-2}[(1+t^2)^{\frac{1}{2}}e^{z\cdot 2\arctan t}-(1+zt)]. \quad \text{(II.9)}$$

With the help of $\bar{w}_\sigma(z,t)$ one may now set up $(\iota^4-\frac{1}{2})^{-1}$ in the way indicated above. For the case $\sigma=\frac{1}{2}$ it reads

$$\langle z/2|(\iota^4-\tfrac{1}{2})^{-1}|z'/2\rangle=(N_{\frac{1}{2}}(z)N_{\frac{1}{2}}(z'))^{\frac{1}{2}}\sum_{\nu=0}^{\infty}(\nu+2)$$

$$\times(1/\nu!)^2\frac{\partial^{2\nu}}{\partial t^\nu\partial t'^\nu}\bar{w}_{\frac{1}{2}}(z,t)\bar{w}_{\frac{1}{2}}(z',t')\Big|_{t=t'=0}. \quad \text{(II.10)}$$

To calculate it we write first the series (II.1) with $\bar{w}$ instead of w and with a factor $\eta^{\nu+2}$ in its νth term:

$$\sum_{\nu=0}^{\infty}\frac{\eta^{\nu+2}}{(\nu!)^2}\frac{\partial^{2\nu}}{\partial t^\nu\partial t'^\nu}\bar{w}_{\frac{1}{2}}(z,t)\bar{w}_{\frac{1}{2}}(z',t')\Big|_{t=t'=0}$$

$$=\frac{\eta^2}{2\pi}\int_0^{2\pi}\bar{w}_{\frac{1}{2}}(z,\eta^{\frac{1}{2}}e^{i\varphi})\bar{w}_{\frac{1}{2}}(z',\eta^{\frac{1}{2}}e^{-i\varphi}). \quad \text{(II.11)}$$

From this the series in (II.10) is easily obtained by $\partial/\partial\eta$, for $\eta=1$. Of course, $\bar{w}_\sigma(z,t)$ obeys a simple differential equation of first order. A somewhat lengthy integration process, whose details will not be of interest, leads then to the formulas (5.4), (5.5) of the text. The author has checked formula (5.5) by insertion of the first three polynomials (4.9) into the integral equation of the U-functions:

$$U_{\iota\mathrm{K}}=(\iota^4-\tfrac{1}{2})\int_{-\infty}^{+\infty}\langle\mathrm{K}|(\iota^4-\tfrac{1}{2})^{-1}|\mathrm{K}'\rangle U_{\iota\mathrm{K}'}d\mathrm{K}'. \quad \text{(II.12)}$$

The evaluation of the integral may be based on the following formula, after a suitable rationalization by a transformation like Eq. (3.6),

$$\frac{1}{4}\int_{-\infty}^{+\infty}\frac{e^{izsz'}}{\cosh\frac{1}{2}\pi z'}\{\ \}dz'$$

$$=\left[e^{is\epsilon}+\frac{is(1-e^{is\epsilon}\cosh\epsilon)}{\sinh\epsilon}\right](\cosh\epsilon)^{-z}, \quad \text{(II.13)}$$

where the $\{\ \}$ indicate the bracketed expression in Eq. (5.5). Developing both sides in powers of ϵ and equating the coefficients of equal powers, one obtains the necessary expressions. Formula (II.13) holds for every real ϵ; it may be evaluated in a complex z' plane by a displacement of the path of integration from the real axis towards $z'=+i\infty$ (for $\epsilon>0$) resp. $z'=-i\infty$ (for $\epsilon<0$) and summation of the residues at the complex zeros of the hyperbolic functions.

20th Anniversary

of the

AMERICAN INSTITUTE OF PHYSICS

OCTOBER 23–27 HOTEL SHERMAN CHICAGO, ILLINOIS

A Joint Meeting of the American Institute of Physics and its Founder Societies

- **AMERICAN PHYSICAL SOCIETY (OCT. 25–27)**
- **OPTICAL SOCIETY OF AMERICA (OCT. 23–25)**
- **ACOUSTICAL SOCIETY OF AMERICA (OCT. 23–25)**
- **SOCIETY OF RHEOLOGY (OCT. 24–26)**
- **AMERICAN ASSOCIATION OF PHYSICS TEACHERS (OCT. 25–27)**

The American Crystallographic Association, an Affiliated Society of the American Institute of Physics, will participate in the Anniversary Meeting.

On Thursday, October 25, there will be an all-day symposium organized upon the theme "physics today", which will feature invited papers by:

ENRICO FERMI—The Nucleus
E. U. CONDON—The Atom
J. C. SLATER—The Solid State
HARVEY FLETCHER—Acoustics
EDWIN H. LAND—Optics
K. K. DARROW—Physics as Science and as Art

A JOINT BANQUET on Thursday evening, October 25, will have Senator Brien McMahon and K. T. Compton as guest speakers.

AN INDUSTRIAL EXHIBIT of scientific instruments and apparatus will provide manufacturers with an excellent opportunity to show their products to men who are responsible for many of the major scientific and technological advances of the past twenty years.

A PLACEMENT SERVICE for the benefit of employers and potential employees will be available during the meeting, and space in the Hotel Sherman will be reserved for this purpose.

Address inquiries to: The Secretary, American Institute of Physics, 57 East 55th Street, New York 22, New York

Some Quantum-Mechanical Divergences of a Simple Field

W. SOLLFREY* AND G. GOERTZEL
New York University, New York, New York
(Received April 26, 1951)

In order to study the sources of quantum-mechanical divergences, an elementary model, consisting of a one-dimensional vibrating string elastically coupled to a harmonic oscillator, is studied in detail. Following a preliminary discussion of the classical eigenfunctions of the coupled system for both a finite and an infinitely long string, the system is quantized by the standard methods of boson field theory. The permissible experiments upon the system are investigated from the viewpoint of regarding the measuring apparatus as providing initial conditions for the system. It is shown that certain infinities are of mathematical origin, and arise from breakdown of perturbation theory. Others are physical, and are the result of prescribing impossible requirements for the measuring apparatus. Cut-off methods which remove the infinities are presented.

I. INTRODUCTION

WHILE quantum mechanics has been highly successful in treating systems of mass points, the extension of its methods to continuous systems has always been beset with divergence difficulties. The present paper is an attempt to obtain an understanding of one source of these divergence difficulties by considering a very simple continuous system.

One of the simplest possible types of continuous systems is that type which is described by the wave equation in one dimension. Examples of such are the transmission line and the transverse vibrations in a plane of a uniform string. For definiteness we shall consider the latter. However, an isolated vibrating string is almost too simple, because it becomes difficult to determine just what are the physically realistic questions to ask. Therefore, in order to be able to describe appropriate experiments, it was felt desirable to couple a harmonic oscillator to the string. This system is still sufficiently simple that its equations of motion can be solved explicitly. While the classical theory of vibrating strings has been the subject of innumerable investigations, the corresponding quantum theory has only been considered very briefly.[1]

The subject matter of this paper is then a study of the classical and quantum-mechanical properties of a vibrating string coupled to a harmonic oscillator. It is not pretended that this study is complete. Rather, we hope we have formulated the problem and have made some start on its solution. For convenience, we have divided the problem into two parts, the study of a string of finite length and the study of a string of infinite length.

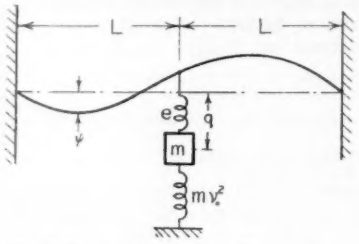

FIG. 1. The quantized string-oscillator system.

II. CLASSICAL MECHANICS OF THE FINITE STRING

A sketch of the system under consideration is given in Fig. 1. The variables describing the system are the displacements of the string and of the oscillator, denoted by $\psi(x, t)$, $q(t)$, and their conjugated momenta $\pi(x, t)$, $p(t)$. The units of length and time are so chosen that the string density per unit length and its tension are unity, with the string then of length $2L$ and fixed at its end. The oscillator, of mass m and fundamental frequency ν_0, is coupled to the string at its midpoint by a spring whose elastic constant is e. The equations of motion of this system are:

$$\begin{aligned}[(\partial^2/\partial x^2)-\partial^2/\partial t^2]\psi(x,t)&=e\delta(x)[\psi(0,t)-q(t)],\\ [(\partial^2/\partial t^2)+\nu_0^2]q(t)&=e/m[\psi(0,t)-q(t)].\end{aligned}\tag{1}$$

Only those solutions of these equations which are even in x will be coupled to the oscillator, and hence only such solutions will be considered. If an even solution of these equations of the form $\psi(x,t)=\psi_\omega(x)e^{i\omega t}$, $q(t)=q_\omega e^{i\omega t}$ is assumed, thereby defining the eigenvalues and eigenfunctions of the system, it is found that ω must satisfy the transcendental equation:

$$\begin{aligned}2\omega(\omega^2-\nu_0'^2)\cos\omega L+e(\omega^2-\nu_0^2)\sin\omega L&=0,\\ \nu_0'^2&=\nu_0^2+e/m,\end{aligned}\tag{2}$$

and for these eigenvalues the corresponding eigenfunctions are

$$\begin{aligned}\psi_\omega(x)&=\sin\omega_n(L-|x|)/N_\omega^{\frac{1}{2}}\sin\nu_n L,\quad \nu_n=(n-\tfrac{1}{2})\pi/L,\\ q_\omega&=-e\sin\omega_n L/mN_\omega^{\frac{1}{2}}\sin\nu_n L(\omega_n^2-\nu_0'^2).\end{aligned}\tag{3}$$

The quantities ν_n introduced here are the eigenvalues of the system without coupling, that is, when e is zero.

* Submitted in partial fulfillment of the requirements for the degree of Doctor of Philosophy in the Graduate School of Arts and Science of New York University.

[1] N. Rosen, Phys. Rev. **71**, 833(A) (1947); **76**, 202(A) (1949). M. Moshinsky, Phys. Rev. **81**, 347 (1951).

The eigenfunctions appropriate to that system are

$$\psi_\nu(x)=\cos\nu_n/\sqrt{L}, \quad q_\nu=\delta_{\nu n}\nu_0/\sqrt{m}. \tag{4}$$

The eigenfunctions in both (3) and (4) are so normalized that

$$\int_{-L}^{L}\psi_1(x)\psi_2(x)dx+q_1q_2=\delta_{12}. \tag{5}$$

The normalization constant N_ω appearing in Eq. (3) is given by

$$N_{\omega_n}=L+\frac{e\sin^2\omega_nL[\omega_n{}^4+(\nu_0{}'^2-3\nu_0{}^2)\omega_n{}^2+\nu_0{}^2\nu_0{}'^2]}{2\omega_n{}^2(\omega_n{}^2-\nu_0{}'^2)^2}. \tag{6}$$

The equations of motion (1) may be derived from the least action principle:

$$\delta\int_{-L}^{L}dx\int_{t_0}^{t_1}dtL(x,t)=0, \tag{7}$$

in which the lagrangian density $L(x,t)$ is given by:

$$2L(x,t)=\dot\psi^2-(\partial\psi/\partial x)^2+\delta(x)[m\dot q^2-m\nu_0{}^2q^2-e(\psi(0,t)-q)^2], \tag{8}$$

and the corresponding hamiltonian is

$$2H=\int_{-L}^{L}[\pi^2+(\partial\psi/\partial x)^2]dx+(p^2/m)+m\nu_0{}^2q^2+e(\psi(0)-q)^2. \tag{9}$$

The system variables ψ, π, etc., may be expanded both in a fourier expansion using the functions of (4), or by a normal mode expansion using the eigenfunctions (3). The fourier expansion yields

$$\psi(x,t)=\sum_1^\infty\psi_\nu(x)a_\nu(t), \quad q(t)=a_0(t)/\sqrt{m},$$
$$\pi(x,t)=\sum_1^\infty\psi_\nu(x)b_\nu(t), \quad p(t)=m^{\frac12}b_0(t), \tag{10}$$

and when these expansions are inserted into the hamiltonian (9), one obtains

$$2H=\sum_0^\infty[b_\nu{}^2+\nu^2a_\nu{}^2]+e\left[\sum_1^\infty\frac{a_\nu}{L^{\frac12}}-\frac{a_0}{m^{\frac12}}\right]. \tag{11}$$

The eigenfunctions (3), being the normal modes of the system, provide that representation for which the hamiltonian is diagonal when the system variables are expanded in terms of the basis (3). This fundamental property enables one to find the eigenfunctions (3) by assuming that there exists a matrix T which diagonalizes the hamiltonian (11), and then solving the equations that result. The conditions on the matrix T are

$$\omega^2\delta_{\omega\omega'}=\sum_0^\infty\nu^2T_{\omega\nu}T_{\omega'\nu}+e\left[\sum_1^\infty\frac{T_{\omega\nu}}{L^{\frac12}}-\frac{T_{\omega\nu_0}}{m^{\frac12}}\right]\times\left[\sum_1^\infty\frac{T_{\omega'\nu}}{L^{\frac12}}-\frac{T_{\omega'\nu_0}}{m^{\frac12}}\right]. \tag{12}$$

We may further assume that the matrix T represents an orthogonal transformation, so we impose on T the further conditions:

$$\sum_0^\infty T_{\omega\nu}T_{\omega\nu'}=\delta_{\nu\nu'}. \tag{13}$$

The solution of these equations may be found directly, or we may use the fact that the elements of T are the fourier components of the coupled system eigenfunctions with respect to the uncoupled system eigenfunctions, and evaluate the appropriate integral. Either method yields the result:

$$T_{\omega_n\nu_k}=\frac{e\sin\omega_nL(\omega_n{}^2-\nu_0{}^2)}{(LN_{\omega_n})^{\frac12}\sin\nu_nL(\omega_n{}^2-\nu_0{}'^2)(\omega_n{}^2-\nu_k{}^2)},$$
$$T_{\omega_n\nu_0}=-\frac{e\sin\omega_nL}{(mN_{\omega_n})^{\frac12}\sin\nu_nL(\omega_n{}^2-\nu_0{}'^2)}. \tag{14}$$

The evaluation by fourier components is simpler here, while the direct solving of the equations is simpler when one treats an infinite string. We shall next take up the classical theory of the latter.

III. CLASSICAL MECHANICS OF THE INFINITE STRING

The equations of motion for the infinite string are the same as (1), but the boundary condition that the displacement vanishes at the ends must of course be lifted. As before, only even solutions shall be considered. Instead of the fourier series representation (10), we use the fourier integral representation:

$$\psi(x,t)=\int_0^\infty a(\nu,t)\cos\nu x d\nu/\sqrt{\pi},$$
$$a(\nu,t)=\int_{-\infty}^\infty\psi(x,t)\cos\nu x dx/\sqrt{\pi}, \tag{15}$$

and a similar expansion for $\pi(x,t)$. This gives rise to the hamiltonian, analogous to (11):

$$2H=\int_0^\infty[b\nu^2(\nu)+\nu^2a^2(\nu)]d\nu+b_0{}^2+\nu_0{}^2a_0{}^2+e\left[\int_0^\infty[a(\nu)d\nu/\sqrt{\pi}]-a_0/\sqrt{m}\right]^2. \tag{16}$$

The matrix T satisfies the system of equations, similar

to (12) and (13):

$$\omega^2\delta(\omega-\omega') = \int_0^\infty \nu^2 T(\omega,\nu)T(\omega',\nu)d\nu + \nu_0^2 T(\omega,\nu_0)T(\omega',\nu_0) + e\left[\int_0^\infty [T(\omega,\nu)d\nu/\sqrt{\pi}] - T(\omega,\nu_0)/\sqrt{m}\right] \times\left[\int_0^\infty [T(\omega',\nu)d\nu/\sqrt{\pi}] - T(\omega',\nu_0)/\sqrt{m}\right], \quad (17a)$$

$$\int_0^\infty T(\omega,\nu)T(\omega,\nu')d\omega = \delta(\nu-\nu'), \quad (17b)$$

$$\int_0^\infty T(\omega,\nu)T(\omega,\nu_0)d\omega = 0, \quad (17c)$$

$$\int_0^\infty T^2(\omega,\nu_0)d\omega = 1. \quad (17d)$$

These equations can be solved directly, but the solutions involve singular terms. The result for T is

$$T(\omega,\nu) = \omega[(\omega^2-\nu_0'^2)\delta(\omega-\nu) + e(\omega^2-\nu_0^2)P/\pi(\omega^2-\nu^2)]/[F(\omega)]^{\frac{1}{2}},$$
$$T(\omega,\nu_0) = -e\omega/[\pi m F(\omega)]^{\frac{1}{2}}, \quad (18)$$
$$F(\omega) = \omega^2(\omega^2-\nu_0'^2)^2 + e^2(\omega^2-\nu_0^2)^2/4.$$

The symbol P denotes that in integrals the principal value is to be taken. The zeros of $F(\omega)$ represent resonances between the string and the oscillator. $F(\omega)$ has no real zeros, but there are two pure imaginary zeros and four complex ones.

IV. QUANTIZATION OF THE SYSTEM

The quantization of the finite string is considered first. The quantum theory retains the equations of motion for the variables when they are expressed in the Heisenberg representation, but interprets the variables as operators We introduce the commutation relations:

$$[\psi(x,t), \pi(x',t)] = i\delta(x-x'), \quad [q(t), p(t)] = i, \quad (\hbar=1). \quad (19)$$

All other commutators vanish when the variables are taken at the same time. The equations of motion (1) may be obtained by transcribing the hamiltonian (9), and then using the commutation relations and the quantum-mechanical equation of motion $i\dot{F}=[F,H]$, where F denotes any quantity not explicitly dependent upon the time. The fourier amplitudes introduced by the expansion (10), and the corresponding amplitudes for an expansion in the eigenfunctions (3), which latter set of amplitudes are denoted by $A_\omega(t)$, $B_\omega(t)$, will satisfy the commutation relations, derived from (19) and the orthogonality of the eigenfunctions:

$$[a_\nu(t), b_{\nu'}(t)] = i\delta_{\nu\nu'}, \quad [a_0(t), b_0(t)] = i, \quad [A_\omega(t), B_{\omega'}(t)] = i\delta_{\omega\omega'}. \quad (20)$$

All other commutators involving separately variables of the coupled system or of the uncoupled system taken at the same time vanish. A system of creation and destruction operators, u_ν^* and u_ν, respectively, is defined by

$$a_\nu = (2\nu)^{-\frac{1}{2}}(u_\nu+u_\nu^*), \quad b_\nu = (\nu/2)^{\frac{1}{2}}i(u_\nu^*-u_\nu), \quad (21)$$

with similar relations for a_0, b_0, A_ω, B_ω. In terms of these operators, the hamiltonian may be expressed as

$$H = \tfrac{1}{2}\sum_0^\infty \nu(u_\nu^* u_\nu + u_\nu u_\nu^*) + \tfrac{1}{4}e\left[\sum_1^\infty \frac{(u_\nu+u_\nu^*)}{(\nu L)^{\frac{1}{2}}} - \frac{(u_0+u_0^*)}{(\nu_0 m)^{\frac{1}{2}}}\right]^2, \quad (22)$$
$$H = \tfrac{1}{2}\sum_0^\infty \omega(U_\omega^* U_\omega + U_\omega U_\omega^*) = \sum_0^\infty \omega(U_\omega^* U_\omega + \tfrac{1}{2}).$$

We thus see the appearance of the zero-point energy $\sum \frac{1}{2}\omega$. The hamiltonian, of course, is arbitrary to within an additive constant. In the usual theories the zero-point energy is taken to be the zero-point energy in the absence of interaction, which here would be represented as $\sum \frac{1}{2}\nu$. We shall instead take the zero-point energy to be $\sum \frac{1}{2}\omega$, the zero-point energy in the presence of the interaction. These two sums are not only unequal, they differ by an infinite amount. With this choice of the additive constant, the hamiltonian becomes

$$H = \sum_0^\infty \omega U_\omega^* U_\omega = \sum_0^\infty \omega N_\omega, \quad (23)$$

where the operator N_ω is that operator whose expectation value in any state denotes the number of quanta of frequency ω in that state.

A complete set of eigenstates for this hamiltonian is given by the eigenstates of the number operator N_ω, describing states with a fixed number of quanta in each of the normal modes of the coupled system. These states may all be derived from the coupled system vacuum state vector, which shall be denoted by Φ_0, by the application of creation operators U_ω^*. The hamiltonian (23) is so arranged that its expectation value is zero in the state Φ_0, and is positive in all the other eigenstates, whence it is a positive definite operator. Another complete set of states, which, however, are not eigenstates of the hamiltonian (23), are the eigenstates of the number operator N_ν, which states are eigenstates of the uncoupled system hamiltonian, after the subtraction of the zero-point energy of the latter. This latter set of states is customarily used for prescribing initial conditions. We shall return to this point

after briefly considering the quantization of the system when the string is infinite in length.

For the infinite string, the commutation relations (20) are replaced by continuous spectrum commutation relations in which the Kronecker δ-symbol is replaced by the Dirac δ-function. The sums appearing in (22) and (23) are replaced by integrals, derived from (16) in the same manner as (22) is derived from (11). The creation and destruction operators are introduced in the same way, and so are the sets of states.

Now that the basic formalism is set up, we shall try to use it to answer some questions.

V. EXPERIMENTS ON THE FINITE STRING

The attempt to answer some questions must necessarily involve the introduction of a measuring apparatus and a determination of how the measurement is to be described in the formalism. The measuring apparatus may be expected to prescribe the state of the system at some time, and then the equations of motion serve to carry the system through time. Thus, the apparatus provides suitable initial conditions for the system.

Almost universally, the initial conditions in an experiment described quantum mechanically are represented as the eigenstates of the hamiltonian without coupling. A typical experiment to be described within the framework of the formalism might go as follows: At time $t=0$ the system is prepared in a state Φ which corresponds to the oscillator being in some definite excited state and no quanta present in the string—all in terms of the hamiltonian with $e=0$. We may then ask what is the probability of finding the system in some definite state of the uncoupled system hamiltonian at a later time.

Before one goes to any great lengths in carrying out such a computation, he should investigate whether it is possible, in the light of the hamiltonian with coupling, to prepare such a state as considered, or whether impossible requirements will have to be placed on the measuring apparatus. We therefore shall investigate what requirements are called for.

A first question we may ask is the expectation value of the energy in the initial state. This should clearly be finite. The state Φ, as indicated, may be derived from the uncoupled system vacuum state vector, which shall be called Φ_0', by application of the creation operator u_0^*, so it is sufficient that the state Φ_0' have finite energy. We recall that the hamiltonian has been reordered so that its energy is zero in the state Φ_0, and it may easily be shown that the state Φ_0' contains an infinite number of quanta in the various normal modes of the coupled system, so its energy is not obviously finite. However, the detailed calculations yield for the expectation value, denoted by $\langle H\rangle_{0'}$,

$$\langle H\rangle_{0'}=\tfrac{1}{4}\sum_{0}^{\infty}\sum_{0}^{\infty}T_{\omega\nu}{}^{2}(\omega^{2}-2\omega\nu+\nu^{2})/\nu. \qquad (24)$$

The orthogonality relations for T enable the terms involving $2\omega\nu$ and ν^2 to be summed over ν and ω respectively, and Eq. (12) for T enables the term involving ω^2 to be summed over ω. There results:

$$\langle H\rangle_{0'}=\tfrac{1}{4}[2\sum_{0}^{\infty}\nu-2\sum_{0}^{\infty}\omega+e\sum_{1}^{\infty}(1/\nu L)+e/\nu_0 m]. \qquad (25)$$

The three series are separately divergent at high frequencies, the first two quadratically, the third logarithmically. However, approximations to the roots of Eq. (2) at high frequencies show that the divergences completely compensate each other, so the entire expression (25) is finite. This finite result is a result of the reordering of the complete hamiltonian by subtracting the zero-point energy of the coupled system, rather than the customary method of subtracting the zero-point energy of the uncoupled system. If the latter zero-point energy had been subtracted, only the third series in (25) would remain, and we would conclude that the state Φ_0' had a logarithmically infinite energy, rather than the finite value (25).

A second question is as to the magnitude of the rate of change of the initial state wave function. This quantity is proportional to the expectation value of the square of the hamiltonian in the initial state, using Schrödinger representation. For considerations of finiteness, again only the vacuum state Φ_0' need be considered. The expectation value may be computed by the same method as before, and after much reduction we obtain the result:

$$\langle H^2\rangle_{0'}=\langle H\rangle_{0'}{}^{2}+\tfrac{1}{4}e^{2}[\sum_{1}^{\infty}(1/\nu L)+1/\nu_0 m]^{2}. \qquad (26)$$

This expression diverges like the square of a logarithm, so that the state Φ_0' will have an infinite time rate of change. Physically, this infinity would seem to indicate that the state Φ under consideration could not be prepared, since it would tend to jump discontinuously into some other state or set of states. On the other hand, one is led by strong arguments to consider such a state as the initial state.

A way out of this difficulty presents itself if one considers the measuring apparatus. To prepare a state which will tend to change infinitely, rapidly one must have at one's disposal a measuring apparatus with infinite band width. Such a property is also required if we realize that we have specified the absence of quanta from the string at all frequencies including the very highest, and the statement that such quanta are absent implies that we measure or in some way detect their absence. Such measuring apparatuses are not normally at the disposal of physicists.

An alternate viewpoint, not directly involving the band width of the measuring apparatus, but rather its time response, is available. The attempt to measure very high frequencies is equivalent to measuring very short time intervals. It is clear that no measurement can take place in zero time, since no apparatus can act with

infinite speed. Thus, it is perhaps desirable to consider what happens if the preparation of the initial state takes place with finite rapidity. One is then led to introduce a function to describe the time behavior of the measuring apparatus. We would then consider an initial state of the form:

$$\Phi'(t)=K\int_{-\infty}^{\infty}g(t-t')\Phi(t')dt'. \tag{27}$$

Here we have temporarily gone over to Schrödinger representation, and K is a normalizing "constant." From the known time behavior of states in the Schrödinger representation, this expression may be transformed into

$$\Phi'=K\left[\int_{-\infty}^{\infty}g(t')e^{-iHt'}dt'\right]\Phi=W\Phi. \tag{28}$$

Now the usual specification of measurements corresponds to $g(t)=\delta(t)$. We may insert a small parameter τ into g, so that it corresponds to measurements taking place over a small but finite time, and then determine the modifying operator W. A reasonable program would then be to compute the result of a thought experiment, retaining the parameter τ in the analysis. The operator W will mainly affect the high frequency parts of the states, and it will provide an automatic high frequency cutoff for the system. After the appropriate transition probabilities have been obtained, one idealizes them by letting τ approach zero. These considerations are similar to those of Stueckelberg.[2]

VI. EXPERIMENTS ON THE INFINITE STRING

Consideration of the possibility of preparing an initial state with no quanta in the uncoupled system leads to the same infinity at high frequencies for the mean square value of the hamiltonian as before. Furthermore, even the expectation value of the energy itself is infinite, this time because of a divergence of logarithmic type at low frequencies. This may be expected from a consideration of the third sum in Eq. (25). If one allows L to approach infinity, the sum is replaced by an integral from zero to infinity, while the L in the denominator is replaced by π, so the limit is infinite. We may further observe that a computation of the energy per unit length for a finite length string shows that the energy is uniformly distributed in the state Φ_0' and of order e/L, so the entire energy of the string may be expected to be of order $e\log L$ and hence to diverge as L becomes very large.

This low frequency divergence may again be interpreted in terms of the characteristics of the measuring apparatus. In order to insure that in an infinitely long string there is an absence of low frequency quanta, it is necessary to have a measuring apparatus which extends over the string length. Such a measuring apparatus cannot be easily constructed. The method of taking this into account in describing a physical problem has not yet been discovered, although some possibilities are being considered. The methods are related to the fluctuation considerations of Welton.[3]

VII. PERTURBATION THEORY CONSIDERATIONS

We shall discuss here the relation of the exact formula (25) to what might be expected from perturbation theory. Suppose we assume that the coupling constant e, which in these units is a frequency, is small compared with all other frequencies involved; and, in fact, that it is small compared with the lowest frequency of the string. Then we may expand the eigenvalues ω in powers of e. The result for (25) correct to the second order in e is

$$\langle H\rangle_{0'}=\tfrac{1}{4}e^2[0.136L +([\log(\nu_0L/\pi)+1.963]/\pi\nu_0{}^2m)+1/4\nu_0{}^3m^2]. \tag{29}$$

The constants 0.136 and 1.963 appearing here are respectively $7\zeta(3)/2\pi^3$ and $C+2\log 2$, where $\zeta(3)$ is the value of the Riemann zeta-function $\zeta(z)$ for $z=3$ and C is Euler's constant. The three terms in (29) represent the string self-energy due to its being partially bound at its midpoint, the coupling energy between the string and the oscillator, and the change in the oscillator fundamental frequency.

The formula (29) is derived under the assumption that the expansions in powers of e are valid, which is only satisfied if the string is not too long. Since the lowest frequency the string can transmit is $\pi/2L$, when L is so great that this quantity is no longer large compared with e, the expression breaks down. Therefore, we may expect that the result of interchanging the limit processes e becoming small and L becoming large will give different answers. The formula (29) corresponds to keeping the string length fixed and then making e small. If we keep e fixed and let the string length become very large, so there are many string modes with frequencies below e, we obtain as an approximation to (25):

$$\langle H\rangle_{0'}=\tfrac{1}{4}\{e[\log eL-0.667] +e^2(1/\pi)\,[\log(2\nu_0/\pi e)/\pi\nu_0{}^2m]+e^2/4\nu_0{}^3m^2\}. \tag{30}$$

The constant 0.667 is $\frac{1}{2}(\pi-1)-(C+\log 2)/\pi$. We see that the self-energy of the string, which for small eL is of order e^2L, is only of order $e\log(eL)$ for eL large. This corresponds to the partial binding becoming less effective as the string length increases, which is reasonable, since a very long string will not be very much affected by what happens at one point. However, for very low frequencies, which practically correspond to bodily displacing the string, the binding effect is important, and it is these low frequencies which give rise to the term $e\log(eL)$ in (30).

The coupling energy, which is of order $e^2\log(\nu_0L/\pi)$ when eL is small, is of order $e^2\log(2\nu_0/\pi e)$ when eL is large. Hence, the coupling energy remains finite as the string length tends to infinity. However, because of the

[2] E. G. C. Stueckelberg, Phys. Rev. **81**, 130 (1951).

[3] T. A. Welton, Phys. Rev. **74**, 1157 (1948).

appearance of $\log e$, the coupling energy is not analytic in e if we make the transition to small values of e after letting L become very large. If we expand the coupling energy in a power series in e, we will obtain an infinite coefficient for every term beyond the second. This corresponds to a purely mathematical breakdown of the perturbation theory, and the apparent infinities have no physical significance. Calculation of the mean energy for the infinitely long string, using a low frequency cutoff, leads to the same result as (30) except that the constant 0.667 is changed to $0.682=(1+\log\pi)/\pi$. This latter calculation shows that the major contribution to the energy arises from a set of damped vibrations whose time behavior is approximately as $\exp(-et)$, and that the oscillator is in resonance with these vibrations. The energy content of these damped vibrations is of order $e^2\log e$.

The details of the derivation of Eqs. (29) and (30) will be found in the Appendix.

VIII. CONCLUSIONS

We have shown in the above that the *a priori* physically sensible system of a vibrating string elastically coupled to a harmonic oscillator leads to some nontrivial problems and divergences owing to the possibility of mathematical breakdown of the perturbation theory or the ascribing of impossible properties to the measuring apparatus. On the other hand, this problem was carefully chosen so as to assure that the hamiltonian of the system is sensible. This is primarily assured by its positive definiteness. Hence, one would not expect that the above considerations, even when carried to their ultimate, would lead to correct solutions and treatment for all hamiltonians. It seems likely that the hamiltonian of quantum electrodynamics is not positive definite; it is probably infinite in having a negatively infinite eigenvalue.

The authors would like to take this opportunity to express their appreciation for the encouragement and interest shown by Professor K. O. Friedrichs of the Mathematics Department of New York University in this research. Further work along the above lines is now progressing under the support of the ONR.

APPENDIX

We shall now discuss the reductions whereby (25) is simplified to the forms (29) and (30). In the case where (29) is valid, e is treated as so small that all frequencies involved are large compared with it. We may then expand the roots of (2) in powers of e, and obtain successive approximations by equating the powers of e on both sides of (2). The result of this straightforward calculation is given to the second order in e by:

$$\omega_n=\nu_n+(e/2\nu_nL)+[e^2/2m\nu_nL(\nu_n^2-\nu_0^2)]-e^2/4\nu_n^2L^2,$$
$$\omega_0=\nu_0+(e/2\nu_0m)-(e^2/8\nu_0^3m^2)-e^2\,(\tan\nu_0L)/4\nu_0^2m. \tag{A1}$$

When these expansions are inserted into (25), the terms of order zero and one cancel from the resulting expression, leaving

$$\langle H\rangle_{0'}=\frac{e^2}{4}\Big[\sum_1^\infty\Big\{\frac{L}{(2\pi^2(n-\tfrac12)^2}-\frac{L^2}{\pi^2m(n-\tfrac12)[(n-\tfrac12)^2-(\nu_0L/\pi)^2]}\Big\}$$
$$+\tfrac12\nu_0^3m^2+(\tan\nu_0L)/2\nu_0^2m\Big]. \tag{A2}$$

The second term in the summation may be simplified by an algebraic identity, which reduces it to the form:

$$-\frac{L}{\pi^2\nu_0m}\sum_1^\infty\Big[\frac{1}{(n-\tfrac12)^2-(\nu_0L/\pi)^2}-\frac{1}{(n-\tfrac12)(n-\tfrac12+\nu_0L/\pi)}\Big]. \tag{A3}$$

The first sum appearing here is simply evaluated by observing that the fourier coefficients of $\sin y(\pi-x)$ are proportional to $1/[(n-\tfrac12)^2-y^2]$, determining the constant of proportionality, and then setting $x=0$. It is then found that this sum exactly cancels the last term in (A2). The remaining series are well-known transcendental functions. The series involving the inverse cubes of the odd integers is evaluated by adding and subtracting the even terms, whence the sum becomes a constant multiple of the sum of the inverse cubes of the integers, which by definition is the Riemann zeta-function evaluated at $z=3$. The constant of proportionality is found immediately to be 7, whence this sum becomes $7\zeta(3)L/2\pi^3$.

The sum appearing as the second term of (A3) may be evaluated in terms of the logarithmic derivative of the gamma-function. The series may be split into two sums, each of which has a general term of the form $1/[n(n+z)]$. The latter sums are then found by the formula:

$$\sum_1^\infty 1/n(n+z)=[\psi(z)+C]/z. \tag{A4}$$

Here $\psi(z)$ denotes the logarithmic derivative of the gamma-function and is not to be confused with the string displacement function. Upon collecting the several formulas, we have for the expectation value of the energy the result correct to order e^2:

$$\langle H\rangle_{0'}=\tfrac14e^2\Big[\frac{7\zeta(3)L}{2\pi^3}+\frac{C+2\psi(2\nu_0L/\pi)-\psi(\nu_0L/\pi)}{\pi\nu_0^2m}+\frac{1}{4\nu_0^3m^2}\Big]. \tag{A5}$$

If the string length is many oscillator wavelengths, we may use the asymptotic formula $\psi(z)\to\log z$, and (A5) reduces to (29).

The expansion of the eigenfrequencies ω_n breaks down when e and ω_n are of the same order of magnitude. Suppose the string is so long that there are many string vibrations whose frequency is less than e. We assume, however, that as before e is small compared with ν_0 and that the string length is many oscillator wavelengths. Then for the very low frequencies we use an expansion in inverse powers of e, or rather of eL. Since under these conditions the roots are very close together, we will lose nothing by setting $eL/2$ equal to $k\pi$, where k is an integer. Then an approximation to the roots of (2) which is quite accurate when $\omega L\ll k\pi$, and is only off by 20 percent when $\omega L=k\pi$, is

$$\omega_nL=n\pi-(n/k)+n/k^2\pi. \tag{A6}$$

In the low frequency terms of the series in (25) we may use the approximation (A6). The sum becomes an arithmetic progression, which may be summed immediately. We thus have, upon neglecting higher powers of $1/k$,

$$\frac{2}{L}\sum_1^k\Big[(n-\tfrac12)\pi-\Big(n\pi-\frac{n}{k}+\frac{n}{k^2\pi}\Big)\Big]+e\sum_1^k\frac{1}{(n-\tfrac12)\pi}$$
$$=\frac{2}{L}\Big[\frac{-\pi(k-1)}{2}+\Big(\frac1k-\frac{1}{k^2\pi}\Big)\frac{k(k+1)}{2}\Big]+\frac{e}{\pi}\sum_1^k\frac{1}{(n-\tfrac12)}$$
$$=e\Big[\frac{-(\pi-1)}{2}+\frac1\pi\sum_1^k\frac{1}{(n-\tfrac12)}\Big]. \tag{A7}$$

When k is a large number, an approximation to this last series is

$$\sum_1^k 1/(n-\tfrac12)=\log k+(2\log2+C)+O(1/k). \tag{A8}$$

Consequently, the total contribution from the low frequency terms is

$$e[(1/\pi)\log(eL)-\tfrac12(\pi-1)+(\log2+C)/\pi]. \tag{A9}$$

In the high frequency terms, we may again use the approximation (A1). We then obtain the equivalent of Eq. (A2), except that the lower limit on the sums is $k+1$. The series involving the inverse

cubes of the odd integers now is of higher order in $1/k$ than are already neglected terms, and hence it may also be neglected. In the second series we make the transformation (A3), add and subtract the terms from 1 to k, and cancel the final term of (A2). The high frequency contribution is now:

$$2e^2\left[\frac{L}{2\pi^2\nu_0 m}\left\{\sum_1^k \frac{1}{(n-\frac{1}{2})^2-(\nu_0 L/\pi)^2} + \sum_{k+1}^{\infty}\frac{1}{(n-\frac{1}{2})(n-\frac{1}{2}+\nu_0 L/\pi)}\right\}+\frac{1}{8\nu_0^3 m^2}\right]. \quad \text{(A10)}$$

In the first series we may neglect the first term in the denominator in comparison with the second, because of the assumption that the coupling constant e is small compared with the fundamental oscillator frequency ν_0. The resulting expression may be summed. and it is of order e^3 and thus is to be neglected. We add and subtract the terms from 1 to k in the remaining series. The sum from one to infinity is equal to the middle term in (A5). In the sum from 1 to k that we subtract, the $n-\frac{1}{2}$ may be neglected compared with $\nu_0 L/\pi$. This last sum then becomes

$$-\frac{1}{2\pi\nu_0^2 m}\sum_1^k\frac{1}{(n-\frac{1}{2})}=-\frac{1}{2\pi\nu_0^2 m}[\log(eL)+\log 2+C]. \quad \text{(A11)}$$

Hence the total contribution from high frequency terms is;

$$2e^2\left[\frac{\log(\nu_0 L/\pi)+2\log 2+C}{2\pi\nu_0^2 m}-\frac{\log(eL)+\log 2+C}{2\pi\nu_0^2 m}+\frac{1}{8\nu_0^3 m^2}\right]$$
$$=e^3\left[\frac{\log(2\nu_0/\pi e)}{\pi\nu_0^2 m}+\frac{1}{4\nu_0^3 m^2}\right]. \quad \text{(A12)}$$

When this is combined with the low frequency contribution (A9), the formula (30) is obtained.

PHYSICAL REVIEW VOLUME 83, NUMBER 5 SEPTEMBER 1, 1951

Oscillator Strengths for the α- and β-Bands in Alkali Halide Crystals*

D. L. DEXTER
Department of Physics, University of Illinois, Urbana, Illinois
(Received May 21, 1951)

The oscillator strengths for the α- and β-absorption bands are calculated for NaCl. These bands, investigated experimentally by Delbecq, Pringsheim, and Yuster in KI, lie on the long-wavelength tail of the first fundamental absorption band and are interpreted by use of a model according to which valence electrons of the adjacent halide ions are raised to bound states in the fields of negative ion vacancies (α-transitions) and F-centers (β-transitions). The oscillator strengths turn out to be only slowly varying with the assumed wave functions and are about 1.9 and 0.6 for the α- and β-bands, respectively.

I. INTRODUCTION

RECENT experiments of Delbecq, Pringsheim, and Yuster[1] have shown the existence of two new absorption bands in the long-wavelength tail of the first fundamental absorption band in KI. Pringsheim *et al.* point out the unlikelihood that the α- and β-bands are caused by V-centers[2] and suggest that "The presence of certain well-defined singularities in sufficient numbers, such as negative ion vacancies or F-centers, may affect the first fundamental frequency of the crystal in such a way that new well-defined absorption bands corresponding to perturbed transitions of the valency electrons of the adjacent halide ions appear superimposed on the tail of the fundamental absorption band."[1]

In the present paper the oscillator strengths of the α- and β-bands are evaluated for NaCl, assuming models in which Cl^- ion $3p$ electrons make transitions to bound levels in the field of a negative ion vacancy for the α-band and in the field of an F-center for the β-band. It is found that the oscillator strength of each band is of the order unity and that the results are rather insensitive to the assumed final-state wave functions.

II. DISCUSSION OF WAVE FUNCTIONS

In order to determine the dipole matrix elements needed for the calculation of the oscillator strengths, the following four wave functions will be required.

Let ψ_1 be the wave function of an otherwise perfect crystal of NaCl containing a single negative ion vacancy. As discussed in a previous paper[3] the wave function of a $3p$ electron in a Cl^- ion may be written as an analytical approximation of the Hartree wave function[4]

$$\varphi_{3p}=r(e^{-r/A}-Ce^{-r/B}), \quad (1)$$

where $A=a_0/1.1$, $B=a_0/8$, $C=23.2$, and $a_0=\hbar^2/me^2$; ψ_1 may be approximated by a permutation of the products of such functions. Specific changes in these one-electron functions due to the presence of the vacancy will be neglected, and the presence of the positive ions may be ignored for the moment.

The excited state of this crystal is described by a wave function, ψ_2, representing a configuration in which any one of the 72 surrounding $3p$ electrons is in a $1s$

* Research supported by the ONR.
[1] Delbecq, Pringsheim, and Yuster, J. Chem. Phys. **19**, 574 (1951). See also, E. Burstein and J. J. Oberly, Phys. Rev. **79**, 903 (1950), and H. Dorendorf, Z. Physik **129**, 317 (1951).
[2] F. Seitz, Phys. Rev. **79**, 529 (1950), and references therein.
[3] D. L. Dexter, Phys. Rev. **83**, 435 (1951).
[4] D. R. Hartree and W. Hartree, Proc. Roy. Soc. (London) **A156**, 45 (1936).

state about the negative ion vacancy and a positive hole is left on one of the 12 nearest Cl^- ions (at distance $7.5a_0$). This configuration is similar to that of an F-center in a photochemically excited crystal, but differs in one important respect. The usual F-center electron's wave function is determined by an effective "nuclear charge" characteristic of the crystal with the surrounding ions in the equilibrium positions they take when an electron is present; however, in the present case, according to the Franck-Condon principle, the nuclear charge will be characteristic of the ionic configuration before the absorption act. The potential due to a negative ion vacancy in an otherwise perfect crystal[5] is e/Kr, where K is the static dielectric constant (5.62 for NaCl); and hence the wave function of the excited electron is

$$\varphi_{F'}(\mathbf{r})=g(\mathbf{r})\exp(-r/Ka_0), \tag{2}$$

where $g(\mathbf{r})$ is the lattice function in the conduction band.[6] Thus, ψ_2 may be written as one of 72 sums of products of Eq. (2) with the functions (1). We shall use ψ_1 and ψ_2 for calculating the oscillator strength for the α-band.

The function ψ_3 is the wave function describing a crystal in the vicinity of a normal F-center. According to this model, it is the ground-state wave function for the transition corresponding to the β-band and can be written as a sum of products of Eq. (1) and an F-center wave function,

$$\varphi_F(\mathbf{r})=g(\mathbf{r})\exp(-r/\gamma_F). \tag{3}$$

Tibbs[7] has calculated an F-center wave function in NaCl, and for small distances the coefficient of $g(\mathbf{r})$ can be approximated by $\exp(-r/3a_0)$. For large distances, however, φ_F must have its high frequency dielectric constant value[3] $\exp(-r/K_0a_0)g(\mathbf{r})$ ($K_0=2.25$ in NaCl). We shall approximate φ_F by a single function (3) and examine the variation of oscillator strength with γ_F.

The crystal with a positive hole in one of the surrounding Cl^- ions and an extra electron in the F-center is described by ψ_4. As in the discussion of ψ_2, however, this is not a usual F'-center, because the surrounding ions have not yet moved to new equilibrium positions for times of interest here. If we assume both electrons to be bound to the negative ion vacancy in $1s$ orbits, an estimate of ψ_4 can be made by use of the variational method[8] as applied to the He atom. Minimizing the expectation value of the hamiltonian with respect to the binding parameter Z, we find

$$Z=\tfrac{1}{2}(2z-5/8K_0), \tag{4}$$

where z is the effective nuclear charge of the vacancy for binding one electron and Z is defined by

$$\varphi_{F'^0}(\mathbf{r})=g(\mathbf{r})\exp(-Zr/a_0). \tag{5}$$

From the discussion of φ_F and consideration of the fact that $\varphi_{F'^0}$ has a larger spread than φ_F it appears that $z=1/K_0$ is a good approximation, so that $Z=1/3.27$. It will be shown that the oscillator strength is insensitive to choice of Z. Thus, ψ_4 can be written as one of a sum of products of the functions (1) and two functions (5).

III. MATRIX ELEMENTS AND OSCILLATOR STRENGTHS

The matrix elements we need for the oscillator strengths[9] are of the form $\int\psi_0^*\mathbf{r}\psi_j d\tau$, where ψ_0 is the initial wave function and ψ_j a final-state wave function. For the α-band this becomes $\int\psi_1^*(\mathbf{r})\mathbf{r}\psi_2(\mathbf{r})d\tau$, which reduces to $\int\varphi_{2p}^*\mathbf{r}\varphi_{F'^0}d\tau$. These two center integrals have been evaluated analytically by using elliptic coordinates and by treating the function $g(\mathbf{r})$ as a constant. From inspection of $\varphi_{2p}^*\mathbf{r}\varphi_{F'^0}$ it is clear that there is a roughly spherical region about each ion (although not about the vacancy) in which cancellation occurs because of $g(\mathbf{r})$ so that to take $g(\mathbf{r})$ into account it is necessary to subtract the contribution to the integral arising from each of these regions. In view of the approximate constancy of $g(\mathbf{r})$ in the important parts of the crystal (except for these small regions) it is felt that this method is sufficient to give a good approximation to the matrix elements. These small contributions were evaluated analytically by treating $\exp(-r/Ka_0)$ as constant over each small region.

TABLE I. Values of f_β for various choices of wave functions (3) and (5).

γ_F \ Z	1/3.00	1/3.27	1/5.62
2.25	0.605	0.612	0.544
3.0	0.646	0.680	0.748

The energy of the α-transition, according to a simple cycle and by comparison with the experimental results on KI, should be about 6.8 ev. Then, using this energy and the matrix elements described in the preceding paragraph, we can evaluate f_α, the oscillator strength between a state with a vacancy and no holes and a state with an electron of either spin in the vacancy and a hole on any adjacent Cl^- ion, for $K=5.62$ in Eq. (2). It turns out to be $f_\alpha=1.89$. To show how f_α varies with damping length in Eq. (2) we may state the values of f_α for $K=3$ and $K=7.3$, i.e., 1.23 and 1.22, respectively. The reason for the slow variation is that the two centers are $7.5a_0$ apart, so that the magnitude of the function (2) near the Cl^- ion site is

[5] N. F. Mott and R. W. Gurney, *Electronic Processes in Ionic Crystals* (Oxford University Press, London, 1948), p. 85.

[6] S. R. Tibbs, Trans. Faraday Soc. **35**, 1471 (1939). For further use and discussion of this function see reference 3.

[7] See reference 6 and J. H. Simpson, Proc. Roy. Soc. (London) **A197**, 269 (1949).

[8] See, for example, L. I. Schiff, *Quantum Mechanics* (McGraw-Hill Book Company, Inc., New York, 1949), p. 172.

[9] See, for example, F. Seitz, *Modern Theory of Solids* (McGraw-Hill Book Company, Inc., New York, 1940), p. 148.

not strongly dependent on damping length in this size range of K. The oscillator strengths for transitions to excited states are negligibly small because of the very wide extent of the excited state wave functions.

The β-band matrix elements were treated similarly except that in this case only half of the electrons can make transitions, because of the spin of the electron already in the F-center, and except that each one-electron integral is multiplied by the overlap integral of φ_F and $\varphi_{F'}$*. The value of f_β is the oscillator strength between a state with an F-center and no holes and a state with 2 electrons in the vacancy and a hole on any adjacent Cl^- ion, γ_F is the damping length of the F-center wave function (3), and Z/a_0 is the inverse damping length in Eq. (5). The energy of the β-band is taken to be 7.2 ev for NaCl. Table I shows the oscillator strength f_β for wave functions in the interesting size range. There is very little variation of f_β with wave functions of this approximate extent, because as $1/Z$ increases and the one-electron dipole matrix element increases (until $Z\sim 1/6$), the overlap integral decreases. This calculation then indicates that $f_\alpha = 1.9$ and $f_\beta = 0.6$.

It does not seem advisable at this time to attempt to compare these results with the experimental data obtained for KI, because the oscillator strength of the F-band is not known for KI and because comparison of areas in the α-, β-, and F-bands is made difficult with the steep rise of the fundamental absorption band superimposed on the α- and β-bands. Nevertheless, assuming the oscillator strength of the F-band to be about 0.6 or 0.7 in KI, the experimental areas of the α- and β-bands are not inconsistent with oscillator strengths of the order of those calculated here. At first sight, it might seem surprising that f_α and f_β should be as large as f_F, but the relative smallness of the matrix elements for the β- and α-band transitions are compensated for by the large numbers of electrons that can take part in these transitions and by the high energy of the transitions.

The author is indebted to Dr. W. R. Heller for bringing the work of Delbecq, Pringsheim, and Yuster to his attention and for helpful discussions. He would also like to express his appreciation to Professor Pringsheim for a discussion of the experimental results before their publication and to Professor Seitz for his kind interest in this work.

Note added in proof: Dr. LeRoy Apker has kindly informed me of evidence, obtained by himself and Dr. E. Taft from the photoelectron emission experiments, which has a bearing on the β-bands in Rb I and KI. In their paper on Rb I near 85°K [Phys. Rev. **81**, 698 (1951)] they show a separate peak (a few tenths of an ev removed from the position of the maximum yield) which they suggested might be associated with the decreasing transparency of the film. Further preliminary results on KI near 85°K also show this separate peak. However, their additional experiments on optical interference appear to rule out the optical effect as being important in this region; in view of the absorption measurements described in reference 1, Apker and Taft now interpret the separate peak as being associated with the β-band. One would expect to find a peak in the photoelectric yield corresponding to the β-band for two reasons: (1) Because of the increase in the absorption coefficient on the tail of the fundamental band, the light is absorbed closer to the surface, so that the electrons which are eventually released have a shorter distance to travel within the crystal, and thus have a higher probability of getting out of the crystal; (2) inasmuch as F′ centers, containing electrons of lower binding energy than F center electrons, are formed by irradiation in the β-band, subsequent ionization of the F′ centers by excitons results in electrons of relatively high energy in the conduction band, which again increases the external photoelectric yield.

It should perhaps be emphasized at this point that this calculation has neglected entirely the effects of the positive hole left at the Cl^- ion site adjacent to the vacancy, and has assumed that the positive hole diffuses away. A more exact calculation, which appears difficult to perform, should take into account the effect of the positive hole on the electrons' wave functions. As Professor Seitz first pointed out to Drs. Apker and Taft, if the positive hole remains in the vicinity of the vacancy, one of the F′-center electrons could perhaps recombine with the positive hole, the energy of the transition being used to ionize the remaining electron. This two-center Auger process would likewise increase the photoelectric yield at an energy close to that of the β-band, and could perhaps be distinguished from the two-quanta process mentioned above by the temperature and light intensity dependence of the external yield.

The Quantum-Mechanical Equations of Motion and Commutation Relations

C. R. PUTNAM
Institute for Advanced Study, Princeton, New Jersey
(Received May 18, 1951)

It has been shown by Wigner that the equations of motion of a quantum-mechanical system with a hamiltonian $H=\frac{1}{2}p^2+V(q)$ need not imply the commutation relation $i[p, q]=1$. Particular examples are furnished by the free particle and the harmonic oscillator. On the other hand, Wigner points out that the above commutation rule does follow from the equations of motion if $V(q)$ is of the form $V=aq+b$ or $V=aq^2$. In the present note, this latter result is generalized to the case of an arbitrary potential $V=aq^n+b$, where n is an odd integer; the last-named potentials are, in fact, particular cases of those satisfying a general criterion contained in the article.

CONSIDER a one-dimensional quantum-mechanical system possessing a hamiltonian $H=H(p, q)$ of the form

$$H=\tfrac{1}{2}p^2+V(q). \tag{1}$$

(It is assumed that the particle has unit mass and that units are chosen so that Planck's constant is unity.) The question as to whether the equations of motion

$$\dot{q}=p, \quad \dot{p}=-\partial V/\partial q \quad (\cdot=d/dt), \tag{2}$$

or, equivalently,

$$i[H, q]=p, \quad i[H, p]=-\partial V/\partial q, \tag{2'}$$

imply, as a consequence, the commutation relation

$$i[p, q]=1, \tag{3}$$

has been considered by Wigner.[1] (As is customary, the symbol $[A, B]$ denotes the commutator $AB-BA$.) Wigner has shown that, if $V=q^2$, so that Eq. (1) is the hamiltonian for the one-dimensional harmonic oscillator, then Eq. (2) fails to imply Eq. (3), at least if certain requirements for operations with infinite matrices are assumed to be valid. Furthermore, he points out that Eq. (2) also fails to imply Eq. (3) for the case of the free particle ($V\equiv 0$) but that Eq. (2) does imply Eq. (3) in certain instances (see above). In the present paper an attempt is made to motivate the above results.

In the sequel, the symbols p and q and, more generally, "functions" A, B, C, $\cdots$, of p and q, are to be regarded as formal algebraic elements constituting a vector space over the complex numbers.[2] In addition it will be supposed that the product AB of two elements A, B is defined and that the distributive laws and the associative law

$$A(BC)=(AB)C \tag{4}$$

are valid. By an inverse, if it exists, of an element A will be meant an element A^{-1} with the property that $AA^{-1}=A^{-1}A=1$. (The above conditions all hold, of course, for finite or for infinite, but bounded, matrices; their validity, in certain quantum-mechanical instances, in which infinite, but unbounded matrices appear, apparently can be justified for physical reasons. It should be mentioned, however, that, for the case of infinite matrices, although all products appearing in Eq. (4) may exist, still Eq. (4) may fail to hold.[3]) It is to be emphasized that the above symbols are, in general, not to be interpreted as operators defined only on certain domains but only as "operators" insofar as the preceding assumptions are fulfilled.

Finally, by $V_q=\partial V/\partial q$ will be meant the function of q obtained by formal differentiation of $V=V(q)$. It is assumed, as is usual, that p and q are functions of the variable t, that the usual differentiation rules hold, and that, if $A=A(p, q)$, then

$$\dot{A}=i[H, A] \quad (\cdot=d/dt). \tag{5}$$

The following will be proved:

Theorem I. Suppose that both p^{-1} and q^{-1} exist. If the potential function $V=V(q)$ of (1) has the form

$$V=aq^n+b, \tag{6}$$

where a and b are constants, $a\neq 0$, and n is an odd integer, then Eq. (3) is a consequence of Eq. (2).

The proof of I will be obtained as a consequence of a more general result; namely:

Theorem II. Suppose that p^{-1} exists and that q commutes (under multiplication) with V and V_q. Suppose that there exist two sequences $a_1, a_2, \cdots$ and $b_1, b_2, \cdots$ of complex numbers and two sequences $j_1, j_2, \cdots$ and $k_1, k_2, \cdots$ of non-negative integers with the property that

$$\sum_\alpha (a_\alpha q+b_\alpha)V^{j_\alpha}V_q^{2k_\alpha}=0, \tag{7}$$

with the understanding that $V^0=V_q{}^0=1$. In addition, suppose that for the above system of constants,

$$\text{either } (\textstyle\sum_\alpha a_\alpha V^{j_\alpha}V_q^{2k_\alpha})^{-1} \text{ exists or both } q^{-1} \text{ and } (\textstyle\sum_\alpha b_\alpha V^{j_\alpha}V_q^{2k_\alpha})^{-1} \text{ exist.} \tag{8}$$

Then Eq. (2) implies Eq. (3).

The theorem II will be proved below. That II implies I is readily seen. For suppose V is defined by Eq. (6), so that $V_q=naq^{n-1}$; it is clear that q commutes

[1] E. P. Wigner, Phys. Rev. **77**, 711 (1950).

[2] For the axioms of such a space, see, for instance, H. Weyl, *The Theory of Groups and Quantum Mechanics* (E. P. Dutton and Company, Inc., New York, 1932), pp. 1–2.

[3] A. Wintner, *Spektraltheorie der Unendlichen Matrizen* (S. Hirzel, Leipzig, 1929), p. 131.

with V and V_q. If $n=2k+1$ and $j=2k-1$, one obtains

$$q(V-b)^j-\text{const}\,V_q^{2k}=0. \tag{9}$$

This follows from the equality $nj+1=2k(n-1)$. Relation (9) is seen to be of the form (7) where $\sum_\alpha a_\alpha V^{i\alpha}V_q^{2k\alpha}=(V-b)^j=(aq^n)^j$. Since q^{-1} exists by hypothesis, the first (as well as the second) condition of Eq. (8) holds and *II* implies *I*.

Proof of II. Let

$$B=i[p, q]. \tag{10}$$

It is to be shown that $B=1$. Since p commutes with p^2 and q commutes with V, Eq. (2′) can be written, in virtue of Eq. (1), as

$$i[p^2, q]=2p, \quad i[V, p]=-V_q. \tag{11}$$

The addition and subtraction of the quantity $ipqp$ to the left side of the first equation of (11) yields

$$pB+Bp=2p. \tag{12}$$

Multiplication of this equation by p on the left yields $p^2B+pBp=2p^2$, while multiplication on the right yields $pBp+Bp^2=2p^2$. Hence, we have $p^2B-Bp^2=0$. Differentiation of B of Eq. (10) with respect to t gives $\dot{B}=i(\dot{p}q+p\dot{q}-\dot{q}p-q\dot{p})$. An application of Eq. (2), together with the assumption that q commutes with V_q, then implies $\dot{B}=0$. Hence, by Eqs. (5) and (1), and the equation $p^2B-Bp^2=0$, it follows that

$$BV-VB=0. \tag{13}$$

Differentiation of Eq. (12) with respect to t and the use of Eq. (2) yield $BV_q+V_qB=2V_q$. Multiplications of this last equation by V_q on the left and on the right followed by a comparison of the resulting two equations give $BV_q^2-V_q^2B=0$. It readily follows from this relation and Eq. (13) that

$$BV^j-V^jB=0, \quad BV_q^{2k}-V_q^{2k}B=0 \tag{14}$$

holds for $j, k=0, 1, 2, \cdots$.

Assume first that $(\sum_\alpha a_\alpha V^{i\alpha}V_q^{2k\alpha})^{-1}$ exists for some system of constants specified in *II*. Multiplications of Eq. (7) by B on the left and on the right followed by a comparison of the resulting equations and the use of Eq. (14) imply $BqC=qBC$, where $C=\sum_\alpha a_\alpha V^{i\alpha}V_q^{2k\alpha}$; hence, since C^{-1} exists by assumption, one obtains $Bq=qB$. Since $\dot{B}=0$, differentiation of the last equation with respect to t and the use of Eq. (2) imply $Bp=pB$. It now follows from Eq. (12) and the assumption that p^{-1} exists that $B=1$, which was to be shown.

Next, suppose that q^{-1} and $(\sum_\alpha b_\alpha V^{i\alpha}V_q^{2k\alpha})^{-1}$ exist. Then multiply Eq. (7) by q^{-1} on the left so as to obtain

$$\sum_\alpha(a_\alpha+b_\alpha q^{-1})V^{i\alpha}V_q^{2k\alpha}=0.$$

Proceeding as above, one obtains $Bq^{-1}=q^{-1}B$. Multiplication of this equation by q on the left followed by a multiplication of the resulting equation by q on the right yields $Bq=qB$ as before. The remainder of the proof is identical with that given above and the proof of *II* is complete.

APPENDIX

I. It is interesting to note that certain polynomial potentials V, other than those given by Eq. (6) when n is odd, may also imply that Eq. (3) follows from Eq. (2). In fact, $V=aq^3+bq$, where at least one of the constants a, b is not zero, is such a potential. In order to see this, one need only verify that V satisfies

$$3VV_q^2+q(bV_q^3-27aV^2-4b^3)=0$$

and hence, provided that p^{-1} and the inverse of the parenthetical expression exist, satisfies the conditions of *II*.

II. Suppose that $V=q^n$, where n need not be an integer, is defined. Then, by Eq. (14), the relations

$$Bq^{jn}=q^{jn}B, \quad Bq^{2j(n-1)}=q^{2j(n-1)}B$$

hold. Thus, if (say) q^n is defined for $n=j^{-1}$ or if $n=(2j)^{-1}+1$, $j=\pm1, \pm2, \cdots$, the relation $Bq=qB$ holds and, provided p^{-1} exists, Eq. (2) implies Eq. (3) (see the last part of the proof of *II*).

Notice: Placement Register

The American Institute of Physics will conduct a Placement Service Register in connection with its 20th Anniversary Meeting in Chicago, Illinois, October 23–27, 1951, at the Hotel Sherman. Records of physicists seeking positions and descriptions of open positions will be available for inspection. Interviews will be arranged between registrants and employer representatives who are present. Employers should send to the Institute descriptions of openings which they wish to have posted on 8½×11 paper in multiple copies (15 required), or post them upon arrival at the meeting. Registrants seeking jobs should apply to the Institute for registration forms and further information by mail. In order to insure its inclusion at this Register, all material must be received at the Institute office, 57 East 55th Street, New York 22, New York, by October 1, 1951.

Letters to the Editor

PUBLICATION of brief reports of important discoveries in physics may be secured by addressing them to this department. The closing date for this department is five weeks prior to the date of issue. No proof will be sent to the authors. The Board of Editors does not hold itself responsible for the opinions expressed by the correspondents. Communications should not exceed 600 words in length.

A Search for Emission of Electron Pairs from Nuclei

G. C. PHILLIPS, D. B. COWIE, AND N. P. HEYDENBURG
Carnegie Institution of Washington, Department of Terrestrial Magnetism, Washington, D. C.
(Received July 9, 1951)

THE (p, α) process for F^{19} is known[1] to yield electron pairs from a 6.05-Mev excited state of O^{16}. That these electrons are of a nuclear origin appears to be established by their momentum distribution[2] and their angular correlation.[3,4] In analogy electron pairs that might result from the residual nuclei of (p, α) disintegrations were sought using anthracene crystals and 5819 photomultipliers for detectors. Fast amplifiers from each phototube fed a coincidence circuit whose resolving time was 10^{-8} sec. To check the apparatus, the $F^{19}(p, \alpha)O^{16}$ pairs were detected[4] using 2-Mev protons and are shown in Fig. 1. Thick targets of B, Na, Al, and P were bombarded with 1.55-Mev protons from the electrostatic generator. No true coincidences of soft radiation could be detected. A 7.9-Mev collimated proton beam from the cyclotron was used to bombard thick targets of Li, Be, Al, Ag, elemental enriched B^{10} (96 percent, obtained from the isotopes division, AEC, Oak Ridge), normal B, and C in a 1-mm wall aluminum chamber. The anthracene crystals were placed at 0° and 90° to the beam direction. A selsyn system allowed the insertion of aluminum absorbers between the 90° crystal and the ¼-inch target spot. The coincidence yields per μcoulomb of protons per 0.045 steradian,[5] corrected for accidental counting rates and room background are shown in Fig. 2. The accidental counting rates were determined by the insertion of lengths of coaxial cable in one channel, while the background due to the circulating beam was measured by turning off the deflector voltage. This background remained at about 5 counts per μcoulomb, while the accidental rate with zero absorber varied with target materials: F, 10; Li, 6; Al, 4; natural B, 2; B^{10}, 1; all others one.

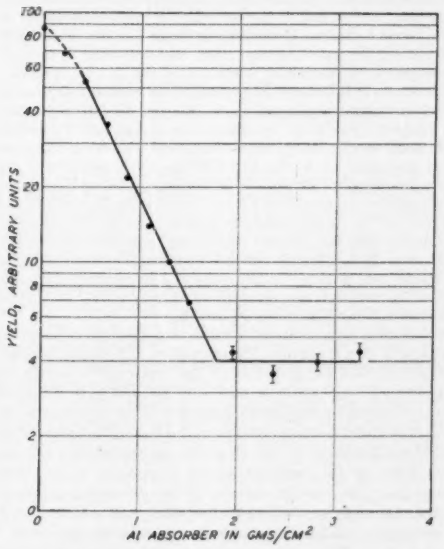

FIG. 1. The coincident yield as a function of aluminum absorber in front of one detector for the $F^{19}(p, \alpha, \gamma)O^{16}$ reaction, using a thin CaF_2 target and 2-Mev protons.

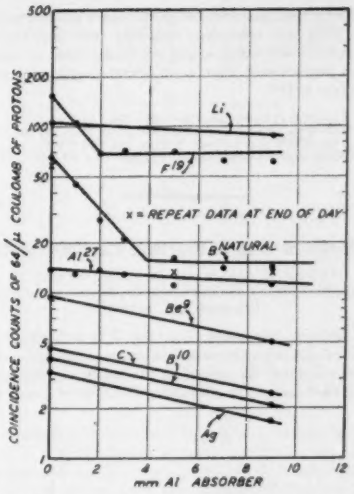

FIG. 2. Coincident yields as a function of aluminum absorber in front of one detector for the target elements indicated, using 7.9-Mev protons.

Since the single counting rates were high for all the targets, it can be anticipated that some photomultiplier fatiguing and saturation occurred. This possibility, resulting in a decreased energy sensitivity of the detectors, probably makes range measurements of no great quantitative significance. Assuming that this energy sensitivity is constant, however, the B^{11} shows electrons of total kinetic energy about 6 Mev, and a total energy for an electron pair of 7 Mev.

The lack of soft, true coincidences for Li and Al, whose capture gamma-energies should bracket the capture gamma-rays from B^{11}, and whose intensity was greater than for B^{11}, shows that the soft coincidences are probably not the result of externally or internally converted electron pairs. The effect cannot be attributed to scattered electrons between the crystals since a 142-mC radium-beryllium source placed at the target position gave a true rate of 56 and an accidental rate of 468. Thus this radiation gave single rates about 10 times greater than, and a true rate only comparable to, the target rates.

A search for radioactive coincidences was made for B^{10} and natural B^{11} targets by obtaining delay time-counting rate curves, or by shutting off the cyclotron rf simultaneous with starting a count. The delay curve for B^{11} was the same as for F^{19}, and for both boron targets no coincidences were observed after the shut off. This seems to eliminate $\beta-\gamma$- or $\gamma-\beta$-radioactivity as the cause of the soft component unless the life-time of the second component is comparable to 10^{-6} sec.

No angular correlations were taken; however, qualitatively the same soft component yield was observed at various angular separations.

It appears that B^{11} bombarded by protons produces a soft, true coincident radiation that cannot be due to $\beta-\gamma$-, $\gamma-\beta$-radio-

activity ($>10^{-6}$ sec half-life) nor from γ-rays producing pairs of electrons. This soft coincident radiation may indicate a pair emitting state in Be^{9} which would not be expected to have even parity and hence would have a considerably different character than the state in O^{16}.

[1] Streib, Fowler, and Lauritsen, Phys. Rev. **59**, 253 (1941).
[2] Chao, Tollestrup, Fowler, and Lauritsen, Phys. Rev. **79**, 108 (1950).
[3] Devons, Hereward, and Lindsey, Nature **164**, 586 (1949).
[4] G. C. Phillips and N. P. Heydenburg, Phys. Rev. **83**, 184 (1951).

The Ratio of L to K Electron Capture for Os^{185}

MAURICE M. MILLER AND ROGER G. WILKINSON
*Department of Physics, Indiana University, Bloomington, Indiana**
(Received June 25, 1951)

THE relative intensities of L and K x-radiation following orbital electron capture and subsequent internal conversion have been measured for several of the heavy elements, and the results for Os^{185} seem to be of interest. The ratio of L to K x-radiation was determined from the pulse height distributions obtained with a scintillation spectrometer. Typical K and L peaks are shown in Fig. 1. The amplifier gain was adjusted to make the statistical spread of the lines large in comparison with the 1.5-volt acceptance width of the differential discriminator. The intensity ratio is then obtained simply by comparison of the areas under the peaks, since for the crystal thickness used (0.4 to 0.8 cm) the efficiency of x-ray detection is essentially 100 percent if the "escape" peak area is added to the main peak area.[1]

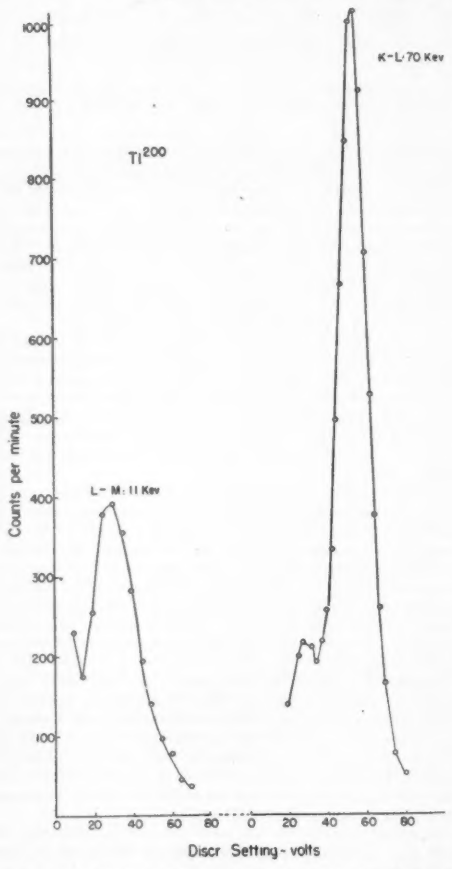

FIG. 1. Pulse height distributions for K and L x-radiation of Tl^{200} obtained with a 5819 RCA photomultiplier and a NaI(Tl) crystal. The peaks are studied in the same discriminator range by using greater amplifier gain for the L x-radiation.

The measured ratio of L to K x-radiation for Os^{185} was 0.40 $\pm$0.05. The estimated error arose mainly from the uncertainty of the gamma-ray background upon which the L peak lies, and also from the uncertainties in the amount of absorption of the L radiation in the source, the aluminum reflector, and the mineral oil film on the crystal. In the other decays investigated, the corresponding ratio was approximately 0.50 for Re^{184}, 0.58 for Tl^{199}, and 0.65 for Tl^{200}.

In the case of Os^{185}, the disintegration scheme (Fig. 2) has been studied by ordinary spectrometer methods[2] and the conversion of the 0.65- and 0.88-Mev gamma-rays is found to be negligibly small. The observed K and L x-rays arise only from orbital electron capture, and it is therefore possible to estimate the relative amounts of K and L capture. In order to deduce the L to K capture ratio from the observed ratio, it is necessary to know what fraction of the total L radiation is due to K capture. This requires a knowledge of the fluorescent yield, $(f_L)_K$, for transitions to the L levels following K capture. In addition, the fluorescent yield, $(f_L)_L$, for transitions to the L level following L capture, and the yield f_K for transitions to the K level must be known. If P_L and $P_K=1-P_L$ denote the probabilities of L and K capture, respectively, then the measured ratio, L/K, of the x-ray intensities is

$$L/K=[P_K(f_L)_K+P_L(f_L)_L]/P_Kf_K.$$

From this expression the ratio of L to K capture, P_L/P_K, can be calculated.

The fluorescent yields $(f_L)_K$ and $(f_L)_L$ can be evaluated from known x-ray data and from Kinsey's[3] calculated values of the partial fluorescent yields and radiationless transfer coefficients for the levels L_I, L_{II}, and L_{III}, providing the relative excitation of the L levels is known. The ionization of the L levels following K capture will be quite different from that following L capture. Following K capture alone, ionization of the L_I, L_{II}, and L_{III} levels occurs in 0, 25, and 50 percent of the events, respectively. These percentages are based on the K_α and K_β intensity ratios for tungsten ($Z=74$) as determined by Duane and Stenström[4] and should be very nearly correct for $Z=75$. Following L capture alone, ionization of the L_I, L_{II}, and L_{III} levels would be in the approximate ratio 100:10:1. After correcting the partial fluorescent yields, as suggested by Kinsey, one obtains $(f_L)_K=0.24$ and $(f_L)_L=0.28$. No explicit measurements of f_K for $Z=75$ are known. Germaine[5] finds the yield to be 0.90 for transitions following K capture in At^{211}, although this is lower than the predicted value of Massey and Burhop.[6] In the range of Z in question, the variation of f_K with Z is not expected to be very rapid,[6] so that an estimate of 0.85$\pm$0.05 seems reasonable.

From these considerations a value of 0.35$\pm$0.15 is found for the ratio of L to K capture. The calculation of Rose and Jackson[7] interpolated at $Z=76$ gives 0.14 for the square of the ratio of the $2s$ to $1s$ wave functions at the nuclear radius. The L_I to K capture ratio is obtained by multiplying this quantity by the square of the ratio of neutrino energies involved in the L_I and K capture if the transitions are allowed. This factor can be appreciably different from unity, as the experimental results indicate, if very little energy is available for the capture. It is to be concluded that the orbital capture energy feeding the 0.88-Mev level in Re^{186} (Fig. 2) is sufficiently small to account for an appreciable amount of L capture. In addition, the energy-dependent factor is somewhat different from unity even for capture feeding the 0.65-Mev level. In fact, if one assumes that the measured L to K capture ratio

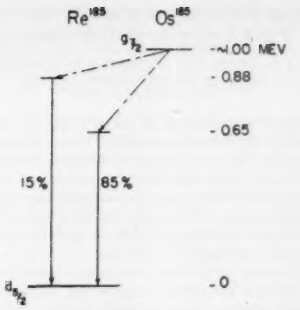

FIG. 2. Disintegration scheme of Os^{185}.

and the disintegration scheme are correct, the atomic mass difference between Os^{185} and Re^{185} may be estimated. This turns out to be about 1.0 Mev if the transition to the 0.88-Mev level is assumed to be first-forbidden, and slightly lower for an allowed transition.

The fraction of the total K capture to the ground state has been reported[8] to be no greater than 0.10. The amount of L capture feeding the excited states could not be estimated at that time and hence was not considered. The presence of L capture changes this value to 0.20, but does not essentially alter the interpretation of this transition as first-forbidden, in agreement with the shell model.

* This work was assisted by the joint program of the ONR and AEC.
[1] West, Meyerhof, and Holstadter, Phys. Rev. **81**, 141 (1951).
[2] Bunker, Canada, and Mitchell, Phys. Rev. **79**, 610 (1950).
[3] B. B. Kinsey, Can. J. Research **26**, Sec. A (1948).
[4] W. Duane and W. Stenström, Proc. Natl. Acad. Sci. U. S. **6**, 477 (1920).
[5] Lawrence S. Germaine, Phys. Rev. **80**, 937 (1950).
[6] H. S. W. Massey and E. H. S. Burhop, Proc. Roy. Soc. (London) **A153**, 661 (1936).
[7] M. E. Rose and J. L. Jackson, Phys. Rev. **76**, 1540 (1949).
[8] M. Miller and R. Wilkinson, Phys. Rev. **82**, 981 (1951).

The Radiations of Tl^{199} and Tl^{200}

HARVEY I. ISRAEL AND ROGER G. WILKINSON
*Indiana University, Bloomington, Indiana**
(Received July 6, 1951)

THE internal conversion electron spectrum of $Hg^{199,200}$ resulting from the orbital electron decay of $Tl^{199,200}$ has been studied with a small 180° shaped field spectrometer. The thallium isotopes were produced by alpha-particle bombardment of gold in the Indiana University cyclotron, and were separated from the target material by standard chemical procedure. Carrier-free sources were obtained by electrodeposition of the thallium from a solution containing no gold or mercury. With a plating current of 150 ma, the major part of the activity was deposited on the platinum electrode within one to two hours. The deposit was removed from the electrode with nitric acid and laid down by evaporation on a thin zapon film.

A survey of the negatron spectrum showed the presence of twenty-five internal conversion lines, all of which decayed in intensity with either the 7-hour half-life of Tl^{199} or the 27-hour half-life of Tl^{200}. An analysis of the conversion lines of Tl^{199} shows that they arise from nine gamma-rays of energies 49, 78, 103, 157, 206, 245, 332, 454, and 490 kev. For Tl^{200} the observed conversion lines correspond to six gamma-rays of energies 365, 577, 622, 829, 1210, and 1360 kev. The figures quoted are accurate to within one percent.

In the case of Tl^{199} the results are in agreement with those of Hole,[1] who has found gamma-rays at 155 and 360 kev associated

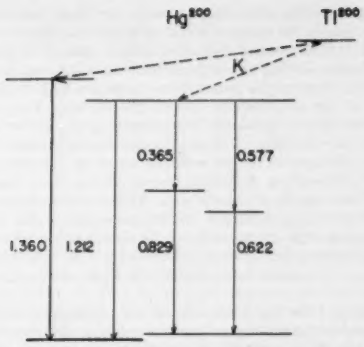

FIG. 1. A possible disintegration scheme for Tl^{200}. It is to be noted that the 1.212-Mev gamma-ray is not the cross-over for the cascade gamma-rays. The assignment of the 15-kev discrepancy as shown is arbitrary.

with an isomeric 43-minute activity in Hg, which has been assigned[2] to Hg^{199}. Scintillation spectrometer studies offer further evidence that these gamma-rays are coupled. It is found that the 157- and 332-kev gamma-rays are of about the same intensity and are probably in cascade. The 490-kev gamma-ray may be interpreted as the cross-over for these transitions. Similarly, the 245- and 206-kev gamma-rays are about equal in intensity and may be regarded as a cascade pair, with the 454-kev gamma-ray resulting from the alternative cross-over transition.

The first five gamma-rays of Tl^{199} listed above have essentially the same energies as those reported in a study[3] of the beta-decay of Au^{199} to Hg^{199}. It therefore appears that the decay scheme proposed by Beach *et al.* should be altered to take into account the higher levels which are evident in the K-capture process. Further work on this matter is in progress.

The energies of the gamma-rays of Tl^{200} are consistent with the tentative decay scheme shown in Fig. 1. While the absorption work of Cuffey[4] in this laboratory supports this picture, further study of the conversion electron spectrum in the low energy region and a complete study of the photoelectron spectrum are necessary before this scheme can be considered as certain.

No positrons were found in the case of either Tl^{199} or Tl^{200}.

* This work was assisted by the joint program of the ONR and AEC.
[1] N. Hole, Arkiv. Mat. Astron. Fys. **36A**, No. 9 (1948).
[2] "Nuclear data," Natl. Bur. Standards (U. S.) Circ. 499 (1950).
[3] Beach, Peacock, and Wilkinson, Phys. Rev. **76**, 1585 (1949).
[4] William Cuffey (to be published).

Electron Mobilities in Liquid Argon*

M. S. MALKIN AND H. L. SCHULTZ
Sloane Physics Laboratory, Yale University, New Haven, Connecticut
(Received July 16, 1951)

THE work of Gerritsen,[1] of Davidson and Larsh,[2] and of Hutchinson[3] has shown that conductivity pulses due to ionizing radiation may be observed in liquid argon. Using a parallel plate chamber immersed in liquid argon, we have measured the mobility of electrons resulting from the ionization of liquid argon by the alpha-particles of ThC and ThC′.

The chamber was similar to that described by Davidson and Larsh,[2] with the plates ¼ inch in diameter and separated by various sizes of spacers made of Teflon. The source ThB was collected on the bottom plate by recoil. Commercial tank argon, supplied by Linde, and stated to be 99.91 percent pure, was liquefied by means of a small heat exchanger immersed in liquid air. Further purification was not undertaken.

Pulses resulting from electron collection were amplified and used to trigger the sweep of a fast synchroscope. They were also applied to the vertical deflection plates through a length of coaxial cable serving as a 0.2-microsecond delay line. The combined rise time of the preamplifier, amplifier, and vertical amplifier of the synchroscope is 0.02 microsecond. This is short compared with the pulse rise times observed, which were between 0.2 and 0.4 microsecond. Using a Kodak Retina camera (1 sec at f:3.5), photographs of the resulting traces at different counter voltages were taken. A straight line parallel to the average slope of the trace was drawn on the print. This line was extended from zero to maximum amplitude, and the projection of this line onto the time base line corresponded to the rise time. The sweep speed was approximately 6 inches per microsecond. In determining the rise time, corrections were made for the slight nonlinearity of the sweep.

To correct for the penetration of the alpha-particles into the chamber, the center of gravity of the resulting electron cloud was calculated. The center of gravity of the electrons produced by the 8.78-Mev alpha-particle of ThC′ is 0.038 mm from the source plane. The drift space is the distance from the center of gravity to the collecting electrode. From these data the drift velocity and the mobility were computed.

In Fig. 1, the mobility U *versus* the field is plotted for two plate separations (0.185 and 0.107 cm). The dotted curve is

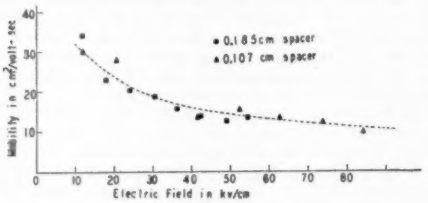

FIG. 1. Electron mobility U *vs* electric field E in liquid argon. The dashed curve is calculated for U proportional to $E^{-\frac{1}{2}}$ and fitted at one point.

calculated, assuming the mobility to be proportional to $E^{-1/2}$, where E is the field strength. The agreement here is well within the experimental accuracy, estimated to be about 15 percent.

Based on kinetic theory considerations, the formula for the mobility is

$$U=c^{3/4}(mM)^{-1/4}(e\lambda)^{1/2}E^{-1/2},$$

where m is the electron mass, M the mass of the argon atom, e the electronic charge, λ the mean free path. The constant c, which various corrections make uncertain, lies between $\frac{1}{2}$ and $\frac{2}{3}$. The value of λ may be calculated from this formula. The collision cross section q may be calculated from the general relation:

$$Nq\lambda=1,$$

where N is the number of argon atoms per cc. According to the reasoning which leads to the mobility formula above, the mean energy of the electrons is about 10 ev. The collision cross section obtained in this manner for electrons of 10 volts mean energy is about 100 times smaller than the published values[4] for the gas.

Preliminary results in solid argon indicate an electron multiplication by a factor greater than 10, in agreement with Hutchinson's work. The mobility in the solid is much greater than that in the liquid. Conductivity pulses have also been observed in liquid helium, and measurements are being continued in solid argon and liquid and solid helium.

We wish to thank Professor H. Margenau for numerous discussions concerning the theoretical aspects of the problem.

* Assisted by the joint program of the ONR and AEC.
[1] A. N. Gerritsen, Physica **14**, 381 (1948).
[2] N. Davidson and A. E. Larsh, Jr., Phys. Rev. **77**, 706 (1950).
[3] G. W. Hutchinson, Nature **162**, 610 (1948).
[4] R. S. Brode, Revs. Modern Phys. **5**, 263 (1933).

The Angular Distribution in the Photodisintegration of the Deuteron at Low Energies

G. R. BISHOP, L. E. BEGHIAN, AND H. HALBAN
Clarendon Laboratory, Oxford, England
(Received July 9, 1951)

THE angular distribution of the protons and neutrons produced in the photodisintegration of the deuteron has been determined by a number of authors[1-3] and for several γ-ray energies. So far the precisions of these measurements do not permit the establishment of agreement or disagreement between theory and experiment. The main difficulty arises from the low intensity obtained in experiments where sufficient angular definition of the photonucleons was provided.

We have made measurements with a new method, giving higher intensities. In this method one makes use of the fact that the energy of the photonucleons depends on the angle relative to the disintegrating γ-ray at which they are ejected (conservation of the linear momentum of the γ-ray). The energy of a photoproton in laboratory coordinates is:

$$E_p=\tfrac{1}{2}(E_\gamma-E_T)+\frac{E_\gamma^2}{8Mc^2}+\frac{E_\gamma}{2}\left(\frac{E_\gamma-E_T}{Mc^2}\right)^{\frac{1}{2}}\cos\theta.$$

The number of photoprotons ejected into unit solid angle at angle θ is:

$$I_\theta=(a+b\sin^2\theta),$$
$$a=\sigma_m,\quad b=\tfrac{3}{2}\sigma_e,$$

where θ is the angle between the photoproton and the incident quantum in center-of-mass coordinates. Combining these two equations we obtain the relation for Y_x, the number of protons per unit energy interval at energy x,

$$Y_x=A\{a+b-(b/\alpha^2)(x-d)^2\},$$

where $\alpha=\frac{1}{2}E_\gamma[(E_\gamma-E_T)/Mc^2]^{\frac{1}{2}}$, $d=\frac{1}{2}(E_\gamma-E_T)$, and A is a factor depending on the γ-ray flux, the number of deuterium nuclei per unit volume, and the wall effect. Table I shows the expected energy spread for the three γ-ray sources used in our measurements.

Originally this effect was established qualitatively with a deuterium-filled ionization chamber.[4] For the present measurement we used a proportional counter, to eliminate the positive ion effects, and to reduce the amplifier noise to negligible proportions.

The counters consisted of a long cylinder of copper or aluminium closed at each end by caps carrying Kovar-glass seals. The center wire was passed through these seals and connected to the first valve of an amplifier. Great care was taken to insure that the wires were central. X-ray radiographs showed that the wires were axial to within 1/10 mm. The sensitive volume of the counter was defined by thickening the center wire in the usual way. The end effects were reduced to 1 percent by using a long counter 30 cm in length, of diameter 2.54 cm, and placing the source at the middle.

The pressure of deuterium in the counter had to be adjusted for each γ-ray energy so as to avoid too high a γ-ray background on the one hand and too large a wall effect on the other.

The output pulses were examined with a kicksorter of the Wilkinson type. Distributions from each counter under various conditions of pressure and relative γ-background were in excellent agreement. Pulse heights were expressed relative to a standard pulse; the energy calibration in kev was established using the fact that the peak of the distribution occurs at the average photoproton energy [Eq. (1)]. Agreement to 0.5 percent was obtained

TABLE I. Expected energy spread for the gamma-ray sources used.

Source	Energy of protons	Spread of energy
Na^{24}	$E_p=(265.5\pm32.9\cos\theta)$ kev	±12.4%
ThC''	$E_p=(194\ \pm26.6\cos\theta)$ kev	±13.7%
Ga^{72}	$E_p=(138.5\pm21.6\cos\theta)$ kev	±15.6%

for the ratios of average pulse height to the expected ratio of average photoproton energy. For sources of about 10 mC, distributions were recorded with counting rates at the peak of about 60/min. A least squares fit parabola was calculated for each distribution; a dozen distributions were investigated for each γ-ray energy.

Corrections are made for the finite channel width of the kick-sorter, and for the spread in pulse height caused by the statistical nature of the multiplication process.[5] A correction for non-centrality of the wire was investigated by calculating the change in field strength it produces and using measured curves of multiplication *versus* high voltage. The correction never amounted to more than 0.05 percent of the average pulse height. The most serious correction is that made for the statistics of the multiplication process. This increases the final value of σ_m/σ_e for Na^{24} by 10 percent, for ThC'' by 8 percent and for Ga^{72} by 6 percent. The errors calculated for curve fitting are ± 3 percent each for Na^{24} and Ga^{72}, and ± 2 percent for RdTh.

Final answers (assuming validity of the above-mentioned correction for statistical spread) are listed in Table II.[6-8]

TABLE II. Ratio of photomagnetic cross section to photoelectric cross section.

Source	σ_m/σ_e Present work	Previous experiments	Meson theories[a]	Effective range theory[b,c]
Na^{24}	0.247 ± 0.007	0.30 ± 0.02[d]	0.234	0.254
ThC''	0.360 ± 0.008	0.39 ± 0.12	0.369	0.395
Ga^{72}	0.600 ± 0.02	0.61 ± 0.04	0.585	0.67

[a] See reference 6.
[b] See reference 7.
[c] See reference 8.
[d] Average of references 1.

We wish to thank Lord Cherwell for all the encouragement given to us. This work was made possible by a grant from the Paul Foundation Fund of the Royal Society.

[1] F. Genevese, Phys. Rev. **76**, 1288 (1949). E. P. Meiners, Phys. Rev. **76**, 259 (1949). N. O. Lassen, Phys. Rev. **74**, 1533 (1948); **75**, 1099 (1949). W. M. Woodward and I. Halpern, Phys. Rev. **76**, 102 (1949). B. Hamermesh and H. Wattenberg, Phys. Rev. **76**, 1408 (1949).
[2] C. A. R. Graham and H. Halban, Revs. Modern Phys. **17**, 297 (1945).
[3] Bishop, Halban, Shaw, and Wilson, Phys. Rev. **81**, 219 (1951).
[4] Bishop, Collie, Halban, Hedgran, Siegbahn, du Toit, and Wilson, Phys. Rev. **80**, 211 (1950).
[5] O. R. Frisch, *Statistics in Multiplicative Processes.*
[6] I. Hansson and L. Hulthén, Phys. Rev. **76**, 1163 (1949). We are obliged to Dr. Nagel, who communicated to us the latest corrections to this theory.
[7] H. Bethe and C. Longmire, Phys. Rev. **77**, 647 (1950).
[8] E. E. Salpeter, Phys. Rev. **82**, 60 (1951).

The Angular Distribution of V^0-Particle Decay Products*

W. B. FRETTER
Department of Physics, University of California, Berkeley, California
(Received July 16, 1951)

IN a series of 20,000 cloud-chamber photographs taken at sea level approximately 800 penetrating showers were seen in 16 months and in these there were 37 V^0-particles and 8 $V^{\pm}$-particles. The arrangement of lead in the cloud chamber was changed from time to time in the hope of making the detection of V-particles more probable. In a multi-plate chamber it is essential to have the plates widely spaced since the particles are observed to decay in the gas. It is also important to have a triggering arrangement that trips on low energy penetrating showers as well as high energy events. The high energy events are usually so complicated as to make the observation of V-particles very difficult.

The cloud chamber has seven $\frac{1}{2}$-inch lead plates spaced $2\frac{1}{2}$ inches apart, illuminated depth 5 inches and useful width 16 inches. The counter arrangement required that one (and only one) counter be tripped in the top tray of 5 one-inch counters and the two lower 2-inch counters side by side simultaneously be tripped. Many electron showers are eliminated by the anticoincidence.

A study has been made of 26 V^0 events in which the plane of the V^0 appeared to contain the point where the original event occurred. In many cases the ionization and scattering of the particles, together with the angles made with the line of the V^0 indicated that the decay particles must have had quite different masses. The events were then analyzed on a simple assumption, namely, $V^0 \rightarrow p + \pi^-$. Curves were drawn giving the angular distribution of the proton and meson in the laboratory system for various values of the velocity β_0 of the V^0 and for various angles φ^* of emission of the particles in the moving system. Two mass values of the V^0 were chosen: $2170m_e$ and $2390m_e$, and separate sets of curves were drawn for each assumed mass value.

The procedure was then to take the measured values of angles in the laboratory system and try to find a single set of values of β_0 and φ^* for each observed pair of angles. It turned out that in all cases except one it was possible to determine the identity of the particles just by knowing the angles; the proton almost always makes the smaller angle. Thus for a given choice of the mass of the V^0 a set of values of β_0 and φ^* was obtained. It was immediately clear that something was wrong since only three out of 26 values of φ^* were less than 90°. Thus under these assumptions the protons had to come out predominantly in the backward direction in the moving system, and changing the mass of the V^0 to $2390m_e$ had no effect on the situation (although the β_0 values had to change). The difficulty is that the measured angles are more nearly equal to each other than is to be expected when the masses of the particles differ as much as do those of a proton and meson.

The possibility arises that some of the processes are $V^0 \rightarrow \pi^+ + \pi^-$ and that this distorts the angular distribution. Another possibility is that the process is a three-body decay and, as Leighton, Wanlass, and Alford[1] have pointed out, the coplanarity is coincidental. As pointed out by T. D. Lee, a possible three-particle decay is $V^0 \rightarrow p + \mu + \nu$. With an excitation energy of about 140 Mev and a lifetime of 10^{-10} sec, the coupling constant turns out to be 2×10^{-48} erg cm^3. It is somewhat remarkable that this coupling constant is of the same order of magnitude as that used in the β-decay of the nucleons and the μ-mesons and the interaction of the nucleons with the μ-mesons.[2,3] It can also be shown that the neutrino and the meson tend to come out in the same direction because of phase space limitations. This would have the effect of reducing the momentum of the meson in the moving system and thus removing the difficulty with the angular distribution.

A trial calculation has been made to check this, using the simplifying assumption that the neutrino and meson go off in the same direction and share the momentum equally. The angular distribution inferred under these assumptions is spherically symmetrical in the moving system.

I am indebted to Dr. Tsung Dao Lee for stimulating discussions and for communicating some results of his calculations on the theoretical aspects of this problem.

* Assisted by the joint program of the ONR and AEC.
[1] Leighton, Wanlass, and Alford, Phys. Rev. **83**, 843 (1951).
[2] J. Tiomno and J. A. Wheeler, Revs. Modern Phys. **21**, 153 (1949).
[3] Lee, Rosenbluth, and Yang, Phys. Rev. **75**, 905 (1949).

Erratum: Magneto-Optics of an Electron Gas with Guided Microwaves

[Phys. Rev. **82**, 956 (1951)]

L. GOLDSTEIN, M. LAMPERT, AND J. HENEY
Federal Telecommunication Laboratories, Inc., Nutley, New Jersey

PARTS of the caption to Fig. 1 should read as follows: Gas: Ne+1 percent A at 1 mm Hg. Signal pulse 50 μsec after 5 μsec dc discharge pulse.

Li^9—New Delayed Neutron Emitter*

W. L. Gardner, N. Knable, and B. J. Moyer
Radiation Laboratory, Department of Physics, University of California, Berkeley, California
(Received July 9, 1951)

AN investigation has been made of a new delayed neutron activity from targets bombarded in the Berkeley 184-inch cyclotron beam. When the daughter product of a beta-decay is neutron unstable, the neutron comes out immediately. Because the decay in neutron intensity is then the same as that of the beta-particle, this process is usually referred to as delayed neutron emission. Only one other delayed neutron emitter, N^{17}, is known[1] outside of the fission products.

Deuteron bombardment of Be and of elements immediately above it, and proton bombardment of B and of elements immediately above it, give rise to such neutrons displaying a decay in intensity with a 0.168-sec half-life.

The targets were 1¼-in. diameter cylinders of approximately 3-in. length, placed in the external beam of the cyclotron. A BF_3 ion chamber embedded in paraffin surrounded the target. A low noise triode preamplifier was used which was coupled into a standard linear amplifier, giving an over-all gain of 5×10^6. The neutron detection efficiency for RaBe neutrons was 5 percent.

The half-life measurement was made by irradiating the target for several seconds, shutting the cyclotron off, and recording the decaying neutron activity by photographing the pulses displayed on an oscilloscope. The activity was followed over more than 5 half-lives, and a complete record of the position of each event in time was secured on the film. The resolution of the equipment was 10 μsec. About 500 pulses per cycle were obtained with a boron target under deuteron bombardment. The results of these measurements give a half-life as shown in Fig. 1 of $T_{\frac{1}{2}}=0.168\pm0.004$ sec. The cross section for this reaction for deuterons on boron is approximately 4 millibarns.

The elements from Li through N were surveyed for this activity, using both protons and deuterons. The relative yields/atom for the various elements are:

	Li	Be	B	C	N	Ratio B/Be
deuterons	<2	45	100	10	3	2.2
protons	<2.5	<2.5	100	13	5	>40.

A Cu target was also used as one type of background determination. The relative copper to boron yield/atom ratio was less than 1 percent. From the above table it is seen that the relative yield under deuteron bombardment is appreciable beginning with Be, while under proton bombardment the yield is not significant until boron is used. That is, within the accuracy allowed by the background; this activity is induced by deuterons on Be, but not by protons. An examination of the isotope chart indicates the most likely reaction to be

$$Be^9+d\rightarrow Li^9+2p$$

under deuteron bombardment.

The fact that under proton bombardment the lightest element to yield the neutrons is boron is also consistent with the Li^9 assignment, assuming

$$B^{11}(p,3p)Li^9.$$

The Li^9 decay scheme is assumed to be

$$Li^9\rightarrow Be^{9*}+\beta^-$$
$$Be^{9*}\rightarrow Be^8+n.$$

Evidence for an excited level in Be^9 which is unstable to neutron emission has been given by Davis and Hafner.[2] The Be^8 breaks up immediately into two alphas, and, the possibility of investigating the neutron-alpha-coincidence as a corroboration of this decay scheme is being considered.

Li^9 and the above decay scheme hold an analogous position in the isotope chart to that of N^{17}. A mass calculation of Li^9 by Barkas[3] permits a threshold for this reaction to be estimated as $\leqq$18.5 Mev. Experimental data on this point were secured by moving a Be target in along the radius of the cyclotron gap with a deuteron beam. The excitation function is shown in Fig. 2. Theoretical indications that this function is of the form $N=k_1(E-E_t)^2$ are further substantiated by the fact that a straight line is a good fit to the experimental points replotted as $\sqrt{N}=k(E-E_t)$. The threshold determined from this intercept is 19±1 Mev, which is in agreement with the calculated threshold. The Li^9 mass indicates that an electron energy of ~11 Mev is quite likely. An attempt to measure a high energy electron in coincidence with the neutron has not yet been successful.

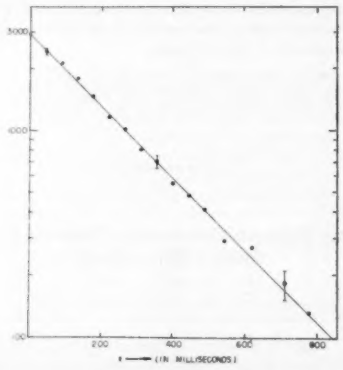

FIG. 1. Neutron decay.

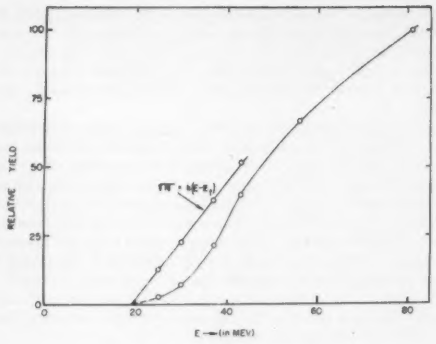

FIG. 2. Excitation function.

* This work was performed under the auspices of the AEC.
[1] L. Alvarez, Phys. Rev. **75**, 1127 (1949).
[2] K. E. Davis and E. M. Hafner, Phys. Rev. **73**, 1473 (1948).
[3] W. H. Barkas, Phys. Rev. **55**, 691 (1939).

Beta-Ray Spectrum of K^{40}

Myron L. Good
*Department of Physics, Duke University, Durham, North Carolina**
(Received July 12, 1951)

THE beta-ray spectrum of K^{40} has been measured by observing the distribution in size of the light flashes which are generated in a crystal of KI-Tl by the natural radioactivity of the

potassium content of the crystal. The crystal, 5.26 g of optically perfect Harshaw KI (0.5 percent Tl added to the melt) gave a total K^{40} beta-count of about 2000 counts/minute. The crystal gave pulses about one-fifth as large as NaI-Tl pulses of the same energy. The energy resolution width was greater than that of NaI-Tl by the square root of the pulse size ratio.

The Jordan and Bell amplifier was used, modified to employ delay line pulse shaping. At the pulse width used (3 μsec) the slow components of the light decay in KI-Tl[1] yielded delayed pulses of about the same size as the thermionic emission background of the photomultiplier tube. This indicated that the mean time interval between photoelectrons of the slow components was greater than the amplifier pulse width, so that the delayed pulses were essentially of single-electron size. These slow component pulses were too small to affect the experiment. The fast component, on the other hand, decayed in much less than the amplifier rise time used (1 μsec).

The energy calibration and resolution width were determined from the photopeak of the annihilation radiation of Cu^{64}. Background ($\approx$1 percent) was measured with the aid of a NaI-Tl crystal. The small ($\approx$2 percent) effect of the detection by the crystal of its own K^{40} gamma-radiation (1.46 Mev) was calculated, using the known gamma-ray rate,[2] the geometry, and a pulse-height distribution obtained with an external gamma-ray source (K^{42}, 1.51 Mev).[3] The beta-ray distribution was corrected for resolution.[4] A further distortion of the spectrum exists, caused by those beta-particles which emerge from the surface of the crystal. A method was developed whereby this distortion could be approximately calculated, using an empirical electron range-energy curve. The energy distribution was then corrected for this effect, and a Kurie plot analysis made.

An "allowed" plot of the data, not corrected for resolution or the above-mentioned surface effect, is shown in Fig. 1. The convexity of this plot is a good indication that the deviation from an allowed shape is real. The "allowed" plot of the corrected data Fig. 2 ($c=1$), is quite nonlinear. The result of applying the unique axial vector or tensor theoretical correction factor corresponding to the known spin change of four, and assuming a parity change, is shown in Fig. 2 ($c=c$). The fit to a straight line is quite good, in agreement with recent measurements.[5-7] However, the deviations from linearity are much smaller in the present experiment. This confirmation, by a different method, of agreement with theory for a third-forbidden transition, further strengthens the evidence for the correctness of either the axial vector or tensor interaction in beta-decay.

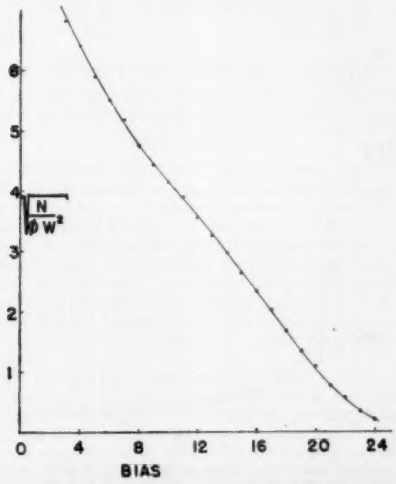

FIG. 1. "Allowed" Kurie plot of uncorrected data.

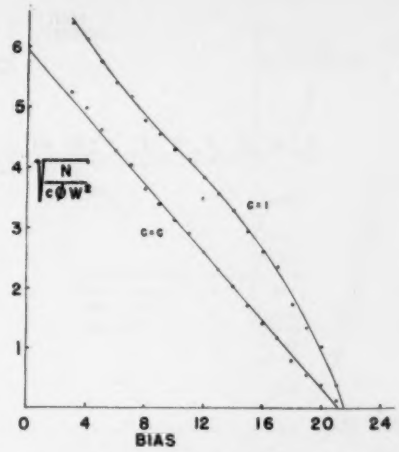

FIG. 2. Kurie plot analysis of corrected data.

The end point energy obtained is 1.28$\pm$0.03 Mev, somewhat lower than previous measurements.[5-7]

The linearity of the Kurie plot allows an extrapolation of the total counting rate to zero energy to be made easily. In this way the beta-decay rate was measured as 27.1$\pm$0.6 betas/sec/gram K, or $\lambda_\beta = 4.67\pm0.15\times10^{-10}$ yr^{-1} (using the relative abundance K^{40}/K of $1.19\pm0.01\times10^{-4}$ given by Nier[8]). This has been corrected for all the effects mentioned above, using integral forms of the corrections. The value is in agreement with that of Sawyer and Wiedenbeck,[9] who also used a 4π geometry. They obtained 28.3$\pm$1.0 betas/sec/gram K.

The author wishes to express his indebtedness to Dr. Henry W. Newson for his helpful supervision of this work.

* This work was supported in part by contracts with the ONR and AEC.
[1] Smallers, May, and Freedman, Phys. Rev. **79**, 940 (1950).
[2] G. A. Sawyer and M. L. Wiedenbeck, Phys. Rev. **76**, 1535 (1949).
[3] K. Siegbahn, Arkiv. Mat. Astron. Fys. **34B**, No. 4 (1947).
[4] G. E. Owen and H. Primakoff, Phys. Rev. **74**, 1406 (1948).
[5] Bell, Weaver, and Cassidy, Phys. Rev. **77**, 399 (1950).
[6] D. E. Alburger, Phys. Rev. **78**, 629 (L) (1950).
[7] L. Feldman and C. S. Wu, Phys. Rev. **81**, 298 (1951).
[8] A. O. Nier, Phys. Rev. **77**, 789 (1950).
[9] G. A. Sawyer and M. L. Wiedenbeck, Phys. Rev. **79**, 490 (1950).

Contribution to the Theory of Impurity Centers in Silicon

WALTER BALTENSPERGER
Swiss Federal Institute of Technology, Zürich, Switzerland
(Received July 9, 1951)

AN electron bound to an impurity is usually treated like a hydrogen atom in which the electrostatic force is reduced by the dielectric constant ϵ of the crystal.[1] We shall use a more detailed treatment for a phosphorus impurity in silicon.

The electron moves in the field of the ion, in the dipole field of the polarized atoms, and in the periodic field of the crystal. The atoms are polarized by the ion and electron charge and by all other dipoles. The polarizability of a silicon atom $\alpha = 3.81A^3$ is obtained from the equation of Clausius-Mosotti with $\epsilon = 13$. The

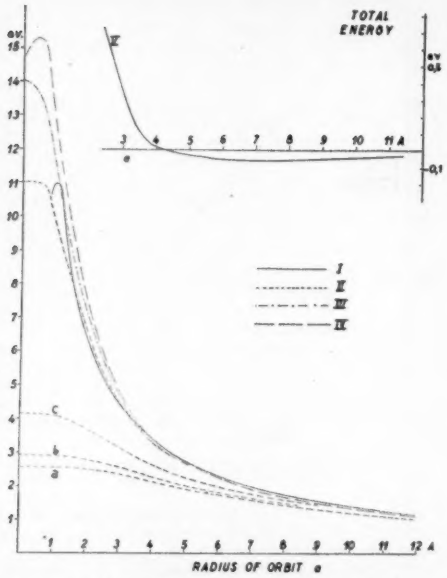

FIG. 1. (I) Negative energy of the electron bound to a free phosphorus atom. (II) Energy of the electron in the dipole field arising from the ion charge. There are contributions from the continuum of distant (>5.16A) dipoles (a), from 12 dipoles at 4.49A (b−a), from 12 dipoles at 3.38A (c−b), and from 4 dipoles at 2.27A (II−c). (III−II) Energy arising from the difference of polarizability of a P-ion with respect to a Si-atom. (IV−III) Energy in the periodic potential of the crystal. (V) Total energy = IV−I. The minimum is −0.065 ev at $a=7$A.

28 nearest silicon atoms are considered explicitly; those farther away are treated as a continuum. The dipole moments due to the ion and the inner field are calculated making use of symmetry. For the electron-dipole field we take an approximation of the radial component of the ion-dipole field, namely,

$$F(d)=(e/d^2)\beta(d);\quad \beta(d)=\begin{cases}1-(d/C)^3 & \text{for } d<5.16\text{A};\quad C=5.37\text{A}\\ 1/\epsilon=0.077 & \text{for } d>5.16\text{A}\end{cases}$$

and then assume that the electron-dipole field is the same expression, where d is the distance from the electron.

The method consists in minimizing the energy for the hydrogen-like wave function $\psi(r)=(\pi a^3)^{-1/2}e^{-r/a}$ with respect to the radius a.

The sum of kinetic energy $\hbar^2/2ma^2$ and potential energy $-e^2/a$ of the electron in the field of the ion must be slightly altered to give an ionization potential of 10.9 ev for free phosphorus (curve *I* of Fig. 1). This first energy is negative. The other energy terms are all positive. Second term: the energy of the electron in the dipole field arising from the ion charge (curve *II*) leaves a weak bond for $a=7$A and a stronger one for $a=1$A. Third term: the energy of the electron in the dipole field arising from the electron itself is different in the bound and conducting states. Namely, the bound electron acts on the phosphorus ion, whose polarizability is taken to be smaller than that of a silicon atom by a factor $(14/15)^3$. For calculation of the resulting repulsion from the ion (*III–II*) cut-off radii $R_{P+}=1.10$A for a phosphorus ion and $R_{Si}=1.17$A for a silicon atom are assumed, within which there are no forces between the electron and the dipole. Incidentally, the potential energy of a conduction electron in the field of the dipoles which it induces becomes −10.0 ev, corresponding to an image-force barrier. Fourth term: it is found that a periodic potential in the crystal changes the energy only for small a (*IV–III*).

In the above model the minimum of the total energy is −0.065 ev for $a=7$A, in essential agreement with experiment[2] and with the simple theory. It is only by taking all effects together that a bond with small a is excluded; but once the orbit is large, the phenomenological theory holds.

I wish to express my gratitude to Professor W. Pauli for his kind support, to Professor G. Busch for suggesting the problem, and to Dr. R. Schafroth for much helpful advice.

[1] H. C. Torrey and C. A. Whitmer, *Crystal Rectifiers* (McGraw-Hill Book Company, Inc., New York, 1948), p. 65.
[2] G. L. Pearson and J. Bardeen, Phys. Rev. **75**, 865 (1949).

A Scattering Approximation

A. L. LATTER
Physics Department, University of California, Los Angeles, California
(Received July 12, 1951)

SCATTERING of a plane wave by a square well potential has been treated in an approximation comparable in simplicity to the Born approximation but with the added feature of being exact at low energies as well as high.

One proceeds from the integral formula for the scattering amplitude:

$$f(\theta)=(mV_0/2\pi\hbar^2)\int \exp(-i\mathbf{k}'\cdot\mathbf{r})\psi(\mathbf{r})d\mathbf{r}; \qquad (1)$$

V_0 is the depth of the well, m is the reduced mass, and the integral is over the domain $r<a$, where a is the radius of the well; and $\psi(\mathbf{r})$ is the exact wave function inside the well, i.e.,

$$\psi(\mathbf{r})=\Sigma_l a_l(2l+1)i^l j_l(\alpha r)P_l(\cos\theta), \qquad (2)$$

where α is the interior wave number and the coefficients a_l are found as usual by matching logarithmic derivatives:

$$a_l^{-1}=x^3[\,[j_l(y)n_l'(x)-(y/x)j_l'(y)n_l(x)]-i[j_l(y)j_l'(x)-(y/x)j_l'(y)j_l(x)]\,], \qquad (3)$$

where $x=ka$; $y=\alpha a$.

It is now observed that the series (2) is summable if one substitutes for the spherical bessel functions in Eq. (3) their asym-

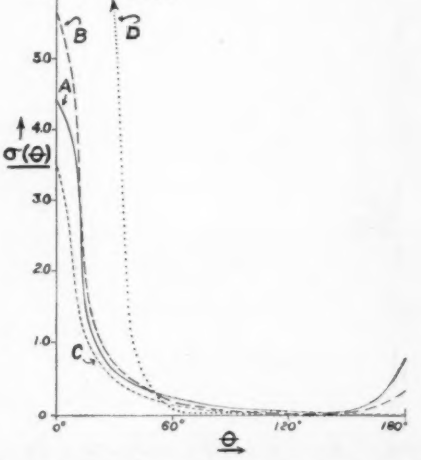

FIG. 1. Differential cross section in barns per steradian: A. exact; B. approximation based on Eq. (5); C. approximation based on Eq. (5) with $a_1=a_0$; D. Born approximation.

ptotic forms[1] valid for $x, y \gg l$. The result is

$$a_{2n} = a_0 = e^{-i\alpha}[\cos y - i(x/y)\sin y]^{-1},$$
$$a_{2n+1} = a_1 = e^{-i\alpha}[(x/y)\cos y - i\sin y]^{-1},$$

and

$$\psi(\mathbf{r}) = \tfrac{1}{2}(a_0+a_1)\exp(i\boldsymbol{\alpha}\cdot\mathbf{r}) + \tfrac{1}{2}(a_0-a_1)\exp(-i\boldsymbol{\alpha}\cdot\mathbf{r}). \quad (4)$$

This approximation is exact only for $l=0$ and becomes progressively less accurate as l increases. However, since partial waves for which $l \gg x$ do not contribute appreciably to the scattering, the inaccuracy will be slight for all but a few partial waves in the transition region $l \approx x$.

Now whereas the Born approximation makes use of the incident plane wave as the trial function in Eq. (1), we prefer at this point to use the approximate wave function (4), which, inserted into Eq. (1) and integrated, yields

$$f(\theta) = \tfrac{1}{2}(a_0+a_1)g(\theta) + \tfrac{1}{2}(a_0-a_1)g(\pi-\theta). \quad (5)$$

The function $g(\theta)$ is just a modified Born approximation for the scattering amplitude, starting with the function $\exp(i\boldsymbol{\alpha}\cdot\mathbf{r})$ instead of $\exp(i\mathbf{k}\cdot\mathbf{r})$. For a square well one has

$$g(\theta) = (2mV_0a^2/\hbar^2)j_1(Ka)/Ka,$$

which is the familiar Born result[2] except now

$$K = [(\alpha-k)^2 + 4\alpha k\sin^2\tfrac{1}{2}\theta]^{\frac{1}{2}}.$$

As an example, the case $V_0 = 30$ Mev, $a = 4.26\times10^{-13}$ cm, an incident energy of 18.26 Mev, and mass m equal to a nucleon mass was worked out using Eq. (5) and compared with the exact solution[3] as shown in Fig. 1. Also shown is the Born approximation and a simplified form of Eq. (5) in which a_1 is set[4] equal to a_0.

Finally, the total cross sections were computed to be as follows: A. Exact: 2.7 barns; B. Approximation based on Eq. (5): 3.0 barns; C. Approximation based on Eq. (5) with $a_1 = a_0$: 1.7 barns; D. Born approximation: 12.1 barns.

[1] Recently Robert W. Hart, J. Acoust. Soc. Am. **23**, 323 (1951), independently observed that the exterior solution could be summed in this way. He interprets his approximation directly to find the cross section. We, however, shall require of ours only that it be a good initial trial function in the integral formula.

[2] See L. I. Schiff, *Quantum Mechanics* (McGraw-Hill Book Company, Inc., New York, 1949), first edition, p. 167.

[3] We wish to thank Dr. R. E. LeLevier for supplying us with the exact calculations, which involved seven partial waves significantly.

[4] The comparison suffers somewhat in this example from the fact that the $l=1$ wave is nearly in resonance.

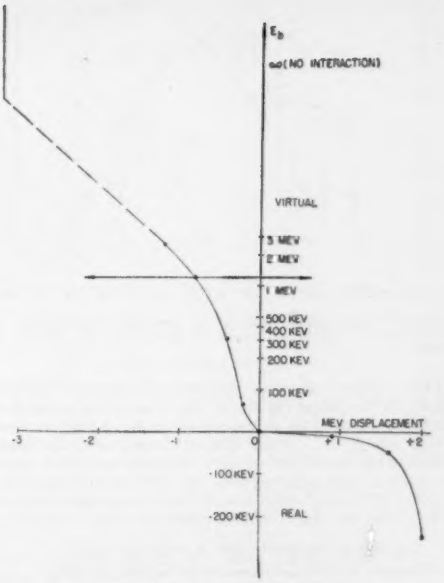

FIG. 1. Plot of effective displacement of theoretically computed spectra (see reference 1) resulting from the process $\pi^- + D \to 2n + \gamma$, as a function of the binding energy E_B of the lowest level of the $n-n$ system.

π^- Absorption in D_2 and the $n-n$ Force*

R. LEE AAMODT, WOLFGANG K. H. PANOFSKY, AND R. PHILLIPS
Radiation Laboratory, Department of Physics, University of California, Berkeley, California
(Received July 16, 1951)

WATSON and Stuart[1] have recently published detailed theoretical calculations concerning the gamma-ray spectrum from the process $\pi^- + D \to 2n + \gamma$ previously observed.[2] The resultant spectrum is clearly sensitive to the $n-n$ interaction at low energies. Since the analysis was based on unpublished data, it appears advisable here to state the experimental status concerning this spectrum. The present data allow considerable latitude regarding the $n-n$ interaction parameters. It is clear, however, that a not immeasurable improvement of the data could lead to quite conclusive evidence concerning the stability of the di-neutron.

When the curves of Watson and Stuart[1] are "folded" into the resolving power of the pair spectrometer used in the absorption experiments,[2] the resultant curves for various values of the $n-n$ interaction show a negligible difference in shape but are effectively displaced along the energy scale. Figure 1 shows a curve of this effective displacement plotted against the binding energy of a hypothetical di-neutron, real or virtual. Figure 2 shows the theoretical spectrum, with the resolution folded in, of the curve corresponding to zero binding. Marked on the abscissa is the value of $E_0 = [(\pi^- + p)^2 - n^2]/2(\pi^- + p)$; here π^-, p, and n are the rest energies of the particular particles. E_0 is thus the expected value of the gamma-ray from the process $\pi^- + p \to n + \gamma$. Measurement of the gamma-ray process in H on the same spectrometer will thus determine the value of E_0 without specific reference to the π^- mass. Plotted on Fig. 2 also is the theoretical shape of the gamma-ray line from $\pi^- + p \to n + \gamma$, i.e., the resolution of the instrument. The value of the binding energy will then simply result by comparing the separation of the gamma-ray peaks of the two processes with that plotted in Fig. 2 and then reading E_B

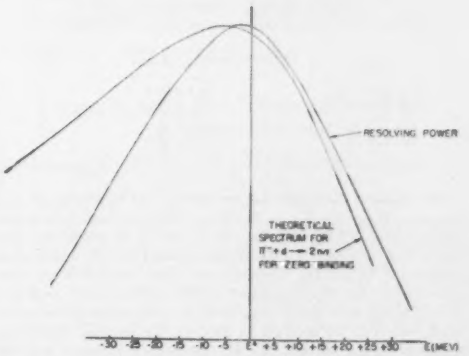

FIG. 2. Theoretical γ-spectra of the processes: $\pi^- + D \to 2n + \gamma$ and $\pi^- + H \to n + \gamma$; these spectra include the resolution.

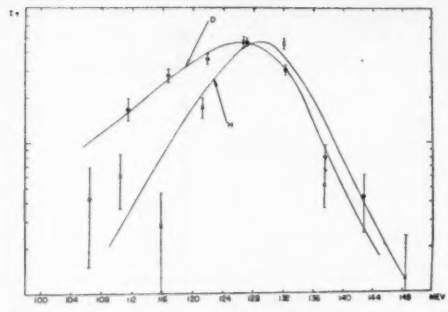

FIG. 3. Experimental data on the processes $\pi^- + D \rightarrow 2n + \gamma$ and $\pi^- + H \rightarrow n + \gamma$. The theoretical curves giving the best fit are also given.

of Fig. 1. Figure 3 shows the experimental hydrogen and deuterium data. On comparing Fig. 2 and Fig. 3 we estimate that the D data are displaced by an amount of 0.8 Mev±1.5 Mev toward lower energy, i.e., virtual binding. Accordingly, the nominal value of the lowest state of the $n-n$ system is 1.2 Mev virtual; in terms of these data the probability is 25 percent that a real di-neutron of binding energy greater than 10 kev exists; the probability is only 10 percent that the binding is in excess of 150 kev.

* This work was performed under the auspices of the AEC.

[1] K. M. Watson and R. N. Stuart, Phys. Rev. **82**, 738 (1951).
[2] Panofsky, Aamodt, and Hadley, Phys. Rev. **81**, 565 (1951).

Pressure Broadening of an Ammonia Inversion Line for Foreign Gases

J. WEBER
*U. S. Naval Ordnance Laboratory, Silver Spring, Maryland, and University of Maryland, College Park, Maryland**

(Received July 18, 1951)

DURING the course of a microwave spectroscopic investigation of the isotopic exchange reaction between ammonia and deuterium,[1] the microwave collision diameters of a number of molecules were determined from collision broadening of the microwave 3,3 line of NH_3. The results are given in Table I.

TABLE I. Microwave collision diameters.

Gases	Microwave collision diameter, in cm	Probable error (%)
NH_3 and NH_3	13.8×10^{-8}	1
NH_3 and NH_2D	13.1×10^{-8}	2
NH_3 and H_2	3.28×10^{-8}	1
NH_3 and D_2	3.65×10^{-8}	1
NH_3 and O_2	4.18×10^{-8}	2

The collision diameters for deuterium and hydrogen are not the same; their ratio is 1.11. Smith and Howard[3] have interpreted the broadening of the NH_3 lines by O_2 and H_2 as arising from the interaction between the NH_3 dipole moment and the quadrupole moments of O_2 and H_2. Anderson[3] has shown that the interaction between the NH_3 dipole moment and the induced dipole moments of O_2 and H_2 is too small to account for observed collision diameters, but that the interaction between the induced dipole moments of O_2 and H_2, and the NH_3 quadrupole moment[4] is of the right order of magnitude. The latter interaction represents a much harder force law (energy $\propto 1/r^7$) than the interaction between the NH_3 dipole moment and the permanent quadrupole moments of H_2 and O_2 (energy $\propto 1/r^4$). The fact that the diameter for D_2 is significantly larger than for H_2 supports the idea of the longer range NH_3 dipole-hydrogen quadrupole interaction. The quantum-mechanical theory predicts that the collision diameter for NH_3 dipole-hydrogen quadrupole interaction should be inversely proportional to the cube root of the molecular velocities. On this basis, diameter $(NH_3\text{-}D_2)$/diameter $(NH_3\text{-}H_2) = [(1.8^4)]^{\frac{1}{3}} = 1.10$, in very good agreement with the value 1.11 above.

Further evidence for the NH_3 dipole and hydrogen or oxygen quadrupole interactions is the fact that the cross sections calculated by Anderson for these processes is significantly less than those above. We therefore conclude that the experimental evidence is strongly in favor of the NH_3 dipole—O_2 or H_2 quadrupole interaction as the important one in this type of broadening.

The collision diameter for NH_3-NH_2D collisions is observed to be smaller than for NH_3-NH_3 collisions. This can be understood in the following way. Rotational resonance effects will be different. In addition, for dipole-dipole collision broadening the effective dipole moment of a given molecule is the component in the direction of the total angular momentum axis, and this must be averaged over all quantum states. This average can be expected to be different for an asymmetric top (NH_2D) than for a symmetric top (NH_3), because both the statistics and wave functions are different.

For the symmetric top having a rotational quantum number J, all states except the one for which K is zero contribute to the average dipole moment. The one for which K is zero does not contribute because it corresponds to rotation about an axis normal to the dipole moment. Consider the Poinsot motion of the asymmetric top. For a given energy there will in general be several quantum states corresponding to rotation about the largest moment of inertia axis and several corresponding to rotation about the smallest moment of inertia axis (which is approximately normal to the dipole axis for NH_2D), and these states hardly contribute to the broadening at all. Therefore, for a given J, all states except one contribute to broadening for the symmetric top, but several states do not contribute in asymmetric top broadening. A calculation of the dipole moment in the direction of the total angular momentum axis averaged over all states was made for NH_2D and NH_3. The result for NH_2D was approximately 2 percent less than for NH_3. The lack of rotational resonance for NH_3-NH_2D collisions should also tend to make the collision diameter slightly less than that for NH_3-NH_3.

The combination of slightly smaller average effective dipole moment and lack of rotational resonance accounts for the fact that the observed collision diameter for NH_3-NH_2D is 5 percent smaller than that for NH_3-NH_3 collisions.

A ten-foot K-band wave-guide cell was employed for all of the measurements. The cross sections for NH_3 and NH_2D were determined by simultaneous measurement of line breadth, absorption coefficient, and pressure, at pressures of about 40 microns. The values for H_2, D_2, and O_2 were determined by making absorption coefficient measurements at NH_3 partial pressures of the order of 0.5 mm. At lower pressures there is more adsorbed NH_3 on the wave-guide walls than in the gas phase. If the system has both metal and glass, pressure equilibrium of the gas mixture is reached more quickly than composition equilibrium, inasmuch as there is usually a very small orifice in the wave guide through which exchange can take place. The concentration of NH_3 in metal parts of a system will be less than in the glass portions. In addition, errors are sometimes introduced as a result of increased adsorption of NH_3 as the gas mixture is compressed in a McLeod gauge. In the above measurements these effects were made small by working at higher pressures, and coating the wave guide with Glyptal to give a nonmetallic surface. Less than 7 percent of the NH_3 was on the walls, and the composition of gas in the wave guide was determined by direct measurements on a sample taken from the wave guide into a cold trap.

Absorption coefficients were determined from crystal current readings before and after introduction of gas into the wave guide,

using a mirror-type galvanometer. Under good conditions absorption coefficients determined in this way are reproducible to 0.1 percent. The ratio of absorption coefficients for different mixtures has only a second-order dependence on the crystal law. The crystal law was known to be approximately 2.2 power from calibrated attenuator measurements.

Mix ratios of 10 to 1 and 3 to 1 were employed for H_2, and mix ratios of 3 to 1 and 6 to 1 for O_2. No dependence of collision diameter on mix ratio was observed.

I wish to thank Mr. Susumu Otsuka for able assistance in making certain calculations in the course of this work.

* Department of Electrical Engineering.
[1] J. Weber and K. J. Laidler, J. Chem. Phys. (to be published).
[2] W. V. Smith and R. Howard, Phys. Rev. **79**, 132 (1950).
[3] P. W. Anderson, Phys. Rev. **76**, 647 (1950).
[4] P. W. Anderson, Phys. Rev. **80**, 511 (1950).

Decay of 10.7-min Co^{60m}

M. Deutsch* and G. Scharff-Goldhaber
Brookhaven National Laboratory, Upton, New York†
(Received July 19, 1951)

THE 10.7-min excited state of Co^{60m} is known to decay predominantly by a highly converted isomeric transition of 0.0589 Mev[1] to the ground state (Fig. 1). A small fraction of the disintegrations is known to decay directly to the first excited state of Ni^{60} at 1.331 Mev.[2] This fraction has been reported only as "less than 10 percent."[3] We have redetermined this quantity by comparing the number of cobalt K x-rays with the number of 1.33-Mev γ-rays from Co^{60m} prepared by neutron bombardment of spectroscopically pure Co metal in the BNL reactor, and find a beta-decay branch of (0.28±0.06) percent. The comparison was made by the use of calibrated proportional and scintillation counters.

The efficiency of the argon-filled proportional counter for the K x-rays of Cr, Fe, and Cu was determined by coincidence measurements using the radioactive decay of Mn^{54}, Co^{57}, and Zn^{65}. The x-ray pulses were selected by means of a differential pulse height analyzer. The efficiency thus determined includes the solid angle, window absorption and fluorescent yield as well as the intrinsic efficiency for the K x-ray. The observed variation of efficiency with x-ray energy is consistent with that expected from the variation of fluorescent yields and absorption coefficients. The efficiency for cobalt K x-rays obtained by interpolation was $(2.0 \pm 0.3)\times 10^{-2}$ count per K-shell excitation.

The efficiency of the NaI scintillation counter for 1.3-Mev γ-rays was measured by the use of a small aliquot of a standard solution containing Co^{60}(5.2 yr). This solution was supplied by the Bureau of Standards. The value of $(1.0\pm 0.15)\times 10^{-2}$ for the gamma-ray efficiency was in line with the values obtained for the 0.84-Mev and 1.14-Mev gamma-rays from coincidence measurements on Mn^{54} and Zn^{65}.

The ratio of gamma-ray to x-ray counting rates due to a source of Co^{60m} was 1.7×10^{-3}. Using the above values for the efficiencies, we obtain $(3.4\pm 0.7)\times 10^{-2}$ for the ratio of γ-rays to K-conversion processes. Allowing for a $K{:}L$ conversion ratio of 4.55,[1] the branching ratio of direct beta-decay to the isomeric transition is $(2.8\pm 0.6)\times 10^{-3}$.

A search was made for a 2.9-Mev beta-transition to the ground state of Ni^{60}, using an anthracene scintillation spectrometer. No evidence for beta-rays of more than 1.56-Mev energy was found, and we can set an upper limit of one ground state beta-transition in 10^6 isomeric transitions. The value of logft for the 1.56-Mev transition is 7.15, that for the 2.9-Mev transition >9.67; for the 5.2-yr beta-transition the value of logft is 7.46. Both of the observed β-transitions could therefore be first-forbidden or possibly allowed. The shape of the 0.32-Mev spectrum and the absence of $\beta-\gamma$ angular correlation preclude a spin change of 2 in this transition. Thus the spin of the Co^{60} ground state must be 5 (or 4).

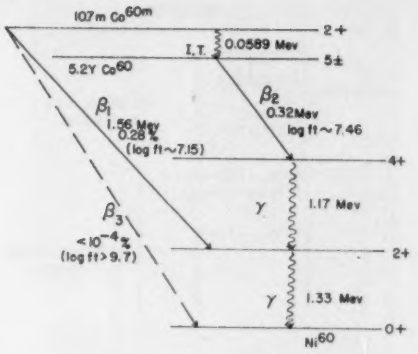

FIG. 1. Proposed disintegration scheme for Co^{60}.

The lifetime of the isomeric transition requires a spin change[4] of 3, making the spin of the 10.7-min state 2 (or 1). Because of the absence of a ground state beta-transition, spin 2 and even parity appears to be the best assignment for this state. The 1.56-Mev transition seems therefore to be allowed.

The parity of the ground state of Co^{60} is not uniquely determined by our results. The isomeric transition is compatible with either an E3 or M3 transition.[4] The lifetime of the beta-transition suggests a parity change. Shell theory would predict states of even parity from combinations $f_{7/2}$ and $f_{5/2}$ or $f_{7/2}$ and $p_{3/2}$. Our knowledge of the decay of Co^{60} is summarized in Fig. 1.

From the observed intensities of the hard gamma-radiation of the 5.2-yr and 10.7-min activities in the same sample we can compute the ratio of the neutron capture cross sections for production of the two states of Co^{60}. For a 10-min bombardment the intensity ratio was 8.9×10^{-3}. Allowing for the growth of the Co^{60} ground state from the 10.7-min isomer and for the ratio of hard gamma-rays to isomeric transitions in the 10.7-min period as reported above, we find $\sigma(5.2\text{ yr})/\sigma(10.7\text{ min}) = 1.4\pm 0.6$. The much larger value reported by Seren *et al.*[5] is probably due to failure to observe the isomeric transition.

We wish to thank E. der Mateosian for valuable help in some of these experiments and R. L. Chase and A. Del Duca for the design and construction of the coincidence circuit.

* Permanent address: Massachusetts Institute of Technology, Cambridge, Massachusetts.
† Work carried out under the auspices of the AEC.
[1] R. L. Caldwell, Phys. Rev. **78**, 407 (1950).
[2] K. Way *et al.*, Natl. Bur. Standards Circ. 499 (unpublished).
[3] Deutsch, Elliott, and Roberts, Phys. Rev. **68**, 193 (1945).
[4] M. Goldhaber and A. W. Sunyar, Phys. Rev. **83**, 906 (1951).
[5] Seren, Friedlander, Turkel, Phys. Rev. **72**, 888 (1947).

Experiments on the Ultrasonic Unmixing of Liquid Solutions

Charles A. Boyd and Robert J. Zentner
Naval Research Laboratory, Department of Chemistry, University of Wisconsin, Madison, Wisconsin
(Received July 16, 1951)

IN a Letter to the Editor, Frei and Schiffer[1] reported on experiments which indicated that gross partial unmixing of solutions such as glycerin dissolved in water could be brought about by setting up standing ultrasonic wave patterns in the solution. In view of the present interest in this subject, it seems worth while to report the results of some of our experiments along these lines.

The apparatus used is shown in Fig. 1. The position of the test cell and that of the reflector were adjustable so as to obtain good

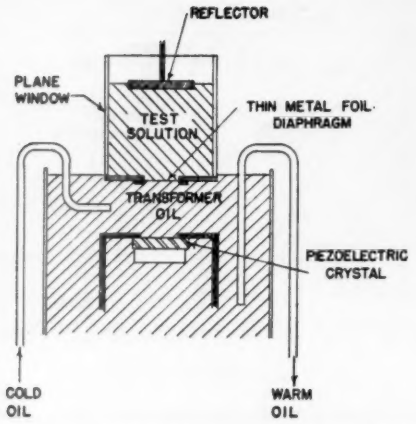

FIG. 1. Schematic diagram showing experimental arrangement for studying ultrasonic effects on solutions.

standing wave patterns in the solution, and these were observed by means of an optical schlieren system through the plane windows. The piezoelectric crystal was driven at a resonant frequency of approximately 400 kc/sec by an oscillator having an output of 500 watts. It was necessary to cool the transformer oil which coupled the crystal to the test cell in order to prevent excessive heating.

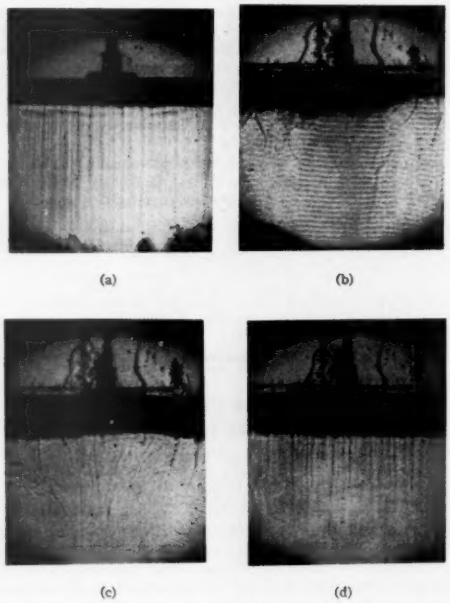

FIG. 2. Effect of ultrasonic irradiation on glycerin-H_2O solutions. Schlieren photographs taken at 1/50 sec. (a) Cell before ultrasonic generator was turned on. T =23.6°C. (b) Generator on 10 minutes. Temperature in front of reflector =29.4°C. (c) Generator on 20 min, then turned off. Temperature in front of reflector =29.3°C. (d) Six minutes after generator turned off. Temperature in front of reflector =27°C.

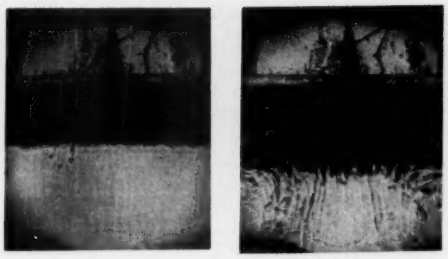

FIG. 3. Effect of heating reflector plate in position with photoflood lamp. (a) Reflector heated by photoflood, initial T =26.7°C. T in dark zone =35.7°C. (b) Dark zone diffusing away after photoflood turned off.

The solutions used in the experiments were approximately 50 percent by weight of glycerin dissolved in water.

A typical run is illustrated in Fig. 2. It was noticed that as the runs progressed, a dark cloud, as seen in the schlieren system, indicating a zone of different refractive, index would form in front of the reflector plate. This persisted after the ultrasonic generator was turned off. Samples taken from this region and analyzed, indicated an increase of approximately 6 percent in the glycerol content over that measured in the bulk of the solution. However, a local temperature increase directly in front of the reflector of approximately 6°C was noted.

In order to check upon the influence of this temperature increase on the concentration of the solution in the vicinity of the reflector, another series of runs were made in which the back of the reflector was coated with lampblack and heated locally by focusing a spot of light on it. The ultrasonic generator was not turned on during these runs. Figure 3 illustrates a typical run made in this manner. The same type of dark cloud was formed, and analyses showed a glycerin concentration increase comparable with that obtained in the ultrasonic runs.

Additional experiments were also made in which samples were withdrawn by means of capillary pipette directly from the nodes and antinodes of the standing waves. While small variations were observed from sample to sample, no direct and consistent correlation between position and concentration was found.

On the basis of these experiments, it seems likely that the solution separations reported by Frei and Schiffer were caused by secondary thermal effects due to ultrasonic local heating.

[1] H. Frei and M. Schiffer, Phys. Rev. **71**, 555 (1947).

Radioactive I^{122}

JOHN N. YOUNG,* M. L. POOL, AND D. N. KUNDU
Ohio State University, Columbus, Ohio
(Received July 13, 1951)

AN activity with a 4-minute half-life in the iodine fraction obtained by bombarding antimony with high energy alpha-particles was reported.[1] The decay was by positron emission with an energy of 2.9±0.1 Mev. The suggested reaction was $Sb^{121}(\alpha, 3n)I^{122}$.

If the above suggested assignment be correct, then it should be possible to produce this isotope by bombarding tellurium with protons. For this purpose Hilger tellurium metallic powder, Lab. No. 2433B, was bombarded with 7.4-Mev protons. By using a Geiger tube placed in a magnetic field so that positive and negative beta-particles could be observed selectively, a 3.6-minute half-life positron activity, as well as the 25-minute negation activity[2] of I^{128}, were obtained.

In order to find out which particular isotope of Te had acted as the target nucleus for producing the 3.6-minute activity, it was

necessary to use a Te sample with a different isotopic composition. This was accomplished by using enriched tellurium in which the content of Te^{122} had been increased from the natural abundance of 2.46 to 79.4 percent. Using 7.4-Mev protons again, the 3.6-minute activity was produced 46.5 times larger in intensity than the 25-minute activity, whereas in the previous case where Hilger material had been used the 3.6-minute activity was 1/4.4 times as large. The ratio of these two relative numbers, 46.5 and 1/4.4, which is 205, is very close to the ratio of the abundances of Te^{122} and Te^{123} for the two bombarded samples, namely, 210. It is thus concluded that the 3.6-minute activity is made from Te^{123}.

The 3.6-minute activity must then be attributed to either I^{122} by the (p, n) reaction or to I^{123} by the (p, γ) reaction.

Though in general the (p, n) reaction proceeds with a larger yield than the (p, γ) reaction, nevertheless it was considered desirable to examine the relative branching of these two reactions on other neighboring isotopes of Te. In particular, Te^{124} and Te^{125} had been bombarded with protons of the same energy. In both cases it was observed that the (p, n) reaction proceeded very readily whereas the (p, γ) reaction did not, with any appreciable yield.

It seems, therefore, reasonable to conclude that the strong 3.6-minute activity be assigned to I^{122}.

By absorption measurements the maximum energy of the positron spectrum was found to be 3.08±0.1 Mev.

* Major, USAF, Institute of Technology, Wright Patterson Air Force Base, now at Sandia Base, Sandia, New Mexico.

[1] L. Marquez and I. Perlman, Phys. Rev. **78**, 189 (1950).
[2] "Nuclear data," Natl. Bur. Standards Circ. 499 (1950).

Resonant Absorption of Oxygen at 2.5-Millimeter Wavelength*

ROY S. ANDERSON, CHARLES M. JOHNSON, AND WALTER GORDY
Department of Physics, Duke University, Durham, North Carolina
(Received July 16, 1951)

A SINGLE resonant absorption peak of oxygen has been theoretically predicted to occur near 2.50-millimeter wavelength.[1] Because of the difficulties of making measurements in this region of the spectrum, the line has not previously been observed. With the millimeter wave harmonic generators previously described[2] and with the Zeeman modulation spectrograph developed in this laboratory[3] for detecting the resonant lines of oxygen in the 5-mm wave region, we have succeeded in detecting and accurately measuring the 2.5-mm line. Its position and line breadth are given in Table I. Figure 1 shows a recorder tracing of the line both at room temperature and at the temperature of dry ice. The line position deviates only 25 Mc from that predicted by Van Vleck[4] with Schlapp's formula.[4] Because of the low intensity of the line, an accurate measurement of its breadth could not be made. However, from measurements as accurate as we could make, the breadth appears to be greater than for the other lines in the millimeter region.[5]

The 2.5-mm line corresponds to the $J=0\rightarrow1$, $K=1$ transition in the spin-type triplet. The Zeeman pattern for this transition is particularly simple, and has been completely resolved. It consists of two components, of equal intensity, corresponding to $\Delta M=\pm1$, which are shifted equally one to higher and one to lower frequencies by the magnetic field, and a third component corresponding to $\Delta M=0$ which is not displaced by the field. The undisplaced line cannot be detected with the Zeeman modulation method used here. Hence, only the two lines corresponding to $\Delta M=\pm1$ were observed. The recorder tracing of these components is shown in Fig. 2. Figure 3 shows the measured displacements of these lines as a function of field strength. It is seen that the displacement is directly proportional to the field up to the highest value employed (22 gauss). Thus it appears that the first-order Zeeman treatment (weak field case) should account satisfactorily for the splitting. However, the g factor observed, 1.22±0.05, does not correspond to that predicted, 1.00, for the normal Zeeman effect of Hund's case (b). So far we have been

TABLE I. $J=0\rightarrow1$, $K=1$ line of oxygen.

Frequency Mc/sec	Line breadth parameter	Zeeman displacement of each component ($\Delta M=\pm1$) Mc/gauss
118,745.5 ±0.3	0.12 cm^{-1}/atmos ($T=193°K$)	1.70

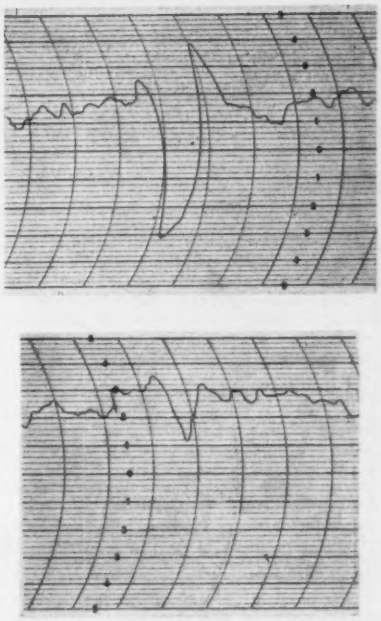

FIG. 1. Recorder tracings of the $J=0\rightarrow1$, $K=1$ transition of oxygen occurring at 118,745.5 Mc. The upper recording shows the line at dry ice temperature and the lower at room temperature.

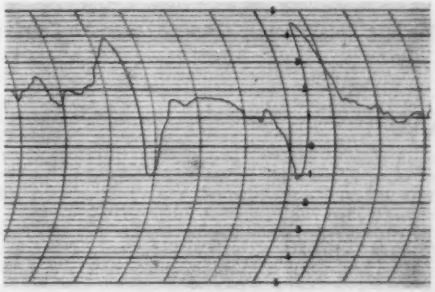

FIG. 2. Recorder tracing of the $J=0\rightarrow1$, $K=1$ transition of oxygen, showing the Zeeman splitting of the line into $M=+1$ and $M=-1$ components. The field in this case was 22 gauss.

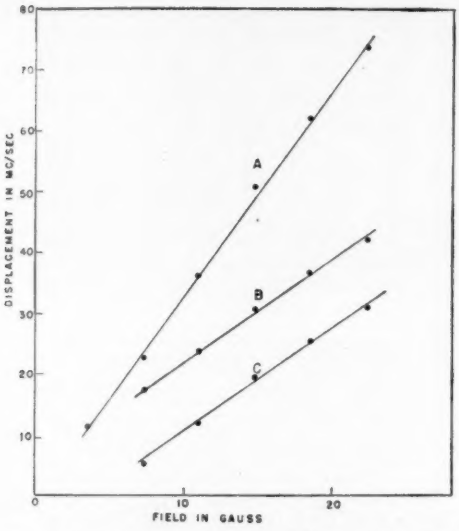

FIG. 3. Measured Zeeman displacements as a function of field strength for the $\Delta M = \pm 1$ components of the $J = 0 \rightarrow 1$, $K = 1$ transition of O_3; (A) total separation of components, (B) displacement of high frequency components, (C) displacement of low frequency components.

unable to account for this discrepancy. Neglecting possible systematic errors of unknown origin, the disagreement lies well outside the estimated range of errors. It is surprising that the strong field magnetic resonance measurements of Beringer and Castle[6] and the strong field Zeeman measurements in the optical region by Schmid, Budó, and Zemplén[7] yield a g factor in agreement with the weak field case of the present measurement. Because of the apparent inconsistency further measurements of the weak field Zeeman effect are being made.

We wish to thank Dr. Allan Henry for a helpful communication.

* The research reported in this paper has been made possible through sponsorship extended by the Geophysical Research Directorate of Air Force Cambridge Research Laboratories.

[1] J. H. Van Vleck, Phys. Rev. **71**, 413 (1947).
[2] Gilliam, Johnson, and Gordy, Phys. Rev. **78**, 140 (1950).
[3] Burkhalter, Anderson, Smith, and Gordy, Phys. Rev. **79**, 651 (1950).
[4] R. Schlapp, Phys. Rev. **51**, 342 (1937).
[5] Anderson, Smith, and Gordy, Phys. Rev. **82**, 264 (1951).
[6] R. Beringer and J. G. Castle, Jr., Phys. Rev. **81**, 82 (1951).
[7] Schmid, Budó, and Zemplén, Z. Physik **103**, 250 (1936).

Nuclear Relaxation in Gases by Surface Catalysis

F. BLOCH
Stanford University, Stanford, California
(Received July 16, 1951)

WHILE the interaction between the rotational motion and the nuclear moment provides, in the case of diatomic and polyatomic gases, an effective mechanism for the establishment of thermal equilibrium,[1] it is necessary for nuclear induction experiments with noble gases to provide a catalyst in order to obtain sufficiently short relaxation times. The admixture of oxygen was originally suggested for this purpose[2] and has since been successfully used[3] for He^3. However, the partial pressure of oxygen must be chosen here as high as 10 atmospheres to attain even a relaxation time $T_1 \cong 1$ sec, and appreciably shorter relaxation times which are otherwise desirable would require excessive pressures. It seemed worth while, therefore, to consider another mechanism, which can lead to short relaxation times without an increase of pressure. Such a mechanism can be realized if the sample consists of a fine powder of a paramagnetic substance with the gas under investigation filling the space between the powder particles. Even with a densely packed powder, there will still be about half of the total volume available for the gas, so that under the same pressure the reduced amount of sample substance within the volume of the receiver coil does not cause serious reduction of the signal. Because of the molecular magnetic moments of the powder, there exist strong irregular magnetic fields within atomic distances from the surface of the powder particles. Consequently, the impact of a gas atom upon a surface causes a similar reorientation of the nuclear moment as is otherwise achieved in an impact with a molecule of admixed oxygen, and one can therefore expect that this mechanism can likewise contribute effectively towards establishment of thermal equilibrium.

To obtain a quantitative treatment of this surface catalysis, it is necessary to consider the self-diffusion of the gas in the space between the powder particles. It requires a slight generalization of the macroscopic differential equations which we gave earlier[4] with the difference that the components of the polarization vector $\mathbf{M}$ must be considered as functions not only of the time but also of the space coordinates. We shall assume that the mean change of the nuclear moment $\boldsymbol{\mu}$ by an impact on the surface is

$$\langle \delta\boldsymbol{\mu} \rangle_{Av} = -w(\langle \boldsymbol{\mu} \rangle_{Av} - \boldsymbol{\mu}_0), \tag{1}$$

where w measures the transition probability in an impact and $\boldsymbol{\mu}_0$ is the equilibrium value of $\langle \boldsymbol{\mu} \rangle_{Av}$. The rate of change of the total moment, contained in a gas volume V with the arbitrary boundary surface B can then be written in the form

$$\frac{d}{dt}\int_V \mathbf{M} d\tau = D\int_{B_1} \operatorname{grad}_\sigma \mathbf{M} d\sigma - \frac{w\bar{v}}{4}\int_{B_2} (\mathbf{M}-\mathbf{M}_0) d\sigma + \int_V \left[\gamma[\mathbf{M}\times\mathbf{H}] - \frac{\mathbf{M}_{tr}}{T_2'}\right] d\tau. \tag{2}$$

The first integral on the right side extends over the part B_1 of B which is situated within the gas and represents the contribution due to diffusion with the coefficient D. The second integral represents the effect of impacts, taking place over the part B_2 of B which is formed by the surface of powder particles; it follows from (1), since the mean number of impacts per unit area and unit time is given by $n\bar{v}/4$ (n = number of gas atoms per unit volume, $\bar{v}$ = mean velocity) and since $n(\langle \boldsymbol{\mu} \rangle_{Av} - \boldsymbol{\mu}_0) = \mathbf{M} - \mathbf{M}_0$. The last integral represents the additional change of $\mathbf{M}$ within V due to the external field $\mathbf{H}$ and a possible field inhomogeneity ΔH, affecting the transverse part $\mathbf{M}_{tr}$ of $\mathbf{M}$ and measured by $1/T_2' = \gamma \Delta H$. An equivalent differential form of (2) is

$$\partial \mathbf{M}/\partial t = D\nabla^2\mathbf{M} + \gamma[\mathbf{M}\times\mathbf{H}] - \mathbf{M}_{tr}/T_2' \text{ within the gas,} \tag{3}$$

$$0 = D \operatorname{grad}_\sigma \mathbf{M} + \tfrac{1}{4}w\bar{v}(\mathbf{M}-\mathbf{M}_0) \text{ on the surface.} \tag{3a}$$

In (2) and (3a) the subscript σ indicates the external normal component to the boundary B_1 and to the powder surface, respectively.

The variation of $\mathbf{M}$ in space can be neglected if the order of magnitude d of the distance between powder particles is sufficiently small. Extending V over the total volume of the gas, so that $B_2 = S$ is the total surface of the powder particles, one obtains then from (2) the same differential equations for the time dependence of $\mathbf{M}$ as were obtained before (see reference 2) if

$$T_1 = 4V/w\bar{v}S \tag{4}$$

and

$$T_2 = T_1T_2'/(T_1+T_2') \tag{4a}$$

are taken as longitudinal and transverse relaxation times, respectively. The necessary smallness of d implies merely that the time d^2/D, which is of the order of the time between impacts upon different particles, is small compared with either T_1 or T_2 and is well realized under normal conditions.

The effectiveness of this mechanism can be best estimated by comparing (4) with the value $(T_1)_{O_2}$ which one would obtain with a given partial pressure $(p)_{O_2}$ of admixed oxygen. Assuming the

magnetic moment per molecule and the distance of closest approach in an impact to be approximately the same for the powder and for oxygen the transition probability w will likewise be approximately the same in the two cases. One can then write

$$(T_1)_{O_2} \cong w\nu, \tag{5}$$

where ν is the number of collisions per unit time of a gas atom with an oxygen molecule. Expressing this number in terms of the gas kinetic cross section σ with oxygen, the pressure $(p)_{O_2}$ and the mean velocity v, which is likewise taken to be approximately the same in the two cases, one obtains from (4) and (5)

$$T_1 \cong (T_1)_{O_2}(4V\sigma A/SV_m)(p)_{O_2}, \tag{6}$$

where A is Avogadro's number, V_m the mole volume at one atmosphere, and where $(p)_{O_2}$ is measured in atmospheres.

A case to which (6) applies is a fine powder of Fe_2O_3, used here recently as a surface catalyst for xenon.[5] From an electron microscope picture V/S was estimated to be about 10^{-6} cm. With $\sigma \cong 10^{-15}$ cm², the "equivalent oxygen pressure" $(p)_{O_2}$ for which $(T_1)_{O_2} = T_1$ is here found from (6) to be about 10 atmospheres; this is in qualitative agreement with the observed equivalent pressure of approximately 30 atmospheres.

[1] N. Bloembergen, Leiden thesis, 1948, pp. 103–110, unpublished.
[2] F. Bloch, Phys. Rev. **70**, 460 (1946).
[3] H. Anderson, Phys. Rev. **76**, 1460 (1949).
[4] See reference 2, Eqs. (38).
[5] W. G. Proctor and F. C. Yu, Phys. Rev. **78**, 471 (1950).

On the Origin of Magnetism in Iron Sulfides with Various Sulfur Contents

TOKUTARO HIRONE, *Research Institute for Iron, Steel, and Other Metals, Tôhoku University*
AND
NOBORU TSUYA, *Faculty of Technology, Tôhoku University, Sendai, Japan*
(Received June 25, 1951)

MAGNETIC,[1] electrical,[2] and thermal[3] behavior of a series of iron sulfides $FeS_x (1 \leq x < 2)$, together with their crystal structures,[4] have been studied by many investigators. It is especially noteworthy that the magnetic behavior is sensibly affected by the excess sulfur content in the substances.[1] A theoretical discussion of these magnetic characteristics is given below based on the following ideas: The formation of S- and γ-type superlattices of ions (explained later in this paper) is inferred from the nonmagnetic interactions between Fe^{++} (4 Bohr magnetons) and Fe^{+++} (5 Bohr magnetons) ions. Furthermore, assuming the exchange integral J between adjacent net planes perpendicular to the hexagonal axis to be negative, it may be shown that antiferro- or ferrimagnetism occurs for the superlattice type γ or S_x, respectively.

We shall consider at first the case $x = 1.12$, for which the value of spontaneous magnetization is largest. In this case the lattice on which Fe ions are situated can be divided into two simple hexagonal sublattices (1) and (2) whose lattice constants in the direction of the hexagonal axis are twice as large as that of the original one (see Fig. 1). By an appropriate choice of the above-mentioned interaction coefficients, it is shown that below a certain temperature T_s, which is somewhat higher than 325°C, there occurs an ordered arrangement (superlattice S) of Fe^{++} and Fe^{+++}, in which the sublattice (1) contains only Fe^{++}, while the sublattice (2) contains both Fe^{+++} and Fe^{++} [see Fig. 1(a)]. Since the exchange integral J between the sublattice (1) and (2) is negative, the directions of aligned spins on the two sublattices become antiparallel* with each other below 325°C ($= T_\beta$). So the total magnetic moment is given by the difference of the magnetic moments of two sublattices, and this magnetism, therefore, is a ferrimagnetism† introduced by Néel.[5] Using the approximational method of Bragg and Williams, the results obtained agreed satisfactorily with the observed values of the spontaneous magnetization as well as with its temperature dependence and with the anomalous specific heat.[3] When x became greater than 1.12, the phase of FeS_2 appeared[6] to mix with the former.

The range $1 \leq x \leq 1.04$ corresponds to the antiferromagnetic case. Using appropriate interaction coefficients, one can find the formation of another kind of superlattice γ which has a Curie point T_γ, ($T_s < T_\gamma$) and is more stable than the superlattice S. The coexistence of these two superlattices is also excluded. In the case of the superlattice γ, the lattice can be divided into new sublattices, in which the Fe ions are distributed in another kind of ordered configuration. For instance, three interpenetrating hexagonal sublattices are assumed, two of which (1′) contain Fe^{++} ions only, while the remaining one (2′) contains also Fe^{++} ions. Or, assuming two monoclinic sublattices, the one (1″) contains Fe^{++} alone [see Fig. 1(b)]. Hence, in the new superlattice γ, Fe^{+++} ions are equally distributed among the former sublattices (1) and (2), so that in this case only antiferromagnetism, whose Curie point is T_β, can be observed. The occurrence of a "knick" in the curve of magnetic susceptibility χ *vs* temperature at about 135°C ($= T_\alpha$) may be understood by Haraldsen's idea or by the change of value of J due to the remarkable change of lattice constant near this temperature. This change may be caused by the order-disorder transformation of the vacant lattice points.

Next, in the range $1.05 \leq x \leq 1.09$, another peak γ was found in the curve of susceptibility *vs* temperature. For this range it is shown that such relations as $T_s < T_\gamma$ and $T_\alpha < T_\gamma$ were obtained by using the interaction parameters interpolated from those of the above two cases ($x = 1.12$ and $1 \leq x < 1.04$). Under such a condition the susceptibility χ at first increases with the fall of temperature according to the relation $\chi \sim (T - T_s)^{-1}$, but reaches a maximum value at T_γ. Since the formation of the superlattice γ counteracts the small unbalance of ionic arrangement between the sublattices (1) and (2) caused by the application of external magnetic field, χ decreases rapidly. The calculated behavior of χ agrees with that of the observed γ-anomaly.

The cause of Λ-type ferromagnetism found at $x = 1.10$ is now considered. For this case such a relation as $T_s \gtrsim T_\gamma \gg T_\alpha$ is very probable. From this relation it follows that, as before, the spontaneous (ferri-) magnetization occurring at T_s may be completely destroyed at a temperature slightly lower than T_γ, because at this

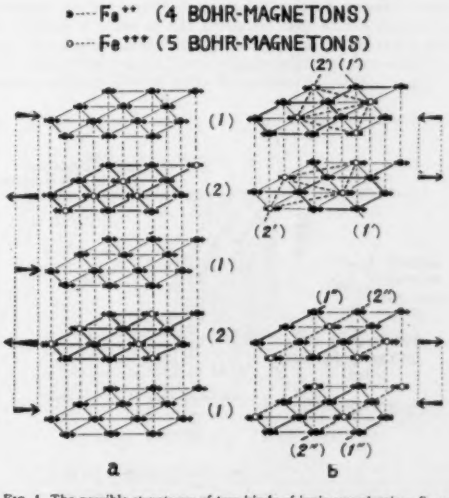

FIG. 1. The possible structures of two kinds of ionic superlattices S- and γ-type. The solid circles represent Fe^{++} ions and the open circles represent Fe^{+++} ions. Small arrows indicate the direction of the magnetic moment of each ion and large ones those of sublattices. (a): S-type ionic superlattice appearing when the substance is ferrimagnetic. (b): γ-type ionic superlattice appearing when the substance is antiferromagnetic.

temperature the second kind of superlattice γ mentioned above becomes more stable than the superlattice S. At $x=1.11$ the curve of magnetization *vs* temperature[4] takes the ordinary Weiss form with a Λ-shaped peak just below the Curie point. The magnetic behavior at this concentration may also be explained by assuming the existence of two phases, one of which is mentioned above (ferrimagnetic phase of Λ-type), the other one being already shown in the case of $x=1.12$.

The details of this calculation will be given in *The Science Reports of the Tôhoku Imperial University*.

The authors wish to express their sincere thanks to Professor H. Watanabe for his valuable discussions.

[1] M. Ziegler, thesis, Zürich (1915); H. Haraldsen, Z. anorg. u. allgem. Chem. **231**, 78 (1937).
[2] H. Watanabe and N. Tsuya, Science Repts. Tôhoku Imp. Univ. **2**, 503 (1950).
[3] R. Ueda, Busseiron Kenkyû **33**, 55 (1950). Measurements by S. Nagasaki, H. Watanabe, and the members of our laboratory are now in progress.
[4] H. Haraldsen, Z. anorg. u. allgem. Chem. **264**, 169 (1941); **264**, 195 (1941).
* Direct detection of this antiparallelism may be given by a magnetic scattering of neutron beam experiment.
† This conclusion was independently announced by K. Yoshida and by us at the meeting of the Physical Society of Japan, April 1, 1951.
[5] L. Néel, Ann. phys. **3**, 137 (1948).
[6] R. Juza and W. Biltz, Z. anorg. u. allgem. Chem. **205**, 237 (1932).

A Method for Reducing the Doppler Breadth of Microwave Absorption Lines

GEORGE NEWELL, JR.,* † AND R. H. DICKE
Palmer Physical Laboratory, Princeton University, Princeton, New Jersey
(Received July 2, 1951)

OF the various contributions to microwave line widths, the natural width is negligible, while collision and saturation broadening can be indefinitely reduced, leaving only the Doppler width.

The scheme discussed here permits only those molecules with a specified Doppler shift to radiate coherently and constructively. Normally, the microwaves scattered by molecules interfere constructively only in the direction of propagation of the incident wave. However, by introducing a spatially periodic, low frequency perturbing electric field, molecules can be made to scatter constructively in the backwards direction as well; further, only those molecules with a definite velocity contribute to the reflected wave.

Figure 1 shows the vacuum cell which is the heart of the scheme.

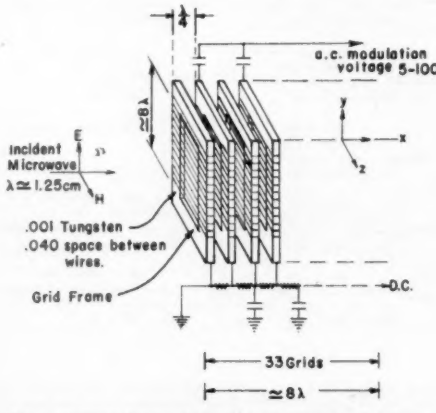

FIG. 1. Schematic diagram of the "Stark reflection" cell showing electrical connections to the grids. The E vector of the microwave radiation, the Stark field vector, and the grid wires are mutually perpendicular.

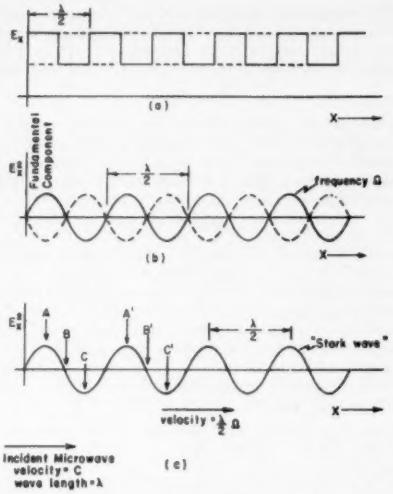

FIG. 2. (a) Instantaneous magnitude of the X component of the Stark field as a function of distance in the cell along the direction of microwave propagation. (b) Fundamental spatial fourier component of the square of the X component of the Stark field. This is a standing wave of frequency Ω and wavelength $\lambda/2$. (c) The Stark wave moving in the direction of propagation of the incident microwave radiation.

It consists of 33 parallel grids separated by $\lambda/4$ and electrically connected to produce a modulating field periodic in space and time superposed upon a uniform static electric field. Figure 2(a) is a plot of the instantaneous X component of the electric field produced by the grid structure. Through the quadratic Stark effect the resonant frequency of the molecules is shifted in proportion to the square of the total field strength; thus only the X component of the weak oscillating field contributes appreciably. Further, only the fundamental spatial fourier component of the square of the field need be considered. This is plotted in Fig. 2(b) and is seen to be a standing wave of frequency Ω and wavelength $\lambda/2$. It may be considered as the superposition of two waves, here called "Stark waves," running with a velocity $\Omega\lambda/2$. The modulation frequencies used, 5 to 100 kc, gave velocities comparable to molecular velocities.

For weak fields the two Stark waves act independently, and they will be discussed separately. Figure 2(c) shows the one moving in the direction of the incident radiation. There exists in the gas a class of molecules moving with this wave. Suppose the frequency of the microwave radiation is adjusted until the molecules at B, B', etc., are at resonance. Because of the Stark effect, molecules at A and C will be slightly off resonance, resulting in phase shifts of opposite sign in the radiation scattered by them, leading to constructive reflection.

From a slightly different point of view the class of molecules moving with the "Stark wave" may be considered as a moving medium of stratified index of refraction. Because of anomalous dispersion, molecules at A, A', etc., give the crests of the Stark wave an anomalously high index of refraction. Those at C contribute a low index. The result is a set of constructive reflections from the laminae of the moving medium when the Bragg condition is satisfied. The higher spatial fourier components of the Stark wave cannot satisfy the Bragg condition and cannot reflect constructively.

The remaining molecules drift with respect to the Stark wave. If their radiation is damped by collisions in a time T, the phases which they radiate average over this time. Thus only molecules drifting by less than one period with respect to the Stark wave in

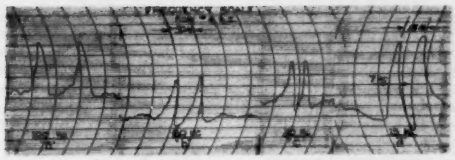

FIG. 3. The ammonia 3-3 line using the "Stark-wave" modulation method with several different modulation frequencies. (100, 60, 30, and 15 kc for (a) to (d), respectively). Pressure $\simeq 4\times10^{-4}$ mm Hg, dc field $=9.7$ v/cm, peak ac field $\simeq 7$ v/cm.

this time can contribute to a lamination and thus to the reflection. This condition requires that just those molecules whose Doppler shifts lie within an interval equal to the collision width contribute to the reflection.

The reflection takes place in a moving system. The Doppler effect shifts the molecular response from its natural frequency ω_0 to $\omega_0+\frac{1}{2}\Omega$, while the reflected frequency is lower than the incident by Ω and can be easily detected. The second Stark wave contributes a response at $\omega_0-\frac{1}{2}\Omega$ and on the opposite side band. Thus two narrow responses separated by a frequency Ω are obtained. These might be separately detected in a single side band receiver.

The ammonia 3-3 line using the "Stark-wave" modulation method is shown in Fig. 3 for several different modulation frequencies. Within the experimental uncertainty of 10 to 20 percent in sweep rate, the frequency separation of the two components equals the modulation frequency. Line widths as low as 7 to 10 kc were obtained.

The lower limit to the line width obtainable with a given cell is caused by collisions with the side walls. Collisions with end walls are not serious, since one component of the molecular velocity is controlled and can be chosen small. A crude estimate of the wall collision rate for ammonia at 300°K in a 10-cm cube yields a width of approximately 2 kc. This limitation may be overcome either by increasing the transverse dimensions of the cell or by limiting the transverse velocities of the molecules by using a very crude molecular beam.

The most serious limitation on any method of reducing line widths is the problem of intensity. Under similar conditions the "Stark-wave" method will yield the same signal strength as ordinary Stark modulation. However, the gas collision and saturation width must be reduced by the same ratio, R, as the Doppler width: the necessary reduction in pressure and incident power causes a loss in signal power proportional to R^4. This can be offset by increasing the dimensions of the cell.

* N.R.C. Predoctoral Fellow, 1946–1949.
† The work outlined here is the basis of a Ph.D. thesis to be submitted to Princeton University by George Newell, Jr. Experimental work is continuing under Signal Corps contract.

Dipolar Broadening in Antiferromagnetic Substances

NOBORU TSUYA, *Faculty of Technology, Tôhoku University, Sendai, Japan*
AND
YOSHIHIKO ICHIKAWA, *Faculty of Science, Tôhoku University, Sendai, Japan*
(Received June 11, 1951)

MICROWAVE resonance absorption in antiferromagnetic substances was studied experimentally by Trounson and others[1] using samples of Cr_2O_3, and it was found that the amount of absorption decreased abruptly when they were cooled through their Curie point. Especially in the powdered specimen, two peaks with broad width appeared below the Curie point, one of which shifted to the side of lower frequency with the fall of temperature. Recently, Okamura and his co-workers[2] made resonance measurements using sintered specimens of MnO, MnS, etc. They showed that the amount of absorption decreased with the fall of temperature, and that the line width increased rapidly, whereas the resonance field (g-factor) remained still unchanged on passing through the Curie point. A theoretical consideration concerning the above-mentioned phenomena is given below, referring to Kittel's suggestion quoted in reference 1.

The interaction between the microwave field and the spin system contains a factor S_x, the x-component of the total spin operator, and this causes a transition in which the total spin quantum number remains unchanged. We consider from this standpoint a system of spins in which each spin orients parallel or antiparallel to the direction of external field. (This is just like the case in which the c axis of an MnF_2 crystal[3] is placed parallel to the magnetic field.) Neglecting the anisotropic energy, the second moment of the resonance frequency is given by

$$\langle\nu^2\rangle=-\frac{\mathrm{spur}[(\mathcal{H}S_x-S_x\mathcal{H})^2\exp(-\mathcal{H}/kT)]}{h^2\,\mathrm{spur}[S_x^2\exp(-\mathcal{H}/kT)]}, \quad (1)$$

where the notation is that of Van Vleck.[4] The approximate line width is thus given by

$$\Delta H_{\frac{1}{2}}=2.35\times3^4\times8^{-1}g^4\beta^6\hbar^{-2}\{a+b(\lambda_1^4+\lambda_2^4+\lambda_3^4)\}^{\frac{1}{2}}\times F(T/T_c), \quad (2)$$

with

$$F(T/T_c)=\langle S_x^2\rangle^{\frac{1}{2}}[(n-1)\{1+\langle S_y^2\rangle^2/\langle S_x^2\rangle^2\}+0.322\{\langle S_x^4\rangle+\langle S_y^4\rangle-\langle S_y^2S_z^2\rangle\}/\langle S_x^2\rangle^2]^{-\frac{1}{2}}, \quad (3)$$

where n is the number of nearest neighbors and $\langle S_x^2\rangle=S(S+1)-SB_S(S\xi)$ etc., in which $B_S(S\xi)$ is a Brillouin function and ξ is determined from the equation $(S+1)T\xi=3T_cB_S(S\xi)$. Thus, it was found that the resonance field (g factor) is unchanged[5] at both sides of the Curie temperature T_c. To clarify the temperature dependence of the half-line width $\Delta H_{\frac{1}{2}}$, the function $F(T/T_c)$ in the above formula is shown in Fig. 1.

The effect of superexchange narrowing causes an increase of the ratio of the width at absolute zero to that at the Curie point. If the values of the exchange interactions estimated from Néel's theory[6] are put in the above formula, the calculated line widths are found to be several hundred oersted, These values are a little smaller than

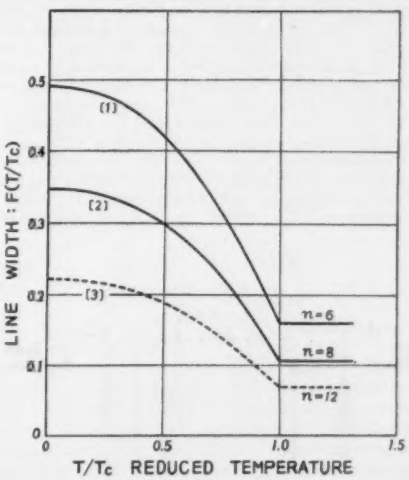

FIG. 1. Calculated factor $F(T/T_c)$, putting $S=5/2$, involved in the half-line width $\Delta H_{\frac{1}{2}}$, represented as a function of the reduced temperature T/T_c using Eq. (3). Curve [1] stands for the case of the simple cubic lattice, [2] for the body-centered cubic lattice, and [3] for the face-centered cubic lattice. The broken line for the f.c.c. lattice indicates that Eq. (2) does not hold rigorously for this lattice, because this lattice cannot be divided into two interpenetrating sublattices. Therefore, in this case we put $n=12$ formally in Eq. (3).

the observed ones. However, the effect of anisotropy energy in the actual crystal might make these values larger. Because the total absorption may be proportional to the magnetization of the specimen[7] and because of the above-mentioned line broadening, the intensity of absorption may decrease rapidly with the fall of temperature through the Curie point. The details of this discussion will be published later in *The Science Reports of the Tôhoku Imperial University*.

The authors wish to express their cordial thanks to Dr. T. Hirone, Professor of Tôhoku University, for valuable discussions throughout the course of this investigation.

[1] Trounson, Beil, Wangsness, and Maxwell, Phys. Rev. **79**, 542 (1950).
[2] Okamura, Torizuka, and Kojima, Phys. Rev. **82**, 285 (1951).
[3] M. Griffel and J. Q. Stout, Phys. Rev. **76**, 144 (1949); J. Chem. Phys. **18**, 1455 (1950).
[4] J. H. Van Vleck, Phys. Rev. **74**, 1168 (1948).
[5] This behavior arises from the fact that the exchange operator commutes with the total spin operator.
[6] L. Néel, Ann. phys. **3**, 137 (1948).
[7] K. W. H. Stevens, Phys. Rev. **81**, 1058 (1951).

Measurement of the F^{19} Magnetic Moment

T. Kanda, Y. Masuda, R. Kusaka, Y. Yamagata, and J. Itoh
Department of Physics, Osaka University, Osaka, Japan
(Received July 17, 1951)

A PRECISION measurement of the ratio of the magnetic moment of the proton to that of the fluorine nucleus in HF aq (22 percent solution) has been carried out using the magnetic resonance method.

The detector circuit is shown in Fig. 1. This circuit, known as "Inoue's circuit," had been used for detecting small changes in capacitance. In this circuit, a parallel resonance circuit which is composed of a variable capacitance and a coil is connected to the grid of a pentode tube (6J7) and the high frequency voltage was fed directly to the screen grid. When this circuit resonates by varying the capacitance, a very sharp change in the plate current is realized, so it can be used to detect a small change in capacity or inductance in this resonance circuit. Nuclear resonance will be detected by this circuit when a sample is introduced in the inductance coil, as the inductance of the coil changes by a small amount at the resonance. This detector was followed by a lock-in amplifier and recording milliammeter. Two similar sets were used, one for detecting proton resonance and the other for fluorine, both samples being HF aq. The magnetic field was produced by an electromagnet whose pole face was 15 cm square, with a gap of 4 cm. The modulation cycle was tuning fork controlled 200 cps.

The oscillator frequency for the fluorine resonance was crystal controlled at 8.0 Mc/sec, and in the magnetic field where the fluorine resonates at this frequency, the proton resonance occurs at about 8.5 Mc/sec. We set the oscillator for the proton slightly higher than this value and swept the magnetic field slowly from a higher value to a lower, so that we obtained first the proton resonance and next the fluorine resonance. Then the frequency of the self-oscillator for the proton was quickly lowered by a few kc/sec; and, as the magnetic field became lower, another proton resonance was recorded. By measuring the frequency difference of the two proton resonances and the distance on the recording paper between the two proton resonances and the fluorine resonance, we could interpolate the frequency of the proton resonance at the exact field strength for the fluorine resonance.

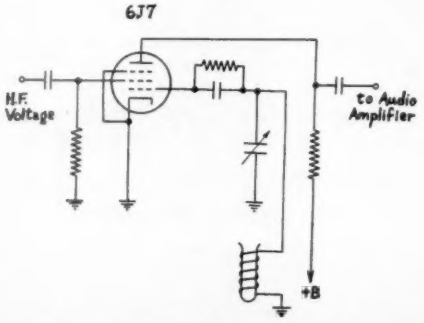

FIG. 1. Circuit diagram of the resonance detector.

TABLE I. Experimental results.

Run	μ_F/μ_H
2	0.940831
7	0.940825
9	0.940818
11	0.940803
12	0.940792
17	0.940815
18	0.940784
26	0.940820
28	0.940829
29	0.940830
38	0.940811
40	0.940807
	Mean 0.940814 ± 0.000009

To measure the frequency, the beat with a 500-kc/sec crystal oscillator calibrated by a 8-Mc/sec standard frequency (J.J.Y.) was measured by a bridge-type audio frequency meter.

The results of 12 independent runs are given in Table I. The stated uncertainty is three times the usual probable error.

The ratio of the magnetic moment of the fluorine nucleus to that of the proton with the sample of HF aq is, without diamagnetic correction,

$$\mu_F/\mu_H = 0.940814 \pm 0.000009.$$

It is in exact agreement with, but a little more accurate than, the value of Siegbahn and Lindström,[1] which is 0.940816 ± 0.000015.

Details of the experiment will be published elsewhere.

[1] K. Siegbahn and G. Lindström, Arkiv Fysik **1**, 6, 193 (1949).

Erratum: On the Evaluation of the *S*-Matrix

[Phys. Rev. **81**, 455 (1951)]

F. Coester
State University of Iowa, Iowa City, Iowa

IN the recursion formula Eq. (3) a class of terms has been overlooked. The correct formula is

$$\begin{aligned} F_n(k_1\cdots,l_2\cdots) = {} & F_{n-1}(k_1-1\cdots,l_2\cdots) + \sum_{m=1}^{n-1}(k_m+1) \\ & \times\{2F_{n-1}(\cdots k_m+1, k_{m+1}-1\cdots,l_2\cdots) \\ & + F_{n-1}(\cdots k_m+1\cdots,\cdots l_{m+1}-1\cdots)\} \\ & + \sum_{m\le\frac{1}{2}(n-1)}(k_m+2)(k_m+1) \\ & \times F_{n-1}(\cdots k_m+2\cdots k_{2m+1}-1\cdots,l_2\cdots) \\ & + \sum_{\substack{m_1<m_2 \\ m_1+m_2\le n-1}}(k_{m_1}+1)(k_{m_2}+1) \\ & \times 2F_{n-1}(\cdots k_{m_1}+1,\cdots k_{m_2}+1\cdots k_{m_1+m_2+1}-1\cdots,l_2\cdots). \end{aligned} \tag{3}$$

Hence

$$F_n(k_1\cdots,l_2\cdots) = n!\prod_{m=1}^{n}\frac{1}{k_m!\,l_m!\,m^{l_m}}. \tag{4}$$

High Energy Protons Emitted from Carbon at 90° to a 240-Mev Proton Beam*

G. M. TEMMER
Department of Physics, University of Rochester, Rochester, New York
(Received June 22, 1951)

THE differential cross section for the emission of protons at right angles to the 240-Mev circulating proton beam of the Rochester synchrocyclotron has been determined for carbon as a function of the outgoing proton energy. The energy interval from 60 Mev to 190 Mev has been studied thus far.

The energy spectrum was obtained by sampling the population of track endings in 100-micron Kodak NTA nuclear emulsions embedded at different depths of a copper absorber, a method similar to that used in meson production experiments.[1] A knowledge of the track density can then be translated into an energy distribution by use of range-energy curves[2] and from the known geometry. The absorber was inserted into the cyclotron tank at an average distance of 4.5 inches vertically beneath a graphite target and was shielded by four inches of copper from the direct proton beam. The carbon target was about 7 Mev thick to the incident beam and no thicker than 0.6 Mev to the emerging protons of lowest energy. The incident proton current necessary to affix absolute values to the cross sections was determined by the well-known carbon activation method, using a value of 48 millibarns for the $C^{12}(p, pn)C^{11}$ cross section at 240 Mev.[3]

Table I gives the values of the differential cross section per unit energy range per carbon nucleus as a function of the proton energy. A plot of the experimental points[4] is shown in Fig. 1. The rectangles indicate the extent of the probable errors in both the energy and cross-section values. The probable errors given for the latter are purely statistical; no attempt has been made to incorporate possible systematic errors. Furthermore, the entire absolute value scale has been assigned an error of ±50 percent. The principal uncertainty in the energy scale arises from the radial oscillations of the proton beam and multiple traversals of the target, contributing an estimated ±8 Mev. Range straggling in the absorber was calculated using the high energy approximation given by Livingston and Bethe[5] and was found not to exceed ±1.2 Mev.

A correction has been applied for nuclear absorption of the protons in the copper absorber, using the inelastic neutron cross sections for copper determined in "poor geometry" experiments at 95 Mev[6] and 270 Mev,[7] and one-half the total neutron cross section measured at 42 Mev;[8] corrections for intermediate energies were obtained by interpolation. This correction varied from 6 percent to 25 percent between the lowest and highest detected proton energies.

Neutron interactions in the copper absorber give rise to charged particles which contribute undesirable track endings in the emulsions. To estimate the extent of this background effect, two methods of approach were used. First, the number of neutron stars observed in the emulsion yields a value for the effective neutron flux at various depths, assuming that the star production cross section is of the order of the inelastic neutron cross section. One can then estimate the number of spurious track endings which will be produced in an effective layer of absorber adjacent to the photographic plate. Second, a plate was exposed behind four inches of copper (range of 240-Mev protons ~2.5 inches). All tracks which are seen to stop are then attributable to neutron background. Again correcting for nuclear absorption, one arrives at a figure for spurious track endings. Both of these estimates yielded a background approximately equal to one-third of the observed value of the cross section at the highest proton energies investigated. However, because of the inherent uncertainties involved in comparing different exposures in a circulating beam, it is believed that the values above ~150 Mev may be largely due to background. The break in the energy distribution in that vicinity lends support to this view.

TABLE I. Energy distribution of 90° protons from carbon. Cross sections are corrected for nuclear absorption but not for background. Uncertainties are purely statistical.

Proton energy (Mev)	No. of tracks observed	$(d^2\sigma/d\Omega dE) \times 10^{28}$ (cm²/Mev-steradian)
61.2	168	4.69 ±0.36
73.1	195	4.89 ±0.36
83.6	159	3.17 ±0.25
93.5	149	2.17 ±0.16
103.1	114	2.01 ±0.19
113.8	150	1.45 ±0.12
132.1	109	0.81 ±0.10
143.8	70	0.59 ±0.07
155.7	70	0.52 ±0.06
167.5	64	0.54 ±0.07
179.8	52	0.51 ±0.07
191.8	35	0.50 ±0.08

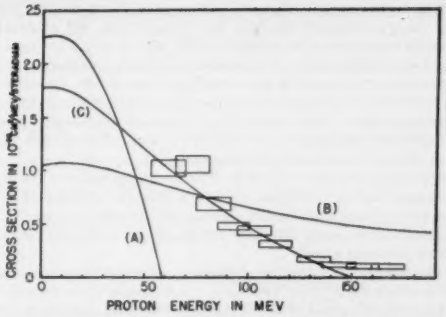

FIG. 1. Comparison of experimental points with theoretical energy distributions for protons emitted at right angles, based on different models for complex nuclei: (A) degenerate Fermi gas, $E_{max}=22$ Mev, $V=30$ Mev; (B) distribution of Chew and Goldberger (see reference 10), characteristic energy $E_p=18$ Mev; (C) same as (B) with the additional assumption of a cut-off at $E_c=72$ Mev. Rectangles denote experimental points multiplied by 2.2.

The particles whose track endings are observed are believed to be mostly protons because (a) particles with higher charge, even with maximum energy compatible with conservation laws, have ranges which are smaller than those observed here, (b) mesons are produced about 100 times less abundantly at our energies,[1,9] (c) high energy deuterons are emitted preferentially forward, but do presumably constitute a small fraction of the particles observed. However, for a given proton energy value the deuteron energy would be about 35 percent higher.

The presence of protons at right angles to the beam with energies up to ~150 Mev and possibly beyond sheds some light on the high momentum nucleons present in the carbon nucleus. The necessity for high momenta was pointed out by Chew and Goldberger[10] when they attempted to interpret the production of high energy deuterons reported by Hadley and York.[11] High energy photoprotons from carbon have also been observed[12] and again seem to require high target nucleon momenta for their interpretation.[13] There is also some evidence along these lines derived from π^+ meson production in carbon.[14]

It should be noted that the upper limit of the secondary proton spectrum predicted by the degenerate Fermi gas model with 22-Mev maximum energy for single nucleon-nucleon encounters is 59 Mev. A target nucleon energy of 72 Mev is required to account for 150-Mev protons at 90° in single collisions. Although favorable secondary collisions within the nucleus make high energy protons energetically possible, they are not believed to be the primary mechanism contributing to the high energy "tail" of the observed distribution, in view of the fact that the nucleon-nucleon collision mean free path is only slightly less than the diameter of the carbon nucleus (6.4×10^{-13} cm). The magnitude of the observed cross section lies close to the values predicted by simple theoretical models based on single encounters only, which necessarily repre-

sent upper limits, since the cross section integrated over all angles and energies yields 0.378 barn for carbon, while the observed inelastic cross section for neutrons of 270 Mev is only 0.144 barn.[7] The theoretically expected distribution for single collisions with a degenerate Fermi gas[15] is shown in Fig. 1, curve (A). Curve (B) represents the theoretical distribution expected on the basis of the momentum distribution deduced by Chew and Goldberger[10] from the deuteron pick-up process.[11] Curve (C) was calculated like (B) with the additional empirical assumption of a cut-off in the momentum distribution at 72 Mev. The rectangles indicate the experimental values multiplied by 2.2. Within the accuracy of the experiment some distribution such as that leading to curve (C) adequately represents the data, except for the very high energy points discussed above.

The differential diffraction scattering cross section for carbon at 90° is about 4×10^{-29} cm²/steradian when calculated according to the model of Fernbach *et al.*[16] It is planned to extend measurements into the region of elastically scattered protons in order to look for this contribution.

I am grateful to Dr. J. B. French for helpful discussions and to John Lowe, Jr., for most of the microscopy involved.

* Work performed under the auspices of the AEC.
[1] C. Richman and H. A. Wilcox, Phys. Rev. **78**, 496 (1950).
[2] Aron, Hoffman, and Williams, AECU 663 (UCRL 121), unpublished.
[3] Aamodt, Peterson, and Phillips, UCRL 526, unpublished.
[4] Ordinates of the experimental points are shown multiplied by 2.2 for purposes of comparison with theory.
[5] M. S. Livingston and H. A. Bethe, Revs. Modern Phys. **9**, 283 (1937).
[6] J. DeJuren and N. Knable, Phys. Rev. **77**, 606 (1950).
[7] J. DeJuren, Phys. Rev. **80**, 27 (1950).
[8] R. H. Hildebrand and C. E. Leith, Phys. Rev. **80**, 842 (1950).
[9] S. B. Jones and R. S. White, Phys. Rev. **78**, 12 (1950).
[10] G. F. Chew and M. L. Goldberger, Phys. Rev. **77**, 470 (1950).
[11] J. Hadley and H. F. York, Phys. Rev. **80**, 345 (1950).
[12] D. Walker, Phys. Rev. **81**, 634 (1951).
[13] J. S. Levinger, quoted in reference 12.
[14] E. M. Henley and R. H. Huddlestone, Phys. Rev. **82**, 754 (1951).
[15] I am indebted to Dr. J. B. French for the derivation of the general expression involved.
[16] Fernbach, Serber, and Taylor, Phys. Rev. **75**, 1352 (1949).

Calculations Concerning the Measurement of the Energy of Charged Particles by Small Angle Scattering*

HARTLAND S. SNYDER
Brookhaven National Laboratory, Upton, Long Island, New York
(Received June 22, 1951)

A COMMON method for determining the energy of particles in photographic emulsions is to measure the mean absolute angle between successive chords on a track. For the papers by Snyder and Scott[1] and by Scott and Snyder[2] various tables of distribution functions were computed and relations determined from which one can find the relationships among the mean absolute angle $\bar{\alpha}$ between successive chords on a track, the momentum p of the particle, the velocity v of the particle, the chord length s, and the composition of the matter through which the particle is passing. Defining the scattering constant K, which is a function of $s_0=s/\beta^2(\beta=v/c)$, by

$$K(s_0)=\bar{\alpha}pv/s^{\frac{1}{2}}, \tag{1}$$

one obtains

$$K(s_0)=\sqrt{2}(\bar{\alpha}'/z^{\frac{1}{2}})(\eta_0 pv/\lambda^{\frac{1}{2}}), \tag{2}$$

in which $\bar{\alpha}'=\alpha/\eta_0$ is a function of z. The quantities z, λ, and η_0 are

TABLE I. Calculated values of the scattering constant $K(s_0)$.

z	s_0	$\bar{\alpha}'/z^{\frac{1}{2}}$	$K(s_0)$
100	0.0801	0.912	22.96
400	0.3205	1.001	25.20
1600	1.282	1.085	27.32
6400	5.128	1.153	29.02
25600	20.51	1.219	30.69

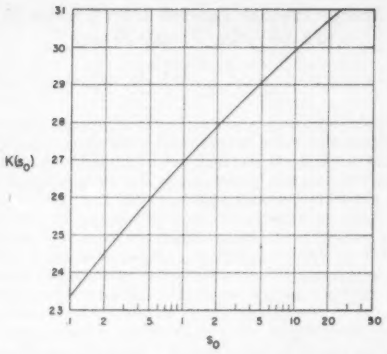

FIG. 1. Graph of $K(s_0)$ against s_0 on a semilogarithmic scale. The scattering constant K is given in units of Mev-deg/$(100\mu)^{\frac{1}{2}}$. The quantity $s_0=s/\beta^2$ is given in units of 100μ.

defined by

$$z=2s/\lambda, \tag{3}$$

$$1/\lambda=(4\pi/\beta^2)(\hbar/mc)^2\sum N_iZ_i^{4/3}, \tag{4}$$

and

$$\eta_0^2\beta^2p^2/\lambda=4\pi e^4\sum N_iZ_i^2. \tag{5}$$

The meanings of the symbols in these equations are given in the above-mentioned papers. For the values of $\sum N_iZ_i^2$ and $\sum N_iZ_i^{4/3}$ the composition of a standard Ilford emulsion was used, and the corresponding values were found to be 3.704×10^{26}/cm³ and 3.33×10^{24}/cm³. Substituting numerical values in Eqs. (2) and (3), one obtains[3]

$$z=1248s_0 \tag{6}$$

if s_0 is measured in units of 100μ, and

$$K(s_0)=25.18\bar{\alpha}'/z^{\frac{1}{2}} \tag{7}$$

if K is measured in units of Mev-deg/$(100\mu)^{\frac{1}{2}}$. The values of $\bar{\alpha}'$ were computed for various values of z from tables available at Brookhaven National Laboratory. The results of this calculation are given in Table I. These values of $K(s_0)$ are also plotted against s_0 on a semilogarithmic scale in Fig. 1.

From these values of K and measured values of $\bar{\alpha}$, one can obtain by use of Eq. (1) the value of pv (in Mev) for the particle.

* Research carried out under contract with the AEC.
[1] H. S. Snyder and W. T. Scott, Phys. Rev. **76**, 220 (1949).
[2] W. T. Scott and H. S. Snyder, Phys. Rev. **78**, 223 (1950).
[3] The relation (6) among z, s, and β is valid only for large β, approximately for $\beta>\frac{1}{2}$, because the Born approximation was used in determining the effect of screening on the mean free path, λ. If a better value of λ is used, then Eq. (3) should be used to determine z. Since K is a function of z only, a graph of K as a function of z enables one to determine the appropriate value of the scattering constant for any given case. Actually, a precise value of λ is not very important, since a change in λ by a factor of four changes the scattering constant by about five percent.

Neutron Deficient Europium and Gadolinium Isotopes*

R. W. HOFF, J. O. RASMUSSEN, AND S. G. THOMPSON
Radiation Laboratory and Department of Chemistry, University of California, Berkeley, California
(Received July 12, 1951)

A STUDY has been made of the light europium and gadolinium isotopes produced by bombardment of samarium and europium oxides with energetic protons, deuterons, and helium ions. In addition to the natural oxides, electromagnetically concentrated isotopes of samarium were used as target materials.[1] In some of the bombardments chemical separations of the target

TABLE I. Observed radiations.

Isotope	Type of radiation	Half-life	Radiation characteristics	Produced by	Bombarding particle energy	Chemical separation
Eu^{145}	*EC*, e^-	5±1 days	0.2 Mev e^-	recoil nuclei from α-decay of Tb^{149}	—	—
				$Sm^{147}(p, 3n)Eu^{145}$	50 Mev	Ion exchange column
Eu^{146}	*EC*, e^-	38±3 hrs	0.4 Mev e^-	$Sm^{147}(d, 3n)Eu^{146}$	19 Mev	no
				$Sm^{144}(\alpha, 2n)Gd^{146}$		
				$(\alpha, pn)Eu^{146}$	25 Mev	no
Eu^{147}	*EC*, e^-, no β^+	24±2 days	2.88±0.1 Mev α 0.2 Mev e^- $\alpha/EC \sim 10^{-5}$	$Sm^{147}(p, n)Eu^{147}$	8.5 Mev	Ion exchange column
Eu^{148}	*EC*, e^-, γ no β^+	50±2 days	0.38 Mev e^-	$Sm^{148}(p, n)Eu^{148}$	8.5 Mev	no
Eu^{149}	—	<1 hr or >50 days	—	$Sm^{149}(p, n)Eu^{149}$	8.5 Mev	no
Gd^{149}	*EC*, e^-, α, γ	9±1 days	3.0±0.15 Mev α 0.35 Mev e^-	$Eu^{151}(p, 3n)Gd^{149}$	28–32 Mev	sodium amalgam
				$Sm^{147}(\alpha, 2n)Gd^{149}$	28–30 Mev	no
				$Sm^{152}(\alpha, xn)Gd^{149}$	36 Mev	sodium amalgam

materials were not considered necessary because of restrictions on the number of possible isotopes produced due to the use of low energy bombarding particles and enriched isotopes. When necessary, separations of europium and samarium were made using a cation exchange resin column (Dowex-50, pH of citrate=3.3–3.5) at elevated temperatures as described in a recent article by Thompson, *et al.*[2] Separations of europium and gadolinium were made using a sodium amalgam reduction method[3] to overcome the difficulty of their separation in a cation exchange column. The conversion electron energies were determined from aluminum and beryllium absorption data. A search for positron emission in most of the nuclides studied here was made using a 180° beta-ray spectrometer of low resolution (see Table I).

The decay of europium isotopes with mass numbers 147 and 148 was observed after proton bombardments of enriched samarium isotopes (see Table I). The (p, n) reaction is probably virtually the only nuclear reaction induced by 8.5-Mev protons on samarium. The threshold of the $(p, 2n)$ reaction is estimated to be 9–10 Mev for $Sm^{147-149}$ using neutron binding energies calculated from the semi-empirical mass equation[4] and estimated electron capture decay energies. This assumption is borne out by the experimental observation that when rare earth samples consisting of a single relatively pure isotope are bombarded with 8.5-Mev protons, only one radioactive species is produced in high yield. The decay of Eu^{149} formed in a proton bombardment of Sm^{149} has not been observed, thus making it possible to set limits on the half-life of Eu^{149}. Our assignment of the 50-day activity to Eu^{148} is in disagreement with the assignment of a 53-day activity to Eu^{147} by Marinsky and Glendenin,[5] who based their assignment on calculations using the Bohr-Wheeler equations. Eu^{147} showed rare alpha-decay branching[6] ($\alpha/EC \sim 10^{-5}$) with a particle energy of 2.88±0.1 Mev as measured with the differential alpha-pulse analyzer.[7]

Another isotope of europium, Eu^{146}, was observed as recoil nuclei from the alpha-decay of Tb^{149}. The terbium was produced in a 150-Mev proton bombardment of gadolinium oxide and isolated using a cation exchange column separation. The Eu^{146} has also been produced in a 50-Mev proton bombardment of $Sm_2{}^{147}O_3$.

The radionuclide, Eu^{146}, was observed after a helium ion bombardment of $Sm_2{}^{144}O_3$. A series of samarium oxide targets were placed between a series of stacked platinum foils which degraded the energy of the helium ions through a range from 36 Mev to 13 Mev. Decay of the samples showed the 38-hour activity was formed in greatest abundance with 25-Mev helium ions. At this approximate energy an (α, pn) reaction or $(\alpha, 2n)$ reaction followed by electron capture decay was considered the predominant mechanism for the production of the nuclide.[8] The 38-hour period was also observed after a 19-Mev deuteron bombardment of enriched $Sm_2{}^{147}O_3$, thus ruling out a possible assignment to Gd^{146} but consistent with an assignment to Eu^{146}.

A gadolinium isotope, Gd^{149}, has been observed as a product in a number of different bombardments. Natural europium oxide was bombarded with protons in a stacked foil arrangement which produced a proton energy range from 32 Mev to 8 Mev. The Gd^{149} was produced in largest yield with 28- to 32-Mev protons, and therefore, a $(p, 3n)$ reaction was assumed as the predominant mechanism in the production of this isotope. This 9-day period, belonging to Gd^{149}, was also produced in a helium ion bombardment of enriched $Sm_2{}^{147}O_3$ also placed between stacked platinum foils. The helium ion energy range through the target was 36 Mev to 13 Mev. The 9-day activity was produced in largest yield with 28- to 30-Mev helium ions, and an $(\alpha, 2n)$ reaction was assumed as the predominant mechanism for the production of this isotope. Measurements with the differential alpha-pulse analyzer gave indication of alpha-branching of this isotope with a particle energy of 3.0±0.15 Mev.

This work is being continued and a more complete report will be published at a later date.

We wish to express our appreciation to J. G. Hamilton, T. M. Putnam, G. B. Rossi, and the crew of the 60-inch Crocker Laboratory cyclotron, J. T. Vale and the crew of the 184-inch cyclotron, and R. D. Watt and the crew of the proton linear accelerator for their cooperation. We also wish to thank the Isotope Research and Development Division of the Y-12 Research Laboratory, Oak Ridge, Tennessee, for making available to us the enriched isotopes which made much of this work possible. It is a pleasure to acknowledge the continued interest of Dr. G. T. Seaborg.

* This work was performed under the auspices of the AEC.

† $Sm_2{}^{144}O_3$ (72 percent), $Sm_2{}^{147}O_3$ (81 percent), $Sm_2{}^{148}O_3$ (76 percent), $Sm_2{}^{149}O_3$ (71 percent).

‡ Thompson, Ghiorso, and Seaborg, Phys. Rev. **80**, 781 (1950).

§ W. W. Meinke, AEC Declassified Document AECD-2738 (August, 1949), unpublished.

‖ C. F. v. Weizsacker, Z. Physik **96**, 431 (1935); N. Bohr and J. A. Wheeler, Phys. Rev. **56**, 426 (1939); E. Fermi, *Nuclear Physics* (The University of Chicago Press, Chicago, 1950), p. 7.

¶ J. A. Marinsky and L. E. Glendenin, *Radiochemical Studies: The Fission Products* (McGraw-Hill Book Company, Inc., New York, 1951), Paper No. 336, National Nuclear Energy Series, Plutonium Project Record, Volume IX.

** Rasmussen, Thompson, and Ghiorso, to be published.

†† Ghiorso, Jaffey, Robinson, and Weissbourd, *The Transuranium Elements: Research Papers* (McGraw-Hill Book Company, Inc., New York, 1949), Paper No. 16.8, National Nuclear Energy Series, Plutonium Project Record, Volume XIVB.

‡‡ E. L. Kelley and E. Segrè, AEC Unclassified Document AECU-88 (November, 1948), unpublished.

Atomic Arrangements in Gold-Nickel Solid Solutions*

P. A. FLINN AND B. L. AVERBACH
Massachusetts Institute of Technology, Cambridge, Massachusetts
(Received July 17, 1951)

MEASUREMENTS of diffuse x-ray scattering from gold-nickel solid solutions have given results which differ markedly from the predictions of the simple statistical theory. This system shows a continuous solid solubility in a face-centered cubic lattice above 840°C; below this temperature two other face-centered cubic lattices, one rich in nickel and the other in gold, coexist. Above 840°C, therefore, the solid solution is expected to contain nickel-rich and gold-rich clusters which act as nuclei for the subsequent precipitation.

Mr. L. Seigle, of this laboratory, has shown by means of thermodynamic measurements that this system exhibits positive deviations from Raoult's Law and has positive heats of mixing. This is also interpreted as an indication that the equilibrium arrangement for the solid solution above 840°C is one which exhibits a preference for Ni-Ni and Au-Au nearest neighbor pairs. In contrast to this, the copper-gold system, above the critical temperature, exhibits positive deviations from Raoult's Law and has negative heats of mixing. X-ray measurements have shown that the equilibrium atomic arrangement in this system is one in which Cu-Au pairs are preferred.

The diffuse scattering expected from a nickel-gold solid solution containing clusters has been calculated. Such a powder pattern should show an intense small angle scattering which falls smoothly to a minimum and exhibits a weak secondary peak in the vicinity of the first lattice reflection.

Measurements of diffuse x-ray scattering from nickel-gold solid solutions have been made by both photographic and Geiger-counter spectrometer techniques. Results have been obtained for alloys containing 10 percent to 90 percent gold, and measurements have been made at 900°C as well as on specimens quenched from 900°C to room temperature. The general form of the observed scattering curve does not change on quenching and is similar for all of the compositions studied. A microphotometer trace of a typical diffraction photograph is shown in Fig. 1(a). This is a transmission powder photogram from a thin foil of Ni_2Au_2 quenched from 900°C and made in a vacuum camera with monochromatic Co Kα-radiation. The diffuse peak, which occurs at approximately $\theta=17°$, is clearly visible. For comparison, a microphotometer trace from a similar powder photogram of Cu_2Au is shown in Fig. 1(b). The short-range order peak in the latter film occurs at a much smaller diffraction angle.

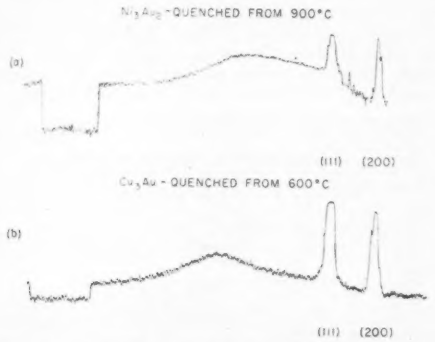

FIG. 1. Microphotometer traces of photograms of Cu_2Au and Ni_2Au_2.

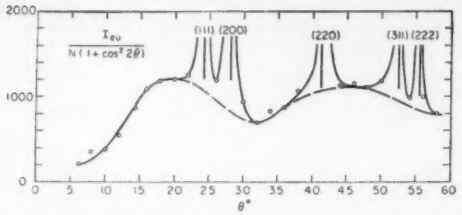

FIG. 2. Diffuse scattering in electron units from Ni_2Au_2 quenched from 900°C.

Quantitative measurements of the diffuse scattering have been made by means of a Geiger-counter spectrometer. Figure 2 shows the results for a sample of Ni_2Au_2 quenched from 900°C; the intensity in electron units was obtained by standardization with the scattering from paraffin. The form of the scattering is beyond the range of the photogram.

The diffuse scattering for Ni_2Au_2 differs considerably from that predicted by the clustering hypothesis, since there is no evidence of small angle scattering. On the other hand, the intensity distribution does not fit the form required for short range order of the Cu_2Au type. Attempts have been made by means of direct synthesis and by the use of the fourier transform to describe the results in terms of local order coefficients. Such a fit has not been possible.

These results indicate that there is no clustering of like atoms in these solid solutions. The exact atomic arrangement, however, will await further interpretation of the diffuse x-ray scattering, and further experiments with single crystals of the alloys.

* This work was performed under the auspices of the AEC.

Double Beta-Decay as a First-Order Process*

ROLF G. WINTER
Department of Physics, Carnegie Institute of Technology, Pittsburgh, Pennsylvania
(Received April 26, 1951)

THERE are two types of double beta theories which use Fermi hamiltonians. In one, no neutrinos are actually emitted, and half-lives of the order of 10^{15} years are obtained for $3mc^2$ available kinetic energy.[1–4] In the other, two neutrinos are emitted, and the half-life is 10^{24} years for $3mc^2$ available kinetic energy.[5,6] By analyses for the products of double beta-transitions, lower limits of about 10^{19} years were found for the half-lives[6,7] of Te^{128} and U^{238}, while a positive result of 10^{21} years was found for the half-life[8] of Te^{130}. If the last datum is correct, the two-neutrino hypothesis is untenable. Also, it may be questioned whether the no-neutrino picture is correct, for the transitions examined would all have to be forbidden. Therefore, it may be interesting to consider other approaches. Of course, the data are not sufficiently good to force the adoption of a new theory. In particular, the work of Fireman[3,4] is still unexplained. Also, it is to be expected that the transitions are somewhat forbidden, for the nuclei considered are far from being mirror nuclei.

To the Fermi hamiltonian will be added a term which couples two electrons to the nucleus in the same manner as that used in Fermi theory to couple one electron and one neutrino to the nucleus. This term is to contain a bilinear combination of creation operators which create two electrons in antisymmetric states only. Let this term be

$$2^{-\frac{1}{2}}g'\{(\Psi^\dagger\Omega_\alpha\delta\Psi^*)\Omega_\gamma Q+\text{complex conjugate}\}.$$

g' is a constant to be evaluated from experiment. Q is Q_1Q_2, an operator which changes two neutrons into two protons. Ω_e and Ω_N are both linear combinations of the five operators occurring in beta-theory; Ω_e operates on the electron wave functions while Ω_N operates on the nuclear wave functions. Ω_N is to be interpreted as $\Omega_{N1}+\Omega_{N2}$. δ is a matrix making $\delta\Psi^*$ a spinor. Writing

$$\Psi=\Sigma_m a_m\psi_m$$

and using the Jordan-Wigner anticommutation relation

$$a_m^*a_n^*+a_n^*a_m^*=0,$$

one obtains, as the perturbing hamiltonian for the creation of one electron into state m and another into state n,

$$2^{-\frac{1}{2}}g'\{(\psi_m^\dagger\Omega_e\delta\psi_n^*-\psi_n^\dagger\Omega_e\delta\psi_m^*)\Omega_NQ\}.$$

For the tensor and pseudovector interactions,

$$\psi_m^\dagger\Omega_e\delta\psi_n^*-\psi_n^\dagger\Omega_e\delta\psi_m^*=0$$

while for the scalar, vector, and pseudoscalar interactions,

$$\psi_m^\dagger\Omega_e\delta\psi_n^*-\psi_n^\dagger\Omega_e\delta\psi_m^*=2\psi_m^\dagger\Omega_e\delta\psi_n^*.$$

For these last three interactions, in the "allowed" approximation for plane wave electrons, the transition probabilities are:

Scalar: $w_S(\epsilon_m,\theta)d\epsilon_m d\theta$

$$=(\epsilon_m\epsilon_n+1)\left\{1-\frac{\alpha\cos\theta}{\epsilon_m\epsilon_n+1}\right\}F.$$

Vector: $w_V(\epsilon_m,\theta)d\epsilon_m d\theta$

$$=(\epsilon_m\epsilon_n+1)\left\{1+\frac{\alpha\cos\theta}{\epsilon_m\epsilon_n+1}\right\}F.$$

Pseudoscalar: $w_{PS}(\epsilon_m,\theta)d\epsilon_m d\theta$

$$=(\epsilon_m\epsilon_n-1)\left\{1-\frac{\alpha\cos\theta}{\epsilon_m\epsilon_n-1}\right\}F.$$

Here

$$F=\frac{4\pi^2(mc^2)^5}{c^6h^7}g'^2\alpha\sin\theta\frac{\epsilon_m\epsilon_n}{(1+\epsilon_m)(1+\epsilon_n)}d\epsilon_m d\theta,$$

$$\alpha=(\epsilon_m^2-1)^{\frac{1}{2}}(\epsilon_n^2-1)^{\frac{1}{2}},\quad \epsilon_n=\epsilon_0-\epsilon_m.$$

ϵ_m is the energy of an electron in the state m, and ϵ_0 is the nuclear mass difference, both in units of mc^2. θ is the angle between the electrons.

Integrating over ϵ_m and assuming that $\epsilon_0=5$, $|H^2|=1$, and the half-life $=10^{21}$ years, one finds that

$$G'=g'(1/mc^2)(mc/h)^3=10^{-24}.$$

It is interesting that the Fermi G is 10^{-11} for the lightest mirror nuclei; it may not be inconsistent to say that G' is G[3].

A fair approximation for the half-life as a function of ϵ_0 for $\epsilon_0>3$ is

$$\tau=2\times10^{24}\text{ years}/[\epsilon_0^2(\epsilon_0^2-4)(\epsilon_0-2)].$$

The term considered here will also make possible the emission of two electrons followed by the absorption of one of these electrons with the emission of a neutrino—that is, a second-order contribution to single beta-decay. However, in the integration over the momentum of the virtual electron, the integrand goes to zero rapidly when the wavelength of the electron becomes of the order of the nuclear diameter. It can then be seen that this contribution to single beta-decay is perhaps 10^{-30} as large as the first-order process.

I should like to acknowledge very helpful discussions with Professors L. Wolfenstein and J. Ashkin.

* This work was partially supported by the AEC.

[1] W. H. Furry, Phys. Rev. **56**, 1184 (1939).
[2] Bruno Touschek, Z. Physik **125**, 108 (1948–49).
[3] E. L. Fireman, thesis, Fine Library, Princeton University, Princeton, New Jersey, 1948 (unpublished).
[4] E. L. Fireman, Phys. Rev. **75**, 323 (1949).
[5] Maria Goeppert-Mayer, Phys. Rev. **48**, 512 (1935).
[6] M. G. Inghram and J. H. Reynolds, Phys. Rev. **76**, 1265 (1949).
[7] Levine, Ghiorso, and Seaborg, Phys. Rev. **77**, 296 (1950).
[8] M. G. Inghram and J. H. Reynolds, Phys. Rev. **78**, 822 (1950).

The Interpretation of Isomeric Transitions

STEVEN A. MOSZKOWSKI
Argonne National Laboratory and University of Chicago, Chicago, Illinois
(Received June 18, 1951)

THEORETICAL calculations.—The half-life of nuclear isomeric states as a function of gamma-ray energy, nuclear radius, and type and multipole order of radiation has been calculated. As a simple model, it is assumed that the radiation is due to a single proton moving in the potential well of the rest of the nucleus. Radial integrals which appear are replaced by the proper power of the nuclear radius R. Because of cancellation of nuclear wave functions, this is expected to give a considerable overestimate of the values of the radial integrals and thus an underestimate of the half-life.

The half-life τ_γ for change of nuclear spin I from $L+\frac{1}{2}$ to $\frac{1}{2}$ is calculated to be

$$\tau_\gamma{}^{EL}=0.693\left[\frac{2(L+1)}{L(1\cdot3\cdot5\cdots2L+1)^2}\frac{e^2}{\hbar c}\omega\left(\frac{\omega}{c}R\right)^{2L}\right]^{-1},$$

for electric 2^L-pole radiation (EL), (1)

$$\tau_\gamma{}^{ML}=\tau_\gamma{}^{EL}\left[\frac{\hbar}{mcR}\left(\mu L-\frac{L}{L+1}\right)\right]^{-2},$$

for magnetic 2^L-pole radiation (ML). (2)

This is the theoretical half-life for gamma-emission[1] not including the effect of internal conversion. Here μ denotes magnetic moment due to intrinsic spin. The angular frequency of the radiation is ω. The mass of the proton is m. Equations (1) and (2) are nearly unchanged for any other transition for which the nuclear spin decreases by L; if the spin increases by L, the above half-lives are multiplied by the factor $(2I_{\text{initial}}+1)/(2I_{\text{final}}+1)$. Figure 1 shows both the theoretical estimates and the experimental values of the half-life of odd-A nuclei, the latter corrected for internal

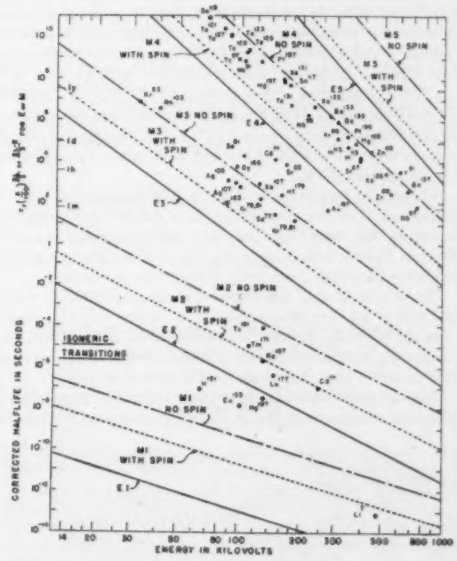

FIG. 1. Corrected half-life of odd-A isomeric transitions as function of energy. The points show experimental values of half-lives corrected for internal conversion (using theoretical values), and to $A=100$. The lines indicate theoretical predictions from the single-proton model, according to Eqs. (1) and (2), for $A=100$. (Nuclear radius, $R=1.5\times10^{-13}A^{\frac{1}{3}}$ cm.)

conversion (using theoretical values[1,2]) and to $A=100$. There are two lines for each magnetic multipole order. For the line labeled "no spin," only the contribution of orbital proton motion to transitions has been considered ($\mu=0$). The other line, indicated by "with spin," has been calculated on the assumption that in addition to orbital motion all of the magnetic moment due to intrinsic proton spin contributes to the interaction responsible for the transition ($\mu=2.79$).

Interpretation of Data.—There is a very well-defined group of transitions with half-lives and internal conversion data corresponding to magnetic 2^4-pole radiation, also[4] called $l=5$, involving a spin change of 4 and change of parity ($\Delta I=\pm 4$, yes). These transitions occur for odd nucleon numbers 39 to 49 and for 67 to 81, as predicted by the shell model.[5] Most of the transitions have half-lives which, when corrected for internal conversion, $A=100$, and energy, lie within a factor of 10 of each other. When the spins of initial and final state are considered, this agreement is improved to within a factor of 3. The half-lives fall near the "no spin" line and are larger by a factor of the order of 100 than for the "with spin" line. This is probably not due to the absence of a spin effect but happens because the spin effect is counterbalanced by cancellation of wave functions in the radial integral.

There is another not so well-defined group of shorter half-lives, also called $l=4$. The interpretation of experimental conversion coefficients and K/L ratios for the Kr^{83} and Ag^{107} transitions[2,3,6,7] favors an assignment of electric 2^3-pole radiation ($\Delta I=\pm 3$, yes) for both cases. It is likely that many of the other transitions in this group are also electric 2^3-pole. Figure 2 shows decay schemes for these cases. The single particle shell model is modified in that one postulates the existence of levels whose spins are determined by coupling spins of several odd nucleons. Thus 3, 5, or 7 nucleons in a $g_{9/2}$ orbit couple to give a state of 7/2 even, in addition to the expected state of 9/2 even. The electric 2^3-pole transitions occur for 43, 45, or 47 odd nucleons exactly where there are 3, 5, or 7 $g_{9/2}$ particles according to the shell model. They are not found for 39, 41, or 49 odd nucleons where there is one particle or one hole in the $g_{9/2}$ shell. A magnetic dipole gamma-ray should follow these transitions wherever the ground state is 9/2 even, as happens for Kr^{83} and Tc^{99}. The half-lives of these electric 2^3-pole transitions are 1000 or more times larger than the theoretical formula. For a many-particle transition to or from a $(g_{9/2})^2 7/2$ level, the effect of cancellation in the radial integral is probably large enough to account for a factor as large as this.

In regard to very short-lived states, a few transitions are well established as electric quadrupole ($\Delta I=\pm 2$, no). It is probably significant that those transitions with half-lives shorter than the theoretical predictions occur in the region of neutron and proton numbers where large quadrupole moments are prevalent.[8]

The half-life of only one magnetic dipole transition ($\Delta I=\pm 1$, no), that of Li^7, has been measured.[9] It agrees well with theory when the full value of proton magnetic moment is considered. No cancellation is expected for this case because the initial and final state probably have very similar radial wave functions.

Many of these conclusions have been reached independently by Goldhaber and Sunyar.[10] The author wishes to thank Dr. Maria G. Mayer for suggesting this problem and for valuable guidance throughout the course of the work.

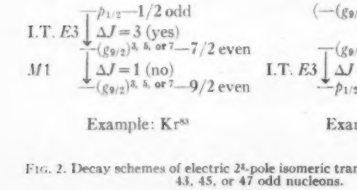

FIG. 2. Decay schemes of electric 2^3-pole isomeric transitions for nuclei with 43, 45, or 47 odd nucleons.

[1] The problem of gamma-ray half-lives was previously considered in some detail by Weisskopf with resulting estimates of τ_γ^{EL} same as given in Eq. (1), $\tau_\gamma^{ML}=\tau_\gamma^{EL}(\hbar/mcR)^{-2}$. J. M. Blatt and V. F. Weisskopf, Chapter XII of a forthcoming book on nuclear structure (John Wiley and Sons, Inc., New York).

[2] Rose, Goertzel, Spinrad, Harr, and Strong, Tables of K-Shell Conversion Coefficients, unpublished.

[3] P. Axel and R. F. Goodrich, Internal Conversion Data, ONR report (1950), unpublished.

[4] P. Axel and S. M. Dancoff, Phys. Rev. **76**, 894 (1949).

[5] M. G. Mayer, Phys. Rev. **78**, 16 (1950).

[6] I. Bergström, Phys. Rev. **81**, 638 (1951).

[7] E. Segrè and A. C. Helmholz, Revs. Modern Phys. **21**, 271 (1949).

[8] Townes, Foley, and Low, Phys. Rev. **76**, 1415 (1949).

[9] L. G. Elliott and R. E. Bell, Phys. Rev. **76**, 168 (1949).

[10] M. Goldhaber and A. W. Sunyar, Phys. Rev. **83**, 906 (1951).

Variation of Dielectric Constants of Ionic Crystals with Pressure

SUMNER MAYBURG
Westinghouse Atomic Power Division, Pittsburgh, Pennsylvania
(Received July 11, 1951)

RECENTLY, Rao[1] has disagreed with certain calculated results in my paper on the effect of pressure on the low frequency dielectric constant of ionic crystals.[2] In addition, Rao presents a Born-Madelung type theory by which he obtains good agreement with my experimental values.

It is the purpose of this letter to point out that the disagreement between Rao and myself can be completely explained by a difference in our definitions of compressibility. I define the compressibility of a material by

$$\chi=-\partial \ln V/\partial p. \tag{1}$$

The results of Rao's calculations indicate that he defines the compressibility as

$$\chi=-(1/V_0)\partial V/\partial p. \tag{2}$$

In (1) and (2), V is the volume at the pressure p and V_0 is the volume at zero pressure. The difference between (1) and (2) becomes important when one wants to determine the change of compressibility with pressure, $\partial\chi/\partial p$, from the data of Bridgman which are in the form

$$(V_0-V)/V_0=ap-bp^2, \tag{3}$$

where a and b are constants for a given material. Then, Eq. (1) leads to

$$(\partial\chi/\partial p)_{p=0}=-2b+a^2, \tag{1a}$$

while Eq. (2) yields

$$(\partial\chi/\partial p)_{p=0}=-2b. \tag{2a}$$

The difference between (1a) and (2a) is by no means negligible and may be as much as 25 percent.

Using the compressibility as defined by Eq. (1), I have recalculated the quantity $\partial \ln K/\partial p$ from the Born-Madelung equation used by Rao; the equation is

$$K-K_0=\text{constant}\ \rho^{4/3}\chi \tag{4}$$

TABLE I. Calculated and observed values of $-\partial \ln K/\partial p$.

	$-\partial \ln K/\partial p$ [from (4)]	$-\partial \ln K/\partial p$ [observed]
LiF	0.29×10^{-5} bars^{-1}	$0.448\pm0.028\times10^{-5}$ bars^{-1}
NaCl	0.72	0.98 ±0.06
KCl	0.59	1.05 ±0.08
KBr	0.66	1.17 ±0.09
MgO	0.13	0.320±0.019

where K is the low frequency dielectric constant, K_0 is the optical constant, ρ the density, and χ the compressibility. In Table I are listed the values of $\partial \ln K/\partial \rho$ calculated from (4) and (1) next to the experimental values of $\partial \ln K/\partial \rho$. The calculated values of $\partial \ln K/\partial \rho$ differ from those of Rao by the term $a(K-K_0)/K$, which arises from the difference between (1a) and (2a).

Equation (4) is derived assuming that the inner field polarizing the dielectric is independent of pressure. Since the values of $-\partial \ln K/\partial \rho$ obtained from (4) do not account for all the change in the dielectric constant, it seems consistent to expect that the inner field is not constant but does decrease with increasing pressure. This conclusion agrees with the one reached in my original paper using the theories of Hojendahl and Mott and Littleton.

[1] D. A. A. S. Narayana Rao, Phys. Rev. **82**, 118 (1951).
[2] S. Mayburg, Phys. Rev. **79**, 375 (1950).

Radiative Transition Probabilities in Nuclei

V. F. Weisskopf
Physics Department, Massachusetts Institute of Technology, Cambridge, Massachusetts
(Received July 20, 1951)

CONSIDER a transition from nuclear state a to nuclear state b with emission of a quantum of multipole radiation of angular momentum l (2^l-pole) and z component m. The transition probability per unit time is given by[1]

$$T(l,m)=\frac{8\pi(l+1)}{l[(2l+1)!!]^2}\frac{\kappa^{2l+1}}{\hbar}|A(l,m)+A'(l,m)|^2, \quad (1)$$

where $\kappa=2\pi\nu/c$ is the wave number of the emitted radiation, and the quantities A, A' are the multipole matrix elements caused by the electric currents and by the magnetization (spins), respectively. We find for electric radiation

$$A(l,m)=Q(l,m)=e\sum_{k=1}^{Z}\int r_k{}^l\, Y_{lm}{}^*(\theta_k,\phi_k)\,\varphi_b{}^*\varphi_a\, d\tau, \quad (2)$$

$$A'(l,m)=Q'(l,m)=-\frac{i\kappa}{l+1}\frac{e\hbar}{2Mc}\sum_{k=1}^{A}\mu_k \times\int r_k{}^l\, Y_{lm}{}^*(\theta_k,\phi_k)\,\mathrm{div}(\varphi_b{}^*\mathbf{r}_k\times\boldsymbol{\sigma}_k\varphi_a)\, d\tau, \quad (3)$$

where φ_a and φ_b are the wave functions of the nuclear states, M is the mass of each nucleon, $\mathbf{r}_k=(r_k,\theta_k,\phi_k)$ is the position vector of the kth nucleon, $\boldsymbol{\sigma}_k$ is its Pauli spin vector, and μ_k is its magnetic moment in nuclear magnetons. The sum in (2) extends over the protons, the sum in (3) over both protons and neutrons. These expressions are approximations valid for $\kappa R\ll 1$, where R is the nuclear radius.

The corresponding expressions for magnetic multipole radiation are

$$A(l,m)=M(l,m)=-\frac{1}{l+1}\frac{e\hbar}{Mc}\sum_{k=1}^{Z} \times\int r_k{}^l\, Y_{lm}{}^*(\theta_k,\phi_k)\,\mathrm{div}(\varphi_b{}^*\mathbf{L}_k\varphi_a)\, d\tau, \quad (4)$$

$$A'(l,m)=M'(l,m)=-\frac{e\hbar}{2Mc}\sum_{k=1}^{A}\mu_k \times\int r_k{}^l\, Y_{lm}{}^*(\theta_k,\phi_k)\,\mathrm{div}(\varphi_b{}^*\boldsymbol{\sigma}_k\varphi_a)\, d\tau, \quad (5)$$

where $\mathbf{L}_k=-i\mathbf{r}_k\times\boldsymbol{\nabla}_k$ is the orbital angular momentum operator (in units of $\hbar$) for the kth nucleon.

We can estimate these matrix elements by the following exceedingly crude method. We assume that the radiation is caused by a transition of one single proton which moves independently within the nucleus, its wave function being given by $u(r)Y_{lm}(\theta,\phi)$. In addition we also assume that the final state of the proton is an S state.[3] We then obtain

$$Q(l,m)\sim[e/(4\pi)^{\frac{1}{2}}][3/(l+3)]R^l \quad (6)$$

where the integral $\int r^l u_b(r)u_a(r)r^2dr$ over the radial parts of the proton wave functions was set approximately equal to $3R^l/(l+3)$. The other matrix elements are estimated by replacing div by R^{-1}. We get the rough order-of-magnitude guess

$$M(l,m)\sim[e/(4\pi)^{\frac{1}{2}}][3/(l+3)][\hbar/Mc]R^{l-1}, \quad (7)$$

$$M'(l,m)\sim[e/(4\pi)^{\frac{1}{2}}][3/(l+3)]\mu_P[\hbar/Mc]R^{l-1}, \quad (8)$$

where μ_P is the magnetic moment of the proton ($=2.78$). $Q'(l,m)$ can be neglected compared to $Q(l,m)$. We therefore get a ratio of roughly

$$(1+\mu_P{}^2)(\hbar/McR)^2\sim 10(\hbar/McR)^2$$

between the transition probability of a magnetic multipole and an electric one of the same order. This ratio is energy-independent in contrast to widespread belief.

Inserting these estimates into (1) we get for the transition probability of an electric 2^l-pole

$$T_E(l)\cong\frac{4.4(l+1)}{l[(2l+1)!!]^2}\left(\frac{3}{l+3}\right)^2\left(\frac{\hbar\omega}{197\ \mathrm{Mev}}\right)^{2l+1} \times(R\text{ in }10^{-13}\text{ cm})^{2l}\ 10^{21}\ \mathrm{sec}^{-1} \quad (9)$$

and for a magnetic 2^l-pole

$$T_M(l)\cong\frac{1.9(l+1)}{l[(2l+1)!!]^2}\left(\frac{3}{l+3}\right)^2\left(\frac{\hbar\omega}{197\ \mathrm{Mev}}\right)^{2l+1} \times(R\text{ in }10^{-13}\text{ cm})^{2l-2}\ 10^{21}\ \mathrm{sec}^{-1}. \quad (10)$$

The assumptions made in deriving these estimates are extremely crude and they should be applied to actual transitions with the greatest reservations. They are based upon an extreme application of the independent-particle model of the nucleus and it was assumed that a proton is responsible for the transition. On the basis of our assumptions the electric multipole radiation with $l>1$ should be much weaker for transitions in which a single neutron changes its quantum state. No such differentiation is apparent in the data.

In spite of these difficulties it may be possible that the order of magnitude of the actual transition probabilities is correctly described by these formulas. We have published these exceedingly crude estimates only because of the rather unexpected agreement with the experimental material which was pointed out to us by many workers in this field.

The author wishes to express his appreciation especially to Dr. M. Goldhaber and Dr. J. M. Blatt for their great help in discussing the experimental material and in improving the theoretical reasoning.

[1] We use the notation $(2l+1)!!=1\cdot3\cdot5\cdots(2l+1)$.
[2] This latter assumption can be removed; the corrections consist in unimportant numerical factors.

Nuclear Magnetic Resonance in Metals: Temperature Effects for Na^{23}

H. S. Gutowsky
Noyes Chemical Laboratory, Department of Chemistry, University of Illinois, Urbana, Illinois[*]
(Received July 2, 1951)

KNIGHT reported[1] that nuclear magnetic resonance frequencies are higher in metals than in chemical compounds. It has been proposed[2] that such frequency shifts are primarily the result of the contribution of conduction electrons to the magnetic field at the nuclei in the metal. This note gives an account of some related preliminary results including temperature and chemical effects, and also detailed line shape studies. Our experiments have been at fixed frequency using equipment and procedures outlined previously.[3,4]

The effect of temperature on the Na^{23} magnetic resonance shift in the metal, relative to a sodium chloride solution, is given in

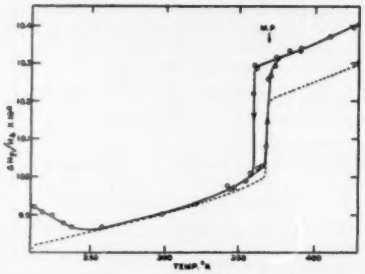

FIG. 1. Temperature dependence of the magnetic field required at fixed frequency for the Na^{23} nuclear resonance in the metal. ΔH_r is the difference in applied fields; the field required for resonance in the metal is subtracted from H_a, the resonance field for Na^{23} in aqueous NaCl. The dashed line is a theoretical curve representing the effect of thermal expansion on paramagnetic susceptibility.

Fig. 1. The sample, from National Distillers Chemical Corporation, was a 25 percent sodium dispersion in Nujol mineral oil; particle sizes ranged from 1 to 60μ, averaging 15μ. ΔH_r is the applied field, H_a, for resonance in aqueous NaCl, less that required for the metal. The resonance shift, $\sigma \equiv 10^4 \times \Delta H_r/H_a$, is relatively insensitive to temperature, varying by 5 percent from 210° to 425°K. Moreover, as suggested by Dr. C. P. Slichter in one of our discussions, most of the temperature dependence can be ascribed to volume effects. The alkali metals show a small increase with temperature in paramagnetic susceptibility, which Stoner attributes[5] to thermal expansion, on the basis of a free electron model. By analogy, the resonance shift would be $\sigma_T = (V_T/V_0)^{\frac{1}{3}}\sigma_0$, where the subscripts T and 0 refer to the given and a reference temperature, respectively, and V is the atomic volume. The dashed line in Fig. 1 represents this function, the reference temperature being chosen to be 25°C. The value of σ_0 is taken to be 9.9, the experimental relative value of σ at 25°C. It is seen that the values computed at higher temperatures with the equation $\sigma_T = (V_T/V_0)^{\frac{1}{3}} \times 9.9$ are lower than the observed σ by an amount that is proportional to the temperature effect on σ. This indicates that $\sigma = 9.9$ measured with respect to the NaCl solution is not the absolute σ value. The experimental values should all be increased by 2, and the theoretical equation changed to $\sigma_T = (V_T/V_0)^{\frac{1}{3}} \times 11.9$, to put everything on an absolute scale and get the two curves to agree. The hysteresis in the resonance shift below the melting point probably results from super-cooling. The low temperature increase starting at 250°K appears to be real; similar results have been obtained for Li[7].

The temperature dependence of the Na^{23} resonance line width in the metal is given in Fig. 2. The transition at 190°K is presumably

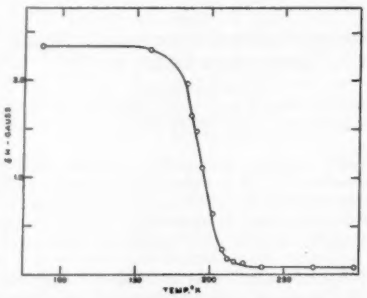

FIG. 2. The Na^{23} nuclear magnetic resonance line-width transition in the metal. The transition is consistent with an activation energy for self-diffusion of 9.5±1.5 kcal/g-atom. The measure of line-width used here is the peak-to-peak separation of the derivative of the absorption line.

associated with self-diffusion. An activation energy for self-diffusion of 9.5±1.5 kcal/g-atom is estimated[8] from the temperature and slope of the transition. The high temperature apparent line width of about 0.05 gauss is determined by field inhomogeneities and modulation effects. An independent analysis of the diffusion process is provided by the relaxation time measurements of Norberg and Slichter, which are presented and discussed in the accompanying letter.[7]

A comparison of Figs. 1 and 2 suggests that the low temperature increase in the resonance shift is perhaps associated with the diffusion process. For Na^{23} the increase in resonance shift starts at 255°K, a temperature about 65° above the line-width transition; in the case of Li^7 the increase starts at a temperature about 85° above the line-width transition at 255°K. The time average magnetic resonance field at the nuclei could change as the diffusion rate becomes less than the Larmor frequency. In fact, the relaxation time data[7] and also the line-width observations for Na^{23} indicate the diffusion frequency is about 1 Mc at 250°K.

Various room temperature observations have been made. The Cu^{63} and Cu^{65} resonance shifts in the metal with respect to $Cu_2Br_2(s)$ were observed to be[1] 23.46×10^{-4}, within experimental error of ±0.5 percent. Also, a chemical shift[4] of 0.56×10^{-4} was found between $Cu_2Cl_2(s)$ and $Cu_2Br_2(s)$ for Cu^{63} and Cu^{65} with an experimental error of ±5 percent; $Cu_2Br_2(s)$ required the higher applied magnetic field. The Al^{27} resonance in Al^{+3} aqueous solution and in anhydrous $AlCl_3(s)$ occurred in applied fields 0.81 and 1.32×10^{-4} higher than in AlO_3^- solution. Such chemical effects are an additional problem in the theoretical analysis[3] of resonance shifts in metals. The 20 percent factor suggested above for Na^{23} may reflect chemical effects; also, the temperature dependence itself complicates the issue.

Sodium, aluminum, and copper crystallize in cubic lattices for which electric quadrupolar broadening of the resonance line should be absent.[6] However, detailed line shape plots for the Na^{23} dispersion at 85°K and for Al^{27}, Cu^{63}, and Cu^{65} in the powdered metals at room temperature gave experimental second moments of about 0.95, 11.7, 7.2, and 5.8 gauss[2] compared with theoretical second moments on the basis of magnetic dipolar broadening alone[3] of 0.66, 7.5, 5.1, and 3.4 gauss[2], respectively. The high experimental values may result from anisotropy in the conduction electron shift in resonance frequency. Also, such anisotropy might generate electrical field gradients at the nuclei and lead to quadrupolar broadening. Experiments designed to determine the relative importance of the two factors include observation of metals with nuclear spin of $\frac{3}{2}$, the investigation of the dependence of second moments on applied field, and single-crystal studies.

The assistance of R. E. McClure with many of the measurements is gratefully acknowledged, as is the computation of several of the second moments by B. R. McGarvey and D. W. McCall. Equipment was provided mainly by a grant-in-aid from Research Corporation.

* Supported in part by the ONR.

[1] W. D. Knight, Phys. Rev. **76**, 1259 (1949).
[2] Townes, Herring, and Knight, Phys. Rev. **77**, 852 (1950).
[3] Gutowsky, McClure, and Hoffman, Phys. Rev. **81**, 635 (1951).
[4] H. S. Gutowsky and R. E. McClure, Phys. Rev. **81**, 276 (1951).
[5] E. C. Stoner, Proc. Roy. Soc. (London) **A152**, 672 (1935).
[6] H. S. Gutowsky and G. E. Pake, J. Chem. Phys. **18**, 162 (1950).
[7] R. E. Norberg and C. P. Slichter, Phys. Rev. **83**, 1074 (1951).
[8] R. Bersohn, Ph.D. thesis, Harvard University, Cambridge, Massachusetts (1949).

Nuclear Relaxation Times in Metallic Na^{23}

R. E. NORBERG AND C. P. SLICHTER
*Department of Physics, University of Illinois, Urbana, Illinois**
(Received July 2, 1951)

NUCLEAR magnetic relaxation times T_1 (spin-lattice) and T_2' (spin phase-memory) have been measured in metallic sodium as a function of temperature from −58°C to +80°C using the spin-echo method.[1] The apparatus was a modified version of

that used by one of the authors to investigate hydrogen-palladium systems.[2] The sample was a dispersion of sodium in mineral oil as described in the accompanying letter.[3]

Within experimental error, T_1 appears to be inversely proportional to the absolute temperature, in agreement with the theory of Heitler and Teller[4] regarding nuclear relaxation by interaction with the conduction electrons. From Korringa's theory[5] and Knight's measurement[6] of the frequency shift between Na^{23} resonances in the metal and in a salt, one calculates that T_1 due to conduction electrons should equal 11.7 milliseconds at room temperature, in excellent agreement with the measured value of 9.2 milliseconds. A 20 percent increase in the shift, such as Gutowsky proposes in the accompanying letter,[3] would lower the theoretical T_1 to a value even closer to the experimental result.

The T_2' data are shown in Fig. 1. Over the entire temperature range covered, T_2' is temperature dependent and is larger than the rigid lattice value by an order of magnitude. These results are in agreement with those of Gutowsky[3] which indicate that the line-width is narrower than the rigid lattice value for all temperatures above -100°C. The spin echo results show that T_2' increases markedly with temperature from the lowest temperature at which spin echoes were observed (-58°C) to about -25°C, where T_2' becomes of the order of T_1. For higher temperatures, T_2' goes as $1/T$ within experimental error and is of the order of T_1, indicating that spin-lattice relaxation determines the line-width in the high temperature range.

Using a simple theory, the observed low temperature behavior of T_2' can be explained as the combined effect of spin-lattice line broadening and nuclear dipolar broadening. T_2' is assumed to be given by the equation

$$1/T_2' = (1/T_2) + 1/T_2^a, \tag{1}$$

where T_2 is the phase-memory time determined by dipolar interactions alone, and T_2^a is that determined by spin-lattice interactions alone. The expression provides a better fit to the data than does the addition of second moments.

The large values observed for T_2' indicate that there is a motion of the sodium nuclei. Taking the motion to be self-diffusion of the nuclei, one may calculate the line narrowing on the basis of the theory of Bloembergen, Purcell, and Pound.[7] The calculation assumes the metal to be a liquid in which the atoms come no closer than a distance r, and predicts an exponential temperature dependence of T_2 according to the law

$$\frac{1}{T_2} = \frac{4}{5}\frac{\gamma^4\hbar^2 I(I+1)Ne^{E/RT}}{rD_0}, \tag{2}$$

where γ is the nuclear gyromagnetic ratio, I is the nuclear spin, N the number of atoms per unit volume, and the diffusion constant, D, has been written in the customary form $D = D_0 e^{-E/RT}$. For numerical work r was taken to be the rigid-lattice nearest-neighbor distance 3.7A. The liquid theory should give the temperature dependence of T_2 rather well, but be less reliable in giving the actual magnitude of T_2.

To compare Eqs. (1) and (2) with experiment, T_2^a was taken to be a constant (10.8 milliseconds), since T_2^a is a much more slowly varying function of temperature than T_2. The work of Nachtrieb[8] has been utilized in the comparison. He has measured the coefficient of self-diffusion for sodium by means of radioactive tracers and finds $D = 0.320e^{-10460/RT}$ cm²/sec. Extrapolating his measurements to -56°C gives $D = 0.74\times10^{-11}$ cm²/sec. The nuclear resonance data at this temperature, where the T_2^a correction is small, yield $D = 1.3\times10^{-11}$ cm²/sec. The order of magnitude agreement is considered satisfactory, since the theory is somewhat crude.

To compare the temperature dependence of the nuclear resonance data with Nachtrieb's results, a theoretical T_2' curve was constructed. Equations (1) and (2) and the constant T_2^a were used to calculate a value of T_2 at -56°C from the data. This value of T_2, together with T_2^a and Nachtrieb's value of the activation energy, determined the theoretical T_2' curve shown in Fig. 1. Curves corresponding to values of activation energy 20 percent higher and lower are also shown. The agreement of both the temperature dependence and the order of magnitude of D with Nachtrieb's results confirms the hypothesis of diffusion narrowing. Similar work is currently in progress on the Li^7 relaxation times.

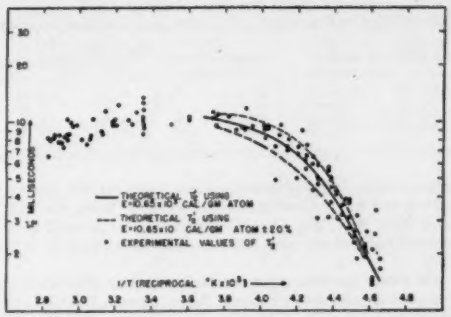
MILLISECONDS
THEORETICAL T_2' USING E=10.65±10⁷ CAL/GM ATOM
THEORETICAL T_2' USING E=10.65±10 CAL/GM ATOM ±20%
EXPERIMENTAL VALUES OF T_2'
1/T (RECIPROCAL °K ×10³)
2.8 3.0 3.2 3.4 3.6 3.8 4.0 4.2 4.4 4.6 4.8

FIG. 1. Temperature dependence of T_2' for metallic Na^{23}.

The authors are indebted to Dr. Nachtrieb for sending them his experimental results in advance of publication. Much of the electronic equipment was built by Mr. L. S. Kypta.

* This work was supported in part by the ONR.

[1] E. L. Hahn, Phys. Rev. **80**, 580 (1950).
[2] R. E. Norberg, thesis, University of Illinois (1951), unpublished.
[3] H. S. Gutowsky, Phys. Rev. **83**, 1073 (1951).
[4] W. Heitler and E. Teller, Proc. Roy. Soc. (London) **A155**, 629 (1936).
[5] J. Korringa, Physica **16**, 601 (1950).
[6] W. D. Knight, Phys. Rev. **76**, 1259 (1949).
[7] Bloembergen, Purcell, and Pound, Phys. Rev. **73**, 679 (1948).
[8] N. Nachtrieb, private communication.

Nuclear Absorption of Negative Pi-Mesons at Different Energies

G. BERNARDINI, E. T. BOOTH, AND L. LEDERMAN
Physics Department, Columbia University, New York, New York
(Received July 9, 1951)

ILFORD G-5, 400-, and 600-micron nuclear emulsions were exposed to the 70- and 105-Mev external π^- meson beams of the Nevis cyclotron, and the analysis of the interaction with emulsion nuclei was continued.[1,2] To extend the energy range, additional plates were exposed to the 70-Mev beam behind 8″ of lithium plus ½″ of carbon. The energy of the mesons crossing these plates was 30–50 Mev, as determined by plural scattering and grain density

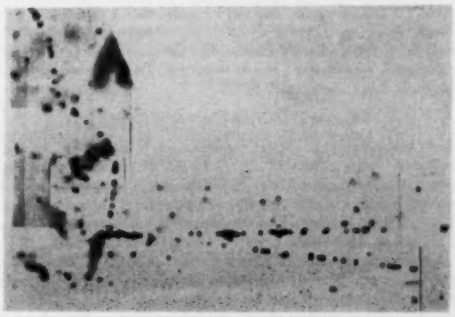

FIG. 1. Backward elastic scattering ($E = 105$ Mev, $\Theta = 173°$) with recoil and slow electron at the vertex (observed by Mrs. N. Bernardini).

TABLE I. Energy dependence of nuclear events.

Energy (in Mev)	Σl (in cm)	Stars	Stops	Elast. scatt. (>30°)	Inelast. scatt.
30– 50	2145±21	49 (15)	8	8 (17)	2 (6)
70– 80	1438±14	44 (11)	4	4 (4)	7 (8)
60– 90	1000±50	19 (7)	4	3 (6)	6 (8)
100–110	2761±28	76 (16)	18	15 (20)	22 (32)

measurements. It was possible to obtain plates covered by such a uniform and well-collimated flux that scanning "along the track" (with 90×, 80×, and 43× oil objectives) was as rapid as the conventional area scanning, and was employed exclusively in this work.

The actual numbers of the nuclear interactions observed in the total path of meson track followed, Σl, are given in Table I. In this classification we define "elastic scattering" as an event in which the incident and scattered pi-meson differ in energy by less than 15 percent. Occasionally, these may be accompanied by a short black prong or slow electron (10–100 kev) at the vertex. "Inelastic scatterings" are defined as events in which the scattered meson demonstrates, by grain density and plural scattering measurements, an energy loss >15 percent of the energy of the incident meson. When the outgoing track is shorter than 700 microns, only its grain density can be determined and the distinction between mesons and protons is not completely certain. The figures enclosed by brackets in columns 5 and 6 include these doubtful scatterings. In the third line, the data obtained in the old (60–90 Mev) meson beam[1] are also reported. The bracketed figures in column 3 give the number of stars having a proton prong of at least 30 Mev.

The angular distribution of the elastic scatterings <30° strongly suggests that most of these can be considered as shadow and coulomb scattering or $\pi-\mu$-decays. Since the results are quite insensitive to the choice of this cut-off angle, we assume that the remaining events are true interactions of pi-mesons with the nuclear matter in the emulsion. Table II gives the total number Σn

TABLE II. Corrected mean free path.

Energy (Mev)	$I(e)$ (percent)	$I(\mu)$ (percent)	$\Sigma'(l)$ (cm)	Σn	λ_{geom} (cm)	λ_{obs} (cm)
30– 50	(3±2)	(8±4)	1910±100	80	15.6	24.0±3.0
70– 80	(10±2)	(9±3)	1165± 55	60	19.1	19.4±2.6
60– 90*	(10±5)	(10±5)	800±100	37		21.5±4.2
100–110	2	(5±3)	2610±100	146	20.4	18.0±1.3

* Old meson beam.

of these and the corresponding total mean free paths. In the $I(e)$ and $I(\mu)$ columns, the relative fractions of the electrons and μ mesons of the different beams are given. These fractions were estimated principally by counter experiments.[2] Further and consistent data were provided by cloud chamber runs[4] and by analysis of track characteristics. The $\Sigma' l$ column gives the corrected path length of π^- meson observed. The geometrical mean free path, λ_{geom}, is taken to be

$$\lambda_{geom}=1/\Sigma_i N_i \pi h^2[(A^{\frac{1}{3}}/\mu c)+(1/p)]^2,$$

where the summation is over the emulsion constituents. This includes the finite extent of the pi-meson wave packet. At high energy, $\lambda_{obs}\cong\lambda_{geom}$; at low energy there is a transparency of ~30 percent. Since probably less than 25 percent of the collisions involve the light elements, this transparency is believed to originate in an energy dependence of the character of the interactions. Table III gives the absolute cross sections in barns for the various types of interactions as a function of energy. In this table, the bracketed figures of Table I were employed. The stoppings are included with stars because of the information in the π^+ interactions (to be published), which strongly indicate that these are stars containing only neutron prongs.

TABLE III. Cross sections, in barns.*

Energy	Stars and stops	Elast. scatt. 30°	Inelast. scatt.	Total
30– 50	0.62	0.19	0.06	0.87
60– 90	0.76	0.10	0.19	1.05
100–110	0.75	0.16	0.25	1.16

* Obtained from $\sigma=(21/\lambda)$ barns.

The definite increase with energy of the relative frequency of catastrophic processes (absorption and inelastic scattering) with respect to the elastic scatterings can partially explain the discrepancy between the results, here presented, and those of Bradner and Rankin.[5] However, in the energy interval (30–50 Mev) corresponding to the Berkeley experiment, the relative star frequency found by us is still twice that given by the Berkeley authors.

The general features of the stars do not change with the π^- energy, and it is evident that a large fraction of the absorbed energy is carried away by neutral particles (neutrons). However, a clearer analysis of the pion absorption mechanics will be possible through the comparison of these results with data now being assembled on the π^+ interactions.

We should like to acknowledge the invaluable assistance of Mr. Harrison Edwards, Mr. J. Spiro, and the Nevis staff, and to express appreciation to Mrs. N. Bernardini, Mrs. D. Lee, and Miss E. Wimmer for the scrupulous care taken in the scanning. Mrs. J. Bielk did excellent work in processing of the plates.

[1] Bernardini, Booth, Lederman, and Tinlot, Phys. Rev. **80**, 924 (1950).
[2] Bernardini, Booth, Lederman, and Tinlot, Phys. Rev. **82**, 105 (1951).
[3] The authors wish to thank Professors A. Sachs and J. Steinberger, and Dr. P. Isaacs for informing them of their results. See also Chedester, Isaacs, Sachs, and Steinberger, Phys. Rev. **82**, 958 (1951).
[4] Lederman, Booth, Byfield, and Kessler, **83**, 685 (1951).
[5] H. Bradner and B. Rankin, Phys. Rev. **80**, 916 (1950).

Probable Emission of a Beryllium-8 Nucleus in the Fast Neutron Fission of Thorium-232

E. W. TITTERTON
Research School of Physical Sciences, Australian National University, Canberra, Australia
(Received July 9, 1951)

IN the course of recent photographic plate experiments on the fast neutron fission of thorium-232 using 2.5-Mev D–D neutrons,[1] an event was observed in which two light particle tracks emanate from the point of fission in addition to the two heavy fragments. The event is very similar to that observed earlier by Goward, Titterton, and Wilkins[2] in the course of experiments on the photofission of uranium. The explanation suggested in the photofission case was that the event represented ternary fission with the emission of a Be^8 nucleus. If the same explanation is applied to the present event, the α-particles are found to have energies of 10.0 and 9.6 Mev, respectively, and are inclined at 9° each other. Calculation shows that the energy release in the to disintegration of such a Be^8 nucleus into the two α-particles is 120±10 kev. This is somewhat higher than the measured value for the instability of the ground state of Be^8 given by Hemmendinger[3] as 103±10 kev, by Tollestrup, Fowler, and Lauritsen[4] as 89±5 kev, and more recently by Carlson[5] as 72±5 kev. Nevertheless, it seems reasonable to interpret the event as representing the fast neutron ternary fission of a thorium-232 nucleus, the third fragment being a Be^8 nucleus in its ground state emitted with an energy of 19.6±0.5 Mev at an angle of 62° to the fission fragment of smaller charge.

That such events are very rare is indicated by the fact that the two discussed above are the only ones observed in investigations including examination of 600,000 slow neutron events in-

duced in U^{238}, 12,000 fast neutron events in U^{235}, 14,000 fast neutron events in Th^{232}, 10,000 photofission events in U^{238}, and 2500 photofission events in Th^{232}.

This work was carried out while the author was still at A.E.R.E., Harwell, and thanks are due to the Director, Sir John Cockcroft, F.R.S., for permission to publish.

[1] E. W. Titterton, Phys. Rev. **83**, 673 (1951).
[2] Goward, Titterton, and Wilkins, Nature **164**, 661 (1949).
[3] A. Hemmendinger, Phys. Rev. **75**, 1267 (1949).
[4] Tollestrup, Fowler, and Lauritsen, Phys. Rev. **76**, 428 (1949).
[5] R. R. Carlson, Phys. Rev. **83**, 203 (1951).

Inter-Ionic Distances and Line Widths in Paramagnetic Resonance Absorption

H. KUMAGAI, K. ŌNO, I. HAYASHI, H. ABE, J. SHIMADA, H. SHŌNO, AND H. IBAMOTO*
Institute of Science and Technology, Tokyo University, Tokyo, Japan
(Received July 3, 1951)

IN a previous letter,[1] we have reported some of the results of our precise observations on the line width in microwave paramagnetic resonance absorption by manganese sulfates, in conjunction with the theory of dipolar broadening by Van Vleck.[2] Since then, measurements on several salts containing copper ions were added to our data, which can be compared with theory more thoroughly than before.

Results are summarized in Table I. The widths in the table are

TABLE I. Paramagnetic absorption lines (9970 Mc).

Salts	Single crystal or powder	Shape of absorption line	Range of half-width by crystal orientation (Oersted)	Range of g-values
$Mn(NH_4)_2(SO_4)_2\cdot 6H_2O$ (diluted)	single	several peaks not completely resolved	~70	—
$Mn(NH_4)_2(SO_4)_2\cdot 6H_2O$	single	several peaks scarcely resolved	1000–2000	—
$MnSO_4\cdot 5H_2O$	single	one peak, intermediate shape of gaussian and resonance curve	—	—
	powder	one peak, intermediate shape of gaussian and resonance curve	1250	2.06
$MnSO_4\cdot 4H_2O$	single	one peak, intermediate shape of gaussian and resonance curve	980–1500	2.00–2.07
	powder	one peak, intermediate shape of gaussian and resonance curve	1140	2.04
$MnSO_4\cdot H_2O$	powder	one peak, resonance curve	305	2.00
$MnSO_4$	powder	one peak, resonance curve	655	2.00
$Cu(NH_4)_2(SO_4)_2\cdot 6H_2O$	single	two peaks, like gaussian curve	~230	2.0 –2.3
$Cu(NH_4)_2Cl_2\cdot 2H_2O$	single	one peak, resonance curve	90–230	2.05–2.20
$CuK_2Cl_4\cdot 2H_2O$	single	one peak, resonance curve	110–250	2.05–2.20
$CuSO_4\cdot 5H_2O$	single	one peak, resonance curve	50–220	2.04–2.24
	powder	—	300	—
$CuCl_2\cdot 2H_2O$	single	one peak, resonance curve	55–70	2.03–2.23
$CuSO_4\cdot H_2O$	powder	one peak, gaussian curve	310	2.19

obtained at half the maximum χ'' irrespective of the line shapes. As the g-values of salts containing $Mn^{++}(^6S)$ are almost isotropic, the half-width in polycrystals of $MnSO_4\cdot H_2O$ and $MnSO_4$ have definite meanings. In the cases of $Cu(NH_4)_2(SO_4)_2\cdot 6H_2O$ and diluted $Mn(NH_4)_2(SO_4)_2\cdot 6H_2O$, the curves are composed of several peaks which can be decomposed to one, and the widths of each are shown in the table. As the line shapes of polycrystals of $CuSO_4\cdot H_2O$ are almost gaussian, it is probable that g-values are nearly isotropic in the single crystal.

We shall consider the line widths for the same kind of paramagnetic ions contained in various salts which have different inter-ionic distances. According to Van Vleck's theory,[2] the widths $(\Delta H)_{\frac{1}{2}}$ owing to dipolar coupling in this case are given approximately as follows:

$$(\Delta H)_{\frac{1}{2}}\sim 1/r^3,$$

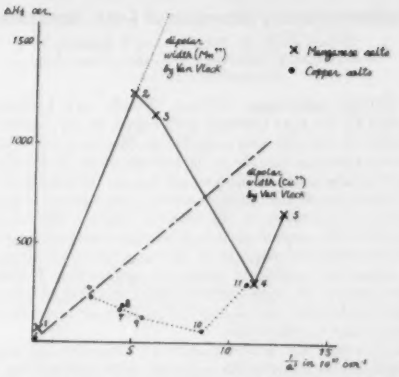

FIG. 1. Half-widths of salts of Mn^{++} and Cu^{++} and calculated dipolar widths. 1. $Mn(NH_4)_2(SO_4)_2\cdot 6H_2O$ diluted; 2. $MnSO_4\cdot 5H_2O$; 3. $MnSO_4\cdot 4H_2O$; 4. $MnSO_4\cdot H_2O$; 5. $MnSO_4$; 6. $Cu(NH_4)_2(SO_4)_2\cdot 6H_2O$; 7. $Cu(NH_4)_2Cl_2\cdot 2H_2O$; 8. $CuK_2Cl_4\cdot 2H_2O$; 9. $CuSO_4\cdot 5H_2O$; 10. $CuCl_2\cdot 2H_2O$; 11. $CuSO_4\cdot H_2O$.

where r is the mean inter-ionic distance, and the line shape is assumed to be gaussian. As a first approximation, we consider the arrangement of ions as simple cubic with lattice constant a; then we can put $(\Delta H)_{\frac{1}{2}}\sim(1/a^3)$. The values of a are given by $a^3\rho=M/N$ where ρ is the density, M the molecular weight related to the single ion of the salt, and N the Avogadro number.

In Fig. 1 the values of $(\Delta H)_{\frac{1}{2}}$ from Table I are plotted against $1/a^3$. The widths indicated in the figure for single crystals are means of those for different orientations. The dotted and dashed straight lines indicate the widths for Mn^{++} and Cu^{++} owing to dipolar broadening, by Van Vleck's calculation.[2] For smaller values of $1/a^3$, the widths are almost equal to those expected by dipolar broadening in both cases of Mn^{++} and Cu^{++}. But when ions are nearer, the width becomes much smaller than those corresponding to the straight lines, because of the effect of exchange interaction. These results agree with the fact that Δ, the departure from Curie's law in the static susceptibility, is 0.7°, 3°, 2°, and 24° for $Mn(NH_4)_2(SO_4)_2\cdot 6H_2O$, $MnSO_4\cdot 5H_2O$, $MnSO_4\cdot 4H_2O$, and $MnSO_4$, respectively, and that Δ is mainly due to the exchange effect for manganese salts.[3] It is remarkable that the widths become broader again for the smallest value of a, which can be seen in the cases of $MnSO_4$ and $CuSO_4\cdot H_2O$. In any case, the curves shown in Fig. 1 may have important bearing on the nature of dipolar and exchange interactions of paramagnetic ions.

* Department of Chemistry, Faculty of Science, Ōsaka University, Ōsaka, Japan.
[1] Kumagai, Ōno, Abe, Shōno, Tachimori, Ibamoto, and Shimada, Phys. Rev. **82**, 954 (1947).
[2] J. H. Van Vleck, Phys. Rev. **74**, 1168 (1948).
[3] J. H. Van Vleck and W. G. Penny, Phil. Mag. **17**, 961 (1934).

Erratum: Angular Distribution of Protons from the D(*d*, *p*)T Reaction at 10.3-Mev Bombarding Energy

[Phys. Rev. **82**, 782 (1951)]

J. C. ALLRED, D. D. PHILLIPS, AND LOUIS ROSEN
University of California, Los Alamos Scientific Laboratory, Los Alamos, New Mexico

THE captions of Fig. 1 and Fig. 2 should be interchanged. This applies also to the angle designations on the histograms, i.e., $\theta=132.5°$ lab for Fig. 2 and $\theta=12.8°$ for Fig. 1. In addition, these angles should be transposed in the references of the text to the figures.

Antiferroelectric Structure of Lead Zirconate

E. SAWAGUCHI, H. MANIWA, AND S. HOSHINO
Tokyo Institute of Technology, Oh-okayama, Tokyo, Japan
(Received June 25, 1951)

A CLOSE resemblance between $PbZrO_3$ and ferroelectric $BaTiO_3$ has been reported[1] with respect to the variation of the dielectric constant with temperature. However, any decisive evidence supporting exclusively the ferroelectricity of $PbZrO_3$, for example spontaneous polarization, has not yet been observed, for both ferroelectrics and antiferroelectrics may reveal a similar temperature dependence of the dielectric constant. On the other hand, all the phenomenological facts recently observed,[2] especially those concerning the response of this material to a biasing dc field, cannot be understood unless we assume that $PbZrO_3$ is antiferroelectric. Of course, the more direct and ultimate proof for its antiferroelectricity can be provided by the x-ray analysis of the superstructure[3] of this crystal.

The structure has been examined by oscillation and powder photographs. We found lattice repetitions with periods of $4a_0$, $4b_0$, and $2c_0$ in the three directions of cubic edges in the perovskite lattice, respectively ($a_0=4.15$A, $b_0=4.15$A, $c_0=4.10$A). Hitherto, the crystal of this substance has been reported to be seemingly tetragonal[4] or monoclinic;[5] but the present x-ray pattern and detailed optical observations on a very minute untwinned crystal by means of a polarization microscope have revealed that it is orthorhombic. The orthorhombic unit cell has spacings $a=5.87$A, $b=11.74$A, and $c=8.20$A, and contains eight molecules. The main characteristic spots corresponding to the superstructure have indices ($h\neq 0$, $k=2n+1$, $l=2p$). The other spots, with odd l, are so faint that they are hardly noticeable except on oscillation photographs of small oscillation angle (<5 degrees), so that 4.10A, half of the c spacing, may be adopted as the approximate value of the c translation. It also turns out that the crystal has two glide reflection planes, and the space group may be either $D_{2h}(9)$ or $C_{2v}(8)$.

In the case of D_{2h}, each Pb ion is supposed to be displaced along the orthorhombic $+a$ or $-a$ axis as shown exaggerated in Fig. 1. The displacement is calculated to be about 0.2A. If, on the other hand, the symmetry is C_{2v}, all the Pb ions can make a certain shift along the c axis in addition to the antiparallel displacement described above. If this common shift along the c axis is of considerable magnitude, the crystal may be ferroelectric in the c direction. In fact, however, the relative spot intensities show that the c shift must be negligibly small, so that the main part of the dipole moment must lie in the $a-b$ plane bearing an antiferroelectric arrangement. This conclusion suggests a reason for the fact that in $PbZrO_3$ the ratio c_0/a_0 is less than 1, in contrast to the situation in $BaTiO_3$.

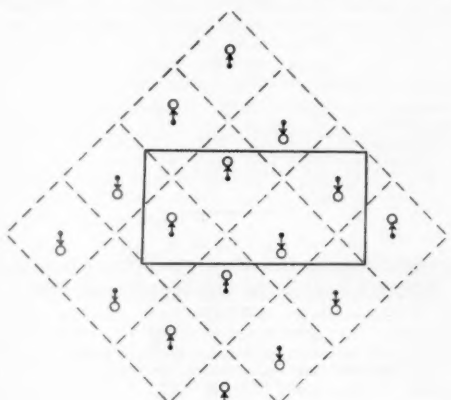

FIG. 1. Antiferroelectric structure of $PbZrO_3$; arrows represent the direction of shifts of Pb ions; the solid line shows an orthorhombic unit cell.

We wish to thank Professors Y. Takagi and S. Miyake for valuable advice and discussions, and Dr. G. Shirane for helpful discussions and for kindly lending us his powder photograph.

[1] S. Roberts, J. Am. Ceram. Soc. **33**, 63 (1950).
[2] Shirane, Sawaguchi, and Takagi, J. Phys. Soc. Japan **6**, 208 (1951); Sawaguchi, Shirane, and Takagi, J. Phys. Soc. Japan (to be published).
[3] A. Hoffmann, Z. physik. Chem. **B28**, 65 (1935).
[4] H. D. Megaw, Proc. Phys. Soc. (London) **58**, 133 (1946); R. Ueda and G. Shirane, J. Phys. Soc. Japan **6**, 209 (1951).
[5] Naray-Szabo, Naturwiss. **31**, 203 (1943).

Piezoelectric Effect in Lead Zirconate

SHEPARD ROBERTS
General Electric Research Laboratory, Schenectady, New York
(Received July 13, 1951)

CERAMIC disks of pure lead zirconate prepared as formerly described by the author[1] were polarized by applying an electric field while cooling from 250°C to 100°C. One disk was polarized with a dc field of about 250 v/mm, while a second disk was polarized with unidirectional pulses 800 v/mm in amplitude. The values for d_{33} measured in both disks under static compression at ambient temperature were approximately 10^{-12} coulomb per newton. This value is just barely detectable in our apparatus, although the results were definitely reproducible and the observed effect reversed when the disk was turned over. The polarity of the field induced by compression is the same as that of the original polarizing field in lead zirconate just as in barium titanate.

The smallness of the effect was at first puzzling, but can now be understood in reference to the structure analysis of Sawaguchi, Maniwa, and Hoshino.[2] Of the two allowable symmetry classes, the choice C_{2v} is consistent with the observed piezoelectric effect.

[1] S. Roberts, J. Am. Ceram. Soc. **33**, 63 (1950).
[2] Sawaguchi, Maniwa, and Hoshino, Phys. Rev. **83**, 1078 (1951).

Erratum: Low States of Li^7 in Intermediate Coupling

[Phys. Rev. **81**, 910 (1951)]

H. H. HUMMEL AND D. R. INGLIS
Argonne National Laboratory, Chicago, Illinois

WE are grateful to Igal Talmi of Zürich for pointing out errors in the $\pi-\nu$-Majorana interaction listed in Table I. The total Majorana interactions in that table should read, respectively, $L+K$, $(2L/9)+10K/3$, $-\frac{1}{3}L+5K$, $-\frac{1}{3}L+6K$, $L+11K/3$, $(-2L+16K)/3$ (for $\tau=3/2$), $(4L+10K)/3$ (for $\tau=1/2$), the last value being calculable from trace invariance with isotopic spin. The consequent changes in the asymptotes on the right side of Fig. 3 are small and the general conclusions of the paper remain unaltered.

Concerning the Mechanism of Electron-Ion Recombination. II

MANFRED A. BIONDI
Westinghouse Research Laboratories, East Pittsburgh, Pennsylvania
(Received June 29, 1951)

DURING the past few years, experiments[1,2] on the decay of electron density from an initially ionized gas have revealed a recombination between thermal electrons and positive ions whose

rate exceeds the theoretical prediction[3] for radiative recombination by several orders of magnitude. This discrepancy has led to the supposition[4] that the observed recombination involves nonradiative capture of an electron by a molecular ion, followed by dissociation into two (or more) neutral fragments, one of which is in an excited electronic state.

In the first paper of the above title,[5] the hypothesis of dissociative recombination was analyzed from the standpoint of recent data obtained in this laboratory. It was found that our data in helium and neon was consistent with the dissociative scheme provided that helium molecular ions were formed and persisted in high vibration states during our measurements. Qualitative theoretical estimates indicated that the assumption of vibrational persistence, while somewhat extreme, was still conceivable.

In order to demonstrate conclusively the dependence of the observed recombination on the presence of molecular ions, it was proposed to study the decay of electron density in samples of helium and neon containing small admixtures of argon (0.1 percent). The argon atoms would be rapidly ionized by helium or neon metastables, so that the chief positive charge carriers would be atomic argon ions; however, the concentration of argon would be too small to permit appreciable formation of molecular argon ions, A_2^+, during our measurements. These experiments are the subject of the present paper.

Previously described[5] microwave and optical techniques were used to measure the electron density and radiation emitted during the afterglow following a discharge. The gas samples were Airco reagent grade helium, neon, and argon. The ultra-high vacuum system[6] used did not contribute significant contamination to the samples.

Typical experimental data for pure argon are presented in Fig. 1. These data fit quite well the relationship

$$1/n_- = (1/n_0) + \alpha t, \tag{1}$$

where n_- is the electron density and α the recombination coefficient. Equation (1) is characteristic of a recombination loss of electrons; the value $\alpha = 8.8 \times 10^{-7}$ cc/sec obtained from the curve is in fair agreement with previous measurements.[1]

Corresponding experimental data for the helium-argon mixture are shown in Fig. 2. In this case the data obey a decay equation of the form

$$n_- = n_0 \exp(-t/T) \tag{2}$$

characteristic of ambipolar diffusion loss of electrons and A^+ ions. The decay constant, T, is related to the ambipolar diffusion coefficient, $D_a{}^A$, by

$$T = \Lambda^2/D_a{}^A, \tag{3}$$

where Λ is the characteristic diffusion length of the container and has the value 0.735 cm. From our values of $D_a{}^A$, which exhibit the correct pressure dependence as shown by Fig. 3, we compute[1] the

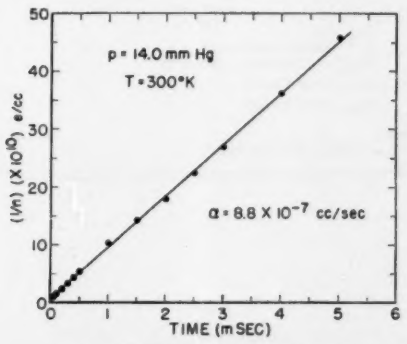

FIG. 1. Decay of electron density in pure argon.

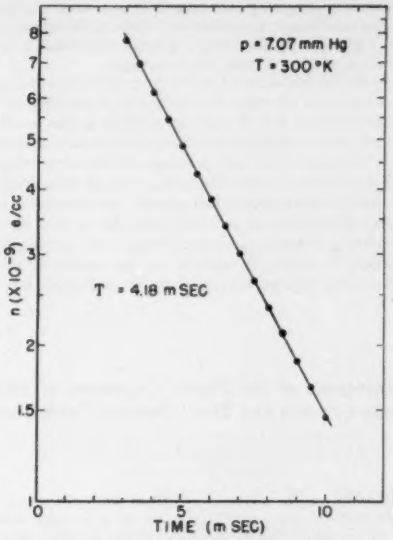

FIG. 2. Decay of electron density in helium-argon mixtures (0.1 percent argon).

mobility of our alleged A^+ in helium as $\mu_+ = 22.4$ cm/sec per volt/cm (at 291°K and 760 mm Hg). This value lies within 2 percent (experimental error) of the curve of mobility *versus* mass number for various ions in helium[7] (see Fig. 8 of reference 1), indicating strongly that the ion under observation is indeed A^+.

Detailed consideration of experimental errors in the data of Fig. 2 permit us to set an upper bound for recombination loss. It is found that the recombination coefficient must be $< 10^{-9}$ times that obtained in pure argon. Data similar to that shown in Fig. 2 were taken over the pressure range 1.6–7.2 mm Hg, and in all cases the above conclusion was substantiated. In addition, radiation measurements, which previously gave a photon yield consistent with a value of $\alpha \sim 10^{-6}$ in pure argon, show a 1000-fold decrease in intensity in the argon admixture experiments. It is not necessary to assign this yield to atomic ion recombination, since it is quite possible that in these admixture experiments the concentration of molecular positive ions $\sim 10^{-3} n_-$. The recombination of these molecular ions with electrons would then explain our radiation yield.

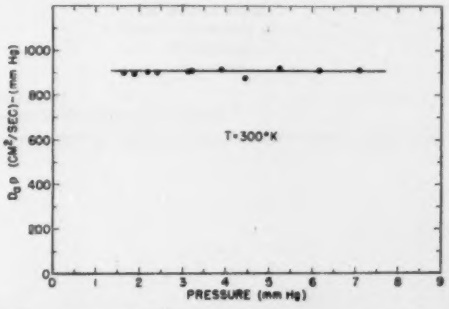

FIG. 3. Ambipolar diffusion coefficient of argon ions in helium at 300°K.

Experiments using 0.1 percent argon in neon were also carried out. These experiments gave identical results to the helium-argon studies, again showing the absence of large recombination under conditions in which molecular ions are absent.

Following the initial report of the large recombination coefficients, a variety of processes were considered as possible recombination mechanisms. For example, in addition to the previously mentioned radiative capture and dissociative capture of electrons by molecular ions, three-body processes involving two electrons and an ion, various plasma effects (e.g., cut-off of coulomb potential in an ionized medium), and negative ion formation in noble gases were all considered in an effort to find the source of the large recombination. These considerations, which were necessitated by the difficulty in finding an electron capture mechanism efficient enough to yield the observed recombination coefficients, may now be discarded. All available evidence indicates that the recombination is a two-body process involving an electron and a molecular ion and that the mechanism is probably dissociative recombination.

The author is greatly indebted to T. Holstein for suggesting these admixture experiments as a conclusive demonstration of the role of molecular ions in the observed recombination.

[1] M. A. Biondi and S. C. Brown, Phys. Rev. **75**, 1700 (1949); **76**, 1697 (1949).
[2] Holt, Richardson, Howland, and McClure, Phys. Rev. **77**, 239 (1950); Johnson, McClure, and Holt, **80**, 376 (1950).
[3] Bates, Buckingham, Unwin, and Massey, Proc. Roy. Soc. (London) **A170**, 322 (1939).
[4] D. R. Bates, Phys. Rev. **77**, 718 (1950); **78**, 492 (1950).
[5] M. A. Biondi and T. Holstein, Phys. Rev. **82**, 962 (1951).
[6] The system and techniques are based on material described by D. Alpert, Rev. Sci. Instr., to be published.
[7] R. J. Munson and A. M. Tyndall, Proc. Roy. Soc. (London) **A172**, 33 (1939).

Measurement of the Elastic Constants of Silicon Single Crystals and Their Thermal Coefficients

H. J. McSkimin, W. L. Bond, E. Buehler, and G. K. Teal
Bell Telephone Laboratories, Murray Hill, New Jersey
(Received June 29, 1951)

INTEREST in the properties of silicon single crystals arising from their use as semiconductors has led us to make measurements of the elastic constants of two single crystals. Measurements of velocities of propagation for both shear and longitudinal waves were made in the crystals as described in a recent paper by McSkimin.[1] Frequencies in the range 8–12 Mc/sec were used.

The three independent elastic constants were evaluated, a density of 2.331 (measured by pycrometer) being used. Data and formulas used are summarized in Table I. Two crystals were measured—as indicated—with data obtained from the larger one being used to determine the elastic constants. Check measurements were made for the smaller crystal; and despite the less accurate "pulse overlap" technique used for two of the measurements, velocity agreement to within 0.15 percent was obtained.

Both crystals were of a high degree of crystalline perfection as shown by etching and x-ray tests.

[1] H. J. McSkimin, J. Acoust. Soc. Am. **22**, 413 (1950).

TABLE I. Data for silicon single crystals ($\rho = 2.331$; $\alpha = 7.63 \times 10^{-6}$).

Direction of propagation	Direction of particle motion	Type of mode	Equation for velocity	Velocity at 25°C in cm/sec	Velocity temp. coeff.
			(Crystal 1)		
110 $t = 9.0140$ mm	$1\bar{1}0$	Shear	$V_1 = \left(\frac{0.5C_{11} - 0.5C_{12}}{\rho}\right)^{\frac{1}{2}}$	4.682×10^5	—
001 $t = 5.9746$ mm	110	Shear	$V_2 = (C_{44}/\rho)^{\frac{1}{2}}$	5.843×10^5	-16.3×10^{-6}
001	001	Long.	$V_3 = (C_{11}/\rho)^{\frac{1}{2}}$	8.474×10^5	-26.2×10^{-6}
110	110	Long.	$V_4 = \left(\frac{0.5C_{11} + 0.5C_{12} + C_{44}}{\rho}\right)^{\frac{1}{2}}$	9.167×10^5 (calculated)	—
			(Check crystal 2)		
110 $t = 3.2215$ mm	$1\bar{1}0$	Shear	V_1	4.682×10^5	-42.3×10^{-6}
110	001	Shear	V_2	5.834×10^5 (29°)	—
110	110	Long.	V_4	9.152×10^5 (30°)	—

Elastic constants (25°C)
$C_{11} = 1.6740 \times 10^{12}$ dynes/cm²
$C_{12} = 0.6523 \times 10^{12}$
$C_{44} = 0.7957 \times 10^{12}$

Elasticity-temp. coeff.
$K_{C_{11}} = -75.3 \times 10^{-6}$ parts per °C
$K_{C_{12}} = -24.5 \times 10^{-6}$
$K_{C_{44}} = -55.5 \times 10^{-6}$

Uncertainties for crystal 1
l—0.02%; freq.—0.01%; elastic constants—0.26%; ρ—0.10%; velocities—0.08%